Lecture Notes in Electrical Engineering 1061

Jatindra Kumar Deka
P. S. Robi
Bobby Sharma *Editors*

Emerging Technology for Sustainable Development

Select Proceedings of EGTET 2022

Springer

Lecture Notes in Electrical Engineering

Volume 1061

The book series *Lecture Notes in Electrical Engineering* (LNEE) publishes the latest developments in Electrical Engineering—quickly, informally and in high quality. While original research reported in proceedings and monographs has traditionally formed the core of LNEE, we also encourage authors to submit books devoted to supporting student education and professional training in the various fields and applications areas of electrical engineering. The series cover classical and emerging topics concerning:

- Communication Engineering, Information Theory and Networks
- Electronics Engineering and Microelectronics
- Signal, Image and Speech Processing
- Wireless and Mobile Communication
- Circuits and Systems
- Energy Systems, Power Electronics and Electrical Machines
- Electro-optical Engineering
- Instrumentation Engineering
- Avionics Engineering
- Control Systems
- Internet-of-Things and Cybersecurity
- Biomedical Devices, MEMS and NEMS

For general information about this book series, comments or suggestions, please contact leontina.dicecco@springer.com.

To submit a proposal or request further information, please contact the Publishing Editor in your country:

China

Jasmine Dou, Editor (jasmine.dou@springer.com)

India, Japan, Rest of Asia

Swati Meherishi, Editorial Director (Swati.Meherishi@springer.com)

Southeast Asia, Australia, New Zealand

Ramesh Nath Premnath, Editor (ramesh.premnath@springernature.com)

USA, Canada

Michael Luby, Senior Editor (michael.luby@springer.com)

All other Countries

Leontina Di Cecco, Senior Editor (leontina.dicecco@springer.com)

**** This series is indexed by EI Compendex and Scopus databases. ****

Jatindra Kumar Deka · P. S. Robi · Bobby Sharma
Editors

Emerging Technology for Sustainable Development

Select Proceedings of EGTET 2022

Springer

Editors
Jatindra Kumar Deka
Department of Computer Science
and Engineering
Indian Institute of Technology Guwahati
Guwahati, Assam, India

P. S. Robi
Department of Mechanical Engineering
Indian Institute of Technology Guwahati
Guwahati, Assam, India

Bobby Sharma
Department of Computer Science
and Engineering
Assam Don Bosco University
Guwahati, Assam, India

ISSN 1876-1100 ISSN 1876-1119 (electronic)
Lecture Notes in Electrical Engineering
ISBN 978-981-99-4361-6 ISBN 978-981-99-4362-3 (eBook)
https://doi.org/10.1007/978-981-99-4362-3

This Springer imprint is published by the registered company Springer Nature Singapore Pte Ltd.
The registered company address is: 152 Beach Road, #21-01/04 Gateway East, Singapore 189721, Singapore

Contents

Design of Modern Technology Lighting System for Automobiles 1
Sundeep Siddula

A Critical Examination of Remote-Controlled Aircraft Technology in Terms of Their Operation in All-Weather Conditions 9
S. K. Vishnoo Prathap and Vikramjit Kakati

A Review of Materials Suitable for Tissue-Engineered Bone Scaffolds 19
Shreeprasad S. Manohar, Chinmoy Das, and Vikramjit Kakati

Abrasive Wear Behaviour of Reformer HP40Nb Steel 31
Leena Harshal Nemade, P. S. Robi, and Pankaj Biswas

Conceptualization, Design, and Development of a Pedal Propelled Vehicle to Collect and Dispose Residential Solid Waste 41
Vikramjit Kakati and Sidharth Borkataky

UAV for Remote Sensing Applications: An Analytical Review 51
Victor Saikhom and Manoranjan Kalita

A Review of Numerical Models for Sediment Dynamics 61
Borneeta Dutta, Pankaj Srivastava, and Annapurna Boruah

Thermal Analysis of an Office Building Using Passive Cooling Design in Aizawl, Mizoram 69
Haudingliana Hauzel, B. C. Vanlalhruaitluanga, Lalrindika, Lalsangzela Sailo, and Sylvia Romawizuali

Geochemical Evolution of Spring Water Sources in West Phaileng, Mizoram 79
Lalsangzela Sailo, Munna Das, and H. Vanlalhruaia

A Review on Nearshore and Offshore Fish Cage Developments in Open Seas 89
Abdul Shareef Shaik and Nasar Thuvanismail

Water Pollution: A Review 101
Nandkishore Dadsena and Sindhu J. Nair

Experimental Study on Low-Cost and Lightweight Building Materials Developed Using Waste Materials 111
Hillol Kashyap, Fazlur Rahman, Nishat Tashnim, Kaushik Kashyap, Shubam Deb, and Debshri Swargiary

A Study on Square and Rectangular Hollow Steel Section Subjected to Torsion 119
Thounaojam Bidyaraj Singh and Khwairakpam Sachidananda

Utilization of Reclaimed Asphalt Pavement (RAP) and Use of Plastic Waste in Road Construction: Literature Review 127
Tuleshwar Choudhary and Madhumati K. Yadav

Utilizing Plastic Waste in Construction Materials: A Review 135
Kasturima Das

Analysis of Seismic Forces for Earthquake-Resistant Constructions 145
Kakade Maheshkumar Anant and P. S. Charpe

Strength Performance Study of Concrete with Partial Replacement of Sand with ROBO SAND and Cement with GGBS 165
Mrinal Kanti Sen, Supran Chakravarty, and T. R. Girija

Analysis and ANN Modeling of Water Quality of Ramsar Site of Assam 175
Tina Gogoi and T. R. Girija

Determination of Optimum K Value for K-means Segmentation of Diseased Tea Leaf Images 187
Anuj Kumar Das and Syed Sazzad Ahmed

Recent Advancement and Challenges of Deep Learning for Breast Mass Classification from Mammogram Images 197
Lal Omega Boro and Gypsy Nandi

Brain Tumour—Augmentation, Segmentation and Classification Using Deep Learning—A Review 209
Ranadeep Bhuyan and Gypsy Nandi

Student Placement Prediction Using Machine Learning Algorithms 231
Samarth Sajwan, Rudraksh Bhardwaj, Revaan Mishra, and Shruti Jaiswal

Development of Machine Learning Based Daily Peak Load Forecasting System for Winter Season in the State of Meghalaya in India 243
Balarihun Mawtyllup and Bikramjit Goswami

IoT Based Cattle Monitoring System 251
Hirokjyoti Kalita, Vivek Kumar Poddar, Deep Kumahr, Raju Rajak, Nupur Choudhury, and Rupesh Mandal

Estimation of Water Quality Parameters for Deepor Beel Using Landsat 8 Data 263
Sonia Sarmah and Bikramjit Goswami

Improved Detection of Large-Sized Pedestrians Using Non-linear Scale Space and Combination of HOG and Dense LDB Features 273
Amlan Jyoti Das, Navajit Saikia, and Abhishek Das

Cyberthreat Detection Using Machine Learning 287
Simanta Rajbangshi, Chemkai Wangpan, Ayushman Chaudhury, Nupur Choudhury, and Rupesh Mandal

Medicinal Plant Classification Using Neural Network 297
Avilie Khate and Bobby Sharma

Driving Behavior Analysis Using Deep Learning on GPS Data 309
Saurabh Kumar Singh, Utkarsh Anand, Anurag Patel, and Debojit Boro

Blockchain-Based Marketplace for Farmers Using Perun Payment System 323
Sujit Sangram Sahoo, Mahesh Mohan Hosmane, and Vijay Kumar Chaurasiya

Sentiment Analysis on COVID-19 Tweets: Machine Learning Approach 339
Janrhoni M. Kikon and Rubul Kumar Bania

Adder Design Using Reversible Logic 349
Gunajit Kalita, Navajit Saikia, and Amit Sravan Bora

Anti-Spoofing System for Face Detection Using Convolutional Neural Network 361
Sumedha Sutradhar, Nazrul Ansari, Manosh Kumar, Nupur Choudhury, and Rupesh Mandal

Utilizing Greenhouse Technology Towards Sustainable Agriculture Using IoT "TechFarm" 373
Darsana Sandilya, Charlina Bharali, Angom Ringku, and Bobby Sharma

Enabling Technologies for Effective E-Waste Management 383
Ezan Abdullah and Khushaima Hilal

Modeling and Simulation of Successful Signal Transmission Without Information Loss in Axon 397
Biswajit Das, Satyabrat Malla Bujar Baruah, and Soumik Roy

An ECG Acquisition/Local Server Unit for Remote Patient Consultation 411
Bidyut Bikash Borah, Satyabrat Malla Bujar Baruah, Debaraj Kakati, and Soumik Roy

Proximity Coupled Planar MIMO Antenna for LTE-46/LTE-U Bands of Sub-6 GHz 421
P. Krishna Kanth Varma and Nagesh Kallollu Narayaswamy

Effective Facemask Detection Using a Few Learning-Based Recognition Methods 433
Atlanta Choudhury and Kandarpa Kumar Sarma

Development and Implementation of Voice-Controlled 3D Movement of Robotic Arm Based on Embedded System 445
Alakesh Sarkar, Partha Bhowal, Nityananda Hazarika, Ram Kishore Roy, Hidam Kumarjit Singh, and Tulshi Bezboruah

PRI Modulation Classification in EW Systems Using Deep Learning . . . 453
Purabi Sharma and Kandarpa Kumar Sarma

JSCC-UFMC in Multi-User Antenna Diversity Using Hybrid Beamforming for Millimeter Wave Wireless Communications 463
Surajit Deka and Kandarpa Kumar Sarma

Dual-Band Omnidirectional Parasitic Dielectric Resonator Antenna 475
Roktim Konch, Sivaranjan Goswami, Kumaresh Sarmah, and Kandarpa Kumar Sarma

Development of Near-Real-Time Solar Generation Prediction Technique Using Weather Data 483
Navareen Sohkhlet and Bikramjit Goswami

Monitoring Soil Wetness Using Ground-Based L-Band Scatterometer 493
Bikramjit Goswami

An Enhanced Blockchain Consensus Mechanism Using Proof-of-Work and Proof-of-Stake 501
Kausthav Pratim Kalita, Jerry Casper Kharbhih, Debojit Boro, and Dhruba Kumar Bhattacharyya

A Remote Health Monitoring System for the Elderly Based on Emerging Technologies 513
C. M. M. Mansoor, Sarat Kumar Chettri, and H. M. M. Naleer

Blockchain with Adjustable Proof-of-Work Consensus Mechanism for Mobile Devices 525
Kausthav Pratim Kalita, Eric Rani, Debojit Boro, and Dhruba Kumar Bhattacharyya

LoRa-Enabled IoT Framework for Flash Flood Crisis Management 537
Rupesh Mandal, Bobby Sharma, and Dibyajyoti Chutia

Crowd Size Estimation: Smart Gathering Management 547
Ishita Swami and Nimish Sunil Das

Determination of Crop Suitability Based on Soil pH Using Image Processing and ANN 563
Vidya I. Hadimani, Keerti Naregal, Roopa Hubballi, and Savita Bakare

About the Editors

Jatindra Kumar Deka received a Ph.D. degree in computer science from IIT Kharagpur, India, in 2001. He is currently a Professor at the Department of Computer Science and Engineering, IIT Guwahati, India. He is involved in academic as well as industry-sponsored research related to VLSI testing and design for testability. He has authored over 50 research papers. His research interests include formal modeling and verification, CAD for VLSI and embedded systems, and data mining. His publications involved topics including fault diagnosis, integrated circuit testing, logic testing, network-on-chip, integrated circuit reliability, automatic test pattern generation, built-in self-test, logic circuits, logic design, logic gates, low-power electronics, quantum gates, scheduling, system-on-chip, VLSI, benchmark testing, circuit testing, computer-aided instruction, design for testability, electronic engineering computing, failure analysis, fault location, fault tolerance, fault-tolerant computing, integrated circuit design, etc.

P. S. Robi completed his Ph.D. from the Department of Metallurgical Engineering and Materials Science in 1995. He joined IIT Guwahati as an Assistant Professor in the Department of Mechanical Engineering in 1997. He served IIT Guwahati in various capacities, viz., Head, Department of Mechanical Engineering, Dean (Research and Development and presently serving as Deputy Director. He's actively involved in teaching undergraduate and post-graduate courses related to Materials and Manufacturing. His research interest is materials development and manufacturing. His areas of specialization include the development of micro-alloyed aluminum alloys, creep studies of high-temperature alloys, thin-strip casting technology, powder metallurgy, smart materials, deformation mechanism maps, etc. He has published around 60 papers in international journals and conference proceedings. He has completed 13 research projects. He has supervised 6 Ph.D. theses and 32 M.Tech. theses and presently supervising 7 Ph.D. theses.

Bobby Sharma had completed her B.E. in Computer Science and Engineering, a Master's degree in Information Technology, and Ph.D. in Computer Science and

Engineering. She is currently serving as Associate Professor and Head of the Department of Computer Science and Engineering, School of Technology, Assam Don Bosco University. Before that, Dr. Sharma was associated with Dibrugarh University. She has more than 45 publications in journals and conference proceedings in computer networks, artificial intelligence, network security, machine learning, IoT, network security, compiler design, data science, etc. She has been involved with nine research projects and several innovation activities. Currently, she is guiding six Ph.D. research scholars in the stream of Computer Science and Engineering.

Design of Modern Technology Lighting System for Automobiles

Sundeep Siddula

Abstract Road accidents are the most unfortunate things to happen for people. This road accident takes place when a vehicle gets collided with another vehicle, pedestrian, animal, or other stationary obstruction, such as a tree or building. While road safety is improving day by day, the procedure debris moderate and misaligned with enacted targets, this moderate development is partly due to the active and complicated nature of road traffic and safety performance. This article aims at design and implementation of automatic road reflectors which reduces eye strain to the road users and the road accidents. This suggests automating the traditional road reflectors, so that it senses the intensity of ambient light and work accordingly which is alike the auto-brightness feature in mobiles. So, by the implementation of automatic road safety reflectors, we can reduce the accidents and provide road safety for the road users same as the use of automatic street lighting nowadays.

Keywords Road reflectors · Ambient light · Enacted targets · Eye strain

1 Introduction

In the world, road accidents are one of the leading causes of death.[1] Among 199 countries in the world, India ranks number one in the number of road accident deaths and records for almost 11% of the accident-related deaths in the world (Clanton 2012). Approximately more than 4.4 L road accidents were reported during the year 2019 according to the 2019 reports for the road accidents in which 1.5 L are dead and 4.5 L are injured. However, road safety is improving across many countries, andthe progress remains slow and misaligned with established targets.

[1] Research scholar, “A review on road accident and related factors”, Anna university Chennai.

S. Siddula (✉)
Department of Electrical and Electronics Engineering, Vignana Bharathi Institute of Technology, Hyderabad, India
e-mail: sundeep.siddula@gmail.com

J. K. Deka et al. (eds.), *Emerging Technology for Sustainable Development*,
Lecture Notes in Electrical Engineering 1061,
https://doi.org/10.1007/978-981-99-4362-3_1

From Table 1, in 2019, the time frame between 18:00 and 21:00 h which is during night accounts the maximum number of road accidents, recording 19.3 percent of the total number of road accidents in India, and this is in line with the pattern seen over the past 5 years (Elvik et al. 2017). These road accidents mostly include accidents due to the high intensity of light in the surroundings due to the high power lights of the vehicles. Because of these high power lights, when vehicles travel in the opposite direction due to the reflection of light, the path of the road is not visible clearly, and because of direct reflection of light into the driver's eyes as a natural reflex, they tend to close their eyes which leads to a high probability of accidents happening (SaraMoridpur 2018).

So, in order to minimize the no. of road accidents happening to some extent and to provide a solution to this problem, all the high power lights of the vehicles are replaced with the automatic road safety reflector light (Aslam Musthafa et al. 2017). This automatic road safety reflector light is an electrical device that measures the intensity of light and works according. The simple function of this device is when there is a high intensity of light in the surroundings it decreases its light intensity, and if there is low intensity of light in the surroundings, it increases its intensity of light (Rumar 2016).

Thus, by maintaining a balanced amount of light on the roads during dark, the drivers can comfortably focus on the roads and drive safe (Fotios and Gibbons 2017).

2 Constructional Details

The basic block diagram is shown in Fig. 1.

Battery

A battery is a device that transform chemical energy directly to electrical energy. An electrical battery is a amalgam of one or more electro-chemical cells. Battery used in the automatic road safety reflector light is a 9 V battery. This battery provides the necessary power supply to the device (Abdul Kader Riyaz et al. 2017).

Diode

A diode is a semi-conductor electronic device that fundamentally acts as a one-directional switch for current. It allows current only to flow in one direction easily, but restricts the current to flow in opposite direction acting as a switch (Okrah et al. 2021). The diode takes input from battery through anode and cathode and diode is connected to the voltage regulator.

Voltage Regulator

A voltage regulator is a component of the input power supply unit that ensures a consistent voltage supply with in all the operational conditions (Siddula et al. 2022a; b). It synchronizes voltage during variations in loads and power fluctuations. Electronic circuits require voltage regulators due to their requirement of a stable voltage

Table 1 Road accidents reported in different time interval of a day during 2015–2019 in India

	2015		2016		2017		2018		2019	
Time	No . of accidents	% share in total accidents	No. of accidents	% share in total accidents	No. of accidents	% share in total accidents	No. of accidents	% share in total accidents	No. of accidents	% share in total accidents
6.00–9.00 h (day)	55,5 18	11.1	54,522	11.3	51,551	11.1	51,489	11.0	49,165	10.9
9.00–12.00 h (day)	81,964	16.8	75,771	15.8	71,426	15.4	70,211	15.0	66,767	14.9
12.00–15.00 h (day)	79,616	15.9	73,380	15.3	71,594	15.4	71,392	15.3	67,623	15.1
15.00–18.00 h (day)	87,819	17.5	85,834	17.9	82,686	17.7	81,619	17.5	78,513	17.5
18.00–21.00 h (night)	86,836	17.3	84,555	17.6	85,686	18.4	86,986	18.6	86,452	19.3
21.00–24.00 h (night)	51,425	10.3	50,970	10.6	49,567	10.7	49,162	10.5	48,370	10.8
0.00–3.00 h (night)	27,954	5.6	25,976	5.4	25,050	5.4	25,407	5.4	23,573	5.3
3.00–6.00 h (night)	30,291	6.0	29,644	6.2	27,580	5.9	26,571	5.7	25, 187	5.6
Time not known	NA	NA	NA	NA	NA	NA	4207	0.9	3352	0.7
Total 24 h	501,423	100	480,652	100	464,910	100	467,044	100	449,002	100

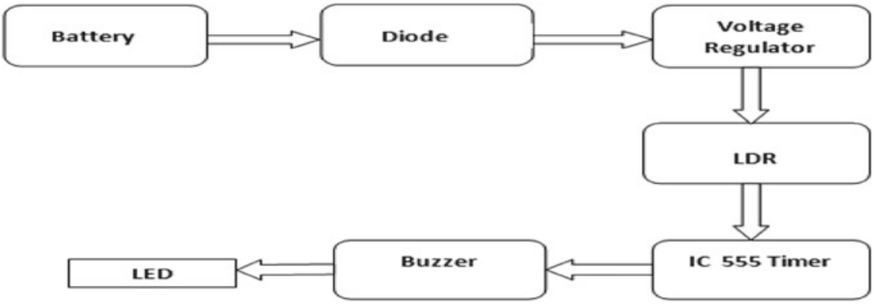

Fig. 1 Basic block diagram of automatic road safety reflector light

supply to avoid damage (Microcontroller 2017). The voltage regulator gets input from cathode of diode, and the output of the voltage regulator is given to LDR (Siddula et al. 2021b).

LDR

The light-dependent resistor (LDR) is an electronic component used in different electric circuits. LDR works upon the photoconductivity principle (Pushpanjali et al. 2016). Photoconductivity is the technique in which the conductivity of the material depends on the intensity of the light it is imbibing. LDR is a photoconductive material that provides a large change in resistance to changes in light level. It is also called a photoresistor. Due to their dependence on light intensity, they are also called light-sensitive devices (Sanal and Taneja 2018). The LDR is used as a sensor in this automatic road safety reflector light to sense the light intensity available and work accordingly. The voltage regulator output is given as input to the LDR.

IC 555 Timer

An IC 555 timer converts analog to digital signal and consists of eight pins where each pin has its function. The IC 555 timer generates pulses, and it is a high-stable controller which is capable of producing accurate timing pulses (Sensors Advanced Research in Electrical and Electronic Engineering Volume 1, Number 2 2014). It is mainly used for alarm generations, time delays, oscillator applications, etc.

The internal structure of IC 555 timer is made up of transistors and resistors, but those can be broken up into various components. Figure 1, shows the various components of IC 555 timer. It consist of two comparators, flip-flop, inverter, two transistors, and a voltage divider. The voltage divider is made up of three 5 kilo ohms resistors connected in series. The voltage divider is connected to power pin (Vcc) and ground pin which is pin no. 8 and 1, respectively. The voltage divider divides the input voltage and feeds both the comparators. Since, the resistors are all the same range, the input voltage or Vcc is divided with the negative terminal of comparator-1 getting two-third of input voltage and the positive terminal of comparator-2 getting one-third of input voltage (Siddula et al. 2021a). The positive terminal of comparator-1 is connected to pin-6 which is threshold, and the negative terminal of the comparator-2 is connected to pin-2 which is trigger. The comparators supply input to the flip-flop.

LED

The light-emitting diode (LED) is a semi-conductor electronic device that releases infrared light (or) visible light when provided with current. The LEDs are used as the final output in automatic road safety reflector light. The working of the LED depends upon the light intensity in its surroundings (Clanton 2012). LED function depend upon the output of the IC 555 timer.

Buzzer

The buzzer consists of two pins, each pin is attached to supply and ground respectively. It is made of central-ceramic disc surrounded by a metal-vibration disc. When supply is provided, current passes with in the buzzer which causes the ceramic disk to shrink or enlarge. Due to this, the metal-vibration disc gets vibrated and the noice is produced. By altering the buzzer's frequency, the vibration speed can be changed, which leads to the change in pitch of the resulting noice.

3 Working/Operation

The automatic road safety reflector lighting system works on the principle of photoconductivity. When two vehicles traveling on roads in opposite directions approach each other during the nighttime with their automatic road safety reflector lighting system ON, the excess amount of light in the surroundings is sensed by the LDR. Now, the LDR produces a voltage greater than two-third of the supply voltage which is given as input to the IC 555 timer. As the IC 555 timer is connected with the LED, it reduces the intensity of light (as shown in Fig. 2b) of the vehicles. And when there is low or dim or less light available in the surroundings, the LDR senses the intensity of that light and produces a voltage less than one-third of the supply voltage as input to the IC 555 timer. Due to which the intensity of light increases (as shown in Fig. 2c) in the vehicles. Thus, the automatic road safety reflector light installed in the vehicles compromises its light intensity depending upon the available light in its surroundings, So that the drivers driving the vehicles during nights can comfortably view the vehicles approaching in opposite directions and pass over without any trouble. In such a way by using the automatic road safety reflector lighting system road safety can be provided and road accidents can be reduced to some extend. The operation is explained in Fig. 2a–c.

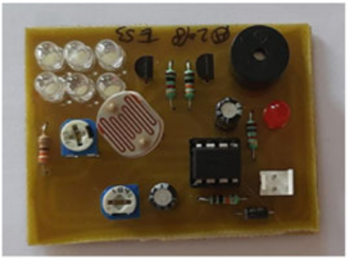

A Circuit with no supply
(circuit when in off state)

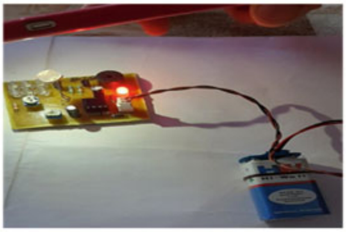

B Circuit with excess surrounding light.
(when excess surrounding light is sensed by LDR the device decreses its light intensity.)

C Circuit with low intensity of surroundings light.
(when low intensity of surrounding light is sensed by LDR the device increases its intensity)

Fig. 2 Hardware Implementation

4 Hardware Implementation

See Fig. 2.

5 Conclusion

This paper concludes that by using modern technologies like automation and executing automatic road reflectors lighting system can minimize the road accidents to some extend. Not only it provides road safety by compromising light during night, it also decreses eye strain for the road users because of the balanced light in the surrounding. Thus, it can be concluded that by implementing the automatic road reflectors, some count of the road accidents are reduced and it also provides security.

Appendix

Equipment	Type/rating	Quantity
LDR		1
Battery	9v	1
LED	Red and White	7
Integerated circuits	555	1
Diode	IN4007	1

References

Abdul Kader Riyaz M, Arun Jeyakumar S, Abdul Hameed Sharik M, Tamilarasi A (2017) Graphene coated LED based automatic street lighting system using Arduino

Aslam Musthafa R, Bala Krishnan T, Seetha Raman N, Shankar M, Swathi R (2017) Automatic headlight beam controller. Special issue published in Int J Trend Res Dev (IJTRD)

Clanton N (2012) Outdoor lighting design with LEDS. PowerPoint Webinar

Elvik R, Hoye A, Vaa T, Sorensen M (2017) Handbook of road safety measures. Emerald Group Publishing Limited

Fotios S, Gibbons R (2017) Road lightning research for drivers and pedestrians. School of Architecture, The university of sheffield, Sheffield

Microcontroller (2017) IEEE international conference on power, control, signals and instrumentation engineering (ICPCSI-2017)

Okrah SK, Williams EA, KumassahF (2021) Design and implementation of automatic headlight dimmer for vehicles using light dependent resistor (LDR)

Pushpanjali GM, Mali PS, Naman RR (2016) Automatic headlight dipper with respect to upcoming vehicles|| response. Int J Emerg Technol (Special Issue on ICRIET-2016)

Rumar K (2016) Vehicle lighting and the aging population. The University of Michigan Transportation Research Institute

Sanal M, Shiv T (2018) Automatic brightness control using LDR

SaraMoridpur (2018) The road markings and their impact on driver behaviour and road safety. ISO 26262 Road vehicles—functional safety

SundeepSiddula, VenkataRamarao K, Mohammad Hasheer SK (2022) Analysis and design approach of footstep power generation using pressure sensors. In: Proceedings of third international conference on communication, computing and electronics systems, lecture notes in electrical engineering vol 844, https://doi.org/10.1007/978-981-16-8862-1_34

Siddula S, Pariyar A, Geetha Kumari P (2021a) Solar panel position monitoring system for maximum power generation. In: Lecture notes in electrical engineering (LNEE), vol 700. Springer Publisher, pp 1159–1167, ISBN 978-981-15-8221-9

Siddula S, Chandra Mouli MP, Bhavya Sree M, Harinadh K, Ramya Shree P (2021b) Utilization of sensor for energy generation using pressure or vibrations. In: Machine learning and autonomous systems, vol 269. Springer Publisher, pp 1–8. ISSN: 978-981-16-7996-4

Siddula S, Mallika M, Srujan C, Vignesh Y, Sai Surya Y (2022a) Advance eye blink sensor controller based wheel chair. In: IEEE 2nd international conference on advance computing and innovative technologies in engineering (ICACITE)-2022a. 978-1-6654-3789-9/22/$31.00 ©2022a IEEE. https://doi.org/10.1109/ICACITE53722.2022.9823704

Siddula S, Maneesha V, Anjali K, Sai Priya S, Divya Teja K (2022b) Design of advanced car driving controller system. In: IEEE 2nd international conference on advance computing and innovative technologies in engineering (ICACITE)-2022b. 978-1-6654-3789-9/22/$31.00 ©2022b IEEE. https://doi.org/10.1109/ICACITE53722.2022.9823856

A Critical Examination of Remote-Controlled Aircraft Technology in Terms of Their Operation in All-Weather Conditions

S. K. Vishnoo Prathap and Vikramjit Kakati

Abstract Remotely piloted aircraft (RPAs) or drones are commonly referred to as unmanned/autonomous aerial vehicles. Over the past 5–6 years, there has been a boom in the use of these vehicles in civil and defense applications worldwide. Despite very protective use guidelines, RPAs are used for surveillance and remote-sensing purposes worldwide, and few delivery services are active. On the Indian Subcontinent, the use of drones/RPAs is limited to government organizations and a few private operators that work with educational institutions. Using a case study from India, the paper explores the various requirements, current objectives, technology, and future challenges for RPA/drone operations that can be conducted in all-weather conditions. India's technology and future benefits are also examined in the paper. Additionally, this paper examines the options for monitoring civil aviation applications related to remote sensing, cargo transport, search and rescue services, and civil surveillance. The utilization of RPAs for the novel COVID-19 pandemic in India has also been reported.

Keywords RPA · All-weather operation · Civil aviation

1 Introduction

Remotely piloted aerial vehicles (RPAVs) are abundantly finding applications due to their low-cost, less maintenance, and multi-terrain launch capabilities. In India, RPAVs, also known as unmanned aerial vehicles (UAVs) according to the Government of India, can be classified into nano, micro, small, medium, and a large class of UAVs. Classification is also done by employing utilization and configurations (see Fig. 1). There are two types of UAVs, low-altitude platforms and high-altitude platforms. In UAV terms, regulations are set with the appropriate height by which a UAV can operate. In India, drones/RPAs are regulated by the Director-General of Civil

S. K. V. Prathap (✉) · V. Kakati
Department of Mechanical Engineering, Assam Don Bosco University, Guwahati, Assam, India
e-mail: du2020phd0051@dbuniversity.ac.in

J. K. Deka et al. (eds.), *Emerging Technology for Sustainable Development*, Lecture Notes in Electrical Engineering 1061,
https://doi.org/10.1007/978-981-99-4362-3_2

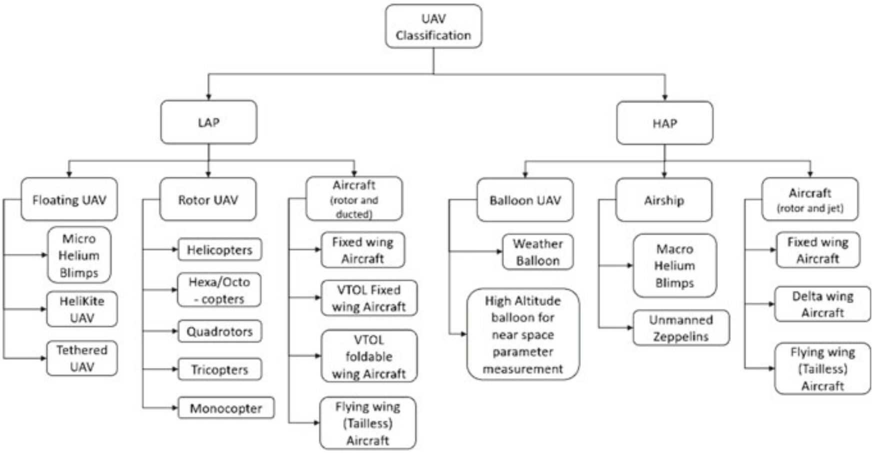

Fig. 1 Classification of UAV based on utilization and configuration

Aviation (DGCA) under the Ministry of Civil Aviation, Government of India. For regulating the usage of UAVs/RPAs in Indian airspace, the Government of India drew up the Drone Rules 2021 and paved the way for the ease of deployment of drones based on the requirements, and RPAs manual was also drafted with specific rules and regulations to be followed by public and private end-users of this technology.

Drone technology has developed tremendously in recent years (Shakhatreh et al. 2018), and the DGCA has taken a number of initiatives to make use of drones/ RPAs in commercial airspace in India. The use of drones for delivery has gained popularity in recent years. The DGCA has granted manufacturing permissions for a few companies, though there are many private players in India, such as start-ups and university-based research centers. There are, therefore, few logistics firms using drones for their operations. In India, e-commerce players such as Amazon are trying to implement the Amazon air delivery program and are yet to become certified.

Sources indicate that drones are used more in Eurasia when compared to other parts of the world (see Fig. 2).

Following the COVID-19 pandemic outbreak, local police have utilized quadrotor drones/RPAs as surveillance tools during lockdowns. Through this, the police were able to undertake non-contact patrols. In addition, drones fitted with radiometric thermal imaging sensors were used to measure the temperature of individuals in a crowd by flying at a lower altitude. The flight distance of a drone varies from 2 to 4 km, depending on the payload and objectives of the mission. While India's market and drone industry are still developing, there is immense potential for growth in the local market. India's drone market is expected to grow 18% between 2017 and 2023. It has been reported by Unearth Insight that there are about 100 start-ups in India engaged in the drone business. The drone market can create jobs for UAV operators, engineers, scientists, and data analysts. The Federation of Indian Chambers of Commerce & Industry projects that the UAV market in India will reach US$ 885.7 million by 2021.

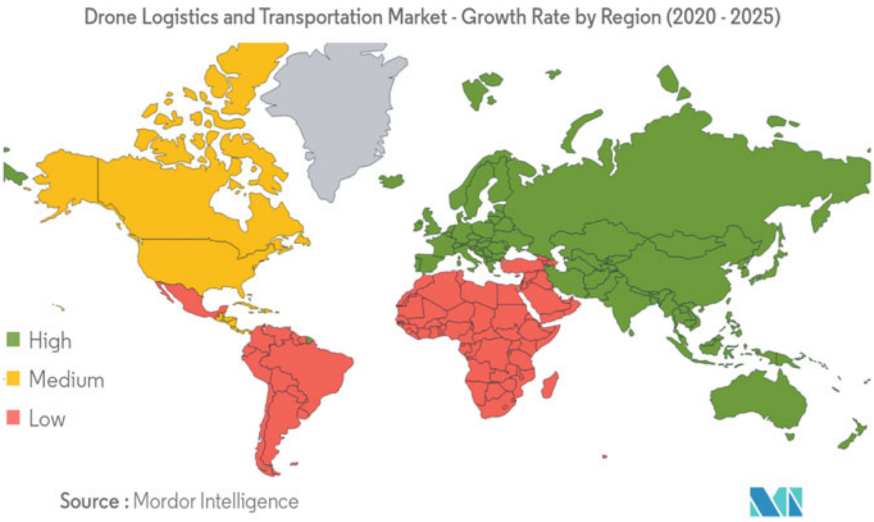

Fig. 2 Drone transportation and logistics market around the world. *Source* Mordor intelligence

2 Application of RPAVs and Their Constraints in India

2.1 Search and Rescue Operations

- Drones are utilized in natural and artificial disasters to find lost persons.
- Drones may be used on land or sea for rescue operations by surveying the field of last known contact.
- Search teams can navigate capsized shafts and natural tunnels/caverns using small, scalable drones.
- Drones can locate people buried under avalanche debris in the mountains.

Challenge: Drones are only sparsely used by national disaster relief organizations in India and are limited to police and national disaster management personnel. This hinders private companies from fully participating and requires more clearance in order to have access.

2.2 Remote Sensing

- It is possible to collect information/data from ground-based systems using UAVs.
- Using UAVs equipped with sensors, disaster monitoring, water quality monitoring, environmental monitoring, drought monitoring, and mineral survey analysis are possible.

- They are also used in agriculture, forestry, and water resources. Several datasets can be gathered for crop monitoring, yield estimates, disease detection, image processing and analysis for crop classifications, forest cover surveys, deforestation surveys, survey of water bodies and underground reservoirs, etc.

Challenge: Drones are widely used in India for remote sensing, especially by remote sensing centers and national disaster relief organizations, but weather conditions limit their flight capabilities.

2.3 Construction and Infrastructure Inspection

- With the appropriate instrumentation/sensors and optical scanners, drones have the potential to be used for pipeline inspections, powerlines inspections, cooling tower inspections, and boiler inspections.
- Using software such as ArcGIS, drones can also be used for construction site surveys, terrain modeling, landscape design, and urban planning.

Challenge: Sense and avoid technology and optical sensor technology needs to be developed for all scalable drones.

2.4 Precision Agriculture

- UAVs are used for crop management, weed detection, irrigation scheduling, disease classification, and pesticide spraying.
- Generally, in agriculture, soil and crop health monitoring is done with ground-based array of sensors and also needs to cover the entire field which is expensive to install. But with UAVs and remote sensing technology, it is easy to cover the entire field and also can be deployed on regular intervals to monitor.
- Similarly, drones are used to take inventory of crops and fruits before harvesting, which provides farmers with precise information about their crops and fruits.
- They are also utilized to protect crops from animals using ultrasonic devices.

Challenge: Low-cost affordability for farmers.

2.5 Goods Delivery

- Food packages, e-commerce supplies, and medical supplies can be transported using UAVs.
- It can also pick up an item from point A and deliver it to point B.
- It can be utilized for commercial transport of goods nationwide.

Challenge: Terrain awareness technology, satellite-based tracking systems, and all-terrain landings are needed to be developed.

2.6 Traffic Monitoring and Situation Awareness

- UAVs can undertake the task of fieldwork support teams monitoring, road surveying, traffic level monitoring, and accident monitoring.
- Smart and reliable UAVs can help automate information transfer on highways and local roads.
- Traffic police can use drones to chase suspects on foot or ground vehicles. It may produce ease in surveillance and also replace traditional cameras.

Challenge: Basic infrastructure for charging and docking with Internet access is developed at designated areas, national highways, and state highways.

2.7 Pandemic Monitoring and Control

- UAVs were used for spraying sanitizer fluid in local municipal areas.
- Pedestrian and traffic monitoring during curfews and lockdowns were essential for non-contact patrolling.

3 Requirement of All-Weather Operational RPAVs

The Indian Subcontinent is situated in a diverse geographical part of Asia, where the weather and terrain vary from state to state. Considering the cold and high-altitude Himalayan Mountain ranges in the northern and northeastern part of India, the hot desert region of Western India, the arid Deccan Plateau region of Central India, and the humid coastal regions of Southern India, the weather pattern varies based on the location. Also, the altitude at ground level varies with the mean sea level toward the north of the country. Also, current RPAVs require proper infrastructure to take-off and land accordingly. As of now, the RPAVs cannot fly in harsh weather conditions. Furthermore, the technology available for all-weather operations is not quite mature. There are many gaps to bridge in order to create a sophisticated machine or vehicle that can fly in severe weather conditions (see Fig. 3).

An RPAV needs to meet the following criteria to be able to operate in any weather.

- Subsystem environmental control and structural integrity (impact resistant and waterproof)
- High endurance capability
- Multi-terrain and vertical take-off and landing (VTOL)

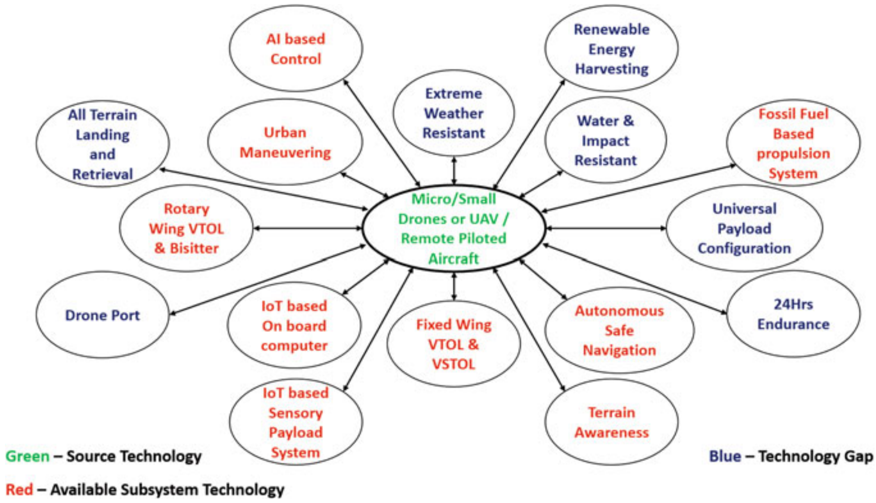

Fig. 3 Current technology status of RPAVs

- RPAV infrastructure availability
- RPAV configuration (overall sizing parameters).

4 Current Technology Development

Based on the current needs of technical requirements to be met for an actual all-weather vehicle, the following are some innovations that are considered as part of the requirements.

4.1 Subsystem Environmental Control and Structural Integrity

RPAVs have different classes and vary in size. They tend to travel in different altitudes, and the weather conditions also vary. The electronic systems inside the hull require ambient temperature monitoring (Pang et al. 2018; Wang et al. 2015; Tanda 2020). Also, they should be leak-proof in case of wet weather conditions and if the vehicle travels on water and air medium (Zufferey et al. 2019). The current technology has been tested by submerging a quadrotor UAV in a water medium. Current material science enables a leak-proof mechanism built and tested and satisfies one significant aspect for all-weather capability (Meng et al. 2018). Internet of Things (IoT)-based sensors (Xu et al. 2022) are also reliable for data analytics in RPAV vital parameter monitoring and ambient temperature monitoring and cooling. Therefore, the aspect of the ambient environment inside the RPAV and its integrity in terms of structures have improved without compromises.

4.2 High Endurance Capability

The energy systems in current RPAVs have a limit in terms of energy density and also energy utilization. The aspect of long endurance has been achieved through endurance by introducing the battery dumping concept (Chang and Yu 2015), solar energy power system (Cestino 2006), introducing fuel cell systems (Swider-Lyons et al. 2011), and optimization of the structures to improve flight capabilities (Bakar et al. 2021). Also, consideration of inclusion of a secondary power system (Chiesa et al. 2011).

4.3 Multi-terrain and Vertical Take-Off and Landing (VTOL)

Vertical landing and take-off technology of aircraft have been available since the 1970s. Also, the procedure has been implemented in the current RPAVs by having multiple multi-rotor platforms (Idrissi et al. 2022) and also introducing morphing vehicle structures like tilt-rotor, tail sitter configuration, etc. (Yuksek et al. 2016; Shanmugam et al. 2016a; Gomez and Garcia 2011; Bilgen et al. 2009; Guiler and Huebsch 2005). On the other hand, multi-terrains are still under the conceptualization stage and yet to develop a mature mechanism/technology as they now rely upon sensor-based landing (Templeton et al. 2007).

4.4 RPAV Configuration

The significant technological developments in the structure of RPAVs are related to morphed wings (Shanmugam et al. 2016b) and increased aerodynamic stability with the incorporation of hybrid variants (combination of fixed-wing and multi-rotor) (Tielin et al. 2017). This technology benefit applications in remote regions and partially comply with the all-weather operation requirements.

4.5 Infrastructure

There are still many areas around the world where drone ports are in the planning stages, and they are not yet operational. In some parts of Rwanda, Africa drone ports[1,2] have been established, but they lack the innovative technology that will allow drone traffic to be recognized. Currently, the main requirements that need to be addressed are the lack of dedicated tracking systems and docking systems for energy storage.

5 Conclusion

Technology is not available for all-weather capability as a combined package. There has been no consideration for the following aspects: (a) deserts and snow conditions, (b) hail storms and winds greater than 10 m/s, and (c) mountain valley and coastal region environmental conditions. There is, therefore, a need to develop an RPAV with universal applications. In all regions of India and around the world, the subsystems should cater to all-weather operation requirements. In addition, drones need to be equipped with the requisite infrastructure to enable cross-country operations. Satisfying these needs can lead to the development of a pure universal all-weather RPAV.

References

Bakar A, Ke L, Liu H et al (2021) Design of low altitude long endurance solar-powered UAV using genetic algorithm. Aerospace 8. https://doi.org/10.3390/aerospace8080228

Bilgen O, Kochersberger KB, Inman DJ (2009) Macro-fiber composite actuators for a swept wing unmanned aircraft. Aeronaut J 113(1144):385–395. https://doi.org/10.1017/s0001924000003055

Cestino E (2006) Design of solar high altitude long endurance aircraft for multi payload & operations. Aerosp Sci Technol 10:541–550. https://doi.org/10.1016/j.ast.2006.06.001

Chang T, Yu H (2015) Improving electric powered UAVs' endurance by incorporating battery dumping concept. In: Procedia engineering. Elsevier Ltd, pp 168–179

Chiesa S, Farfaglia S, Fioriti M, Viola N (2011) Design of all electric secondary power system for future advanced medium altitude long endurance un-manned aerial vehicles. Proc Inst Mech Eng Part G J Aerosp Eng 226(10):1255–1270. https://doi.org/10.1177/0954410011420914

Gomez JC, Garcia E (2011) Morphing unmanned aerial vehicles. Smart Mater Struct 20(10):103001. https://doi.org/10.1088/0964-1726/20/10/103001

Guiler R, Huebsch W (2005) Wind tunnel analysis of a morphing swept wing tailless aircraft. In: 23rd AIAA applied aerodynamics conference. https://doi.org/10.2514/6.2005-4981

Idrissi M, Salami M, Annaz F (2022) A review of quadrotor unmanned aerial vehicles: applications, architectural design and control algorithms. J Intell Robot Syst 104:22. https://doi.org/10.1007/s10846-021-01527-7

Meng L, Hirayama T, Oyanagi S (2018) Underwater-drone with panoramic camera for automatic fish recognition based on deep learning. IEEE Access 6:17880–17886. https://doi.org/10.1109/ACCESS.2018.2820326

[1] Droneport—Norman Foster Foundation.

[2] Zipline—Instant Logistics (flyzipline.com).

Pang L, Zhao M, Luo K et al (2018) Dynamic temperature prediction of electronic equipment under high altitude long endurance conditions. Chin J Aeronaut 31:1189–1197. https://doi.org/10.1016/j.cja.2018.04.002

Shakhatreh H, Sawalmeh A, Al-Fuqaha A et al (2018) Unmanned aerial vehicles: a survey on civil applications and key research challenges. https://doi.org/10.1109/ACCESS.2019.2909530

Shanmugam P, Raja S, Parammasivam KM, Zohra F (2016a) A study on VGTM actuation system for multi axis morphing wing of UAV. In: 34th AIAA applied aerodynamics conference. https://doi.org/10.2514/6.2016-3414

Shanmugam P, Km P, Raja S (2016b) Realization of efficient multi-axis morphing wing mechanism for a VTOL-UAV through LMA and IMU based approach

Swider-Lyons KE, Mackrell JA, Rodgers JA et al (2011) Hydrogen fuel cell propulsion for long endurance small UAVs. In: AIAA centennial of naval aviation forum "100 years of achievement and progress"

Tanda G (2020) Cooling solutions for an electronic equipment box operating on UAV systems under transient conditions. Int J Therm Sci 152:106286. https://doi.org/10.1016/j.ijthermalsci.2020.106286

Templeton T, Shim DH, Geyer C, Sastry SS (2007) Autonomous vision-based landing and terrain mapping using an MPC-controlled unmanned rotorcraft. In: Proceedings 2007 IEEE international conference on robotics and automation. https://doi.org/10.1109/robot.2007.363172

Tielin M, Chuanguang Y, Wenbiao G, Zihan X, Qinling Z, Xiaoou Z (2017) Analysis of technical characteristics of fixed-wing VTOL UAV. In: 2017 IEEE international conference on unmanned systems (ICUS). https://doi.org/10.1109/icus.2017.8278357

Wang T, Tseng KJ, Zhao J (2015) Development of efficient air-cooling strategies for lithium-ion battery module based on the empirical heat source model. Appl Therm Eng 90:521–529. https://doi.org/10.1016/j.applthermaleng.2015.07.033

Xu R, Zhang W, Wong NH et al (2022) A novel methodology to obtain ambient temperatures using multi-rotor UAV-mounted sensors. Urban Clim 41:101068. https://doi.org/10.1016/j.uclim.2021.101068

Yuksek B, Vuruskan A, Ozdemir U et al (2016) Transition flight modeling of a fixed-wing VTOL UAV. J Intell Robot Syst Theory Appl 84:83–105. https://doi.org/10.1007/s10846-015-0325-9

Zufferey R, Ortega Ancel A, Farinha A et al (2019) Consecutive aquatic jump-gliding with water-reactive fuel. Sci Robot 4

A Review of Materials Suitable for Tissue-Engineered Bone Scaffolds

Shreeprasad S. Manohar, Chinmoy Das, and Vikramjit Kakati

Abstract Biomedical and regenerative medicine has significantly contributed to developing new, specific techniques and technologies to improve patient care. A significant leap has been made with innovative materials, cell development, scaffold design, and fabrication in tissue engineering. The tissue engineering process focuses on regenerating tissues that have been lost accidentally or encounter defects such as osteosarcoma, osteoporosis, and osteoarthritis. India has a high number of people who suffer from bone diseases. An estimated 15–20% of the population suffers from osteoporosis. Bone scaffolds are proving to be an excellent treatment for osseous anomalies and defects. Scaffolds are porous, three-dimensional structures that enhance the growth of new tissues. Bone scaffolds are designed to facilitate osteoinductive cells' growth, expansion, and migration on their surface. The purpose of this paper is to review possible polymeric materials for bone scaffolds and provide a suitable combination in terms of cost of material and cost of technology for tissue-engineered bone scaffolds.

Keywords Tissue engineering · Bone scaffold · Osteoinductive cells · Porous structure · Polymeric material

S. S. Manohar (✉) · V. Kakati
Assam Don Bosco University, Assam, Guwahati, India
e-mail: ssmanohar@dbit.in

S. S. Manohar
Don Bosco Institute of Technology, Mumbai, India

C. Das
Department of Orthopaedics, Tezpur Medical College & Hospital, Tezpur, Assam, India

J. K. Deka et al. (eds.), *Emerging Technology for Sustainable Development*,
Lecture Notes in Electrical Engineering 1061,
https://doi.org/10.1007/978-981-99-4362-3_3

1 Introduction

1.1 Tissue Engineering

The goal of tissue engineering is to enhance tissue function by combining engineering and life sciences. A tissue engineering procedure aims to regenerate damaged or diseased tissue in the body attached to the extracellular matrix (ECM). The ECM is made up of a network of carbohydrates and proteins. ECM configuration varies with tissue, and it also includes structural proteins like elastin, collagen, etc., adhesive proteins such as laminin or fibronectin, and proteoglycans. As proteins, proteoglycans carry molecules of sugar attached in the form of polysaccharide complexes (Kusindarta and Wihadmadyatami 2018; Zheng 2019; Biazar 2018). Two sugar units make up a polysaccharide called glycosaminoglycan (GAG). GAGs are commonly used as lubricants and shock absorbers in the body due to their ability to attract water. Based on the sugar type, GAG is categorized into five categories: chondroitin sulfate, epamin sulfate, heparin sulfate, and hyaluronic acid (Zhang et al. 2019).

Collagen and hyaluronic acid are components of cartilage's ECM and GAG. The ECM of bone is primarily composed of collagen and hydroxyapatite. In contrast, the ECM of the skin is composed of collagen, elastin, and proteoglycans (Chocholata et al. 2019).

A scaffold is a structure made of specific materials that can be manufactured artificially and implanted in the body. The scaffolding promotes cell interactions inside the body and helps to form new native functional tissues. The design of scaffolds focuses on having predefined porosity. In the same way that the native ECM in the body mimics the porous structure of the scaffold, it triggers cell proliferation, cell migration, and differentiation. Cells continuously reabsorb and sediment more ECM in the body. Bone, for example, grows in response to load. Healthy bones are also reabsorbed and sublimated. However, the resorption and sedimentation rates are roughly equal in normal bone. When a bone disease like osteoporosis occurs, this balance is disrupted. A tissue engineering scaffold is conventionally designed to degrade as the cells release enzymes within the body. Ideally, these scaffolds should be replaced with a natural ECM produced by the body's cells (Abraham 2014; Wang 2020).

Tissue engineering was introduced in the 1980s and quickly became popular among researchers. In the early stage of the study, specific cells, such as stem cells, were mixed with chemicals to observe cell growth under controlled conditions (Chia and Wu 2015). Some implants have been used to treat human diseases since ancient times. Dentures and dental implants have been used in various cultures worldwide for centuries. The ancient Egyptians used gold wires to bind the surrounding teeth structures as early as 2500 BC. The French civilization mastered wrought iron implants on corpses around 200 AD. The Maya civilization made nacre teeth from calcium carbonate from seashells around 600 A.D.; the present-day process is called osseointegration (Abraham 2014). The Honduran dynasty made stone implants around 800 AD (Wang 2020). Almost every era in human history has used tissue engineering and implants in some form or another. It is a massive motivation for current researchers, and tissue engineering is on the rise due to the advancement of technology (Qi 2013). In vitro studies on scaffolds began around 25 years ago, focusing primarily on bone tissue engineering. Various materials and technologies have been used since then for bone scaffolding. The scaffolds are fabricated using electrospinning, solvent casting, porogen leaching, gas foaming, phase separation, fiber mesh, melt molding, bonding, membrane lamination, and freeze-drying, as well as rapid prototyping (Velasco et al. 2015).

1.2 Role of 3D Printing in Biomedical Applications

Tissue engineering has been given a significant boost with rapid prototyping. Although it is still in its infancy, it has already shown great potential in aerospace, medical, manufacturing, automobile, and construction owing to its rapid development.

Rapid prototyping is broadly considered an additive manufacturing technology. As of late, it has also been called 3D printing in a broad sense. The 3D printing is an important development in tissue engineering because of its ability to manufacture intricate shape parts very efficiently and precisely. Exoskeletons, jawbones, bones, and various tissues and organs are currently being created with 3D printing. This field has many possibilities, from making anatomical samples for study to creating a human organ that will function flawlessly inside the patient's body (Zhang et al. 2019).

The process of 3D printing involves creating a three-dimensional (3D) model using a computer-aided design (CAD) package. Then, the 3D solid model is converted into a valid surface format (.stl or .obj). Slicing software then uses the surface file to create all inner details, including infill pattern, infill density, layer height, wall count, etc., to convert a surface file into a layer file. A 3D printer uses this layer definition to build the part layer by layer (Chocholata et al. 2019). All 3D printing technologies can create intricate geometric shapes, making them especially suitable for biomedical and tissue engineering applications. In general, porous scaffolds can be manufactured using various 3D printing technologies (Hospodiuk et al. 2017). Currently, there are approximately 40 different 3D printing technologies in existence. Each technology is based on a different approach (An et al. 2015).

2 Polymers in Tissue Engineering

In tissue engineering applications, polymer materials are used to fabricate scaffolds. Polymer material selection depends on various properties, such as molecular weight, shape, lubricity, chemistry, hydrophilicity, hydrophobicity, solubility, and biodegradability. The 3D printed polymer scaffolds have good mechanical strength, biodegradability, and porous structure. Natural polymers and synthetic polymers are the two main categories of polymers. Polymers are further classified into proteins, polysaccharides, and polynucleotides. The three types of synthetic polymers are copolymers, microbial polymers, and bioactive ceramics (see Fig. 1) (Dhandayuthapani et al. 2011).

2.1 *Essential Properties Required in Polymers for 4D Printing*

Pore sizes from 20 to 1500 μm are used primarily in tissue engineering applications to mimic the natural bone structure. For significant bone growth, it is recommended that the pore size be 80 to 120 mm. Pore sizes less than 80 μm affect the migration of cells, while larger pores, more than 500 μm, affect the attachment of cells as the specific surface area decreases. Pore size optimization facilitates many cell sites and increases bone ingrowth (Murphy and O'brien 2010).

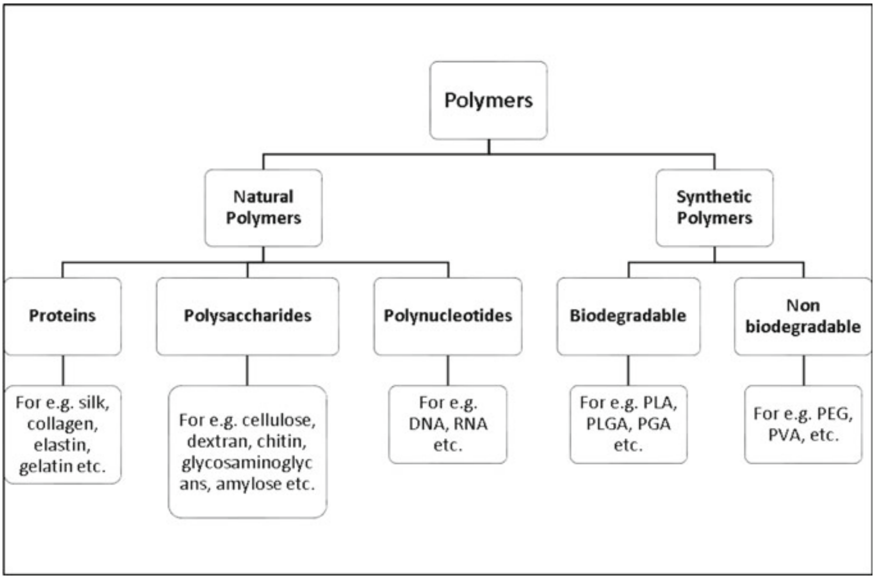

Fig. 1 Classification of polymers

Biocompatibility refers to a material's ability to react with a specific host response in a given situation. Specifically, it refers to the suitability of the polymer material to the body and its fluids. Polymeric bone scaffolds should be biocompatible to increase bone tissue interaction with the scaffold material (Arif 2019).

Biodegradability results from a chemical process that produces a sharp division of covalent bonds. Polymers degrade by hydrolysis, which is typically a chemical process occurring in the presence of water molecules. When biology is concerned, biodegradable polymers refer to a material that degrades over time once it is implanted inside the patient (Ratner and Bryant 2004; Cameron and Kamvari-Moghaddam 2008).

Cytotoxicity is defined as the addition of foreign elements to the body that causes cells to become toxic. An implant material should not contain or exhibit cytotoxicity; the polymeric bone scaffold should be non-toxic (Gregor 2017).

Chemical bonding at surfaces is necessary for cell attachment, proliferation, and migration.

Mechanical strength, for a bone scaffold, is essential. In order to place the scaffold at an appropriate location within the patient's body, the scaffold should resist a certain amount of compressive stress to support adjacent bones, if needed (Subia et al. 2010).

Printability refers to the ease with which a material can be 3D printed. A polymer material should be very printable (Dhandayuthapani et al. 2011).

2.2 Natural Polymers

Plants, animals, and microorganisms are all sources of natural polymers, also known as renewable resources. Different sources of these organisms possess complex structures with different physiological functions. Polymers of this type are typically created by adding or condensing groups together. Regular polymers possess remarkable properties. Material properties are often determined by the material's structure rather than by molecular formation (Bassas-Galia et al. 2017). Composite polymers with enhanced properties are developed by studying and mimicking natural polymer structure and function. Natural polymers can frequently be developed from proteins. Many proteins, such as gelatin, soy protein, silk, casein, and keratin, have demonstrated excellent qualities. In combination with polymers, these proteins have improved shear and flexural strength, toughness, elasticity, and tensile modulus (Gupta and Nayak 2015).

An extended shackle of polymeric carbohydrate molecules, polysaccharides are composed of monosaccharides linked by o-glycosidic chains. Polysaccharides perform a variety of physiological functions. A few examples of polysaccharides are starch, cellulose, alginate, chitosan, glycosaminoglycans (GAGs), hyaluronic acid, pullulan, and dextran (Aravamudhan et al. 2014).

Polynucleotides are covalently bonded chains of nucleotide monomers. Polynucleotides include deoxyribonucleic acid (DNA) and ribonucleic acid (RNA). Research is being conducted on gene therapy using bio-nano composite DNA and RNA (Noreen et al. 2020).

2.3 Synthetic Polymers

The advantages of synthetic polymers over natural polymers have been well documented. A synthetic polymer possesses desired mechanical properties, process control capabilities, and reliability. Synthetic polymers can be engineered to achieve the desired chemical bonding, cell interaction, porosity, and surface roughness characteristics. Synthetic polymers exhibit controlled resorption and biocompatibility, which are highly desirable properties when designing bone scaffolds (Gunatillake et al. 2003). They are more uniform and exhibit predictable responses to chemical and mechanical properties. Synthetic polymers can exhibit non-toxic behavior toward surrounding tissues, making them a preferred choice over natural polymers. In general, synthetic polymers can be classified according to their ability to degrade biologically and their inability to degrade biologically.

Synthetic polymer scaffolds can be created using a variety of methods, e.g., gas leaching, salt leaching, electrospinning, solvent casting, gas foaming, and 3D printing. The 3D printing is the most suitable technique for constructing bone scaffolds because it can deliver the desired shape and ensure adequate porosity (Bolívar-Monsalve 2021). In addition to providing cell attachment sites, 3D-printed bone scaffolds can mimic the shape of the bone. As this scaffold is implanted in a patient, it can be resorbed easily and promote bone growth. This section discusses highly suitable synthetic polymers in 3D printing using the fused deposition modeling (FDM) technique. FDM is used because it is cost-effective and can be used with biodegradable materials.

According to Table 1, polylactic acid (PLA) shows favorable chemical composition for bone scaffold application as its FTIR spectroscopy results. The contact angle of PLA is < 90° making it hydrophilic, which can provide enough cell sites for bone tissues to grow. PLA has a moderately high glass transition temperature in 45–60°C compared with the average human body temperature. When PLA is used as a bone scaffold, it can retain its solid form and provide adequate mechanical strength to the adjacent bones. The tensile modulus of PLA is between 0.35 and 3.5 GPa which ensures enough load-bearing capacity when used as a bone scaffold implant in the lower limb.

Table 1 Polymer properties

Polymer	FTIR IR spectroscopy (cm^{-1})	Contact angle (°)	Glass transition temperature (°C)	Tensile modulus (GPa)	Resorption period (weeks/months/years)	References
PLA	Peak-2929 sharp-1756 and 1090	74.3° ± 11°	45–60	0.35–3.5	1–2 years	Subia et al. (2010) and Zhang et al. (2020)
PGA	Sharp-1751	66.1° ± 8°	35–45	6–7	6–12 months	Subia et al. (2010), Zhang et al. (2020), Narayanan et al. (2018) and Benkaddour et al. (2013)
PCL	Peak-3500 sharp-1750	140° ± 5°	60	0.2–0.4	Up to 2 years	Zhang et al. (2020), Chieng et al. (2014) and Vrandečić et al. (2010)
PEG	Peak-3446	63° ± 5°	(− 56) to (− 52)	0.12–0.266	Non-biodegradable in pure form	Lee et al. (2009) and Cai et al. (2019)
PPF	Peak-3540	60.6° ± 8.2°	30–32	0.21–0.24	6–8 weeks	Karfarma et al. (2019), Kharazmi (2015), Liu et al. (2019) and Jiang et al. (2015)
PVA	Peak-3280	60.6° ± 5°	85		Up to 2 months	Jiang et al. (2015), Mohammadi et al. (2015) and Wondu et al. (2019)
PU	Peak-3352	66° ± 5°	− 35	0.091	Up to 3 months	Ranjan (2020) and Ranjan et al. (2018)

2.4 Fabrication of Polymer Composites Using FDM

Ranjan et al. demonstrated through in vitro studies that PLA-HAp-chitosan composite in proportions of 91-8-1 (by % of weight) was used to 3D print bone scaffold using the FDM technique. This composite bone scaffold exhibited good biocompatibility and bioactivity from the Ra profile and serum stability test (Ranjan 2020; Ranjan et al. 2018). Ales Gregor et al. 3D printed PLA scaffolds and performed in vitro studies to showcase porosity of 30–60% promotes cell attachment proliferation. It provides more cell sites for a natural ECM to grow (Gregor 2017). Ricardo Donate et al. suggested the use of additives which includes HAp, β-TCP, etc., to increase mechanical properties of PLA and enhance its osteoconductivity, use of surface treatments like alkali and plasma treatment to increase the hydrophilicity of PLA, and use of bioactive substances like chitosan, calcium phosphate, collagen, alginate, etc., to enhance cell bioactivity in PLA (Donate et al. 2020). Bruna Teixeira et al. suggested that the FDM technique is suitable to 3D print PLA scaffolds and exhibit structural properties comparable to cancellous bone (Marianna et al. 2016). To showcase good compressive strength, Zhang et al. created optimized PLLA (L-PLA)/nano-HA (nHA) composites with cost-effective FDM technology to 3D print PLLA/nHA porous bone scaffolds. It also exhibited good osteogenic properties when compared with HA ceramic scaffold and cancellous bone (Zhang 2021). Mazzanti et al. studied the mechanical properties of polymers like polyolefins when mixed with natural fillers and showcased significant improvement (Mazzanti et al. 2019).

FDM is the most widely used 3D printing technology across the globe. However, still, the cost of FDM 3D printers is comparatively higher. To overcome this barrier, open-source 3D printers have been manufactured in several parts of the world and getting more popular. These open-source FDM 3D printers work on open-source software that includes slicing software, e.g., Ultimaker Cura, slice 3r, etc., open-source community setup provides free access to users for different 3D models, designs, e.g., Thingiverse, Backster, etc. (Alagoz and Hasirci 2020). FDM is specifically useful in tissue engineering to print porous scaffolds used for bones. FDM can produce scaffolds with good mechanical properties and structural integrity in making bone scaffolds. It is possible to design patient-specific defects using MRI or C.T. scan data. Additionally, the infill structures can match the defect sites and encourage cell attachment and migration.

3 Conclusion

According to research, FDM outperforms all available 3D printing techniques in cost-effectiveness, a wide range of polymers, a harmless mode of operation, and specific tissue engineering applications, such as bone scaffolding. Materials such as PLA, PGA, and polylactic-co-glycolic acid (PLGA) are readily available in clinical grade. Several of these materials can be mixed with other natural polymers to produce biocompatible, biodegradable composite polymers; in vitro studies were conducted to determine cytotoxicity, biodegradation rate, percentage porosity, mechanical strength, and geometrical properties of these materials. In all of these studies, satisfactory results have been achieved concerning cell proliferation, migration, and differentiation. Additionally, functional scaffold prototypes were tested for statistical control and assembly applications, and the results were satisfactory. Using FDM, it is also possible to fabricate ceramic composites, which has been satisfactory. In conclusion, the material of the scaffold and fabrication techniques plays a significant role. A number of studies have demonstrated that FDM can be a cost-effective alternative in the 3D printing of bone scaffolds of various sizes and shapes.

4 Future Scope

The field of tissue engineering is experiencing rapid growth with the development of additive manufacturing. The development of new bio-printers equipped with increased efficiency, widening the variety of materials available, and improving accuracy. Despite all this progress, there remain some challenges to overcome. The high cost of these bio-printers and materials and technologies like SLA, SLS, and binder jet printing has a significant and somewhat limiting effect on the conduct of research. Moreover, most studies are in vitro studies, more emphasis should be placed on in vivo studies, and clinical trials should be carried out.

The field of multi-material printing is still nascent. Accelerating research toward this area is essential in developing multi-polymer printing, multi-metal printing, etc. Improved surface structures, layer adhesions, and cell interactions would allow customized implants to be used in surgeries.

References

Abraham CM (2014) A brief historical perspective on dental implants, their surface coatings and treatments. Open Dent J 8:50–55

Alagoz AS, Hasirci V (2020) 3D printing of polymeric tissue engineering scaffolds using open-source fused deposition modelling. Emerg Mater 3:429–439

An J, Teoh JEM, Suntornnond R, Chua CK (2015) Design and 3D printing of scaffolds and tissues. Engineering 1:261–268

Aravamudhan A, Ramos DM, Nada AA, Kumbar SG (2014) Natural polymers: polysaccharides and their derivatives for biomedical applications, natural and synthetic biomedical polymers. Elsevier, pp 67–89

Arif U (2019) Biocompatible polymers and their potential biomedical applications: a review. Curr Pharm Des 25:3608–3619

Bassas-Galia M, Follonier S, Pusnik M, Zinn M (2017) Natural polymers: a source of inspiration. In: Bioresorbable polymers for biomedical applications: from fundamentals to translational medicine

Benkaddour A, Jradi K, Robert S, Daneault C (2013) Grafting of polycaprolactone on oxidized nanocelluloses by click chemistry. Nanomaterials 3:141–157

Biazar E (2018) 3D bioprinting technology for body tissues and organs regeneration. J Med Eng Technol 42:187–202

Bolívar-Monsalve EJ (2021) Engineering bioactive synthetic polymers for biomedical applications: a review with emphasis on tissue engineering and controlled release. Mater Adv 2(14):4447–4478

Cai Z, Wan Y, Becker ML, Long YZ, Dean D (2019) Poly(propylene fumarate)-based materials: synthesis, functionalization, properties, device fabrication and biomedical applications. Biomaterials 208:45–71

Cameron RE, Kamvari-Moghaddam A (2008) Synthetic bioresorbable polymers. In: Degradation rate of bioresorbable materials: prediction and evaluation, pp 43–66

Chia HN, Wu BM (2015) Recent advances in 3D printing of biomaterials. J Biol Eng 9:1–14

Chieng BW, Ibrahim NA, Yunus WMZW, Hussein M (2014) Poly(lactic acid)/poly(ethylene glycol) polymer nanocomposites: effects of graphene nanoplatelets. Polymers 6:93–104

Chocholata P, Kulda V, Babuska V (2019) Fabrication of scaffolds for bone tissue regeneration. Materials 12:568

Dhandayuthapani B, Yoshida Y, Maekawa T, Kumar DS (2011) Polymeric scaffolds in tissue engineering application: a review. Int J Polymer Sci 2011. Article ID 290602, (19 pages)

Donate R, Monzón M, Alemán-Domínguez ME (2020) Additive manufacturing of PLA-based scaffolds intended for bone regeneration and strategies to improve their biological properties. E-Polymers 20:571–599

Gregor A (2017) Designing of PLA scaffolds for bone tissue replacement fabricated by ordinary commercial 3D printer. J Biol Eng 11:1–21

Gunatillake PA, Adhikari R, Gadegaard N (2003) Biodegradable synthetic polymers for tissue engineering. Eur Cells Mater 5:1–16

Gupta P, Nayak KK (2015) Characteristics of protein-based biopolymer and its application. Polym Eng Sci 55:485–498

Hospodiuk M, Dey M, Sosnoski D, Ozbolat IT (2017) The bio link: a comprehensive review on bioprintable materials. Biotechnol Adv 35:217–239

Jiang L, Nath C, Samuel J, Kapoor SG (2015) An enhanced microstructure-level finite element machining model for carbon nanotube-polymer composites. J Manuf Sci Eng Trans ASME 137(2):021009, (11 pages)

Karfarma M, Esnaashary MH, Rezaie HR, Javadpour J, Naimi-Jamal MR (2019) Poly(propylene fumarate)/magnesium calcium phosphate injectable bone composite: effect of filler size and its weight fraction on mechanical properties. Proc Inst Mech Eng Part H J Eng Med 33:1165–1174

Kharazmi A (2015) Structural, optical, opto-thermal and thermal properties of ZnS-PVA nanofluids synthesized through a radiolytic approach. Beilstein J Nanotechnol 6:529–536

Kusindarta DL, Wihadmadyatami H (2018) The role of extracellular matrix in tissue regeneration. Tissue Regen

Lee KW, Wang S, Yaszemski MJ, Lu L (2008) Physical properties and cellular responses to crosslinkable poly(propylene fumarate)/hydroxyapatite nanocomposites. Biomaterials. 29(19):2839–2848

Liu P, Chen W, Liu C, Tian M, Liu P (2019) A novel poly (vinyl alcohol)/poly (ethylene glycol) scaffold for tissue engineering with a unique bimodal open-celled structure fabricated using supercritical fluid foaming. Sci Rep 9:9534–9534

Marianna C, Bruna T, Daniel K, Mara TR (2016) Structural evaluation of PLA scaffolds obtained by 3D printing via fused deposition modelling (FDM) technique for applications in tissue engineering. Front Bioeng Biotechnol 4:995–997

Mazzanti V, Malagutti L, Mollica F (2019) FDM 3D printing of polymers containing natural fillers: a review of their mechanical properties. Polymers 11:1094

Mohammadi A, Barikani M, Barmar M (2015) Synthesis and investigation of thermal and mechanical properties of in situ prepared biocompatible Fe_3O_4/polyurethane elastomer nanocomposites. Polym Bull 72:219–234

Murphy CM, O'brien FJ (2010) Understanding the effect of mean pore size on cell activity in collagen-glycosaminoglycan scaffolds. Cell Adhes Migr 4:377–381

Narayanan G, Shen J, Boy R, Gupta BS, Tonelli AE (2018) Aliphatic polyester nano- fibres functionalized with cyclodextrins and cyclodextrin-guest inclusion complexes. Polymers 10:1–26

Noreen A, Sultana S, Sultana T, Tabasum S, Zia KM, Muzammil Z, Jabeen M, Lodhi AZ, Sultana S (2020) Natural polymers as constituents of bionanocomposites. In: Micro and Nano Technologies, Bionanocomposites. Elsevier, pp 55–85

Qi L (2013) Application of visible light-based projection stereolithography for live cell-scaffold fabrication with designed architecture. Biomaterials 34:331–339

Ranjan N (2020) On 3D printed scaffolds for orthopaedic tissue engineering applications. SN Appl Sci 2:1–8

Ranjan N, Singh R, Ahuja IPS, Singh J (2018) Fabrication of PLA-HAp-CS based biocompatible and biodegradable feedstock filament using twin-screw extrusion. In: Additive manufacturing of emerging materials, pp 325–345

Ratner BD, Bryant SJ (2004) Biomaterials: where we have been and where we are going. Annu Rev Biomed Eng 6:41–75

Subia B, Kundu J, Kundu SC (2010) Biomaterial scaffold fabrication techniques for potential tissue engineering applications [Internet]. Tissue Eng. InTech

Velasco MA, Narváez-Tovar CA, Garzón-Alvarado DA (2015) Design, materials, and mechanobiology of biodegradable scaffolds for bone tissue engineering. BioMed Res Int 2015. Article ID 729076, (21 pages)

Vrandečić NS, Erceg M, Jakić M, Klarić I (2010) Kinetic analysis of thermal degradation of poly(ethylene glycol) and poly(ethylene oxide)s of different molecular weight. Thermochim Acta 498:71–80

Wang Z (2020) Design and characterization of hydroxyapatite scaffolds fabricated by stereolithography for bone tissue engineering application. Proc CIRP 89:170–175

Wondu E, Lule Z, Kim J (2019) Thermal conductivity and mechanical properties of thermo- plastic polyurethane-/silane-modified Al_2O_3 composite fabricated via melt compounding. Polymers 11:1103

Zhang B (2021) 3D printed bone tissue regenerative PLA/HA scaffolds with comprehensive performance optimizations. Mater Des 201:109490–109490

Zhang L, Yang G, Johnson BN, Jia X (2019) Three-dimensional (3D) printed scaffold and material selection for bone repair. Acta Biomater 84:16–33

Zhang G, Zheng G, Ren T et al (2020) Dopamine hydrochloride and carboxymethyl chitosan coatings for multifilament surgical suture and their influence on friction during sliding contact with skin substitute. Friction 8:58–69

Zheng XQ (2019) 3D bioprinting in orthopaedics translational research. J Biomater Sci Polym Ed 30:1172–1187

Abrasive Wear Behaviour of Reformer HP40Nb Steel

Leena Harshal Nemade, P. S. Robi, and Pankaj Biswas

Abstract In the engineering industry, mechanical damage done by abrasive wear is probably the most dominant. In the present study, the two body abrasive wear characteristics of reformer steel (HP40Nb) are investigated. The design of experiments was done by using Taguchi technique. For performing the experiments, three parameters each of three levels were chosen. The L27 orthogonal array was selected. The combined effect of parameters on specific wear is studied, and interactions of parameters on specific wear are also studied.

Keywords Reformer HP40Nb steel · Abrasive wear · Taguchi technique

1 Introduction

Abrasive wear is the most commonly occurring wear mechanism in machine elements, and it constitutes the major portion of the total material loss due to abrasive wear. Wear represents one of the most significant opearting costs for an economy of Industrial firms.

Eyre (1976) has estimated that among total wear occurred in industrial situations, abrasive wear is around 50%, whereas other wear types adhesive, erosion, fretting and chemical, all together contribute 35% only. In the engineering industry, probably the most common cause of mechanical damage is abrasive wear. As abrasive wear contributes about half of the total wear experienced in industrial situations, it is essential to set standards for evaluating such a wear phenomenon to understand the long life of machine parts and to save energy and resources. HP grade (25Cr, 35Ni and 0.4C) of the centrifugally cast creep-resistant austenitic stainless steel alloys

L. H. Nemade (✉) · P. S. Robi · P. Biswas
Department of Mechanical Engineering, IIT Guwahati, Guwahati, India
e-mail: leena.nemade@dbuniversity.ac.in

L. H. Nemade
Department of Mechanical Engineering, School of Technology, Assam Don Bosco University, Guwahati, India

J. K. Deka et al. (eds.), *Emerging Technology for Sustainable Development*,
Lecture Notes in Electrical Engineering 1061,
https://doi.org/10.1007/978-981-99-4362-3_4

has been used in a wide extent for fabrication of the tubes in reforming operations (Liu and Chen 2011). HP grade (25Cr, 35Ni and 0.4C) of centrifugally cast creep-resistant austenitic stainless steel alloys has been widely used for the tubes fabrication in reforming operations. The catalyst tube assembly can amount to the quarter of the total cost of the furnace, and hence, optimization of its design from chemical, thermal, as well as mechanical points of view is a great motivation. It is seen in the past research that wear behaviour of reformer steel has not been studied. In the present paper, two body abrasive wear characteristics of reformer steel (HP40Nb) are investigated.

Abrasive wear induces several morphological changes in the abraded surface. Different researchers have studied wide range of variables that can influence the abrasive wear of materials (Bhushan 2013; Hawryluk et al. 2014; Narayanaswamy et al. 2016). Optimization of the process parameters in order to reduce the wear is the prime purpose in these works.

It is understood from the literature that the correlation between the parameters in dry sliding wear is individualistic and not simple. To reduce specific wear rate and coefficient of friction, it is important to select the optimum parameter of combination. Taguchi technique is an important approach to deal with reaction affected by numerous variables. It is developed for process enhancement and identification of preferable combination of the variables for a given feedback. As compared with the full factorial design of experiments, the Taguchi approach remarkably reduces the number of experiments that are essential to imitate the feedback function. Understanding the possible interaction between the factors is the most significant advantage of this technique (Çoban and Demirer 2014; Kıvak 2014; Stojanović et al. 2017; Serrao et al. 2016; Uvaraja and Natarajan 2012; Baradeswarana et al. 2013; Ghalme et al. 2016; Radhika and Raghu 2015; Ghosh et al. 2013; Ganesh et al. 2014; Sivaraosa et al. 2014; Agarwal et al. 2013; Rajesh et al. 2012; Jou et al. 2014; Singha and Pradhan 2014). Çoban et al. optimized the material type, sliding speed and applied load in order to reduce the drop in specimen weight and coefficient of friction due to abrasive wear of polyamide6 and Wollastonite composite materials (Çoban and Demirer 2014). Kıvak optimized the milling machining parameters such as surface roughness and flank wear of Hadfield steel with PVD- and CVD-coated carbide inserts (Kıvak 2014). The outcome of various factors like load, sliding speed and sliding distance on wear rate of aluminium hybrid composites was studied by Stojanović et al., and they optimized the tribological properties by using Taguchi technique (Stojanović et al. 2017). Taguchi method is an effective tool to design the experiments in order to optimize the wear parameters or to predict the abrasive wear behavior of different materials (Serrao et al. 2016; Uvaraja and Natarajan 2012; Baradeswarana et al. 2013; Ghalme et al. 2016; Radhika and Raghu 2015). When multiple performance characteristics to be optimized, it can be converted into a single grey relational grade, in order to avoid complications (Ghosh et al. 2013; Ganesh et al. 2014). Optimization of parameters in different processes such as machining, laser machining and injection moulding is done successfully with Taguchi method along with response surface methodology (Sivaraosa et al. 2014; Agarwal et al. 2013; Rajesh et al. 2012; Jou et al. 2014; Singha and Pradhan 2014).

Table 1 Chemical composition of reformer steel

C	Si	Mo	Cr	Ni	Nb	Ti	Fe
0.4%	1.3%	0.037%	23.6%	34.9%	0.8%	0.037%	Bal

2 Experimental Procedure

2.1 Material Used

The material used for the experiments is centrifugally cast reformer tubes HP40Nb micro-alloyed austenitic stainless steel obtained from Numaligarh Refineries Limited, Assam, India. It was supplied in the form of tube with thickness 15.3 mm and inside diameter of 106 mm and had been exposed to high temperatures up to 923 K for 11 years. The chemical composition of the steel is given in Table 1.

The HP40Nb cylindrical specimens (Φ 6 mm, length 30 mm) were cut by using wire EDM. The abrasive wear tests were conducted as per ASTM G 99 standard by using a wear and friction monitor tester, model TR-201 by M/S DUCOM, Bangalore, India. The experiments were conducted in dry sliding condition and atmospheric air at normal temperature. The machine has pin on disc setup to measure wear. It has an arm to attach pin, a fixture to accommodate disc of diameter 100 mm, 6–8 mm thickness. For measuring the friction force, it has an electronic force sensor, and for displaying parameters, printing or storing data for analysis purpose a computer software (WINDUCOM) is attached along with the system.

Effect of different operating parameters such as disc speed (150, 200 and 250 rpm), normal load (10, 15 and 20 N), a fixed sliding distance 1000 m. was studied on HP40Nb pin sample against the disc. Silicon carbide abrasive grit papers of different particle sizes (i.e., 320, 400 and 600 grit) were pasted on the disc. To create the two-body abrasive environment, the stationary pin was subjected to abrade against the abrasive disc. The specimen was thoroughly cleaned with acetone in prior and post the wear test. The weight of specimen pin was measured by electric weight balance of accuracy 0.0001 g prior to and after the experiment. The measured density of the specimen is $\rho = 7.709\ \text{g/cm}^3 = 0.007709\ \text{g/mm}^3$.

2.2 Design of Experiments

The Taguchi technique is employed to design the experiments for abrasive wear study. The parameters with their levels taken as given in Table 2. The L27 orthogonal array was selected.

The experiment has 27 tests, i.e., each row in the L27 orthogonal array, and the specific parameters are assigned to the columns. The first, second and the fifth

Table 2 Parameters and levels

Level	(A) Grit size (G)	(B) Load (*N*)	(C) Disc speed (RPM)
1	600	10	150
2	400	15	200
3	320	20	250

Table 3 Column-wise parameters and interactions

Column no	1	2	3	4	5	6	7	8	9	10	11	12	13
Parameter	A	B	AB	AB^2	C	AC	AC^2	BC	BC^2	D	E	F	G

column are designated as A, B and C which is allocated to grit-type, load and RPM, respectively, with the other columns are allocated to their interactions as per Table 3.

The specific wear rate of material is studied as response. The tests were reproduced, resulting in a total of 81 tests, in order to evaluate the analysis of the variance of the results. The input and output parameters are as given in Table 4.

3 Wear Test Results and Taguchi Analysis

The Taguchi analysis, ANOVA and general linear regression is done to find out the effect and impact of each parameter as well as by considering the interaction between the parameters and its reaction on the specific wear rate.

The percentage contribution of the different process variables to the selected performance characteristic is analysed by ANOVA. Considering different factors, the signal- to-noise (*S/N*) ratio was computed for the specific wear rate responses. The *S/N* ratios were calculated using the Eq. (1) in MINITAB software with smaller is better option.

$$SN = -10n \log \ln\left(\sum y^2\right) \tag{1}$$

where n is the number of observations and y is the observed data. The *S/N* ratios and the mean weight loss are plotted for each factor against each of its levels with the smaller is better condition the specific wear rate.

Table 4 Input and output parameters

Sr. no	Grit	Load (*N*)	RPM	Wt. loss (g)	*Ks* (mm^3/Nm)	SNRA (Wt. loss)	SNRA (*ks*)
1	3	2	1	0.2012	0.0017400	13.9274	55.1890
2	1	1	2	0.0057	0.0000739	44.8825	82.6271
3	1	3	2	0.0100	0.0000649	40.0000	83.7551
4	3	2	3	0.2039	0.0017633	13.8117	55.0735
5	3	3	2	0.2244	0.0014554	12.9795	56.7404
6	2	2	1	0.0184	0.0001591	34.7036	75.9666
7	3	1	2	0.1690	0.0021922	15.4423	53.1824
8	3	1	1	0.1790	0.0023220	14.9429	52.6828
9	3	1	3	0.1857	0.0024089	14.6238	52.3636
10	1	1	3	0.0047	0.0000610	46.5580	84.2934
11	2	2	2	0.0415	0.0003589	27.6390	68.9005
12	1	3	3	0.0127	0.0000824	37.9239	81.6815
13	1	1	1	0.0040	0.0000519	47.9588	85.6967
14	2	3	3	0.0899	0.0005831	20.9248	64.6851
15	2	1	2	0.0163	0.0002114	35.7562	73.4979
16	2	1	3	0.0419	0.0005435	27.5557	65.2960
17	2	3	1	0.0332	0.0002153	29.5772	73.3391
18	2	3	2	0.0626	0.0004060	24.0685	67.8295
19	1	2	2	0.0086	0.0000744	41.3100	82.5685
20	3	3	3	0.2334	0.0015138	12.6380	56.3986
21	1	3	1	0.0135	0.0000876	37.3933	81.1499
22	1	2	1	0.0225	0.0001946	32.9563	74.2171
23	2	1	1	0.0109	0.0001414	39.2515	76.9910
24	3	3	1	0.2154	0.0013971	13.3351	57.0955
25	3	2	2	0.1841	0.0015921	14.6989	55.9606
26	2	2	3	0.0628	0.0005431	24.0408	65.3024
27	1	2	3	0.0073	0.0000631	42.7335	83.9994

3.1 S/N Ratio Analysis: Specific Wear Rate Versus Grit, Load (N), RPM

The response table for the means and *S/N* ratio specific wear rate versus grit, load (*N*), RPM is given in Table 5. Grit has the highest influence over specific wear rate, followed by RPM and load.

Figure 1 shows main effects plots of (a) *S/N* ratios and (b) interaction plot for *S/N* ratios: *ks* (mm^3/Nm) versus grit, load (*N*) and RPM, and it shows the similarity in the results obtained in response.

Table 5 Response table: *ks* (mm^3/Nm) versus grit, load (*N*) and RPM

S/N ratios (smaller is better condition)			
Level	Grit	Load (*N*)	RPM
1	82.22	70.02	70.65
2	70.20	68.18	69.45
3	54.97	69.19	67.29
Delta	27.26	1.83	3.36
Rank	1	3	2

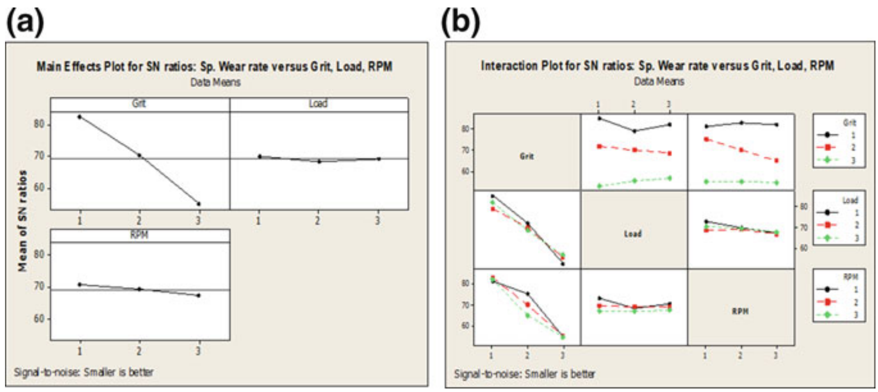

Fig. 1 Main effect plots of **a** *S/N* ratios and **b** interaction plots of *S/N* ratios: *ks* (mm^3/Nm) versus grit, load (*N*) and RPM

The rank order obtained in response for *S/N* ratio is grit size followed by RPM and load, respectively. The interaction plot is as shown Fig. 1. It can be seen that there is interaction between grit and load according to the interaction plot.

3.2 Regression Analysis: Sp. Wear Rate Versus Grit, Load (N), RPM

In order to establish the correlation between wear parameters grit, sliding distance, load and RPM with the sp. wear rate, regression was done. Equation (2) shows the correlation between the wear parameters and specific wt. loss due to wear.

The regression equation is

$$ks = -0.000880 + 0.000868\,\text{Grit} - 0.000121\,\text{Load}(N) + 0.000070\,\text{RPM} \quad (2)$$

Equation (2) shows the correlation between the wear parameters and specific wt. loss due to wear.

Table 6 ANOVA for specific wear rate (mm^3/Nm)

Source	*df*	Seq SS	Adj SS	Adj MS	*F*	*P*	*P* %
Grit	2	0.0000157	0.0000157	0.0000079	2106.17	0.000	91.28
Load	2	0.0000003	0.0000003	0.0000001	37.73	0.000	1.74
Grit × load	2	0.0000004	0.0000004	0.0000002	52.95	0.000	2.33
Grit × load × load	2	0.0000005	0.0000005	0.0000002	66.70	0.000	2.91
RPM	2	0.0000001	0.0000001	0.0000000	14.22	0.002	0.58
Grit × RPM	2	0.0000000	0.0000000	0.0000000	5.45	0.032	0.00
Grit × RPM × RPM	2	0.0000001	0.0000001	0.0000000	15.33	0.002	0.58
Load × RPM	2	0.0000000	0.0000000	0.0000000	0.04	0.956	0.00
Load × RPM × RPM	2	0.0000000	0.0000000	0.0000000	0.12	0.886	0.00
Error	8	0.0000001	0.0000001				0.58
Total	26	0.0000172					100

$S = 0.0000611267$, $R\text{-Sq} = 99.83\%$, $R\text{-Sq(adj)} = 99.44\%$
df degrees of freedom, *Seq SS* sequential sum of squares, *Adj SS* adjusted sum of squares, *Adj MS* adjusted mean squares

3.3 ANOVA: Specific Wear Rate Versus Grit, Load (N), RPM

Table 6 shows each parameters percentage contribution of among which grit size have the highest contribution followed by load and RPM. However, the contribution of interaction between the parameters is also significant, since its *P* value is less than 0.005.

The most significant parameter is Grit size, followed by Grit x Load x Load, Grit x Load, Load, RPM and Grit x RPM x RPM respectively.

4 Conclusion

1. With an increase in grit size, the specific wear rate also increased.
2. From the experimental simulation, the two-body abrasive wear mechanism was studied. The most significant parameter is found as abrasive grit size on abrasive wear of HP40Nb reformer steel, followed by RPM and load.

3. The effect of the interaction between the parameters is also studied. The interaction in between the parameters also found significant on the specific wear rate.
4. The specific wear rate was lowest for the combination of parameters such as lowest grit size, lowest load and lowest RPM, i.e., A1B1C1.
5. Taguchi analysis was successfully applied in order to find out the optimum parameters to minimize abrasive wear of HP40Nb reformer steel.

References

Agarwal G, Patnaik A, Kumar Sharma R (2013) Parametric optimization and three-body abrasive wear behavior of sic filled chopped glass fiber reinforced epoxy composites. Int J Compos Mater 3(2013):32–38

Baradeswarana A, Elayaperumal R, Franklin I (2013) A statistical analysis of optimization of wear behaviour of al-Al_2O_3 composites using Taguchi technique. Proc Eng 64:973–982. www.sciencedirect.com

Bhushan B (2013) Introduction to tribology, 2nd edn. John Wiley & Sons, Ltd., Publication

Çoban A, Demirer F (2014) Fiçici, optimization of wear parameters of polyamide-6 composite materials filled with wollastonite particles. Period Eng Nat Sci 2:1

Eyre TS (1976) Wear characteristics of metals. Tribol Int 9:202–212

Ganesh R, Chandrasekaran K, Ameen M, Kumar RP (2014) "Optimization of the process parameters for dry sliding wear of an AL 2219-SICP composite using the Taguchi-based grey relational analysis. Mater Technol 48:361–366

Ghalme S, Mankar A, Bhalerao YJ (2016) Optimization of wear loss in silicon nitride (Si_3N_4)—hexagonal boron nitride (hBN) composite using DoE—Taguchi method. Springer Plus

Ghosh S, Sahoo P, Sutradhar G (2013) Tribological performance optimization of Al-7.5% SiCp composites using the Taguchi method and grey relational analysis. Hindawi Publishing Corporation. J Compos 2013:1–9

Hawryluk M, Marciniak M, Misiun G (2014) Possibilities of investigating abrasive wear in conditions close to those prevailing in industrial forging processes. Maintenance Reliab16(4):600–607

Jou YT, Lin WT, Lee WC, Yeh TM (2014) Integrating the Taguchi method and response surface methodology for process parameter optimization of the injection molding. Appl Math Inf Sci 8(3):1277–1285

Kıvak T (2014) Optimization of surface roughness and flank wear using the Taguchi method in milling of Hadfield steel with PVD and CVD coated inserts. Measurement 50:19–28

Liu CJ, Chen Y (2011) Variations of the microstructure and mechanical properties of HP40Nb hydrogen reformer tube with time at elevated temperature. Mater Des 32:2507–2512

Narayanaswamy B, Hodgson P, Beladi H (2016) Comparisons of the two-body abrasive wear behaviour of four different ferrous microstructures with similar hardness levels. Wear 350–351:155–165

Radhika N, Raghu R (2015) Evaluation of dry sliding wear characteristics of LM 13 Al/B4C composites. Tribol Indus 37(1):20–28

Rajesh S, Rajakarunakaran S, Pandian RS (2012) Modelling and optimization of sliding specific wear and coefficient of friction of aluminium based red mud metal matrix composite using Taguchi Method and response surface methodology. Mater Phys Mech 15:150–166

Serrao B, Prabhu R, Chiranth BP, Mohammed Y (2016) Application of Taguchi method to predict the abrasive wear behavior of CP titanium. J Mech Eng Autom 6(5A):13–17

Singha V, Pradhan SK (2014) Optimization of WEDM parameters using Taguchi technique and response surface methodology in machining of AISI D2 steel, science direct. Proc Eng 97:1597–1608. www.sciencedirect.com

Sivaraosa S, Milkey KR, Samsudin AR, Dubey AK, Kidd P (2014) Comparison between Taguchi method and response surface methodology (RSM) in modelling CO_2 laser machining, Jordan. J Mech Indus Eng 8(1):35–42

Stojanović B, Veličković S, Babić M, Bobić I (2017) Optimization of tribological properties IN A356/10SIC/5GR hybrid composite using Taguchi method. In: 15th international conference on tribology—Serbiatrib '17

Uvaraja VC, Natarajan N (2012) Optimization on friction and wear process parameters using taguchi technique. Int J Eng Technol 2:4

Conceptualization, Design, and Development of a Pedal Propelled Vehicle to Collect and Dispose Residential Solid Waste

Vikramjit Kakati and Sidharth Borkataky

Abstract The most exhibited consequence of the population explosion is seen within the style of solid waste disposal issue. This is because of incorrect analysis of waste disposal sites, setting up and transportation. This project deals with the designing of a vehicle that is powered by human energy to drive it. The vehicle has been designed to gather and manage dispose of the solid waste of approximately 500 L with proper, healthy way. The aim of this project is to overcome the effort and to provide safe and easy disposal of domestic solid waste. The existing design for the three-wheeler vehicles for collection of municipal waste is in a poor condition. The safety issues, improper and unhealthy transportation of the waste, etc., are several key issues in the current waste assortment tricycles in the country. It is of the utmost requirement to design and develop a vehicle which is safe, comfort in riding, cost-effective, etc. There are many designs of human-powered vehicles, but they have some issues related to human comfort, proper and safe and hygienic way of transporting wastes.

Keywords Solid waste · Collection · Transportation · Household waste · Municipal waste · Residential

1 Introduction

Garbage, trash, rubbish, or refuse is waste material that is discarded by humans, usually due to a perceived lack of utility. The household waste collection is destitute in India since the vehicle carrying the garbage does not have any proper covering, it creates a very filthy surrounding by dropping the waste while transporting. As mentioned by Hanrahan et al. (2006) "There is an urgent need for much improved

V. Kakati (✉)
Assam Don Bosco University, Guwahati, Assam, India
e-mail: vikramjit.kakati@dbuniversity.ac.in

S. Borkataky
Senior Application Specialist CFD, New Delhi, India

J. K. Deka et al. (eds.), *Emerging Technology for Sustainable Development*,
Lecture Notes in Electrical Engineering 1061,
https://doi.org/10.1007/978-981-99-4362-3_5

medium-term planning at the municipal and state level so that realistic investment projections can be developed and implemented." Issues related to waste management in the content of Indian cities still requires a pathfinder as most of the solid waste management (SWM) planners and executers are still in the dark that which part of the SWM rule 2016 needs to be addressed in the primary stage. Indian's current population of 1200 million will continue to grow at the rate of 3–3.5% per annum. With the per capita waste generation which is increasing by 1.3% per annum, the yearly increase in waste generation is around 5% annually. A review of the literature of SWM in India highlights that institutional/financial issues are the most important factors that are limiting improvements in SWM. To know the actual cost of SWM services in India, an attempt has been made to analyze the extensive cost data of SWM that was first published in 2005 by National Institute of Urban Affairs (2016). Some of the unaddressed and unresolved issues in municipal waste management in India are listed below.

2 General Issues

(a) Non-revenue expenditure
(b) Collection procedures
(c) Transfer of waste
(d) Management

3 Issues (Metro Cities)

(a) Location of landfill sites (LFS)
(b) Travel time to LFS
(c) Road width

Presently, there are mainly three types of vehicles that are being used for transportation of MSW as shown in Fig. 1.

(1) Type-1
(2) Type-2
(3) Type-3

It is observed that the above data does not address the hazardous surrounding created during transporting of the waste. Also, the vehicle for transportation is generic one and lack in mechanism for pick up and drop of the waste.

Any process which seeks to find the best possible solution to a problem is called optimization. According to Scardina (1996), mechanism optimization is the repeated

Fig. 1 Types of vehicles are being used for transportation of MSW

analysis of randomly determined mechanism to find the best design. The best solution will satisfy the design constraints and produce the minimum value for the objective function. For design optimization problems, there are five steps formulation procedure (Arora 2010):

I. Project/problem statement
II. Data and information collection
III. Identification/definition of design variables
IV. Optimization criterion
V. Formulation of constraints.

In most of the current type-3 design bed of the tricycle truck is 0.4 m from the ground, because of which the contents are dumped into the ground.

This situation exposes the operators to unhealthy conditions and this method also involves much labor.

According to Krajewski et al. (2022) the concentration of organic dust in the raw MSW is 7.7 mg/m^3. The lift-tipping mechanism which was developed by Fiagbe et al. (2011a), was considered and employed. The actuation of the mechanism was achieved by employing a power screw with a worm and wheel connection. The cycling paddle was used in such a way that it can lift and lower the mechanism as well as move the tricycle in the forward direction. The system dimensions and parameters are chosen to minimize modification on the existing tricycle framework.

With respect to tricycle bin, the length of the lifting bar and lift support bar are 1.2 m each. The length of the tipping arm is 0.45 m. However, the vehicle does not address factors like spillage of the garbage and other environment hazards that may arise during garbage dumping.

Apart from the lift-tipping kinematic mechanism available, there are many other mechanisms available for collecting solid household waste. These mechanisms are also reliable and help in proper and healthy transportation of the waste to the municipal dustbin. These vehicles have more power, better durability, and require less human effort as most of the components are motorized. The carriage bin behind can be fixed in any pickup vehicles. They can have a capacity of 1–1.5 cubic meter which are lifted by using two hydraulic cylinders for the purpose of dumping. To prevent overturning while dumping, the vehicles are provided with a stabilizer at the rear end. The hydraulic power pack receives power from the flywheel of the vehicle. Although these vehicles provide more efficient and easier mode of transportation, the cost factor for these vehicles is quite high since the use and maintenance of the hydraulic system is high, and their manufacturing is done in large quantities, and most of the manufacturers sell them in large quantities because of which the weak section of the society who indulged in the garbage collection activity cannot purchase them.

The current project will focus on the designing of a garbage collecting and transporting vehicle considering the safe operational environment and considering various ergonomic factors. The proposed vehicle will transport the waste without spilling it and it will have a mechanism to dump the waste directly into the municipal garbage bins available in the municipal area (Fornace et al. 2016). Complaints were recorded during field study that the present garbage disposing vehicle spreads fetid to the surroundings due to non-availability of close garbage-carrying containers. This results in health and environmental hazards. Considering those conditions, it has been felt that one improvised garbage collection vehicle is very much essential in the present context and hence it has been decided to design and develop an improvised garbage collection vehicle.

Minimal research has been done on garbage-dumping and collecting vehicles. The fact is that there is no proper garbage dumping vehicle or proper waste-dumping methods from municipal household to the collecting bins provided by the municipality which are usually having a height of around one meter. The research showed that areas where the bins are provided become very unhygienic due to waste spill as well as a disturbing smell.

4 Concept Generation

A pilot study of the possible areas of design intervention in the field of garbage collection was carried out and was found that the process of collection and dumping was very unhygienic and it causes spilling of the waste on the ground. Therefore, there was a need for the development of a mechanism which could lift the carriage bin to the desired height and dump the contents of the bin directly to the collecting bin without spilling it outside. For this purpose, different mechanisms were thought of which could lift the carriage bin. The height of the collection bin from the ground is 0.960 mm. It has a length of 3075 mm and a breadth of 1956 mm. According to these dimensions of the collecting bin, two mechanisms were idealized which could lift the bin to a height corresponding to the height of the collecting bin.

4.1 Ideation of First Mechanism

For the purpose of lifting, in the first mechanism that was conceptualized was a scissor-type mechanism. In this mechanism, for direct dumping of the garbage into the collection bin, it requires a height of 1250 mm from the ground level. Then only, the garbage container can be tilted properly for the perfect unloading of the garbage into the collection bin.

The scissor mechanism mainly consists of the following components: frame, lifting bar, lifting support bar, tipping arm, and bin support bar. The mechanism is operated with the help of a power screw. The power screw relates to the link (b). As the power screw is operated, the link (b) moves forward. The link (b) is pivoted with link (c) which in turn is pivoted with link (d) and link (d) is pivoted with link (e). The link is pivoted to link (e) at its end and the link is pivoted at a fixed point on the link (a). The carriage bin is lifted and tilted at the back side of the tricycle.

4.2 Ideation of Second Mechanism

The second mechanism that was idealized consists of a winch, a set of pulleys and two cables. The cables which are tied to the frame of the pulley passes through the pulleys to the winch which is operated manually. In this mechanism, the carriage bin is lifted and tilted sideways of the tricycle and into the collecting bin. Eleven pulleys are used in the mechanism, ten pulleys with the single way and one with double way. As the winch is operated, the carriage tilts from its mean position and goes to a position where all the contents of the bin are dumped directly to the collecting bin. The winch is provided with a ratchet for locking purpose, such that when the carriage bin is at the highest position it does not fall back by itself (Artobolevsky 1976).

4.3 Ideation of Third Mechanism

After various considerations on the two mechanisms that were conceptualized, the second mechanism was hence adopted and focused upon as the tilting of the bin was done sideways, so the chances tilting of the tricycle were reduced since the center of gravity (C.G.) of the cycle remains in the center (Fiagbe et al. 2011b).

In the first concept, the weight factor could not be cut out with modification, so with additional modification and introduction of a proper mechanism, the effort required to lift the collecting bin was reduced to a great extent, making the product possible for usage and keeping the cost factor in mind. And to make it more efficient, a winch mechanism was added to help in the tilting, and to make sure that the bin would not fall back, a locking mechanism was provided (Artobolevsky 1976).

5 Design Process and Prototyping

The designing was carried out taking into account the various problems which are faced by the operator in the existing such type of vehicles. The present tricycle, apart from not having a proper mechanism for dumping the waste, also faces difficulty of using it in different weather conditions, as for instance during a rainy season the operator cannot use the tricycle as it has no proper cover on the carriage bin, so the garbage gets wet/soaked and becomes heavy due to this very reason. To overcome this problem, it has been decided to provide weather and stench-resistant cover on the carriage. In most of the existing models, the carriage is welded with the chassis of the tricycle, because of which if any modification is to be done then the entire chassis and the carriage part must be altered. The carriage of those vehicles is made of plain tin sheets which get corroded easily and requires replacement quite often (Urunkar and Deshpande 2014). In the proposed design, the carriage bin has its own frame which is supported with the help of four columns which are fixed to the main chassis of the tricycle, due to this the carriage bin can be tilted while dumping of garbage and while maintenance it does not affect the chassis of the mainframe as it can be removed for maintenance and attached back. In the mechanism, the winch used is fixed with two square bars which are welded to the columns of the main chassis. The bin has two hinges in two extreme edges of the carriage frame on the side to be tilted, where the two cables used in the tricycle are tied. The pulleys that are used for guiding the cables are placed horizontally and vertically in such a way that they reduce the effort required for lifting the bin.

5.1 Prototype 1

Based on the concept of the scissor mechanism, a small prototype was prepared using scrap materials to analyze the working of the mechanism. The cross-links were thought of to be operated using a winch and a cable. Also, two pulleys, one simple pulley and one spring controlled, were incorporated for tilting the bin.

When the winch is operated, the cable gets rolled causing the cross-link to rise. The bin is connected to the spring-loaded pulley with another cable which also passes through the simple pulley. As the winch is operated, the cross-links rises, the cable which is connected to the bin and the spring-loaded pulley gets stretched. After the cross-link reaches a certain height, the cable connected to the bin gets fully stretched which on further stretching starts pulling the bin from the lower end causing it to tilt. The bin rests on a stage and when the cross-links are at the mean position the spring-loaded pulley keeps the cable coiled.

5.2 Prototype Two

Another small prototype was prepared using mechanical components corresponding to the scissor mechanism. Two pulleys, a pair of cables, and a winch were used to operate the mechanism. One cable is longer than the other. The longer cable is used for raising the cross-links, and the shorter one is used for titling the bin. One end of the longer cable is attached to the links which pass through one of the pulleys and to the winch. The other cable is attached to the pulley and to the bottom end of the bin, a pulley is also used to guide the cable to the winch, and also a stage is provided for resting the bin.

The movable end of the cross-links is connected to a shaft carrying bearings which can roll on the stage. As the winch is operated, the cable which is connected to the winch and cross-links gets stretched and causes the link to rising. Due to the rising of the links, the cable which is connected to the bin and the winch, because of it being shorter in length, keeps on stretching and starts tilting the bin when the links reach a particular height.

5.3 Prototype Three

The third prototype was prepared based on the concept of a power screw. Here, the main driving mechanism is not a winch as in the previous prototypes but a power screw, which is operated with the help of the pedal of the tricycle.

5.4 Prototype Four

This prototype is operated using a winch, unlike the third prototype. Here, not only a pair, but eleven pulleys are used. This mechanism requires less effort for tilting the carriage bin as when the winch is used, the cables are stretched to the maximum which creates a tension on the cables, thus making it easier to tilt the bin. Upon design analysis with the help of 3D modeling tools it has been learned that this model satisfies the necessary design parameters, and hence, this prototype model has been selected for creating a functional prototype. In his concept, a bin with tilting mechanism will fulfil the purpose of this study.

6 Fabrication of Functional Prototype

6.1 Dimensional Mapping

In product design process, the dimensional mapping is a significant activity.

6.2 Materials

The main chassis of the vehicle was fabricated with mild steel members and the waste collection bin was fabricated by using fiber glass. Fiber glass was used to make it lightweight and weather resistant. As per the shape of the bin, the weight is acting downwards along the middle portion of the bin as shown in Fig. 2.

For riding comfort, the sitting arrangement was ergonomically fabricated and one fiber roof was provided (Fig. 4).

After fabrication of various modules those were joined accordingly and carried out successful testing of the working prototype. The final fabricated working prototype is shown in Fig. 4.

7 Conclusion

The main objective of this work is effective collection and the disposal of residential solid waste in the urban area. The covered lightweight bin and tilting mechanism fulfill the objective of the research. This tilting mechanism prevents spillage of solid waste in the open area during unloading, and hence, a clean working environment can achieve.

Fig. 2 Bin with tilting mechanism

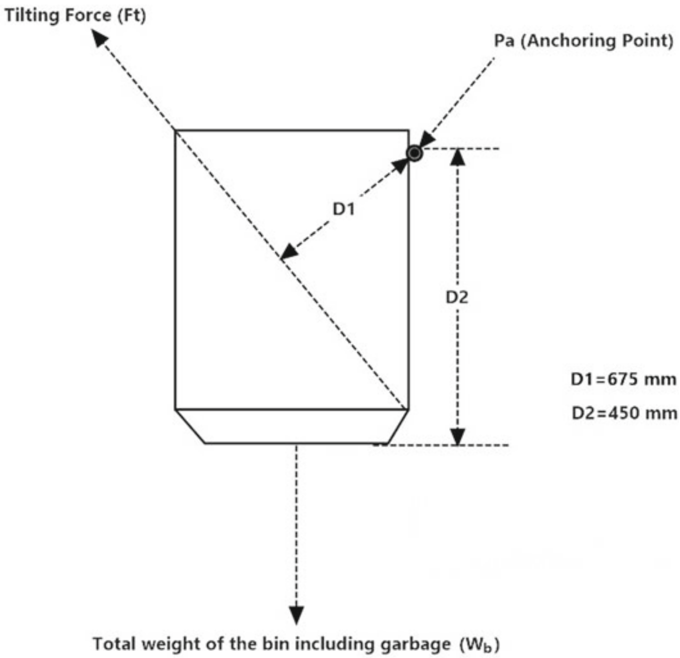

Fig. 3 Free body diagram of the bin

Fig. 4 Final working prototype

References

Arora JS (2010) Formulating design problems as optimization problems. In: System engineering. Wiley Online Library

Artobolevsky I (1976) Mechanisms in modern engineering design, vol 1. MIR Publishers

Fiagbe YA, Sackey MN, Agbeko E (2011a) Kinematic design of lift- tipping mechanism for small solid waste collection truck. J Univ Sci Technol 31(2):135–141. https://doi.org/10.4314/just.v31i2.69402

Fiagbe Y, Mensah MY, Sackey M, Andoh P (2011b) Municipal solid waste tricycle truck with lift-tipping mechanism for improved sanitation. J Ghana Inst Eng 31(2):135–141. https://doi.org/10.4314/just.v31i2.69402

Fornace KM, Abidin TR, Alexander N, Brock PM, Grigg MJ, Murphy AC, William T, Menon J, Drakeley C, Cox J (2016) Association between landscape factors and spatial patterns of *Plasmodium knowlesi* infections in Sabah, Malaysia. Emerg Infect Dis 22(2):201–209

Hanrahan D, Srivastava S, Ramakrishna AS (2006) Improving management of municipal solid waste in India: overview and challenges. World Bank Publications—reports 19463

Krajewski JA, Tarkowski S, Cyprowski M, Szarapińska-Kwaszewska J, Dudkiewicz B (2022) Occupational exposure to organic dust associated with municipal waste collection and management. Int J Occup Med Environ Health 35(2):289–301

National Institute of Urban Affairs (2016) The solid waste management rules were inaugurated in 2016

Scardina MT (1996) Optimal synthesis of force-generating planar four-link mechanisms. Virginia Polytechnic Institute and State University

Urunkar R, Deshpande PP (2014) Study of drive mechanisms of bicycle, tricycle or like vehicles to optimize operating performance-a review. Int J Eng Res Appl 4(1):214–219

UAV for Remote Sensing Applications: An Analytical Review

Victor Saikhom and Manoranjan Kalita

Abstract Unmanned aerial vehicles (UAV) have occupied a pertinent space in the field of remote sensing in recent years. UAVs are powered aircraft with pre-programmed flight planning. They are operated remotely. UAVs also known as drones can propose a practical and sustainable alternative to traditional platforms when it comes to procuring cost-effective high-resolution remote sensing data, greater versatility and operational flexibility. The practical use of UAV remote sensing in various fields like environmental studies, disaster management, flood monitoring system, archaeology, land-use dynamic monitoring, meteorological disaster monitoring, fighting COVID-19 pandemic, etc., is considered to have enhanced the application domains. Moreover, the effective use of UAVs for acquiring digital elevation model (DEM) data renders analytical advantages in a wide range of remote sensing applications. The need of the hour is to examine and religiously work on the diverse research aspects and trends of UAV remote sensing to augment its regular use. This paper reviews and examines the innumerable benefits and significance of the use of UAV platform for remote sensing applications in various fields.

Keywords Digital elevation model (DEM) · Remote sensing applications · Research trends · UAV

1 Introduction

Remote sensing (RS) system works on various state-of-the-art technology such as data acquisition, data transmission, data processing and data storage system. It comprises of five components which are remote sensor system, platform carrier, data transmission system and positioning and control system. RS technology's most mature technology is believed to be satellite remote sensing technology (Ninghao et al. 2019). Satellite and aircraft platform-based remote sensing technologies

V. Saikhom (✉) · M. Kalita
Department of Civil Engineering, Assam Don Bosco University, Guwahati, Assam, India
e-mail: victorsaikhom@gmail.com

J. K. Deka et al. (eds.), *Emerging Technology for Sustainable Development*,
Lecture Notes in Electrical Engineering 1061,
https://doi.org/10.1007/978-981-99-4362-3_6

have improved considerably in respect of spatial and temporal resolution; thereby augmenting their aptness for high-resolution mapping (HRM) applications. The importance of satellite surveys is that they map huge regions and areas. However, the resolution for HRM is even coarse for some large scale mapping, and after a certain point, it is very difficult to procure detailed features. Furthermore, cloud cover hindrance is a regular phenomenon in many regions. Aircraft surveys, on the other hand, are more flexible, but it can be sometimes a very costly affair. To counter these shortcomings, delivery platforms like unmanned aerial vehicles (UAVs), unmanned airships, etc., have been a boon in this vast field of remote sensing applications. Some shortcomings of traditional RS platforms can be solved by UAVs. In manned aircrafts, caution should be kept while operating heights. However, there is no such problem in case of UAVs about operating heights and dangers which comes with it. UAVs have a varied range of flying heights and also low flying cost. Their operation is flexible. The take-off and the landing sites are also flexible. UAVs at any time can create secondary measurements efficiently. Furthermore, UAVs are suitable to map a small area with an ultra-high-resolution, typically with ground sampling distance (GSD) varying from 0.01 to 1 m and accuracy of sub-centimetres (Alessandro et al. 2015). With these observations, it is pertinent to critically review the umpteen usage of UAV for remote sensing (RS) applications. This paper examines the applications of UAVs for RS.

2 UAV Technology

UAVs are powered aircraft with pre-programmed flight planning. They are operated remotely. UAVs also known as drones can propose a practical and sustainable alternative to traditional platforms when it comes to procuring cost-effective high-resolution remote sensing data with greater versatility and operational flexibility. UAVs can capture imagery in conjunction with field observations. This brings a probable solution to the common remote sensing problem arising from the variations while acquiring ground and remote sensing data.

The categorization of UAVs are based on key features such as flying attitude, weight, endurance, range and payload (Korchenko and Illyash 2013; Dalamagkidis 2015). Furthermore, in India according to the maximum all-up weight inclusive of payload, UAV laws are divided into the following: “Nano unmanned aircraft system: weighing less than or equal to 250 g; Micro unmanned aircraft system: weighing more than 250 g, but less than or equal to 2 kg; Small unmanned aircraft system: weighing more than 2 kg, but less than or equal to 25 kg; Medium unmanned aircraft system: weighing more than 25 kg, but less than or equal to 150 kg; and Large unmanned aircraft system: weighing more than 150 kg” (Draft Drones Rules 2022). As the UAVs can operate in low flying altitude, they can efficiently give a detailed information of objects with as low as below one decimetre (ultra-high resolution) spatial resolution. This can accurately bring about semantic and geometrical analysis for a rationally broader area. Furthermore, UAV in conjunction with autopilot systems and Global Positioning System/inertial measurement unit (GPS/IMU) can effortlessly take photogrammetric image blocks. Data acquisition with the aid of UAV can capture high-resolution photogrammetric images or full motion videos (Yao et al. 2019). In the present times with the advancement of photogrammetry, three-dimensional geometric information like DSMs and triangular meshes are some important products for UAV-based RS applications. These UAV platforms are found to be more flexible than traditional platforms. So, they have a unified access to ortho-photograph and DSM products (Li et al. 2017). Additionally, the availability of low-cost and lightweight sensors like hyperspectral and multispectral cameras has opened up new avenues for UAVs to bring out multi-source data fusion solutions of higher spatial and temporal resolution.

3 Methodology

The study has adopted analytical method to critically study the available literature. It reviews and examines the umpteen benefits and importance of the use of UAV platform for remote sensing applications in various fields. The study is based on primary, secondary sources, research journals and online sources.

4 Digital Elevation Model from UAV

Digital elevation model (DEM) has been a vital input in geographical research particularly in analysing quantitative landscape. For developing a good-quality DEM, accuracy plays a critical role. If the accuracy of DEM does not meet the required criteria, the project has to be redesigned, thereby affecting the costs and efficiency. The accuracy of DEM depends on the source and resolution of the data samples observed (Hanuphab et al. 2012). The use of UAVs for acquiring DEM data has benefited in a wide range of remote sensing applications which are cost effective. They can provide speedy deployment on-demand flood mapping for various projects. For such a reliable and accurate study, an accurate topography information and digital elevation model (DEM) are needed. Camera-equipped unmanned aerial systems (UAS) and digital aerial photogrammetry (DAP) analysis techniques are also increasingly used in the present times. Initially, UASs were created and developed for military establishments. Later on, they were developed to market for various commercial purposes. One important advantage of UAS compared to other manned counterparts is that by flying at lower altitudes it can take high-quality image and spatial resolution; at the same time, it can reduce its dependency on cloud situations (Shi et al. 2016). Relatedly, UAS can be deployed more easily, and hence, it allows many flights. This creates a platform to monitor and observe highly dynamic vegetation when compared to such traditional RS platforms like aircraft and satellites (Turner et al. 2012).

Currently, for generating DEM, light detection and ranging (LiDAR) is believed to be the most widely used remote sensing technology (Rusli et al. 2019). LiDAR is used to generate DEM which are georeferenced, and the sensor's position is examined by the use of IMU data and GPS. Presently, a more advanced, TanDEM-X imagery is becoming more common to obtain high-quality DEM. For acquiring field data, real-time kinematic–Global Positioning System (RTK-GPS) method can be used for Global Navigation Satellite System (GNSS) (Lee and Ryu 2017). The use of root mean square error (RMSE) for TanDEM-X imagery can deliver and contribute to a vital design and concept of future SAR missions (Tridon et al. 2016).

The use of UAV for data acquisition has become a most viable method pertaining to its cost effectiveness. Moreover, many organizations have their own drone/UAV. The benefits of using UAV for acquiring data in the fields like urban planning, flood modelling, forestry and environment-related research and study are numerous, and this will be discussed in this paper at a later stage. By incorporating UAV and TanDEM-X, the 3D data processing results can be high in quality (Rusli et al. 2019). This can be highly effective in analysing terrain mapping. Another important benefit of using UAV is that it is flexible. It can capture data which can be customized on a person's preference.

Unquestionably, the benefits of the use of UAV for data acquisition are numerous. With the usage of UAV for acquiring data in DEM and subsequent applications, it will highly improve the effectiveness of DEM in producing high-quality results.

5 Applications of UAV Remote Sensing

Today, the use of UAV platforms in remote sensing applications is increasingly seen in various fields. UAV remote sensing is used in the following areas: land supervision, inspection and precaution of geological disasters, land-use change dynamic monitoring, earthquake disaster rescuing and evaluation, meteorological disasters monitoring, evaluation and monitoring of flood disaster, cadastral surveying and topographic mapping (Ma et al. 2005). Some of the applications are discussed in the sections below:

1. Land-use dynamic monitoring: The use of high-resolution and multi-temporal images of UAV remote sensing can extract and analyse information ranging through different periods. This information is essential to detect changes which are pertinent in the study of land-use monitoring.
2. Monitoring and evaluation of flood disaster: In this case, flood disaster is monitored and evaluated by comparing and analysing multi-temporal images. It can thus monitor the development and altering facets of flood. This aids in the prediction of probable trend of flood disaster.

3. Meteorological disaster monitoring: UAV remote sensing can record images which can monitor meteorological disaster. This helps in finding the areas that are affected, assessing damage, evaluate the extent of disaster and can offer instant and speedy rescuing operations.
4. Disaster relief and evaluation of earthquake: In the management of earthquake disaster, UAV remote sensing can swiftly procure images of the earthquake area. It can assess earthquake-strike extent, damage of building structures, distress severity of buildings, etc. This can aid in extending faster relief and rescue operations.
5. Forest-fire prevention and insect pest monitoring: UAV remote sensing can be used to control and fight fire disasters. It can be used to conduct fire prevention patrol and determine fire point location, fire detection and fire suppression command. UAV remote sensing can also be used to monitor and evaluate the condition of the forest damaged by insect pest and its extent.
6. Assessment and prevention of mud-rock flow, landslide: In the geological disaster like mud flow and landslide, UAV remote sensing can analyse and assess the severity conditions of disaster and their spatial distribution. This can contribute to the government's relief works. For speedy relief works, obtaining disaster information is prerequisite. So, UAV remote sensing images can collect disaster information faster. They can collect information of disaster and can also procure basic data of forecasting to monitor disaster.
7. Topographic and cadastral surveying and mapping: Acquiring nadir viewed images with permissible frontal and side overlapping viewed from different locations/angles integrated with ground control points (GCPs), interior and exterior orientation parameters on the images can be assessed and calculated. The derivatives are used for topographic mapping and cadastral surveying.
8. Environmental remote sensing: This comprises of the collection, acquisition and interpretation of information about the land, atmosphere and oceans remotely. The data collected through this process can be effective in predicting the weather conditions and in tracking hurricanes, coastal dynamics observation, detection of pollutants and mapping coastal land cover, inclusive of tidal wetlands, agriculture, urban areas and forests (Jensen 2007). For environmental change studies, satellites in the conventional way have been instrumental in offering large area coverage, a reliable revisit time and a multispectral imaging. However, they are devoid of spatial resolution which is the requisite of various applications. Currently, satellite data with high spatial resolution are available. However, these applications operated by airborne sensors are suitably adapted for various applications like wetlands mapping, land-use mapping, tracking oil slicks and coastline delineation. To cite an example, an aircraft overflight can be remotely used to observe a coastal wetland to enhance the finding of emergent and submerged aquatic vegetation (SAV) during low tide. Additionally, a low-altitude aircraft through its hyperspectral or multispectral imagers can be used to accurately map SAV, coral reef habitats and wetland (Purkis 2005). So, this imagery can be incorporated with locational information based on Global Positioning System (GPS) information and further employed as layers in a

Geographic Information System (GIS) for a variety of modelling and mapping applications. Manned aircraft overflights can be found to be expensive. In this regard, the use of unmanned aerial platforms can in a way minimize the cost. In the long run, this proves to be a boon for organizations considering the delivering of a cost-effective platform. According to Lechner et al. "GPS-guided unmanned aerial vehicles (UAVs) have the capacity to obtain ultra-high spatial resolution (< 10 cm) imagery of specific landscape features with revisit times determined by the operator as opposed to fixed satellite revisit times (Lechner et al. 2012)." Considering the observations in the preceding reviews, UAVs are continuously and effectively being used in various environmental studies.

9. Archaeology: UAVs are widely used in archaeology to survey sites due to its easy usage and the quality data measurements (Themistocleous 2014). Researchers have effectively used UAVs to work on cultural heritage archaeological sites in the Mediterranean (Rinaudo et al. 2012), Hungary, Germany and Cambodia (Seitz and Altenbach 2011). Concurrently, researchers have used aerial imagery to create a 3D reconstruction of the cultural site (Fiorillo et al. 2012).
10. Civil construction and monitoring: In the present times, UAV is increasingly used in in monitoring the civil construction projects particularly to inspect the progress of the work done. Similarly, it is also used to monitor and inspect the GSM towers, gas pipelines, high-tension electric power lines, water pipelines, etc. (Liu et al. 2014; Deng et al. 2014; Mohamadi 2014). To give an example, thermal infra-red (TIR) cameras are used for identifying the hotspots of bad conductivity in the high-tension power lines (Larrauri et al. 2013).
11. Hydrology: UAVs have been effectively used for flood monitoring, assessment and management because of their innate ability to capture images (Popescu et al. 2017; Aicardi et al. 2017; Feng et al. 2015). Researches show that UAV with the capability of integrating with various types of payload such as hyperspectral sensors can be used for collecting hydro-chemical data to monitor phosphorus, chemical oxygen demand, chlorophyll-a content, nitrogen total-suspended solid, biological oxygen demand, turbidity and plastic floats in water (Kwon et al. 2020; Wei et al. 2019; Balsi et al. 2021). Relatedly, fixed-wing UAV platform can also be used to map snow depth distribution at a centimetre scale in a research conducted over an alpine area in northern Italy. This was done by repeated UAV data acquisition during peak snow accumulation periods. The snow depth and volume were estimated and validated by subtracting the elevation models generated using UAV photogrammetric techniques (Michele et al. 2016; Bühler et al. 2016).

Relatedly, UAV remote sensing is also used in various other fields like mineral resources investigation, customs inspection, to monitor forest cover, marine resources and environment monitoring, traffic management and transportation planning in urban areas through aerial photography. It can also be effectively used to monitor and assess hazard zone and pollution on toxic zone. The year 2020 has experienced the uncertainty of the pandemic in world history. The need of the hour is contactless delivery and transportation. During these unprecedented times, UAV remote sensing/

drones showcase a promising alternative to deliver essential goods like COVID-19 viral tests (Kunovjanek and Wankmüller 2021). Presently, drones are also effectively used to deliver medicines, sanitizers, masks and food items to people's home. This eased in effective COVID-19 pandemic fight to a certain extent.

6 Conclusion

In the recent times, UAV remote sensing applications have come to occupy a vital place in the field of remote sensing. Indisputably, the practical use of UAV remote sensing in various fields like environmental studies, disaster management, flood monitoring system, archaeology, land-use dynamic monitoring, meteorological disaster monitoring, fighting COVID-19 pandemic, etc., is considered to have enhanced the application process. The need of the hour is to examine and religiously work on the umpteen research prospects of UAV remote sensing. Further, this can be translated into effective practical applications. Some of the research aspects of UAV remote sensing identified by this analytical review are: attitude measurement in the process of capturing remote sensing images, augmenting to achieve accuracy in navigation, the integration of real-time remote sensing images splicing, automatic detection of image objects using deep learning/machine learning (DL/ML) techniques, data transmission of multi-sensors, GPS difference, etc. This will make significant contributions toward the research trends and practical use of UAV remote sensing.

References

Aicardi I et al (2017) A methodology for acquisition and processing of thermal data acquired by UAVs: a test about subfluvial springs' investigations. Geomatics Nat Haz Risk 8(1):5–17

Alessandro M et al (2015) Intercomparison of UAV, aircraft and satellite remote sensing platforms for precision viticulture. Remote Sens 7:2971–2990. https://doi.org/10.3390/rs70302971

Balsi M et al (2021) High-resolution aerial detection of marine plastic litter by hyperspectral sensing. Remote Sens 13(8):1557. https://doi.org/10.3390/rs13081557

Bühler Y et al (2016) Mapping snow depth in alpine terrain with unmanned aerial systems (UASs): potential and limitations. Cryosphere 10:1075–1088. https://doi.org/10.5194/tc-10-1075-2016

Dalamagkidis K (2015) Classification of UAVs. In: Valavanis KP, Vachtsevanos GJ (eds) Handbook of unmanned aerial vehicles. Springer, Dordrecht, pp 83–91

De Michele C et al (2016) Using a fixed-wing UAS to map snow depth distribution: an evaluation at peak accumulation. Cryosphere 10:511–522. https://doi.org/10.5194/tc-10-511-2016

Deng C et al (2014) Unmanned aerial vehicles for power line inspection: a cooperative way in platforms and communications. J Commun 9(9):687–692

Draft Drones Rules (2022) https://www.civilaviation.gov.in/sites/default/files/Draft_Drones_Rules_14_Jul_2021.pdf. Accessed 8 Feb 2022

Feng Q, Liu J, Gong J (2015) Urban flood mapping based on unmanned aerial vehicle remote sensing and random forest classifier—a case of Yuyao, China. Water 7(4):1437–1455

Fiorillo F, Jimenez B, Remondino F, Barba S (2012) 3D surveying and modeling of the archaeological area of Paestum. Ital Virtual Archaeol Rev. 4:55–60

Hanuphab T, Suwanprasit C, Srichai N (2012) Effects of DEM resolution and source on hydrological modeling. In: The 33rd Asian conference on remote sensing, pp 26–30

Jensen JR (2007) Remote sensing of the environment: an earth resource perspective. Prentice-Hall, Upper Saddle River, New Jersey

Korchenko AG, Illyash OS (2013) The generalized classification of Unmanned Air Vehicles. In: Proceedings of the 2013 IEEE 2nd international conference actual problems of unmanned air vehicles developments proceedings (APUAVD), Kiev, Ukraine, vol 12, pp 28–34 (2013)

Kunovjanek M, Wankmüller C (2021) Containing the COVID-19 pandemic with drones—Feasibility of a drone enabled back-up transport system. https://www.sciencedirect.com/science/article/pii/S0967070X21000779. Accessed 8 Feb 2022

Kwon YS et al (2020) Drone-based hyperspectral remote sensing of cyanobacteria using vertical cumulative pigment concentration in a deep reservoir. Remote Sens Environ 236:111517. https://doi.org/10.1016/j.rse.2019.111517

Larrauri JI, Sorrosal G, González M (2013) Automatic system for overhead power line inspection using an unmanned aerial vehicle—RELIFO project. In: Proceedings of international conference on unmanned aircraft system (ICUAS), pp 244–252

Lechner AM, Fletcher A, Johansenand K, Erskine P (2012) Characterizing upland swamps using object-based classification methods and hyper-spatial resolution imagery derived from an unmanned aerial vehicle. In: Proceedings of the XXII ISPRS congress annals of the photogrammetry, remote sensing and spatial information sciences, vol I-4, pp 101–106, ISPRS, Melbourne, Australia

Lee S, Ryu J (2017) High-accuracy tidal flat digital elevation model construction using TanDEM-X science phase data. Appl Earth Obs Remote Sens 10(6):2713–2724

Li W, Wu G, Zhang F, Du Q (2017) Hyperspectral image classification using deep pixel-pair features. IEEE Trans Geosci Remote Sens 55(2):844–853

Liu P et al (2014) A review of rotorcraft unmanned aerial vehicle (UAV) developments and applications in civil engineering. Smart Struct Syst 13(6):1065–1094

Ma LJ et al (2005) The general research on applications of aerial remote sensing. J Guangxi Meteorol 2005(26):180–181

Mohamadi F (2014) Vertical takeoff and landing (VTOL) small unmanned aerial system for monitoring oil and gas pipelines. U.S. Patent 8 880 241, Nov. 4

Ninghao Y et al (2019) A review: UAV-based remote sensing. IOP Conf Series Mater Sci Eng 490:062014. https://doi.org/10.1088/1757-899X/490/6/062014

Popescu D et al (2017) Unmanned aerial vehicle systems for remote estimation of flooded areas based on complex image processing. Sensors 17(3) (2017)

Purkis SJ (2005) A 'reef-up' approach to classifying coral habitats from IKONOS imagery. IEEE Trans Geosci Remote Sens 43:1375–1390

Rinaudo F, Chiabrando F, Lingua A, Span A (2012) Archaelogical site monitoring: UAV photogrammetry can be an answer. ISPRS Int Arch Photogramm Remote Sens Spatial Inform Sci XXXIX-B5:583–588

Rusli N, Majid MR, Razali NFAA, Yaacob NFF (2019) Accuracy assessment of DEM from UAV and TanDEM-X imagery. https://ieeexplore.ieee.org/document/8696088. Accessed 8 Feb 2022

Seitz C, Altenbach H (2011) Project ArchEye—the quadracopter as the archaeologist's eye. ISPRS Int Arch Photogramm Remote Sens Spatial Inform Sci XXXVIII-1/C22:297–302

Shi Y, Thomasson JA, Murray SC, Pugh NA, Rooney WL, Shafian S (2016) Unmanned aerial vehicles for high-throughput phenotyping and agronomic research. PLoS ONE 2016:11

Themistocleous K (2014) The use of UAV platforms for remote sensing applications: case studies in Cyprus. https://www.researchgate.net/publication/269319902_The_Use_of_UAV_Platforms_for_Remote_Sensing_Applications_Case_Studies_In_Cyprus. Accessed 8 Feb 2022

Tridon DB, Bachmann M, Martone M, Schulze D, Zink M (2016) The future of TanDEM-X : final DEM and beyond. In: Proceedings of EUSAR 2016 11th European conference on synthetic aperture radar, pp 541–545

Turner D, Lucieer A, Watson C (2012) An automated technique for generating georectified mosaics from ultra-high resolution unmanned aerial vehicle (UAV) imagery, based on structure from motion (SFM) point clouds. Remote Sens 2012(4):1392–1410

Wei L et al (2019) Inland waters suspended solids concentration retrieval based on PSOLSSVM for UAV-borne hyperspectral remote sensing imagery. Remote Sens 11(12):1455. https://doi.org/10.3390/rs11121455

Yao H, Qin R, Chen X (2019) Unmanned aerial vehicle for remote sensing applications—a review. https://www.mdpi.com/2072-4292/11/12/1443. Accessed 8 Feb 2022

A Review of Numerical Models for Sediment Dynamics

Borneeta Dutta, Pankaj Srivastava, and Annapurna Boruah

Abstract Sediment dynamics plays a very important part in erosion, floods and morphological changes in the river. The sediment dynamics can be analysed by studying the basin and river parameters. There are different techniques to investigate the sediment dynamics. Numerical modelling of rivers for studying sediment dynamics is rapidly being utilized to investigate river pattern changes, and the information acquired from these studies is used by environmental managers and decision makers. There are a lot of numerical models present for these studies. But all of these models vary in some way or the other. They may vary in their intricacy, inputs and outputs, advantages and disadvantages and so on. In light of these issues, this research examines various numerical models and their approaches with regard to sediment dynamics. Upgradation of these numerical models from the time it was first presented has been discussed in the paper. A summary of some specific numerical models is given. The purpose of this paper is to understand different numerical models and the usage of these models in a given research, so that the sediment dynamics of a river can be studied.

Keywords Sediment dynamics · Numerical model · Sediment transport

1 Introduction

The creation, distribution and transport of sediments are described by sediment dynamics. The morphology, banks and floodplains form according to sediment movement mechanisms, such as bank and bed erosion and shoaling/accretion. When compared to the use of physical models, the use of numerical models for finding solutions connected to sediment dynamics is pretty recent. Numerical models were first studied in early 1970s. Numerical models are computational simulations to solve a problem, and from these solutions, the required interpretations are given.

B. Dutta (✉) · P. Srivastava · A. Boruah
University of Petroleum and Energy Studies, Dehra Dun 248007, India
e-mail: 500078624@stu.upes.ac.in

J. K. Deka et al. (eds.), *Emerging Technology for Sustainable Development*,
Lecture Notes in Electrical Engineering 1061,
https://doi.org/10.1007/978-981-99-4362-3_7

With the increasing trend of using computational tools, numerical models thus have been greatly explored in the last 50 years. A range of numerical models for studying sediment factors have been explored, but there has been not a review where the development of the models and modification of these models have been given. The main goal of this review is to lay out a resource that future model users can utilize to guide their research in deciding which model to use for their study. Thus, this is achieved by reviewing the numerical models which are mainly used for studying sediment dynamics and how further new features have been added to these models.

2 Model Types

Here, the models are divided according to the numerical schemes that they use. The most common numerical schemes are finite difference method (FDM), finite element method (FEM) and finite volume method (FVM). Then, these models are categorized accordingly under one-dimensional models (1D), two-dimensional models (2D) and three-dimensional models (3D) (Table 1). Below, these models are discussed and reviewed.

2.1 Finite Difference Method (FDM)

By calculating derivatives with finite differences, FDM is implemented to solve differential equations. This numerical scheme is used by all the three 1D, 2D and 3D models.

The 1D models are generally drafted in a Cartesian coordinate system. In short tidal basins, 1D models provide an accurate description of the dynamics and the friction coefficient is larger than in the 2D models (Prooijen and Wang 2013). The 1D models are much simple to use as they require low data. The 2D and 3D models are computationally much expensive than 1D models. It is seen that models usually undergo a lot of modifications from the start when they are first developed. HEC-RAS was developed as a 1D model which was used for steady flow and water surface profile calculations in 1995 by US Army Corps of Engineers. Gradually, this model had new features added such as 1D HEC-RAS (Hydrologic Engineering Centre, River Analysis System) software which was adopted for developing the hydrodynamic model for unsteady flow regime (Nistoran et al. 2017). A 1D unsteady flow model (UNET, part of HEC-RAS 3.0) in a generalized likelihood uncertainty estimation (GLUE) structure was investigated (Pappenberger et al. 2005). The finding suggests that this study might provide excellent flood likelihood maps in the course of the event and could be linked to a GLUE stopping basis. The HEC-RAS model (Yang et al. 2006) and GIS tools to describe floodplains were employed. With its revised computational procedures, the HEC-RAS river network model provides improved simulations, assists in the import and export of GIS data, approves for uncomplicated

Table 1 Model name, type of model which tells whether it is 1, 2 or 3 dimensional in nature, flow of sediment, type of sediment and numerical methods

SN	Model	Model type	Flow	Sediment type	Numerical method
1	MIKE21 (1993)	2D	Unsteady	Cohesive sediment	FDM
2	ROMS (1994)	3D	Unsteady	Non-cohesive	FDM
3	USTARS (1997)	2D	Quasi-unsteady		FDM
4	MIKE3 (1997)	3D	Unsteady	Cohesive sediment	FDM
5	FAST 2D (1998)	2D	Unsteady	Non-cohesive	FVM with structured grids
6	DELFT 2D (1998)	2D	Unsteady	Cohesive	FDM
7	CCHE2D (1999)	2D	Unsteady	Non-cohesive sediment	FEM
8	FAST3D (1998)	3D	Unsteady	Non-cohesive	FVM with structured grids
9	SHYFEM (2004)	2D	Unsteady	Cohesive	FEM
10	NETSTARS (2013)	2D	Quasi-steady	Both	FDM
11	SISYPHE (2015)	2D and 3D	Unsteady	Both	FEM, FVM
12	SedFoam-2.0 (2017)	3D	Steady	Non-cohesive	FVM, Reynolds-averaged Navier–Stokes (RANS) equations, Exner equation
13	HEC-RAS (2017)	1D	Unsteady	Non-cohesive	FDM
14	DEM (2019)	2D and 3D	Quasi-steady	Non-cohesive	FVM
15	UMHYSER-1D (2020)	1D	Unsteady and steady	Both	FVM

and rapid cross-section interpolation, and provides for 3D analysis of river reach and cross-section information. HEC-RAS model and Qual2K model were merged to simulate the tidal results on river water character (Fan et al. 2009).

In medium-scale domains, 2D depth-averaged modelling is primarily used (Huybrechts et al. 2010). The depth-averaged solutions are obtained using these models (i.e. shallow water equations). The 2D model MIKE 21 employs the FDM in a Cartesian coordinate system. The most important input parameter is the bathymetry. Initially, MIKE 21 was described as the model used for study of hydraulics and hydraulic related events in estuaries, coastal waters and seas (Warren et al. 1992). Flood attacks can also be studied (Patro Chatterjee et al. 2009).

The 2D model USTARS (1997) was developed to treat the shortcomings of GSTARS. Generalized stream tube model for alluvial river simulation (GSTARS) was initially launched in 1986, and GSTARS 2.0, with better algorithms, was launched in 1998. Then, GSTARS 2.1, revised GSTARS 2.0 and GSTARS 3 were released with more modified features. The stream tube theory was used, and this incorporates the ability of simulating the motion of suspended load and bed load, and the reactions between them (Hong-Yuan Lee et al. 1997). It is applicable to both steady and unsteady flow patterns. It is mainly used for sediment routing.

The 3D models are used when 2D models cannot discuss some specific hydrodynamic/sediment transport processes in hydraulic engineering problems. The 3D models commonly apply numerical approaches like FDM, FEM, or FVM to address the continuity and Navier–Stokes equations, as well as the sediment mass balance equation. The 3D model ROMS (1994) was developed at the Rutgers University, University of California, Los Angeles. It is now best applied to those systems which are mappable at high resolution. Options for higher-order stencil are available now (Shchepetkin and McWilliams 2005). The performance of turbulence closures was assessed in ROMS in terms of idealized sediment transport applications (Warner et al. 2005). In a recent study, ROMS was used where river run off was introduced in the continuity equation (Dey et al. 2020). For the study of bathymetry and also studying the geomorphic reaction to measure of sea level and climatic change, ROMS can be used (Ganju and Schoellhamer 2009).

Delft 3D used FDM and was developed by Delft Hydraulics, 1999. The limitation of Delft 2D is overcome by Delft 3D model, i.e. the model can be applied to different sizes of the sediments. Delft 3D and ROMS are both built on the result of the Reynolds-averaged Navier–Stokes equations. In case of Delft 3D and ROMS, the differences might occur in bed friction velocities.

Thus, it is seen that these models have undergone a lot of modifications from the time they were developed.

2.2 Finite Element Method (FEM)

The FEM is a key numerical approach for working out partial differential equations in two or three spatial variables. In seeking a solution, the FEM breaks down a complicated structure into smaller, more manageable components known as finite elements.

In this study, it is seen that not many models use FEM as their numerical scheme; here, 2D models use FEM. CCHE2D model was first presented in 1999 which is a 2D model and uses FEM as a numerical scheme (Jia and Wang 1999). This model may be applied to investigate steady and unsteady free surface flow, sediment transport and morphological dynamics in natural rivers. A channel confluence was studied and bifurcation using the CCHE2D model (Khan et al. 2000).

SHYFEM is a 2D FEM that was created at ISMAR-CNR (Institute of Marine Sciences—National Research Council) and is an open source for the Venice lagoon.

A comparative evaluation of ten Mediterranean lagoons were also carried out using the SHYFEM 3D numerical model (Umgiesser et al. 2014). It uses a semi-implicit approach for time integration, which unites the benefits of both the explicit and implicit schemes.

2.3 Finite Volume Method (FVM)

The FVM uses algebraic equations to express and evaluate partial differential equations. The little volume around every node point on a mesh referred is described as "finite volume." Here, some 1D, 2D and 3D models which use FVM as a numerical scheme are discussed.

The unsteady model for the hydraulics of sediments in rivers 1D (UMHYSER-1D) is a 1D hydromorphodynamic model with FVM which was created to indicate water surface studies in a single river or a multi-river system with various flow arrangements which facilitates for cohesive or non-cohesive sediment transport (AlQasimi and Mahdi 2020). It can deal with both subcritical and supercritical conditions. Internal boundary conditions are computed. Even on a modest scale, bed armouring can be done and performed excellently. It cannot, though, directly model lateral sediment transport.

SISYPHE is TELEMAC-MASCARET modelling system's modern sediment transport and bed evolution module. It can be used both as a 2D and 3D models, and FVM is used. To upgrade the sediment transport module SISYPHE, some parts of the FAST computer code (developed by University of Karlsruhe, Germany, KIT and TUM) were adjusted into the TELEMAC environment to remove the errors from complicated real river applications (Reisenbüchler et al. 2017). Instead of 2-class mixtures, SISYPHE (Lepesqueur et al. 2019) was employed for 10-class mixes and distributed sediment density instead of uniform sediment density. The sediment representation was refined in order to improve sediment movement and riverbed evolution forecasts.

Discrete element method (DEM) was constructed with a multi-layer's concept (Bui et al. 2019). It was first forwarded by Cundall and Strack (1979) to model the mechanical actions of granular flows and to calculate the forces and movement of every particle. It can be used both as a 2D and 3D models, and FVM is used. DEM was applied to reproduce a huge quantity of particles in transport and interaction (Bravo et al. 2014). DEM was used to investigate evolving sediment transport for non-cohesive landforms. Granular sedimentation (Zhao et al. 2014) was examined through DEM–CFD (computational fluid dynamics) combined simulations. The mechanical and hydraulic aspects of the fluid–solid mixing system are investigated.

The mathematical model SediMorph is 3D FVM. The German Federal Waterways Institute (BAW), Hamburg, created this modern 3D morphodynamics numerical model in collaboration with the Institute of Hydro Sciences at the German Federal Armed Forces University in Munich. It was studied for sediment transport along with the hydrodynamic model called TELEMAC-2D (Ramsankaran et al. 2010).

SediMorph operates on a user-defined sediment classification via a classification file for the sediments. SediMorph (Silva et al. 2015) was used to investigate the variance in the fine sediment dynamics in estuarine and coastal environments. It operates in conjunction with the hydrodynamic model TELEMAC-3D (Marques et al. 2010).

SedFoam-2.0 (Chauchat et al. 2017) is a 3D two-stage flow solver that can be used in sediment transport. It solves two-phase flow equations in three dimensions for sediment transport, with the possibility of selecting permutations of turbulent and granular stress models. SedFoam (Santana et al. 2019) was used to execute the parameterization of results of secondary flows of the event, 3D modelling of the flow field and local scour. FVM is used here.

A lot of modifications have been clearly made in the models from the time it was first developed, e.g. after MIKE21 (1993), MIKE 3 was developed by the Danish Hydraulic Institute in 1993. This can be used to simulate 3D free surface flows as well as sediment or water quality procedures. It is a finite difference model in an orthogonal grid system. It can quantify the fine grain sediment dynamics. It is seen that numerical models have also undergone a lot of modifications in terms of algorithms since the early years of its use. Some of the models from the 1990s uses finite difference method to solve the shallow water equations (Falconer et al. 1990). For different types of mode of sediment transport like bed load, suspended load and sheet flow, a numerical model where creation, growth and removal of bed ripple was suggested.

3 Conclusion

Usually, the models are 1D, 2D or 3D. The selection of these models should be based on the nature of the research. A realistic approach should be taken, so that the output produced by the model is almost accurate. Field studies should be done in order to have less errors, i.e. both model output and field output should be consistent. There should always be scope for development of the modelling technique. The environment setting should also be considered from which the samples were drawn. Best results can be obtained from the models with high efficiency. It is hard to determine the precision of quantitative evaluation of source contributions as the absolute values provided by the model might sometimes differ, so this has to be corrected at the earliest stage. It is seen that the disadvantages of the numerical models can be overcome with certain modifications, e.g. the large computational cost of FEM can be solved by applying the high-order elements or the differential quadrature elements, which lessens the number of the elements in the double loops. The development of a numerical model with low complexities is required. Considerable work is necessary to upgrade numerical models by improved data collection. If there is unavailability of records, the study is limited to only certain experiments.

Acknowledgements The authors would like to thank University of Petroleum and Energy Studies, Dehradun, for the support.

Conflict of Interest The authors stated that there is no conflict of interest for the research.

References

AlQasimi E, Mahdi TF (2020) A new one-dimensional numerical model for unsteady hydraulics of sediments in rivers. SN Appl Sci 2. https://doi.org/10.1007/s42452-020-03284-y.

Bravo R, Ortiz P, Pérez-Aparicio JL (2014) Incipient sediment transport for non-cohesive landforms by the discrete element method (DEM). Appl Math Model 38:1326–1337. https://doi.org/10.1016/j.apm.2013.08.010

Bui VH, Bui MD, Rutschmann P (2019) Advanced numerical modeling of sediment transport in gravel-bed rivers. Water 11. https://doi.org/10.3390/w11030550

Chauchat J, Cheng Z, Nagel T, Bonamy C, Hsu T-J (2017) SedFoam-2.0: a 3D two-phase flow numerical model for sediment transport. Geosci Model Dev Discuss 10:1–42. https://doi.org/10.5194/gmd-2017-101

Cundall PA, Strack DL (1979) A discrete numerical model for granular assemblies

Dey SP, Dash MK, Sasmal K, Jana S, Raju NJ (2020) Impact of river runoff on seasonal sea level, Kelvin waves, and East India Coastal Current in the Bay of Bengal: a numerical study using ROMS. Regional Stud Mar Sci 35:101214. https://doi.org/10.1016/j.rsma.2020.101214

Falconer RA, Owe' PH, Scienti'c Ofleer B (1990) Numerical modelling of suspended sediment fluxes in estuarine waters

Fan C, Ko CH, Wang WS (2009) An innovative modeling approach using Qual2K and HEC-RAS integration to assess the impact of tidal effect on River Water quality simulation. J Environ Manage 90:1824–1832. https://doi.org/10.1016/j.jenvman.2008.11.011

Ganju NK, Schoellhamer DH (2009) Calibration of an estuarine sediment transport model to sediment fluxes as an intermediate step for simulation of geomorphic evolution. Cont Shelf Res 29:148–158. https://doi.org/10.1016/j.csr.2007.09.005

Hong-Yuan Lee B, Hsieh H-M, Yang J-C, Ted Yang C (1997) QUASI-two-dimensional simulation of scour and deposition in alluvial channels

Huybrechts N, Villaret C, Hervouet J-M (2010) Comparison between 2D and 3D modelling of sediment transport: application to the dune evolution

Jia Y, Wang SSY (1999) Numerical model for channel flow and morphological change studies

Khan AA, Cadavid R, Wang Y (2000) Simulation of channel confluence and bifurcation using the CCHE2D model

Lepesqueur J, Hostache R, Martínez-Carreras N, Montargès-Pelletier E, Hissler C (2019) Sediment transport modelling in riverine environments: on the importance of grain-size distribution, sediment density, and suspended sediment concentrations at the upstream boundary. Hydrol Earth Syst Sci 23:3901–3915. https://doi.org/10.5194/hess-23-3901-2019

Marques WC, Fernandes EHL, Moller OO (2010) Straining and advection contributions to the mixing process of the Patos Lagoon coastal plume, Brazil. J Geophys Res Oceans 115. https://doi.org/10.1029/2009JC005653

Nistoran DG, Ionescu C, Pătru G, Armaş I, Omrani ŞG (2017) One dimensional sediment transport model to assess channel changes along Olteniţa-Călăraşi reach of Danube River, Romania. Energy Proc 67–74 (Elsevier Ltd). https://doi.org/10.1016/j.egypro.2017.03.1062

Numerical modeling of sediment transport for various mode Masanobu ONO (1), Ichiro DEGUCHI (2) and Torn SAWARAGI (3)

Pappenberger F, Beven K, Horritt M, Blazkova S (2005) Uncertainty in the calibration of effective roughness parameters in HEC-RAS using inundation and downstream level observations. J Hydrol 302:46–69. https://doi.org/10.1016/j.jhydrol.2004.06.036

Patro Chatterjee S, Mohanty R, Singh NS, Raghuwanshi SC, Patro S, Chatterjee C, Mohanty S, Singh R, Raghuwanshi NS (2009) Flood inundation modeling using MIKE FLOOD and remote sensing data. J Indian Soc Remote Sens 37:107–118

Ramsankaran R, Maerker C, Malcherek A (2010) Numerické modelovanie hydrodynamických javov a transportu sedimentov počas prívalových zrážok v občasných tokoch. J Hydrol Hydromech 58:36–48. https://doi.org/10.2478/v10098-010-0005-1

Reisenbüchler M, Bui M-D, Rutschmann P (2017) Implementation of a new layer-subroutine for fractional sediment transport in SISYPHE Zur Verfügung gestellt in Kooperation mit/provided in cooperation with: TELEMAC-MASCARET Core Group.

Santana LD, Alberto J, Vargas E (2019) Numerical modelling of local scour around cylindrical piers including secondary flows effects

Shchepetkin AF, McWilliams JC (2005) The regional oceanic modeling system (ROMS): a split-explicit, free-surface, topography-following-coordinate oceanic model. Ocean Model 9:347–404. https://doi.org/10.1016/j.ocemod.2004.08.002

Silva PD, Lisboa PV, Fernandes EH (2015) Changes on the fine sediment dynamics after the Port of Rio Grande expansion. Adv Geosci 39:123–127. https://doi.org/10.5194/adgeo-39-123-2015

Umgiesser G, Ferrarin C, Cucco A, de Pascalis F, Bellafiore D, Ghezzo M, Bajo M (2014) Comparative hydrodynamics of 10 Mediterranean lagoons by means of numerical modeling. J Geophys Res Oceans 119:2212–2226. https://doi.org/10.1002/2013JC009512

van Prooijen BC, Wang ZB (2013) A 1D model for tides waves and fine sediment in short tidal basins—application to the Wadden Sea. Ocean Dyn 63:1233–1248. https://doi.org/10.1007/s10236-013-0648-7

Warner JC, Sherwood CR, Arango HG, Signell RP (2005) Performance of four turbulence closure models implemented using a generic length scale method. Ocean Model 8:81–113. https://doi.org/10.1016/j.ocemod.2003.12.003

Warren R, Bach HK, Warren IR (1992) MIKE 21: a modelling system for estuaries, coastal waters and seas

Yang J, Townsend RD, Daneshfar B (2006) Applying the HEC-RAS model and GIS techniques in river network floodplain delineation. Can J Civ Eng 33:19–28. https://doi.org/10.1139/l05-102

Zhao T, Houlsby GT, Utili S (2014) Investigation of granular batch sedimentation via DEM–CFD coupling. Granular Matter 16:921–932. https://doi.org/10.1007/s10035-014-0534-0

Thermal Analysis of an Office Building Using Passive Cooling Design in Aizawl, Mizoram

Haudingliana Hauzel, B. C. Vanlalhruaitluanga, Lalrindika, Lalsangzela Sailo, and Sylvia Romawizuali

Abstract Due to climate change, the overheating risk of the buildings becomes alarming worldwide, thus increasing energy demand for thermal comfort of the inhabitant. This study was conducted to provide overheating risk reduction measures using passive cooling design for both existing buildings and those yet to be constructed. Simulations were done in Revit software and Autodesk Insight, and the results were compared with the first simulation to see its effect. The building study typology is an office building of Mizoram University. The simulations were done using thermal wall absorptance, thermal transmittance through glazing, wall and roof insulation using expanded polystyrene and polyurethane, natural shading by trees and changing the window-to-wall ratios (WWR) by measuring the heating and cooling loads from Revit and also through optimizations done in Insight. This study concluded that the best thermal comfort measure can range from building to building. Since the building used in this study is an office building, having high WWR, the windows played the most important role in the overheating of the building. This study highlights the significance of thermal comfort and overheating risk measures.

Keywords Thermal comfort · Passive cooling design · Overheating risk

1 Introduction

The thermal comfort of a building signifies the satisfactory perception of an individual concerning the built-in environment and is considered as one of the most important conditions for occupants' comfort and health. Climate changes and extreme temperatures are crucial problems faced worldwide. In tropical countries, climate change will

H. Hauzel · B. C. Vanlalhruaitluanga · Lalrindika · L. Sailo (✉)
Department of Civil Engineering, School of Engineering and Technology, Mizoram University, Aizawl, Mizoram 796009, India
e-mail: zelasailo@gmail.com

S. Romawizuali
School of Architecture and Planning, Mizoram University, Aizawl, Mizoram 796009, India

J. K. Deka et al. (eds.), *Emerging Technology for Sustainable Development*, Lecture Notes in Electrical Engineering 1061,
https://doi.org/10.1007/978-981-99-4362-3_8

have an adverse effect on the world's poorest and most vulnerable inhabitants (James Cook University 2017). From studies, it is found that 43% of the world's population are located in tropical areas, which is likely to exceed 50% by 2050 (James Cook University 2017, 2020; UNDESA 2019). Cooling access risks are being faced by at least 1 billion people worldwide, and more than 2.2 billion are likely to purchase inefficient cooling devices, resulting in a dramatic increase in energy and associated carbon emissions (SEforALL 2020). Over the last few years, there has been increasing studies on the thermal performance of building and cooling design for a reduction in energy consumption of building which accounts for about 40% globally. In a warm tropical climate like India, key design parameters include roof insulation, balcony openings for natural ventilation are the most influencing parameters, and window shading and wall materials are very effective in reducing building cooling loads. The buildings in North East India having a very pleasant climate lack analysis and studies on the building performance, where natural ventilation and passive design intervention can play a major role in the reduction of energy use.

2 Methodology

2.1 Locations and Climate Scenarios

The building model as shown in Fig. 1 was designed as per IS 456, IS 875 to be constructed in Mizoram University, Aizawl, Mizoram, which has a little more extreme weather than other parts of Mizoram. Mizoram has moderate weather compared to other states of India. However, Mizoram University, due to its low distance from mean sea level, experiences a little more extreme weather conditions than other parts of Aizawl. The ambient temperature during summer is about 20–29 °C and during winter 11–21 °C which is very comfortable to dwell in. Due to this reason, we have decided to plan thermal comfort measures which are effective and affordable at the same time.

2.2 Thermal Simulations

The thermal performance of the building was simulated with existing environmental conditions. The office-type building is of two-storey height, and a flat accessible roof was used for analysis, and the building plan is shown (Fig. 1). An office building was selected because Mizoram University (MZU) is an institutional campus where the most common buildings are office-type buildings, and the typology of these official buildings is very similar to the others. The BIM software, Revit 2020.2.7, was used for modelling and performing thermal and solar analysis along with the Web version of Autodesk Insight specifically for performing window-to-wall ratio

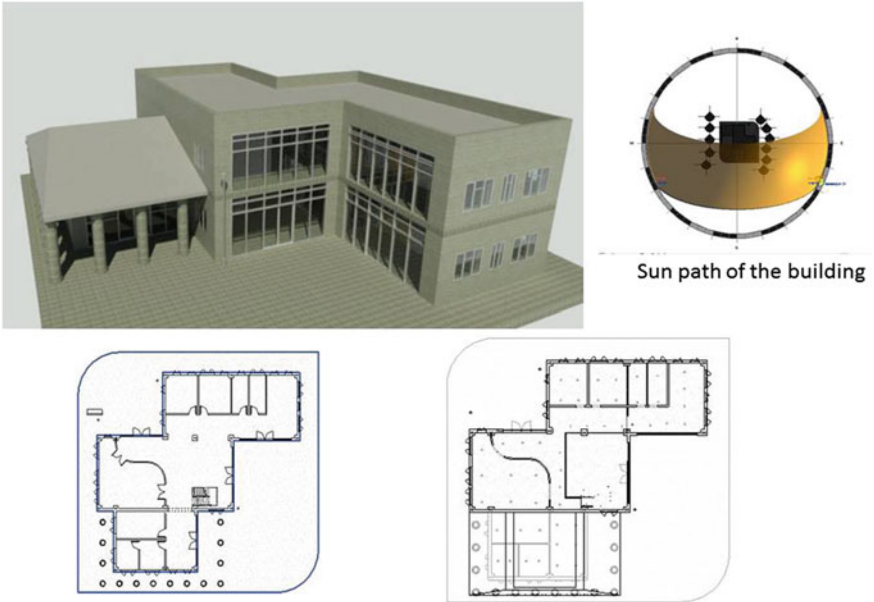

Fig. 1 Office building in Mizoram University campus and sun path of the building

(WWR)-related optimizations. Many other optimizations are available in the Web version of Autodesk Insight, but in this study, we will only consider the WWR. In Revit, the materials were changed from the properties palette by assigning the appropriate materials. If the required materials were not found, new materials were created with similar thermal properties. The material U-values were taken from green rating for integrated habitat assessment (GRIHA) (2017) as given in Table 1.

2.2.1 Passive Cooling Design Measures

The passive cooling strategies include natural ventilation, wall absorptance, buffering semi-outdoor space, solar heat gain coefficient of windows and window-to-wall ratios (WWR) is simulated and were divided into eight cases as mentioned below.

Original Building

In this case, we used normal building materials without considering thermal comfort measures. Standard RCC concrete was used in the walls and roofs, but due to their differences in exposure to heat, they have different U-values, i.e. thermal heat gain coefficient. So, the U-values were altered in the properties palette in Revit software as necessary. The U-values of the materials used for this study were obtained from

Table 1 Detailed list of cases and materials used for considered elements (Material *U*-values taken from GRIHA website) (GRIHA 2017)

Case	Element	Material	Thickness (mm)	Area m^2	*U*-value (W/m^2 K)
1	Wall	Brick wall	90	376	2.03
	Flat roof	RCC roof	101.6	259	3.3
	Sloped roof	RCC roof	101.6	147	3.3
	Glass	Single glazing	3.175	–	5.9050
2	Wall	AAC blocks	101.6	376	0.79
	Flat roof	RCC roof	101.6	259	3.3
	Sloped roof	RCC roof	101.6	147	3.3
	Glass	Single glazing	3.175	–	5.9050
3	Wall	Brick walls + EPS	90 + 90	376	2.03 + 0.389 = 0.326
	Flat roof	RCC roof	101.6	259	3.3
	Sloped roof	RCC roof	101.6	147	3.3
	Glass	Single glazing	3.175	–	5.9050
4	Wall	Brick wall	90	376	2.03
	Flat roof	RCC roof	101.6	259	3.3
	Sloped roof	RCC roof	101.6	147	3.3
	Glass	Double glazing	6.35	–	1.9873
5	Wall	Brick wall	90	376	2.03
	Flat roof	RCC roof + Polyurethane	101.6 + 101.6	259	3.3 + 0.356 = 0.3214
	Sloped roof	RCC roof + Polyurethane	101.6 + 101.6	147	3.3 + 0.356 = 0.3214
	Glass	Single glazing	3.175	–	5.9050
8	Wall	AAC blocks	101.6	376	0.79
	Flat roof	RCC roof + Polyurethane	101.6 + 101.6	259	3.3 + 0.356 = 0.3214
	Sloped roof	RCC roof + Polyurethane	101.6 + 101.6	147	3.3 + 0.356 = 0.3214
	Glass	Double glazing	6.35	–	1.9873

GRIHA. The original building heat gain and thermal loads summary is shown in Fig. 2.

Autoclaved Aerated Concrete Blocks (AAC Blocks)

Brick walls are the most commonly used walls in Mizoram; however, they have quite a high *U*-value, making the interior of the building hot during summers. In this case,

Building Summary	
Inputs	
Building Type	Office
Area (mm²)	533,828,894
Volume (m³)	1,336.35
Calculated Results	
Peak Cooling Total Load (W)	109,170.9
Maximum Cooling Capacity (W)	107,382.7
Peak Heating Load (W)	42,229.3
Checksums	
Cooling Load Density (W/m²)	204.51
Cooling Flow Density (LPS/m²)	14.81
Cooling Flow / Load (L/(s·kW))	72.44
Cooling Area / Load (m²/kW)	4.89
Heating Load Density (W/m²)	79.11
Heating Flow Density (LPS/m²)	5.21

Fig. 2 Thermal analysis of original building and summary

all the external wall materials were changed from RCC walls to AAC blocks. AAC blocks were selected for use in this case due to their low cost and low thermal heat gain coefficient (U-value). The Brazilian building code outlines three alternatives when assessing the wall absorptance by a simulation method: (i) light colour ($a = 30\%$), (ii) medium colour ($a = 50\%$) and (iii) dark colour ($a = 70\%$) (Gamero-Salinas et al. 2021), a low wall absorptance was found to be the most effective and economic strategy in hot humid climates (Cheng et al. 2005).

Brick Walls Overlaid with Expanded Polystyrene (EPS)

AAC blocks are not always the best choice, especially for small residential buildings where their use of them may not be very cost-effective. Also, in existing buildings where low U-value materials were not used, but thermal comfort measures were in demand, a coating of insulating materials had to be used. So, in this case, a 90 mm layer of EPS was applied on top of the normal brick wall material on all the external walls. EPS is a white foam plastic material produced from solid beads of polystyrene. It is primarily used for packaging, insulation, etc. It is a closed-cell, rigid foam material produced from styrene and pentane (Kim et al. 2022). This case was considered for existing buildings that required thermal comfort to a large extent.

Double Glazing

In this case, all glass used in the model was changed from single glazing to double glazing. Double glazing, also known as insulating glass (IG), consists of two or more glass window panes separated by a space to reduce heat transfer across a part of the building envelope.

Reinforced Cement Concrete (RCC) Roofs Overlaid with Polyurethane

The type of roofs used in Mizoram are usually basic RCC roofs, a few of which have layers of insulation above the base layer. For this study, a 101.6 mm thick layer of polyurethane was added above the basic RCC of both flat and sloped roofs to reduce the amount of heat entering the building through the roof.

Natural Shading Environment

In this case, natural shading was provided by adding trees to the surrounding environment in Revit and the other parts of the building with high exposure to heat. From the Revit software, the sun path was calculated according to the location of the building. Trees were planted on the sides which received the most sunlight to give it shading. This is a very cost-effective, efficient and eco-friendly way of providing thermal comfort which is applicable not only on new buildings but also on existing buildings.

Window-to-Wall Ratio

Window-to-wall ratio (WWR) is a very important parameter to consider for the thermal comfort of buildings. Studies indicate that high WWR leads to more amount of heat entering inside the building as common glass used in building windows do not reflect much heat and sunlight. So, we can decrease the WWR to provide thermal comfort. Based on ASHRAE 90.1 (2019), a WWR of 40% was defined as the maximum allowable value. The Web version of Insight was used to optimize the WWR, and the results were observed. After simulating the original building for thermal loads, the passive cooling design strategies were incorporated in each unit by changing variables. Sensitivity analysis was performed for finding the best suitable results in the thermal performance of the building in cooling and heating loads. The best options available for thermal comfort of the occupants and lowering the energy consumption were identified and discussed, and the cumulative of all the simulation was performed.

3 Results and Discussions

3.1 Original Building

The original building (Fig. 1) with *U*-values (Table 1) was simulated as shown in Fig. 2. It was observed from the simulation of an MZU office building, designed with high WWR, accounts for about 30% which is the maximum load in the building. The roof and walls of the building account for about 25% since both the units are exposed to direct sunlight. The passive design strategies help in the reduction of loads to building, and sensitivity analysis of each component was studied and further discussed in the section below:

Even without regarding any passive cooling strategies, the result shows that overheating risk is not relatively high as compared to other parts of the world due to the moderate climate of Mizoram.

3.2 Autoclaved Aerated Concrete Blocks (AAC Blocks)

This section reveals the relative influence in the thermal property of a building on the risk of overheating when using AAC block for wall masonry. AAC blocks were used for this study due to their lightweight, low-cost and effective heat insulation.

After changing the brick walls to AAC blocks, the result shows significant changes in the walls with a decrease of 5295 W (4.81%) in the cooling load and a decrease of 3918.3 W (11.98%) in the heating loads which has better performance.

3.3 Brick Walls Overlaid with Expanded Polystyrene (EPS)

In this section, we determine the changes in the thermal property when brick walls are coated with EPS. The results show a significant drop in the cooling load by 5602.9 W (4.84%) and a decrease in the heating load by 5586.7 W (13.32%).

Here, bricks walls are used instead of AAC blocks in consideration that most existing buildings in India are constructed with brick walls. Therefore, the walls of existing buildings can be coated with EPS to provide thermal insulation.

3.4 Double Glazing

This section shows the result when glasses of all windows from Fig. 1 are changed from single glazing to double glazing. Double-glazed units have twice the insulation capability as single-glazed units. Not only can they insulate heat, but they can also store heat in winter and are harder to break than normal glass (Pachano and Bandera 2021).

From the simulation result, we find that the cooling loads in the windows decrease drastically by 18,223.4 W (10.53%) and the heating loads by 1905.9 W (6.13%). Hence, we can conclude that double glazing is empirically better for thermal comfort as compared to the single-glazing glass window.

3.5 RCC Roofs Overlaid with Polyurethane

In this section, a 101.6 mm layer of polyurethane was added on all roofs, and the brick walls were changed to AAC walls. The results of the thermal analysis show a drastic decrease in the cooling load by 23,260.2 W (21%) with a decrease of 6792 W (22.24%) in the heating loads. So, it was concluded that adding a layer of polyurethane was very effective for this building. From a previous study (Liu et al. 2020), it was found that solar protection was not the best option for providing indoor thermal comfort. Other studies conclude that the *U* value of roofs should be prioritized rather than walls for thermal comfort (Hashemi and Khatami 2017). But which element to prioritize depends on the type of building, the location and the climate. As we have seen in the simulation results, a lot of improvement was found by adding insulation layers on the roofs.

3.6 Natural Shading Environment

In this section, we target to lower the cumulative insolation of the building using natural shading. This is done by planting trees near the east and west faces of the building area as shown in Fig. 3. The shading provided by the branches of trees is very effective for cooling the parts of the building having higher exposure to heat.

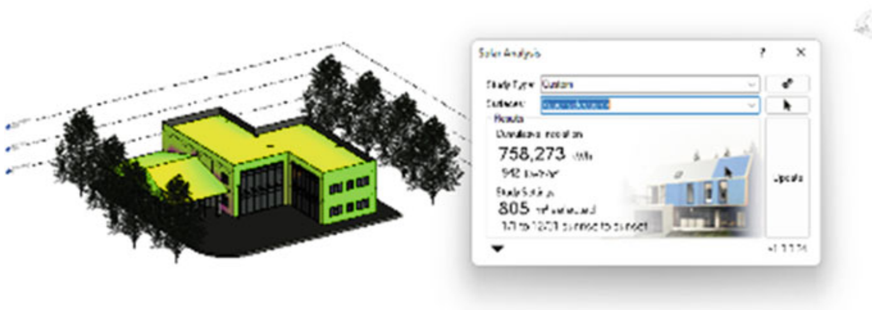

Fig. 3 Result of solar analysis after providing natural shadings

Here, the solar analysis result shows that the cumulative insolation decreases from 839,656 to 758,273 kWh which is very efficient. Hence, we conclude that natural shading provided by trees is an effective way to achieve thermal comfort.

3.7 Window-to-Wall Ratio (WWR)

This section reveals the influence of changing the WWR of the building from the original building (Fig. 1) using thermal analysis. Depending on the typology of the building, decreasing the WWR can be effective as well as ineffective for reducing the overheating risk. The results obtained from Insight show that changing the WWR does not change the overheating risk to a large extent.

3.8 Compilation of Thermal Comfort Methods

In this section, we utilize all the major changes obtained from the above results by using AAC block for all the walls, changing all the windows to double glazing, adding a layer of polyurethane (90 mm) to all the roofs and surrounding the building with trees. Hence, in hot climatic areas, all of the above simulations can be implemented to reduce the overheating risk for a building.

4 Conclusions

This study reveals the results of the influence of passive cooling design methods on the overheating risk reduction of an office building located in MZU, Aizawl, Mizoram, which has moderate climate.

The study concluded that the best thermal comfort measure can differ in various typologies and functions of a building. Since the building used in this study is an office building, having high WWR, the windows played the most important role in the overheating of the building. This study highlights the significance of thermal comfort and overheating risk measures to increase inhabitant comfort levels and also reduce the energy consumption of the building.

References

ASHRAE (2019) ANSI/ASHRAE/IES Standard 90.1-2019. Energy standard for buildings except low-rise residential buildings, Atlanta, GA. www.ashrae.org.

Cheng V, Ng E, Givoni B (2005) Effect of envelope colour and thermal mass on indoor temperatures in hot humid climate. Solar Energy 78:528–534. https://doi.org/10.1016/j.solener.2004.05.005.

Gamero-Salinas J, Monge-Barrio A, Kishnani N, López-Fidalgo J, Sánchez-Ostiz A (2021) Passive cooling design strategies as adaptation measures for lowering the indoor overheating risk in tropical climates. Energy Build 252:11421

GRIHA Council and The Energy and Resources Institute (2017) GRIHA for existing buildings. India https://www.grihaindia.org/manuals

Hashemi A, Khatami N (2017) Effects of solar shading on thermal comfort in low income tropical housing. Energy Proc Elsevier B.V. 235–244. https://doi.org/10.1016/j.egypro.2017.03.025

James Cook University (2017) State of the tropics, sustainable infrastructure in the tropics. James Cook University Townsville, Australia. https://www.jcu.edu.au/__data/assets/pdf_file/0004/473503/

James Cook University (2020) State of the tropics. State of the Tropics 2020 Report, Townsville, Australia. https://www.jcu.edu.au/__data/assets/pdf_file/0007/1146292/SOTT-Report-2020-Web-FINAL.pdf. Accessed 10 June 2021

Kim S, Seo J, Jeong H, Kim J (2022) In situ measurement of the heat loss coefficient of thermal bridges in a building envelope. Energy Build 256:111627. https://doi.org/10.1016/j.enbuild.2021.111627

Liu S, Ting Kwok Y, Ka-Lun Lau K, Ouyang W, Ng E (2020) Effectiveness of passive design strategies in responding to future climate change for residential buildings in hot and humidHong Kong. Energy Build 110469. https://doi.org/10.1016/j.enbuild.2020.110469

Pachano JE, Bandera CF (2021) Multi-step building energy model calibration process based on measured data. Energy Build 252:111380. https://doi.org/10.1016/j.enbuild.2021.111380

SEforALL, Chilling Prospects (2020) Tracking sustainable cooking for all-2020. Vienna. https://www.seforall.org/system/files/2020-07/CP-2020-SEforALL.pdf

UNDESA (2019) Revision of world population prospects. https://population.un.org/wpp/DataQuery/. Accessed 10 June 2021

Geochemical Evolution of Spring Water Sources in West Phaileng, Mizoram

Lalsangzela Sailo, Munna Das, and H. Vanlalhruaia

Abstract As water demand is rising due to the increase in the population and urbanization, the use of spring water as supplementary water sources becomes imminent. Mizoram state, which is located in the North Eastern part of India, located at the top of a ridge where the main sources of water are generally streams, spring and rainfall. As many of the springs are reportedly drying up lately, this may be due to the anthropogenic and the local effect of climate change as the area received intense rain during monsoon and longer dry period of little or no rain during winter, which may result in the very low discharge or drying up during this time of year. The general lithology consists of alternations of siltstone, shale, and sandstone, wherein the porosity of the rocks is very limited. Identifying the recharge of spring water is of prime importance for sustainable management strategies. The hydrogeological strata and the geochemical composition in mountain scale study were conducted, and it was observed that water is young and immature type, and the lower residence time of the water relates with MFR mountain front recharge mechanism being the major portion of groundwater recharge. Artificial recharge is a necessity for the growing populations which demands more water and as more storage of water is needed to save water in times of water surplus for use in times of water shortage.

Keywords Spring water · Geochemical modeling · Recharge

1 Introduction

The growth in population and urbanization has led to sharp increase in global demand for freshwater for drinking, sanitation, agricultural, energy production, industry, and environmental protection (FAO 2011; WWAP 2012). Due to declining availability of freshwater because of groundwater depletion, surface water pollution, and

L. Sailo (✉) · M. Das · H. Vanlalhruaia
Department of Civil Engineering, Mizoram University (MZU), Aizawl 796004, India
e-mail: zelasailo@gmail.com

J. K. Deka et al. (eds.), *Emerging Technology for Sustainable Development*,
Lecture Notes in Electrical Engineering 1061,
https://doi.org/10.1007/978-981-99-4362-3_9

climate change impacts, sustainability is potentially threatened (IPCC 2007). Similarly, the water problem in Mizoram is not new, especially during lean season even though the state receives ample of rainfall during monsoon season of about 3000 mm (SAPCC 2012). During lean season from November to March, maximum stress is experienced at end as long rainless period, the stream-flow decreases substantially reducing soil moisture, lowering of water table, and depleted surface storage. The term “low flow” described the decrease in streamflow due to depleting groundwater reserve in the basin (Markovich et al. 2019). The understanding of low flow situation is crucial for water supply, irrigation, drainage, maintaining environmental flow, fishery, hydropower, etc. (Nikic and Radonja 2009).

Springwater is the groundwater discharge to the land surfaces creating a visible flow (Author Kresic 2007). From time immemorial, the spring water (‘Tuikhur’ in Mizo) is the main source of water supply for drinking and domestic purpose. Still today, most of the rural population and remote location in urban or habitation areas where piped connection is difficult depends entirely on spring water which accounts to about 47% of household (Sailo et al. 2017). Most of the rural settlements in Mizoram are located on the mountain tops and mountain slopes; although isolated drinking water projects have been implemented by the government, many communities are experiencing increasing hard-ship to meet their water demands.

The hydrological processes in mountains have been studied by numerous researchers at hillslope scale, focusing the response of rainfall to streams discharge (McGlynn et al. 2002; Wilson and Guan 2004). The water resources in the downstream of mountains are controlled by two important processes viz the baseflow from the mountain and mountain block recharge (Welch and Allen 2012; Yao et al. 2017). The groundwater in mountainous regions is different from the plain areas or lower relief areas in three main ways: (a) the position of water table is much higher and the hydraulic gradient is much steeper which influence the flow path and discharge rate (Forster and Smith 1988; Somers and McKenzie 2020), (b) the complex hydrogeological strata near the surface due to high energy depositional environment and glacial deposition (Cairns 2014), (c) deeper groundwater circulation due to high relief of the topography, which can even recharge regional and continental scale of flow (Forster and Smith 1988).

The recent reports on drying up or lowering of discharge of various springs sources in the many places have led acute water shortage in many places (Sailo et al. 2017; Public Health Engineering Department 2020). Numerous factors including population growth, agricultural intensification/practices, economic development, land use/land cover change, and climate change impacts might be responsible for water shortage. However, understanding the linkage between mountain water sources and aquifers, and predicting recharge are required to manage groundwater resources in this region as most of the habitation is located in top hills and ridges.

The mountains and hillocks in these areas have thin top layer soils that can store less water, and due to high vegetation along the mountains lead to potential reduction via evapotranspiration. But the fast flow along the faults and fractures in the bedrock may also limit evapotranspiration loss. The bedrock geology showed the prevalence of faults and fractures in many places mostly due to tectonics activities. This paper aims to identify the recharge mechanisms in the West Phaileng area using hydrogeochemical composition and formulating the dominant conceptual processes that is of recharge.

2 Study Area

The study area West Phaileng is a block situated in Mamit district in Mizoram. The area is identified as water-challenged sites for research-based solutions by Water Technology Initiative (WTI) of Technology Mission Division (TMD) of Department of Science and Technology (DST), Govt. of India. Even though the study sites receive average annual rainfall of 2794 mm during monsoon season, there is extreme water scarcity problem during post-monsoon. Most of the rainwater flows as runoff due to soil type and slope of area which is a common problem in hilly region of North East India. The area is situated in rural area where majority of the land use is classified as mild/less dense forest and moist deciduous bamboo forest. The effect of recent development, deforestation, and build up areas has also aggravated the runoff characteristic on the mountains which is the main source of groundwater recharge (Fig. 1).

2.1 Hydrogeology

The terrain of West Phaileng is considered to be tectonically young and immature. The general lithology consists of a sequence of siltstone, shale, and sandstone, wherein the porosity of the rocks is very limited. This has significantly reduced the water-yielding capacity of the aquifers (Lalfakzuala and Chamliana 2003). The thin top soil is mostly silty loam soils which extend to about 2–4 m in most places overlying the shales rock beneath which are moderately to highly fracture. The occurrence of groundwater in such a terrain is mainly restricted to weak zones such as fractures, lineaments, and weathered residuum (Central Ground Water Board 2013). These tectonic elements create seepage conduits, which are sources of springs. The hill slopes contain a range of springs and seepages, while a good number of them are perennial and tapped for local water supply. The spring's discharges in most cases reduce severely starting from December to January (Central Ground Water Board 2013).

2.2 Sample Collection and Analysis

A total of 11 samples were collected out of which nine were spring water samples and two tube well samples having a depth of about 60–70 m below ground level, from

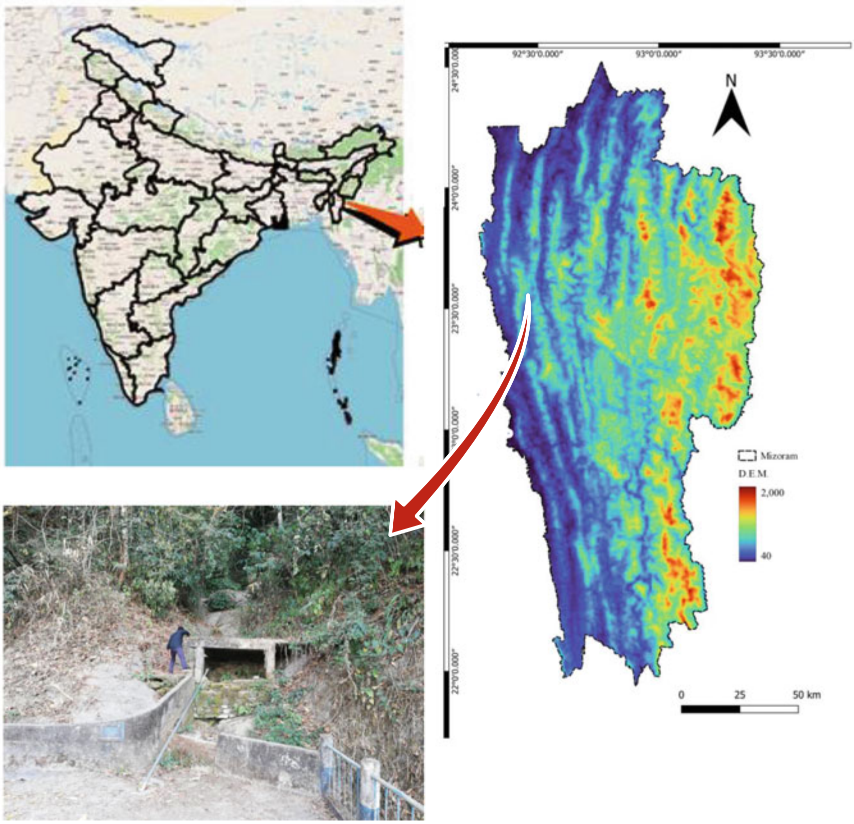

Fig. 1 Study area of West Phaileng, Mizoram

March 2020 till date quarterly. The geographical locations were determined using a handheld Global Positioning System (GPS), Garmin eTrex10. Two samples were collected from each source, one acidified sample ($pH < 2$) using 1:1 HCl and another non-acidified sample in 500 ml plastic sampling bottle. The tube well samples were purged and pumped for about 5 min to avoid contamination by stale water. The physical parameters viz pH, temperature, and electrical conductivity were measured directly at site using portable YSI Pro plus multi-parameter. APHA (1990) recommended standard methods were used for the measurement of dissolved ion concentration in the samples. The major anions, viz alkalinity, were measured using titration method, chloride (Cl^-) using argentometric method, sulfate (SO_4^{2-}) using turbidimetric method, phosphate (PO^{3-}) using ascorbic acid method in spectrophotometer, and nitrate (NO^-) with UV spectrophotometer—Shimadzu UV1800.

Geochemical Composition and PHREEQC. A computer model PHREEQC Interactive, Version 3 (2013) developed by U.S Geological Survey's was used in speciation model, which is considered appropriate due to its similar applicability elsewhere.

Geochemical modeling is used as a tool to perform a wide variety of low-temperature aqueous geochemical calculations. PHREEQC determine the saturation status of minerals in various solutions and mixtures. A saturation index (SI) is defined as log (IAP/K). The state of saturation of a mineral in aqueous solution can be expressed using a saturation index, where IAP is the ion activity product of the ions in solution obtained from analysis. A positive saturation index (SI) indicates super-saturation or precipitation of secondary minerals, and a negative SI indicates under-saturation or dissolution of minerals. An SI index of $\pm$ 0.5 indicates equilibrium conditions. Calcite, dolomite, and gypsum SI can be a good proxy of the saturation level of these minerals in groundwater.

3 Results and Discussion

3.1 Hydrogeochemistry

The major ionic composition of spring water and tube well samples collected from the study area are presented in Table 1. The pH of the water sample were in neutral range and are under oxidized condition. The major cations in the sampled groundwater are Na^+ (mean 19.5 mg/l), Mg (12 mg/l), Ca^{2+} (10.4 mg/l), and alkalinity (HCO^-) which is the major anion with mean concentration of 94.2 mg/l as $CaCO_3$, whereas Cl^- (14.7 mg/l) and SO^{2-} (2.8 mg/l) forming minor anions. The hydrogeochemical composition of groundwater is shown as Piper diagram (Fig. 3). Considerable spatial variations were observed in the concentration of groundwater cations and anions in the study area.

The hydrogeochemical composition is mainly controlled by precipitation, evapotranspiration, rock–water interaction, and biogeochemical condition. Gibbs (1970) suggested three mechanisms that control the chemistry of the water using simple Gibbs diagram as shown in Fig. 2. The water samples fall under rock dominance.

3.2 Geochemical Modeling

The geochemical modeling of using PHREEQC suggests the under-saturation of various mineral phases such as dolomite, gypsum, siderite, and halite. The high degree of sub-saturation of gypsum ($CaSO_4$) is likely to be due to the low concentration of Ca^{2+} in the samples along with low $SO_4{}^{2-}$ in the area. The calcite minerals are slightly under-saturated with SI values of 0.11 to − 0.9. Similarly, carbonate minerals dissolution viz calcite ($CaCO_3$) and dolomite ($CaMg(CO_3)_2$) was also observed (Fig. 3).

The geochemical modeling of using PHREEQC suggest the under-saturation of various mineral phases such as dolomite, gypsum, siderite, and halite. The high

Table 1 Groundwater quality parameters in mg/l showing the values of mean and standard deviation

Parameters	Mean	SD
pH	7.7	0.1
EC (μs/cm)	224.8	119
ORP (mV)	122.8	7.6
Alkalinity	94.2	51
Cl^-	14.7	4.2
SO_4^{2-}	2.8	1.9
NH_4	2.4	2.32
NO_3	13.1	7.4
PO_4^{3-}	0.39	0.32
Ca^{2+}	10.4	11.3
Mg^{2+}	12	8.8
Na^+	19.5	6.02
Mn	0.98	0.7
Fe	2.1	2.5

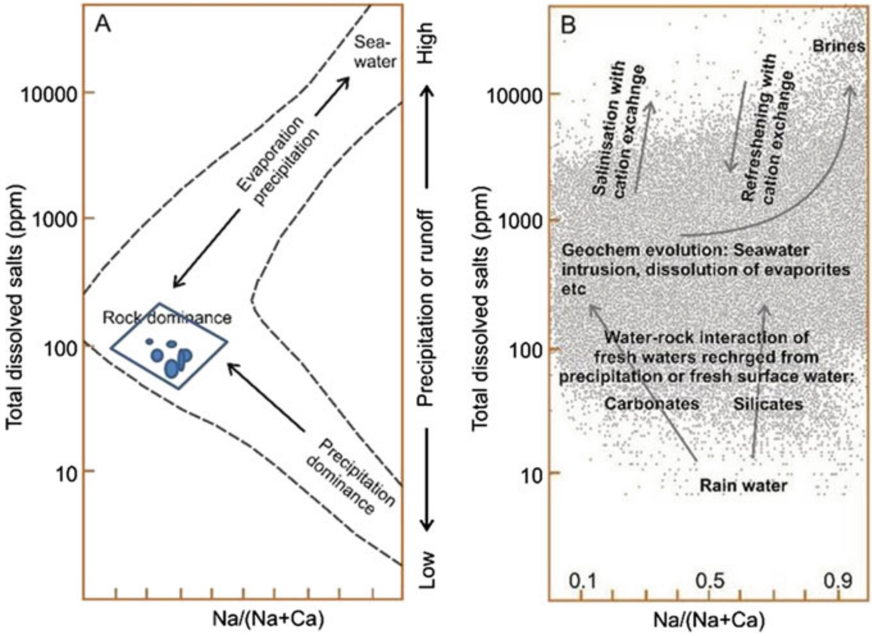

Fig. 2 Gibbs diagram for water sample of West Phaileng

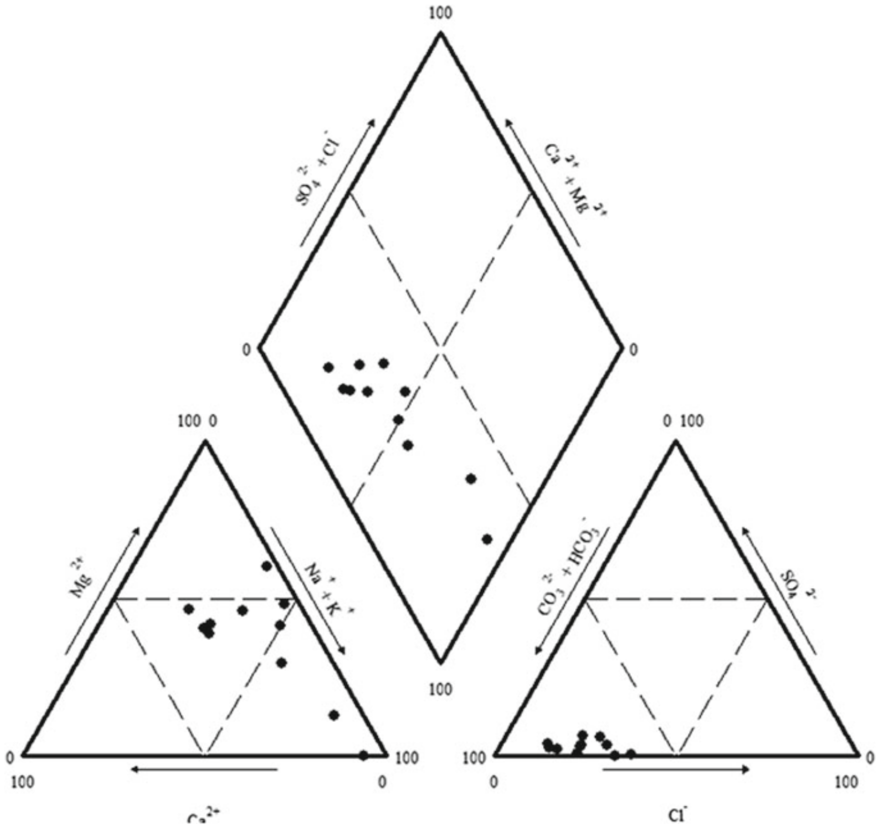

Fig. 3 Piper diagram of water samples from West Phaileng

degree of sub-saturation of gypsum ($CaSO_4$) is likely to be due to the low concentration of Ca^{2+} in the samples along with low SO^{2-} in the area. The calcite minerals are slightly under-saturated with SI values of 0.11 to − 0.9. Similarly, carbonate minerals dissolution viz calcite ($CaCO_3$) and dolomite ($CaMg(CO_3)_2$) was also observed.

The second process discussed here that can influence the chemical evolution of groundwater is simple mixing. A common simple mixing involves the mixing of water from different groundwater systems (shallow and deep) due to the large number of faults and cracks in the rocky aquifer of the region. Direct input from the anthropogenic sources is also suspected.

Conceptual Flow Model: The primary source of water in Mizoram is rainwater. Numerous people depends on spring water for their drinking and domestic purposes. The spring water discharge solely depends on hydrology of the mountainous catchments to provide freshwater, lesser is known about the key hydrological processes in these systems, i.e., mountain block recharge (MBR) and mountain front recharge (MFR). A mountain block comprises of mountain mass inclusive of soil, bedrock, and vegetation and water. MBR processes require closer look in all hydrologic processes which include spatial and temporal distribution of precipitation, evapotranspiration, runoff and interflow, and flow through fractures and faults. The MFR refers to the groundwater infiltration/recharge of flow from streams along the mountain front adjacent to the basin (i.e., the MFR is positioned somewhere between MBR and the basin floor) (Wilson and Guan 2004). Various researcher reported MFR to be dominating processes in mountain recharge systems accounting to about (73–97%) (Welch and Allen 2012; Markovich et al. 2019), but clear distinction of quantifying mountain front recharge remains ambiguous and difficult to compare (Wilson and Guan 2004).

The mountain front recharge (MFR) is categorized into two: (1) the basin-centered methods which include Darcy's law groundwater flow application along the mountain front and calibration of groundwater models in the basin aquifer (Wilson and Guan 2004) or (2) mountain-centered view take into account the precipitation amounts on the mountains relating to MFR rates and do not consider the hydrogeolical process of the subsurface such as comparing geochemical or isotopic characteristics of precipitation over the mountains with groundwater and also empirical equation developed between precipitation and MFR for the mountain, subtracting estimated evapotranspiration from precipitation.

In this context, we assume that similar recharge mechanism of MFR is predominant in the study area. Since, this also coincide with the spring discharge or hydrograph which suggested that the recharge time, i.e., time to infiltrate along the mountain and discharge on to the spring water is relatively fast comparing the thin soil overlain by semi-consolidated to consolidated silty, clayey, and shale stones. The potential existence of secondary porosity is suggested with the spring discharge after an event of precipitation. The extent of mountain block recharge leading to regional groundwater recharge may be predominant during lean season (November to March). During the month of March, the local people experience water scarcity since the discharge on these spring water has been reduced so much that it is about 1–3 l per minute. And the hydro chemistry of groundwater also suggested that the water is not aged and relatively young water from the mountain recharge as sources to the spring water which contain low ionic concentrations.

4 Conclusion

The evaluation of hydrochemical data from West Phaileng show that weathering due to organic/microbial decomposition and silicate weathering as major process influencing the composition of spring water. The spring water is observed to be in oxic condition, low EC, and less ionized, showing the water relatively fresh and young comparing to tube well sample with a depth of about 60 m. The relative abundance of cations and anions are in the order: $Na^+ > Ca^{2+} > Mg^{2+} > Fe > Mn$ and $HCO_3^- > Cl^- > NO_3 > SO_4^{2-} > NH_4 > PO_4^{3-}$, respectively. The hypothetical conceptual groundwater recharge model was formulated in view of the geology, geochemical characteristic of the spring water and spring water discharge increment after few hours of rainfall event. The water at the springs and groundwater from tube wells are classified as young and immature type, and the lower residence time of the water relates with MFR mountain front recharge mechanism being the major portion of groundwater recharge. Thus, under climate change scenario, the reduction of runoff in high-intensity rainfall event will increase the availability and sustainability of spring water in the area.

References

Author Kresic N (2007) Hydrogeology and Ground water modeling, 2nd edn. CRC press

APHA (1990) Standard method for the examination of water and wastewater. 21st Edition. American Public Health Association/American Water Works Association/Water Environment Federation, Washington DC

Cairns DW (2014) Simulation of groundwater flow in mountain watersheds (Master's Thesis). University of Lethbridge, Lethbridge, ALTA, Canada

Central Ground Water Board, CGWB (2013) Ground water information booklet, Aizawl District Mizoram. Technical report series: D, CGWB, North East Region. Ministry of Water Resource, Guwahati

FAO (2011) FAOSTAT. Food and agriculture organization of the United Nations. http://www.fao.org/3/a-i2697e.pdf

Forster C, Smith L (1988) Groundwater flow systems in mountainous terrain: 2. Controlling factors. Water Resour Res 24(7):1011–1023. https://doi.org/10.1029/WR024i007p01011

Gibbs RJ (1970) Mechanisms controlling world water chemistry. Science 170:1088–1090

IPCC (2007) In: Core Writing Team, Pachauri RK, Reisinger A (eds) Climate change 2007: synthesis report. contribution of working groups I, II and III to the fourth assessment report of the intergovernmental panel on climate change. IPCC, Geneva, Switzerland

Lalfakzuala C, Chamliana J (2003) Report on detail hydrological mapping of Aizawl City (core area). Geology and Mining Wing, Directorate of Industries, Government of Mizoram

Markovich KH, Manning AH, Condon LE, McIntosh JC (2019) Mountain-block recharge: a review of current understanding. Water Resour Res 55:8278–8304. 10.1029/2019WR025676

McGlynn BL, McDonnel JJ, Brammer DD (2002) A review of the evolving perceptual model of hillslope flowpaths at the Maimai catchments, New Zealand. J Hydrol 257:1–26

Nikic Z, Radonja P (2009) Modelling the influence of hydrogeological parameters on low flow in hilly and mountainous regions of Serbia. Hydrol Sci J 54:484–496. https://doi.org/10.1623/hysj.54.3.484

Public Health Engineering Department (2020) Ground water depletion survey report, Mizoram. Ground water report assessment cell. PHE Department, Mizoram

Sailo L, Ramthansanga F, Hussain S (2017) Feasibility study of recharge of spring water in Aizawl, Mizoram. IGWC, New Delhi

SAPCC (2012–2017) Mizoram State action plan on climate change. Directorate of Science and Technology. Governmentof Mizoram, Mizoram, India. https://forest.mizoram.gov.in/uploads/attachments/eaca54828e34ef7b4472fd5c985fd31b/pages-202-sapc-mizoram-2012-17.pdf

Somers LD, McKenzie JM (2020) A review of groundwater in high mountain environments. Wires Water 2020(7):e1475. https://doi.org/10.1002/wat2.1475

Welch LA, Allen DM (2012) Consistency of groundwater flow patterns in mountainous topography: implications for valley bottom water replenishment and for defining groundwater flow boundaries. Water Resour Res 48:W05526. https://doi.org/10.1029/2011WR010901

Wilson JL, Guan H (2004) Mountain-block hydrology and mountain-front recharge. In: Phillips F, Hogan J, Scanlon B (eds) Groundwater recharge in a desert environment, the southwestern United States. AGU, Washington, DC. https://doi.org/10.1029/009WSA08

WWAP (2012) The United Nations world water development report 4: managing water under uncertainty and risk. UNESCO, Paris

Yao Y, Zheng C, Andrews C, Zheng Y, Zhang A, Liu J (2017) What controls the partitioning between baseflow and mountain block recharge in the Qinghai-Tibet Plateau? Geophys Res Lett 44:8352–8358. https://doi.org/10.1002/2017GL074344

A Review on Nearshore and Offshore Fish Cage Developments in Open Seas

Abdul Shareef Shaik and Nasar Thuvanismail

Abstract Despite the fact that cage culture has been in practice for centuries, commercialization has only begun in the last few decades. Farmers are keen to relocate to offshore locations since most nearshore sites are entirely utilized, with limited potential for additional fish production and environmental groups are raising concerns about pollution, conservation, and recreation. The cage culture system classifies into nearshore and offshore farming. In this review, the nearshore cage system investigates on cage materials, classifications, and net shapes. It provides a brief overview of cage deformation, velocity reduction, cage hydrodynamic features, motion responses, mooring line tension of single cage and grid system. The definitions of offshore and the design challenges that must overcome to relocate offshore are discussed. The offshore system analyses distinct designs in open cages depending on submergence depth and closed contaminant tanks under harsh environmental conditions. An assessment is carried out on experimental studies, in-situ tests, and numerical and analytical methods of the cage culture system. The evolution, development, and present scenario of sea cage culture in India are also reviewed.

Keywords Cage culture · Nearshore cages · Offshore cage systems · Design challenges · Cage culture in India

1 Introduction

Cage culture has been in practice for centuries in freshwaters and open seas. Even though fish farming started in the early 2000 BC in China, it has been officially recorded in a book on 475 BC (Villaluz 1953; Lovell 1989). The trend of seafood

A. S. Shaik (✉) · N. Thuvanismail
Department of Water Resources and Ocean Engineering, National Institute of Technology Karnataka, Mangalore, Karnataka 575025, India
e-mail: abdul82984@gmail.com

N. Thuvanismail
e-mail: t.nasar@nitk.edu.in

J. K. Deka et al. (eds.), *Emerging Technology for Sustainable Development*, Lecture Notes in Electrical Engineering 1061,
https://doi.org/10.1007/978-981-99-4362-3_10

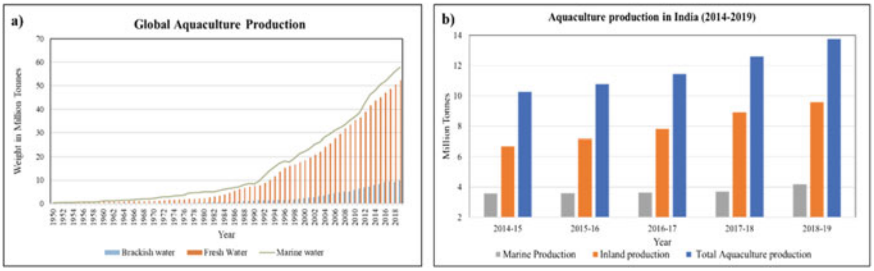

Fig. 1 **a** Global aquaculture production (2020) and **b** aquaculture production in India (*Source* FAO 2020; Department of Fisheries 2020)

consumption increased continuously from the 1950s and has risen exponentially since the 1990s because seafood is the cheapest and healthiest protein available for developing and poor countries. The current global population is 7.8 billion, with a projected increase to 9.8 billion by 2050; global food supply pressures may endure (UNFPA 2021). Currently, aquaculture and capture fisheries provide 16% of the global consumption of animal protein. The global consumption of fish has increased by 122%, and aquaculture production excluding aquatic plants increased by 527% since 1990. Total export value of fish increased to USD 160 billion in 2018 from USD 36 billion in 1990 (FAO 2020). The aquaculture system provides nutrition and supports livelihood for 10% of the world population, and 97% of people are from developing and poor countries. Effective management will improve the long-term viability of capture fisheries and aquaculture operations, potentially increasing world output by 15% by 2030 (FAO 2020). China now dominates the global aquaculture business, accounting for three-quarters of the market in terms of value and volume and India ranked as the second (Society 2015). Figure 1 shows the global aquaculture production and Indian aquaculture production of brackish water, fresh water, and marine water over the past decades.

2 Nearshore Cage System

The nearshore cage culture production system consists of a floating collar, net materials, ballast, and mooring system. Square cages with steel frames and HDPE circular cages are most commonly installed around the globe. The floating surface collar provides the required buoyancy to the cage system and serves as a working platform. HDPE and nylon are the most commonly used net materials for both primary and external net in cage systems. Predator-X, Kikko-net, UR-30, Bekaert, copper-alloy, and Econet are the latest net materials; besides single net can sustain predator attacks. These materials have anti-fouling properties, providing greater water exchange in and around the cage and decreasing regular inspections.

Ballast is essential to maintain maximum net volume when the cage is subjected to wave and current loadings. The bottom collar type ballasting shows better performance than sinker weights. The mooring system holds the cage in required position and at required depth using mooring lines, chains, and anchors. Moorings also reduce the excessive forces on the cages caused by waves, wind, and currents. Mooring design depends on type of cage, exposure, and precision for desired position. The nearshore cage system studies are divided into these primary sections in this review: cage volume deformation, mooring line tension, and motion responses.

2.1 Cage Volume Deformation

Abundant experimental studies have been conducted on cages with a collar, net, and bottom weights in uniform flow and waves. Deformation of the net increases with an increase in current velocity, and it decreases with increase in bottom weights. The higher bottom weights have a propensity to retain geometry (Lader and Enerhaug 2005). The net deformation for diamond mesh with sinker weight is greater than square mesh and vice versa when bottom collar sinker system is provided. The bottom collar-sinker design is practically suitable for reducing cage net volume deformation (Zhao et al. 2007). Higher solidity net has been studied under uniform flow and concluded that cage deformation depends less on net solidity than flow velocity and bottom weights (Moe-Føre et al. 2016). Cage with copper alloy net acting as a rigid structure and net volume deformation is considerably low (Cha and Lee 2018). Scaled model square fish cages are studied under uniform flow with different mesh materials, types, and sizes. The wire-netting-only model cage had the least geometric distortion and volume loss, suggesting its extraordinary potential for open-sea fish cultivation (Qu et al. 2019). A comparative study has been done between floating and submerged cages under waves and currents. The submerged cage shows better performance for higher wave amplitudes and currents (Xu et al. 2013).

Numerical approaches based on the lumped mass method are developed by Yucheng et al. (2006), Huang et al. (2006), Zhao et al. (2009) and (Zhao et al. (2009) considered rigid body dynamics along with lumped mass method. Results show a 10–15% relative error with experimental data of Lader and Enerhaug (2005). Later, Lee et al. (2008) developed a mathematical model depends on the mass-spring model and considered the shielding effects, and Fig. 2 represents the numerical simulations results of defamation of flexible nets. A statistical approach is developed to study the net cage volume reduction coefficient in irregular waves using wave incident angle, and the coefficient increases as wave angle increases (Xu et al. 2011). A finite element method tools such as ABAQUS, AQUASIM, and FLUENT have been used to study the cage volume deformation (Xu et al. 2013; Moe et al. 2010; Berstad et al. 2012). The collar deformation increases with increase in wave heights combined with currents. The failure of the collar can be prevented by providing connecting components with a lower diameter to thickness ratio (Huang et al. 2018; Liu et al. 2019).

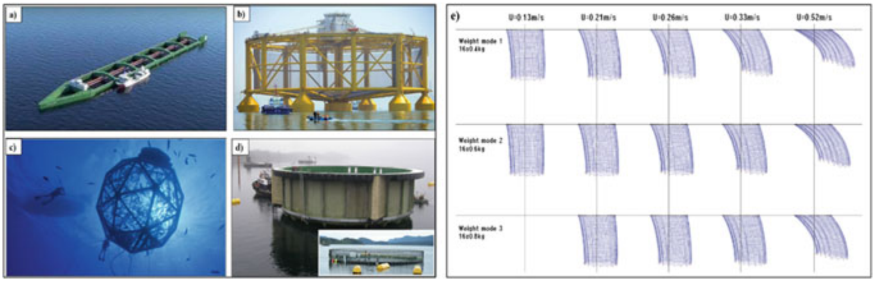

Fig. 2 Types of offshore cages **a** floating cages, **b** semisubmersible cage, **c** submerged cage, **d** closed containment tank, and **e** numerical simulation results of deformation of model cage for different sinker weights and currents (*Source* Lee et al. 2008; https://www.aquaculturealliance.org/advocate/floating-closed-containment-aquaculture/; https://www.intrafish.no/nyheter/byggestart-to-maneder-utsatt-men-havfarmen-skal-komme-tidsnok/2-1-433034; https://www.kongsberg.com/zh-hans/kmagazine/2017/9/sustainable-ocean-technology; https://aquafisheries-expo.com/cambodia/news/innovative-anchoring-for-the-aquaculture-industry-1-52.html)

2.2 Motion Responses

The responses of the single-point mooring system studied in uniform flow and net solidity are considered as a key parameters. The submergence investigations indicate a major unstable phase in the cage responses at higher velocities (DeCew et al. 2010). The responses of the gravity cages were studied under regular and irregular waves. The responses of cage decrease with an increase in frequencies. Wave incident angle significantly affects surge whereas negligible effect on heave motion (Zhao et al. 2009, 2012; Xu et al. 2011). The heave motion of the collar is very similar for each multiple cage arrangement, and surge motion is higher on seaward side for each arrangement (Xu et al. 2012). Heave, surge, and pitch motions are more significant for floating cages than submerged cages (Xu et al. 2013). A buoyancy distribution method has been introduced to find instantaneous buoyancy, which helps estimate vertical motions in small wave amplitudes. The drag forces and interaction between floater and net significantly affect horizontal motions under waves and currents (Li et al. 2013). A relative error of the box-shaped cage's responses is much less under both pure waves and steady currents (Zhao et al. 2013). The responses of the flatfish cage increase with increase in wave period and wave heights, and it led to a large response when a current was added along with waves (Cui et al. 2013).

2.3 Mooring Line Tension

Mooring line tension of cage increases with increase in current velocity, wave heights, wave periods, and magnitude of tension doubles when waves are added to the currents. Numerical methods are developed based on lumped mass method, Morison force model and also considered rigid body kinematics to study mooring line analysis (Huang et al. 2006; Zhao et al. 2009; Lee et al. 2008; Cui et al. 2013; Cifuentes and Kim 2017). In laboratory experiments, the tension in ropes is measured by load cells and strain gauges (Huang et al. 2006; Chen et al. 2019). Multiple cage arrangements and grid mooring systems been studied under waves and currents, considering wave incident angle, net solidity and wave steepness as parameters. Mooring line tension for single cage is maximum at wave incident angle is 30° and minimum is at 45° for grid mooring system. Mooring line tension increases with increase in wave steepness for floating cages and higher velocities, not showing a significant effect. The net solidity exhibits minimal effect on mooring line tension. Among all configurations, 2×4 configuration is best suitable in economic way, and length of the grid lines should be taken in consideration (Xu et al. 2011, 2012, 2013; Zhao et al. 2015; Bjelland et al. 2015). The mooring line tension of the column-shaped cage is smaller than the box-shaped cage (Zhao et al. 2013). The cable tension can be reduced by providing supporting buoys with proper spacing in between them, and damage of the structure can be prevented. The presence of stiffer mooring lines leads to higher mooring line tensions (Cha and Lee 2018; Liu et al. 2019).

3 Offshore Cage System

The definitions of offshore are provided based on parameters of depth, distance, visibility from the shore, waves, and accessibility (Holmer 2010; Shainee et al. 2012; CEA 2018; NS 2009). Besides these definitions, James (2013) proposed offshore farming site conditions based on real-time restrictions. The offshore farming site should be located within exclusive economic zone (EEZ up to 200 NM), and the preferable distance is 25 NM from the coastline. Water depth should be within the range of 25–100 m for effective mooring lines, and a current speed of 0.1–1 m/s is preferable for open sea cages. Further, the offshore site depends on onshore facilities like feed, maintenance, storage, processing unit, and transportation.

3.1 Types of Offshore Cages Systems

Floating cages: Flexible collar cages were first introduced in the 1970s and are now widespread all over the globe. High-density polyethylene (HDPE) is a widely used material for collars and nets. HDPE cages have the advantages of longer design life and resistance to biofouling, weathering, rotting, and it has deformation problems for higher waves and currents. Floating rigid cages are made up of solid frame structures with high strength, stability, stiffness, and buoyancy. The design concept is entirely different from that of flexible cages. These cages are built to withstand harsh sea conditions, and because they are large structures, facilities such as feed storage, oil storage, and harvest cranes can be accommodated (Cardia and Lovatelli 2016; Malcolm 2004; Scott and Muir 2000).

Submerged cages: Submerged cages operate at a certain depth below the water surface to avoid harsh environmental conditions exist in the surface. These cages can be brought up to the surface for maintenance and harvesting purposes. The effects of winds, waves, and currents are significantly less for submerged cages than surface cages even in storm conditions and can avoid surface debris. Scaled models and prototype cages have been studied and deployed in the sites (Scott and Muir 2000).

Semi submerged cages: Semi-submerged cages float on the water surface and can be submerged at required depth to avoid the high energy regimes. Few types of semisubmersible offshore platforms are mentioned in Fig. 2. Tension leg cage (TLC) is a semisubmerged flexible structure that can be submerged by strong currents during storm conditions, leading to minor damage for fish and cages. Semisubmersible rigid cage design is entirely different which it is designed to withstand strong waves and currents rather than avoid them. Semisubmersible rigid cage consists of a robust framework, ballast tanks to alter the water depth of cage and grid system to provide autonomous service, feed facilities (Scott and Muir 2000).

A floating cylindrical structure mainly focused on growing and farming fishes and was designed to resist various climatic conditions, including waves of more than 5 m in height. Responses of the cage showed good behaviors for all sea conditions. A time-domain coupled numerical model was developed to evaluate the hydrodynamic performance of two bodies connected by cables (Jurado et al. 2018). A novel concept for an open-sea aquaculture system that is flexible, submersible, and uses single-point mooring is proposed and investigated. A typical design of gravity cages suffers from a decrease of two-thirds of the volume under strong currents, and the present cage model retains more than 70% of the volume during extreme storms (Milich and Drimer 2019).

A floating platform with a heaving buoy-based wave energy converter (WEC) integrated with a series of net cages is proposed to use the richness of fisheries and wave energy resources in offshore sea areas. It is designed to have an autonomous and self-sufficient breeding function (Shi et al. 2019). A coupled well boat–fish farm system is studied under currents and long-crested waves in time domain. The simulated results indicate that the mooring lines can withstand severe conditions and collar stresses reached to yield limits even in moderate sea conditions (Shen et al. 2019). Laboratory studies have been conducted on a vessel-shaped cage with a single-point mooring system under waves and currents. The tension on the mooring line can be minimized by lengthening the chain or connecting sinker weights to the chain. Motion responses of the cages are higher in combined wave-current action than wave-only action (Li et al. 2017).

Hydrodynamic characteristics of a semisubmersible offshore fishing farm are studied under regular waves experimentally, and different draughts are considered. The mooring line tension and motion responses, such as heave, surge, and pitch, increase proportionally to the wave height. The windward mooring line tension reduces as the draught increases. However, the presence of the net raised the heave

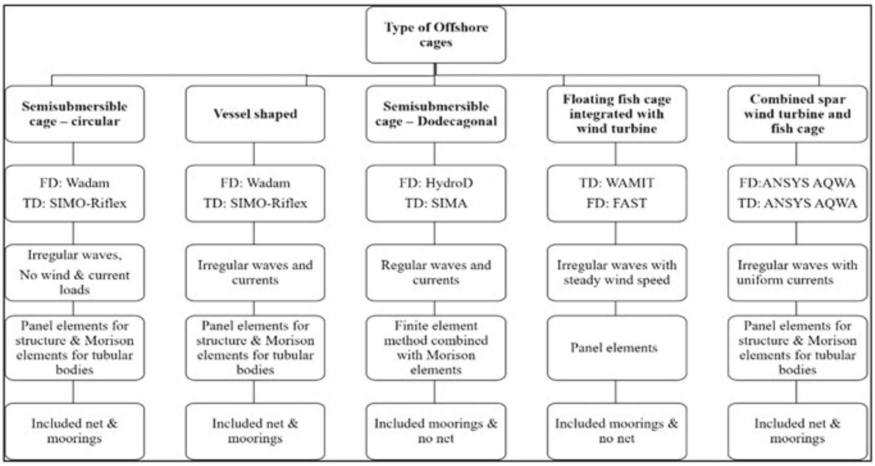

Fig. 3 Numerical simulations of different offshore fish farming cages (*Source* Li et al. 2017; Li and Ong 2017; Dou 2018; Lei et al. 2020; Chu and Wang 2020). *TD* time domain analysis, *FD* frequency domain analysis

and pitch of the fish farm marginally (Huang et al. 2020). Numerical studies have carried out on different types of prototype offshore farming cages, and these are the few studies mentioned in Fig. 3.

Closed containment tanks: Closed containment tank technology's principal purpose is to safeguard the output from parasites, sea lice, and other carnivores. A well-designed closed containment tank can maintain sufficient oxygen, temperature, and disposal of organic waste with a recirculating water system. Maximum production can be achieved in closed tanks than open cages by controlling the basic physical parameters. Apart from most advantages, capital cost, operational and maintenance costs are high (Scott and Muir 2000; Tidwell 2012). When the cage is exposed to waves, the water within the tank begins to oscillate, causing a sloshing effect that is harmful to both the fish and the cage system. The resonance phenomenon will occur if cage excitation frequencies are near the natural periods, and extensive research should be carried out to overcome these challenges of the closed tanks (Lader et al. 2017; He et al. 2018).

4 Sea Cage Culture System in India

Central Marine Fisheries Research Institute (CMFRI) began sea cage farming at India with cooperation from the Ministry of Agriculture and the National Fisheries Development Board (NFDB) in Visakhapatnam, Andhra Pradesh (Gopakumar 2009). Indian total maritime fish landings were about 3.49 million tons in 2018. According to CMFRI data, there are 3200 sea cages available throughout the Indian coast, with an annual output capacity of 4500 tons. The total fisheries production contributes 1.07% to Indian GDP (Department of Fisheries 2020). The ICAR-CMFRI estimation reveals that even if 1% of India's nearshore waters are utilized adequately for cage farming, an annual output capacity of 3.2 million tons can be achieved by installing 820,000 cages (Singh 2020).

CMFRI has researched In-situ cages and provided economic analysis of two major species (cobia and sliver pompano). The total capital costs for both cobia and silver pompano are 7.11, 5.71 lakhs, and net profits for these both species are 2.09 and 1.64 lakhs, respectively. CMFRI-Karwar Research Center developed a low-cost sea cage as per the interest of local fishing farmers, and it costs around 10,000/- rupees with a life expectancy of 5 years. The cage frames are fabricated with galvanized iron (1.5″ pipe, B-class) and fiber barrels provided for the buoyancy. The capital costs can be recovered within one crop for GI cages and take 4–5 crops for HDPE cages. The metal cages are showing better performance than HDPE cages, and most of the states are using these low-cost cages effectively (Philipose 2013). The government of India provides subsidies for this farming as part of the Blue Revolution (Gopalakrishnan et al. 2018).

5 Conclusions

The main objective of the cage culture is to meet consumers' everlasting demand for fish, and industry has been developed to outcome that appetite. A comprehensive review of the development of nearshore and offshore cages is provided in this paper. The cage volume deformation, drag forces on net, motion responses, and mooring line tension are the major parameters that challenged the design of the cage system. Net deformation increases with an increase in current velocity, and it can be reduced by providing bottom sinker weights up to some extent. The drag force on cage net is directly proportional to current velocity, and with an increase in net solidity, drag force increases. Motion responses of the cage system and floating collar are studied, and heave and pitch are the significant responses considered. Single-point mooring and grid mooring systems are inspected for different arrangements. The mooring line tension is always greater for seaward side than leeside, and attached buoys can help minimize mooring line tension.

Experimental, analytical, and numerical studies on various models are discussed in this review. Motion responses, mooring line tension, environmental loads, and forces on the net and structures are the major challenging parameters in offshore cage culture. Cage farming should consider environmental conditions, the health of fish, exposure to sea, diseases, species growth, harvesting, and logistic services to the market. Sustainable offshore farming can be achieved by developing autonomous/self-governing cages that do not depend on land facilities and multipurpose projects like cages integrated with wave energy converters, wind turbines, and breakwaters.

References

Berstad AJ, Walaunet J, Heimstad LF (2012) Loads from currents and waves on net structures. In: Volume 7: ocean space utilization; ocean renewable energy. American Society of Mechanical Engineers, pp 95–104. https://doi.org/10.1115/OMAE2012-83757.

Beveridge MCM (2004) Cage aquaculture, 3rd edn. Wiley-Blackwell

Bjelland HV, Føre M, Lader P, Kristiansen D, Holmen IM, Fredheim A, Grøtli EI, Fathi DE, Oppedal F, Utne IB, Schjølberg I (2015) Exposed aquaculture in Norway. In: OCEANS 2015—MTS/IEEE Washington, pp 1–10. https://doi.org/10.23919/OCEANS.2015.7404486

Cardia F, Lovatelli A (2016) Aquaculture operations in floating HDPE cages

CEA (2018) Offshore finfish aquaculture

Cha BJ, Lee GH (2018) Performance of a model fish cage with copper-alloy net in a circulating water channel and wave tank. Ocean Eng 151:290–297. https://doi.org/10.1016/j.oceaneng.2018.01.053

Chen YY, Yang BD, Chen YT (2019) Applying a 3-D image measurement technique exploring the deformation of net cage under wave–current interaction. Ocean Eng 173:823–834. https://doi.org/10.1016/j.oceaneng.2019.01.017

Chu YI, Wang CM (2020) Hydrodynamic response analysis of combined spar wind turbine and fish cage for offshore fish farms. Int J Struct Stab Dyn 20. https://doi.org/10.1142/S0219455420501047

Cifuentes C, Kim MH (2017) Numerical simulation of fish nets in currents using a Morison force model. Ocean Syst Eng 7:143–155. https://doi.org/10.12989/ose.2017.7.2.143

Closed Containment Tank. https://www.aquaculturealliance.org/advocate/floating-closed-containment-aquaculture/

Cui Y, Guan CT, Wan R, Huang B, Li J (2013) Numerical simulation of a flatfish cage system in waves and currents. Aquac Eng 56:26–33. https://doi.org/10.1016/j.aquaeng.2013.04.001

DeCew J, Tsukrov I, Risso A, Swift MR, Celikkol B (2010) Modeling of dynamic behavior of a single-point moored submersible fish cage under currents. Aquac Eng 43:38–45. https://doi.org/10.1016/j.aquaeng.2010.05.002

Department of Fisheries (2020) Aquaculture production in India

Dou R (2018) Numerical modeling and analysis of semisubmersible fish-cage. http://hdl.handle.net/11250/2615064

FAO (2020) The state of world fisheries and aquaculture

Floating cage—havfarm. https://www.intrafish.no/nyheter/byggestart-to-maneder-utsatt-men-havfarmen-skal-komme-tidsnok/2-1-433034

Gopakumar G (2009) History of cage culture, cage culture operations, advantages and disadvantages of cages and current global status of cage farming

Gopalakrishnan A, Joseph I, Gopakumar G, Ignatius B, Abdul Nazar AK, Jayakumar R (2018) Guidelines for sea cage farming in India. Towar Blue Revol pp 1–32

He Z, Faltinsen OM, Fredheim A, Kristiansen T (2018) The influence of fish on the mooring loads of a floating net cage. J Fluids Struct 76:384–395. https://doi.org/10.1016/j.jfluidstructs.2017.10.016

Holmer M (2010) Environmental issues of fish farming in offshore waters: perspectives, concerns and research needs. Aquac Environ Interact 1:57–70. https://doi.org/10.3354/aei00007

Huang CC, Tang HJ, Liu JY (2006) Dynamical analysis of net cage structures for marine aquaculture: numerical simulation and model testing. Aquac Eng 35:258–270. https://doi.org/10.1016/j.aquaeng.2006.03.003

Huang XH, Guo GX, Tao QY, Hu Y, Liu HY, Wang SM, Hao SH (2018) Dynamic deformation of the floating collar of a net cage under the combined effect of waves and current. Aquac Eng 83:47–56. https://doi.org/10.1016/j.aquaeng.2018.08.002

Huang XH, Liu HY, Hu Y, Yuan TP, Tao QY, Wang SM, Liu ZX (2020) Hydrodynamic performance of a semisubmersible offshore fish farm with a single point mooring system in pure waves and current. Aquac Eng 90. https://doi.org/10.1016/j.aquaeng.2020.102075

Jurado A, Sánchez P, Armesto JA, Guanche R, Ondiviela B, Juanes JA (2018) Experimental and numerical modelling of an offshore aquaculture cage for open ocean waters. In: Volume 7A: ocean engineering. American Society of Mechanical Engineers. https://doi.org/10.1115/OMAE2018-77600
Kapetsky JM, Jose Aguilar-Manjarrez JJ (2013) A global assessment of offshore mariculture potential from a spatial perspective
Lader PF, Enerhaug B (2005) Experimental investigation of forces and geometry of a net cage in uniform flow. IEEE J Ocean Eng 30:79–84. https://doi.org/10.1109/JOE.2004.841390
Lader P, Fredriksson DW, Volent Z, DeCew J, Rosten T, Strand IM (2017) Wave response of closed flexible bags. J Offshore Mech Arct Eng 139. https://doi.org/10.1115/1.4036676
Lee CW, Kim YB, Lee GH, Choe MY, Lee MK, Koo KY (2008) Dynamic simulation of a fish cage system subjected to currents and waves. Ocean Eng 35:1521–1532. https://doi.org/10.1016/j.oceaneng.2008.06.009
Lei Y, Zhao SX, Zheng XY, Li W (2020) Effects of fish nets on the nonlinear dynamic performance of a floating offshore wind turbine integrated with a steel fish farming cage. Int J Struct Stab Dyn 20:1–31. https://doi.org/10.1142/S021945542050042X
Li L, Fu S, Xu Y, Wang J, Yang J (2013) Dynamic responses of floating fish cage in waves and current. Ocean Eng 72:297–303. https://doi.org/10.1016/j.oceaneng.2013.07.004
Li L, Ong MC (2017) A preliminary study of a rigid semisubmersible fish farm for open seas. In: Volume 9: offshore geotechnics. Torgeir Moan honoring symposium. American Society of Mechanical Engineers. https://doi.org/10.1115/OMAE2017-61520
Li L, Jiang Z, Ong MC (2017) A preliminary study of a vessel-shaped offshore fish farm concept. https://doi.org/10.1115/OMAE2017-61665
Liu HY, Huang XH, Wang SM, Hu Y, Yuan TP, Guo GX (2019) Evaluation of the structural strength and failure for floating collar of a single-point mooring fish cage based on finite element method. Aquac Eng 85:32–48. https://doi.org/10.1016/j.aquaeng.2018.12.007
Lovell T (1989) Nutrition and feeding of fish (1989)
Milich M, Drimer N (2019) Design and analysis of an innovative concept for submerging open-sea aquaculture system. IEEE J Ocean Eng 44:707–718. https://doi.org/10.1109/JOE.2018.2826358
Moe H, Fredheim A, Hopperstad OS (2010) Structural analysis of aquaculture net cages in current. J Fluids Struct 26:503–516. https://doi.org/10.1016/j.jfluidstructs.2010.01.007
Moe-Føre H, Lader PF, Lien E, Hopperstad OS (2016) Structural response of high solidity net cage models in uniform flow. J Fluids Struct 65:180–195. https://doi.org/10.1016/j.jfluidstructs.2016.05.013
NS 9415 (2009) Marine fish farms—requirements for site survey, risk analyses, design, dimensioning, production, installation and operation. Standards Norway
Philipose KK (2013) Development of innovative low cost cages for promoting open sea cage culture along the Indian coast
Qu X, Hu F, Kumazawa T, Takeuchi Y, Dong S, Shiode D, Tokai T (2019) Deformation and drag force of model square fish cages in a uniform flow. Ocean Eng 171:619–624. https://doi.org/10.1016/j.oceaneng.2018.12.016
Scott DCB, Muir JF (2000) Offshore cage systems: a practical overview. In: BBJ. M (eds) Mediterranean offshore mariculture. Zaragoza : CIHEAM, pp 79–89
Semi Submersible Cage. https://www.kongsberg.com/zh-hans/kmagazine/2017/9/sustainable-ocean-technology
Shainee M, Leira BJ, Ellingsen H, Fredheim A (2012) An optimum design concept for offshore cage culture. In: Volume 7: ocean space utilization; ocean renewable energy. American Society of Mechanical Engineers, pp 85–93. https://doi.org/10.1115/OMAE2012-83601
Shen Y, Greco M, Faltinsen OM (2019) Numerical study of a well boat operating at a fish farm in long-crested irregular waves and current. J Fluids Struct 84:97–121. https://doi.org/10.1016/j.jfluidstructs.2018.10.007

Shi H, Dong X, Feng L, Han Z (2019) Experimental study on the hydrodynamic performance of a heaving buoy assembled on a net cage platform. J Ocean Univ China 18:1031–1040. https://doi.org/10.1007/s11802-019-4028-x

Singh G (2020) Why cage-based aquaculture is all the rage in India. https://thefishsite.com/articles/why-cage-based-aquaculture-is-all-the-rage-in-india. Accessed 28 Aug 2023

Society AF (2015) Book of Abstracts. In: Sobana KS, Joseph S, Sukumaran S, Kathirvelpandian A, Kumar RG (eds) 5th International Symposium on Cage Aquaculture in Asia. A. Gopalakrishnan, Kochi, India, p 79

Submerged Cage. https://aquafisheries-expo.com/cambodia/news/innovative-anchoring-for-the-aquaculture-industry-1-52.html

Tidwell JH (2012) Functions and characteristics of all aquaculture systems. In: Aquaculture production systems. John Wiley & Sons, Ltd, pp 51–63. https://doi.org/10.1002/9781118250105.ch3

UNFPA (2021) UNFPA Global Results. In: webpage. https://www.unfpa.org/data/results. Accessed 28 Aug 2023

Villaluz D (1953) Fish farming in the Philippines

Xu TJ, Dong GH, Zhao YP, Li YC, Gui FK (2011) Analysis of hydrodynamic behaviors of gravity net cage in irregular waves. Ocean Eng 38:1545–1554. https://doi.org/10.1016/j.oceaneng.2011.07.019

Xu TJ, Dong GH, Zhao YP, Li YC, Gui FK (2012) Numerical investigation of the hydrodynamic behaviors of multiple net cages in waves. Aquac Eng 48:6–18. https://doi.org/10.1016/j.aquaeng.2011.12.003

Xu TJ, Zhao YP, Dong GH, Gui FK (2013) Analysis of hydrodynamic behavior of a submersible net cage and mooring system in waves and current. Appl Ocean Res 42:155–167. https://doi.org/10.1016/j.apor.2013.05.007

Yucheng L, Yunpeng Z, Fukun G, Bin T, Guohai D (2006) Numerical simulation of the influences of sinker weight on the deformation and load of net of gravity sea cage in uniform flow. Acta Oceanol Sin 25:125–137

Zhao YP, Li YC, Dong GH, Gui FK, Teng B (2007) Numerical simulation of the effects of structure size ratio and mesh type on three-dimensional deformation of the fishing-net gravity cage in current. Aquac Eng 36:285–301. https://doi.org/10.1016/j.aquaeng.2007.01.003

Zhao YP, Li YC, Dong GH, Teng B, Gui FK (2009) Numerical simulation of hydrodynamic behaviors of gravity cage in current and waves. Int J Offshore Polar Eng 19:97–107

Zhao YP, Gui FK, Xu TJ, Chen XF, Cui Y (2013) Numerical analysis of dynamic behavior of a box-shaped net cage in pure waves and current. Appl Ocean Res 39:158–167. https://doi.org/10.1016/j.apor.2012.12.002

Zhao YP, Bi CW, Chen CP, Li YC, Dong GH (2015) Experimental study on flow velocity and mooring loads for multiple net cages in steady current. Aquac Eng 67:24–31. https://doi.org/10.1016/j.aquaeng.2015.05.005

Zhao Y, Xu T, Bi C, Dong G, Liu S (2012) The numerical simulation of hydrodynamics of fishing net cage. In: Hydrodynamics—theory and model. InTech. https://doi.org/10.5772/34780

Water Pollution: A Review

Nandkishore Dadsena and Sindhu J. Nair

Abstract Water is a very important element for living organisms, and it is helpful in the circulation and transmission of nutrients in the biosphere. Due to industrialization, urbanization, and rapid increase in human population, the demand for water has increased sharply, and the quality has declined drastically. Although water has the ability to purify itself, when the concentration of pollutants generated from man-made sources becomes so high that it exceeds the self-purifying ability of water, then the water becomes polluted. Degradation of the physical, chemical, and biological characteristics of water by natural and man-made processes in such a way that it is unsuitable for humans and other biological communities. This is called water pollution.

Keywords Oil spills · Self-purification · Dissolved oxygen · Effluent standard · Aquatic ecosystem · Pollution abatement

1 Introduction

Sources of Water Pollution: On the basis of origin, the water pollutant sources are divided into two major parts.

a. **Point Source Pollution**. It includes such pollution in which the pollutants come from a fixed source of water. Such as the sewage site of the municipal area and the effluent site of the factory.

N. Dadsena (✉)
Environmental Science and Engineering, Bhilai Institute of Technology, Durg, Chhattisgarh, India
e-mail: dadsenank@gmail.com

S. J. Nair
Department of Civil Engineering, Bhilai Institute of Technology, Durg, Chhattisgarh, India
e-mail: sindhuj.nair@bitdurg.ac.in

J. K. Deka et al. (eds.), *Emerging Technology for Sustainable Development*,
Lecture Notes in Electrical Engineering 1061,
https://doi.org/10.1007/978-981-99-4362-3_11

b. **Non-Point Source Pollution**. Under this, such pollution is included in which the pollutants do not effluent from any separate source. In this, the pollutants come from a wide area. For example, the flow of rainwater of the city, the flow of agriculture, washery ghat, open defecation, carcasses of animals, etc.

Point source pollution can be controlled by using appropriate techniques, but nonpoint source pollution is difficult to control.

1.1 Causes of Water Pollution

Mixing of domestic and industrial wastes into water sources.

- Mixing of water containing fertilizers and weeds used in agriculture in the river.
- Oil spill
- Access of chemicals containing radioactive substances to aquatic systems.
- Drain of high-temperature water from the electric power station into the water source.
- Use of river water for bathing and washing.

1.2 Oil Spills

Due to the accident of oil tankers in ocean areas and pollution spread from oil mining in coastal areas, plankton fishes and sea creatures die. More than 100 million tons of oil are transported every year, and about 6.01% of the oil spilled during the transportation is in the sea. In this way, 200 million gallons of oil pollute the ocean water every year. The problem of oil overflow also arises from leakage in the international oil pipeline.

1.3 Effects of Oil Spills

Impact on Local Industries. The impact of oil spill on local industries, such as tourism industry, fishing industry, swimming, and sailing. However, its effect lasts for a limited time.

Effects on Human Health. Food affected by marine aquatic oil is harmful to humans. Due to exposure to fire in the oil-flooded area, problems like respiratory, eye diseases, etc., arise. People living in such areas suffer from the problem of asthma, throat infection, burning eyes, migraine, etc.

Impact on Aquatic Ecosystem. Oil spills have an effect on marine vegetation. It has a direct effect on coral reefs. It has a negative effect on aquatic animals. Millions of species are being destroyed every year due to oil spills. This also affects the food chain.

Control Measures of Oil Spills

1. **Chemical method**. The oil is vaporized through bubbles using detergents, but it also has a negative effect on the aquatic ecosystem.
2. **Physical method**. 98% of oil sludge can be removed by burning oil by combustion process, but this oil overflow must be at least 9 mm level.
3. **Biological method**. Oil zapping developed by TERI is a method of bioremediation in which oil spillage is controlled using bacteria. These bacteria on the oil eat the hydrocarbons present in the oil and convert it into carbon dioxide and water.
4. **Mechanical method**
   (i) **Booms**. In this (in an oil field), a type of wall is made.
   (ii) **Skimmers**. This is non-harmful. Similar to the type of vacuum cleaner that draws out oil.
   (iii) **Sorbent**. In this process, oil is removed by absorption or adsorption.

2 Effects of Water Pollution

2.1 Impacts on Aquatic Ecosystem. Water Pollution Has a Bad Effect on the Physical, Chemical, and Biological Characteristics of the Aquatic Ecosystem

- Due to the excess of polluting substances, the amount of dissolved oxygen (DO) in the water decreases, which leads to the death of some sensitive organisms such as plankton, mollusks, and some fish. Only a few tolerant species, such as annelids and some insects, can survive at low DO. Such organisms are recognized as indicator species of polluted water.
- Biocides, polychlorinated biphenyls (PCBs), and heavy metals such as mercury, lead, cadmium, copper, and silver directly destroy various species of organisms.
- The solution of oxygen in water is low at high temperature, so the waste hot water from industries, when dumped in reservoirs, reduces their DO content. The amount of DO decreases with an increase in salinity and increases with an increase in pressure.

Dissolved Oxygen (DO): It is the amount of dissolved oxygen in the water which is required for the respiration of aquatic organisms. When the amount of DO in water falls below 8.0 mg/1, such water is said to be contaminated. When this quantity falls below 4.0 mg/l, it is said to be highly polluted.

Biological Oxygen Demand (BOD): The amount of oxygen that is required for the biochemical decomposition of organic matter in water. Where BOD is high, DO will be low. The amount of water pollution is measured through BOD. But only biodegradable is detected through BOD, and at the same time, it is a very long process. Therefore, BOD is not used in pollution measurement.

Chemical Oxygen Demand (COD): The amount of oxygen in the water that is required for the oxidation of the total organic matter (soluble or insoluble) present. It is a better option for the measure.

Most Probable Number (MPN): The water in which the pollution of organic wastes such as sewage has the number of bacteria like *Escherichia coli* is found to be high. With the help of MPN test, *E. Coli*, etc., can be identified and measured. High MPN is found in polluted water.

1. The Central Pollution Control Board has considered fluoride, zinc, chromium, heavy metals (mercury, uranium, cadmium, etc.) responsible for drinking water pollution in India.
2. EPA 2010 National Lakes Assessment found high levels of nitrogen and phosphorous pollutants in 20% of India's lakes. This has a direct impact on the aquatic ecosystem. She goes.
3. Accelerate the process of eutrophication, bio-enhancement, etc., in the aquatic ecosystem.
4. The effect of polluted water is also on the coral reef; this increases the incidence of coral bleaching.

2.2 Impact on Human Health

- Due to viruses, bacteria, parasites, and worms present in polluted water, there is a risk of infectious diseases, such as jaundice, cholera, typhoid, diarrhea, hepatitis, and kidney failure. This infected water is unsuitable for drinking, bathing, cooking, etc.
- The use of water containing heavy metals can cause serious health problems. In 1956, Minamata disease killed many people in Japan after consuming mercury-tainted fish. The mercury mixture present in the wastewater is converted into a highly toxic substance methyl mercury by microbial activities, which causes sensibility, deafness, blurring of eyes and mental imbalance in organs, lips, tongue, etc.
- Cadmium pollution causes 'ItaiItai' disease, which causes severe pain in bones and joints and leads to liver and lung cancer. The effects of anemia, headache, muscle weakness, and blueness of gums are seen from the water containing sauce.
- Water containing asbestos fibers causes asbestosis (a form of lung cancer).

2.3 Economic Impact

The economic impact of water pollution is very visible. It is expensive to clean polluted water in comparison with the cost of clean water. Water pollution affects fish and other aquatic organisms. It also has a negative impact on tourism. According to an estimate, there is a direct and indirect loss of $50 billion annually due to water pollution.

3 Control of Water Pollution

Water pollution can be effectively controlled by adopting the following measures.

1. **Domestic sewage**: Domestic sewage contains 99.9% water and 0.1% pollutants. Centralized sewage treatment plants can remove more than 90% of the pollutants of domestic sewage in urban areas.
2. **Industrial wastewater**: Some industries emit common toxic pollutants which can be disposed of by the municipality but some pollutants like oil, grease, heavy metals, etc., must be disposed of by special disposal plants. It should be made mandatory for industrial establishments not to immerse waste from factories in rivers, lakes, and ponds without treatment.
3. **Agricultural wastewater**: The runoff of water in the agricultural sector can be reduced by a number of erosion control systems. Farmers can maintain water quality by not using fertilizers and pesticides excessively and by using bio-fertilizers and bio-pesticides.
4. The general public should be made aware and made aware of water pollution and its ill effects.

Groundwater Pollution: Groundwater gets infected due to the mixing of ground water with the seepage of water containing industrial city and agricultural wastes. Groundwater accounts for about 30% of the total amount of clean water. Groundwater is the primary source of water for 1.5 billion people. The depletion of groundwater creates a serious problem for human beings for other activities including agriculture.

3.1 Effects of Ground Water Pollution

- Due to the high amount of nitrate in drinking water, it combines with the hemoglobin of newborns to form methemoglobin, which hinders oxygen transport. This leads to the death of newborn babies. This disease is called methemoglobinemia or blue baby syndrome.
- Excess of fluoride in drinking water causes a disease called fluorosis. Due to this, the teeth and bones become weak.

- The use of water containing arsenic causes a skin disease called black foot, apart from this arsenic causes diarrhea, hyperkeratosis, peripheral neuritis, and lung and skin cancer.
- The government should make effective laws for the control of water pollution. Although the government had enacted the Water (Conservation and Control of Pollution) Act, 1974, but it needs to be made more effective.

4 Government Efforts to Control of Water Pollution

4.1 Conservation of Water Bodies

Most of India's rivers have become like polluted drains at this time. Half of India's ponds, lakes are victims of pollution, and their water is no longer potable. The work of 'National River Conservation Directorate' working under the Ministry of Environment, Forest and Climate Change is done under the Centrally Sponsored Schemes 'National River Conservation Plan' (NRP) and 'National Plan for Aquatic Ecosystem Conservation' (NPCA). To provide financial assistance to the state governments for the protection of lands.

4.2 Ganga Action Plan (GAP)

One of the country's major rivers and self-cleansing (viruses found in the Ganges eat bacteria like bacteriophage, etc.), Ganga, today almost half of its runoff has become polluted. At present, unprocessed sewage from more than 100 cities with a population of more than 50,000 is discharged into the Ganges, and thousands of dead bodies and burnt remains are discharged into it. About 35% of India's population resides in the Ganges basin. The Ganga Action Plan (GAP) was launched in 1985 by the Central Pollution Control Board constituting the Central Ganga Authority (CGA). GAP-I ran from 1986 to 1993.

4.3 National River Conservation Plan

The Central Ganga Authority (CGA) was renamed as 'National River Conservation Authority (NRCA) in 1995. The Ganga Action Plan was merged with the NRCP. At present, it covers the polluted stretches of 34 rivers in 77 cities spread across 16 states.

The objective of NRCP is to improve the water quality of rivers through pollution abatement works in various cities situated along the banks of polluted rivers. Pollution abatement works done under NRCP include construction of sewage system to stop waste coming into rivers from open drains, installation of water treatment plants to treat wastewater, ban on riverside defecation, improvement of river banks and bathing ghats, participatory awareness, etc.

On the orders of the Comptroller and Auditor General of India (CAG), Environmental Research Laboratory (ERL), Lucknow has divided water into five categories after testing the quality of water.

- **Category A (Category A)**: Suitable for drinking.
- **Class B (Category B)**: Suitable for bathing, swimming, and recreation.
- **Class C (Category C)**: Potable after conventional treatment.
- **Class D (Category D)**: For wildlife and fish suitable.
- **Category E (Category E)**: Suitable for irrigation, industrial cooling, and waste disposal.

4.4 National Plan for Conservation of Aquatic Ecosystem (NPCA)

Earlier, for conservation of wetlands and lakes, centrally sponsored schemes were being implemented by the Ministry of Environment Forest and Climate change

(i) National Wetland Conservation Program.
(ii) National Lake Conservation Plan.

NPCA was started by integrating these two schemes to avoid duplication and better coordination. The cost of the scheme was divided between the central and state governments in the ratio of 70:30 and 90:10 in the case of special states. The plan aims to conserve and rejuvenate wetlands and wetlands to improve water quality and improve biodiversity and ecology through a common regulatory framework. This scheme will reduce the pollution of lakes and help in the rational use of wetland resources. About 150 million people in the world are forced to drink water containing arsenic. Arsenic pollution is a serious threat to people's health in 10 states in India. Arsenic in excess of 0.5 mg per liter is injurious to health.

4.5 Water (Prevention and Control of Pollution) Act, 1974

This act has been made for the prevention and control of water pollution. Through this, various boards have been formed, which prevent and control water pollution. Certain powers and duties have been conferred on the boards by the Act.

Functions and Rights of Central Pollution Control Board

- To advise the Central Government on water pollution.
- Consolidation of functions of State Boards.
- To assist the State Boards in water pollution investigation and research work.
- Training of water pollution experts.
- Providing information related to water pollution to the general public through the media. To collect, integrate, and publish relevant technical and statistical information.
- To fix the standard of water pollutants with the help of the government and to revise them from time to time.
- To run a nationwide program to stop water pollution.

Functions and Powers of the State Pollution Control Board

- Conducting the state government's program to stop water pollution.
- To advise the state government on water pollution.
- To collect and publish water pollution-related information at the state level.
- To conduct research to stop water pollution.
- To assist the Central Board in the training of specialists.
- Inspection of sewage and effluents for treatment.
- Establish and revise the standards of water pollution.
- To find effective and cheap methods of water treatment.
- To find out the uses and uses of sewage and effluents, to devise proper methods of removal of sewage and effluents.
- Establishing treatment standards, informing the government about industries that are emitting harmful effluents.
- Board members, officers, or authorized persons can take samples of water emitted from any industry. Board members, officers, or authorized persons can inspect any industry. No person has the right to knowingly release any poisonous or intoxicating substance into any water stream. Violation of the rules is punishable with imprisonment for a term which may extend to three months, or with fine, or with both. There is a provision of penalty for violation of rules by companies and government entities.

4.6 Namami Gange Programme

₹ 20,000 crores was allocated by the central government in June 2014 for the flagship program named Namami Gange. The purpose of this program is to conserve, rejuvenate, and eliminate pollution of river Ganga. The main pillars of the Namami Gange program are:

1. Sewerage Treatment Infrastructure.
2. River Front Development.
3. Afforestation

4. Biodiversity Development
5. Ganga Gram Yojana
6. Public Awareness
7. River Surface Cleaning.
8. Industrial Flow Monitoring.

5 Conclusion

Today, due to some uncontrolled population explosion in the whole world (except in some countries), industrialization and urbanization, as well as the increase in agricultural production due to excessive demand for food, the demand for water has been continuously increased. And the groundwater has been raised at a dangerous place. As a result, not only the rivers, wells, and ponds are drying up, but the level of pure groundwater accumulated in the ground for thousands of years has also reached a remarkable level today. It is not a big deal that in the coming few years' people should yearn for water. One-third (2/3) of the earth is covered by water, which is proof that water is an inexhaustible natural resource on earth, which can never be lacking. Then, what are the reasons for the scarcity of water in the whole world? Why so much discussion on water? Is water running out of the earth? The answer is clear that water on earth is a priceless gift of nature, which is rarely found on any other planet. Owing to all these considerations, water pollution should be kept in mind to preserve our natural as well as commercial resources for the generations to come, and the problem of water pollution should be prevented and minimized.

References

Abel PD (2002) Water pollution biology. CRC Press

Dojlido J, Best GA (1993) Chemistry of water and water pollution. Ellis Horwood Limited

Dugan P (2012) Biochemical ecology of water pollution. Springer Science & Business Media

Freeman III AM (2010) Water pollution policy. In: Public policies for environmental protection. Routledge, Chica, pp 179–224

Goel PK (2006) Water pollution: causes, effects and control. New Age International

Håkanson L, Bryhn A (1999) Water pollution. Backhuys Publication, Leiden

Hogan CM (2010) Water pollution. encylopedia of earth topic. Cleveland National Council on Science and Environment, Washington, DC

Moss B (2008) Water pollution by agriculture. Philosoph Trans R Soc B Biol Sci 363(1491):659–666

Schwarzenbach RP, Egli T, Hofstetter TB, Von Gunten U, Wehrli B (2010) Global water pollution and human health. Annu Rev Environ Resour 35:109–136

Warren CE (1971) Biology and water pollution control

Experimental Study on Low-Cost and Lightweight Building Materials Developed Using Waste Materials

Hillol Kashyap, Fazlur Rahman, Nishat Tashnim, Kaushik Kashyap, Shubam Deb, and Debshri Swargiary

Abstract Since the large demand has been placed on building material industry especially in the last decade owing to the increasing population which causes a chronic shortage of building materials, the civil engineers have been challenged to convert waste to useful building and construction material. Recycling of such waste as raw material alternatives may contribute in the exhaustion of the natural resources; the conservation of not renewable resources; improvement of the population health and security preoccupation with environmental matters and reduction in waste disposal costs. Different low-cost/waste materials like plastic bottles, polythene, saw dust, styrofoam, fine aggregates and coarse aggregates from different places are taken for regenerating building blocks. Automatic compaction machine has been used to find the compressive strength (fck) of prepared blocks. Based on the experimental investigation on plastic–aggregate blocks, it was found that the blocks with the proportion of 26% plastic, 74% fine aggregate have the highest strength when comparing with all other proportions of the plastic–aggregate blocks. Hence, it was concluded that polyethylene terephthalate (PET) bottle can be used as main constitution for the preparation of paver blocks with the increased strength. Though the compressive strength is low when compared to the concrete paver block, but it can be used in gardens, pedestrian path and cycle way, non-traffic and light traffic road, etc.

Keywords Plastic waste · Fly ash · Water absorption · Compressive strength · PET bottle

H. Kashyap · F. Rahman · N. Tashnim · K. Kashyap · S. Deb · D. Swargiary (✉)
Department of Civil Engineering, Bineswar Brahma Engineering College, Kokrajhar, Assam 783370, India
e-mail: sdebshri@gmail.com

J. K. Deka et al. (eds.), *Emerging Technology for Sustainable Development*, Lecture Notes in Electrical Engineering 1061,
https://doi.org/10.1007/978-981-99-4362-3_12

1 Introduction

In the last decades, due to the modern lifestyle, the progresses in industry and technology had led to an important increase in the amount and type of wastes. The problem of waste accumulation every year is all over the world. These industrial and agricultural wastes are by-products, slag, rice husk ash, fly ash, cement dust, brick dust, sludge, glass, tires, etc. Raju et al. (2019) prepared paver blocks with the utilization of plastic waste, quarry dust, coarse aggregate and ceramic dust in place of cement and concluded that the compressive strength is lower than paver blocks but can be utilized in light construction works like gardening. Sseremba et al. (2006) prepared composite bricks from saw dust using Portland cement as a binder and concluded that the composite bricks cannot be used for high strength external construction materials instead can be used for decoration, interior wall paneling, etc. Shanmugavalli et al. (2017) prepared paver block plastic waste in different proportions with quarry dust, coarse aggregate and ceramic waste to find alternative ways conserving the environment. The replacement of plastic waste for cement provides potential environmental as well as economic benefits. Nivetha et al. (2016) mixed plastic waste with solid waste fly ash and quarry dust in varying proportion and find out the physical and mechanical properties and concluded that solid waste (quarry dust, fly ash and PET) can be used as a main constitutions for the preparation of paver block. Dinesh et al. (2016) added high-density polyethylene (HDPE) and polyethylene (PE) with sand and aggregate at various percentages to obtain high strength bricks that possess thermal and sound insulation properties to control pollution and to reduce the overall cost of construction. The waste represents a major problem for the environment because the air pollution and leaching toxic chemicals like arsenic, boron, cobalt, lead, manganese, mercury, selenium, strontium, hydrocarbon compounds, etc., when are dumped in landfills, quarries, rivers or oceans. The capitalization of waste is difficult because of their variety, as well as their unknown properties over time.

Lately, the environmental sustainability became an important problem from the point of view of natural resources and that of wastes. The construction and the building materials sectors are involved in both processes: Building industry is the largest user of natural materials, and in addition a large amount of waste results from the demolition of constructions.

2 Sample Preparation

Different low-cost/waste materials like plastic bottles, polythene, saw dust, styrofoam, fine aggregates, and coarse aggregates from different places or sites are collected. Then, the stickers and caps of the bottles are separated out manually as it is made up of different types of plastic. The styrofoam and polythene are shredded into small pieces. The plastic bottles are weighed according to the ratio and percentage of the composite samples. Similarly, the filler materials like fine and coarse aggregate, saw dust, etc., are also weighed before mixing all the ingredients.

Samples of plastic–aggregate blocks, plastic–polythene–aggregate blocks, plastic and sawdust blocks, cement–styrofoam–aggregate blocks and cement–styrofoam–fly ash–aggregate blocks were prepared. Composition of those samples are listed in Table 1.

Blocks were made by different methods using different materials of different compositions. Hence, to know their characteristics, behavior, strength and durability, we conducted some tests like compressive strength test using compressive testing machine and water-absorption test on those blocks so that we can find out their usability. These tests can highlight future risks and also check the quality of the construction to fulfill the requirements.

Compressive testing shows how the material will react when it is being compressed. Compression testing is able to determine the material's behavior or response under crushing loads and to measure the plastic flow behavior and ductile fracture limits of a material. Water absorption is used to determine the amount of water absorbed under specified conditions. Water absorption test is done to determine the moisture content of a specimen as a percentage of its dry weight.

3 Results and Discussions

Blocks were made by different methods using different materials of different compositions. Hence, to know their characteristics, behavior, strength and durability, we conducted some tests like compressive strength test and water absorption test on those blocks so that we can find out their usability. Specific weight of the blocks was also considered. These tests can highlight future risks and also check the quality of the construction to fulfill the requirements.

Table 1 represents the highest compressive strength of each and every specimen from our experiment. These specimens' compressive strengths are compared with standard blocks.

The comparison of compressive strength of all our experimented specimen blocks with standard paver blocks and standard burnt clay bricks are shown in Fig. 1. It can be observed that compressive strength of sample S1, i.e., plastic–aggregate block of composition 30% plastic, 35% fine aggregate, 35% coarse aggregate (of size $\leq$ 9.5 mm) (in a 2 kg composition) and of dimension 0.1 × 0.1 × 0.1 cum and specific weight 1750 kg/cum is **10.47 N/mm²** is lower than M30 paver blocks but higher than class 10 burnt clay bricks. So, sample S1 can replace class 10 burnt clay bricks.

Compressive strength of sample S2, i.e., plastic–polythene–aggregate block of composition 12.5% plastic, 12.5% polythene, 75% fine aggregate (in a 3 kg composition) and of dimension 0.07 × 0.07 × 0.07 cum and specific weight 1690 kg/cum is **8.571 N/mm²** is lower than M30 paver blocks but higher than class 7.5 burnt clay bricks. So, sample S2 can replace class 7.5 burnt clay bricks.

Table 1 Sample composition and compressive strength

Specimen	Composition	Sample No.	Dimension	Area (mm^2)	Weight (kg)	Specific weight (kg/cum)	Crushing value (N)	Compressive strength (N/mm^2)
Plastic–aggregate blocks	30% plastic 35% fine aggregate 35% coarse aggregate (of size < 9.5 mm) (in a 2 kg composition)	S1	0.1 × 0.1 × 0.1	10,000	1.750	1750	104,700	10.47
Plastic–polythene–aggregate blocks	12.5% plastic 12.5% polythene 75% fine aggregate (in a 3 kg composition)	S2	0.07 × 0.07 × 0.07	4900	0.580	1690	41,997.9	8.571
Plastic–saw dust blocks	30% plastic 70% saw dust (in a 2 kg composition)	S3	0.07 × 0.07 × 0.07	4900	0.490	1428	65,562	13.38
Cement–styrofoam–aggregate blocks	Cement, styrofoam, and fine aggregate (1:1:1)	S4	0.07 × 0.07 × 0.07	4900	0.724	2110	11,270	2.3
Cement–styrofoam–fly ash aggregate blocks	Cement, styrofoam, fly ash, and fine aggregate (1:2:1.5:1)	S5	0.1 × 0.1 × 0.1	10,000	1.215	1215	9100	0.91

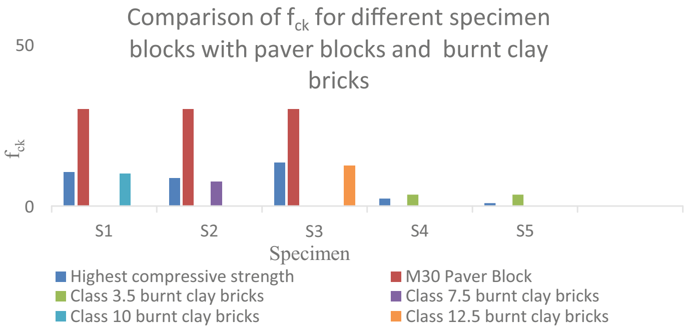

Fig. 1 Comparison of *f* ck for different specimen blocks with paver blocks and burnt clay bricks

Compressive strength of sample S3, i.e., plastic-saw dust block of composition 30% plastic, 70% saw dust (in a 2 kg composition) and of dimension 0.07 × 0.07 × 0.07 cum and having specific weight 1428 kg/cum is **13.38 N/mm²** is lower than M30 paver blocks but higher than class 12.5 burnt clay bricks. So, sample S3 can replace class 12.5 burnt clay bricks.

Compressive strength of sample S4, i.e., cement–styrofoam–aggregate block of composition cement, styrofoam, fine aggregate (1:1:1) and of dimension 0.07 × 0.07 × 0.07 cum and having specific weight 2110 kg/cum is **2.3 N/mm²** is lower than class 3.5 burnt clay bricks. So, sample S4 can be used for light construction works.

Compressive strength of sample S5, i.e., cement–styrofoam–fly ash–aggregate block of composition cement, styrofoam, fly ash, fine aggregate (1:2:1.5:1) and of dimension 0.1 × 0.1 × 0.1 cum and specific weight 1215 kg/cum is **0.91 N/mm²** is lower than class 3.5 burnt clay bricks. So, sample S5 can be used in broken form as aggregate in road construction, foundations.

From Fig. 2, it is clear that the compressive strength (*f* ck) of sample 3 (S3) is highest and that of sample 5 (S5) is lowest.

Similarly, results of lowest % of water absorption test are listed in Table 2.

According to clause 6.2.4 of IS 15658: 2006, water absorption shall not be more than 6 percent by mass and in individual samples, the water absorption should be restricted to 7 percent in case of paver blocks.

Fig. 2 Comparison of *f* ck of all samples

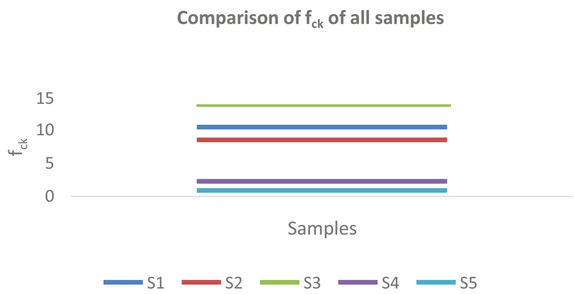

Table 2 Specimen showing lowest % of water absorption

Specimen	Composition	Sample No.	Dimension (cum)	Area (mm^2)	Weight (dry) (kg)	Weight (wet) (kg)	Specific weight (kg/cum)	% of water absorbed
Plastic–aggregate blocks	30% plastic 35% fine aggregate 35% coarse aggregate (of size = 9.5 mm) (in a 2 kg composition)	S1'	0.1 × 0.1 × 0.1	10,000	1.895	1.902	1895	0.36
Plastic–polythene–aggregate blocks	12.5% plastic 12.5% polythene 75% fine aggregate (in a 3 kg composition)	S2'	0.07 × 0.07 × 0.07	4900	0.528	0.531	1539	0.56
Plastic-saw dust blocks	30% plastic 70% saw dust (in a 2 kg composition)	S3'	0.07 × 0.07 × 0.07	4900	0.490	0.501	1428	2.24
Cement–styrofoam–aggregate blocks	Cement, styrofoam, fine aggregate (1:4:2)	S4'	0.1 × 0.1 × 0.1	10,000	1.256	1.281	1256	1.99
Cement–styrofoam–fly ash aggregate blocks	Cement, styrofoam, fly ash, fine aggregate (1:3:4:1)	S5'	0.1 × 0.1 × 0.1	10,000	1.145	1.168	1145	2

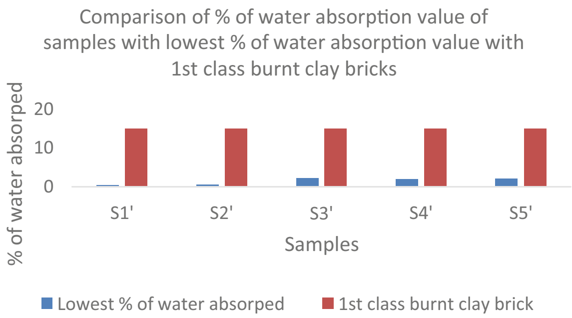

Fig. 3 Comparison of % of water absorption value of samples with lowest % of water absorption value with 1st class burnt clay bricks

From our experiment, each and every specimen has % of water absorption value less than 6%. In Table 2, the samples having lowest % of water absorption value are listed. These samples are denoted by **S1′**; **S2′**; **S3′**; **S4′** and **S5′**. These samples are compared with first class burnt clay brick which has % of water absorption value 15%. This is represented in Fig. 3.

Besides blocks of samples S1, S2, S3, S5, S2′, S3′, S4′ and S5′ have specific weight between the range 300 and 1840 kg/m^3. So, these are considered to be lightweight material.

4 Conclusion

The following conclusions were drawn from the experimental investigation:

1. Blocks composing of 30% plastic, 35% fine aggregate, 35% coarse aggregate (of size $\leq$ 9.5 mm) (in a 2 kg Composition) with weight 1.750 kg and having dimensions 0.1 $\times$ 0.1 $\times$ 0.1 cum and having specific weight 1750 kg/cum can be utilized in outer wall, garden road, exterior use with plastering, etc.
2. Blocks composing of 12.5% plastic, 12.5% polythene, 75% fine aggregate (in a 3 kg composition) with weight 0.580 kg and having dimensions 0.07 $\times$ 0.07 $\times$ 0.07 cum and having specific weight 1690 kg/cum can be used in garden walls, partition walls, etc.

Blocks composing of 30% plastic, 70% saw dust (in a 2 kg composition) of dimension 0.07 $\times$ 0.07 $\times$ 0.07 cum and having specific weight 1428 kg/cum can be used for moderate construction works like cycle way, pedestrian path, etc.

References

Dinesh S, Dinesh A, Kirubakaran K (2016) Utilisation of waste plastic in manufacturing of bricks and paver blocks. Int J Appl Eng Res 2(4):364–368

IS 15658: 2006, clause 6.2.4
Nivetha C, Rubiya M, Shobana S, Viswanathan VRG, Vasanthi R (2016) Production of plastic paver block from the solid waste (quarry dust, flyash and PET). ARPN J Eng Appl Sci 11(2):1078–1079
Raju S, Amarnath M, Anandhakumar M, Elavarasan K, Naveenkumar A (2019) Utilisation of waste plastics as a replacement of cement in paver blocks. Int Res J Eng Tech 6(3):2497–2951
Shanmugavalli B, Gowtham K, Nalwin PJ, Moorthy BE (2017) Reuse of plastic waste in paver blocks. Int J Eng Res 6(2):313–315
Sseremba O (2006) Production of composite bricks from sawdust using Portland cement as a binder. Uganda J Agric Sci 12(1):38–44

A Study on Square and Rectangular Hollow Steel Section Subjected to Torsion

Thounaojam Bidyaraj Singh and Khwairakpam Sachidananda

Abstract Steel members have become one of the most popular building materials in the construction industry owing to its high tensile and compressive strength, high ductility, durability, longer span, aesthetic looks, etc. Steel members can be classified into various types based on the manufacturing process, chemical composition, types of section, etc. Steel members used in construction are subjected to various loading such as tension, compression, bending, and torsion. Only few studies (Ridley Ellis in Rectangular hollow sections with circular web openings fundamental behaviour in torsion, bending and shear. University of Nottingham, 2000; Devi et al. in J Constr Steel Res 162, 2019) have been conducted on steel members subjected to torsion. Based on the literatures, it has been concluded that perforated members have lower torsional load resisting capacity than unperforated members and square steel members are better in resisting torsional stiffness than rectangular steel members.

Keywords Steel · Torsion · Square · Rectangle

1 Introduction

Steel members have become one of the leading building materials in the construction industry owing to its various advantages such as high tensile and compressive strength, high ductility, high durability, longer span, and aesthetic looks. Steel members can be classified into two types based on the type of section (a) Open section (b) Closed section. Hollow steel members are more preferred in construction by architects and engineers as compared to open sections as they have high torsional rigidity, lower drag coefficient, aesthetic looks, internal space, etc. (Wardenier et al. 2010). Thin-walled hollow steel members are generally manufactured in industries by two methods: (a) Hot rolling process (b) Cold forming process. Steel sections

T. B. Singh (✉) · K. Sachidananda
Department of Civil Engineering, National Institute of Technology Manipur, Imphal, India
e-mail: bidyaraj@nitmanipur.ac.in

J. K. Deka et al. (eds.), *Emerging Technology for Sustainable Development*,
Lecture Notes in Electrical Engineering 1061,
https://doi.org/10.1007/978-981-99-4362-3_13

produced by cold forming process have reduced ductility, but mechanical properties like tensile strength and yield strength are increased (Macdonald et al. 1997; Afshan et al. 2013). Based on the chemical composition, commercial steel can be classified into four types (a) Carbon steel (b) Stainless Steel (c) Alloy Steel (d) Tool Steel. In the present day, the austenitic stainless steel grades of EN 1.4301/1.4307 and EN 1.4401/1.4404 are commonly used in constructional works (Gardner 2005). Some of the famous steel structures in the world are the Eiffel Tower, Paris, France: Burj Khalifa, Dubai: Taipei 101, Taiwan: Empire State Building, New York, United States, etc. These structural members are subjected to various types of loadings such as tension, compression, bending, torsion, and other various load combinations. A lot of researchers have conducted studies on steel members subjected to tension (Barth et al. 2002; Sujiatanti et al. 2020), bending (Moen and Schafer 2009; Dissanayake et al. 2021), and compression (Kulatunga and Macdonald 2013; Maiorana et al. 2009). However, studies conducted on members subjected to torsion loading are limited unlike tension, compression, and bending as only few studies have been found (Ridley Ellis 2000; Devi et al. 2019).

2 Literature Review

Ridley-Ellis (2000) conducted a study on the fundamental behaviour of rectangular hollow steel (RHS) section with circular web openings when subjected to torsion, bending, and shear. He carried out experimental investigation on full-scale torsion testing and small-scale torsion testing on four different hot finished bars, each two with same section sizes (RHS $200 \times 100 \times 8$ and RHS $150 \times 150 \times 6.3$) of different grades. The study considered the influence of the number and size of holes upon resistance and stiffness in bending, shear, and torsion and combined analytical finite element modelling with large- and small-scale pseudo-static (short-time static loading) laboratory testing. The experimental results were compared against the finite element predictions and were found to match relatively. Based on the comparison between the performance of perforated and unperforated RHS members, it was concluded that huge reduction in torsional capacity (of up to 60%) was caused due to large web openings, and significant reduction in stiffness (of up to 40%) was also observed.

Devi et al. (2019) conducted experimental and numerical investigation on behaviour of cold-formed steel hollow section members subjected to torsional loading. Experimental investigations were carried out on YSt-310 cold formed steel square hollow section (SHS) members, and the numerical investigation was carried out using the finite element software Abaqus (2009). A comparative study between perforated and unperforated square hollow section members was carried out. From the study, it was found that the perforated members were less effective in resisting the torsional load.

Peen et al. (2019) investigated the behaviour of hollow circular section with multiple perforations under compression, flexure, and torsional loading. They conducted both experimental study and finite element simulation with the use of LUSAS (FEA Ltd. 2005). In their study for torsional load case, they recorded the strain gauge reading along with the torsional moment. They compared the experimental and finite element model results based on the graph plotted between torsional moment and strain recorded for both the unperforated and perforated models. It was concluded that the principal major and minor strains between experimental and finite element results were in good agreement within the elastic range, but finite element results yielded higher torsional moment in the nonlinear range for the unperforated specimen. For the perforated model, slight discrepancies were reported in the results between experimental and finite element analysis results. The study was carried out in order to produce lighter structural members. The main emphasis of the study was given within the material linear range, and hence, the modelling results were considered reliable.

Janarthanan and Mahendran (2021) carried out numerical analysis on behaviour of thick unlipped channel section subjected to combined bending and torsional load. They observed the effects of loading eccentricity along with the effect of span. From their analysis, they found that the effect of torsion was more critical in short-span channel beams as compared to long-span channel beams when the members were subjected to same loading eccentricity. They concluded that when unlipped channel section was subjected to eccentric loading, there was a significant reduction in the bending capacity of the system owing to additional torsional moment acting on the section. They have also proposed interaction equations for combined bending and torsion for unlipped channel section when the members get subjected to positive and negative loading eccentricities.

Devi and Singh (2021) conducted a study on circular hollow section member subjected to torsional loading in an attempt to develop continuous strength method design equation. The study was carried out on four different grades of steel (carbon steel, duplex stainless steel, austenitic stainless steel, and ferritic stainless steel). In order to develop the design equations, nonlinear analysis was first carried out using finite element models and was validated against experimental results. They carried out a comparative analysis of torsional capacity among the finite element results, proposed design equation of continuous strength method, and existing torsion design equations from AISC 360-16 (2016), EN 1993-1-1 (2005a), EN 1993-1-5 (2005b), and EN 1993-1-4:2006 (2015). A graph between the torsional capacity ratios of finite element result to the predicted result against the relative torsional cross-section slenderness was plotted to assess the comparison. From their study, they found that torsional capacity was over predicted by AISC 360-16 design equation for slender section of all the four different grades of steel. It was concluded that the proposed design equation offered better prediction results as compared to existing design equations for circular hollow section member subjected to torsion.

3 Methodology

The study of square and rectangular hollow section subjected to torsion have been analysed by both experimental (Ridley Ellis 2000; Devi et al. 2019) and numerical analysis (Janarthanan and Mahendran 2021; Devi and Singh 2021; Vipej et al. 2000) with the use of software like Abaqus. In the experimental test, first the material properties of steel have to be found out by tensile test in terms of stress and strain. Then, the boundary condition of torsion has to be applied with the required twisting force as an experimental set-up. For parametric study of the materials, experimental set-up has to be repeated. To avoid the repeated set-up and huge expenditure for the experiment, numerical analysis can also be done for the parametric study of materials. But before the analysis, the numerical model needs to be validated using the material properties obtained from the tensile testing. For providing the torsional force, the boundary conditions have to be applied. In these papers, both the experimental as well as the numerical analysis results have been analysed in the following section.

4 Result and Discussion

For the study, only few papers, namely Ridley-Ellis (2000), Devi et al. (2019), have been taken to study the effect of torsional force on SHS and RHS for both perforated and unperforated structural steel member. Based on the literatures, few results have been highlighted as shown in Figs. 1, 2 and 3. From Figs. 1 and 2, for different grades of steel S275J2H and S355J2H, it is seen that the torsional capacity of SHS is having more resistance as compared to RHS. The reason may be that the webs of SHS contributed a smaller proportion in the total resistance of the cross-section to the applied torsion. As per the study carried out by Devi et al. (2019), it has been reported that the effect of single and double perforations in stocky steel section almost remains same up to a certain perforation area (up to perforation diameter of about 15 mm) as can be referred from Fig. 3, but the effect of presence of perforation is prominent after perforation diameter of about 15 mm which can been noticed from the same figure. The reason may be that the perforation may be lying in the ineffective portion of the section.

5 Conclusion

From the studies of the steel members under torsional forces, the following conclusions have been made as follows

1. The perforated members have lower torsional load resisting capacity as compared to unperforated members.

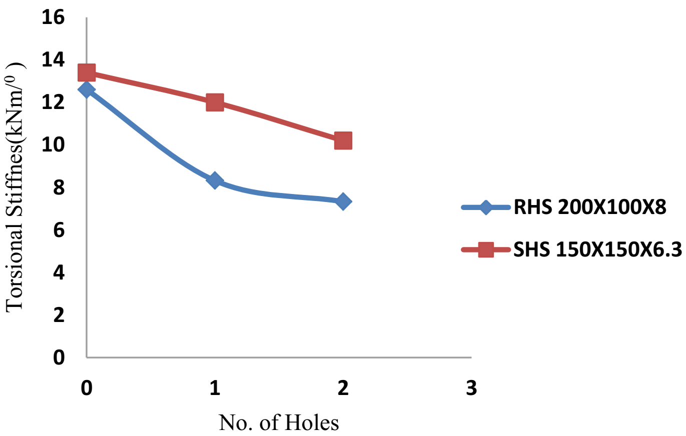

Fig. 1 Comparison of torsional stiffness between the RHS and SHS of steel grade S275J2H (Ridley Ellis 2000)

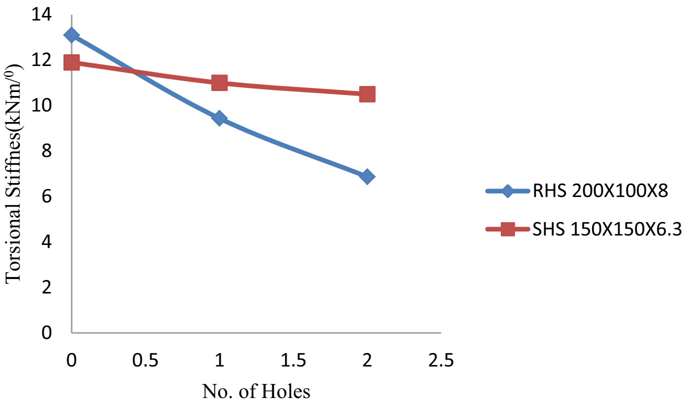

Fig. 2 Comparison of torsional stiffness between the RHS and SHS of steel grade S355J2H (Ridley Ellis 2000)

2. The torsional resisting capacity was slightly affected due to change in position of perforation which could be neglected due to insignificant effect.
3. The reduction of torsional stiffness in steel specimen with square cross-section was lesser as compared to that with rectangular cross-section when there were perforations in the specimen.

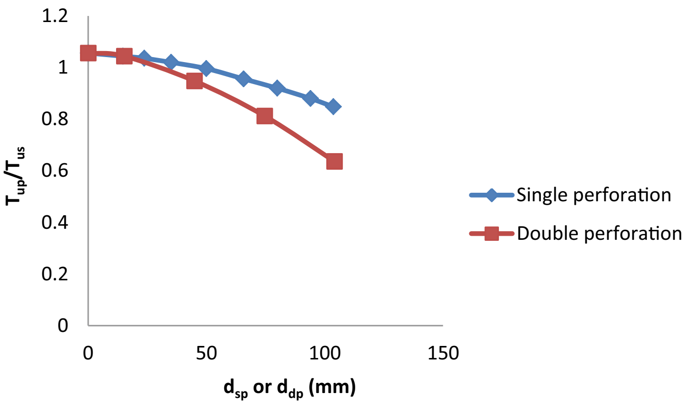

Fig. 3 Variation of normalized T_{up} with perforation diameter for stocky section (Devi et al. 2019)

References

Abaqus (2009) Abaqus/standard user's manual volume I–III and Abaqus CAE Manual, Version 6.9-EFI Dassault Systemes Corp. Providence, USA, 2009W

Afshan S, Rossi B, Gardner L (2013) Strength enhancements in cold-formed structural sections—part I: material testing. JCSR 83:177–188

ANSI/AISC 360-16 (2016) Specification for structural steel buildings. American Institute of Steel Construction

Barth KE, Orbison JG, Nukala R (2002) Behavior of steel tension members subjected to uniaxial loading. J Constr Steel Res 58(5–8):1103–1120

Devi SV, Singh TG, Singh KD (2019) Cold-formed steel square hollow members with circular perforations subjected to torsion. J Constr Steel Res 162:105730

Devi SV, Singh KD (2021) The continuous strength method for circular hollow sections in torsion. Eng Struct 242:112567

Dissanayake DMMP, Poologanathan K, Gunalan S, Tsavdaridis KD, Wanniarachchi KS, Nagaratnam B (2021) Bending-shear interaction of cold-formed stainless steel lipped channel sections. Structures 30:1042–1055

EN 1993-1-1:2005a (2005a) Eurocode 3: design of steel structures-part 1-1: general rules and rules for buildings

EN 1993-1-5:2005b (2005b) Eurocode 3: design of steel structures-part 1-5: plated structural elements. Eur Comm Stand Brussels

EN 1993-1-4:2006+A1 (2015) Eurocode 3: design of steel structures—part 1–4: general rules—supplementary rules for stainless steel

FEA Ltd. (2005) LUSAS, user manual, version 13.7, Surrey, UK

Gardner L (2005) The use of stainless steel in structures. Prog Struct Eng Mater: 45–55

Janarthanan B, Mahendran M (2021) Behaviour and strength of unlipped channel sections under combined bending and torsion. J Constr Steel Res 182:106648

Kulatunga MP, Macdonald M (2013) Investigation of cold-formed steel structural members with perforations of different arrangements subjected to compression loading. Thin-Walled Struct 67:78–87

Macdonald M, Taylor GT, Rhodes J (1997) The effect of cold forming on the yield strength of thin gauge steel-hardness test approach. Thin Walled Struct 29:243–256

Maiorana E, Pellegrino C, Modena C (2009) Elastic stability of plates with circular and rectangular holes subjected to axial compression and bending moment. Thin-Walled Struct 47(3):241–255

Moen CD, Schafer BW (2009) Elastic buckling of thin plates with holes in compression or bending. Thin-Walled Struct 47(12):1597–1607

Peen Y, Keong CK, Hassanshahi O (2019) Behaviour of hollow circular section with multiple perforations under compression, flexure and torsion. Lat Am J Sol Struct 16(2)

Ridley Ellis D (2000) Rectangular hollow sections with circular web openings fundamental behaviour in torsion, bending and shear. Ph.D. thesis. University of Nottingham

Sujiatanti SH, Tanaka S, Shinkawa S, Setoyama Y, Yanagihara D (2020) Experimental and numerical studies for buckling and collapse behaviors of a cracked thin steel panel subjected to sequential tensile and compressive loading. Thin-Walled Struct 157:107059

Vipej S, Konjengbam D, Singh D (2020) Numerical investigation on torsional behaviour of lean duplex stainless steel semi-elliptical hollow section members. Int J Steel Struct 2000. https://doi.org/10.1007/s13296-020-00358-w

Wardenier GJ, Packer J, Zhao JA, van der Vegte XL (2010) Hollow sections in structural applications

Utilization of Reclaimed Asphalt Pavement (RAP) and Use of Plastic Waste in Road Construction: Literature Review

Tuleshwar Choudhary and Madhumati K. Yadav

Abstract Nowadays there is concern about the environment, and ecology has ended up a worldwide issue and is putting nearly each industry accentuation on the use of eco-friendly materials, technology, etc. The road construction field is one of them. There has been a colossal increment in the cost of bituminous asphaltic material. As we all know, "day-by-day the mines are vanishing with broad mining work and as recycling". Recycling materials can be utilized in a few development areas as well as in road development. In expansion, much consideration is centered on the utilization of recovered black-top asphalt material in modern asphalt pavement design. So, reusing is a choice by which there are more concerns. As coordinated to moderate and decrease characteristic assets, natural effect can be of utilizing new asphalt binders. One more major issue on earth is plastic waste. Plastic waste has many bad impacts on soil, surface water, groundwater, and air (due to burning). Scientists and researchers are doing a major concentration on this area to use/reduce plastic waste. Government had banned single-use plastic. Now being fashion on packed food, online food ordering, and packed drinking water bottles. Some packages of food as necessary to protect from moisture and time duration cannot be stopped instantly. Daily plastic waste collection is in millions of tones which is a major issue to handle and dispose of municipals. Plastic waste is now used in road construction at various methods and stages. Utilizing reclaimed asphalt pavement and the use of waste plastic in road construction can solve many environmental problems to a great extent.

Keywords Reclaimed asphalt pavement (RAP) · Marshall stability · Flow · Aggregates · Bitumen · Flexible

T. Choudhary (✉)
Environmental Science and Engineering, Bhilai Institute of Technology, Durg, Chhattisgarh, India
e-mail: tulesh.rgh@gmail.com

M. K. Yadav
Department of Civil Engineering, Bhilai Institute of Technology, Durg, Chhattisgarh, India
e-mail: madhumati.yadav@bitdurg.ac.in

J. K. Deka et al. (eds.), *Emerging Technology for Sustainable Development*,
Lecture Notes in Electrical Engineering 1061,
https://doi.org/10.1007/978-981-99-4362-3_14

1 Introduction

The utilization of reclaimed asphalt pavement (RAP) in various highway projects gets to be currently more prevalent. The materials shown in ancient black-top asphalts have remained in esteem indeed when the asphalts themselves have come to the close of their benefit lives. The use of RAP material was demonstrated to be conservative and ecologically good. In expansion to over, execution of asphalt with legitimately arranged reusing black-top in terms of rutting, fatigue, durability, and thermal resistance, demonstrated to be acceptable. RAP is regularly utilized between 10.0 and 30.0% in the HMA mix. The natural and budgetary limitations are driving the analysts to join a high rate of RAP in the asphalt-based construction of highways. Among them, one of the obstructions to accomplishing the objective is the expanded stiffness of the RAP binder. The objective of this paper is to study RAP with other major environmental solid-waste/waste. The paper gives a brief overview of the recycling of existing methods of bituminous pavement, advantages of using RAP materials, sources, processing of RAP, and uses of waste plastic in flexible road construction.

2 Objectives/Study of the Project

The main objective of the project is to collect and evaluate the information about the findings of various reviews in the field of RAP analysis and to provide better techniques while using RAP materials. In short, they are as follows:

- To observe the behavior of reclaimed asphalt pavement with different blending percentages.
- To carry out various tests adopted for the design of road pavement.
- Study of strength and life of reclaimed asphalt pavement.
- Study in uses of waste plastic in flexible road construction.

3 Salient Features

The RAP aided flexible pavement possesses,

- Remarkable water resistance properties
- Sufficient flexibility
- Lesser absorption of moisture.
- Lesser ruts and repair needed is much lower.
- Smooth-riding surface with very low maintenance.
- Reduces handling and transportation cost.

4 Literature Review

Many studies on the usage of reclaimed asphalt pavement and plastic garbage have been conducted. These studies have demonstrated that they can aid in the 3 understanding of the behavior of recovered asphalt pavement material and plastic debris. The following are some of the research projects:

4.1 Literature Review on Reclaimed Asphalt Pavement (RAP) in Flexible Pavement Constructions

Shah et al. (2007). This paper focuses on testing at low- and high-temperature properties of reclaimed asphalt pavement. Tested a mix of 25% RAP with 3% air voids, and also at 40, 15, and 0% RAP blend. The sample was taken 100 tones after plant stabilization. Design to keep in mind to target 6.5% void content. Tested for creep compliance and tensile strength for low-temperature and high-temperature mix were tested for dynamic modulus. They found as a result that the mix with 40% RAP has the highest strength (Avg. 20% high) among all in temperature with other mixes as the same binder ratio. They conclude that the RAP binder content does not change the mix properties up to the use of 40% RAP. The sample of one source has been tested; this can be eliminated as a sample test on various sources.

Li et al. (2008). They determine the effect and type of RAP mixture properties. Using the methodology of Dynamic Modulus Testing, SCB Fracture Testing. Results found using RAP give higher dynamic modulus value than using without RAP mix. 40% RAP dynamic modulus value in the cold mix is similar to 20% hot asphalt Mix HMA. The RAP-modified mixture has a higher dynamic modulus and stiffer asphalt binder characteristics.

Valdés et al. (2011). They chose a project in Spain Huesca pavement rehabilitation work of highway A-40 length of 5.90 km average daily traffic of 6890 including 8.50% of heavy vehicle. The top layer of 80 mm is being milled from the damaged portion, and using 60% RAP was laid after the milling surface. Over this layer, an intermediate layer is laid with 40% RAP. Over it wearing curse of polymer-modified binder laid without RAP. Uses tests on the material such as stiffness, indirect tensile test, fatigue test, and Fenix test. Core test report after 6 and 12 months of the indirect tensile strength (ITS) has found similar or less than laboratory higher RAP content increases stiffness. Recycled material behavior could be similar to conventional mix. Handling and characterization of stockpiles are very stuff to maintain homogeneously.

Reyes-Ortiz et al. (2012). This paper's main focus is on partial and full replacement of aggregates with RAP. Performed indirect tensile strength on dry and wet mix. They used both 60/70 and 80/100-grade bitumen binders in their experiments. Experiments done on a sample size of 5 no's, with a mean asphalt content of 6.18% with adding new virgin bitumen from 2 to 5%. Sample tested 0, 15, 20, 35, and 100% RAP blending. 60/70 grade bitumen is more susceptible to moisture damage than 80/100-grade bitumen. Research gap of more material combination with RAP.

Pradyumna et al. (2013). The report recommends that the accelerated pavement testing facility (APTF) be utilized to examine the real-world performance of reused 4 asphalts in a more timely and effective manner. A few analysts found that the nearness of RAP increments the stiffness of the blend and diminishes in a few considers. So also fatigue life increments diminish and shift concurring to the temperature. Ductile quality increments or is comparable to virgin blends. Employing a 10% restoring operator as an ideal dosage of recuperated bitumen. Mixing of 20% is way better than virgin and other mixing extents which make strides all properties of the bituminous.

Hussain and Yanjun (2013). The rigidity of the binder is increased by including the RAP binder in the mix. However, when the temperature rises, the effect diminishes. Stiffness and viscosity of bitumen increase with a higher RAP percentage. Under low temperature circumstances, the creep stiffness (*S* value) appears to increase with the increase in the RAP substance, according to the results of BBR. The stiffness, viscosity, and basic temperature of the mix rise when the RAP binder rates are increased.

Izaks et al. (2015). RAP 30% blend with the least bitumen substance was not met the desired air voids ratio. RAP 30% blend with the least bitumen content did not meet the specified esteem of air voids. Air voids diminished in reused blends with an increment of RAP rate, since expanded the fine aggregate within the blend from RAP. RAP 30% blend with the least bitumen substance did not meet the specified esteem of air voids. RAP has no critical impact on volumetric and physical properties of the reused HMA in terms of Marshall stability and flow as well as ruts resistance. It is concluded that it is conceivable to plan high-quality HMA with up to 50% RAP that meets the required volumetric and execution perquisites. Physical parameters (stiffness and fatigue behavior) do not differ significantly between the reused and virgin blends.

Jahangiri et al. (2019). The study in this paper is on study investigation of the rutting and cracking potential of cores samples using modern mixture performance tests. Method for using performance tests on field cores by disk-shaped compact tension (DCT) testing and Illinois flexibility index test (I-FIT). Performed test on eighteen sections of road in the best and worst condition on mixes of 13.2 and 43.7%. The disparities between the DC(T) and IFIT tests are due to variances in test repeatability for these two types of cracking testing.

Ziari et al. (2020). Introducing RAP at 0.0 and 15.0 °C decreases the cracking resistance of the black-top blend. Using 40% RAP on mix fails on cracking resistance when mixing temperatures at (−) 12 and 25 °C. Additional material glass fiber is used in this experiment. Using glass fiber up to 0.12% noteworthy upgrade in resistance against crack initiation and proliferation. Utilizing a technology strategy of mix design and test planning, SCB fracture tests employ crack resistance criteria. At a temperature of 15 °C., the increased stiffness of the mix improved the fracture behavior by incrementing the RAP content and fiberglass.

Montañez et al. (2020). The focus of this outcome is the variability of the physical characteristic’s behavior of different sources of RAP material. They used a sample size of six different ongoing projects in Bogota (Colombia). Performing (i) Characterization of the recovered materials with sieve size investigation black-top cover substance and characterization of the recuperated asphalt. (ii) Characterization of FAM-RAP mixes using linear viscoelastic characteristics, fatigue resistance, permanent deformation resistance, and moisture resistance. They found FAM-RAP mix on RAP sources has proven a major impact on the antagonism to deformation and fatigue in both wet and dry conditions. Lacking identifying threshold limits of RAP contents for quality and durability of mix.

Yousefi et al. (2021). This paper is focusing on RAP with WMA with moisture vulnerability and behavior on resistance to crack and rutting. The test was conducted with 0 and 50% RAP samples. This bitumen of 60/70 is used. Method using semi-circular bending (SCB) fracture moisture susceptibility, dynamic creep, and resilient modulus. Because of the enlarged solidity of the black-top blend, using 50% RAP in the HMA mixture raises the indirect tensile strength (ITS) values of unconditioned and conditioned instances by roughly 13.30% and 23.20%, respectively. Expanded strong modulus within the blends with RAP may well be due to the impacts of stiffer and matured cover in RAP fabric adding 50% RAP to a black-top mix boosts flow, robust modulus, and wetness resistance. This paper employments standard stacking conditions which can be disposed of by different stacking rates and temperatures on break potential.

Al-Ghurabi et al. (2021). The work in this paper focuses on evaluating the influence of RAP particle sizes on the volumetric and physical parameters of HMA when mixing RAP with HMA. The utilizing strategy of Blend plan and arrangement of tests, Characterization of recycled mixtures, and test using Marshal stability and flow tests (ASTM D6926), Indirect Tensile Strength Test (ITS) (AASHTO T283). In comparison with the VMA of the traditional mix, voids in mineral aggregate (VMA) decreased when the fraction of RAP was increased, due to contenting of hardened asphalt and increasing Marshall stability also increment in the percentage of RAP, which produces a steadier blend comparative to a standard blend.

4.2 Literature Review on the Use of Waste Plastic in Superpave Construction

Zoorob and Suparma (2000) used methodology Marshall stability and flow tests, indirect tensile stiffness modulus test, indirect tensile strength test (ITS), creep stiffness, and adhesion test. Uses plastic with hot bitumen rather than use over the hot aggregate and called platisphalt (asphalt with plastic) which gives around 2.5 times more stability than conventional mix on marshal stability test, and also, more flow value is observed which gives more elasticity on mix material. It was discovered that reusable plastic is mostly made of low-density polyethylene and that its use has increased the adaptable asphalt's hardness and fatigue life.

Gawande et al. (2012). They discovered practical techniques to repurpose hard plastic in road construction; for example, when plastic is used as a bitumen modifier, the plastic component may be extended by 5–10% by the weight of bitumen. Because of the presence of changed bitumen, fatigue life and abrasion value be increased.

Chavan (2013). Plastic waste of size 2.36 and 4.75 mm are used with the help of a shredder. Plastic coated aggregate is tested for stripping value and results in zero percent. It is also good in moisture susceptivity. Moisture absorption, aggregate impact value, and crushing value decrease when plastic is added, but specific gravity increases due to plastic filling the voids in specimen or material. Polymer bitumen bland has been discovered to make a significant difference in the authority of plastic-coated aggregate and bitumen.

Mir (2015). Waste plastic ground and made into powder form; 3.0–4.0% of plastics are blended with the asphalt. Plastic increments softening point of bitumen and makes the road hold its adaptability amid winters coming about in its long life. Destroyed plastic squanders act as a solid "binding agent" for tar making the black-top last long. By blending plastic with bitumen, the capacity of the bitumen to resist high temperature Increments increases. The plastic squander is dissolved and blended with bitumen in a specific proportion. Regularly, mixing takes place when the temperature comes to 45.50 °C However, when plastic is combined, the temperature remains constant at 55.0 °C.

Appiah et al. (2017). They used a wet process, using the melt-blending strategy. Taken bitumen (400 g) was warmed on a stove till liquid condition and polymer were gradually included at around 160.0 °C. They used concentration of PP and HDPE extended an increment of 0.5% from 0.5 to 3.0%. The addition of thermoplastic modifiers to regular bitumen alters the behavior of the bitumen mix and affects its rheological characteristics. Generally, high-density polyethylene (HDPE) and polypropylene (PP) modifiers are used, they were watched to show the diverse sums of impact, i.e., expanding the softening point, diminishing penetration value while improving the generally energetic and absolute viscosities of binder.

Kulkarni (2017). In most studies, ten percent of waste plastic is the appropriate level. PVC up to 10% can be used for bituminous asphalt in warm climates to heal mortality, according to research. By powdering and combining, plastic bottles, cups, and other items may be reused.

Duggal et al. (2020). They said about introducing plastic waste in asphalt mix with two processes: Dry and wet mix. Dry blends prepare (a) Aggregates and bitumen are preheated around the temperature of 160.0 °C. (b) Plastic is applied to aggregates, which improves their quality. (c) There will be no harmful gas progress. (d) Utilize of squander plastic more than 15%. (e) Increment properties like porosity, dampness, retention, and soundness. Amp blends prepare (a) Plastic squander is powdered, to begin with, and after that liquefied, it is included to bitumen blend. (b) As it was 6–8% plastic is included in bitumen. (c) Destroyed plastic squander acts as an authoritative operator. (d) When compared to normal bitumen, there is a 2–3 flow increases in Marshall stability.

Hake et al. (2020). SDBC with 10.0% squander plastic showed significantly improved Marshall stability, and bitumen is strengthened with a folio of complete using plastic. They used plastic over the heated graded aggregate and found it works as priming for bitumen binder. Using plastic on the mix from 5 to 15% of the weight of bitumen. Started mix design from 4.50 to 5.75 percentage of bitumen of total mix with an interval of 0.25%. Using the methodology of marshal stability, air voids, flow ratio, voids on mineral aggregate, and flow concerning varying bitumen content. As bitumen percent increases, air voids decrease, but the density of mix, stability, and VMA increase. No major changes in flow value. Optimum bitumen on conventional mix demanded ten percent more bitumen than mix with plastic. Plastic mix sample stability becomes higher than non-plastic mix sample. They watched that by utilizing plastic waste in blends, the road's life is extended, and as a result, the need for support is reduced. According to the extension's cost analysis, they watched that the rate cost lessening for one cum fabric blend is 5.18%.

5 Benefits of Reclaimed Asphalt Pavement (RAP)

There are many benefits of use of reclaimed asphalt pavement and plastic waste. Advantages are as below:

- Construction cost reduction.
- Saving in economy.
- Minimize the problem of disposal of RAP.
- Energy conservation.
- Saving of natural minerals/mines as aggregate.
- Saving on bitumen binder.
- Prevention of unnecessary land disposal.
- Helps in environmental protection.

6 Future Scope

One of the foremost frequently used waste materials is reclaimed asphalt pavement (RAP). The utilization of RAP can help reduce the price of a project and make sure that the project is eco-friendly. Therefore, this study aims to grant an in-depth description of the assembly of RAP to make sure that the rehabilitation and maintenance of pavements, in addition, because the construction of pavements are environmentally friendly and cost-effective. Previous works have shown the advantages of using RAP about its ability to provide equally good or maybe superior results compared to the employment of virgin or original mixes if they are properly produced and applied. This review also demonstrates the critical importance of using RAP in asphalt mixtures. Reclaimed asphalt pavement design with higher RAP content with a combination of other major waste can be done which can solve more environmental problem.

References

Al-Ghurabi SB, Al-Humeidawi BH (2021) Comparative evaluation for the effect of particles size of reclaimed asphalt pavement (RAP) on the properties of HMA. J Phys Conf Ser 1895(1)

Appiah JK, Berko-Boateng VN, Tagbor TA (2017) Use of waste plastic materials for road construction in Ghana. Case Stud Constr Mater 6:1–7

Chavan MAJ (2013) Use of plastic waste in flexible pavements. Int J Appl Innov Eng Manage 2(4):540–552

Duggal P et al (2020) Use of waste plastic in wearing course of flexible pavement. In: Advances in structural engineering and rehabilitation. Springer, Singapore, 177–187

Gawande A et al (2012) An overview on waste plastic utilization in asphalting of roads. J Eng Res Stud 3(2):1–5

Hake SL, Damgir RM, Awsarmal PR (2020) Utilization of plastic waste in bitumen mixes for flexible pavement. Transp Res Procedia 48:3779–3785

Hussain A, Yanjun Q (2013) Effect of reclaimed asphalt pavement on the properties of asphalt binders. Procedia Eng 54:840–850

Izaks R et al (2015) Hot mix asphalt with high RAP content. Procedia Eng 114:676–684

Jahangiri B et al (2019) Performance evaluation of asphalt mixtures with reclaimed asphalt pavement and recycled asphalt shingles in Missouri. Transp Res Record 2673(2):392–403

Kulkarni SJ (2017) Use of plastic in road construction material: towards solid waste minimization. Int J Recent Trends Eng Res 3(01)

Li X et al (2008) Effect of reclaimed asphalt pavement (proportion and type) and binder grade on asphalt mixtures. Transp Res Record 2051(1):90–97

Mir AH (2015) Use of plastic waste in pavement construction: an example of creative waste management. J Eng 5(2):57–67

Montañez J et al (2020) Variability of the mechanical properties of reclaimed asphalt pavement (RAP) obtained from different sources. Constr Build Mater 230:116968

Pradyumna TA, Mittal A, Jain PK (2013) Characterization of reclaimed asphalt pavement (RAP) for use in bituminous road construction. Procedia Soc Behav Sci 104:1149–1157

Reyes-Ortiz O et al (2012) Evaluation of hot mix asphalt mixtures with replacement of aggregates by reclaimed asphalt pavement (RAP) material. Procedia Soc Behav Sci 53:379–388

Shah A et al (2007) Investigation of properties of plant-produced reclaimed asphalt pavement mixtures. Transp Res Record 1998(1):103–111

Valdés G et al (2011) Experimental study of recycled asphalt mixtures with high percentages of reclaimed asphalt pavement (RAP). Constr Build Mater 25(3):1289–1297

Yousefi A et al (2021) Performance evaluation of asphalt mixtures containing warm mix asphalt (WMA) additives and reclaimed asphalt pavement (RAP). Constr Build Mater 268:121200

Ziari H et al (2020) Crack resistance of hot mix asphalt containing different percentages of reclaimed asphalt pavement and glass fiber. Constr Build Mater 230:117015

Zoorob SE, Suparma LB (2000) Laboratory design and investigation of the properties of continuously graded Asphaltic concrete containing recycled plastics aggregate replacement (Plastiphalt). Cement Concr Compos 22(4):233–242

Utilizing Plastic Waste in Construction Materials: A Review

Kasturima Das

Abstract Inefficient solid waste management of plastics and polymeric materials is one among the biggest challenges worldwide, resulting in environmental deterioration. Observations in the domain of plastic waste management have indicated that the process of incineration has become the most widely accepted disposal strategy worldwide. However, due to poor maintenance of incinerators, it releases several harmful gases including dioxins and furans in case of chlorinated and brominated plastic waste thus raising several environmental issues. This challenge has brought alarming concerns regarding minimizing the volume of such wastes released into the environment. This review paper presents an extensive study and proposes a solution to this problem to some extent by reuse, recycling, and efficient conversion of waste materials into alternative application such as utilization of plastic waste in road construction, co-processing of plastic waste in cement kilns etc. Some of such newly employed recycling and conversion techniques of plastic wastes, and possible future alternatives with recommendations are reviewed in this paper, with emphasis given to the recycling potential, specifically in the construction industry.

Keywords Plastic waste · Building blocks · Recycled plastic

1 Introduction

It is a well-known fact that "Waste isn't waste until we waste it." In 1907, about 115 years ago, plastic was invented. In due course of time, plastics proved to be necessary evil, and today the earth is poised on the brink of a severe environmental crisis. The plastic industry has developed considerably since the invention of different types of manufacturing processes for making different kinds of polymers from petrochemical sources. Owing to its basic properties of durability, resistance to chemicals,

K. Das (✉)
Jorhat Engineering College (ASTU), Jorhat, Assam 785007, India
e-mail: kasturimadas@gmail.com

J. K. Deka et al. (eds.), *Emerging Technology for Sustainable Development*, Lecture Notes in Electrical Engineering 1061,
https://doi.org/10.1007/978-981-99-4362-3_15

safety and hygienic nature, relative inexpensiveness to produce, thermal and electrical insulations, and lighter weight than the competing materials, plastics have become indispensable part of the human society. Approximately 50 per cent of plastics are used for single-use disposable applications, such as packaging, agricultural films, and disposable consumer items, between 20 and 25% are used for long-term infrastructure such as pipes, cable coatings, and structural materials; the remaining are used for durable consumer applications with intermediate lifespan, as in electronic goods, furniture, vehicles, etc. Since plastics have only been mass-produced for around 60 years, their longevity within the environment is not known with certainty. Most kinds of plastics are non-biodegradable, and consequently majority of these polymers manufactured today will persist for at least centuries if not millennia. Even degradable plastics may persist for a substantial period of time depending upon local environmental conditions, as the rates of degradation depend upon physical factors, like UV exposure, oxygen availability, and ambient temperature. On the other hand, biodegradable plastics require the presence of suitable micro-organisms. Consequently, degradation rates vary considerably between landfills, terrestrial, and marine environments. Even when a plastic item degrades under the influence of weathering, it first breaks down into smaller pieces of plastic debris, but the polymer itself might not necessarily fully degrade in a considerable timeframe. As a consequence, substantial quantities of end-of-life plastics are accumulating in landfills and as debris in the natural environment, leading to issues with waste management and effects on the environment, leaving the world with the only option of turning garbage into gold.

2 Global and National Scenario of Plastic Waste Generation

Globally, each year nearly 150MT of plastic is produced. Nearly, 80% of the global plastic additives were consumed by USA, China, India, and Eastern Europe. However, South East Asia, especially India and China, has emerged as the global leaders in plastic consumption. As per the September 2017 report by the Central Pollution Control Board (CPCB), which extrapolated data from 60 major cities, India generates around 25,940 tonnes of plastic waste a day. About 94% of this comprises thermoplastic, such as polyethylene terephthalate (PET) and PVC (polyvinyl chloride), which is recyclable. The remaining belongs to thermoset and other categories of plastics, such as sheet moulding compound (SMC), fibre reinforced plastic (FRP), and multi-layer thermocol, which are non-recyclable. According to the latest reports (by Plastindia Foundation) the plastic waste generated across the country is close to 16.5 million tonnes a year. An average of 11 kg has been estimated to be the per capita plastic consumption as of 2021 (Overview of Plastic Waste Management by CPCB 2017) (Fig. 1).

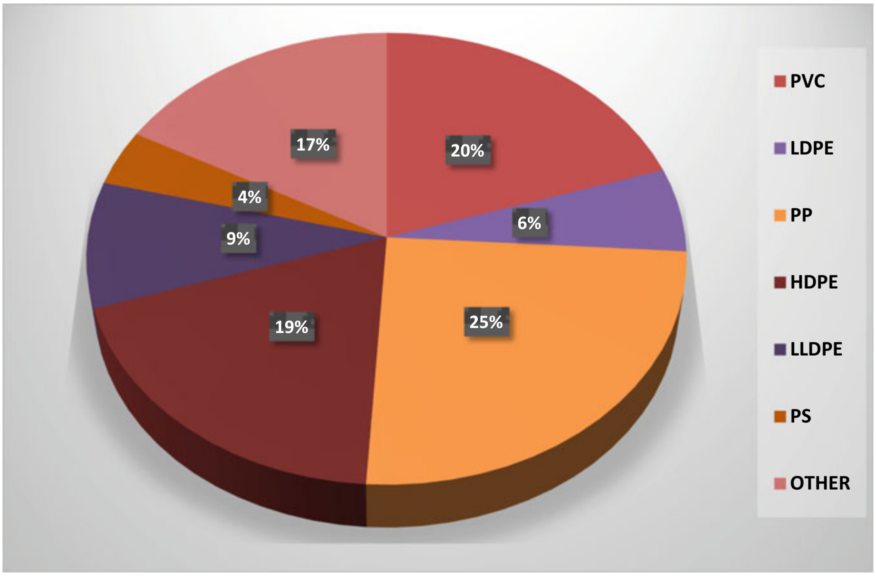

Fig. 1 Consumption of different virgin plastic resins in India

Packaging represents the largest single sector of plastics used in India. The sector accounts for 42% of plastic consumption, and plastic is the material of choice in nearly half of all packaged goods. Apart from use in packaging, plastics are also used in the consumer products such as furniture, housewares, construction, and in industrial sectors. After primary use of this portion of plastics, annually 1.3 MT of waste plastic is generated in India, which is 36% of India's total plastic consumption. Nearly 42% of the total generated plastic waste in India is recycled by approximately 20,000 recycling industries with total potential of 0.37 MT/annum. The rest 58% of the plastic waste generated goes unattended in the landfill sites. A heavy percentage of this waste belongs to the unrecyclable category of plastic. Even if there is a 100% ban on plastic production, the waste so far generated will remain in landfills, harming the environment for years to come (https://www.downtoearth.org.in/news/waste/an-indian-consumes-11-kg-plastic-every-year-and-an-average-american-109-kg-60745).

3 Use of Plastic Waste in the Construction Industry

Plastic is a synthetic or semi-synthetic material that uses polymer as the main ingredient. Owing its unique property, plastics can be moulded, extruded, or pressed into objects of varying shapes and sizes. Discussed in Table 1 are the seven major types of plastics that are extensively used in the present time (https://waste4change.com/blog/7-types-plastic-need-know/).

Table 1 Types of plastic and their plausible uses in the construction industry

Types of plastic	Physical properties	Examples	Recycling potential
Polyethylene terephthalate (PET or PETE)	Lightweight, hard, and flexible Most likely to be picked up by recycling programs		Can be used as fibres in cementitious composites
High-density polyethylene (HDPE)	Rigid, has long virtually unbranched polymer chains Stronger and thicker and relatively more stable than PET and considered a safer option for food and drinks		Can be used for plastic lumber, table, and chairs
Low-density polyethylene (LDPE)	Flexible LDPE is considered a safer plastic option for food and drinks but is difficult to be recycled		Can be used in bricks and blocks
Polyvinyl Chloride (PVC or Vinyl)	Hard and rigid and is the second most frequently used plastic resin in the world Considered as the most hazardous plastic and rarely accepted by recycling programs		Aggregates in cementitious composites
Polypropylene (PP)	Hard and flexible Widely used for hot food containers. It is considered a safer plastic option		Aggregates in asphalt mixture
Polystyrene (PS or Styrofoam)	Hard and brittle PS has a low recycling rate		Insulation material
Mixed forms of plastic	Plastics that may be layered or mixed with other types of plastics, such as bioplastics	Eyeglasses, baby and sports bottles, CD/DVDs, clear plastic cutlery, etc.	Replast blocks, ecobricks, etc.

Recycled plastic material has brought about a paradigm shift in the way a variety of materials are being used within the construction industry. Plastic recycling is, however, a very complex process and sometimes confusing because of the wide range of recycling and recovery processes. These include four categories: primary (mechanical reprocessing into a product with equivalent properties), secondary (mechanical reprocessing into products requiring lower properties), tertiary (recovery of chemical constituents), and quaternary (recovery of energy). Primary recycling is often referred to as closed-loop recycling, and secondary recycling as downgrading. Tertiary recycling is either described as chemical or feedstock recycling and applies when the polymer is de-polymerized to its chemical constituents. Being a low-cost alternative to other materials, the utilization of such recycled plastic in construction helps save energy and landfill space. When combined with virgin plastic, recycled plastic helps reduce cost significantly without compromising on the end goal. Additionally, it is a sustainable construction material that contributes immensely to environmental sustainability through recyclability and energy recovery options. A summary of some secondary products developed using waste plastics as raw materials is presented in Table 2.

4 Comparison of Various Quality Parameters of Plastic Used in the Construction Industry

A detailed comparative study is done regarding the various quality parameters of plastic blended construction materials used in varied applications. Parameters related to plastic blended floor tiles, roof tiles, lightweight concrete, replast blocks, and sand infused plastic bricks are presented in Tables 3, 4 and 5 sequentially.

Table 3 presents a comparative study of the various quality parameters associated with floor tiles manufactured from recycled LDPE, HDPE, and PP (Archit et al. 2019; Hazzan 2003; Konin 2011).

Table 4 presents a comparative study of the various quality parameters associated with roof tiles manufactured from recycled plastics (Rosana 2018).

Table 5 presents a comparative study of the various quality parameters associated lightweight concrete manufactured from recycled PET plastics (Dhawan et al. 2019; Hameed and Ahmed 2019; Pacheco et al. 2012).

One very intriguing concept of recycling plastic waste which eliminates the necessity of sorting and separating the various grades of plastic was put forward by New Zealand-based inventor Peter Lewis, who turned plastic waste into walls. This modular system is at the centre of a US-based company that converts 100% plastic waste into an alternate building block. Table 6 presents the varied quality parameters of replast blocks which are currently in use as building blocks in case of retaining walls, boundary walls, etc. (https://www.engineeringforchange.org/solutions/product/replast/).

Table 2 Products developed by processing plastic wastes

Type of plastic	Other raw materials	Treatment method	Product developed	References
Metallised packaging plastics	Layer of aluminium foil	Thermo-delamination of materials at temperature above 500 °C	High-quality aluminium and hydrocarbon fuel gases	Yin et al. (2019)
Polypropene	5–10% dolomite	Thermochemical method (pyrolysis)	High-calorific fuels	Khoo (2019), Kofi et al. (2019)
HDPE bags	Rubber	Burning at 1000 °C for three hours	Refused fuel	Hashem et al. (2019)
Waste plastic bags	Fly ash (FA) and flame retardant	Simple extrusion and compression moulding technique	Floor and wall tiles and road paver	Dhawan et al. (2019)
PET	–	Cutting into flakes	Lightweight concrete	Hameed and Ahmed (2019)
LDPE or HDPE	–	Shredding and burning	Pellets, flakes, garbage bags, and hoses	Pacheco et al. (2012)
Post-consumer packaging	–	Pyrolysis	Chemicals and fuels	Ragaert et al. (2017)
Mixed forms of plastic	Sand, colorant	Melting and moulding	Roofing tiles	Rosana (2018)
HDPE, PP, and LDPE	Sand (15%)	Crushed, mixed with fillers, and then compressed	Floor tiles	Archit et al. (2019)
Mixed forms of plastic	–	Shredding and compression	Replast blocks	https://www.engineeringforchange.org/solutions/product/replast/
HDPE, LDPE, and PP	Sand	–	Sand-infused plastic bricks	https://worldarchitecture.org/article-links/egmeg/kenyan-startup-founder-nzambi-matee-recycles-plastic-to-make-bricks-that-are-stronger-than-

Table 3 Comparison of quality parameters of conventional and recycled products with regard to floor tiles

Parameter	Recycled product	Conventional product
Density	843 kg/mm^3	2400 kg/mm^3
Weight	57.7322% less	57.7322% more
Peak strength	2175.6 N	2200 N
Static friction factor	0.5	0.512
Floating tendencies	Floats in water	Sinks in water
Burning rate	52 mm/min (std. rate: 100 mm/min)	> 100 mm/min
Price	Comparatively cheaper	Expensive

Table 4 Comparison of quality parameters of conventional and recycled products with regard to roofing tiles

Parameter	Recycled product	Conventional product
Density	925 kg/mm^3	1650 kg/mm^3
Impact resistance	Satisfactory as per IRAM std. 12582-2	Satisfactory as per IRAM std. 12582-2
Specific weight reduction	33% > zinc sheets 40.3% < concrete 51.5% < ceramic	–
Thermal conductivity	99.4% < zinc sheets 72.5% < concrete 49.2% < ceramic	–
Air permeability	Much lower	Comparatively higher
Permeability to water vapour	Satisfactory as per IRAM std. 11632-1	Satisfactory as per IRAM std. 11632-1
Water absorption %	0.3	10
Price	14% < ceramic tiles but higher than zinc sheets	–

Nzambi Matee, a 29-year-old Kenyan woman entrepreneur and inventor, founded the start-up Gjenge Makers Ltd that transforms plastic waste into sustainable, affordable building materials which includes paving tiles, manhole covers, and paving blocks that are stronger than concrete. Matee acquires the waste plastic for free from packaging factories and also buys it from other recyclers. The method involves the company workers acquiring plastic waste, mixing it with sand, and heating it, which results in the brick being approximately five to seven times stronger than concrete. The plastic's fibrous nature makes the bricks an exceptionally durable material and lighter compared to regular bricks. To make the bricks, Matee's team uses the kind of plastic waste that cannot be recycled or processed anymore, including LDPE, HDPE, PP waste, etc. However, it does not use PET, which is usually utilized in plastic

Table 5 Comparison of quality parameters of conventional and recycled products with regard to lightweight concrete

Parameter	Recycled product
Compressive strength	A gradual decrease in compressive strength development occurs with increase in the content of plastic aggregates (both fine and coarse)
Tensile strength	A decrease in the flexural/splitting tensile strength of plastic aggregate concrete is reported. At moderate levels of replacement of natural aggregate with plastic aggregate (less than 20% waste plastic fibre), an increase in the flexural/tensile properties can be achieved
Ductility	The ductility of concrete increases significantly with the addition of plastic aggregate, up to 50%
Workability	Workability increases with increase in the content of coarse recycled waste plastic aggregate increases, up to 50%. Beyond this level, workability decreases. The workability of concrete could also increase or decrease depending on the particle shape, size, roughness, water–cement ratio, and amount of cement paste
Air content	Plastic aggregate results in significant increase of air content in concrete due to its irregular shape, immiscibility of plastic and natural sand, and hydrophobic nature of plastic
Density	Increase in the content of plastic aggregate results in the reduction of the concrete density—the reduction is much more significant with bigger and flakier particles of plastic aggregate
Water absorption	Negligibly low as compared to the conventional concrete

Table 6 Quality parameters of replast blocks

Primary material	All types of plastic
Secondary material	None
Thermal insulation capacity	*K* factor: 0.86
Compressive strength	2.81 MPa
Suitable climates	All types
Lifespan	100 + years
Manufacturer specified performance targets	No glue or adhesives, no crack or crumble, zero waste process, no skilled labour required

bottles and easy to recycle. Table 7 presents a brief idea of the quality parameters involved with the Pavers (https://www.gjenge.co.ke/). Most striking parameter is the strength of the paver block designed, which is 150 N/mm^{2}as compared to 25–30 N/mm^2 in case of the conventional concrete pavers, which indicates, the paver blocks designed using plastic materials tend to be 5–7 times stronger than conventional concrete blocks.

Table 7 Quality parameters of the Gjenge Pavers

Density	3–5 times denser than concrete
Strength	150 N/mm^2
Wear and tear	Far less wear and tear compared to concrete
Price	Nearly 30% cheaper than concrete pavers

5 Conclusion and Future Perspective

Plastics play a significant role in our society, and wastes generated at the end of their usage are inevitable. As such, in order to properly manage these plastic wastes while improving the sustainability of the environment, their use for various construction applications may be a viable option. This overview has indeed explored the current research that has been done on the utilization of several recycled plastic wastes for construction applications. Based on this overview, we can draw the following conclusions.

- The use of plastic waste for construction applications will solve both the solid waste management problem and depleting deposits of raw materials used for construction purposes. In addition, the use of plastic waste in different construction applications supports the sustainability trend of a circular economy.
- The use of plastic waste for construction applications creates a pathway to use these wastes for long-term applications compared to short-term ones, such as recycling into new products which will sooner or later find its way back to the landfill sites.
- Innovative methods developed for manufacturing construction materials using different types of plastic wastes require more research in terms of their relative strength, stability, and durability, in comparison with conventional materials under different environmental conditions.

References

Abota CA (2012) Recycling of plastic wastes in Ghana; a way to reduce environmental problems/ pollutions. University of Ghana, Accra, Ghana

Archit H, Omkar B, Swapneel W, Abhishek S, Rohit B (2019) Comparative analysis of tiles made from recyclable LDPE plastic waste. IJERT 8(2). ISSN: 2278-0181

Bacon F, Holland W, Tikalsky J (2005) Roofing materials made with nylon fibre composites. US20050170141 A1

Berdahl P, Akbari H, Levinson R, Miller WA (2008) Weathering of roofing materials—an overview. Constr Build Mater 22(4):423–433

Dhawan R, Mohan B, Bisht S, Kumar R, Kumari S (2019) Recycling of plastic waste into tiles with reduced flammability and improved tensile strength. Environ Prot 124:299–307

Gaggino R, Positieri MJ, Irico P, Kreiker J, Arguello R, Sanchez MPA (2014) Ecological roofing tiles made with rubber and plastic wastes. Adv Mater Res 844:458–461

Gaggino R, Kreiker J, Filippin C, Sanchez Amono MP, Gonzalez Laria J, Peisino LE (2018) The comprehensive comparison of thermal and physical-mechanical properties of the recycled rubber and plastic roofing tiles versus roofing tiles made with different traditional materials, 7361798
Hameed AM, Ahmed BAF (2019) Employment the plastic waste to produce the light weight concrete. Energy Procedia 157:30–38
Hashem FS, Razek TA, Mashout HA (2019) Rubber and plastic wastes as alternative refused fuel in cement industry. Constr Build Mater 212:275–282
Hazzan EB (2003) A study of plastic moulding techniques in Oyo state. Ladoke Akintola University of Technology, Ogbomoso, Oyo State
Hopewell J, Dvorak R, Kosior E (2009) Plastics recycling: challenges and opportunities. Phil Trans R Soc B 364:2115–2126
https://waste4change.com/blog/7-types-plastic-need-know/
https://worldarchitecture.org/article-links/egmeg/kenyan-startup-founder-nzambi-matee-recycles-plastic-to-make-bricks-that-are-stronger-than-concrete.html
https://www.downtoearth.org.in/news/waste/an-indian-consumes-11-kg-plastic-every-year-and-an-average-american-109-kg-60745. 2018/06/04
https://www.engineeringforchange.org/solutions/product/replast/
https://www.gjenge.co.ke/
Khoo HH (2019) Resources, conservation & recycling LCA of plastic waste recovery into recycled materials, energy and fuels in Singapore. Resour Conserv Recycle 145:67–77
Kibert C (1994) CIB-TG16. In: Proceedings of the first international conference on sustainable construction, Tampa, FL, USA
Kofi S, Kofi E, Dapaah S (2019) Plastic waste to fuel via pyrolysis: a key way to solving the severe plastic waste problem in Ghana. Therm Sci Eng Prog 11:417–424
Konin A (2011) Use of plastic waste as binding material in tiles, materials and structure
Navarro FJ, Partal P, Martinez-Boza FJ, Gallegos C (2010) Novel recycled polyethylene/ground tire rubber/bitumen blends for use in roofing applications: thermo-mechanical properties. Polymer Testing 29(5):588–595
Overview of Plastic Waste Management by CPCB (2017)
Pacheco EBAV, Ronchetti LM, Masanet E (2012) Resources, conservation and recycling an overview of plastic recycling in Rio de Janeiro. Resour Conserv Recycle 60:140–146
Ragaert K, Delva L, Van Geem K (2017) Mechanical and chemical recycling of solid plastic waste. Waste Manage 69:24–58
Vasudevan R, Ramalinga Chandra Sekar A, Sundarakannan B, Thiagarajar College of Engineering (TCE). Madurai on “plastone block—a precast structure made with waste plastics and stone aggregate and its use in toilet construction”
Yin S, Rajarao R, Gong B, Wang Y, Kong C (2019) Thermo-delamination of metallised composite plastic: an innovative approach to generate Aluminium from packaging plastic waste. J Clean Prod 211:321–329
Zhang M (2001) Slate made with plastic mix (PVC; CPVC; PVDC; ABS; ASA y EVA). European Patent

Analysis of Seismic Forces for Earthquake-Resistant Constructions

Kakade Maheshkumar Anant and P. S. Charpe

Abstract Earthquakes are the sign of change in our earth's inner crust. The past earthquake encounters have exhibited gigantic death threats and infrastructure, influencing the social and monetary states of a. However, it is unimaginable to expect to prevent an earthquake, and all today's technology is capable of making infrastructure earthquake safe. With the advancement in our comprehension of the earthquakes, most of the nations have commanded the cooperation of seismic provisions in building plan and engineering. In case of an earthquake, the seismic waves starting from the centre are sent in all the potential bearings. These shock waves propagate as body waves and surface waves through the interior of earth and are profoundly arbitrary in nature. These ground movements cause buildings to vibrate and instigate dormancy powers in the structures. Without a seismic plan, the structure may fall leading to catastrophic events. The seismic plan theory intends to principally ensure life safety and gets the usefulness of the structure. The paper means to make a statement about the earthquake-safe structures in different seismic zones. The impacts of plan and form configuration on irregularly shaped structures are discussed in this study. Seismic activity affects buildings with uneven geometry in diverse ways. The plan geometry is the parameter that determines how well it performs under various loading situations. Using the structural analysis programme STAAD Pro. V8i, the influence of irregularity (plan and form) on structure was investigated. There are numerous elements that influence how a building behaves, and storey drift and lateral displacement are two of the most significant in understanding how a structure behaves. Graphs and bar charts are used to display the results. According to the research, a basic layout and configuration must be selected at the planning stage to reduce earthquake effects.

Keywords Earthquake · Building · Irregular plan · Irregular shape · Seismic forces · Construction techniques

K. M. Anant · P. S. Charpe (✉)
Kalinga University, Raipur, India
e-mail: mak7133@gmail.com

J. K. Deka et al. (eds.), *Emerging Technology for Sustainable Development*,
Lecture Notes in Electrical Engineering 1061,
https://doi.org/10.1007/978-981-99-4362-3_16

1 Introduction

Earthquakes and their devastating effects have been influential in determining recorded civilization, and since the beginnings, acquiring knowledge to foresee or avoid earthquake hazards is still an important component of human search for information (Takagi and Wada 2019). Earthquake-resistant construction has been on radar of technology evolution since the beginning of modern construction techniques. Shock proof and vibration proof de- sign of buildings have been carried out since the old times. However, most of the innovation has been carried out to prevent loss of human beings than techno-economics aspects of these structures. Buildings that are constructed in a modern way are permitted during the event of an earthquake to go through plastic deformation, wherein building supporting structures as well as steel in the joints helps the structure from getting collapsed. This is also the major reason for economic damage as the time it takes for the structures to renovate again and cost for their construction. Thus, for the structures to continue their activity immediately after the event it has become need of the day to design structures so that they can bear the loss caused by earthquake and can sustain their functionality even after that (Ortega et al. 2017; Krinitzsky et al. 1993).

Without significant breakdown, all traditional technologies for earthquake-resistant construction help the structures with the possibility of withstanding enormous seismic forces. These advancements can be arranged into the groups given below:

1. Development strategies that use malleable development materials, like wood and bamboo houses.
2. Development advancements, like constructions with symmetric arrangement and elevation, use robust design styles.
3. Development innovations, like structures with groups and supports, that utilization robust primary setup.
4. Development advances decreasing seismic forces, for example, utilization of lightweight non-structural members (Elnashai and Sarno 2008).

Correlation of different techniques for their seismic reaction is profoundly requested for different various sorts of building developments to augment their safety. This will prevent human, monetary, and structural loss during an earthquake. To better understand the tensile capacity, both mathematical and simulation techniques must be utilized to identify the response of infrastructure (Aiello et al. 2018). For the effects of seismic forces, utilization of distributed multiple tuned mass dampers can be isolated and can be added to the foundation or base of the structures. This innovation can be extended even in low rise structures to give insurance to those structures. Schools, clinics, power plants, and gas/fire stations might get colossal advantages from this innovation (Sayin et al. 2019).

There is a strong interest for new speculation in the development field for concealment of seismic forces which require arrangement of new designs, more robust assessment of reaction of new plans, and materials utilized in structures. New strategies for underlying uprightness assessment are along these lines required for this reason (Artino et al. 2019; Deng et al. 2020; Wang et al. 2018; Patil et al. 2018).

2 Review of Works

This section presents the literature review of work carried out in the field of earthquake-resistant construction so as to reduce seismic forces acting on them. This includes different construction material, structures and configurations, and conventional and modern techniques.

In (Takagi and Wada 2019) the author examines the requirement for new intuition for making building framework to oblige the prerequisites of life saving methodology as well as for monetary and business improvement also. The construction of the structures ought to be with the end goal that they ought to get effectively and immediately reestablished even after a significant seismic earthquake. The present plans permit plastic disfigurements with the goal that they disperse the energy from the earthquake while denying the structural breakdown and loss of human existence. In any case, it sets aside long effort for full recuperation of the structure which brings about tremendous monetary misfortune. Henceforth, there is a need to configuration structure which follows seismic separation component utilizing superstructure innovation.

In (Ortega et al. 2017) the author audits the most regularly utilized strategies for seismic forces safe constructions created by individuals throughout past. They present a contextual analysis of Portugal culture of raising earthquake-safe structures. Notwithstanding, this idea is losing its hold as development business is increasingly more centred around raising the constructions rapidly and at least expense which does not settle for the safety. Subsequently, it is important to readopt the prior demonstrated development innovation.

In (Krinitzsky et al. 1993; Elnashai and Sarno 2008) author examines the basics of earthquake-safe constructions and their plan. They work on different parts of seismic demonstrating, reaction of various constructions for that displaying, strategies to address the interest that it induces and its assessment. They additionally talk about substitute ways to deal with earthquake to lessen the effect of seismic waves on the constructions. The utilization of glass shade allotments is quickly filling in the places of advanced engineering. They have one day represented obliteration in the wake of experiencing earthquake developments. The conduct of such frameworks under seismic forces is examined in these compositions.

The author in Aiello et al. (2018) commits to aim toward upgrading the usefulness of suppliers and designers. Structures might have phenomenal durability against leftover power applying underlying burden, but earthquake involving deficient limit involving earthquake forces against tension and compression. Seismically reinforcing their development is crucial as to get their underlying assurance and to broaden their useful life.

The review introduced in Sayin et al. (2019) adopts the strategy of supporting a notable arrangement of workmanship that has been built in the late nineteenth century, however, abandoned for quite a long while. Around 74% of private properties were built in Italy before 1980, while 25% of the district was marked as seismic. Right around 86% were introduced before 1991, while the essential prohibitive power yield law was passed. Numerous families need any seismic and power security development to build their level of supportability. For supported cement outlined houses, the recommended blended retro-fit approach is primarily founded exclusively on the expulsion of the external layer of double-leaf infill walls (Artino et al. 2019).

Modular steel construction (MSC) includes volumetric components and on-site fabrication assembled off-site. When the ceiling height rises, the effect of the earthquakes is important. An analysis of mid-to-high MSC seismic output is described in Deng et al. (2020). The goal is to facilitate the further widespread application of MSC in earthquake zones.

Masonry work develops for the most part of the world happens by and by and is still in existence. These homes are in charge of high outside loadings demanded with the guide of earthquake, heavy winds, blasts, and so forth. Some advanced seismic retro- fitting and reinforcing structures are developed and applied in these recent years to the construction (Wang et al. 2018).

Indeed, even in India, just about 80% of Delhi's homes, the capital of India, are not earthquake inclined. Parallel strain opposing gadgets, for example, chevron supports, knee supports are situated in total with aluminium shear hyperlinks to limit the effect of the earthquakes on the levied frameworks (Patil et al. 2018).

Multi-storey houses are cause for wind or lateral masses. Structures might be built through a few methodologies to bring down these lateral masses. The conduct of primary diaphragm for the length of the seismic waves on their general yield is being noticed (Jereen et al. 2017).

Because of more than one known attributes, wood frameworks generally delivered excellent seismic by and large execution. The consequences of the last worldwide earthquake have essentially shown that the seismic wooden design can be changed along these lines (Ugalde et al. 2019). Today, wooden constructions target higher statures and face various serious seismic models. As an area of interest in wood designing science, seismic protection technologies (SPTs) have emerged.

Precast cement works with a development technique utilizing strong and quickly erectable pre-assembled individuals to make economical and great designs. The associations between the precast individuals just as between the individuals and the establishment require extraordinary regard for guaranteed seismic execution (Kurama et al. 2018).

The authors of Nath et al. (2018) present extreme strategies for improving the seismic efficiency of houses and bridges. The investigation focuses on the impact of various insulators and dampers on building damage prevention. The multi-level pipe damper (MPD) is a static control device suggested by the authors in Zahrai and Cheraghi (2017) to reduce seismic activity. The seismic performance of structural steel with MPDs is discussed. MPD may be utilized as a maintenance and repair method for structures in severe seismic zones.

During the structure interaction for the rope connect with slant development, it was discovered that there is no reconciliation between the dock and the foundation. When a quake strikes, the design will almost certainly overturn or the foundation turntable will break down. The differentiating pin at the centre of the ball-end turn has significant shearing strength under the 6° and 7° tremor adequacy. The seismic strides for gathering anchor bars at the turntable's edges are proposed in the investigation (Xiao et al. 2019). In the field of wood engineering, the creation of cross-laminated wood (CLT) is be- coming commonplace. As a result, early adopters should avoid developing and constructing CLT systems in earthquake-prone areas. (Tannert et al. 2018) Shows the most recent seismic design of CLT structures.

In (Quezada et al. 2021) author some of the strategies utilized for investigation for earthquake safe plan which incorporate comparable horizontal power strategy and reaction range examination. They likewise give relative investigation of both these techniques. It is seen that assuming R factor is under 6, it is proposed to perform nonlinear reaction history investigation.

The authors of Arya (2018; Mashal and Palermo 2019) suggest an earthquake-resistant masonry building de- sign. These structures are extremely heavy, with no discernible tensile strength and poor wall construction. They recommend that building walls be reinforced vertically with steel to provide them enough flexibility to withstand seismic pressures. Accelerated Bridge Construction (ABC) has been tried in low seismic regions (Shekhar et al. 2018; Saravanan et al. 2018). ABC has only been used in areas with high seismic activity. The linkages attempt to replicate the typical production of plastic hinges within the side of bridge columns by an earth- quake. Seismic isolation devices are used to reduce the effects of earthquakes (Stanikzai et al. 2019; Anwar and Dong 2020). The bottom shear and displacement are reduced, while ground acceleration and inter-storey drift increase.

Blue mussels can be found sticking to rocks and ocean decks up and down the shore of New England. In between of their twin sea shells emerges a stingy outcrop of cabling which helps them to be anchored in their place. Normally, even the most incredibly elevated tides cannot pry them free. To remain appended to their shaky roosts, mussels emit tacky filaments known as byssal strings. A portion of these strings are firm and inflexible, while others are adaptable and flexible. Specialists are attempting to join this specific component into structures to cause the structure to withstand earthquakes.

A team at Blume Earthquake Engineering Centre, USA, led by Deierlein are working on an innovative innovation known as the shaking outline, which comprises of three fundamental parts, namely steel outlines, steel links, and steel wires. During a seismic occasion, energy-dispersal is assigned to a wire while the post-tensioning (PT) links re-establish the edge to its underlying setup. At the point when a seismic tremor strikes, the steel outlines rock all over. The entirety of the energy gets coordinated descending to a fitting that houses a few tooth-like wires. The teeth of the wires grind together and may even fizzle; however, the actual edge stays unblemished. When the shaking has halted, the steel links in the casing pull the structure once again into an upstanding position. Labourers then, at that point, investigate the circuits and supplant any that are harmed. The benefit is that the structure can be reoccupied rapidly after a seismic tremor.

Seismic invisibility is a term used to describe the invisibility of earthquake cloak—A sequence of boreholes is drilled around the perimeter of the structure to be protected.

These boreholes appear to act as a seismic cloak, shielding a building—or maybe a whole city—from the devastating waves of an earthquake. Isolators, dampers, and other vibration response control devices are no longer necessary.

Cardboard can be used as a strong and long-lasting construction material. Several constructions constructed by Japanese architects use polyurethane-coated cardboard tubes as the major frame elements. The Transitional Cathedral in Christchurch, New Zealand, was built from 98 massive cardboard tubes and wooden beams. The cardboard-and-wood construction is exceptionally light and flexible, outperforming concrete during seismic events by a wide margin. It is also less likely to crush those who are within if it does collapse.

Levitating houses—A Japanese company has developed an idea where a house in stable condition rests on a deflated airbag. When the sensors detect a vibration, they switch on the compressor which turns pumps the air into this bag. This airbag lifts the house by 3 cm from its foundation. The structure will hover for the duration of the quake, then the airbag deflates, and the structure settles to its original condition. This technique can be fitted to new homes of appropriate weight and also can be used to retrofit the existing house.

Another research team from ARX PAX (California) has filed a patent for the levitating house. The mechanism is quite different from the Japanese, and this may find wide applications is tall buildings. A three-part foundation system is used to support a structure in this method. A containment vessel, a buffer medium, and a construction platform are what they are. The buffer medium can be a fluid, a gas, or a liquefiable solid, and the building can be built on the construction platform. The containment vessel is subjected to lateral forces which transfer the load to the buffer medium. This medium acts as a damper and significantly reduces the forces being transmitted to the building. The system can levitate the building for around 90seconds which are considered as the average time of the earthquake.

Eco-friendly ductile cementations composite (EDCC) spray—A research team from the University of British Columbia (Vancouver, Canada) has developed a new radical approach to make the buildings resist earthquakes. EDCC combines cement with polymer-based fibres, flash, and other additives in making it eco-friendly and has been engineered at a molecular level to be strong and malleable at the same time. This material when applied as a thin coating (10 mm), was found to have improved seismic resistance of the structure by withstanding an earthquake of intensity 9–9.1 on Richter scale (Tohoku earthquake, Japan, 2011). At present, this technique has been suggested for retrofitting of the existing structures such as an elementary school building in Vancouver.

2.1 Research Gaps Identified in Proposed Research

The focus of this research is to propose technologies to be used in earthquake-resistant construction of buildings and structures so as to reduce the effect of seismic forces acting on them during the actual occurrence of the quake. From the literature review, following research gaps were identified.

(a) Use of dampers for seismic isolation such as multi-tuned mass dampers and multi- level yielding pipe damper is still not fully explored for modern constructions.
(b) There is a need to develop technologies so as to protect timber structures from seismic forces to further improve their design.
(c) Modular steel structure is used in construction as the whole structure may not be feasible to manufacture on-site. As such there is demand in conducting seismic performance in mid-to-high-rise buildings where modular steel structure is used.
(d) There is a huge gap in research concerning retrofitting of old buildings without seismic resistance with modern techniques for their protection from earthquakes. The research gaps show that the seismic performance of the timber structures can further be improved by using modern techniques. The use of modular steel structure which has proven its performance in low-rise buildings is now getting popular with mid-to-high-rise buildings, and thus, there is a need to conduct its analysis. Mass dampers need to be studied in more depth for isolating the building from seismic forces.

2.2 Significance and Scope of the Study

The significance and scope of this work is to evaluate existing methods for earthquake-resistant construction and propose a design which help suppress seismic forces acting on them. Earthquake fundamentals like its occurrence, causes, related terminologies, assessment of the site of occurrence, and ground designs consisting of its motions are studied in detail. Based on this study, various methods to suppress seismic forces acting on the structures were evaluated using numerical and simulation techniques. It was concluded that use of single damper for seismic isolation of buildings proved inefficient in case of major earthquakes. Moreover, non-engineered and masonry buildings which are cheap alternatives to more reformative and complex structures suffer heavy loss during an occurrence of earthquake.

To overcome these disadvantages, use of multiple mass dampers, earthquake-resistant materials and structures, and modular steel structure in low-to-high-rise buildings is suggested. Comparison of various structures and materials was done using numerical and simulation platform, and new design of structures and its material was proposed for reduction of seismic forces acting on them. Moreover, use of mass dampers was studied in depth for its role in seismic isolation of buildings, its response was improved by placing multiple dampers on site, and its performance was evaluated using simulations.

2.3 Objectives of Proposed Study

The aim of this research work is to propose and evaluate construction technologies which help in reducing seismic forces for earthquake-resistant construction. Apart from this below are basic objectives of this project:

- To study literature and analyse techniques used for earthquake-resistant construction.
- To propose the state-of-the-art techniques for reducing seismic forces on building structures.
- To propose materials and structures to be used for non-engineered building constructions for resisting damage due to earthquake.
- To calculate seismic response of proposed techniques and to verify whether the design is complacent according to guidelines specified in IS:4326.

3 System Model

Seismic loading and analysis have grown increasingly important in recent years all around the world. This is primarily owing to the high frequency of big-magnitude earth- quakes that have been seen, especially in large urban areas, and which have generally resulted in terrible loss of life. As a result, more effort has been put into understanding and quantifying the loads that could be encountered during an earthquake. However, depending on the seismicity, soil characteristics, natural frequency of the building, and anticipated usage of the structure, this approach has been improved to allow progressively appropriate designs (Elnashai and Sarno 2008). Buildings have longer durations of vibration and periods of vibration that are mostly orthogonal and tightly spaced. As a result, the equivalent static analysis approach was used to design structures and counteract the effects of earthquakes. In this work, it has been used IS 1893-2002 to do static analysis. It has been created 9 models in STAAD Pro V8i programme to investigate the effects of irregular plan and form configuration. To achieve the expected behaviour, several forms of input data were used to build all nine models. The many forms of data used to create the models are listed Tables 1, 2 and 3.

Table 1 Load data

Live load (kN/m^2)	3
Roof live load (kN/m^2)	1
Floor finish (kN/m^2)	1

Table 2 Seismic definition

Earthquake zone	III
Damping ratio	5%
Importance factor	1
Type of soil	Medium soil
Type of structure	All general RC frame
Response reduction factor	5 [SMRF]
Time period	Program calculated
Foundation depth	2 m
Poison's ratio	0.15

Table 3 Geometric and material data

Density of RCC considered (kN/m^3)	25
Thickness of slab (mm)	160
Depth of beam (mm)	380
Width of beam (mm)	300
Dimension of column	300 mm × 450 mm
Density of infill (kN/m^3)	20
Thickness of out wall (mm)	230
Height of each floor (m)	3.4
Poison's ratio	0.15
Conc. cube comp. strength, fck (N/mm^2)	20,000
Bending reinforcement yield strength, fy (N/mm^2)	415,000
Shear reinforcement yield strength, fys (N/mm^2)	415,000
Beam rebar cover (mm)	30
Column bar size	12 φ

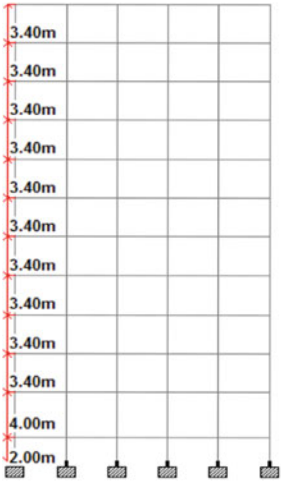

Fig. 1 Elevation of model

These 9 models are created by taking into account plan irregularities, which means that the plan area of each construction is the same, but the geometry differs. The total number of storeys for all sorts of structures is 12. All nine models have the same elevation. The height distribution of each floor is shown Figs. 1, 2, 3, 4, 5, 6, 7, 8, 9 and 10.

4 Results

In STAAD-PRO V8i software, it has been compared the lateral displacement and storey drift of all 9 models with regard to each other. By comparing the results, one may quickly assess the structure's performance and forecast the best shape among all those that withstand earthquake forces. Below is a detailed analysis of each graph.

With plan irregularity, the structure's reaction to seismic pressures changes. The behaviour of the structure in response to these loads is monitored. For storey drift and lateral displacement, we have plotted graphs of individual structure. As a consequence, plus shape structures displaced more, which might be attributed to their lighter weight and thin geometry when compared to other building types. Under the specified loading circumstances, complex-shaped structures showed a substantial reaction in terms of nodal displacement and storey drift when all of the aforesaid elements were taken into account. As a result, we may conclude that basic form geometry of structures should be used to reduce the impacts of seismic activities (Figs. 11, 12, 13 and 14).

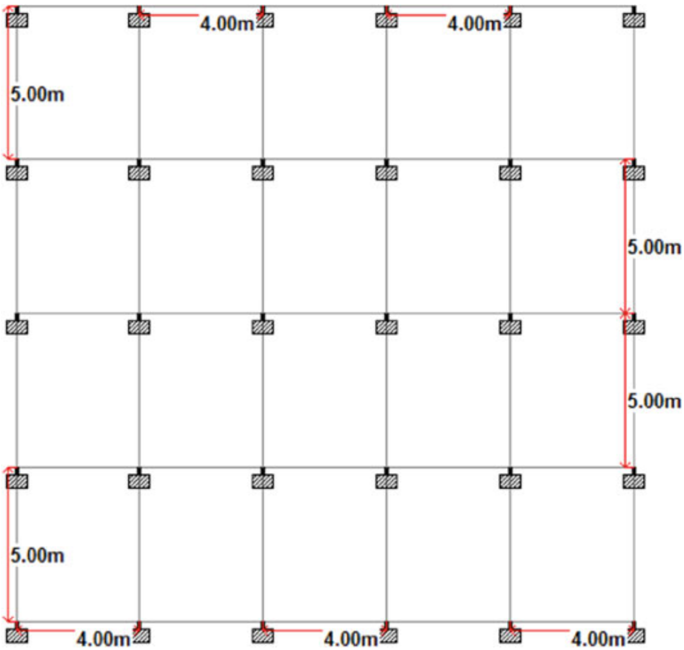

Fig. 2 Regular square (S-1)

Fig. 3 E-shaped (S-2)

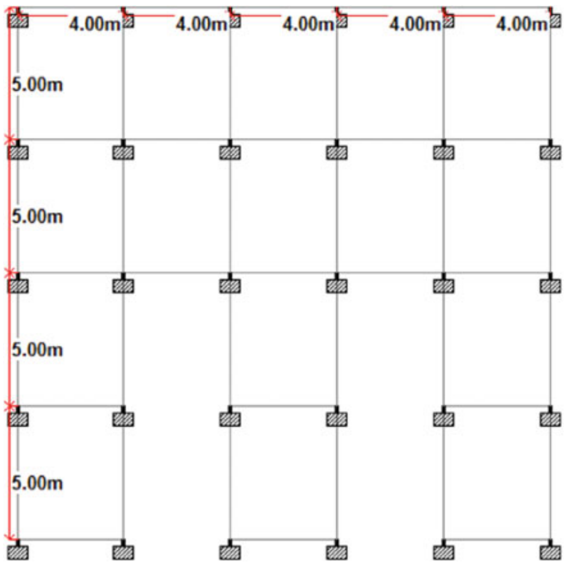

Fig. 4 H shape (S-3)

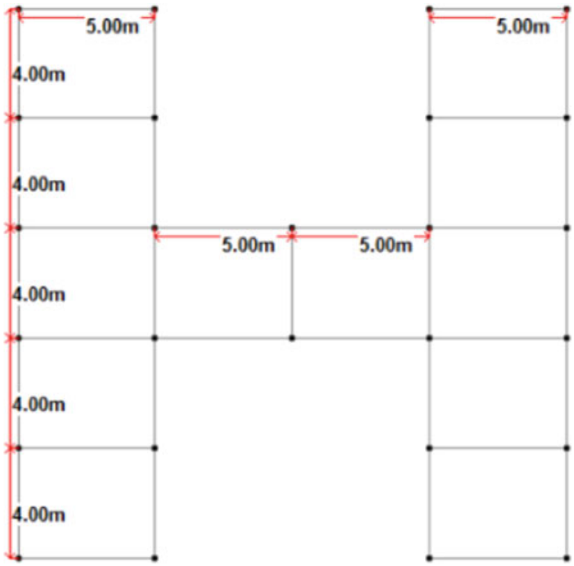

Fig. 5 T-shaped (S-4)

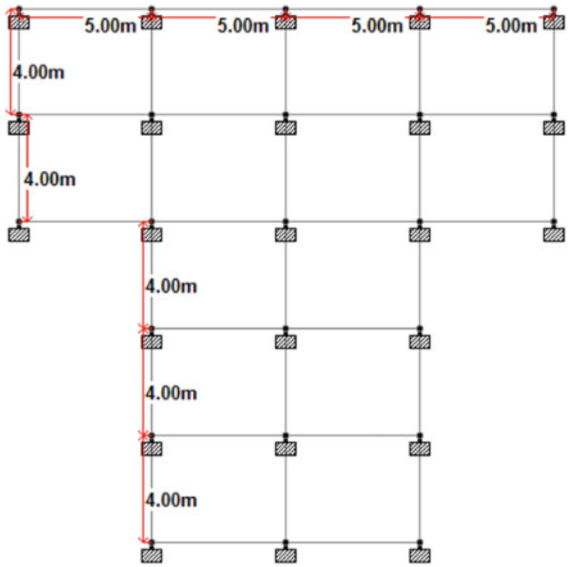

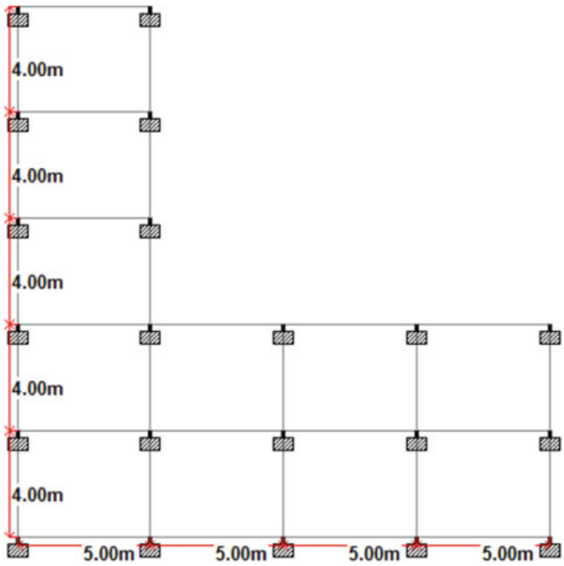

Fig. 6 L shape (S-5)

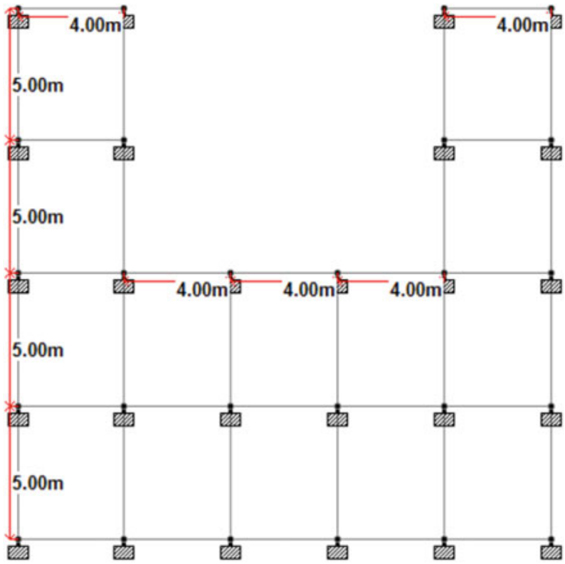

Fig. 7 C-shaped (S-6)

Fig. 8 Plus (+) shape (S-7)

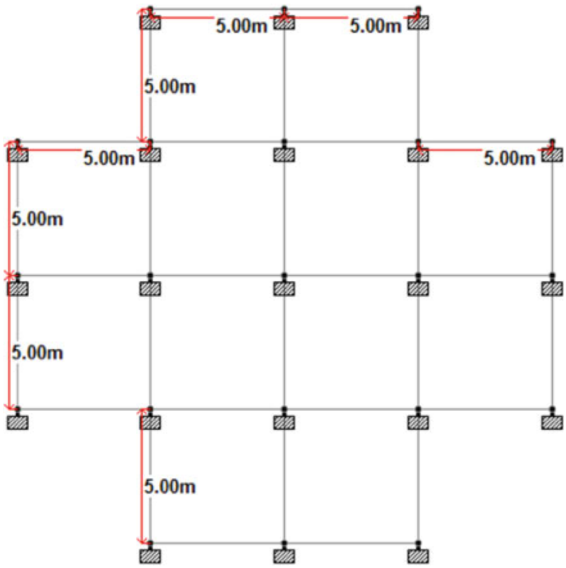

Fig. 9 Square with core (S-8)

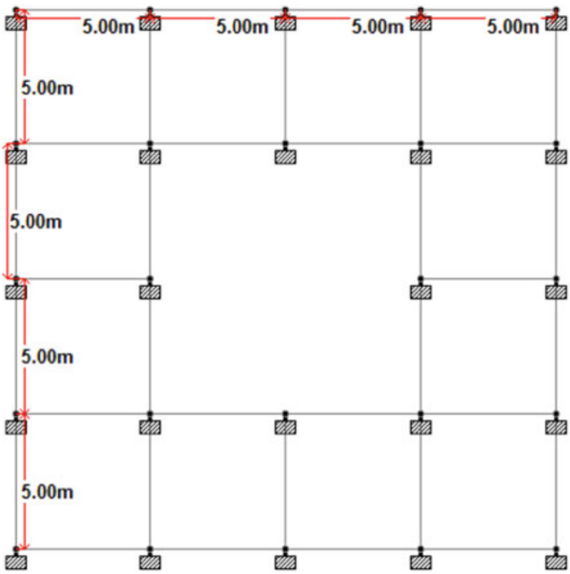

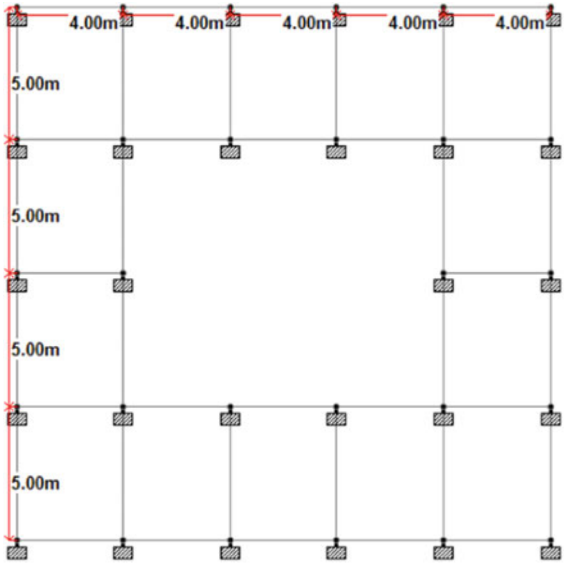

Fig. 10 Rectangle with core (S-9)

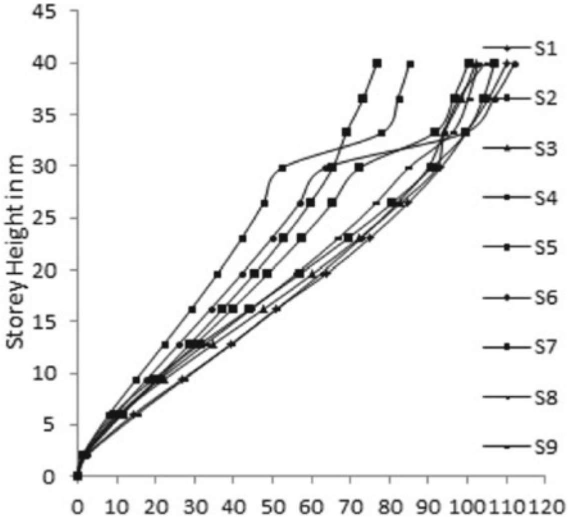

Fig. 11 Nodal lateral displacement in *X*-direction

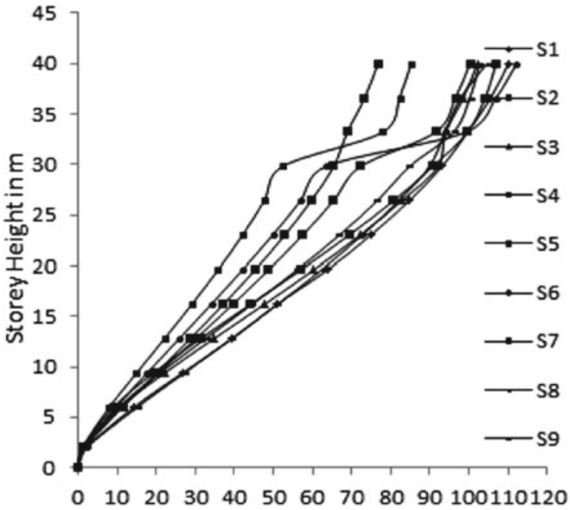

Fig. 12 Nodal lateral displacement in Y-direction

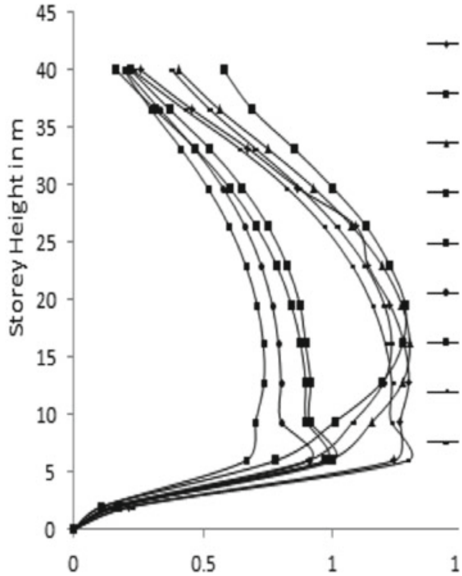

Fig. 13 Storey drift in X-direction

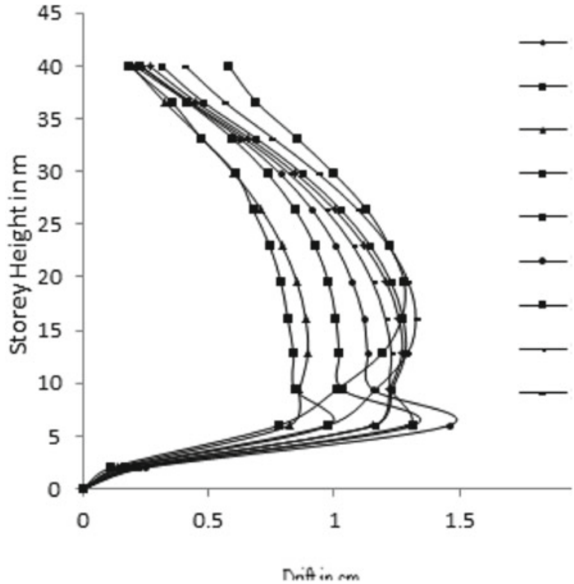

Fig. 14 Storey drift in Y-direction

5 Conclusion

All around the globe, researchers are trying to make low cost and well planned technology for earthquake resistant construction by using easily accessible resources. Like, in Peru, by reinforcing wally with plastic mesh, researchers have made much stronger traditional adobe structures much. In India, Bamboo have been used by engineers to strengthen concrete. And in Indonesia, few homes are built in a way so that they can stand on efficient bearings made by old tires that are filled with either sand or stone.

New innovative watts are in progress and researchers are working everyday on many new technologies that are being tested many times before running into practice. In the previous phase of the performance study, effects on selected models were displayed in the form of a graph and bar chart by comparing various parameters such as nodal displacements and storey drifts. As a result of the findings, the following conclusions may be drawn":

1. Considering the influence of lateral displacement on various forms of the structure's building. In contrast to other remaining basic shaped buildings, plus-shape, L-shape, H-shape, E-shape, T-shape, and C-shape buildings have displaced more in both directions (X and Y) (core-rectangle, core-square, and regular building).
2. While collecting the results from both software as per (IS 1893-2002), the storey drift, which is an important parameter to understand the structure's drift demand, is taken into account. The limiting value of drift for the given structure as per (7.11.1) is 16 cm, which is not exceeded in any of the structures, but L-shaped and C-shaped models showed larger drift than other shaped models".

3. Taking into account all of the previous findings based on the examination of irregular structures, we can conclude that simple geometry attracts less force and performs better during earthquakes. Complex geometries will inevitably be omitted, but they can be sorted into simpler ones by using seismic joints to decrease earthquake effects".

References

Aiello C, Caterino N, Maddaloni G, Bonati A, Franco A, Occhiuzzi A (2018) Experimental and numerical investigation of cyclic response of a glass curtain wall for seismic performance assessment. Constr Build Mater 187:596–609

Anwar GA, Dong Y (2020) Seismic resilience of retrofitted RC buildings. Earthquake Eng Eng Vibr 19(3):561–571

Artino A, Evola G, Margani G, Marino EM (2019) Seismic and energy retrofit of apartment buildings through autoclaved aerated concrete (AAC) blocks infill walls. Sustainability 11(14):3939

Arya AS (2018) Earthquake resistant design of masonry buildings. In: Advances in Indian earthquake engineering and seismology. Springer, Cham, pp 259–271

Deng E-F, Zong L, Ding Y, Zhang Z, Zhang J-F, Shi F-W, Cai L-M, Gao S-C (2020) Seismic performance of mid-to-high rise modular steel construction—a critical review. Thin-Walled Struct 155:106924

Elnashai AS, Sarno LD (2008) Fundamentals of earthquake engineering. Wiley, New York

Jereen AT, Anand S, Issac BM (2017) Seismic evaluation of buildings with plan irregularity. Appl Mech Mater 857:225–230

Krinitzsky EL, Gould JP, Edinger PH (1993) Fundamentals of earthquake-resistant construction, vol 51. Wiley

Kurama YC, Sritharan S, Fleischman RB, Restrepo JI, Henry RS, Cleland NM, Ghosh SK, Bonelli P (2018) Seismic-resistant precast concrete structures: state of the art. Ph.D diss., American Society of Civil Engineers

Mashal M, Palermo A (2019) Emulative seismic resistant technology for accelerated bridge construction. Soil Dyn Earthq Eng 124:197–211

Nath S, Debnath N, Choudhury S (2018) Methods for improving the seismic performance of structures: a review. IOP Conf Ser Mater Sci Eng 377:012141

Ortega J, Vasconcelos G, Rodrigues H, Correia M, Lourenço PB (2017) Traditional earthquake resistant techniques for vernacular architecture and local seismic cultures: a literature review. J Cultural Heritage 27:181–196

Patil R, Naringe A, Kalyana Rama JS (2018) Novel techniques for seismic performance of high rise structures in 21st century: state-of-the art review. IOP Conf Ser Mater Sci Eng 330:012126

Quezada E, Serrano Y, Huaco G (2021) Dynamic amplification factor proposal for seismic resistant design of tall buildings with rigid core structural system. In: Proceedings of the 5th Brazilian technology symposium. Springer, Cham, pp 245–256

Saravanan M, Goswami R, Palani GS (2018) Replaceable fuses in earthquake resistant steel structures: a review. Int J Steel Struct 18(3):868–879

Sayin B, Yildizlar B, Akcay C, Gunes B (2019) The retrofitting of historical masonry buildings with insufficient seismic resistance using conventional and non-conventional techniques. Eng Fail Anal 97:454–463

Shekhar S, Shukla SP, Zafar S (2018) Seismic isolation devices, Oct 2018

Stanikzai MH, Elias S, Matsagar VA, Jain AK (2019) Seismic response control of base-isolated buildings using multiple tuned mass dampers. Struct Des Tall Special Build 28(3):e1576

Takagi J, Wada A (2019) Recent earthquakes and the need for a new philosophy for earthquake-resistant design. Soil Dyn Earthq Eng 119:499–507

Tannert T, Follesa M, Fragiacomo M, Gonzalez P, Isoda H, Moroder D, Xiong H, van de Lindt J (2018) Seismic design of cross-laminated timber buildings. Wood Fiber Sci: 3–26

Ugalde D, Almazán JL, María HS, Guindos P (2019) Seismic pro tection technologies for timber structures: a review. Euro J Wood Wood P rod 77(2):173–194

Wang C, Sarhosis V, Nikitas N (2018) Strengthening/retrofitting techniques on unreinforced masonry structure/element subjected to seismic loads: a literature review. Open Constr Build Technol J 12(1)

Xiao J, Liu M, Zhong T, Fu G (2019) Seismic performance analysis of concrete-filled steel tubular single pylon cable-stayed bridge with swivel construction. IOP Conf Ser Earth Environ Sci 218(1):012087

Zahrai SM, Cheraghi A (2017) Reducing seismic vibrations of typical steel buildings using new multi-level yielding pipe damper. Int J Steel Struct 17(3):983–998

Strength Performance Study of Concrete with Partial Replacement of Sand with ROBO SAND and Cement with GGBS

Mrinal Kanti Sen, Supran Chakravarty, and T. R. Girija

Abstract This study aims at replacing sand and cement with ROBO sand and ground granulated blast furnace slag (GGBS) in the concrete mix. Here, GGBS and ROBO sand are chemically and physically characterized and used to replace cement and sand in different proportions. Tests on workability were conducted for fresh concrete, various strength tests were conducted for hardened M30 grade of concrete, and a comparative study was done with normal concrete and composite concrete with GGBS and ROBO sand in different proportions. Increase in compressive strength after 28 days was observed with 15% GGBS along with 20% ROBO sand. Similar trend was observed in the case of split tensile strength and flexural strength test.

Keywords GGBS · ROBO sand · Partial replacement · Compressive strength · Split tensile strength · Flexural strength

1 Introduction

Materials, which are the essential components of buildings construction, are usually selected through functional, technical, and financial requirements. Mechanical strength of the building is significantly influenced by chemical, physical, and mechanical properties of materials and an appropriate design. Hence, the green buildings design should start with the identification of sustainable materials with similar or enhanced characteristics compared to conventional building materials. With the advancement of "green buildings", there is an increasing trend to identify better techniques for saving both resources and energy. Green building design is comparatively a new episode in the construction industry. Developing nations like India are adopting development schemes that encourage sustainability as a national master plan. As the cost of concrete is very high, for economic purposes, the replacement of concrete ingredient with other materials should be taken care of.

M. K. Sen · S. Chakravarty (✉) · T. R. Girija
Assam Don Bosco University, Azara 781017, India
e-mail: supran.chakravarty@dbuniversity.ac.in

J. K. Deka et al. (eds.), *Emerging Technology for Sustainable Development*,
Lecture Notes in Electrical Engineering 1061,
https://doi.org/10.1007/978-981-99-4362-3_17

Concrete consists of binding material, fine and coarse aggregates, and water (Popovics 1992). Cement, the conventional binding material, is very costly, and its manufacturing process is accompanied by undesirable environmental consequences like release of carbon dioxide (CO_2) (Muradov and Veziroğlu 2005). River sand, the conventional fine aggregate, has become a diminishing resource, and its exploitation resulted in deterioration of river bed and drop in groundwater recharge (Annal and Rachel 2016). Here comes the need of identifying a substitute for these ingredients in the construction field. Studies conducted by Naceri and Hamina (2009) used waste brick to partially replace cement and studied the strength of mortar (Naceri and Hamina 2009). Marthong (2012) partially replaced cement with sawdust ash, to assess the performance of concrete (Marthong 2012). Tamanna et al. (2020) explored the durability and strength of concrete by partially replacing sand with recycled waste glass (Tamanna et al. 2010). Suresh and Nagaraju (2015) conducted tests on compressive strength of concrete with partial replacement of sand with ground granulated blast furnace slag (GGBS) (Suresh and Nagaraju 2015). It has been observed that the maximum of studies is conducted by replacing any one of the ingredients of cement or sand with a single material. So, in this study, an effort has been made to produce concrete using sustainable materials replacing the ingredients of concrete partially. One of the by-products of steel production, namely ground granulated blast furnace slag (Babu and Kumar 2000), was used to partially replace the cement. Also, quarry stone dust (also known as ROBO sand), a by-product obtained during quarrying of stone, was used as an substitute of fine aggregate that entirely replaces the river sand which is superior in quality as compared to river sand in all aspects. Although, a study has been done with 40–60% (with 10% increment) replacement of cement with GGBS and 0–30% (with 5% increment) replacement of sand with ROBO sand (Malagavelli and Rao 2010). However, the drawback of this study is that 0–30% replacement of GGBS with cement is not done yet. The authors have not performed all the tests, such as flexural and split tensile tests. Therefore, in this study, various combinations have been made for mix design of concrete with different proportions of GGBS (such as 0–30%, at 10% increment) and ROBO sand with sand. Characteristics of concrete were studied in fresh state as well as hardened states for all mentioned proportions and arrived at the conclusions.

Concrete is a brittle material, and it is fragile in tension (Akita et al. 2003). The idea of using GGBS and ROBO sand separately to improve building materials' properties is ancient. The studies started with reinforced horsehair plaster with clay bricks and asbestos reinforced ceramics. It is essential to be careful in concrete placement with equal importance as in reinforced concrete to increase the strength and ductility. Nowadays, constituents' materials which are required for manufacturing concrete are expensive due to the unavailability of the same. Non-judicious use of few ingredients of concrete also affects the environment which poses undesirable consequences (Meyer 2009). Scarcity and rising cost of natural river sand which is one of the ingredients of concrete has led to identifying materials to replace the river sand without sacrificing the required properties of concrete in both fresh and hardened condition. Dust produced from granite crushing plants (crusher dust) is

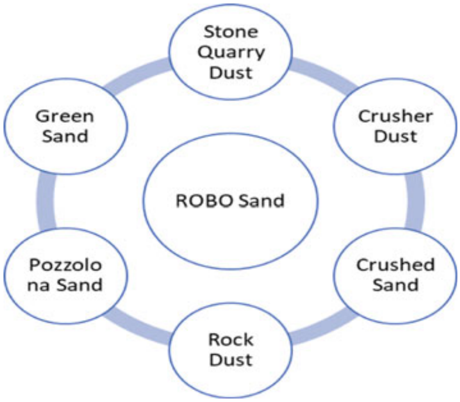

Fig. 1 Different standard terms used for ROBO sand

a suitable replacement for river sand (Mir 2015). It has several names as shown in Fig. 1.

ROBO sand is known to have better performance compared to conventional river sand and is cheaper than river sand, and cement which acts as the binding material in concrete is costly, and its manufacturing is a threat to environment. That is why GGBS which is a by-product of the iron manufacturing process is used to replace cement and is eco-friendly. To some extent, it can act as a cementitious material and can partially replace cement in concrete. GGBS saves 50% of the cost of same quantity of cement, and its replacement is expected to enhance characteristics of fresh as well as hardened concrete. A thorough study is needed for exploring the different proportion of GGBS and ROBO sand and its effect in both the forms of concrete.

The main objective is to study high-performance concrete incorporating GGBS and ROBO sand resulting in required strength characteristics. In the present investigation, the mix design for M30 concrete was done as per the procedure in IS 10262–2009 for both conventional concrete and composite concrete with ROBO sand and GGBS. Tests for compressive strength, split tensile strength, and flexural strength tests were conducted to evaluate the performance of composite concrete, compared with that of the conventional concrete. In this study, 10%, 20%, and 30% by weight of cement and fine aggregates were replaced with GGBS and quarry dust, respectively. Strength tests were conducted after 7 and 28 days of curing.

2 Literature Review

Several indigenous materials are being experimented to substitute the filler material and binding material in concrete. To optimize the cost and to utilize sustainable material from the iron industry effectively, cement can be substituted with GGBS partially in various proportions (Siddique and Bennacer 2012). It is known as a non-toxic and non-metallic by-product of the iron industry, which is environment-friendly and improves the strength, workability, and durability of concrete. Babu and Kumar (2000) presented an effort to quantify the 28 days cementitious efficiency of GGBS in concrete with different proportions and concluded with encouraging results (Babu and Kumar 2000). The strength efficiency factor varied from 1.29 to 0.70 for the proportion of 10–80%. The slump value increases by 60–85 mm when 100% fine aggregate is replaced with copper slag (Pazhani and Jeyaraj 2010). The values are reduced for chloride ion permeability, water absorption, and pH by 29.9, 4.58, and 0.39%, when 30% of cement is replaced with GGBS. When 100% of fine aggregate is replaced with copper slag, the above-mentioned parameters decrease by 77.32, 33.59, and 3.04%.

As studied by Nataraja et al. (2013), it has been stated that the application of GGBS is a suitable substitute to natural fine aggregate from the perspective of various types of strength (Nataraja et al. 2013). An investigation conducted by Patel et al. (2013) concludes that when fine aggregate for M35 concrete is replaced with crusher sand, it in turn increases the total strength of the concrete (Patel et al. 2013). Higher the replacement percentage, higher will be the compressive strength.

River sand, which is the filler material in concrete, has become a diminishing resource and expensive. Hence, the crusher dust (quarry stone dust) can be used as an alternative material for the river sand. Stone dust acquires similar properties as river sand and thus accepted as a building material. It basically contains angular particles with rough texture that pass through 4.75 mm sieve. Many researchers have investigated stone dust for several years to evaluate its characteristics and behavior. Bonavetti and Irassar (1994) observed that with 15% of sand replacement with stone dust, the highest strength was achieved (Bonavetti and Irassar 1994). Analysis by scanning electron microscope showed homogeneous mix with 15% replacement due to the filling of micropores and densification of transition zone. A linear increment of strength is observed with respect to replacement of sand with stone dust up to 15%. Further increase in percentage replacement results in decrease in strength gradually; hence, 15% replacement of sand with stone dust is found optimum.

3 Materials

The materials used in the research are: Portland cement of 43 grade, conforming to Indian Standard IS 12269-1987, aggregates (fine and coarse), ROBO sand, GGBS, and water, as depicted in Fig. 2. Various tests on aggregate are performed following Indian Standard Codes, which are discussed in the following section.

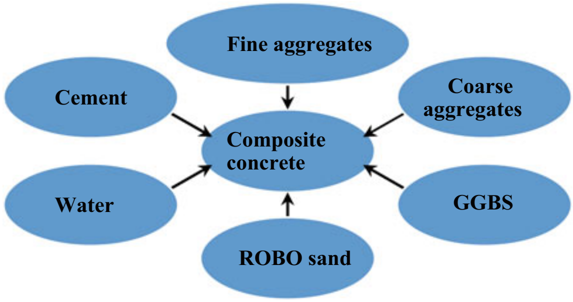

Fig. 2 Composition of composite concrete

3.1 GGBS

GGBS is a by-product obtained during the production of iron and steel. Carefully controlled mixture of iron-ore, coke, and limestone is fed at about 1500 °C temperature. Materials left out once the ore is reduced to iron form a slag which is seen floating on top of the iron. This is periodically taken out as a molten liquid and through rapid quenching in water with immense volumes of water to get the by-product GGBS. Similar to coarse sand, granulated particles are produced by optimizing the cementitious properties through quenching process. Further, the granulated slag is made in to fine powder after drying and grinding.

4 Experimental Study

Tests were carried out on all the ingredients and also on the resulting concrete to study the characteristics to ascertain if the constituents and the prepared concrete provide the expected value.

Fineness of cement was conducted following the procedure explained in IS: 4031 (Part 1)—1996. Standard consistency of cement was obtained using a Vicat plunger. The initial and final setting time of cement was estimated as per IS: 4031 (Part 5)—1988 using Vicat apparatus conforming to IS: 5513—1976. The specific gravity of cement was found out using the Le Chatelier flask with its stopper.

5 Methodology

Concrete specimens were cast replacing 10, 20, and 30% of cement with GGBS, and same percentage of replacement is used to replace the fine aggregate or sand with ROBO sand along with normal concrete mix. While replacing the cement with 10–20% GGBS, the strength of the concrete was observed to be at its highest value. So, to narrow down the precise range of partial replacement, numerous experiments were conducted at various percentages of partial replacement. The result obtained reflects that at 15% partial replacement of cement with GGBS, the concrete achieves an acceptable strength. Hence, in this section the mix design is prepared keeping 15% replacement of cement with GGBS constant. Casted cubes of conventional dimension were examined for 7 and 28 days of compressive strength. Cylindrical concrete specimens of standard dimension, i.e., having diameter of 100 mm and a height 200 mm were tested for 7 and 28 days for split tensile strength. Standard prisms were tested for flexural strength.

5.1 Mix Design

Concrete mix design is the exercise of determining the quantity of selected ingredients to produce a concrete of the required target strength, workability, and durability as possible with economic point of view. In both fresh and hardened states of concrete, assessment concerning the proportion of constituents was carried out. The strength to withstand compressive force for hardened concrete is influenced by characteristics and amount of cement, water, and aggregates. The properties of concrete also depend significantly on the processes of manufacturing such as batching, mixing, placing, compaction, and curing.

In design mix, the proportions are determined, with the exception that the minimum cement content can be laid down which is the most rational approach to select mix proportions with specific materials in mind possessing more or less unique characteristics. This approach results in economical concrete with appropriate properties. The factors influencing the mix design are compressive strength, workability, durability, aggregate size, type of aggregate, and quality control. The mix design considered for this study is having a mix proportion of 1:1.6:2.6, and the water content is 0.45.

6 Results and Discussion

The study has been carried out for a variety of percentages (0%, 10%, 20%, and 30%) of partial replacement of GGBS and ROBO sand with cement and fine aggregate, respectively. As it is mentioned in the previous section that at 15% replacement of cement with GGBS, the concrete attains its highest strength. Hence, in this section the results of various tests such as slump test, compressive test, tensile test, and flexural test were conducted keeping 15% replacement of cement with GGBS constant. A total of 4 class of cube specimen were prepared for this study, such as PC, CC1, CC2, and CC3, where PC denotes plain concrete with 0% replacement, CC1 denotes replacement of cement and sand with 15% GGBS and 10% ROBO sand, respectively, CC2 denotes replacement of cement and sand with 15% GGBS and 20% ROBO sand, respectively, and CC3 denotes replacement of cement and sand with 15% GGBS and

Table 1 Slump values

S. No.	Mix	Slump (mm)
1	PC	80
2	CC1	79
3	CC2	77
4	CC3	74

30% ROBO sand, respectively. In each class, 6 concrete specimen, 3 for 7 days and 3 for 28 days, were tested. A total of 72 concrete specimens were prepared for this study. From the values of Table 1, it can be observed that for replacement of fine aggregates with quarry stone dust or ROBO sand having partial replacement percentages 0% (plain concrete), 10%, 20%, and 30%, all the values of slump are acceptable for normal RCC works having medium workability as per IS 456:2000 as shown in Table 1.

The results of compressive test are represented in Table 2. The compressive strength of all the classes for 7 and 28 days is found to be CC1 < CC3 < CC2 < PC and CC1 < CC3 < PC < CC2, respectively. Comparing the strength of concrete for 7 and 28 days, it is noted that the initial strength gained by the specimen CC2 is lower than that of PC. But after 28 days, the strength of CC2 reaches its ultimate peak value which is 29.86 N/mm2 (more than 99% of the characteristics strength). Hence, it can be concluded that concrete of class CC2 gives relatively more compressive strength than PC.

The results of the tensile test are represented in Table 3. The tensile strength of all the classes for 7 and 28 days is both found to be CC3 < CC1 < PC < CC2. Comparing the strength of concrete for 7 and 28 days, it is noted that the strength of CC2 has increased nearly about 3% and 9%, respectively, compared to PC. Hence, it can be concluded that concrete of class CC2 gives relatively more tensile strength than PC.

Table 2 Compression test

S. No.	Mix	7 days (MPa)	28 days (MPa)
1	PC	19.12	28.76
2	CC1	16.38	27.71
3	CC2	18.09	29.86
4	CC3	17.89	28.26

Table 3 Tensile test

S. No.	Mix	7 days (MPa)	28 days (MPa)
1	PC	3.07	3.63
2	CC1	2.93	3.21
3	CC2	3.16	3.97
4	CC3	2.56	3.09

Table 4 Flexure test

S. No.	Mix	7 days (MPa)	28 days (MPa)
1	PC	4.13	5.09
2	CC1	3.97	4.82
3	CC2	4.47	5.28
4	CC3	3.66	4.57

The results of the flexural test are represented in Table 4. The tensile strength of all the classes for 7 and 28 days is both found to be CC3 < CC1 < PC < CC2, which follows a similar pattern as tensile test. Comparing the strength of concrete for 7 and 28 days, it is noted that the strength of CC2 has increased nearly about 8% and 4%, respectively, compared to PC. Hence, it can be concluded that concrete of class CC2 gives relatively more flexural strength than PC.

7 Conclusion

In this work, the performance of composite concrete with GGBS and quarry stone dust as partial substitute to cement and fine aggregate respectively was explored. Quarry stone dust which is more economical compared to river sand was proved to be the right substitute of river sand, and it satisfies all the specifications of IS Codes and also contained no impurities. The GGBS was observed to be used successfully as a substitute to cement to some extent, thus reducing the amount of CO_2 produced during cement production.

The tests done with design mix of M30 (1:1.6:2.6) with a water–cement ratio of 0.45 revealed that there is a decrease in slump with an increase in the proportion of quarry stone dust which can be attributed by the high-water absorption of quarry stone dust in the initial stage. Compressive strength, split tensile strength, and flexural strength were observed to be increased with 15% GGBS and 20% quarry stone dust after 7 and 28 days. Hence, composite concrete using GGBS and quarry stone dust proved to be successful for solving environmental problems and reducing the need for cement in large quantities. Therefore, the reuse of these by-products from steel industry and quarry in concrete is highly recommended to move toward sustainable development in the construction industry.

References

Akita H, Koide H, Tomon M, Sohn D (2003) A practical method for uniaxial tension test of concrete. Mater Struct 36(6):365–371

Annal AA, Rachel P (2016) Experimental study on behaviour of high performance concrete using GGBS and M sand. Int J Eng Res Technol (IJERT). ISSN: 22780181

Babu KG, Kumar VSR (2000) Efficiency of GGBS in concrete. Cem Concr Res 30(7):1031–1036
Bonavetti VL, Irassar EF (1994) The effect of stone dust content in sand. Cem Concr Res 24(3):580–590
Malagavelli V, Rao PN (2010) High performance concrete with GGBS and ROBO sand. Int J Eng Sci Technol 2(10):5107–5113
Marthong C (2012) Sawdust ash (SDA) as partial replacement of cement. Int J Eng Res Appl 2(4):1980–1985
Meyer C (2009) The greening of the concrete industry. Cement Concr Compos 31(8):601–605
Mir AH (2015) Improved concrete properties using quarry dust as replacement for natural sand. Int J Eng Res Dev 11(3):46–52
Muradov NZ, Veziroğlu TN (2005) From hydrocarbon to hydrogen–carbon to hydrogen economy. Int J Hydrogen Energy 30(3):225–237
Naceri A, Hamina MC (2009) Use of waste brick as a partial replacement of cement in mortar. Waste Manage 29(8):2378–2384
Nataraja MC, Kumar PD, Manu AS, Sanjay MC (2013) Use of granulated blast furnace slag as fine aggregate in cement mortar. Int J Struct Civ Eng Res 2(2):59–68
Patel M, Rao PS, Patel TN (2013) Experimental investigation on strength of high performance concrete with GGBS and crusher sand 3(4)
Pazhani K, Jeyaraj R (2010) Study on durability of high performance concrete with industrial wastes. Appl Technol Innov 2(2)
Popovics S (1992) Concrete materials: properties, specifications, and testing. William Andrew
Siddique R, Bennacer R (2012) Use of iron and steel industry by-product (GGBS) in cement paste and mortar. Resour Conserv Recycl 69:29–34
Suresh D, Nagaraju K (2015) Ground granulated blast slag (GGBS) in concrete—a review. IOSR J Mech Civ Eng 12(4):76–82
Tamanna N, Tuladhar R, Sivakugan N (2010) Performance of recycled waste glass sand as partial replacement of sand in concrete. Constr Build Mater 239:117804

Analysis and ANN Modeling of Water Quality of Ramsar Site of Assam

Tina Gogoi and T. R. Girija

Abstract This paper presents the water quality status of Deepor Beel which is a perennial freshwater lake and the Ramsar site in Assam. Now, its ecological health is being affected by developmental works; this study is aimed to find out the status of water quality so that remedial measures can be initiated to protect it. Various analyses including physical and chemical quantification of important parameters of the water samples were collected from different locations of Deepor Beel. Samples were found to have higher concentration of alkalinity, BOD, iron, TS, TDS, and TSS, in some locations, and DO was found less than the minimum requirement in few locations. Based on the correlation coefficient, alkalinity, acidity, total solids, total suspended solids, DO, and chloride were identified as sensitive parameters which were influencing the BOD level. Iron is the parameter which is least correlated with any of the parameters. An attempt was made to model the ecosystem study by using artificial neural network using the identified sensitive parameters as inputs and BOD as output. The number of hidden neurons was 10, and the transfer functions were tangent and logarithmic sigmoidal functions in the input layer and in the output layer, respectively, for the best configured neural network model.

Keywords Water quality · ANN · BOD · DO

T. Gogoi
Department of Civil Engineering, Scholars Institute of Technology and Management, Garoghuli Rd, GARCHUK, Guwahati, Assam 781035, India

T. R. Girija (✉)
Department of Civil Engineering, School of Technology, Assam Don Bosco University, Assam, India
e-mail: girija.r@dbuniversity.ac.in

J. K. Deka et al. (eds.), *Emerging Technology for Sustainable Development*,
Lecture Notes in Electrical Engineering 1061,
https://doi.org/10.1007/978-981-99-4362-3_18

1 Introduction

Rapid growth of population and the advanced rate of industrialization have resulted in increased demand for freshwater in the last few decades. Human health is affected mostly by the agricultural development activities, and aquatic environment is polluted by non-judicious use of chemical fertilizers and pesticides leading to deterioration of water quality and depletion of aquatic biota and the unsanitary conditions. Most important water resources like lakes, rivers, and reservoirs are affected by the natural factors like climate, acid rain, nuclear fallout, landslide, etc. Discharge of pollutants from different sources, developmental activities, and agricultural activities causes water pollution as well as an increase in sedimentation in the lake basin making it shallow thus reducing the life span of the lake.

The study is conducted on water quality assessment of Jail and Kalwa lakes of Thane, Maharashtra (India), by considering various physicochemical parameters which revealed that Jail Lake is more polluted with higher degree of eutrophication compared to Kalwa Lake (Pejaver and Gurav 2008). Work on water quality index (WQI) in different lakes of Nagpur (Maharashtra, India), in all the three seasons in one year, and it was observed that the human activities and idol immersion during festival season, surface runoff resulting from rainfall, and sewage have contributed considerable pollution to the various lakes in the Nagpur city (Puri et al. 2011). Studies on water quality of the backwater of river Saryu revealed that organic pollutants and inorganic pollutants were within prescribed standard for drinking water (BIS10500:1991) (Sharma et al. 2012). Study on water quality of Chilika Lake, Odisha, revealed that the physicochemical parameters largely affect the complex habitat of the lagoon, and the lagoons are under stress due to luxuriant growth of weeds, fall in salinity, eutrophication, weed infestation, siltation addition of chemical pollutants of urban or agro origin, etc. (Pradhan et al. 2012). Quality assessment of groundwater sources in and around Lonar Lake, in Buldana district of Maharashtra, observed higher concentrations of parameters like heavy metal like iron and inorganic pollutants and nitrate which affected the water quality adversely (Gaikwad and Sasane 2013). The results of water quality analysis of Nagzari Dam of Kinwat district, Maharashtra (India), revealed that there were less variations in water quality, and the tested parameters were meeting the water quality criteria as per ISI (Yannawar et al. 2013). Studies on water quality parameters and impact of various human activities on Pravara River, a tributary of Godavari River of Maharashtra, showed that domestic waste and the various human activities cause the eutrophication. Water quality assessment of the river Brahmaputra in Guwahati city, Assam, revealed that the river water is not fit for beneficial uses of water except for irrigation, industrial cooling, and fish culture (Borthakur et al. 2016). Studies on water quality of River Brahmaputra in Guwahati city of Kamrup district, Assam (India), from five different locations along the river revealed that the water quality of Brahmaputra River is not meeting the water quality criteria of drinking purpose but can be used for agricultural purposes (Kotayk and Sarma 2017). The sources affecting the water quality were sewage discharge, open defecation, idol immersions, municipal wastewaters, septic systems, agricultural runoff, etc. Based on the literature review, it is decided to assess the water quality of Deepor Beel, the second largest lake in lower Brahmaputra Valley of Assam, as not much work has been done on the water quality analysis of this water body. This study intents at assessing the water quality of Deepor Beel and identifying the parameters having good correlation with BOD. An attempt is made to formulate a relationship connecting the sensitive parameters with BOD using artificial neural network of the ecosystem studied.

Contamination of aquatic ecosystems is a serious problem, all over the world, and in this line, enormous studies have been carried out for quality assessment of various lakes throughout India. Up to now, there was no systematic study carried out for the assessment of water quality parameters of Deepor Beel of Assam, India. Therefore, the present work emphasized on the water quality analysis of Deepor Beel, which is a permanent freshwater lake and largest Beel in the Brahmaputra Valley of Lower Assam. Deepor Beel is the only Ramsar site in Assam.

2 Objectives of the Study

- To analyze the water quality of Deepor Beel, Ramsar site wetland and identify the most polluted sampling stations and the probable sources of pollution.
- Temporal variation of pollutants.
- Identifying the sensitive parameters based on correlation coefficient.
- Establish or formulate a relationship between the sensitive parameters by means of artificial neural network (ANN).

3 Environmental System Selected for Study

During Ramsar Convention on wetlands, 1971, Deepor Beel is designated as "Wetlands of International Importance", and in 2002, it was declared as Ramsar site with 40.14 km^2 as Deepor Beel wetland, and 4.14 km^2 area was proposed as a wildlife sanctuary under the Wildlife Protection Act of India, 1972 (Government of Assam, 1989). The Beel which is among the third Ramsar site of the northeastern region of India is also a permanent freshwater lake and largest Beel in the Brahmaputra Valley of Lower Assam. It is located at about 10 km southwest of Guwahati in the Kamrup metro district of Assam in a valley shaped like U, surrounded by highlands in the northern and southern parts and between 26°03′26″–26°09′26″ N latitude and 90°36′39″–90°41′25″ E longitude. Families in the area around Deepor Beel were benefitted directly as well as indirectly by the Beel through fishing and collection of herbaceous plant (Sakia et al. 2014). Basistha and Kalmani rivers and monsoon runoff provide the main source of water for the wetland apart from runoff from the nearby hills which contributes the sedimentation of the wetland which reduces the

Table 1 Details of sampling point

Sampling pts	Latitude/longitude	Location
1	26°6′57.90″ N, 91°40′34.90″ E	Near Boragaon
2	26°6′48.54″ N, 91°39′19.01″ E	Bird Watch Tower, Chakardeo Village
3	26°6′8.44″ N, 91°36′56.24″ E	Azara Railway Station, Rani Gate
4	26°6′52.55″ N, 91°37′18.72″ E	Near Godhuli Bazar, Azara
5	26°8′23.06″ N, 91°39′48.61″ E	Near Assam Engineering Observatory
6	26°8′20.81″ N, 91°40′4.47″ E	Near Tetelia
7	26°8′7.61″ N, 91°37′32.42″ E	Dharapur Chariali
8	26°6′29.52″ N, 91°37′47.35″ E	Near Chakardeo Mikirpara Bazar
9	26°7′27.12″ N, 91°37′43.41″ E	Near Azara Brick Kiln Factory

depth of the Beel. The Beel is surrounded by Rani and Garbhanga reserved forests (> 100 km^2) which has increased its socio-economic importance, and the endangered Asiatic elephants (Elephas maximus) found there are depending on Deepor Beel for their food and water.

4 Sampling Locations Identified

Sample locations are identified covering the possible area of Deepor Beel and on the basis of importance. The selected sampling locations are given in Table 1, and the respective location points are indicated in the map of Fig. 1.

5 Parameters Selected

The parameters selected for water quality analysis were: alkalinity, acidity, BOD, DO, total hardness, calcium, chloride, pH, iron, total solids (TS), total dissolved solids (TDS), and total suspended solids (TSS). The experiments are conducted following the procedure mentioned in APHA standard methods of water and wastewater analysis.

6 Analysis of Results and Interpretation

After the completion of all the experiments, the results are calculated according to the procedure and formulas given in APHA standard methods of water and wastewater analysis and compared with the standard permissible limits given in IS 10500:2004.

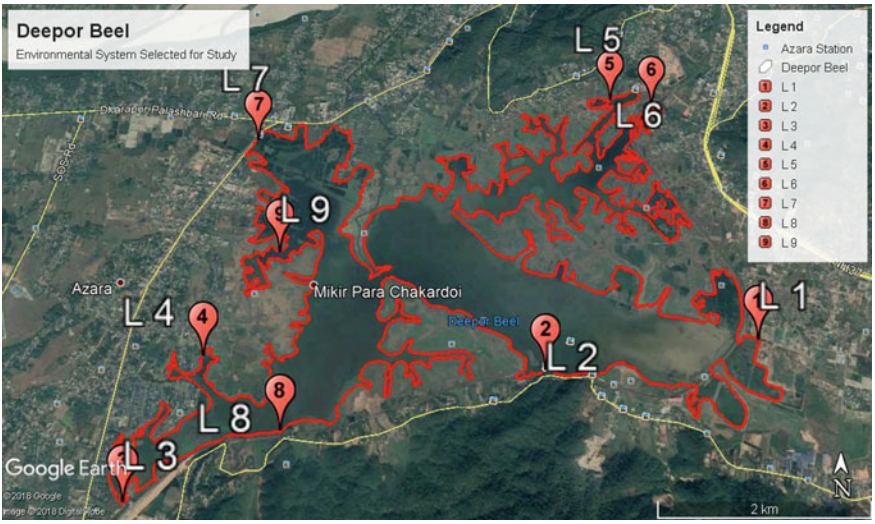

Fig. 1 Map of sampling locations

7 ANN Modeling

The present work is carried out with a feed-forward artificial neural network (ANN) model with six input variables, one output variable, and one layer of hidden neurons as shown in Fig. 3. Majority of the physical, chemical, and biological factors have significant impact on biochemical oxygen demand of water bodies. By making use of ANN model, it was attempted to establish a nonlinear relationship connecting the input parameters (alkalinity, acidity, TS, TSS, chloride, and DO) with BOD.

The Neural Network Toolbox was used for the development of the neural network models. Transfer functions selected were tangent and logarithmic sigmoid functions in the input layer and in the output layer, respectively. The training method chosen was Levenberg–Marquardt as it has the fastest convergence for medium-sized neural networks (Karul et al. 2000). Out of the total generated datasets, 36 sets were selected for training and 9 each for validation and testing. Value of root mean square error (RMSE), coefficient of determination (R2), and Nash efficiency (E) between the predicted output and measures of training and validation and testing datasets determine the performance of the neural network model. It is expected that the network after proper training should give the output with least error for training as well as validation data. After this, its performance for a third set of data (testing data) should be checked. If testing error also performs in the same manner, it can be taken as the best-fit model (Engin et al. 2005). The neural network configuration with ten hidden neurons and with tangent sigmoidal function (tansig) in the input layer and logarithmic sigmoidal function (logsig) in the output layer was finalized. The neural network topology used for BOD prediction is shown in Fig. 3.

Tansig (n) calculates the output according to Eq. (1):

$$n_h = \frac{2}{(1 + \exp(-2 \times n)) - 1} \tag{1}$$

where n_h = output from the hidden layer and, $n = w_1 \times P + b_1$, where W_1 = weight matrix connecting input and the hidden layer, P = input matrix, and b_1 = the bias.

Final output can be expressed in Eq. (2) as:

$$t_m = \text{logsig}(W_2 n_h + b_2) = \frac{1}{(1 + \exp(-W_2(\frac{2}{1+\exp(-2(W_1 P + b_1))})))} \tag{2}$$

where W_2 = the weight matrix connecting the hidden layer and the output layer and b_2 = bias matrix connecting the hidden layer and the output layer (Fig. 2).

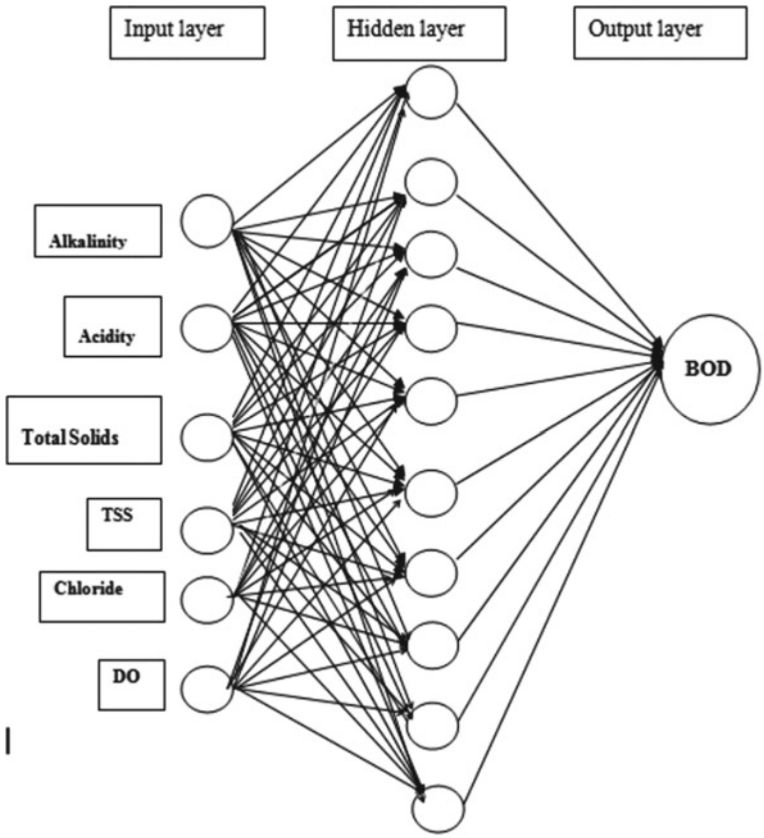

Fig. 2 Neural network configuration used in the study

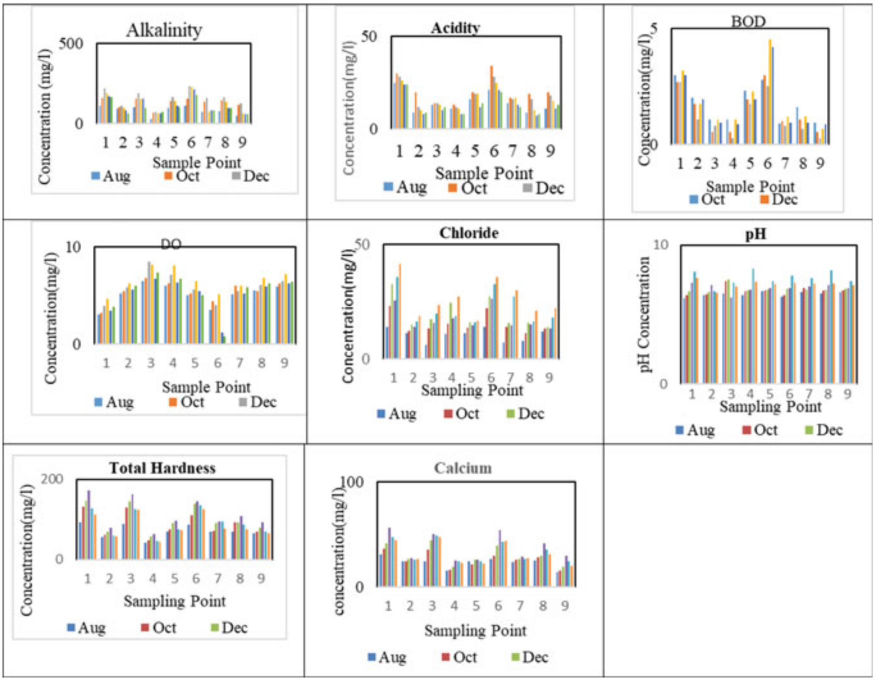

Fig. 3 Concentration of different parameters at various sampling points

8 Results and Discussion

Graphical representation of concentration of all selected parameters at various sampling points is shown in Fig. 3. Alkalinity of the tested samples ranges from 31 to 234 mg/l, and most of them are within the limit (200 mg/l) for potable water except sampling location (1) which is near the Boragaon dumping area and sampling location (6) near Tetelia which is a commercial place, and there is a railway crossing bridge over Deepor Beel. Winter period recorded the maximum value of alkalinity, i.e., 234 mg/l (at sampling location 6) which does not lie within the freshwater limit and minimum in the monsoon period, i.e., 31 mg/l (at sampling location 4). The alkalinity of samples was lesser in the monsoon which may be due dilution of salts like bicarbonate, carbonate, and hydroxide compound of sodium and calcium and higher in the winter due to reduced dilution factor. Acidity of the tested samples ranges from 7 to 34 mg/l. Mineral acidity is not present in any of the tested samples; hence, the samples are not acidic. Phenolphthalein acidity is present in all the samples but in very low concentration. The acidity of the samples was higher after monsoon, which may be because of the waste materials, chemical, etc., carried to the wetland during monsoon flood remains there and lower in the pre-monsoon period which could be due to the dilution by the pre-monsoon shower. Higher concentration of BOD was observed soon after the pre-monsoon shower, and during the winter period, lower concentrations of BOD was observed. The highest value of BOD was 4.53 mg/l at sampling location (6) near Tetelia as mentioned earlier which is a commercial place, there is a railway crossing bridge over Deepor Beel, and it is not within the permissible limit. The lowest value of BOD in the winter period was 0.53 mg/l at sampling location (9) near Azara Brick Kiln factory where mostly green fields are there. The higher values BOD in the pre-monsoon period can be due to the contribution from land flow, and higher concentration after pre-monsoon shower was a clear indication of the contribution of organic pollutants from land. Lower values of BOD during winter period may be due to restricted microbiological population in water under the low temperature. The higher values of DO were recorded in the winter period and lower values in the pre-monsoon period; it may be because of the increasing and decreasing temperatures and due to the presence of more organic matters. The maximum DO in the winter period is 8.2 mg/l at location (3) near Azara Railway Station where not much sources of pollution are there except the station, and it is suitable for aquatic life, and the minimum is 0.8 mg/l at location (6) near Tetelia, it is a commercial place, and there is a railway crossing bridge over Deepor Beel which can be a source for the contribution of organic particles, and it is below the required DO level and is not suitable for the survival of aquatic life. Total hardness of the tested samples ranges from 42 to 172 mg/l and is well below the permissible limit of 300 mg/l. Higher concentration of total hardness is obtained in the winter period and lower in the monsoon period. Lower concentrations in the monsoon period may result from the increasing dilution factor due to the monsoon shower and higher concentrations in winter due to less dilution factor as the water levels have gone down. Calcium content of the tested samples ranges from 14.42 to 56.11 mg/l, and all the tested samples were within the permissible limit, i.e., 75 mg/l. The calcium concentration was higher in the winter season and lower in the rainy season. As the dilution factor was higher in the monsoon period, that might have helped the calcium to get diluted, and in the winter season, calcium got concentrated as the dilution factor was very less. Chloride content of the samples ranges from 5.99 to 41.49 mg/l and is well below the permissible limit of 250 mg/l.

The concentrations of chloride were highest in the pre-monsoon period which may be because of the pre-monsoon shower which might have carried higher chloride content particles from the land to the wetland and lowest in the monsoon period which may be because of the high dilution factor. The pH of the tested samples ranges from 6.2 to 8.3. The pH of the samples collected in the monsoon period is more acidic in nature because of the deposits from the surrounding and the monsoon rainfall, and the samples collected in the period of pre-monsoon period are basic in nature because the low dilution factor as well as the acidity to neutralize base is also less. All the results are within the permissible limit 6.5–8.5. Concentration of iron in the tested samples ranges from 22.67 to 10,335 μg/l. The samples collected in the post-monsoon period contain higher iron concentration because of the deposits from the surrounding areas and industries due to flood; again the iron content is higher in the winter, and it may be because of the groundwater intrusion. Iron shows higher temporal variations among all the parameters. Total solids of the tested samples range from 100 to 2100 mg/l, total dissolved solids range from 100 to 700 mg/l, and total suspended solids range from 0 to 1550 mg/l. Higher concentrations of TS, TDS, and TSS before monsoon concentrations may be due to the pre-monsoon shower which carries all the dust particles, dried plants all around to the wetland, and at the same time water level was also down. Monsoon season observed lower concentrations which may be due to dilution. It was observed that alkalinity, acidity, total solids, total suspended solids, DO, and chloride were identified as sensitive parameters which were influencing the BOD level based on the values of correlation coefficient (Table 2).

9 Artificial Neural Network Model Performance

The study successfully concluded with a feed-forward artificial neural network (ANN) model with six input neurons, one output neuron, and ten hidden neurons. The root mean square errors for the predicted results were 0.1808, 0.2364, and 0.2685 with coefficients of determination of 0.9808, 0.9132, and 0.9563 and Nash efficiency of coefficient 0.981, 0.970, and 0.962 for training data, testing data, and validation data, respectively. Expression for output derived out from the ANN model is of the form,

$$t_m = \text{logsig}(W_2 n_h + b_2) = \frac{1}{(1 + \exp(-(W_2 \times (\frac{2}{1+\exp(-2\times(W_1 P + b_1))}))))}$$

10 Conclusions

- Water samples are tested from nine different locations around the Deepor Beel, wetland recognized as Ramsar site wetland for all the seasons, and concentration of different parameters during different season showed temporal variations.
- Among all the sampling locations, the one near Boragaon (sampling location 1) dumping site and another one near Tetelia (sampling location 6) are the most polluted sites. Sampling location near to a barren land (sampling location 4) without any developmental activities is the least polluted site.
- Among the parameters analyzed, higher concentration has been found in alkalinity, BOD, iron, TS, TDS, and TSS, in some locations, and DO was found less than the minimum requirement in few locations.
- Alkalinity, acidity, total solids, total suspended solids, DO, and chloride were identified as sensitive parameters which were influencing the BOD level.
- Artificial neural network with ten hidden neuron transfer functions of tangent and logarithmic sigmoidal functions in the input layer and in the output layer, respectively, was found to be the best configured neural network model for predicting BOD.

Table 2 Correlation coefficient of all the parameters with BOD

Parameters	Alkalinity	TS	Acidity	TSS	Hardness	TDS	Ca	Cl^-	pH	DO	Iron	BOD
Correlation coefficients	0.64	0.59	0.67	0.59	0.47	0.48	0.44	0.60	0.10	0.91	−0.03	1

- For predicting BOD of a similar ecosystem, the equation derived from ANN model can be used by making use of the weight matrix and bias of the best-fit model.

References

American Public Health Association (2005) Standard Methods for the examination of water and waste water, 12th edn. American Public Health Association, Washington, DC

Borthakur TA, Kumar D, Singhal A (2016) Assessment of water quality of River Brahmaputra in Guwahati City of Assam. In: National conference on sustainable water resources development and management (SWARDAM-2016). ISBN 978-93-85777-75-2

Deshmukh BS, Sathe SD (2013) Physico-chemical characteristics of Pravara River, Maharashtra. J Aquatic Biol Fisheries 2/2014/:101–105

Engin GO, Demir I, Engin SN (2005) Determination of the relationship between sewage odour and BOD by neural networks. Environ Model Softw 20:843–850

Gaikwad RW, Sasane VV (2013) Assessment of ground water quality in and around Lonar lake and possible water treatment. Int J Environ Sci 3(4)

Gorde SP, Jadhav MV (2013) Assessment of water quality parameters: a review. Int J Eng Res Appl 3(6):2029–2035. ISSN 2248-9622

IS 10500 (2004) Indian Standard Specification for drinking water, New Delhi

Karul C, Soyupak S, Cilesiz AF, Akbay N, Germen E (2000) Case studies on the use of neural networks in eutrophication modeling. Ecol Model 134:145–152

Kotayk P, Sarma P (2017) Assessment of water quality index of the Brahmaputra River of Guwahati City of Kamrup District of Assam, India. Int J Eng Res Technol (IJERT) 6(03):536–540. ISSN 2278-0181

Lourakis M, Argyros A (2005) Is Levenberg-Marquardt the most efficient optimization algorithm for implementing bundle adjustment? In: Tenth IEEE international conference on computer vision (ICCV'05), vol 2, pp 1526–1531

Pejaver M, Gurav M (2008) Study of water quality of Jail and Kalwa Lake, Thane, Maharashtra. J Aqua Biol 23(2):44–50

Pradhan V, Mohsin M, Gaikwad BH (2012) Assessment of physico chemicalparameters of Chilika Lake water. Int J Res Environ Sci Technol 2(4):101–103

Puri PJ, Yenkie MKN, Sangal SP, Gandhare NV, Sarote GB, Dhanorkar DB (2011) Surface water (Lakes) qualityassessment in Nagpur city (India) based onWater quality index (WQI). Rasayan J Chemvol 4(1):43–48

Sakia MK, Saikia PK, Bhatta R (2014) Management perspectives for avian population conservation and enrichmentn in Deepor Beel Ramsar Site, North-East India. J Glob Biosci 3(2):428–451

Sharma RK, Soni DK, Agrawal N (2012) A study on physico-chemical parameters of Dah lake water, District-Ballia (U.P.), India. J Appl Natural Sci 4(2):237–240

Yannawar VB, Shaikh PR, Bhosale AB, Nagargoje BN (2013) Water quality assessment of Nagzari Dam of Maharashtra. J Appl Technol Environ Sanitation 3(3):111–116

Determination of Optimum K Value for K-means Segmentation of Diseased Tea Leaf Images

Anuj Kumar Das and Syed Sazzad Ahmed

Abstract Detecting diseases from the leaf images of a plant is an important and challenging task. Various image processing techniques like pre-processing, segmentation, classification, etc., are performed to detect plant diseases from its leaf images. Image segmentation is one of the important steps in the process of disease detection in leaf images of plants. A well segmented image increases the accuracy of prediction. In this paper, we have implemented the K-means algorithm to segment leaf images of tea infected with red rust disease caused by algae. The value of *K* in K-means needs to be set manually. Determining the optimum value of *K* is crucial to obtain a well segmented image. So, the elbow method and silhouette coefficient determination are employed for this purpose.

Keywords K-means · Elbow method · Silhouette coefficient · Segmentation

1 Introduction

Tea is very important crop for the state of Assam, situated in the north-eastern part of India. Tea is mainly cultivated for its leaves to make beverages. Tea plants have a very high economic value. A large population of the state of Assam is dependent on tea crop cultivation. In the annual report of Tea Board of India, the total value of tea export from India was estimated at Rs. 5457.10 Crs (Tea Board India 2021). But diseases of tea plants are one of the major problems that lead to yield loss in tea crops. Diseases that affect tea crops increase the cost of production. So, early detection of diseases in tea plants is crucial. This enables farmers to take effective steps to contain the spread of disease. One of the major hurdles in disease treatment of tea crops is disease recognition. Farmers generally rely on naked eye disease recognition in tea plants. This process of disease recognition needs expert guidance and also it becomes a laborious work since tea crops are generally cultivated in a large area.

A. K. Das · S. S. Ahmed (✉)
Department of CSE, Assam Don Bosco University, Azara, India
e-mail: sazzad@dbuniversity.ac.in

J. K. Deka et al. (eds.), *Emerging Technology for Sustainable Development*,
Lecture Notes in Electrical Engineering 1061,
https://doi.org/10.1007/978-981-99-4362-3_19

In this age of technological advancements, a number of computer technologies can be employed for the purpose of disease detection in tea plants. Today, computer components have become cheap and their processing power has increased manifold. Disease detection based on computer technology is fast, efficient and highly scalable. The images of the tea plants can be used to detect the type of disease affecting the tea plant and also make an estimate of the total area of the leaf image that has been affected by the disease. Image processing and machine learning techniques can be employed for this purpose. One of the major steps involved while detecting diseases in tea leaves is image segmentation.

Segmentation of images is the process of dividing images into homogenous regions based on certain features and properties of the constituent pixels. These regions then can be used for a further image processing and classification tasks. Segmentation is an important image processing technique that can be employed for disease detection in tea leaves. The segmented images are then used for feature extraction and classification. So it's very important that a well segmented image is obtained. This in turn increases the detection accuracy of the classifier. A number of methods exist for image segmentation. Among them K-means (Zheng et al. 2018) clustering is one of the prominent methods for image segmentation. The K-means clustering algorithm clusters the pixels in the image into K clusters.

In our work, we have segmented diseased tea leaves using K-means clustering algorithm. The tea leaves were infected with red rust disease caused by the algae, Cephaleuros parasiticus. One of the drawbacks of the K-means clustering is that the value for K needs to be set manually. Right K value divides the image pixels into clusters of homogeneous regions. This is very important for feature extraction and classification for disease detection in leaf images. So determining an optimum K value is crucial for obtaining a well-clustered image. The elbow method (Nainggolan et al. 2019) and silhouette coefficient (Saputra et al. 2020) determination method are used for this purpose. The optimum K value so obtained is used to segment the image.

The rest of the paper is organized in the following way. Section 2 is the literature review where a brief review of previous work done by different researchers is given. Section 3 contains the proposed methodology. Section 4 demonstrates the experiment performed and contains a brief description of the experimental outcome. Section 5 contains the conclusion and future work.

2 Literature Review

Researchers have proposed different methods for disease detection in plants using the images of leaf and fruits. A brief review of some of these methods is highlighted in this section.

Dhingra et al. (2019) proposed a method for disease detection in basil leaf using the leaf images. For contrast enhancement, contrast limited adaptive histogram equalization (CLAHE) (Reza 2004) algorithm was employed. Segmentation was done using neutrosophic logic. Evaluations of nine classifiers were done to find the best among them for classification. Classifiers evaluated are decision tree, random forest, support vector machine, Ada-Boost, linear models, Naïve Bayes, K-nearest neighbor, artificial neural network and discriminant analysis. Random forest was evaluated to be the best with an accuracy of 98.4%. Singh (2019) proposed a method for disease detection in sunflower. Particle swarm optimization (PSO) (Wang et al. 2018) is used for segmentation. The color co-occurrence method is employed to obtain both color and texture features. Classification was done using the minimum distance classifier. Areni et al. (2019) used Gabor kernel to extract features from cocoa fruit image. The features were stored in a database. Vector image distance is then computed for identification. Ashok et al. (2020) employed discrete wavelet transform and gray level co-occurrence matrix (GLCM) for feature extraction of tomato leaf images. Convolutional neural network (CNN) (Albawi et al. 2017) is then used for classification. The method proposed had less computational time and yielded optimum results. Carneiro et al. (2021) used single-shot detector (SSD) as object detection algorithm for detecting diseases in coffee plants leaf images. The performance of ResNet and Inception were evaluated in the detector. It was found that the Inception-based model had a higher accuracy rate. Islam et al. (2018) proposed method for disease detection in rice. The green pixels of the leaf images are masked with blue pixels and removed. The RGB values in the affected region of the leaf image are calculated. Gaussian Naïve Bayes classifier is used for classification. Hossain et al. (2018) proposed a technique for detection of brown blight and algal diseases in tea leaves. Features were selected based on univariate statistical test. Support vector machine (SVM) is then used for classification purpose. Srivastava et al. (2020) also proposed method for detection of diseases in tea leaf images. GLCM is used for feature extraction. Four types of images, namely healthy, algal, blister and gray mold were used. Four classifiers were used and each one of them classifies the image into one of the four categories. The classifiers were SVM, decision tree, random forest and Ada-boost. Prediction is done based on the majority vote. Zhang et al. (2020) proposed a method for detecting powdery mildew, bacterial angular, scab and gray mold and anthracnose diseases in cucumber leaf images. An IoT-based system is employed for data collection. Sum and difference histogram (SADH) feature vectors are determined based on intensity values of neighboring pixels. K-nearest neighbor (KNN) is used for classification. Bedi and Gole (2021) proposed a hybrid deep learning model for detecting diseases in peach. Convolutional auto encoder (CAE) was used to obtain a compressed domain representation of the images. Numbers of features were reduced due to CAE. Convolutional neural network is then used for classification. Guo et al. (2020) used region proposal network (RPN) for image detection in a complex surrounding of leaf images. Then Chan Vase algorithm is used for image segmentation. The paper examines images having black rot, bacterial plaque and rust diseases. Singh et al. (2017) proposed a method for disease detection in rose, lemon, beans and banana leaf images. They used genetic algorithm for segmentation. Then color co-occurrence method is used for feature extraction. Minimum distance classifier and support machine vector are then used for classification.

In Table 1, we give an overall survey of all the methods under consideration.

Table 1 Survey of leaf disease detection and classification systems

Culture	Features	Techniques	No of images considered	Accuracy (%)	Researchers
Basil	Histogram feature	Neutrosophic logic,	400	98.4	Dhingra et al. (2019)
Sunflower	Color, texture	PSO	Not specified	98	Singh (2019)
Cocoa	Texture	Gabor filter	80	70	Areni et al. (2019)
Tomato	Color	CNN	Not specified	98.1	Ashok et al. (2020)
Coffee	Segmentation	Single-shot detector	285 (training) 257 (testing)	81.5	Carneiro et al. (2021)
Rice	Color	Gaussian Naïve Bayes	60	> 90	Islam et al. (2018)
Tea	Contrast, correlation,	SVM	150 (training) 150 (testing)	93.3	Hossain et al. (2018)
Tea	Texture, color	SVM, decision tree,	2016	96.4	Srivastava (2020)
Cucumber	SADH	KNN	760	94.4	Zhang et al. (2020)
Peach	Spatial and temporal features	Convolution-al autoencoder, CNN	4457	98.3	Bedi, Gole (2021)
Banana, beans	Color, texture	Genetic algorithm	106	95.7	Singh, Misra (2017)

3 Methodology

The proposed method contains the following steps:

1. First pre-processing is done to remove unwanted part of the images. This is done by cropping the image and removing the background.
2. Then contrast limited adaptive histogram equalization (CLAHE) is used for contrast enhancement of the image. CLAHE is a modification of the adaptive histogram equalization method. In adaptive histogram equalization, an image is divided into smaller regions known as tile. Then histogram equalization is performed for each tile in the image for contrast enhancement. In histogram equalization, first images are converted to its histogram representation of the pixels intensity values. Then the histogram is redistributed to form a more uniform histogram of the pixels intensity. But adaptive histogram equalization suffers from the problem of over amplification. This problem is taken care of by CLAHE. In CLAHE the contrast is limited to a predetermined value. After that the individual tiles are combined using bilinear interpolation.

3. An analysis of the K-means is performed to determine the optimum number of clusters. Two types of methods are used for this purpose. They are elbow method and silhouette coefficient. The analysis is done based on the cohesion and separation of the clusters. Cohesion is defined as the intra-cluster relationship of data points. It measures how closely the data points are related to one another inside a cluster. It is given by:

$$\mathrm{Ch} = \frac{1}{n-1}\sum_{i=1}^{k}\sum_{j=1}^{n-1} d\left(c_i, p_j\right) \tag{1}$$

where Ch = cohesion, c_i = cluster center, p_j = data points in cluster c_i, n = number of data points in cluster c_i, $d(c_i, p_j)$ = distance between c_i and p_j.

Whereas separation measures the inter-cluster relationship. It defines how much a cluster is different from another cluster. It is given by:

$$\mathrm{Se} = \frac{1}{n}\sum_{i=1}^{n} d(m, p_i) \tag{2}$$

where Se = separation, m = sample data point, $p_j = n$ number of data points, $d(m, p_i)$ = distance between m and p_i.

The elbow method calculates the cohesion of the clusters (known as inertia) for different values of K. The inertia is plotted along the y-axis and the values of K are plotted along the x-axis. The graph so obtained forms an elbow-like structure. The point where the elbow forms has a minimum deviation in inertia for a low value of K. This value of K where the elbow is formed is the optimal number of clusters required. Silhouette coefficient on the other hand measures the cohesion as well as the separation of the clusters. Its value ranges from -1 to 1. A value close to 1 indicates a greater separability among clusters and a value in negative implies that a data point is assigned to a wrong cluster. For the value of K, having the highest silhouette coefficient is considered to be optimum. Silhouette coefficient (S) is given by:

$$S = 1 - \frac{\text{cohesion}}{\text{seperation}} \quad \text{for cohesion} < \text{seperation} \tag{3}$$

$$S = \frac{\text{seperation}}{\text{cohesion}} - 1 \quad \text{for seperation} < \text{cohesion} \tag{4}$$

Using the optimum K value obtained, the images are segmented with the K-means algorithm. The K-means algorithm is an unsupervised learning algorithm. The algorithm partitions the data into K clusters. In K-means algorithm, first key data points are selected randomly and are made the center of the clusters. Then the Euclidean distance of each data points from the cluster centers are calculated and the nearest data points from the centers are grouped to form the clusters. After that the

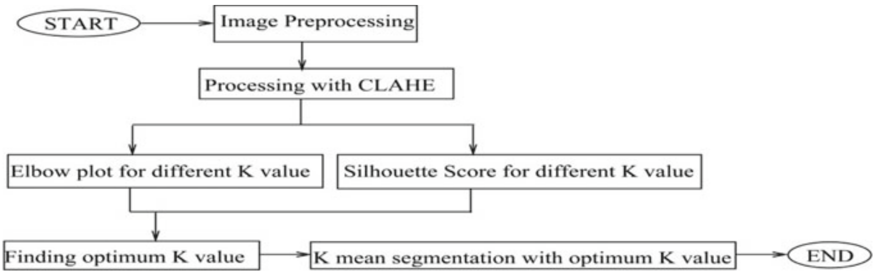

Fig. 1 Flow chart showing proposed method

new mean of data points in each cluster is calculated. The newly calculated mean of a cluster is then made the new center of the cluster. This process is performed iteratively till assignment of cluster centers no longer changes. The Euclidean distance D is given by the following equation:

$$D = \sqrt{\sum_{i=1}^{n} (d_i - c)^2} \tag{5}$$

where c is the cluster center and d_i is the n number of data points.

4. The segmented image obtained can be used for extracting features such as contrast, energy, mean, standard deviation, variance, etc. These features then can be fed to a classifier for classifying the leaf image as diseased or not.

The entire proposed method is depicted in Fig. 1.

4 Experimental Results

We performed experiments as shown in Fig. 1. In this section we give a brief over-view of the experiments performed and results obtained.

4.1 Data Collection

Tea leaves infected with red rust disease were collected from private tea gardens situated at Dudhnoi in Goalpara district of Assam. We have collected around 200 images each for healthy and infected tea leaves. The images of the tea leaves were captured using a digital camera under controlled conditions with uniform lighting. Tomato and apple leaves data were collected from open source platform Kaggle which is a large repository of public datasets.

Fig. 2 Tea leaf infected with rust disease **a** unprocessed image **b** CLAHE image

4.2 Experiment Performed

For the experiment first the images are cropped and the background is removed. The images are then processed with CLAHE algorithm to enhance the contrast of the pixels. To process the images using CLAHE, the images are first converted to $L^*a^*b^*$ color space from RGB. Figure 2 shows the output of an unprocessed image and CLAHE image.

Next we applied the elbow method and the silhouette coefficient determination to find the optimum K value for the K-means segmentation. The inertia for every K clusters is plotted along the y-axis and the number of K clusters is plotted along the x-axis. The silhouette score is also determined for different K values. The optimum value for K is determined using the elbow plot and the silhouette score. The K-means algorithm is then employed to segment the image by setting the value of K to the optimum value obtained. A total of 300 different iterations were performed to obtain the segmented image.

4.3 Observation

Plot for the elbow method is shown in Fig. 3. From the figure it can be seen that the elbow structure is formed at the value for $K = 4$.

The silhouette score for K value is given in Table 2. The highest silhouette score (0.94) is obtained when K value equals 4. So, the optimum value for K is determined to be 4 to get a well segmented image using the K-means segmentation.

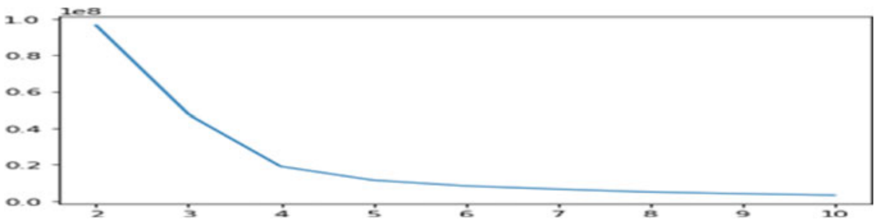

Fig. 3 Elbow plot for different K values

Table 2 Silhouette scores for different K values of the image:

K-value	2	3	4	5	6	7	8
Silhouette score	0.93007	0.92367	0.94116	0.93491	0.91353	0.91366	0.93964

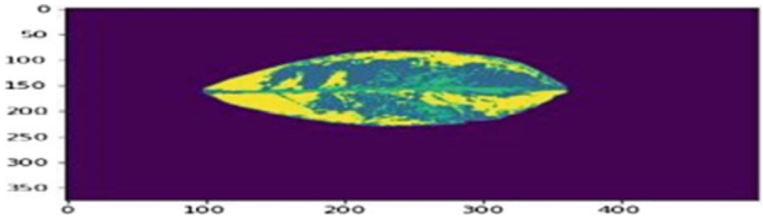

Fig. 4 Plot for segmented image using K-means clustering for $K = 4$

Table 3 Table showing comparative study for leaf images of different plants

Culture	Optimum K value from elbow plot	Silhouette score for optimum K value
Tea	4	0.94
Tomato	5	0.60
Apple	5	0.59

The plot for the segmented image for $K = 4$ is given in Fig. 4. This segmented image can be used for feature extraction and classification for disease detection.

The proposed method was also applied to images of tomato leaf infected with late blight disease and apple leaf infected with scab disease. This was done to show a comparison of the K value obtained from the elbow plot and their respective silhouette score. Table 3 gives this comparison.

From Table 3, it can be seen that the optimum K value is different for different images. The silhouette score for tea is 0.94. A silhouette score close to 1 indicates that well separated clusters were formed and the intra-cluster distances were minimized.

5 Conclusion and Future Work

The segmented images of diseased tea leaf obtained using the K-means algorithm can be used for feature extraction of the different segmented regions of the image. Based on the features extracted, a classifier can classify the regions as diseased or non-diseased. Determining an optimum value for K in K-means algorithm is important for obtaining a well segmented image. A well segmented image is very crucial for obtaining a higher accuracy in disease prediction of leaf images. The analysis performed in this paper predicts a reasonably optimum value for K. Although the validation can be done only after performing the analysis on a dataset of multiple images and then employing an appropriate algorithm for classification. A higher accuracy of prediction so obtained will validate the value of K for tea leaf image.

One of the problems seen during the study was that while applying CLAHE for contrast enhancement, the noise in the images was also amplified. Although CLAHE reduces the problem of noise amplification of adaptive histogram equalization to a considerable amount, still the images need to be processed for better noise removal. This will result in obtaining a better segmented image.

Acknowledgements This research work is being carried out with the help of fund received from AICTE NER-RPS for the project titled "Detection of Tea Leaf Pest Attack in Assam Tea Gardens" via Sanction Letter File No. 8-13/FDC/RPS (NER)/POLICY-1/2020-21 dated March 10, 2021.

References

Albawi S, Mohammed TA, Al-Zawi S (2017) Understanding of a convolutional neural network. In: 2017 international conference on engineering and technology (ICET), 2017 Aug 21. IEEE, pp 1–6

Areni IS, Tamin R (2019) Image processing system for early detection of cocoa fruit pest attack. J Phys Conf Ser 1244(1):012003. IOP Publishing

Ashok S, Kishore G, Rajesh V, Suchitra S, Sophia SG, Pavithra B (2020) Tomato leaf disease detection using deep learning techniques. In: 2020 5th international conference on communication and electronics systems (ICCES). IEEE, pp 979–983

Bedi P, Gole P (2021) Plant disease detection using hybrid model based on convolutional autoencoder and convolutional neural network. Artif Intell Agric 1(5):90–101

Carneiro AL, Silva LD, Faulin MS (2021) Artificial intelligence for detection and quantification of rust and leaf miner in coffee crop. arXiv preprint arXiv:2103.11241

Dhingra G, Kumar V, Joshi HD (2019) A novel computer vision based neutrosophic approach for leaf disease identification and classification. Measurement 1(135):782–794

Guo Y, Zhang J, Yin C, Hu X, Zou Y, Xue Z, Wang W (2020) Plant disease identification based on deep learning algorithm in smart farming. Discret Dyn Nat Soc 18:2020

Hossain S, Mou RM, Hasan MM, Chakraborty S, Razzak MA (2018) Recognition and detection of tea leaf's diseases using support vector machine. In: 2018 IEEE 14th international colloquium on signal processing and its applications (CSPA), 2018 Mar 9. IEEE, pp 150–154

Islam T, Sah M, Baral S, Choudhury RR (2018) A faster technique on rice disease detection using image processing of affected area in agro-field. In: 2018 second international conference on inventive communication and computational technologies (ICICCT), 2018 Apr 20. IEEE, pp 62–66

Nainggolan R, Perangin-angin R, Simarmata E, Tarigan AF (2019) Improved the performance of the K-means cluster using the sum of squared error (SSE) optimized by using the elbow method. J Phys Conf Ser 1361(1):012015. IOP Publishing

Reza AM (2004) Realization of the contrast limited adaptive histogram equalization (CLAHE) for real-time image enhancement. J VLSI Sig Process Syst Sig Image Video Technol 38(1):35–44

Saputra DM, Saputra D, Oswari LD (2020) Effect of distance metrics in determining *k*-value in k-means clustering using elbow and silhouette method. In: Sriwijaya international conference on information technology and its applications (SICONIAN). Atlantis Press, Indonesia, pp 341–346

Singh V (2019) Sunflower leaf diseases detection using image segmentation based on particle swarm optimization. Artif Intell Agric 1(3):62–68

Singh V, Misra AK (2017) Detection of plant leaf diseases using image segmentation and soft computing techniques. Inform Process Agric 4(1):41–49

Srivastava AR, Venkatesan M (2020) Tea leaf disease prediction using texture-based image processing. In: Emerging research in data engineering systems and computer communications. Springer, Singapore, pp 17–25

Tea Board India. The Official Website of Tea Board India, 12 Nov. 2021. http://www.teaboard.gov.in/

Wang D, Tan D, Liu L (2018) Particle swarm optimization algorithm: an overview. Soft Comput 22(2):387–408

Zhang S, Huang W, Wang H (2020) Crop disease monitoring and recognizing system by soft computing and image processing models. Multimedia Tools Appl 79(41):30905–30916

Zheng X, Lei Q, Yao R, Gong Y, Yin Q (2018) Image segmentation based on adaptive K-means algorithm. EURASIP J Image Video Process 2018(1):1

Recent Advancement and Challenges of Deep Learning for Breast Mass Classification from Mammogram Images

Lal Omega Boro and Gypsy Nandi

Abstract Deep learning (DL) has become a critical component of medical image processing. Over time, DL methods have changed. Advances in the field of DL have resulted in a computer-aided diagnosis system (CADs) that is more sophisticated and self-reliant. In medical image analysis, convolutional neural networks (CNN) are becoming increasingly extensively employed as a DL approach. This study aims to survey state-of-the-art approaches of breast mass classification using CNNs. The breast cancer mammography repositories have also been examined. Various limitations that demand further examination are also discussed. We looked at articles published on well-known publishing platforms like Google Scholar, PubMed, Science Direct, and IEEE Xplore to conduct the literature study. These papers are all SCOPUS/SCI/SCIE indexed and focus on using CNN algorithms in mammogram images. We also present the advancements and challenges of CNNs for breast cancer diagnosis. When it comes to medical image processing, using CNNs has proved to be more beneficial to researchers than using a traditional approach. However, better architectures, larger datasets that address class imbalance issues and improved optimization methods are still required.

Keywords Deep learning · Mammograms · Convolutional neural network · Medical image · Classification · Breast masses

1 Introduction

Breast cancer is a form of cancer in which cells in the breast tissue grow rapidly out of control. It is one of the most frequent malignancies in women worldwide, and it is the leading cause of death in women, affecting 2.1 million women each year. Breast cancer claimed the lives of over 685,000 women in 2020, according to the World Health Organization (WHO) (Who.int. 2021).

L. O. Boro (✉) · G. Nandi
Assam Don Bosco University, Guwahati, Assam 781017, India
e-mail: omegaboro7@gmail.com

J. K. Deka et al. (eds.), *Emerging Technology for Sustainable Development*, Lecture Notes in Electrical Engineering 1061,
https://doi.org/10.1007/978-981-99-4362-3_20

According to the Global Cancer Statistic 2020, breast cancer was the most often diagnosed global cancer in 2020, with an anticipated 2.3 million new cases (11.7%), followed by lung (11.4%), colorectal (10.0%), prostate (7.3%), and stomach (5.6%) cancers. Breast cancer affects one out of every four women and accounts for one out of every six cancer deaths worldwide (Sung et al. 2020).

Early detection and treatment of breast cancer can enhance survival rates. Mammography has been increasingly accepted for breast cancer screening and has had a key role in lowering cancer mortality rates by detecting cancer early. Mammography is a breast x-ray as shown in Fig. 1b that can detect malignant tumors that are too tiny to be felt. However, mammographic image interpretation can be difficult, resulting in a false diagnosis of breast cancer by medical specialists because of the variation of the breast tissue, architectural noise induced by dense tissue masking, and the subtlety of some breast cancer types.

In the medical field, CAD systems build on DL techniques like CNNs have made significant breakthroughs. These techniques improve the diagnosis of suspicious lesions (Chougrad et al. 2018) and help in reducing the overall cost of medical care. Transfer learning is frequently utilized in DL applications to construct networks that are often used as a foundation source for new classification tasks (Shen et al. 2019; López-Cabrera et al. 2020). Also, transfer learning is beneficial when used in combination with a fewer number of training images to perform better in a new classification task.

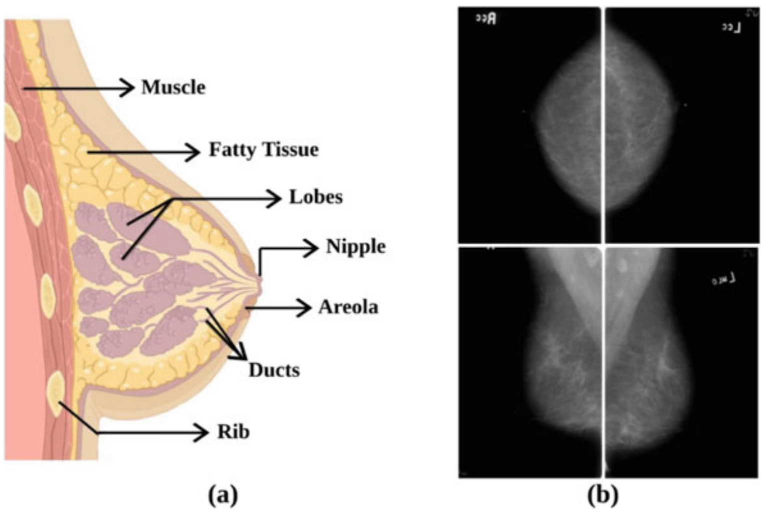

Fig. 1 **a** Anatomy of woman's breast. Most breast cancers begin in the ducts or lobules. **b** Multi-view mammography images from the CBIS-DDSM dataset. The first column presents the right craniocaudal (RCC) view and the right mediolateral oblique (RMLO) view of the breast. The second column presents the left craniocaudal (LCC) view and left mediolateral oblique (LMLO) view of the breast

Table 1 Comparison between popular publicly available mammographic databases

Database	Number of images	Abnormality
MIAS	322	All kinds of lesions and masses
DDSM	2620	All kinds of lesions and masses
INbreast	410	All kinds of lesions and masses
BCDR-FM	3703	All kinds of lesions and masses
BCDR-DM	3612	All kinds of lesions and masses
CBIS-DDSM	10,239	All kinds of lesions and masses

The primary requirement for learning accurate computational models has always been high-quality data. This is also valid for deep models, which must consume a significant amount of training data. The Mammographic Image Analysis Society (MIAS) database (Suckling et al. 2015), the Digital Database for Screening Mammography (DDSM) (Heath et al. 1998), the INbreast database (Moreira et al. 2012), the Breast Cancer Digital Repository (BCDR) (Lopez et al. 2012), the Curated Breast Imaging Subset of DDSM (CBIS-DDSM) (Lee et al. 2017), and the Image Retrieval in Medical Applications (IRMA) (Lehmann et al. 2004) database are the most widely used publicly accessible databases in mammography. We present an overview of the necessary information about each of these databases in Table 1. The public databases provide a mixture of normal, benign, and malignant annotated images and also extensive diversity of patient cases. Many existing studies rely on publicly available databases, and few authors rely on private data obtained from research centers or hospitals.

The review paper is divided into four sections which includes introduction, review of related work, challenges of deep convolutional neural for breast cancer classification and followed by conclusion.

2 Literature Review

Mammograms are among the most successful and efficient ways to diagnose breast cancer early on. The radiologist looks for numerous sorts of abnormalities on the mammography, such as calcification, lumps, and breast density that indicate a high risk of getting breast cancer. Several researchers have sought to automate this process by using a CAD system. In this section, we review the related work that has been carried out for breast mass classification using deep learning.

Shen et al. (2019), for example, created an end-to-end DL-based technique for detecting and classifying cancerous masses. A patch classifier is used as a pre-trained model to recognize local image patches, and the weights of this classifier are then transferred to another classifier for full image classification. The patch-based and complete image-based classifiers were created using the CBIS-DDSM database, and the INbreast database, respectively.

Kooi et al. (2017) proposed a VGG like pre-trained DCNN for discriminating solitary cysts from soft tissue lesions. They used two different datasets and patches of 260 * 260 at 200 microns were extracted in both datasets. They employed tissue augmentation and superimposing these over mass and cysts patches. A massive dataset of possible mass areas from screening mammography is used to train the network. The network is then given with solitary cyst and malignant mass patches from a diagnostic dataset, and features are collected from the hidden layers, with gradient boosting trees (GBT) used for the classification task.

Altan (2021) investigated and compared the results of the CNN and deep autoencoder algorithms for the classification of mass lesions with existing literature. The ROI images of normal (1052 images) and cancer (973 images) were collected from DDSM. These ROI images were augmented using cropping and flipping techniques and resized to 224 * 224 pixels which are then fed into the deep autoencoder and CNN architectures. The deep autoencoder output was fed into the fully connected layer. The classification parameters including learning rate, dropout, and Adam optimization were set the same for both the models with five-fold cross-validation.

The study of López-Cabrera et al. (2020) integrated a pre-trained CNN model, Inception V3 to classify mammograms into multiple classes. The pre-trained CNN model used is composed of five convolutional layers, each followed by a batch normalization layer, two grouping layers, and 11 inception modules. Data augmentation, L2 regularization, batch normalization, and dropout were applied to reduce overfitting. They created three CNNs models based on the Inception V3 architecture and were trained and tested on the mini-MIAS dataset.

Ragab et al. (2019) proposed a methodology for classifying benign and malignant masses using AlexNet and SVM. The proposed method consists of two segmentation techniques such as manually cropping the ROI from the DDSM dataset and segmentation based on threshold and region-based techniques. However, they only applied these two segmentation techniques to the DDSM dataset since the data provided in the CBIS-DDSM dataset are already segmented. Images were resized to 227 * 227 * 3 and augmented using rotation. Features from the segmented region were extracted using AlexNet. They connected the last fully connected layer of AlexNet to the SVM classifier.

Chougrad et al. (2018) investigated the performance of CNN, VGG16, ResNet50, and Inception V3 as pre-trained architectures for classifying mass lesions as benign or malignant. They merged DDSM, BCDR, and INbreast datasets into one dataset resulting to 6116 images from a total of 1529 cases. Lesions were extracted as fixed-size ROIs during preprocessing, and the images were normalized using global contrast normalization and augmented with different transformations. L2 regularization and dropout techniques were applied to reduce overfitting. Five-fold cross-validation was used for training purposes. The MIAS dataset was used to assess the models' performance.

Arevalo et al. (2016) presented a representation learning method based on the hybrid CNN in a supervised way. The dataset includes 736 images which include both MLO and CC views. Preprocessing such as ROI extraction was done on the image by manual segmentation. Data augmentation was applied to enhance the number of the training images, and global and local contrast normalization was also used. They employed CNN for representation learning and SVM for classification. Dropout and max-norm were applied to reduce overfitting.

Carneiro et al. (2017) described a holistic approach that can classify both unregistered CC and MLO views of the mammographic images using CNN pre-trained on ImageNet. The baseline of the proposed model contains five convolutional layers with two fully connected layers and one softmax layer. The model can have 2D or 3D inputs and pre-trained and fine-tuned in four different manners. They used INbreast and DDSM datasets which are preprocessed with local contrast normalization and the otsu method.

Jadoon et al. (2017) presented two methods, convolutional neural network-discrete wavelet (CNN-DW) and convolutional neural network-curvelet transform (CNN-CT) for the classification of mammogram images. Datasets of 2796 patches from IRMA collected from four different sources were used. These mammogram patches were augmented, resized, and enhanced by applying CLAHE. They extracted dense scale-invariant features (DSIFT) for all subbands from both the methods which are then fed as input matrix to the CNN. They employed a softmax layer and SVM to train the CNN for classification.

Li et al. (2019) used an improved DenseNet known as DenseNet-II for the classification task of benign and malignant from the datasets provided by the First Hospital of Shanxi Medical University. These datasets were preprocessed through zero-mean normalization and data enhancement. Like the DenseNet, the improved DenseNet-II neural network model uses 40 layers with a growth rate of $k = 12$, including three dense blocks layers and two transition layers. However, in DenseNet-II, the Inception structure was employed to replace the first 3 * 3 convolutional layer of the DenseNet neural network model. The preprocessed mammogram datasets were inputted into five architectures of CNN, AlexNet, VGGNet, GoogleNet, DenseNet, and DenseNet-II.

Jiao et al. (2018) presented a jointly deep metric learning neural network for the classification of breast masses. The method consists of two layers, CNNs layers and metric learning layers. The CNNs layer used here is a variation of AlexNet and provides deep features representations directly learned from original breast mass images. The classification performance was further improved by adding a parasitic metric learning layer at the back of the CNNs structure. The suggested approach was trained on image instances from the DDSM database and evaluated on the DDSM and MIAS database, respectively.

Sun et al. (2019) proposed a method that integrates multi-view convolutional neural subnetwork (MV-CNN) and multi-view dilated convolutional neural subnetwork (MD-CNN). They added a penalty term to the cross-entropy loss function to reduce the rate of misclassification. The inputted breast mass images for training are resized to 180 * 180 pixels.

Song et al. (2020) classified mammographic masses into normal, benign, and malignant based on the combined features of a DCNN, GLCM, and histogram of the oriented gradient. The experimental dataset includes 11,562 ROIs of mammographic screen digitized images from the DDSM. They studied the performance of two classifiers, SVM and extreme gradient boosting (XGBoost) for the classification task. The performance of XGBoost outperforms SVM.

Cao et al. (2020) proposed the use of a multi-task U-shaped network (MT-UNet) to classify benign and malignant tumors. ResNet50 was used in the proposed technique. The model's main body is made up of four encoding and four decoding modules. The image is preprocessed using the CLAHE method and truncation normalization. To help overcome the problem of overfitting, a regularization technique called label smoothing was used. For training and prediction, a 512-pixel ROI square was cropped from the images of both the DDSM and INbreast datasets. Adam was applied as the optimizer to update the weights of the model during training.

Dhungel et al. (2017) presented an automated CAD system to detect, segment, and classify breast cancer masses based on a deep belief network (m-DBN) model and a Gaussian mixture model (GMM). To minimize false positives, a series of DL approaches are applied. The mass detection hypotheses are then refined using Bayesian optimization. Deep structured output learning was used to segment the observed ROIs, which was subsequently optimized using a level set technique. Finally, they applied a pre-trained classifier for mass classification on the INbreast database.

Al-antari et al. (2018) presented a comprehensive CAD system that uses the you-only-look-once (YOLO) method, a full resolution convolutional network (FrCN), and a pre-trained AlexNet model to identify, segment, and classify breast masses. AlexNet was trained on the INbreast database using Adam optimizer with a learning rate of 0.001.

Gao et al. (2018) proposed a shallow-deep CNN (SD-CNN) in contrast-enhanced DMs (CEDM). The visualization mappings of the convolutional layer in the CEDM images were extracted and combined with low-energy (LE) images using a four-layered shallow-deep CNN. The quality of LE images was increased by this virtual augmentation. ResNet was used to extract characteristics from these virtual merged images in order to classify benign and normal instances. When compared with DMs, using the SD-CNN on CEDM images resulted in a considerable improvement in classification accuracy.

Al-masni et al. (2018) presented a CAD system for detecting and categorizing malignant tumors based on the YOLO DL algorithm. The system employs a ROI-based CNN method that uses convolutional layers and fully connected neural networks. The model was fine-tuned using the DDSM dataset.

Huynh et al. (2016) classified breast cancer tumors using transfer learning and CNN. The authors suggested an approach that merged CNN and handmade characteristics to create an ensemble method (e.g., statistical and morphological features). The ensemble feature matrix was created by combining the features from each method. Five-fold cross-validation was used with the SVM classifier. Using 219 breast lesions, the accuracy of independent methods was compared with the ensemble method. Their findings demonstrated that the ensemble generated superior results than fine-tuned CNN and analytical feature extractor.

Arora et al. (2020) presented an ensemble of transfer learning models that carried out feature extraction which are fed later to a neural network classifier. The model was tested and evaluated with a total of 1318 preprocessed mass ROI images from CBIS-DDSM dataset.

Instead of the typical DCNN pooling approaches, Shu et al. (2020) suggested a deep CNN-based classification method that utilized two pooling structures. A pre-trained DenseNet169 model was used as feature extraction, and their pooling structure replaced the last classification layer. This model, which has a learning rate of 10 to 4, was trained with Adam optimizer, and tested on the INbreast and CBIS-DDSM databases.

Khan et al. (2019) suggested a multi-view feature fusion model. They used four mammography images for each breast. In the preprocessing stage, they used bilateral filter and contrast enhancement techniques. They adapted pre-trained CNN architectures including VGGNet, GoogleNet, and ResNet. By training their own weights, they found VGGNet to be the best CNN architecture for distinguishing cancer and normal mammography images.

Agnes et al. (2020) proposed a method that eliminated the necessity for a separate pooling layer by employing a larger stride convolution operation. The method also used multiple dilated convolution to extract multi-scale features for classification tasks. Images from mini-MIAS were augmented to a total of 4500 images and resized to 192 * 192 pixels. Preprocessing techniques such as median filter, global thresholding, standard morphological, and single-seeded region growing algorithm were applied.

Table 2 summarizes the methods listed above, as well as performance metrics.

2.1 Principal Findings from the Literature

The current study examined 23 papers. All of the papers addressed in this study used DCNN to alter breast cancer diagnosis systems. The need for a robust, dependable, and computationally efficient CAD system has recently been a key concern due to a rise in the number of breast cancer patients. Although DL aids with the challenge of identifying reliable features, it requires a considerable amount of data to train. To overcome overfitting during the training stage, the majority of research in the literature used data augmentation. One of the difficulties researchers have when training CNNs, according to the literature, is the training size of the dataset. The size of the training data, as well as the quality and balance of its classes, have a significant impact on the system's performance. Although most studies use techniques like data augmentation, transfer learning, and dropout to deal with the challenge of training with small sample size, this is still an unsolved topic.

Table 2 Summary of the literature studies

References	Method	Performance metrics
Shen et al. (2019)	VGG16 + ResNet50	AUC (0.98)
Kooi et al. (2017)	Pre-trained DCNN	AUC (0.80)
Altan (2021)	CNN, Deep Autoencoder	Acc (91.44%), AUROC (0.931)
López-Cabrera et al. (2020)	Inception v3	Acc (88.2%)
Ragab et al. (2019)	DCNN-SVM-AlexNet	Acc (79%), AUC (0.88)
Chougrad et al. (2018)	Inceptionv3-MD	Acc (98.94%)
Arevalo et al. (2016)	CNN + SVM	AUC (0.826)
Carneiro et al. (2017)	ConvNet	AUC (0.94)
Jadoon et al. (2017)	CNN-DW and CNN-CT	Acc (81.83%)
Li et al. (2019)	DenseNet-II	Acc (94.55%)
Jiao et al. (2018)	PML	Acc (97.4%)
Sun et al. (2019)	MVMDCNN-Loss	Acc (0.8202)
Song et al. (2020)	SF-XGBoost	Acc (94.80%)
Cao et al. (2020)	MT-UNet	AUC (0.9963), Acc (0.9817)
Dhungel et al. (2017)	m-DBN, GMM, CNN,RF	Acc (0.91), AUC (0.76)
Al-antari et al. (2018)	YOLO, FrCN, CNN	Acc (95.64%)
Gao et al. (2018)	SD-CNN	Acc (0.90), AUC (0.92)
Al-masni et al. (2018)	YOLO, FC-NNs	Acc (99.7%)
Huynh et al. (2016	AlexNet, SVM	AUC (0.86)
Arora et al. (2020)	DCNN-based Ensemble	Acc (0.88), AUC (0.88)
Shu et al. (2020)	DCNN with RGP/GGP	Acc (0.922)
Khan et al. (2019)	MVFF	AUC (0.932)
Agnes et al. (2020)	MA-CNN	Acc (96.47), AUC (0.99)

Notes Acc—Accuracy, AUC—Area under the curve, AUROC—Area under the receiver operating characteristic

3 Challenges of Deep Learning in the Classification of Breast Cancer from Mammogram Images

The scientific issues that must be addressed before the clinical application of the DL-CAD-based system were explored in this section.

Lack of training data: Obtaining enough data to train DL-CAD-based systems for breast cancer with millions of parameters is one of the most significant challenges. However, given the common use of data augmentation, transfer learning, and dropout to deal with the obstacle of training the model with little samples, this may not be a serious concern, but the problem has persisted.

Imbalanced dataset: The imbalance ratio between positive and negative classes in the training samples is a considerably more common problem. A dataset for training a model for identifying cancerous mass might only have a few positive samples but a lot of negative ones. Directly training CNN models on unbalanced datasets may benefit the prediction of more common classes. As a result, it's crucial to think about how the CNN model's accuracy is affected by using balanced and imbalanced datasets.

Technical challenges: There are various obstacles in using transfer learning in deep learning, including architectural selection, the amount of samples required to fine-tune the model, and the number of layers employed on top of the pre-trained model. Furthermore, the effectiveness of transfer learning reduces when the targeted task differs from the source task.

Non-annotated dataset: Another issue that researchers are grappling with is training a model with unannotated data. The input image to the CNN model in a non-annotated dataset is binary tagged as normal or malignant, with no information on the position of the abnormalities. The training of CNNs on non-annotated datasets is still a topic of research.

4 Conclusion

To summarize, using CNNs to extract essential features for automatic breast cancer diagnosis, particularly in dense breasts, could be a promising method. Furthermore, in medical image processing, experts have shown that employing CNNs is more effective than using a traditional method. CNNs appear to provide a way for retrieving features automatically via a self-learning network, enhancing classification accuracy. Better structures, larger datasets that solve issues of class imbalance, and new optimization approaches are still needed.

References

Agnes SA, Anitha J, Pandian SI, Peter JD (2020) Classification of mammogram images using multiscale all convolutional neural network (MA-CNN). J Med Syst 44(1):1–9

Al-Antari MA, Al-Masni MA, Choi MT, Han SM, Kim TS (2018) A fully integrated computer-aided diagnosis system for digital X-ray mammograms via deep learning detection, segmentation, and classification. Int J Med Inform 1(117):44–54

Al-Masni MA, Al-Antari MA, Park JM, Gi G, Kim TY, Rivera P, Valarezo E, Choi MT, Han SM, Kim TS (2018) Simultaneous detection and classification of breast masses in digital mammograms via a deep learning YOLO-based CAD system. Comput Methods Prog Biomed 1(157):85–94

Altan G (2021) A deep learning architecture for identification of breast cancer on mammography by learning various representations of cancerous mass. In: Deep learning for cancer diagnosis. Springer, Singapore, pp 169–187

Arevalo J, González FA, Ramos-Pollán R, Oliveira JL, Lopez MA (2016) Representation learning for mammography mass lesion classification with convolutional neural networks. Comput Methods Prog Biomed 1(127):248–257
Cao H, Pu S, Tan W, Tong J, Zhang D (2020) Multi-tasking U-shaped network for benign and malignant classification of breast masses. IEEE Access 7(8):223396–223404
Carneiro G, Nascimento J, Bradley AP (2017) Automated analysis of unregistered multi-view mammograms with deep learning. IEEE Trans Med Imaging 36(11):2355–2365
Chougrad H, Zouaki H, Alheyane O (2018) Deep convolutional neural networks for breast cancer screening. Comput Methods Prog Biomed 1(157):19–30
Dhungel N, Carneiro G, Bradley AP (2017) A deep learning approach for the analysis of masses in mammograms with minimal user intervention. Med Image Anal 1(37):114–128
Gao F, Wu T, Li J, Zheng B, Ruan L, Shang D, Patel B (2018) SD-CNN: a shallow-deep CNN for improved breast cancer diagnosis. Comput Med Imaging Graph 1(70):53–62
Heath M, Bowyer K, Kopans D, Kegelmeyer P, Moore R, Chang K, Munishkumaran S (1998) Current status of the digital database for screening mammography. In: Digital mammography. Springer, Dordrecht, pp 457–460
Huynh BQ, Li H, Giger ML (2016) Digital mammographic tumor classification using transfer learning from deep convolutional neural networks. J Med Imaging 3(3):034501
Jadoon MM, Zhang Q, Haq IU, Butt S, Jadoon A (2017) Three-class mammogram classification based on descriptive CNN features. Biomed Res Int 15:2017
Jiao Z, Gao X, Wang Y, Li J (2018) A parasitic metric learning net for breast mass classification based on mammography. Pattern Recogn 1(75):292–301
Khan HN, Shahid AR, Raza B, Dar AH, Alquhayz H (2019) Multi-view feature fusion based four views model for mammogram classification using convolutional neural network. IEEE Access 13(7):165724–165733
Kooi T, van Ginneken B, Karssemeijer N, den Heeten A (2017) Discriminating solitary cysts from soft tissue lesions in mammography using a pretrained deep convolutional neural network. Med Phys 44(3):1017–1027
Lee RS, Gimenez F, Hoogi A, Miyake KK, Gorovoy M, Rubin DL (2017) A curated mammography data set for use in computer-aided detection and diagnosis research. Sci Data 4(1):1–9
Lehmann TM, Güld MO, Thies C, Fischer B, Spitzer K, Keysers D, Ney H, Kohnen M, Schubert H, Wein BB (2004) Content-based image retrieval in medical applications. Methods Inf Med 43(04):354–361
Li H, Zhuang S, Li DA, Zhao J, Ma Y (2019) Benign and malignant classification of mammogram images based on deep learning. Biomed Signal Process Control 1(51):347–354
Lopez MG, Posada N, Moura DC, Pollán RR, Valiente JM, Ortega CS, Solar M, Diaz-Herrero G, Ramos IM, Loureiro J, Fernandes TC (2012) BCDR: a breast cancer digital repository. In: 15th international conference on experimental mechanics, vol 1215, 2012 Jul 22
López-Cabrera JD, Rodríguez LA, Pérez-Díaz M (2020) Classification of breast cancer from digital mammography using deep learning. Intel Artif 23(65):56–66
Moreira IC, Amaral I, Domingues I, Cardoso A, Cardoso MJ, Cardoso JS (2012) Inbreast: toward a full-field digital mammographic database. Acad Radiol 19(2):236–248
Ragab DA, Sharkas M, Marshall S, Ren J (2019) Breast cancer detection using deep convolutional neural networks and support vector machines. PeerJ 28(7):e6201
Ridhi A, Rai PK, Balasubramanian R (2020) Deep feature–based automatic classification of mammograms. Med Biol Eng Comput 58(6):1199–1211
Shen L, Margolies LR, Rothstein JH, Fluder E, McBride R, Sieh W (2019) Deep learning to improve breast cancer detection on screening mammography. Sci Rep 9(1):1–2
Shu X, Zhang L, Wang Z, Lv Q, Yi Z (2020) Deep neural networks with region-based pooling structures for mammographic image classification. IEEE Trans Med Imaging 39(6):2246–2255
Song R, Li T, Wang Y (2020) Mammographic classification based on XGBoost and DCNN with multi features. IEEE Access 8(8):75011–75021

Suckling J, Parker J, Dance D, Astley S, Hutt I, Boggis C, Ricketts I, Stamatakis E, Cerneaz N, Kok S, Taylor P (2015) Mammographic image analysis society (mias) database v1. 21

Sun L, Wang J, Hu Z, Xu Y, Cui Z (2019) Multi-view convolutional neural networks for mammographic image classification. IEEE Access 3(7):126273–126282

Sung H, Ferlay J, Siegel RL, Laversanne M, Soerjomataram I, Jemal A, Bray F (2021) Global cancer statistics 2020: GLOBOCAN estimates of incidence and mortality worldwide for 36 cancers in 185 countries. CA Cancer J Clin 71(3):209–49

Who.int. Breast cancer [cited 15 January 2021]. Available from https://www.who.int/news-room/fact-sheets/detail/breast-cancer

Brain Tumour—Augmentation, Segmentation and Classification Using Deep Learning—A Review

Ranadeep Bhuyan and Gypsy Nandi

Abstract Tumour can be detected early and prevented, although this is not always practicable. Image augmentation and segmentation is an important method used to enhance the properties and abilities of deep learning architectures and can be generalised with the regularisation of the image data. This method plays an important role where the number of original training image data is limited and deriving new attributes from image data becomes expensive and time-consuming. This is a general and common issue in medical image analytics, especially when it is about brain tumour classification and prediction. In this paper, we reviewed the recent enhancement in the field of cancer image generation algorithms used over a number of magnetic resonance brain tumour images. For more understanding of the practical and real aspects of most of the algorithms, our work investigates the articles written and submitted on challenges faced for multimodal brain tumour segmentation. This review also verifies which image augmentation techniques were exploited and what were the research impacts on the capabilities with supervised learning scenarios. In the end, we highlighted the use of pre-trained CNN-based architectural methods such as H2NF, GoogleNet, UNet, etc., in order to serialise and synthesise high-quality automated brain tumour examples which can give a boost to the capabilities of deep learning models.

Keywords Brain tumour · Image augmentation · Segmentation · MRI · Deep neural network · Pre-trained CNNs

R. Bhuyan (✉) · G. Nandi
Assam Don Bosco University, Guwahati 781017, India
e-mail: ranadeep.bhuyan@gmail.com

J. K. Deka et al. (eds.), *Emerging Technology for Sustainable Development*,
Lecture Notes in Electrical Engineering 1061,
https://doi.org/10.1007/978-981-99-4362-3_21

1 Introduction

According to the World Health Organisation (WHO), cancer is the second largest cause of death worldwide (World Health Organization 2022). A tumour, unlike cancer, can be benign, pre-carcinoma, or malignant. Benign tumours are distinguished from malignant tumours in that they do not spread to other organs or tissues and can be surgically removed. Gliomas, meningiomas, and pituitary tumours are examples of primary brain cancers. Gliomas are tumours that grow from tissues other than nerve cells and blood vessels in the brain. Meningiomas, on the other hand, come from the membranes that protect and surround the brain and central nervous system, whereas pituitary tumours are lumps inside the skull (Cancer Treatments Centers of America Brain Cancer Types 2019). The most significant distinction between these three tumour forms is that meningiomas are usually benign, but gliomas are almost always malignant. Pituitary tumours, unlike meningiomas, which are slow-growing tumours, can induce additional medical problems, even if they are benign (Asif et al. 2018; Wong 2015). The exact classification between these three types of tumours is a critical stage in the clinical diagnosis process, as seen by the information presented in Asif et al. (2018), Wong (2015).

In this review paper, we studied the brain tumour segmentation models that are accessible in the cited works of various related research work. We also investigated some of the latest strategies that have been employed by researchers who are dealing with issues in multimodal tumour image segmentation during BraTS challenges during 2018 to 2021. The images utilised for the BraTs yearly challenges are the most popular and exhaustive list of brain tumour datasets used to verify existing and advanced technologies for tumour identification and segmentation by augmenting brain MRI images. Furthermore, it includes both low and high-grade lesions (damage or abnormal change in an organism's tissue) (Amit et al. 2017).

The binary classification method, such as malignant or benign, is generally simple; nevertheless, radiologists face a difficult problem in classifying multimodal brain tumours. There are four major (T1, T2, T1CE, and Flair) components of deep learning optimisation techniques, viz, (1) the deep neural network architecture, (2) the per-sample loss function (e.g. dice loss) that determines the stochastic gradient, (3) the population loss function (e.g. empirical risk) that determines how to merge the stochastic gradients into one aggregated gradient, and (4) the optimiser (e.g. Adam network optimiser) that determines how the aggregated gradient is used to update the parameters of the deep neural network at each training iteration. We investigate per-sample loss function, population loss function, and optimiser modifications for use in automatic brain tumour segmentation in this paper.

The participants were supplied multimodal MRI imaging data of brain tumour patients (low and high-grade gliomas, as previously stated) with the image segmentation provided by BraTS challenge. They also provided the grounds for truth multiclass classification indicated in Sect. 3. Various sequences in the collection are referenced to the anatomical format of the subject and interpolated with the same resolution. The key aim is to create a supervised learner capable of performing well on unseen data that is presented throughout the testing period. This paper outlines the augmentation models used with 20 distinct publications in BraTS 2018 in Sect. 4. Our emphasis here is on papers that only state that data augmentation was employed and specifically state what type of augmentation was used. Single-modal augmentation implies that they operate on MRI from a single floor of sequencing and may be used in conjunction with co-registered sequences to enhance multimodal tumour specimens. Lastly, this paper closes in Sect. 5, which summarises the efficiency and drawbacks of the studied augmentation models. In particular, the promising research routes that arise with BraTs are highlighted.

A convolutional neural network (CNN) has lately been highlighted in computer vision studies for both supervised and unsupervised learning. CNNs are used for a variety of tasks and purposes, including image processing, computer vision tasks such as localisation and segmentation, video analysis, detecting obstacles in self-driving cars, and natural language processing. CNN is made up of convolutional, pooling, and fully linked layers. The convolutional layer's principal function is to identify patterns, lines, and edges, among other things. Several kernels produce multiple feature images and perform well in vision tasks like segmentation and classification. Classification, object detection, image segmentation, and image synthesis are all examples of radiological applications. Post that, image transformations are done using various pre-trained CNNs such as MobileNet, InceptionV3, ResNet152V2, Xception, DenseNet201, InceptionResNetV2, and VGG19 in the agriculture area. We discussed augmentation with flip and rotation with a certain probability factor. This study gave a comprehensive comparison of some of the CNN architectures such as InceptionV3, ResNet152V2, H2NF, GoogleNet, DenseNet201, InceptionResNetV2, VGG19, etc. CNN-based computer vision technique involves primarily two things viz, augmentation for predicting missing data and features and segmentations to isolate the problem area for further analyses and prediction. In this review paper, we will discuss these two techniques using some of the latest advanced methods where CNN is the core of those architectures primarily in the medical imaging domain focusing on brain tumours.

2 Data Augmentation in Brain Tumour Segmentation

In general, data preprocessing strategies are used to increase the amount and size of training datasets in order to supply more descriptive training sets to large capacity learning. As a consequence, there is indeed a craze in deep learning reviews wherein data are supplied in the testing planning and scheduling augmentation scenario on the fly (during interference). Test time augmentation increases trained models' robustness by stimulating the formation of homogeneous ensembles, in which $[n + 1]$ systems of similar type are trained on similar training examples voted for a class

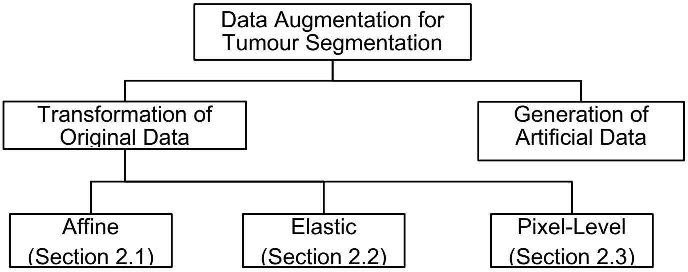

Fig. 1 Taxonomy augmentation for tumours segmentation

label with each incoming test sample where n is the number of automatically generated samples multiplying the number of test instances to be classified. Augmentation techniques for brain tumour segmentation with MRI can be divided into below categories (which is rendered in a taxonomy in Fig. 1).

The models explain different transformations of actual data, which include affine image transformation (Sect. 2.1), elastic transformation (Sect. 2.2), pixel-level transformation (Sect. 2.3), and several other approaches to generate artificial data (Sect. 2.4). In the next subsections, we examine the models associated with each set of these augmenting strategies in depth.

The design feasibility of deep learning models is often compared with their ability for suitable classification when trained with original data. Earlier, those were tested with unknown examples that are mostly noisy or re-created by heuristic methods. In deep networks, testing time enhancement may be used to assess the degree of uncertainty during inference. It brings up fresh and amazing possibilities in the field of medical image analytics, particularly when it comes to monitoring the robustness of deep CNN dependability, both of which are key experimental difficulties, Wang et al. (Zhang et al. 2010). In the case of MRI brain tumour segments, such augmenting may use methodologies that may alter the following example by giving affine, elastic, or pixel-level alteration.

A block diagram depicting combined training and time consumption knowledge augmentation is shown in Fig. 2. This paper is reviewing, augmentation and segmentation and the challenges faces by recent BraTS datasets in 2020 and 2021.

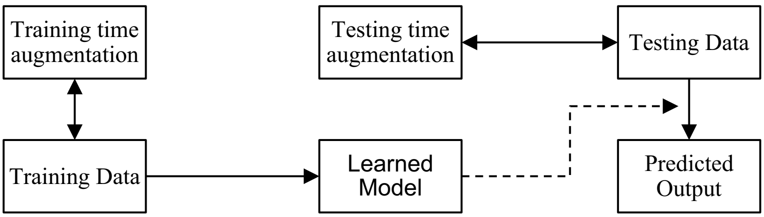

Fig. 2 High-level building blocks for augmentation process

2.1 Affine Transformation of Images for Augmentation

Existing data have been subjected to different processes such as rotation, zooming, crop varieties, as well as flipping to determine the number of training instances used with affine modelling by Pereira et al. (Carver et al. 2019; Castro et al. 2018). They emphasised that certain standardised data augmentation treatments create equivalence class pictures, therefore there may be a few gains for such deep belief network scenarios with future generalisation with unknown test data (examples with non-regularise the issue sufficiently). In addition, they may create inaccurate results when utilising rotation. On the other hand, affine picture modifications are simple to construct both in 2D or 3D, are quite versatile in their hyper characteristics, and may be extensively employed in the evaluation. Figure 3 shows an example of how the use of a basic augmentation model might result in a specified increasing total variety of training samples.

Figure 3 depicts how a basic affine transformation yields new synthetic image patches because different augmentation procedures may be used at various levels of the augment tree. The number of automated instances may be expressly increased. Building rotational training models were critical in boosting the general capability of existing deep models, according to multi-fold cross-validation tests. Our implementation of Friedman's rank tests, which suggest horizontally flipping with more extra rotation, is critical to developing highly specialised deep neural networks inside the patch initial section to validate the quantitative significance of the data. Similarly, in the augmentation phase, Nalepa et al. employed diffeomorphic picture registration (DIR) in combination with a suggested strategy to choose train image pairs for registration by Nalepa et al. (2019b).

2.1.1 Flip Plus Rotation

Flip creates a mirror reflection of the original picture including one or even more axes. Natural photographs may generally be flipped with a horizontal plane, but not with the vertical since the upper and bottom elements of the image are not usually interchangeable. In most circumstances, MRI scans in the long axis of a brain picture

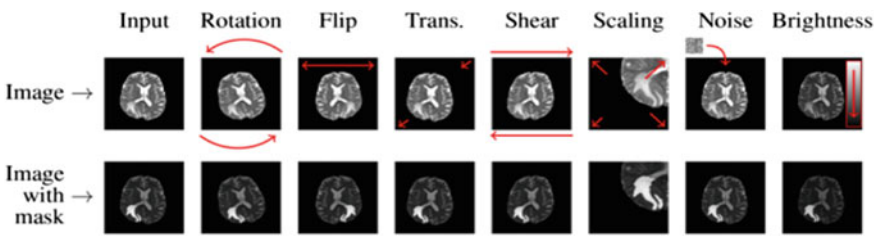

Fig. 3 Applying affine transformation and pixel-level transformations to increase size (Nalepa et al. 2019a)

have two hemispheres and may be considered anatomically comparable. Flipping with the horizontal axis switches the hemispheres from left to right and right to left. This flip may aid multiple deep classifications, particularly for context tumour data, with the constant w.r.t location within the brain picture; otherwise, not reflecting training data is tough (with the brain tumours present only in the left to the right hemisphere). In this situation, the same as rotating its picture by an angle dependent on the centre pixel might be used. This model has been properly interpolated to suit the original picture size. The rotations operation denoted by R (in Eq. 1) is often used with thresholding given to missing pixels where α is the angle of rotation around its centre pixel.

$$R = \left(\frac{\cos\alpha - \sin\alpha}{\sin\alpha \cos t\alpha} \right) \tag{1}$$

2.1.2 Translation

When using padding in compliance, the translating process changes the whole picture by a specified pixel density in the desired direction. This permits the networks to avoid being too focused on traits found mostly in a single spatial location. In the case of rotational MRI scans, the various patients accessible in the training dataset are frequently non-registered translations of images with the specified amount of pixels along a selected axis which is much more than two axes and may produce acceptable viable synthetic images during the augmentation process. Furthermore, this model is not as beneficial for deep architecture as convolutional neural network (CNN), which demonstrates convolution layer and pooling spatially invariant structures internally (Asif et al. 2018).

2.1.3 Cropping Plus Scaling

Choosing input as a scaled image of the original into the training set may assist deep neural networks in learning with useful deep characteristics that are independent of actual scale. This type of operation S may be carried out individually in multiple directions (since we have two dimensions in this case):

$$S = \begin{pmatrix} S_x & 0 \\ 0 & S_y \end{pmatrix} \tag{2}$$

In Eq. 2, S_x and S_y with x- and y-coordinates are the scaling properties. Tumours range in size, and scaling may introduce a variety of enhanced pictures within training sets. Because various deep architectural elements need photographs of the very same size, scaling is usually partnered with cropping to retain the image's true dimensions. This augmented brain tumour sample may tag characteristics of different sizes. Also, cropping might be confined to a field of view with all the critical picture components (Bakas et al. 2017, 2017, 2018).

2.1.4 Shearing

The shearing "H" transformation swaps each pixel of an image in the given direction. That substitute is proportionate to one's distance away that runs parallel to and through the origin.

$$H = \begin{pmatrix} 1 & h_x \\ h_y & 1 \end{pmatrix} \tag{3}$$

In Eq. 3, h_x and h_y are the shear coefficients in the x and y axis, respectively. Furthermore, this mode may reform the forms, as it is seldom used to supplement the MRI image data since this work often wishes to preserve the original shape of data characteristics as described by Frid-Adar et al. (2018).

2.2 Image Augmentation Using Elastic Registration

Image augmentation approaches based on unconditional elastic transformations of training samples may include shape variations (Suicheng et al. 2014). If the reforming area is modified, it will be noisy and dispersed throughout the training set, as shown by Chaitanya et al. (2021). Gu et al. (2014) used a few more flexible transformations to produce a completely unrealistic MRI scan of a brain imaging. If simulated tumours with unknown placements are implanted, the flow would push the segmentation algorithm to become insensitive to contextual input and concentrate on lesion traits by Dvornik et al. (2021). Furthermore, some research suggests that certain intelligence augmentation may damage the effectiveness of procedures in brain tumour delineation, which is a long-pending concern. Chaitanya et al. (2019, 2021) used visual unrealistic instances to boost MRI segmentation and found that it was somewhat counterintuitive, maybe owing to intrinsic structure and reconstruction associated properties of the cardiovascular system. B-splines are more often used in elastic transformations (Huang), (Huang and Cohen 1996; Castro et al. 2018). Diffeomorphic mapping is important in brain pictures because it can preserve topology and regenerate physiologically plausible reformations. The diffeomorphic mapping is given n frequency dimension of a source picture I and converts I to the targeted image as J: I 1 (x, 1) in Fig. 4. That's the correct solution to the differential equation as given in Eq. 4.

$$\frac{\mathrm{d}\varphi(x,t)}{\mathrm{d}t} = v\varphi(x,t), t \tag{4}$$

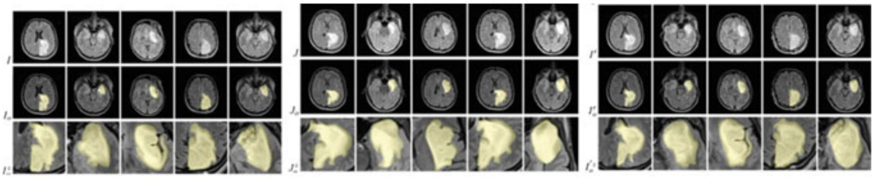

Fig. 4 Diffeomorphic registration on each MRI image to obtain visually possible synthetic images

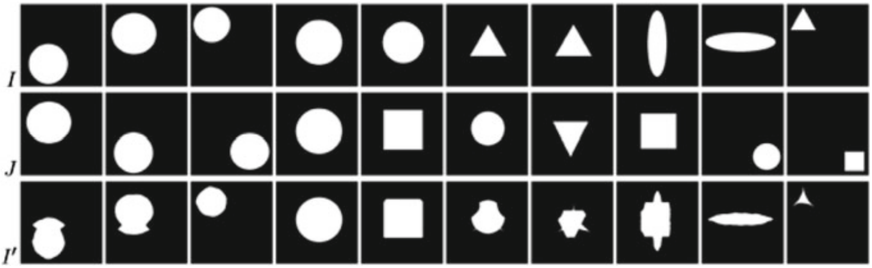

Fig. 5 Diffeomorphic affine registration on basic shapes simple (Nalepa et al. 2019a)

In Eq. 4, where $\varphi(x, 0) = x$ and v is dependent on time of the vector field in the direction of velocity, v: t Rd, (x, t) is a geodesic route "d" specifies spatial domain's dimensionality, and (x, t): t. They directly used controlled free-form distortion in Nalepa et al. (2019b, 2019c) where B-splines described by Tustison et al. (2018) used regularised velocity vector fields.

Nalepa et al. (2019b, 2019c) calculated the B-spline basis functions, for each parametric dimension for N number of pixels, the B-spline functions operate as a regularised solution (Zhang et al. 2010; Yue et al. 2021; Nalepa et al. 2019b).

In Fig. 4, source (I) has a target (J) which depicts brain tumour pictures created by diffeomorphic registration, and such automatically generated data significantly boosts the powers of deeper learning, especially when paired with affine transformation. The resulting (I′) pictures include the topologic information about the original image data (I) as well as visible alterations to the tissue (Nalepa et al. 2019b).

Relevant constructs registering may be used on more than only photos and anatomic features. Figure 5 depicts instances of sample forms that have undergone changes. This data is plainly visible in the created photos as well.

2.3 Data Augmentation Using Pixel-Level

With pixel image transformations, there are augmentation models that cannot modify the geometrical forms of the picture (thus all geometrical properties will not change throughout the augmentation process), but it still influences the intensity values (local or to the entire image). Such a method, in which multiple training photos are retrieved from various places can only help image analytics. As a result, they may have varying intensity values or gradient saturations by default. During pixel-level augmentation, the intensity of pixels is typically disrupted by randomised or zero means noise like standard error according to the precise data dimension with a specified probability, which is known as intensity changes. Other pixel operations include shifting and scale of brightness pixel values by gamma correction and its different versions (Agarwal and Mahajan 2017) via sharpening, blurring, and so on (Galdran et al. 2017). This data augmentation methodology is used for maximum energy and dimensional data since it is simple to apply to certain dimensions by Nalepa et al. (2019c).

2.4 Brain Image Augmentation with Synthetic Data

Various ways of generating artificial datasets (GAD) have been developed to exploit difficulties relating to picture augmentation techniques. Generative adversary networks (GANs), which Goodfellow et al. (2014, 2020) initially reported, are currently being utilised to augment MRI datasets used by Han et al. (2019). The basic purpose of a GAN is used to generate new sample data that the determiner cannot differentiate from the original information. Chaitanya et al. (2021), Lachinov et al. (2020), and Sunita et al. (2022) presented a few unique GAN architectures that use a coarse-to-fine synthesis to capture the variety of train data and generate improved examples. Adversarial networks have also been used for brain tumour text categorisation, tumour diagnostics (Frid-Adar et al. 2018; Han et al. 2019; Yue et al. 2021), and multimodal image synthesis by Yue et al. (2021). Although GANs allow us to begin normalisation, serviceability of profound network architectures about interpolation image transformation (e.g. twisting, expandability, or turning) and shape feature variants, the assimilation of reinforcement methods and the existence of its position of equilibrium stay open problems. Lastly, there really are cases when the generator creates numerous similar samples, which hinders the system's generalised statement, known as the "modal collapse problem" described by Wang et al. (Gibson et al. 2018) (Fig. 6).

In their brain tumour segmentation task Yue et al. (2021) used the aforementioned 3D MI-UNet also outputs four probability maps that, respectively, represent the probability that each voxel belongs to the background. A trained 3D MI-UNet is used to predict the training data and then use the 2D slices of the four multimodal tumour images. They named it as joint 3D + 2D MI-UNet.

In their work Yue et al. (2021) combined three UNet architectures to achieve a higher modality of segmentation and then segment classifications.

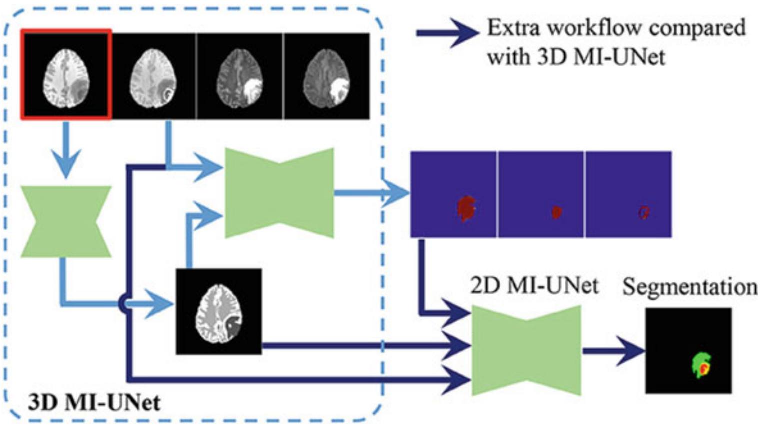

Fig. 6 Joint 3D + 2D MI-UNet (Yue et al. 2021)

3 Segmentation of Image Data

The hospital gathers clinical data from MR tumour scans with the patients' approval during their treatment. Doctors use the acquired MR brain data to assess patients' conditions and provide appropriate and successful treatment strategies. Researchers are not allowed to utilise such data for research without the approval of patients and hospitals due to patient privacy and ethical concerns. Because each hospital collects clinical data at different phases from multiple patients, and the equipment used to gather the data is also diverse, comparing the segmentation performance of all these works is impossible. The revised 3D UNet approach presented by *X* Feng et al. (2018) has greater segmentation accuracy in the total tumour, core tumour, and enhanced tumour based on experimental data alone. The model is made up of two paths: contraction and expansion. The context is mostly captured by the shrinking path, while the expanding path achieves the goal location. Also taken into account are the activation function and loss and data enhancement. As a result, each segmentation metric is helped to raise.

In this paper, we investigated the methodology employed by BraTS 2021 and 2020 participants to distinguish brain tumours from MRI (at least 138 unique ways have been found across multiple years) as well as the enhanced models utilised in these methods, in this work. Each research work had manual data annotation processes by reviewers. The image set is accessible initially by four modalities: pre-contrast T1-weighted (T1), comment T1-weighted (T1c), efforts have been made (T2), and T2 fluid damped reversal recovery (T2) (FLAIR). All pixels are labelled with one of five labels: healthy tissues, Dang tumour (ET), peritoneal oedema (ED), necrotic and tumour core non-enhanced (NCR/NET), or necrotic and non-enhancing tumour core (NCR/NET). The skull was stripped from the scan and interpolated back to the same shape with accurate voxels. Because the research was done in many places and with various scanners, the image quality in this dataset is quite uncommon. The

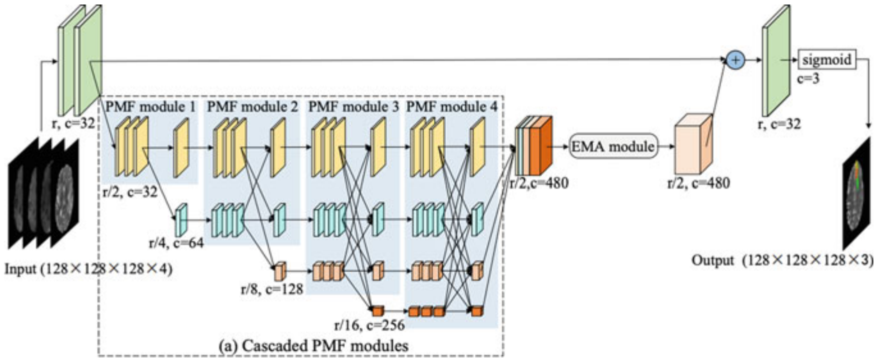

Fig. 7 Hybrid high-resolution and non-local feature network (H2NF-Net) for this challenging task (Jia et al. 2020)

demarcation approach, on the other hand, was very well developed, enabling similar surface markings across several readers (Fig. 7).

In Jia et al. (2020), proposed a hybrid high-resolution and non-local feature network (H2NF-Net) for this challenging task. Compared with the original HNF-Net, the proposed H2NF-Net adds a two-stage cascaded HNF-Net and uses the single and cascaded models to segment different brain tumour sub-regions. Jia et al. evaluated the proposed method on the BraTS 2020 challenge dataset. In addition, they also introduced the detailed implementation information of our second-place solution to BraTS 2020 challenge segmentation task (Fig. 8).

The BraTS dataset was created for this aim as a standardised brain tumour dataset for evaluating the performance of current and novel detection and segmentation techniques. It is the most extensive, diversified, and easily annotated collection. This heterogeneity is critical since it encompasses a wide range of tumour characteristics, and the models trained on BraTS data sets are transferrable to segregating other imaging techniques (Nalepa et al. 2019).

DICE aka F1 score is (2 * Area of Overlap)/(total pixels combined)

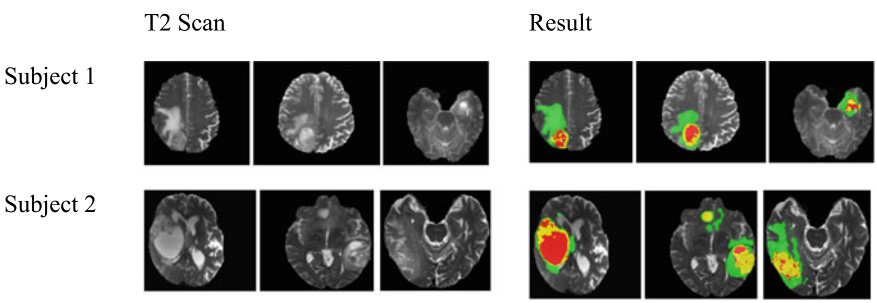

Fig. 8 H2NF-Net for brain tumour segmentation proposal (Jia et al. 2020)

Table 1 Single and cascaded HNF-Net dice factor analysis (Jia et al. 2020)

Method	Dice (%)				95%HD (mm)			
	ET	WT	TC	Mean	ET	WT	TC	Mean
Single*	0.78492	0.91261	0.83532	0.84428	26.60476	4.17888	5.41503	12.06622
Single+	**0.78908**	0.91218	0.84887	0.85004	**26.50355**	**4.10500**	5.14468	11.91774
Cascaded*	0.77647	0.91084	0.85631	0.84787	26.68954	4.38397	**4.93158**	12.00169
Cascaded+	0.77338	0.91022	**0.85701**	0.84687	29.71248	4.30247	4.93369	12.98288
H^2NF-Net	0.78751	**0.91290**	0.85461	**0.85167**	26.57525	4.18426	4.97162	**11.91038**

Table 2 Parameter numbers (M) and FLOPs of both methods (Jia et al. 2020)

Method	Params (M)	FLOPs (G)
Single HNF-Net	16.85	436.59
Cascaded HNF-Net	26.07	621.09

$$\mathrm{DICE}(A, B) = 2\frac{|A \cap B|}{|A| + |B|} \tag{5}$$

In Eq. 5, there A and B are two sections in this study, human and synthetic, 0 DICE 1, and DICE = 1 represents the ideal score of segmentation methods where a deeper layer was trained, so over the BraTS training dataset and utilised for segregating the testing all individual test cases, but at the other hand, recognised 85.7% of tumours (6/7 patients) with an overall whole tumour DICE = 0.84. This little experiment demonstrates segmented algorithms and models are learned and can detect tumour features in MRI data obtained and processed using various techniques, allowing us to get high-quality segments.

Table 1 shows segmentation performances of our method on the BraTS 2020 validation set. DSC: dice similarity coefficient, HD95: Hausdorff distance (95%), WT: whole tumour, TC: tumour core, ET: enhancing tumour core. $*$: ensemble of models trained with five-fold cross-validation, $+$: ensemble of models trained with entire training set.

Jia et al. (2020) also provide the parameter numbers and floating point operation per second (FLOPs) of both single and cascaded HNF-Net, given in Table 2.

3.1 Segmentation of BraTS Images

BraTs 2018 image data is rendered in Fig. 9 with 2 low-grade and 2 high-grade glioma patients, along with corresponding multiclass ground truth citations. It's good the data with different parts of tumours are manifested in different models, e.g. necrotic and unenhanced tumour core is hype intensity in T1c when compared with T1 (Bakas

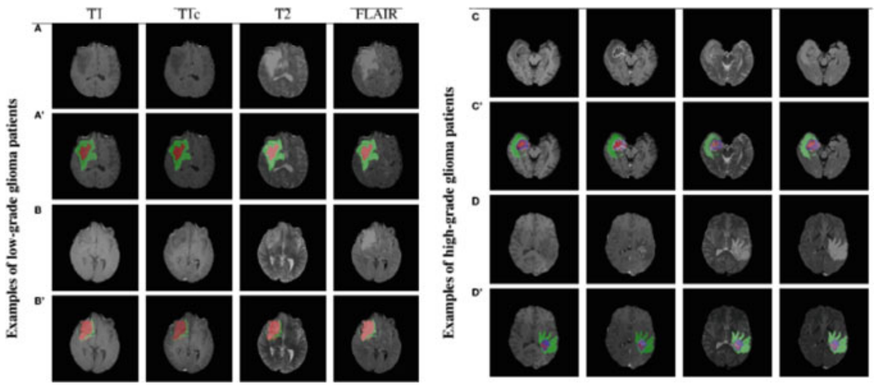

Fig. 9 Examples of low-grade and high-grade glioma tumours BraTS, datasets

et al. 2018). So multimodal analytics comes crucial with full benefits from an existing image with pathological labels.

All of those models were trained using the BraTS 2018 dataset, which also included MRI-DCE data from 285 patients given a diagnosis of gliomas: 210 with top-grade glioblastomas (HGG) and 75 with low-grade glioblastomas (LGG), and validated using a validation set of 66 old undiscovered patients (both LGG and HGG, but the standard was not divulged) by Akbari et al. (Bakas et al. 2017, 2017, 2018).

Figure 10 depicts an example segmentation method produced by both DIR or flip deep networks and the accompanying DICE values. The actual network, built on the same training sets, works together, will identify, and segment huge volume tumours flawlessly. It underperformed for relatively tiny lesions that were there in the training sample (Fig. 10a–c). Similarly, synthesising new training instances aided in boosting the performance of their proposed models in the diagnosis of brain tumours situated in parts of the brain that were not initially included in the database (by applying rotation and flipping). Furthermore, the training dataset's centroid was increased to 16. The combined technique offered statistically significant DICE in the Wilcoxon test by p 0.01, improving when compared with a randomised augmentation method.

4 Brain Tumour Classification

This section explains the approach for detecting a brain tumour using a brain MRI. (1) Tumour versus Non-Tumour Dataset: The online data for tumorous and non-tumorous classification was acquired from an online source (Brain Tumor Detection 2020). There are 154 tumorous MRIs and 91 non-tumorous MRIs in this collection. The sample of tumorous and non-tumorous brain MRI is shown in Figs. 10 and 11. Preprocessing is the process of preparing something before it is used. The intensity

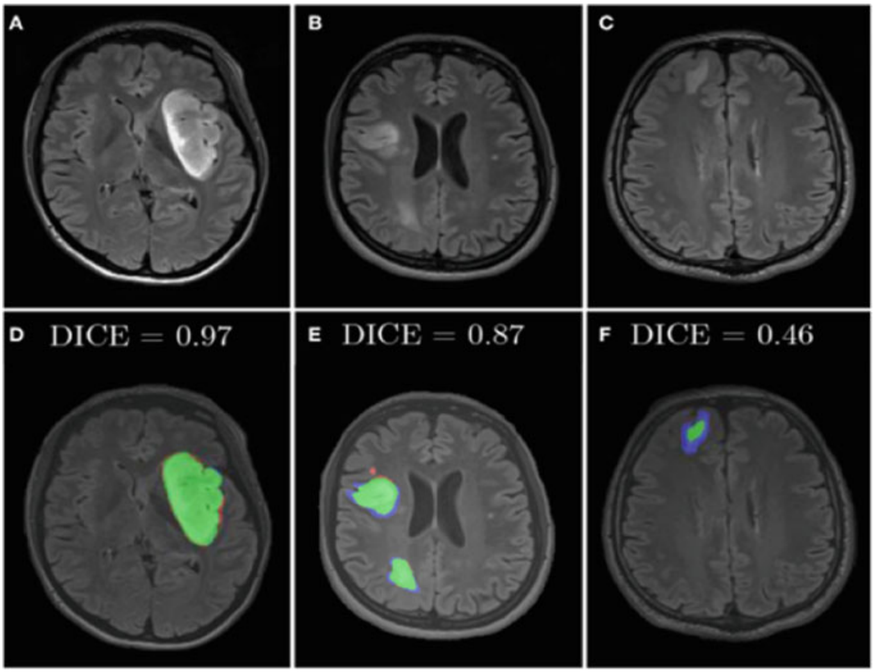

Fig. 10 Brain MRI image segmented using deep network

falls within the range of pixel values translated into the [0 1] range during the normalisation process. Each pixel's intensity is divided by the image's maximum intensity values in this process. By producing a larger source, normalisation might provide binary thresholding. Variations in greyscale value might alter classifications, thus these MRI pictures can help. (3) Skull stripping: Skull stripping is a required step in biomedical image examination for the accurate analysis of brain malignancies from brain MRI (Zhang et al. 2010). The non-brain elements of the brain, such as skin, fat, and the skull, are removed from the MRI.

Sunita et al. (2022) presented brain tumour detection and classification techniques shown in Fig. 2. The three stages of the proposed system as mentioned in Sunita et al. (2022) are brain tumour detection, benign and malignant brain MRI classification, and glioma and meningioma brain MRI classification (Table 3).

Tumours are classified in many dimensions, size shape, fatality, locations, etc. Figures 11 and 12 show a couple of ways to classify them in current studies and diagnoses around the brain tumour research communities. Figure 12 shows a broad classification of brain tumours done by recent American Association of Neurological Surgeons (AANS) publications on their official website.

In this paper, we are studying a couple of classification methods that adhere to WHO and AANS classifications for brain tumours. We studied in depth by Sunita

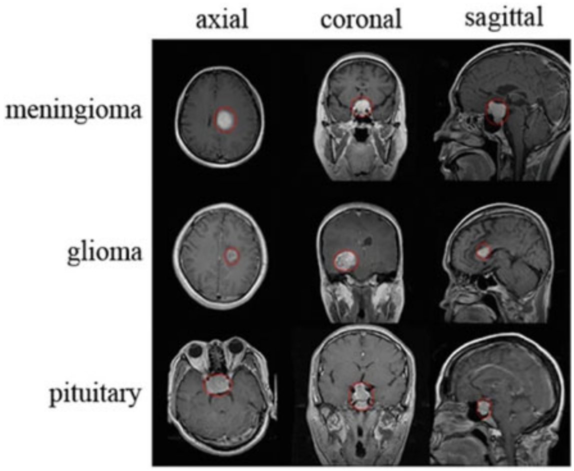

Fig. 11 Classification of tumour-based on location (David 2016)

Table 3 Examples of brain tumour severity and location by WHO

Grade	Characteristics	Tumour type
G-I	Least malignant (benign) Curable via surgery Non-infiltrative Long-term survival Slow growing	Pilocytic astrocytoma Craniopharyngioma Gangliocytoma Ganglioglioma
G-II	Relatively slow growing Mild infiltrative Tend to recur	Diffuse astrocytoma Pineocytoma Pure oligodendroglioma
G-III	Infiltrative Malignant Recur as high grade	Anaplasic astrocytoma Anaplasic ependymoma Anaplasic oligodendroglioma
G-IV	Malignant, infiltrative Rapid growth Aggressive Necrosis prone	Gliobestoma multiforme Pineoblastoma Medulloblastoma Ependynolastoma

et al. (2022) who proposed classification techniques using five deep learning algorithm, they are AlexNet, VGG16, ResNet18, ResNet50, and GoogleNet CNN and did a comparative study with classic deep learning methods.

Figures 13, 14, 15, and 16 are qualitative comparisons for six algorithms that classify the above datasets into malignant and benign, then if malignant then glioma or meningioma classes. Proposed algorithms by Sunita et al., for brain tumour segmentation and classification using their proposed algorithms.

Measurement scales for classification algorithms—Apart from Dice, there are various ways to measure the performance of a classification algorithm or a neural network architecture.

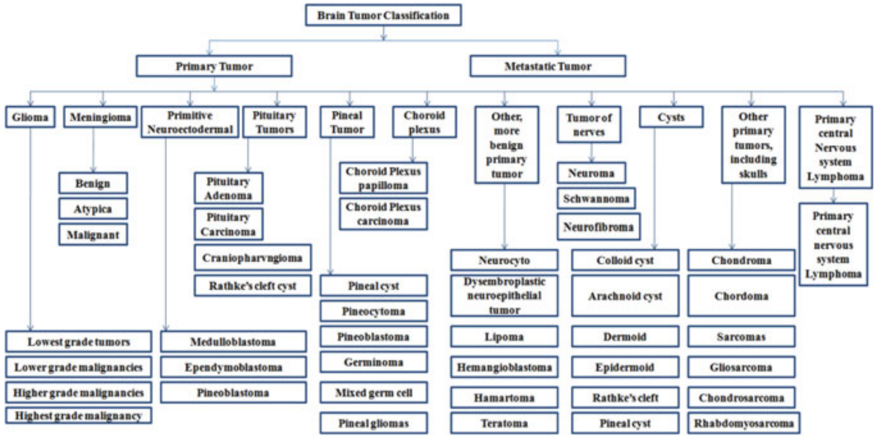

Fig. 12 Detail pathological classification of tumours by American Association of Neurological Surgeons (ANNS 2020)

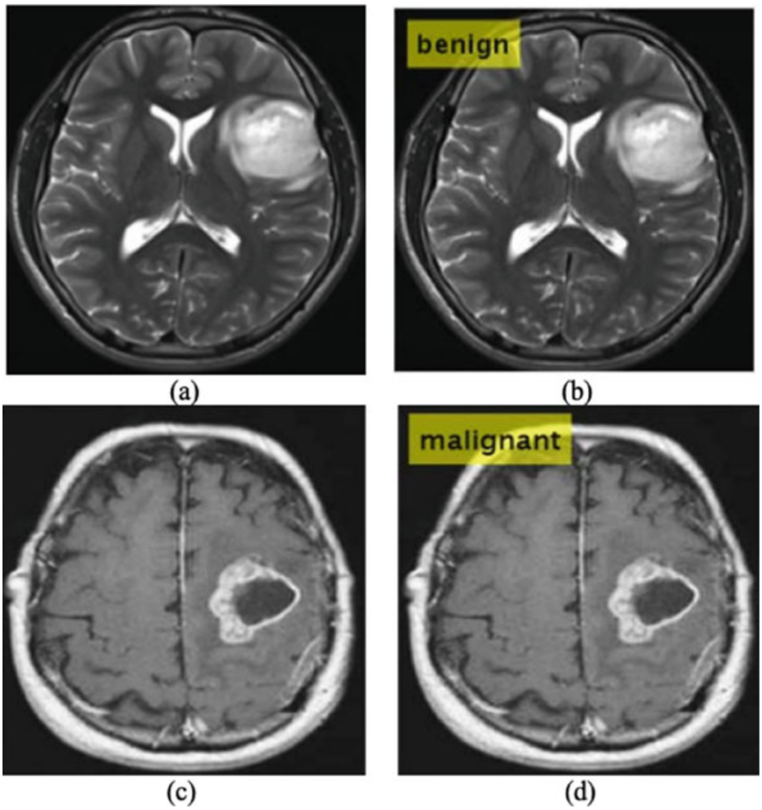

Fig. 13 Classification of cancerous or not

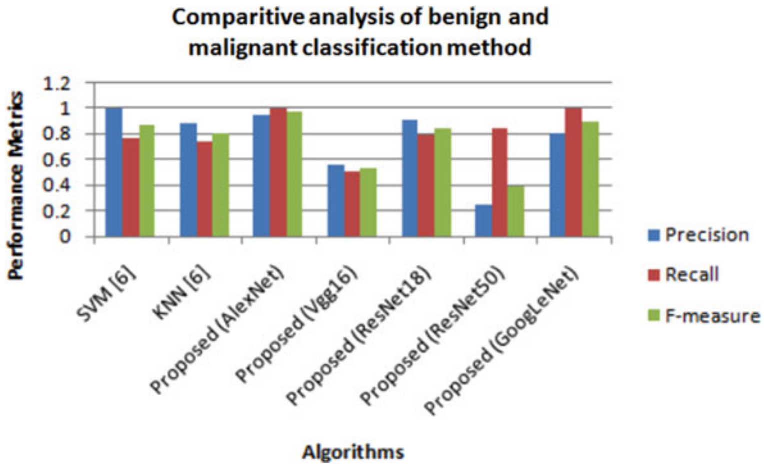

Fig. 14 Computation performance of classification malignant or not (Sunita et al. 2022)

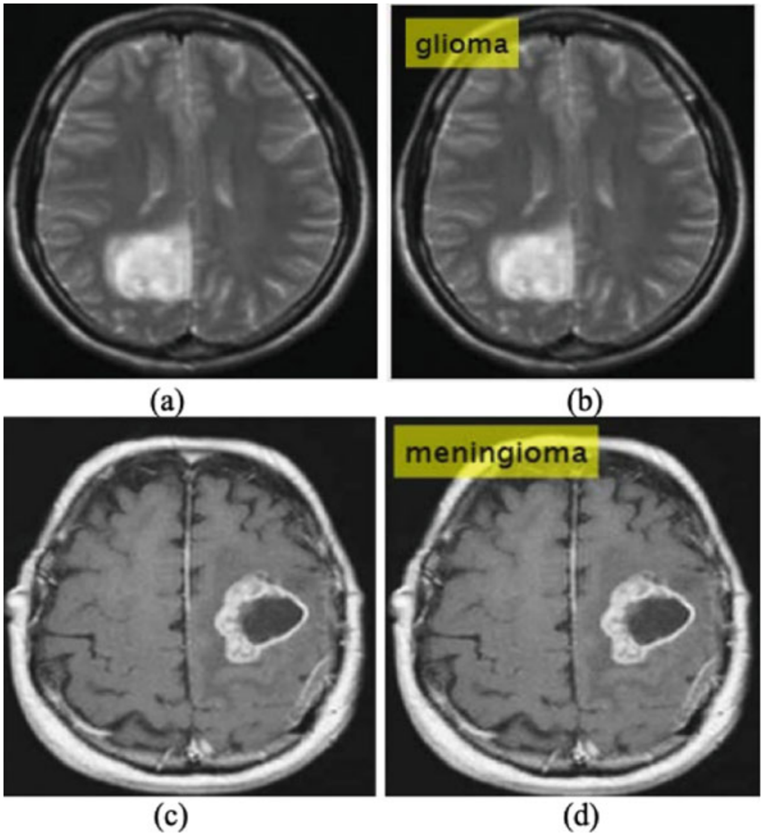

Fig. 15 Classification of malignant types

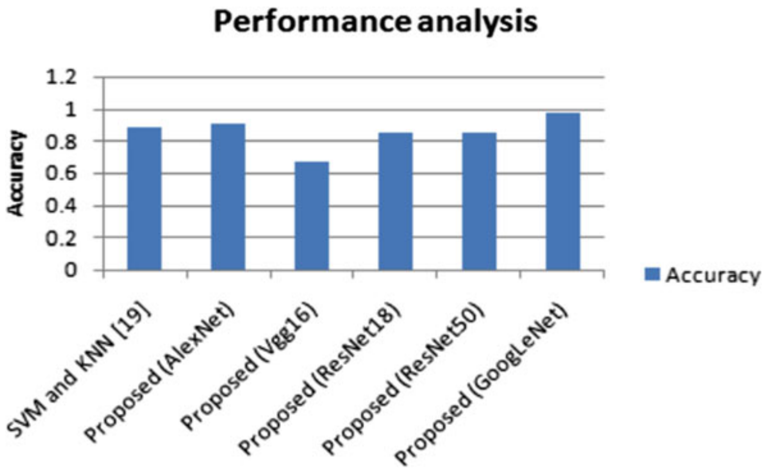

Fig. 16 Computation performance of classification malignant types (Sunita et al. 2022)

True positive (TP) is referred to as a benign identified as a benign (or glioma is identified as glioma). True negative (TN) is referred to as a malignant identified as a malignant (or meningioma is identified as meningioma). False positive (FP) is referring to a benign identified as a malignant (or glioma is identified as meningioma). False negative (FN) refers to as a malignant identified as a benign (or meningioma identifying as glioma).

$$\text{Precision} = \frac{\text{TP}}{\text{TP} + \text{FP}}$$

$$\text{Recall} = \frac{\text{TP}}{\text{TP} + \text{FN}}$$

$$\text{Fmeasure} = \frac{\text{Precision} \times \text{Recall}}{\text{Precision} + \text{Recall}}$$

$$\text{Accuracy} = \frac{\text{TP} + \text{TN}}{\text{TP} + \text{TN} + \text{FP} + \text{FN}}$$

These are generic methods for the performance analysis of multimode image processing algorithms. We found these parameters are calculated in many BraTS technologies from 2018 to 2021 along with accuracy and DICE as discussed in Eq. 5, Sect. 3 of this paper. Sunita et al. (2022) have implemented the above methodologies to compare various parameters for proposed algorithms. The results for those are given in Table 4.

AlexNet shows higher accuracy for the first level of classification of brain tumours as per Table 4 than GoogleNet, while the latter is more precise in multimodal image

Table 4 Performance and accuracy studied for algorithms to compare with classic SVM and KNN (Sunita et al. 2022)

Methods/classes	Benign versus malignant		Glioma versus meningioma		Overall accuracy
	Precision	F-measure	Precision	F-measure	
SVM and KNN	0.88	0.7999	–	–	0.88
AlexNet	**0.9375**	0.9677419	0.8863	0.9285	**0.9047**
VGG16	0.55	0.5238095	0.6591	0.8966	0.6667
ResNet18	0.9	0.8372093	0.9318	0.9010	0.85
ResNet50	0.25	0.3846154	0.8863	0.8965	0.85
GoogleNet	0.8	0.8888889	**0.95**	0.9743	**0.9750**

pixels when input from the previous learning model is taken into account during augmentation processed.

5 Conclusion

Almost all brain tumour segmentation approaches that have emerged in recent research efforts have been evaluated on the BraTS datasets. We found the use of UNets with a charged augmentation approach and examined their effect on clinical MRI images in BraTS 2019 and 20 datasets. Our emphasis in the review was on entire tumour segmentation, since it was a midway step in automation, dynamic contrast, and increased MRI analytics. The parameters of infusion have indeed been filtered for the whole tumour. Furthermore, this information was reviewed by professionals and only the whole tumour regions were marked. Our study expanded and carried out multi-step augmentation by using affine as well as tumour sample reformations. In this study, we looked into state-of-art data (SOA) augmentation methodologies used in the context of MRI segmentation of brain tumours. We took a great effort to thoroughly analyse all BraTS-2019, 20, and 21 research papers, as well as to conduct analytics on data augmentation approaches. Our study took advantage of the fact that affine transformation methods are still commonly employed in everyday activities as they are simple to create and improve, and can provide anatomically plausible brain tumour models. Furthermore, we found several augmentations and segmentation methods that can be combined in multiple procedures to evolve which may result from an elastic transformation. The above approaches can generate synthetic visuals that are intriguing to many researchers and institutions. The study of brain tumour growth and techniques found is genuine. They also must adhere to a real-life distribution of data including ethical AI practices.

References

Agarwal M, Mahajan R (2017) Medical images contrast enhancement using quad weighted histogram equalization with adaptive Gama correction and homomorphic filtering. In: Gahegan M, Mulerikkal JP (eds) 7th international conference on advances in computing and communications 2017, vol 115, pp 509–517. Procedia Comput Sci

Amit G, Ben-Ari R, Hadad O, Monovich E, Granot N, Hashoul S (2017) Classification of breast MRI lesions using small-size training sets: comparison of deep learning approaches. In: Proceedings of medical imaging conference (2017), SPIE, vol 101341H, Orlando

ANNS, Classification of Brain Tumours. https://www.aans.org/en/Media/Classifications-of-Brain-Tumours. Last assessed 2020/06/29

Asif U, Bennamoun M, Sohel F (2018) A multi-modal, discriminative and spatially invariant CNN for RGB-D object labeling. IEEE Trans Pattern Anal Mach Intell 40(9):2051–2065

Bakas S, Akbari H, Sotiras A, Bilello M, Rozycki M, Kirby JS et al (2017) Advancing the cancer genome atlas glioma MRI collections with expert segmentation labels and radiomic features. Nat Sci Data 117(4):170117

Bakas S, Reyes M, Jakab A, Bauer S, Rempfler M, Crimi A et al (2018) Identifying the best machine learning algorithms for brain tumor segmentation, progression assessment and Overall Survival Prediction in the BRATS challenge. In: The dblp computer science bibliography, vol 1811(3), pp 26–29

Bakas S, Hamid A et al (2017) Advancing the cancer genome atlas glioma MRI collections with expert segmentation labels and radiomic features. Sci Data 30(4):170117

Brain Tumor Detection. https://github.com/MohamedAliHabib/BrainTumor-Detection/tree/master/yes. Last assess 2020/06/22

Cancer Treatments Centers of America Brain Cancer Types. Available online https://www.cancercenter.com/cancer-types/brain-cancer/types. Last accessed 2019/11/30

Carver E, Liu C, Zong W, Dai Z, Snyder JM, Lee J, Wen N (2019) Automatic brain tumor segmentation and overall survival prediction using machine learning algorithms. In: Brainlesion: glioma, multiple sclerosis, stroke and traumatic brain injuries, 3rd edn. Springer International

Castro E, Cardoso JS, Pereira JC (2018) Elastic deformations for data augmentation in breast cancer mass detection. In: IEEE EMBS international conference on biomedical and health informatics (BHI), pp 230–234

Chaitanya K, Karani N, Baumgartner CF, Erdil E, Becker A, Donati O, Konukoglu E (2021) Semi-supervised task-driven data augmentation for medical image segmentation. Med Image Anal 34(68):1361–8415

Dvornik N, Mairal J, Schmid C (2021) On the importance of visual context for data augmentation in scene understanding. IEEE Trans Pattern Anal Mach Intell 43:2014–2028

Feng X, Tustison N, Meyer C (2018) Brain tumor segmentation using an ensemble of 3D U-nets and overall survival prediction using radiomic features. Front Comput Neurosci 25(10):2289

Frid-Adar M, Diamant I, Klang E, Amitai M, Goldberger J, Greenspan H (2018) GAN-based synthetic medical image augmentation for increased CNN performance in liver lesion classification. Neurocomputing 321(10):13–162

Galdran A, Alvarez-Gila A, Meyer M, Saratxaga C, Araújo T, Garrote et al (2017) Data-driven color augmentation techniques for deep skin image analysis. Semantic Scholar 22(10):232–983

Gibson E, Li W, Sudre C, Fidon L, Shakir DI, Wang G, Eaton-Rosen Z, Gray R, Doel T, Hu Y, Whyntie T, Nachev P, Modat M, Barratt DC, Ourselin S (2018) NiftyNet: a deep-learning platform for medical imaging. In: Jorge Cardoso M, Vercauteren T (eds) Conference on computer methods and programs in biomedicine, vol 158, pp 113–122

Goodfellow I, Pouget-Abadie J, Mirza M, Xu B, Warde-Farley D, Ozair S, Courville A, Bengio Y (2020) Generative adversarial networks. Commun ACM 63(11):139–144

Gu S, Meng X, Sciurba FC, Ma H, Leader J, Kaminski N, Gur D, Pu J (2014) Bidirectional elastic image registration using B-spline affine transformation. Comput Med Imaging Graph 38(4):306–314

Han C, Murao K, Satoh S, Nakayama H (2019) Learning more with less: GAN-based medical image augmentation. In: 28th conference on information and knowledge management, vol 28, pp 4503–6976

Huang Z, Cohen FS (1996) Affine-invariant B-spline moments for curve matching. In: 5th international conference on IEEE transactions on image processing, vol 5(10), pp 1473–1480

Jia H, Cai W, Huang H, Xia Y (2020) H2NF-Net for brain tumour segmentation using multimodal MR imaging. In: 9th BraTS challenge segmentation. RSNA-ASNR-MICCAI BraTS

Kulkarni SM, Sundari G (2022) A framework for brain tumor segmentation and classification using deep learning algorithm are AlexNet, Vgg16, ResNet18, ResNet50, and GoogLeNet CNN. J Sathyabama Inst Sci Technol 11(8):1–9. Chennai, India

Lachinov D, Shipunova E, Turlapov V (2020) Knowledge distillation for brain tumor segmentation. In: 5th invernation workshop BrainLes and MICCAI. Shenzhen, China, pp 324–332

Louis DN, Perry A, Reifenberger G, von Deimling A, Figarella-Branger D, Cavenee WK, Ohgaki H, Wiestler OD, Kleihues P, Ellison DW (2016) The 2016 world health organization classification of tumours of the central nervous system: a summary. Acta Neuropathol 131:803–820

Nalepa J, Myller M, Kawulok M (2019c) Training- and test-time data augmentation for hyperspectral image segmentation. IEEE Geosci Rem Sens Lett 17(2):1–5

Nalepa J, Lorenzo PR, Marcinkiewicz M, Bobek-Billewicz B, Wawrzyniak P, Walczak M et al (2019a) Fully-automated deep learning-powered system for DCE-MRI analysis of brain tumors. Artif Intell Med 102(101):101769–101800

Nalepa J, Mrukwa G, Piechaczek S, Ribalta Lorenzo P, Marcinkiewicz M, Bobek-Billewicz B, Wawrzyniak P, Ulrych P, Szymanek J, Cwiek M, Dudzik W, Kawulok M, Hayball M (2019b) Data augmentation via image registration. IEEE Geosci Rem Sens Lett 17(2):4250–4254

Wong T-T (2015) Performance evaluation of classification algorithms by k-fold and leave-one-out cross validation. Pattern Recognit 48(9):2839–2846

World Health Organization. Cancer updates online: https://www.who.int/news-room/fact-sheets/detail/cancer. Last accessed 2022/02/22

Zhang Y, Zhong P, Jie D, Wu J, Zeng S, Chu J, Liu Y, Wu EdX, Tang X (2021) Brain tumor segmentation from multi-modal MR images via ensembling UNets. Frontiers Radiol 1(3):1–20

Zhang Y, Dong Z, Wu L, Wang S, Zhou Z (2010) Feature extraction of brain MRI by stationary wavelet transform. In: 10th international conference on biomedical engineering and computer science, vol 12, Wuhan, pp 1–4

Student Placement Prediction Using Machine Learning Algorithms

Samarth Sajwan, Rudraksh Bhardwaj, Revaan Mishra, and Shruti Jaiswal

Abstract One of the most perplexing issues confronting higher education institutions today is how to increase student placement performance. Placement estimation becomes more complex as the number of educational institutions increases. Educational organizations explore more efficient technologies to assist them in improving their decision-making practices, as well as in developing creative methods. Providing new insight into instructional processes is a critical component in resolving quality issues. Machine learning methods are used to extract information from historical data contained in the libraries of educational organizations. Our model will generate a recommendation system that forecasts the placement level of a student. This model assists an organization's selection cell in identifying prospective students, assessing their technical and interpersonal abilities, and assisting them in developing them. Students in their pre-final and final years of B. Tech programs may also use this work to determine their individual placement status and probability of achieving it. This enables them to exert additional effort in order to get placements in organizations with higher hierarchies.

Keywords Machine learning · Regression · Classification · Prediction · Exploratory data analysis

1 Introduction

Higher education is now recognized as an essential component of national development in terms of awareness, community, and globalization (Kadambande et al. 2017). This has a significant impact on higher education output in India, both in terms of quantity and quality of graduates. The key cause of worry is the existing mismatch between higher education production and the country's economic demands (Patil

S. Sajwan · R. Bhardwaj · R. Mishra · S. Jaiswal (✉)
Department of Computer Science and Engineering and Information Technology, Jaypee Institute of Information Technology, Noida, India
e-mail: dce.shruti@gmail.com

J. K. Deka et al. (eds.), *Emerging Technology for Sustainable Development*, Lecture Notes in Electrical Engineering 1061,
https://doi.org/10.1007/978-981-99-4362-3_22

et al. 2017). We will concentrate on student development and graduate throughput in this study.

Universities operate in a fast-paced, competitive world today. The primary challenge confronting contemporary universities is conducting a comprehensive evaluation of their results, recognizing their uniqueness, and developing a plan to capitalize on it (Oloruntoba and Akinode 2017).

Student grading is a time-honored way of assessing and analyzing the academic worth of a student. An unseen problem that hinders a student's progress to get a good placement is avoiding an analysis of several non-academic factors.

Additionally, the university administration is interested in determining which characteristics in the available data are the best predictors of university performance and they want to know if the data collected is sufficient for making reliable predictions, whether any changes to the data collection process are necessary and how to strengthen it, and what additional data to collect to make the analysis results more reliable. This paper will provide an indication of how final grades and other sociocultural and effort-based characteristics, as well as any other major factors in students' academic performance that affect their rate of success, will affect their rate of success and will rank the value of features gained through information gain.

2 Background Study

In recent research done, such as that by Abed and Ajoodha (2020) and Harihar and Bhalke (2020), have classified student placement using various techniques like logistic regression, decision tree classification, multi-layer perceptron, **but have only focused on academic factors, and neglected socioeconomic for placement prediction.**

This section discusses how researchers have used a variety of proven classification algorithms to forecast student academic success:

2.1 SVM Classifier in Student Academic Performance

According to (Pratiyush and Manu 2016) study, as the educational sector expands, new technologies emerge, resulting in an explosion of data. This study incorporates student placement data and employs a support vector machine classification method on training data to determine outcomes and enhances competitive advantage and decision-making through the use of data mining techniques. Kadambande et al. (2017) developed applications for assessing student achievement using data mining techniques, which are now widely used in the field of education, as education has grown in importance in the modern era.

Oloruntoba and Akinode (2017) use support vector machines to predict pupils' academic achievement. The purpose of this research is to discover the association between a student's academic profile before admission and their ultimate academic performance. Similarly, Zainordin and Nabilah (2018) recommended for using SVM to classify pupils based on their overall quality of life and academic achievements. This study categorizes pupils based on their academic performance and general quality of life.

2.2 Naive Bayes Classifier in Student Academic Performance

Shaziya et al. (2015) present a method for forecasting students' semester exam results. The aim of this approach, which is based on the Naive Bayes classifier, is to ascertain what students are likely to achieve in their semester-end grades.

Makhtar et al. (2017) examine student performance in SijilPelajaran Malaysia using a Naive Bayes classifier, one of the classification methods used in data mining, to uncover secret data between subjects that influenced student performance. The Naive Bayes algorithm can be used to classify students' progress in the early stages of the second semester with a precision of 74%.

Razaque et al. (2017) presented an academic data mining application of a classification system based on the Naive Bayes algorithm. It was used to evaluate the academic success of both students and teachers.

Divyabharathi and Someswari (2018) created a model to forecast academic achievement in students. This study employed the Naive Bayes classification methodology.

2.3 Decision Tree Classifier in Student Academic Performance

Raut and Nichat (2017) assess student performance using a decision tree classification technique. The classification methods used to examine performance according to the reach of the knowledge have received considerable attention in this research.

Olaniyi et al. (2017) wrote about a data mining methodology for analyzing student performance. This thesis also investigates the precision of various decision tree methods.

Hasan et al. (2018) use a decision tree algorithm to investigate student academic performance using criteria such as student behavior and academic data. **Neural network classifier in student academic performance.**

According to Binh and Duy (2017), many educational scholars concur, based on learning styles and their guidelines, as well as the fact that students possess a variety of personalities, each with its own unique learning style, which has an effect on student success in all subject areas. The aim of this study was to develop an artificial neural network capable of predicting academic performance based on the learning style of a student.

According to Gerritsen's research (Gerritsen 2017), neural networks have been widely adopted and used in a wide variety of data mining applications, often outperforming classifiers. The primary objective of this study is to determine whether neural networks are an effective classifier for predicting student performance in an educational data mining context using learning management system (LMS) data.

In their study, Okubo et al. (2017) proposed employing a recurrent neural network (RNN) to anticipate students' final grades based on log data maintained in educational systems. This method was utilized in this study to gather data from students and analyze predicting accuracy.

Bendangnuksung (2018) suggested using deep neural networks to predict student performance. The proposed deep neural network uses logistic regression analysis to determine whether students will pass or fail.

Following inferences are drawn from the above study:

- Because of their simplicity, classification-based techniques are commonly used for performance prediction.
- The famous techniques in line for prediction are neural networks, Naive Bayes, and decision trees.
- Students' success is also influenced by socioeconomic factors.

3 Research Methodology

The aim of this study is to develop a structure for academic prediction that will assist students in making more informed choices about their academic future. For the purposes of our work, we will adhere to the structure depicted in Fig. 1. This segment discusses the details of each step of our method.

Step1. Import a Suitable Dataset

Dataset Characteristics: Dataset is taken from Kaggle, the dataset for the model is made up of a selected group of students from a single university.

The dataset that has been used consists of 32 variables, out of which 31 variables are independent (source) variables, and the final variable, i.e., final grade is our target variable.

The dataset has a variety of academic and non-academic factors such as age, sex, father's education level, grades in the first examination cycle, study time, travel time, family size, whether the student stays in a rural or an urban area, type of the job of parents, etc.

Step2. Pre-processing the Dataset

Preprocessing of data is done to make it suitable to work upon by the machine learning algorithms. The two datasets were merged using the **Pandas** library in. The

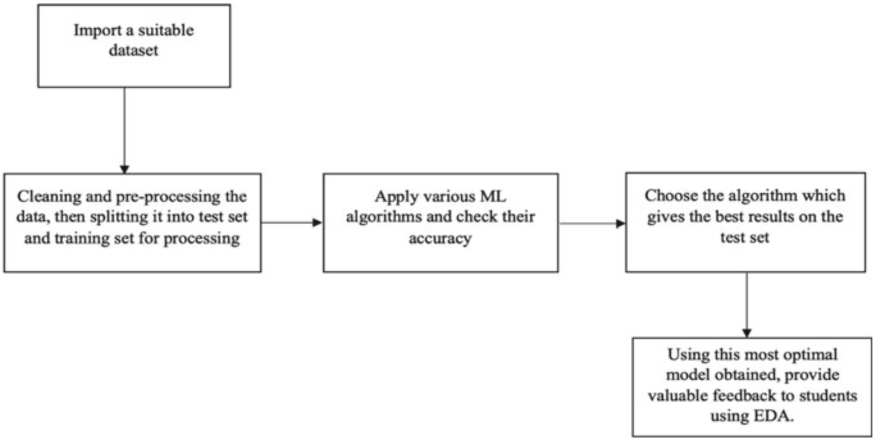

Fig. 1 Proposed methodology

final grade variable is label encoded and the dataset is split into the training set and testing set.

Step3. The Methods and Algorithms of Machine Learning

a. **Support Vector Machine**
   SVM (Hsu et al. 2003) is a well-known and powerful supervised learning technique for pattern classification and regression tasks, as well as associated learning algorithms.
b. **Decision Tree**
   The decision tree (Song and Ying 2015) is a computational classification model whose primary goal is to maximize entropy and information gain.
c. **Random Forest**
   Random forests (Liaw and Wiener 2002), commonly known as random decision forests, are an ensemble learning approach that may be used for classification, regression, and other activities.
d. **Logistic Regression**
   Logistic regression (Menard 2002) is a statistical model that utilizes a logistic function to represent a binary dependent variable in its simplest form, while it has many more complicated variants.
e. **Logistic Regression**
   AdaBoost classifiers (Schapire 2013) are meta-estimators that begin by fitting a classifier to the initial dataset, then fit further copies of the classifier to the same dataset, but with the weights of erroneously classified instances adjusted such that future classifiers focus on tough situations.

f. **Stochastic Gradient Classification**
Stochastic gradient descent (Gardner 1984) is a technique for optimizing an objective function that has the desired smoothness properties. Consider it a stochastic approximation to gradient descent optimization.

4 Implementation

After the preprocessing of the dataset, given below is a step-by-step implementation of our work that is done in Python.

1. Logistic regression is a classification technique that requires putting your most suitable features into making a classifier. As shown in Fig. 2, the highest accuracy is obtained by using 56 features out of 58.
2. One argument that can arise is, in our original dataset we had a total of 33 features, so where did these extra features totaling to 58 come from? The explanation for that is, when we create a classifier for a dataset consisting of categorical features, the logistic regression classifier automatically creates dummy variables for all those categorical features.
3. We found out the adequate number of attributes that provide us the highest accuracy, with the result being **56 features.**

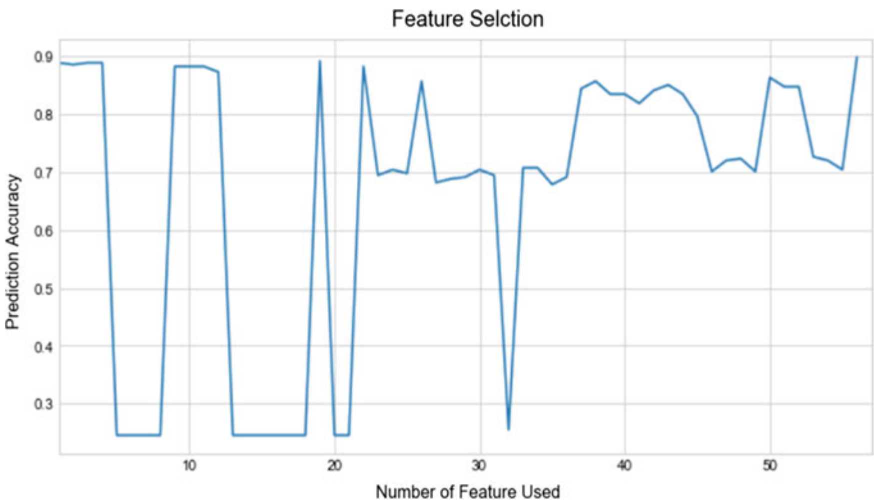

Fig. 2 Plotting of feature selection

5 Experimental Results and Analysis

5.1 Correlation Matrix (Heatmap)

A correlation heatmap was plotted to check the correlation between the predictor variables and the final score variable to understand and get an idea which predictors are more important to use in different classification algorithms. A positive value closer to $+1$ suggests high $+$ve correlation, while a negative value closer to -1 suggests a strong $-$ve correlation. The highest correlation that our final_score variable has is promised by term1_score and term2_score.

A multicollinearity check (correlation between the predictors themselves) is another important aspect. Problems such as overfitting, redundant data variables and an important predictor becoming unimportant can arise due to strong multicollinearity.

As seen in the heatmap shown in Fig. 3, **we have no major multicollinearity in our dataset predictors except the term1 score and term2 score which can be neglected due to their importance for the model.**

5.2 Exploratory Data Analysis (EDA)

In this part of paper, exploratory data analysis of our work is explained.

a. Analysis of final grade of student with the number of students attached to each is shown in Fig. 4a.
b. Analysis of final grade on the basis of alcohol consumption by a student on the weekend is shown in Fig. 4b.
c. Analysis of final grade on the basis of frequency of going out is shown in Fig. 4c.
d. Analysis of final grade on the basis of the desire of the student to receive higher education is shown in Fig. 4d.

6 Conclusion

6.1 The Aforementioned Machine Learning Algorithms Gave us the Following Results

Table 1 depicts the model score, cross validation score, precision, and F1 score of various machine learning algorithms. **The support vector machine classification gives a higher score value for all the metrics than the other models under consideration.**

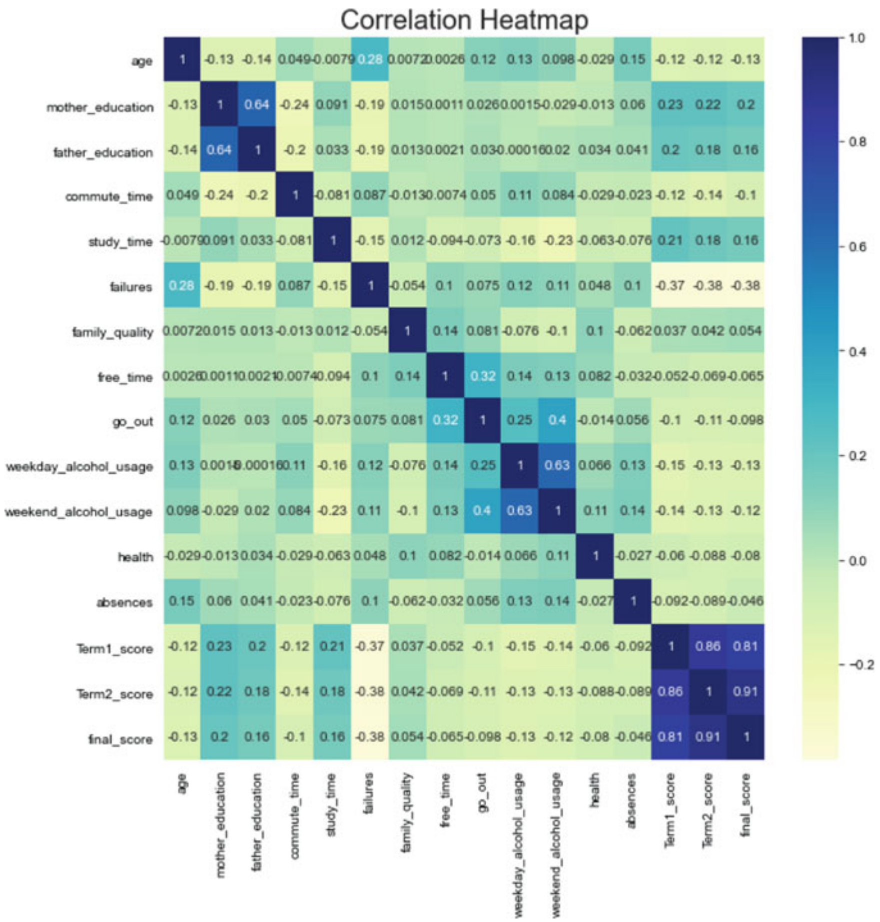

Fig. 3 Correlation heatmap

In all the previously done work discussed, the chances of getting placed have been determined considering only marks and other academic factors.

In our work, we have considered various **socioeconomic factors along with the academic factors for placement prediction.**

One important observation to note is that the results obtained are dataset dependent which means in future, if the college committee decides to increase the entries or the features of the dataset, the accuracy obtained may change.

The reasons due to which SVM gave better results on the dataset as compared to other Machine Learning models that were tried on the same data are:

- In general, SVM models have a good chance of performing better on sparse data when compared with denser data. As shown in the document classification, there may be thousands of features, and only a small proportion of these features may

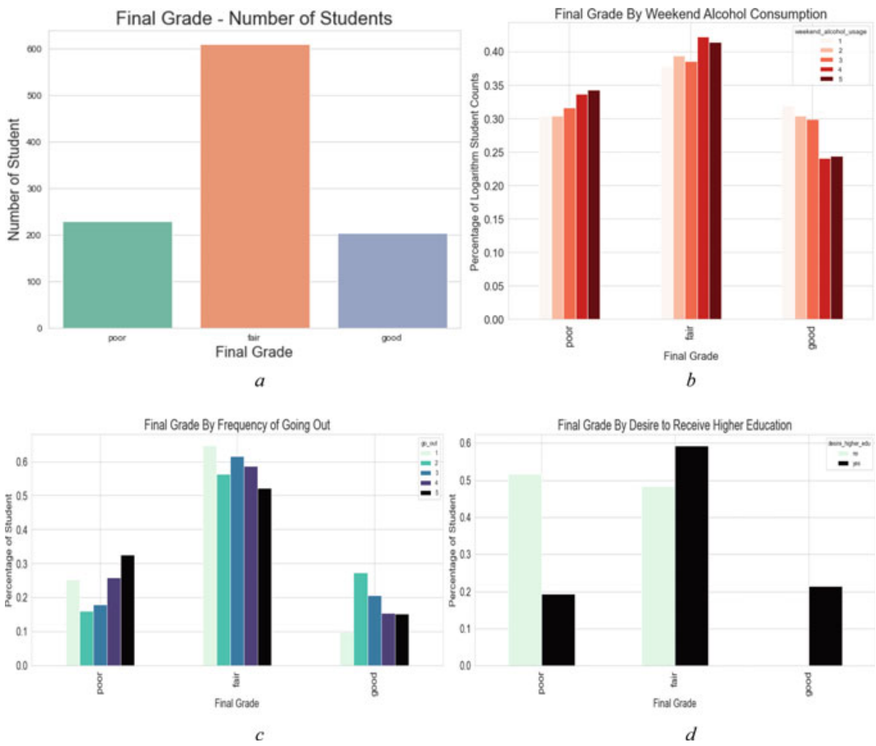

Fig. 4 **a** Number of students versus final grade**. b** Final grade by weekend alcohol consumption. **c** Number of students versus final grade. **d** Final grade by weekend alcohol consumption

Table 1 Model selection

Model used	Model score	Cross validation score	Precision	F1 score
Logistic regression	0.887671232877	0.245222929936	0.871457179110	0.863906310375
Decision tree	0.902739726027	0.875796178344	0.871723581914	0.859868137643
Support vector	0.945205479452	0.891318471338	0.873800965366	0.870632129594
Random forest	0.976712328767	0.847133757962	0.854463038625	0.85330904930
Ada boost	0.750684931507	0.710191082803	0.857058915422	0.82311083976
Stochastic gradient descent	0.620547945205	0.624203821656	0.794460584963	0.668120969269

have a value that is greater than zero in any given document vector. Our dataset became relatively sparse because our data contained several binary variables that were encoded as 0s and 1s.

- When there is a small amount of data, traditional machine learning models such as SVM are typically preferable to deep learning models. This is due to the fact that deep learning models have a large number of weights that must be fine-tuned with data.
- When we have a large number of features, we use a linear SVM kernel because the data has more chances in high-dimensional space to be linearly separable.

References

Abed T, Ajoodha R, Jadhav A (2020, January) A prediction model to improve student placement at a south African higher education institution. In: 2020 international SAUPEC/RobMech/PRASA conference. IEEE, pp 1–6

Bendangnuksung PP (2018) Students' performance prediction using deep neural network. Int J Appl Eng Res 13(2):1171–1176

Binh HT, Duy BT (2017, October) Predicting students' performance based on learning style by using artificial neural networks. In: 2017 9th international conference on knowledge and systems engineering (KSE). IEEE, pp 48–53

Divyabharathi Y, Someswari P (2018) A framework for student academic performance using Naïve Bayes classification. JAET 1–4

Gardner WA (1984) Learning characteristics of stochastic-gradient-descent algorithms: a general study, analysis, and critique. Sig Process 6(2):113–133

Gerritsen L (2017) Predicting student performance with Neural Network. Tilburg University, Netherlands

Harihar VK, Bhalke DG (2020) Student placement prediction system using machine learning. SAMRIDDHI J Phys Sci Eng Technol 12(SUP 2):85–91

Hasan R, Palaniappan S, Raziff ARA, Mahmood S, Sarker KU (2018) Student academic performance prediction by using decision tree algorithm. In: 2018 4th international conference on computer and information sciences (ICCOINS). IEEE, pp 1–5

Hsu CW, Chang CC, Lin CJ (2003) A practical guide to support vector classification

Kadambande A, Thakur S, Mohol A, Ingole AM (2017) Predicting students performance system. Int Res J Eng Technol 4(5):2814–2816

Liaw A, Wiener M (2002) Classification and regression by random forest. R News 2(3):18–22

Makhtar M, Nawang H, Wan Shamsuddin SN (2017) Analysis on students performance using Naïve Bayes classifier. J Theor Appl Inform Technol 95(16)

Manu GPS (2016) Classifying educational data using support vector machines: a supervised data mining technique. Indian J Sci Technol 9:34

Menard S (2002) Applied logistic regression analysis, vol 106. Sage

Okubo F, Yamashita T, Shimada A, Ogata H (2017, March) A neural network approach for students' performance prediction. In: Proceedings of the seventh international learning analytics and knowledge conference, pp 598–599

Olaniyi AS, Kayode SY, Abiola HM, Tosin SIT, Babatunde AN (2017) Student's performance analysis using decision tree algorithms. Ann Comput Sci Ser 15(1):55–62

Oloruntoba SA, Akinode JL (2017) Student academic performance prediction using support vector machine. Int J Eng Sci Res Technol 6(12):588–597

Patil V, Suryawanshi S, Saner M, Patil V, Sarode B (2017) Student performance prediction using classification data mining techniques. Int J Sci Dev Res 2(6):163–167
Raut AB, Nichat MAA (2017) Students performance prediction using decision tree. Int J Comput Intell Res 13(7):1735–1741
Razaque F, Soomro N, Shaikh SA, Soomro S, Samo JA, Kumar N, Dharejo H (2017) Using Naïve Bayes algorithm to students' bachelor academic performances analysis. In: 2017 4th IEEE international conference on engineering technologies and applied sciences (ICETAS). IEEE, pp 1–5
Schapire RE (2013) Explaining adaboost. In: Empirical inference. Springer, Berlin, Heidelberg, pp 37–52
Shaziya H, Zaheer R, Kavitha G (2015) Prediction of student's performance in semester exams using a Naïve Bayes classifier. Int J Innov Res Sci Eng Technol 4(10)
Song YY, Ying LU (2015) Decision tree methods: applications for classification and prediction. Shanghai Arch Psychiatry 27(2):130
Zainordin R, Farah Nabilah AM (2018) Classification of students based on quality of life and academic performance by using support vector machine. J Academia 6(1):45–52

Development of Machine Learning Based Daily Peak Load Forecasting System for Winter Season in the State of Meghalaya in India

Balarihun Mawtyllup and Bikramjit Goswami

Abstract Load forecasting is a technique used by power companies to predict the energy needed to balance the supply and load demand at all times. It is also a mandatory requirement for proper functioning of the electrical power supply industry. Load forecasting is critical to provide decision-making support for power generation. An accurate load forecasting can ensure sufficient power being generated to fulfill actual need of the community and reduce waste of generation. In this paper, a regression-based method is presented for load forecasting in Meghalaya. The efficiency of the methodology is evaluated on the dataset and the predicted values are compared with the actual maximum load demands. The method is found to be effective in accurately forecasting of maximum load demand during the winter season in Meghalaya. This method can be applied to any place in the world having colder climate, with load dependency on heating elements, especially during the winter season.

Keywords Load forecasting · Machine learning · Regression

1 Introduction

Electricity plays an important role in today's world, especially in economic and social development as well as in industrial production. One of the features of electricity is that, once it is produced it is difficult to store. So, to overcome this problem, load forecasting is required, to plan the generation schedules accordingly. Therefore, load forecasting is important and crucial for power utility, in order to reduce power wastage, improve accuracy and maintaining a stable functioning of the power system (He 2017). It helps the power utility to take decisions regarding generating and purchasing of electric power.

Load forecasting has been in existence for decades. Electricity demand forecasting for different seasons is a significant part of power system planning and scheduling. It

B. Mawtyllup · B. Goswami (✉)
Assam Don Bosco University, Guwahati, Assam, India
e-mail: bikramjit.goswami@dbuniversity.ac.in

J. K. Deka et al. (eds.), *Emerging Technology for Sustainable Development*, Lecture Notes in Electrical Engineering 1061,
https://doi.org/10.1007/978-981-99-4362-3_23

is very important for energy generation, transmission, distribution and transactions. The accuracy of load forecasting is directly related to the financial operation of the energy market (Smyl et al. 2112).

Load forecasting primarily depends on three types of models: statistical or econometric model, machine learning model and hybrid model. The seasonal load demand is associated with consumer types, climate and weather variations. Accurate load forecasting is a very complex task, because of frequent load fluctuations due to weather changes and several levels of seasonality. The load trend for a given day is not only dependent on the previous day load usage, but also dependent on the load variations of the previous week and month (Islam 2011).

Nonlinear trend, random changes in load and seasonal variations make forecasting of load very challenging and hence there is a high demand of forecasting models. Load is affected by many external factors such as weather, time, season, demography, economy, electricity price, geographical condition, number of customers, consumer types and their habits (Dudek 2016). Economic operation has become the major requirement in load management and has gained more attention over the years for the power companies and researchers over the world.

Different types of load forecasting methods have been studied and developed over the years by many scientists and engineers. He (2017) in his study opted for a deep neural network-based architecture of a feed-forward model to conduct one day ahead load forecasting. He used convolutional neural network (CNN)-based algorithms to estimate the load consumption pattern. Chen et al. (2018) used a forecasting method based on deep residual network to build the deep neural network structure.

The authors in Smyl et al. (2112) proposed a neural network-based model for short-term load forecasting (STLF) and correlated the performance with other models such as statistical and machine learning (ML) models developed for one day ahead forecasting for 35 countries. Reddy et al. (2017) used time series linear regression model to forecast load for a complex electrical network.

Dudek (2020) proposed a multi-layer perceptron (MLP) model for STLF with Bayesian regularization. The global model is built for forecasting the system load at each hour of the day. Sharma et al. (2022) used the Blind Kalman Filter algorithm to conduct a day ahead load forecasting in IIT Delhi. Amral et al. (2007) used multiple linear regression load forecasting methods for south Sulawesi electricity system, to predict the daily load on dry and rainy seasons.

2 Regression Technique Used in Electrical Load Forecasting

Since the development of machine learning (ML) in the 1990s, different ML methods have evolved over the decades, such as regression analysis, artificial neural networks (ANN), support vector machine (SVM), random forest, linear regression, polynomial regression, etc. Many of these methods have been implemented in load forecasting and in related prediction techniques (He 2017). In this paper, we have used regression models, i.e., linear regression and polynomial regression.

The accuracy of ML-based method depends on the selection of suitable data for training (Singh et al. 2013). In general, regression method produces accurate predictions of the future behavior based on the historical data (Nassif et al. 2201).

In load forecasting dependent variables are load demand and price of the electricity, but independent variables are weather parameters such as wind, temperature, humidity, etc. It has been observed historically that the future value of load demand in some places depend on the predicted ambient temperature. Regression is used to model the relationship of the factors of weather, day type, and customer class of load consumption (Reddy et al. 2017).

Polynomial regression is a type of regression which models the nonlinear dataset using a linear model. It is similar to multiple linear regressions, but it fits into a nonlinear curve between the values of x and corresponding conditional values of y. For a dataset which exists in a nonlinear fashion, linear regression will not best fit to those data points. To cover such data points, polynomial regression is needed. In polynomial regression, the original features are transformed into polynomial features of given degree and then modeled using a linear model. This means the data points are best fit using a polynomial line.

For load forecasting, there are several factors to be considered, mainly historical loads are the main sources. It contains information for prediction of future load, weather factor and time factors. Historical load is one of the main factors to be included, as load usage follows a pattern. Having load history is definitely essential to forecast future load usage.

3 Results and Discussion

The forecasting of maximum load demand in the state of Meghalaya is done by using five years daily data from 2017 to 2021. Also, the ambient temperature values in $\circ$C along with number of consumers, total population and peak load demand in MW are taken as input to the model. The number of consumers is taken from Meghalaya Energy Corporation Limited (MeECL) and actual daily peak load data is obtained from North Eastern Regional Load Dispatch Center (NERLDC). A major part of the dataset is used for training the model and rest of the parts are used for testing and validation. Actual average ambient temperature values are taken as the input day-wise for the state.

The actual methodology of the work is shown in Fig. 1, which is used to build a load forecasting model using regression in the Python environment. The objective is to predict the peak load by using the dataset and the parameters. The data collected is imported into the machine learning program. The training dataset is used to build and analyze the machine learning model. The machine learning algorithm predicts the output by using the trained model. For testing the algorithm, different range of temperature inputs are set to the model, which correspondingly predicted the peak

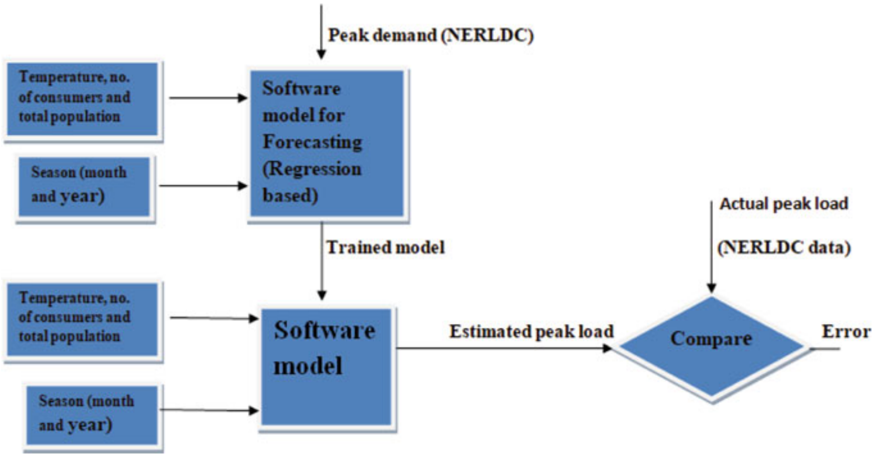

Fig. 1 Block diagram of the methodology used for load forecasting

load values as output. Finally, the accuracy of predicted maximum load demand value is calculated in reference to the actual maximum load demand values.

The goal of the work is to predict the seasonal daily maximum load demand with good accuracy. For a typical range of temperature variation in December, the predicted peak load demand is derived, using the regression techniques. This method is then used to predict the upcoming load value by identifying the relationship between the features of the historical data for December 2021. The trained model is then used to predict the peak load demand and compared with the actual value obtained for each day. For validation of the forecasting model, the temperature forecast values are used as input to the model.

Table 1 gives a comparison between the actual peak load demand and the predicted values. The error percentages calculated for the predicted peak load demand are within 10%. The R^2 value was calculated between the actual and the predicted values of peak demand and the result of R^2 computation is found to be 0.9729.

Figure 2 shows actual and predicted maximum load demands in a bar diagram. From the figure, it is observed that the predicted values of maximum load demand are very close to the actual maximum load demand values.

Table 2 represents the comparison of different load forecasting models in terms of their mean absolute percentage error (MAPE) and root mean square error (RMSE) values. The performance of the proposed method is thus compared with the other existing models like ANN, linear regression, SVM, RF, ANN, RBF and fuzzy logic. The results show a fair standing of the proposed method in comparison with the other existing methods.

Table 1 Comparison between actual and predicted maximum load demand in December 2021

Dates of December 2021	Actual maximum load demand (MW)	Predicted maximum load demand (MW)	Error (%)
1	367	381.03	−3.82
2	386	379.50	1.68
3	381	379.50	0.39
4	377	382.55	−1.47
5	348	382.55	−9.92
6	384	381.03	0.77
7	385	382.55	0.63
8	377	381.03	−1.06
9	377	381.03	−1.06
10	370	382.55	−4.03
11	385	384.07	0.24
12	361	384.07	−6.39
13	379	385.59	−1.73
14	373	385.59	−3.37
15	389	384.07	1.26
16	379	385.59	−1.73
17	388	382.55	1.40
18	384	382.55	0.37
19	384	385.59	−0.41
20	383	387.11	−1.07
21	391	385.59	1.38
22	389	390.16	−0.29
23	394	388.63	1.36
24	401	388.63	3.08
25	368	390.16	−6.02
26	365	391.68	−7.30
27	387	391.68	−1.20
28	393	388.63	1.11
29	398	385.59	3.11

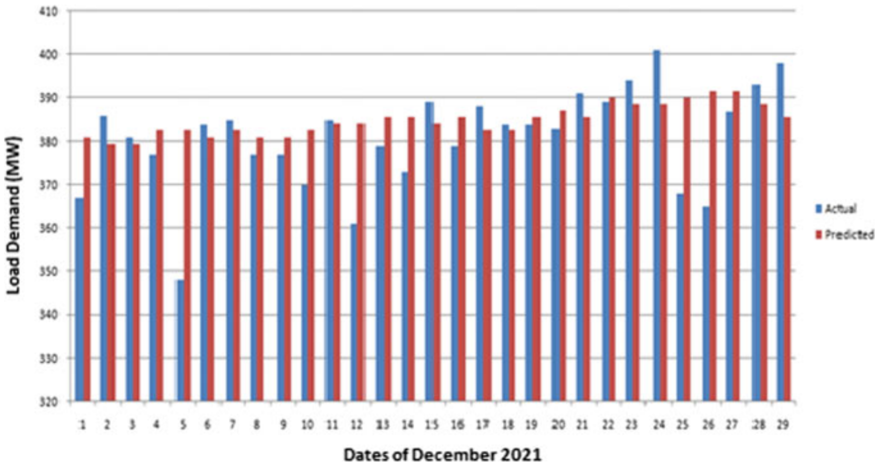

Fig. 2 Actual and predicted maximum load demand for December 2021

Table 2 Comparison of the performance of the proposed model with other existing models

S. No	Method	MAPE	RMSE
1	Linear regression (He 2017)	2.939	–
2	MLR (Amral et al. 2007)	3.52	–
3	SVM (Smyl et al. 2112)	0.234434	106.41
4	RF (Guo et al. 2021)	0.036709	39.2323
5	ANN (Rana and Koprinska 2016)	0.268	–
6	RBF (Hamlich and Eddine Belbounaguia 2019)	3.14	–
7	Fuzzy logic (Ali et al. 2016)	6.9	–
8	Linear regression (our method)	2.34	11.9409

4 Conclusion

Maximum load demand in a grid system is an important forecast parameter for generation scheduling and load planning. The present paper presents a seasonal maximum load demand forecasting method, using forecasted average ambient temperature of a day, number of consumers during the previous month and projected population of the area as input. The regression methods used for forecasting the maximum load demand is optimally chosen based on accuracy of estimation. The method is found to be useful and accurate in estimating the maximum load demand in the state of Meghalaya in India, with a limiting error of 10%. The method is currently tested and validated for five years from 2017 to 2021. Further, this method can be tested for other grids in the world, having similar weather conditions.

References

Ali D, Yohanna M, Puwu MI, Garkida BM (2016) Long-term load forecast modelling using a fuzzy logic approach. Pacific Sci Rev: Nat Sci Eng 18(2):123–127

Amral N, Ozveren CS, King D (2007) Short term load forecasting using multiple linear regression. In: 42nd international universities power engineering conference proceedings. IEEE, Brighton, UK, pp 1192–1198

Chen K, Chen K, Wang Q, He Z, Hu J, He J (2018) Short-term load forecasting with deep residual networks. IEEE Trans Smart Grid 10(4):3943–3952

Dudek G (2016) Pattern-based local linear regression models for short-term load forecasting. Electric Power Syst Res 130:139–147

Dudek G (2020) Multilayer perceptron for short-term load forecasting: from global to local approach. Neural Comput Appl 32(8):3695–3707

Guo W, Che L, Shahidehpour M, Wan X (2021) Machine-learning based methods in short-term load forecasting. Electr J 34(1):106884

Hamlich M, Eddine Belbounaguia N (2019) Short-term load forecasting using machine learning and periodicity decomposition. AIMS Energy 7(3):382–394

He W (2017) Load forecasting via deep neural networks. Procedia Comput Sci 122:308–314

Islam BU (2011) Comparison of conventional and modern load forecasting techniques based on artificial intelligence and expert systems. Int J Comput Sci Issues (IJCSI) 8(5):504

Nassif AB, Soudan B, Azzeh M, Attilli I, AlMulla O (2021) Artificial intelligence and statistical techniques in short-term load forecasting: a review. arXiv preprint arXiv:2201.00437

Rana M, Koprinska I (2016) Forecasting electricity load with advanced wavelet neural networks. Neurocomputing 182:118–132

Reddy MD, Valley RK, Vishali N (2017) Load forecasting using linear regression analysis in time series model for RGUKT, R.K. Valley Campus HT Feeder. Int J Eng Res Technol (IJERT) 6(5):1–5

Sharma S, Chouzenoux É, Elvira V, Majumdar A (2022) A dynamical model for stock forecasting via deep recurrent dictionary learning. HAL Archives. HAL Preprint https://hal.archives-ouvertes.fr/hal-03654152/file/Final_version_Deep_Recurrent_Dictionary_Learning_NoColor.pdf

Singh AK, Ibraheem SK, Muazzam M, Chaturvedi DK (2013) An overview of electricity demand forecasting techniques. Network Complex Syst 3(3):38–48

Smyl S, Dudek G, Pełka P (2021) ES-dRNN: a hybrid exponential smoothing and dilated recurrent neural network model for short-term load forecasting. arXiv preprint arXiv:2112.02663

IoT Based Cattle Monitoring System

Hirokjyoti Kalita, Vivek Kumar Poddar, Deep Kumahr, Raju Rajak, Nupur Choudhury, and Rupesh Mandal

Abstract Internet of Things (IoT) is an evolutionary as well as emerging concept which is in one of the pioneering positions in the transformation of the real-time objects (things) into smart components. It finds its place in a wide range of application domains such as smart grid, healthcare, defence, agriculture, etc. This technology has been successful in creating revolutionary solutions in agriculture in the form of creating artificial greenhouses, precision farming as well as monitoring of livestock. In this article, a novel long range wide area network (LoRaWAN) cattle monitoring and tracking system (CMTS) is proposed which assures a framework that is operated wirelessly over radio frequency having long ranges and lower power consumption. This device not only enables to locate the animal in an unknown area but also proved support in terms of monitoring the vital conditions of the same. The information accumulated by the device is transmitted to the cloud-based server which could be accessed through mobile application for identifying health abnormalities of the animal or location coordinates of the same.

Keywords IoT · LoRaWAN · Livestock monitoring · Long-range network

1 Introduction

IoT is considered as an upcoming technology which is capable of connecting the physical world with the digital advancements for solving real-world problems. This technology is equipped with the interconnections of different intelligent devices

H. Kalita · V. K. Poddar · D. Kumahr · N. Choudhury (✉) · R. Mandal
Assam Don Bosco University, Guwahati, India
e-mail: nupur.choudhury@dbuniver-sity.ac.in

R. Mandal
e-mail: rupesh.mandal@dbuniversity.ac.in

R. Rajak
Pandu College, Guwahati, India

J. K. Deka et al. (eds.), *Emerging Technology for Sustainable Development*,
Lecture Notes in Electrical Engineering 1061,
https://doi.org/10.1007/978-981-99-4362-3_24

and components which are capable of data communication as well as accumulating processes (Lee et al. 2017). Several sectors such as smart farming (Farooq et al. 2019), healthcare, data acquisition (Samie et al. 2016), autonomous vehicles (Philip et al. 2018), smart grids (Al-Turjman and Abujubbeh 2019) as well as other service providers, businesses as well as industries are highlighted by the IoT application (Davcev et al. 2018). The integral processes such as gathering of the data, analysis, and the data processing are facilitated by the use of IoT, which on the other hand promotes smart agriculture and assists the farmers to choose more informed options depending on the scientific calculations and predictions. Smart agriculture or the application domain of IoT in agriculture can be categorized into three different classes: livestock management, greenhouse monitoring and control and precision farming. Current livestock industry is continuously upgraded with the application of IoT which contributes to the interoperability, scalability as well as decision-making for large patches of land or smaller farms. There are certain sensor-based wearable devices which are used for health tracking and monitoring of the animals such as smart collars (Pratama et al. 2019). Livestock management using IoT is not limited to just health monitoring and tracking the vitals, but is also associated with advanced approaches for feeding (Corkery et al. 2013; Ilapakurti and Vuppalapati 2015; Zhang et al. 2016). This domain also includes technology for beehive analysis. Various wireless sensors are created for the monitoring of the odour gas and analyzing the behaviors or the animals (Asikainen et al. 2013; Huircán et al. 2010; Mamduh 2010). A traditional IoT-based framework could be divided into four different parts, i.e. components also termed as things, gateway, technology for communication and cloud computing framework. “Things” comprises of sensors, buzzers, devices, etc., which are capable of communicating independently or without any human intervention (Ursino and Virgili 2020). Protocol translation along with encryption, filtering, data management are taken care of by the IoT gateways. It is also responsible for communication of data which is accumulated by the devices to the cloud framework (Alonso et al. 2020). The primary challenge in this domain is the development of an IoT framework which needs to be created by integrating different technologies. Currently, the advanced mobile networks equipped with 4GLTE too comprises of various deficiencies in terms of delays, limitation in coverages, huge costs and overhead, etc. However there are advanced technologies like LoRaWAN which is capable of long-range communications over several yards, but fails in performance when it comes to obstructed communication for having a selected frequency range. The challenge with long-range communication is that it requires a separate radio spectrum along with a combination of Bluetooth, Wi-Fi, etc., and deployment of frequency gateways for the smooth functioning of the framework. Currently in livestock management, monitoring of cattle is a cumbersome job as huge amount of movement uncertainties are present and enormous manpower is needed to track the animals that go astray. IoT would serve as a solution if these cattle could be monitored and tracked for the information about their whereabouts. Implementation of the IoT LoRaWAN solution could serve as a boon to the monitoring system as it is capable of wireless communication in remote areas and can cover long ranges (Rizzi et al 2017).

This paper proposes a CMTS which is implemented using IoT and smart LoRaWAN-based gateway. It is cost effective as well as can communicate over long ranges. Section 2 gives detailed design of proposed CMTS and its technical description. Brief experimental process flow is provided in Sect. 3. Results and performance of the proposed system are mentioned in Sect. 4. Finally Sect. 5 summarizes the features and concludes the work.

2 Methodology

2.1 Proposed System

As cattle keep roaming in the farms, it is difficult for the workers to observe cattle individually with conventional and traditional approaches. The proposed IoT-based CMTS is a framework that uses various sensors mounted together to monitor the body temperature and heartbeat of each cattle. This device also has a GPS module to get the accurate coordinates of cattles in real time. This device acts as the transmitter node attached to the cattle's neck. In the receiver end, LoRa transceiver, micro controller (esp8266) and 5 V power supply are arranged to process the data which receives from the transmitter side and streamed the data to the cloud servers and also shared with an android application managed by the farm owners. Figure 1 represents the way in which the device is connected with the LoRa gateway which transmits the data stored in the cloud database from which information can be accessed via an android application.

2.2 Block Diagram

This system has two modules, one transmitter node and one receiver node. The transmitter is attached to the cattle's neck with the help of a collar strap. The block diagram of the transmitter and receiver is shown in Fig. 2. For the receiver end there will be a single node which receives signals from all the transmitter nodes.

3 Experimental Process

The concept explained in the block diagrams of both transmitter and receiver nodes are experimental setup, developed for prototype implementation. In the LoRa communication part 433 MHz ISM band is used and only for the prototyping only two such sender node and one receiver node have been developed. Both the sender

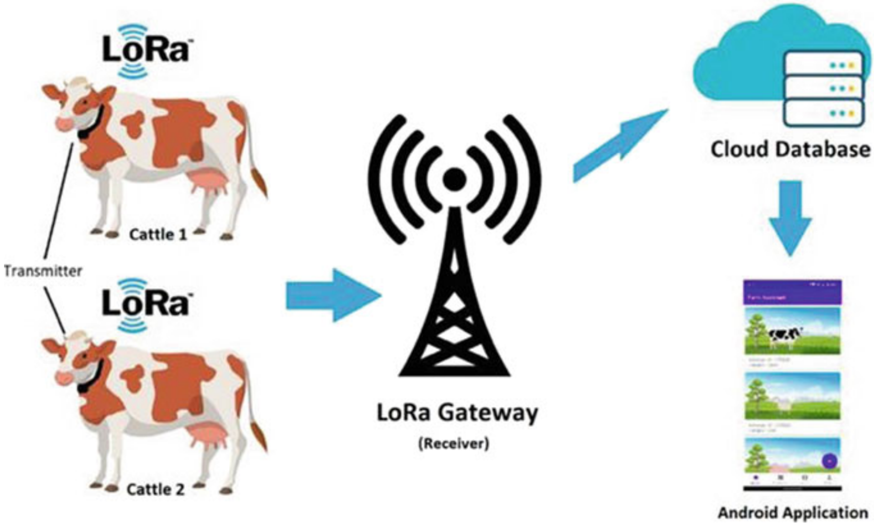

Fig. 1 Representation of proposed IoT-based cattle monitoring system

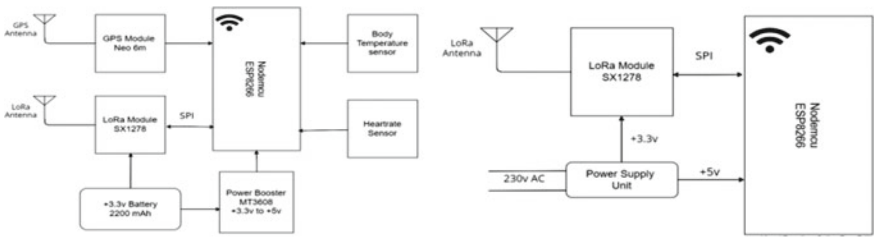

Fig. 2 Block diagram of proposed system's transmitter and receiver node

nodes are programmed to send the packets with an interval of 3 min and their initialization time is different from each other which led to an assumption that both the devices will not send the data packets at the same time. Moreover, the testing is done in rural area where there was no interference present in the same band. In this prototype, no LoRa protocol is being used. As the sender device sends data in every 3 min, which means that in a duration of 24 h around 480 such data packets will be sent. The processes involved are elaborated with the help of a flow diagram.

3.1 1.1 Flow Charts

The process involved at the transmitter node is shown in Fig. 3. At first the system initializes the LoRa module, i.e. the device which is attached with the collar of the cattle. Later on the other components such as GPS module, heart rate sensor and body temperature sensor are initialized. After completing all the initialization process, the data is acquired from all the sensors (GPS, heart rate and body temperature sensor) and verification is done. If the verification process is not successful, then data acquisition will be re-performed. If verification process is successful, then information will be converted into an accessible (CSV) format and sent to the base receiver node via LoRa communication. Once the data has been sent, the sender will wait for an acknowledgement message (ACK) from the receiver and this waiting will be only for 30 s. If there is no acknowledgement message received within 30 s, then once again the data will be sent to the base receiver. And in case it receives acknowledgement message from the base receiver, then the devices sit ideal for 3 min and again go for the data acquisition process followed by sending and waiting for the acknowledgement message. By this methodology the data get transmitted from the sender collar device.

In case of base receiver, node is shown in Fig. 4, at first initialization of the LoRa module took place followed by the initialization of Wi-Fi and the cloud database which will store the real-time location heart rate and the body temperature of the cattle in a database. In this IoT-based cattle monitoring system, Firebase real-time database has been utilized to save the data. After all the initializations process, the device will wait for the data packet sent by the sender. Once the base receiver receives any message from the sender device, it sends an acknowledgement message back to the respective sender device. Then the received message will be decoded into respectively which undergoes through validation check. Once it's validated, GPS coordinates, heart rate and the body temperature along with the current movement status are uploaded into the cloud database immediately, otherwise it will repeat the process flow from receiving data from sender.

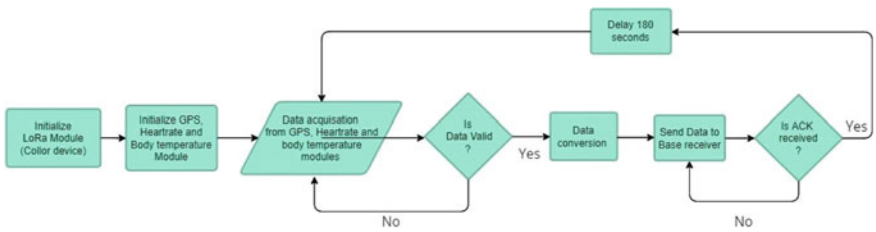

Fig. 3 Flow of the sender node

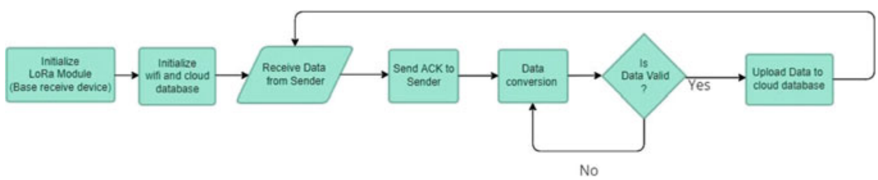

Fig. 4 Flow chart for receiver node

In this methodology an acknowledgement message (ACK) is being shared from the base receiver device and received by the sender device. If the sender device does not receive any acknowledgement, it once again sends the same data packet to the base receiver, which counters the problem of data loss.

3.2 Circuit Diagram

The circuit diagram of the proposed IoT-based cattle monitoring system is implemented using affordable components without compromising on its performance. The transmitter and receiver circuit diagram is shown in Fig. 5, respectively.

The major components of the system:

(a) **NodeMCU Module**: NodeMCU is an open-source platform, based on ESP8266 which can connect objects and lets data transfer using the Wi-Fi protocol and maintains data consistency.
(b) **Lora Module**: LoRa is a low-power, wide area wireless networking protocol built on top of the LoRa radio modulation technique. Usage of LoRa in the proposed system at the transmitter end is to send the sensors data to receiver's end with bi-directional communication protocol with very low power consumption.
(c) **GPS Module**: The global positioning system (GPS) is used in the system to identify the current location of the cattle through NodeMCU that will send the location to the user application.
(d) **Temperature sensor**: The thermistor is used to sense the body temperature of the cattle. Here LM35 is used to calculate the cattle body temperature, i.e. connected to cattle body and NodeMCU.
(e) **Heart Rate**: The heart beat sensor counts the number of heart beats in a minute. It contains an IR pair which detects heart beat from blood flow. Both the IR transmitter and receiver have to be placed in a straight line in order to measure the heart beat rate accurately. Cattle have heart beats in the range of 48–84 beats per minute beyond which indicates stress or animal anxiety.
(f) **Power Supply**: We used a 2200mAh + 3.3v lithium-ion battery to give power to the system.

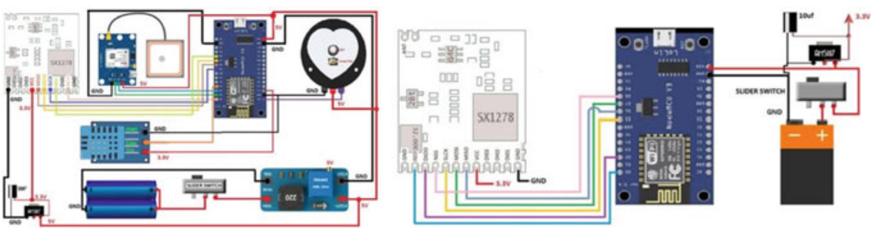

Fig. 5 Circuit diagram of transmitter and receiver system

(g) **Power Booster MT3608**: It is DC to DC converter. The MT3608 is a constant frequency, current mode step-up converter intended for small, low-power applications. It is connected between battery and NodeMCU.

3.3 Experimental Setup

The real-time device implementation of the IoT-based cattle monitoring system is shown in the Fig. 7. With the help of this system monitoring and other physical parameters of cattle in a long-range area have become more convenient. The transmitter's actual device and open circuit board is shown in Fig. 6. Here both NodeMCU and LoRa process the latitude and longitude coordinates received by the GPS module. The temperature and heart rate sensor are also attached to the system to monitor the temperature and heart rate.

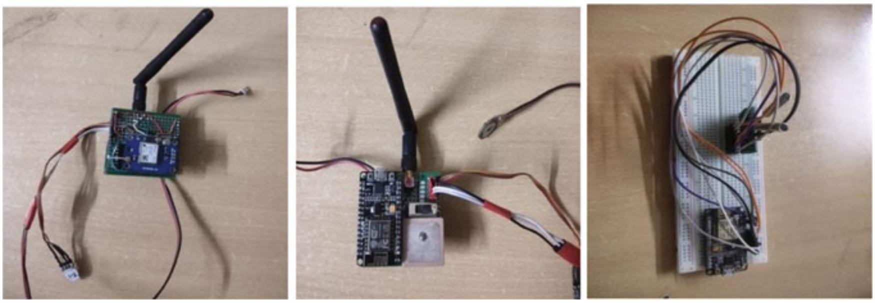

Fig. 6 Experimental set-up of receiver node

Fig. 7 Real-time device implementation cattle monitoring system

This experiment was conducted successfully on a cow in Batasipur area near Monmohinipur village, Dhekiajuli, Assam. The latitude and the longitude of the area are 26.806103 and 92.454193 where the testing was done.

The receiver end set-up is shown in Fig. 6 (rightmost) and here LoRa module and NodeMCU are major components. The location coordinates and others sensor data received through LoRa are processed by the NodeMCU and into the Firebase database. The farm owners can access this data through the mobile application.

4 Results and Discussions

The implementation of proposed system is done and the real-time device is being installed on the cattle with the help of a neck collar. The real-time data acquired with the help of different sensors of the cattle monitoring system are being transmitted from this IoT device which is then received by the base receiver system. A special mechanism has also been added to counter the packet loss while the data are being transmitted from the sender to the receiver. The receiver received the data packets and finally uploads these to the cloud server. A mobile application has been developed which retrieves the data from the cloud server and made available to the user. Through this, the users can track and monitor the vitals of their cattle. The user can monitor the important cattle vitals through the following interface of the application (Fig. 8).

4.1 Live Location and Dashboard Table

Cattle live location is displayed on the user app based on Google Map using GPS module. This helps the user to track the cattle live location where the cattle is currently

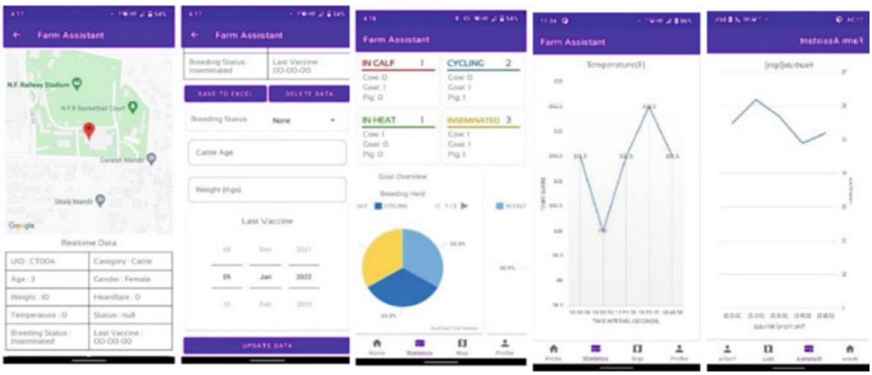

Fig. 8 Android-based dashboard

present. The dashboard table represents all the data that are receiving from sensor like: temperature, heart rate, location, as well as the static data, e.g. cattle age, gender, weight, last vaccine, breeding status, this data is entered by user to maintain as record and this data we can save in excel file.

4.2 Body Temperature

In the current scenario in a large farm, continuous monitoring of cattle temperature manually is impossible, due to this cattle suffer from fever and to avoid that, here temperature sensor is used to monitor continuous temperature of each cattle through the app digitally. Temperature also indicated the infection and stress situation. The status of body temperature will be displayed on the user's app and then the user can take further action. Apart from the cattle's current temperature, the near historical value is also being represented in the graphical format through which the user can get the trend analysis of how the temperature is changing or staying same.

4.3 Heart Rate

The heart rate measures the number of the heart beats per minute. It is not only the speed of the heart rate that is important. The rhythm of the heartbeat is also crucial, and an irregular heartbeat can be a sign of a serious health condition. The heart rate is also being displayed with a graphical representation which will provide the current data and previous data for the trend analysis.

The power consumption of the prototype has also been tested in actual field. The sender node is powered by two 2200mAh lithium-ion cell. The testing was done with following details.

Initial value (when the circuit is switched on)	→	4.149 V
Final value (when device is switched off)	→	4.051 V
Duration of test (9:30 am–3:30 pm)	→	6 h
Total no. of packets sent (every 3 min)	→	120 packets
Usage (4.149–4.051 V)	→	0.098 V (0.1 V approx.)

For sending 120 packets in 6 h the battery loses around 0.1 V. So, in around 60 h the battery loss will be 1 V. Finally the developed prototype will last for around 2 and ½ days.

5 Conclusion

This system is a prototype which utilizes the smart technologies and will try to provide helping hands to the farmers and cattle managers. This kind of approach will be a one-stop solution for the farmers who manage and monitor their cattle with the help of smartphones. This would be an effective choice for all the farmers for increasing the productivity from their cattle as they would be able to monitor them in an effective manner and also keep a track of their health status to avoid any risks. Further the system can also be integrated with machine learning algorithms for creating health related prediction models to improve productivity.

References

Alonso RS, Sittón-Candanedo I, García Ó, Prieto J, Rodríguez-González S (2020) An intelligent Edge-IoT platform for monitoring livestock and crops in a dairy farming scenario. Ad Hoc Netw 98:102047

Al-Turjman F, Abujubbeh M (2019) IoT-enabled smart grid via SM: an overview. Futur Gener Comput Syst 96:579–590

Asikainen M, Haataja K, Toivanen P (2013) Wireless indoor tracking of livestock for behavioral analysis. In: 2013 9th international wireless communications and mo bile computing conference (IWCMC). IEEE, pp 1833–1838

Corkery G, Ward S, Kenny C, Hemmingway P (2013) Monitoring environmental parameters in poultry production facilities. In: Computer aided process engineering-CAPE Forum 2013, 2013. Institute for Process and Particle Engineering, Graz University of Tech nology, Austria

Davcev D, Mitreski K, Trajkovic S, Nikolovski V, Koteli N (2018) IoT agriculture system based on LoRaWAN. In: 2018 14th IEEE international workshop on fac tory communication systems (WFCS). IEEE, pp 1–4

Farooq MS, Riaz S, Abid A, Abid K, Naeem MA (2019) A survey on the role of IoT in agriculture for the implementation of smart farming. IEEE Access 7:156237–156271

Huircán JI, Muñoz C, Young H, Von Dossow L, Bustos J, Vivallo G, Toneatti M (2010) ZigBee-based wireless sensor network localization for cattle monitoring in grazing fields. Comput Electron Agric 74(2):258–264

Ilapakurti A, Vuppalapati C (2015) Building an IoT framework for connected dairy. In: 2015 IEEE first international conference on big data computing service and applications. IEEE, pp 275–285

Islam SR, Kwak D, Kabir MH, Hossain M, Kwak KS (2015) The internet of things for health care: a comprehensive survey. IEEE Access 3:678–708

Köksal Ö, Tekinerdogan B (2019) Architecture design approach for IoT-based farm management information systems. Precision Agric 20(5):926–958

Lee SK, Bae M, Kim H (2017) Future of IoT networks: a survey. Applied Sci 7(10):1072

Mamduh SM, Shakaff AYM, Saad SM, Kamarudin K, Kamarudin LM, Zakaria A, Abdullah AH et al (2012) Odour and hazardous gas monitoring system for swiftlet farming using wireless sensor network (WSN). Chem Eng Trans 30:331–336

Philip BV, Alpcan T, Jin J, Palaniswami M (2018) Distributed real-time IoT for autonomous vehicles. IEEE Trans Industr Inf 15(2):1131–1140

Pratama YP, Basuki DK Sukaridhoto S, Yusuf AA, Yulianus H, Faruq F, Putra FB (2019) Designing of a smart collar for dairy cow behavior mon itoring with application monitoring in microservices and internet of things-based systems. In: 2019 international electronics symposium (IES). IEEE, pp 527–533

Rizzi M, et al (2017) Evaluation of the IoT LoRaWAN solution for distributed measurement applications. IEEE Trans Instrum Measur 66(12): 3340–3349. ISSN: 0018-9456

Samie F, Bauer L, Henkel J (2016) IoT technologies for embedded com- puting: A survey. In: 2016 international conference on hardware/software codesign and system synthesis (CODES+ ISSS). IEEE, pp 1–10

Ursino D, Virgili L (2020) Humanizing IoT: defining the profile and the reliability of a thing in a multi-IoT scenario. In: Toward social internet of things (SIoT): enabling technologies, architectures and applications. Springer, Cham, pp 51–76

Zhang J, Kong F, Zhai Z, Han S, Wu J, Zhu M (2016) Design and development of IoT monitoring equipment for open livestock environment. Int J Simul Syst Sci Tech 17(26):2–7

Estimation of Water Quality Parameters for Deepor Beel Using Landsat 8 Data

Sonia Sarmah and Bikramjit Goswami

Abstract Monitoring the water quality of a wetland is very essential as it forms a major ecosystem in the environment. Although in situ wa-ter quality measurements are precise, high costs limit their applications. Remote sensing has demonstrated high potential as a cost-effective alter-native to traditional water quality monitoring techniques. In this study, the remotely sensed Lansat 8 dataset was used for estimating the water quality parameters of Deepor Beel, Assam. Using in situ data, regression models were created to establish the relation of water quality parameters—pH, total dissolved solids (TDS), and turbidity; with the bands of the Landsat data. For linear regression, R^2 values for all the three parameters were more than 0.70. With R^2 values over 0.90 for all parameters, the decision tree regression model produced more promising results. The analysis also showed that the pH value had a substantial correlation with the NIR band of the Landsat dataset. TDS, on the other hand, had a significant impact on the reflectance of the SWIR 1 and the green bands. For estimation of turbidity, the modified normalized difference water index (MNDWI) and red bands were found to be vital.

Keywords Deepor Beel · Water quality parameters · Remote sensing · Regression

S. Sarmah (✉)
Department of Computer Applications, Assam Don Bosco University, Azara, Guwahati, Assam 781017, India
e-mail: sonia.sarmah@dbuniversity.ac.in

B. Goswami
Department of Electrical and Electronics Engineering, Assam Don Bosco University, Azara, Guwahati, Assam 781017, India
e-mail: bikramjit.goswami@dbuniversity.ac.in

J. K. Deka et al. (eds.), *Emerging Technology for Sustainable Development*,
Lecture Notes in Electrical Engineering 1061,
https://doi.org/10.1007/978-981-99-4362-3_25

1 Introduction

Water quality monitoring is crucial for humanity and preserving the aquatic ecosystem. Wetlands are one of the most significant ecosystems in the world and provide environmental support to a wide range of aquatic life. Apart from recreation and aesthetics, wetlands are also extremely valuable to human life as they aid in natural water quality improvement, flood protection, and prevention of coastline erosion (Liu 1998). Yet, the rapid increase in human population, urbanization, and industrial growth has resulted in the water quality degradation in the major water bodies in the world including wetlands, leading to a global water crisis (Kazi et al. 2009). Water quality monitoring involves measuring the various physical, biological and chemical parameters of water. Based on the measured parameters, the merit of the water is determined for a particular usage. Some of the important parameters for determining water quality include turbidity, pH, total dissolved solids (TDS), dissolved oxygen (DO), bio-chemical oxygen demand (BOD), electrical conductivity, fecal coliform, etc. (Gitelson et al. 1993). In traditional water quality monitoring programs, in situ water samples are collected and are analyzed in standard laboratory systems. This process, though often gives high accuracy, is labor-intensive, time-consuming, and costly. Moreover, monitoring, forecasting, and management of large water bodies may not always be possible due to topographic situations (Gholizadeh et al. 2016; Ritchie et al. 2003).

Recent studies have shown a strong correlation between water quality parameters and satellite data. The researchers have obtained promising results using free open-access satellite data such as Landsat and Sentinel for estimating water quality parameters such as transparency, chlorophyll concentration, turbidity, TDS, etc. (Gholizadeh et al. 2016; Pu et al. 2019; Pereira et al. 2020; Wang and Yang 2019) Using remote sensing, it is also possible to have a spatial and temporal view of surface water quality parameters which helps in effective and efficient monitoring of the water bodies (Pu et al. 2019; Topp et al. 2020). However, the application of remote sensing for water quality monitoring in India in general, and Assam, in particular, has been limited. In Mabwoga et al. (2010), authors assessed selected water quality parameters of Harike wetland using Indian remote sensing satellite (IRS), linear imaging self scanner (LISS) IV multispectral data and found a significant correlation. Though remote sensing has been applied for land use/land-cover analysis of Deepor Beel, water quality monitoring is mostly done using statistical analysis of in situ data. Thus, in this study, an attempt has been made to identify the correlation between some selected water quality parameters (pH, turbidity, and TDS) of the Deepor Beel with Landsat 8 sensor operational land imager (OLI) bands and determine whether remote sensing can be used for studying the water quality of the wetland.

Fig. 1 Map of Deepor Beel

2 Materials and Methodology

2.1 Study Area

Deepor Beel is a permanent and the biggest freshwater lake in lower Assam's Brahmaputra basin. It is the only Ramsar site of Assam and lies 10 km southwest of Guwahati city, between latitudes 26°3′26″–26°9′26″N and longitudes 90°36′39″–90°41′25″E. Figure 1 presents the abstract view map of the lake. Besides diverse fish and birdlife, Deepor Beel also serves as a major natural water reservoir for Guwahati and the surrounding districts (Deka and Goswami 1992; Islam et al. 2014). However, its ecological health is degrading due to its vicinity to a trash disposal site in Boragaon, extensive encroachment for railway line construction and other development projects.

2.2 Water Sample

In this study, we have utilized the water quality parameter levels published by authors in Khongthaw et al. (2019). The authors had collected water samples from six different sites in Deepor Beel on March 29th of 2019, during the daytime. The samples were analyzed for three water quality parameters: pH, turbidity, and TDS; in the Public Health Engineering Department Laboratory, Chanmari Guwahati. Table 1 presents the geographical coordinates of the six sites and the corresponding water quality parameter levels. For Khanamukh and Dharapur, the turbidity level "0" indicates missing values and was excluded in the turbidity analysis model.

Table 1 Water Sampling locations and levels of water quality parameters

S. No.	Site name	Latitude	Longitude	pH	Turbidity (NTU)	TDS (mg/l)
1	Near bird watching tower	26°7′6″ N	91°39′3″ E	6.8	11	70
2	Railway bridge	26°6′45″N	91°39′17″ E	6.7	14	89
3	Khonamukh	26°8′10″ N	91°37′34″ E	6.6	0	71
4	Tateliya	26°7′54″ N	91°38′9″ E	7.5	13	87
5	Dharapur	26°8′21″ N	91°40′7″ E	7.5	0	76
6	Boragaon	26°6′57″ N	91°40′36″ E	7.7	15	92

Source Khongthaw et al. (2019)

2.3 Satellite Dataset

As water sample collection and Landsat data acquisition are asynchronous, it is important to use images of a nearby (if not exact) date to avoid ambiguity. For our study, we used a Landsat 8 OLI dataset acquired on March 28th, 2019 during the daytime. The image was downloaded from Earth Explorer U.S. Geological Survey (USGS). The details of the image are: path/row no—137/42, spatial resolution—30 × 30 m, cloud coverage—2.8%, and quality grade—9 (excellent). The Landsat 8 OLI captures images using 11 bands as shown in Table 2. Out of the 11 bands we used only 8 bands leaving out the panchromatic and thermal bands (band 8, 10, and 11).

Table 2 Landsat 8(OLI) bands

Band	Wavelength (μm)
Band 1—coastal aerosol	0.43–0.45
Band 2—blue	0.45–0.51
Band 3—green	0.53–0.59
Band 4—red	0.64–0.67
Band 5—near infrared	0.85–0.88
Band 6—SWIR 1	1.57–1.65
Band 7—SWIR 2	2.11–2.29
Band 8—panchromatic	0.50–0.68
Band 9—cirrus	1.36–1.38
Band 10—thermal infrared (TIRS)1	10.6–11.19
Band 11—thermal infrared (TIRS)2	11.50–12.51

Source "https://www.usgs.gov"

2.4 Methods

For the initial processing of the dataset, we used the QGIS 3.0 software. Radiometric calibration and atmospheric correction are important preprocessing steps in remote sensing fields to reduce errors caused by sensors, atmospheric scattering, reflection, and absorption. This process involves the conversion of the quantized and calibrated pixel values or the digital numbers (DN) to top of the atmospheric (TOA) reflectance (Teixeira Pinto et al. 2020). For Landsat data products, the conversion of DN to TOA with a correction for the solar angle can be done using Eq. (1).

$$\rho_\lambda = \frac{(\text{Mult}_\rho * \text{DN} + \text{Add}_\rho)}{\sin(\vartheta_{\text{SE}})} \tag{1}$$

Where ρ_λ = TOA with correction for solar angle, Mult_ρ = band-specific multiplicative factor, Add_ρ = band-specific additive rescaling factor, θ_{SE} = local sun elevation angle in degree.

The values for sun's elevation angle, additive, and mulitplicative factors can be extracted from the metadata file accompanying the image file. For the given dataset, the additive factor for the bands is $2.0000E\ \ 05$, multiplcative factor is 0.10 and the sun's elevation angle is 57.133 747 22°. Next, the geographical coordinates of the six water sample collection sites were imported and overlaid on the top of the dataset. For each site, some neighboring water pixels were selected as shown in Fig. 2. It was assumed that the water quality parameters of the neighboring pixels have the same values as that of the water quality parameters of the site. The spectral features of all these pixels were then exported to a CSV file for further processing using Python. The spectral features include the TOA values for the 8 bands. As water quality parameters are affected by natural factors such as soil minerals, vegetation, precipitation, we added three auxiliary bands (i) the normalized difference vegetation index (NDVI), (ii) normalized difference water index, and (iii) modified normalized difference water index (MNDWI) which were calculated using Eqs. (2)–(4). NDVI is utilized to high-light vegetation by maximizing the reflectance in the NIR band and minimizing the reflectance in the red band. In NDWI, the green and the NIR bands are used to recognize the water features with positive values. MNDWI, on the other hand, enhances open water features by using green and SWIR bands (Pereira et al. 2020).

$$\text{NDVI} = \frac{\rho_{\text{NIR}} - \rho_{\text{red}}}{\rho_{\text{NIR}} + \rho_{\text{red}}} \tag{2}$$

$$\text{NDWI} = \frac{\rho_{\text{green}} - \rho_{\text{NIR}}}{\rho_{\text{green}} + \rho_{\text{NIR}}} \tag{3}$$

$$\text{MNDWI} = \frac{\rho_{\text{green}} - \rho_{\text{SWIR}}}{\rho_{\text{green}} + \rho_{\text{SWIR}}} \tag{4}$$

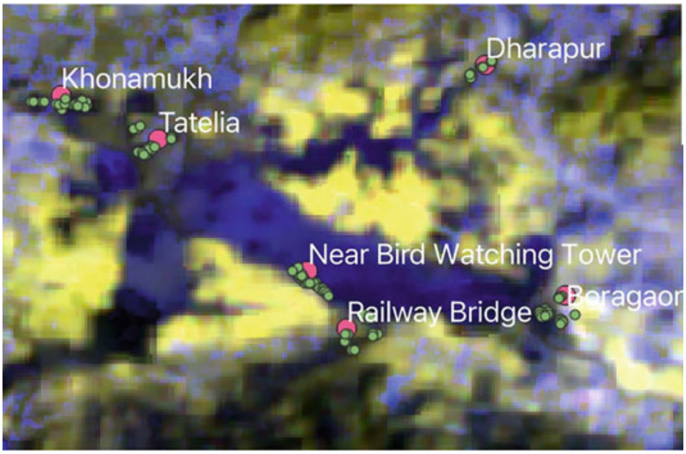

Fig. 2 Sampling points for dataset preparation

where, ρ_{NIR}, ρ_{red}, ρ_{green} and ρ_{swir} are the reflectances in the NIR, red, green, and SWIR-1 bands, respectively.

After removal of the duplicate rows and addition of the auxiliary bands, the resultant dataset had 90 samples and 11 features. Each sample was then assigned with pH, TDS, and turbidity values according to Table 1. The dataset was then analyzed for the three parameters using two different models, namely linear and decision tree regression (Christensen et al. 2000; Pekel 2020). Throughout the experiments, 80% of the samples were used for training and 20% were used for testing. Figure 3 represents the general workflow of the method.

3 Results and Discussion

To study the correlation between the band reflectance values and water quality parameters, linear regression (LR) and decision tree regressions (DTR) were carried out for the three water quality parameters under consideration. Table 3 presents the R^2 values of the respective models for the different water quality parameters. Table 4 gives the coefficients of linear regression and analyzed importance value by decision tree regression for various bands for the respective parameters. In Fig. 4, the comparative graphs for the actual versus the predicted values of the water quality parameters by different models have been shown.

For linear regression, the R^2 value for pH and TDS were above 0.70 and for turbidity, it was 0.928, which indicated a good correlation of the linear model. It could also be seen from Fig. 4a, c and e that predicted values by the linear models were close to the actual values of the water quality parameters. From Table 4, it

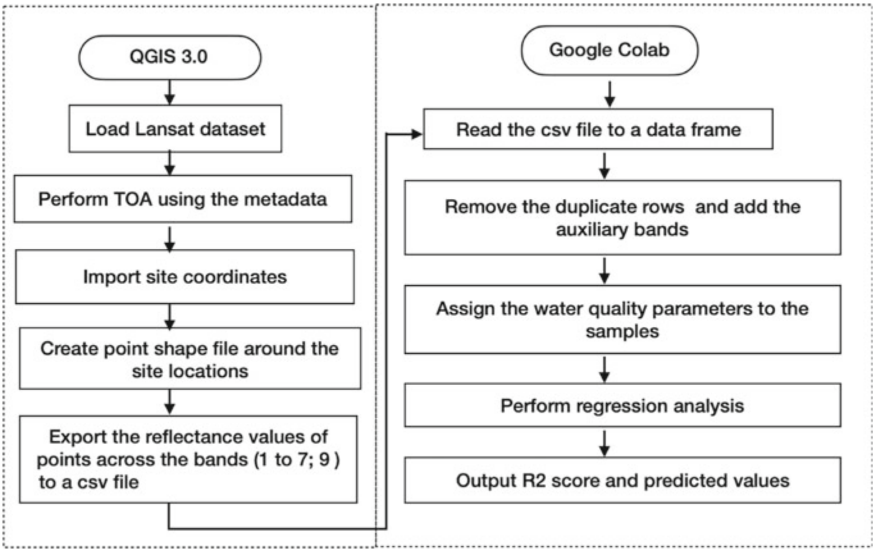

Fig. 3 General workflow diagram of the experiment

Table 3 R^2 coefficient of linear and regression analysis for the water quality parameters

Model	pH	Turbidity	TDS
Linear	0.77	0.928	0.715
Decision tree	**0.90**	**1.0**	**0.91**

The better results are highlighted in bold

Table 4 Analysis report for linear and decision tree regression

Brand	Coefficients of LR			Importance value DTR		
	pH	TDS	Turbidity	pH	TDS	Turbidity
Band1	−2.69E-03	1.13E-02	6.045E-03	0.05	0.09	0
Band2	3.82E-03	−3.10E-02	−1.08E-02	0.02	0	0.02
Band3	−1.53E-02	−2.95E-01	−6.36E-02	0	0.17	0.28
Band4	1.50E-02	2.97E-01	6.55E-02	0	0.15	0
Band5	4.98E-04	3.47E-03	3.56E-03	0.79	0	0.04
Band6	4.83E-04	3.74E-02	−3.09E-03	0	0.54	0
Band7	−8.03E-04	−2.81E-02	2.04E-03	0.08	0	0
Band9	8.70E-03	2.35E-01	6.53E-03	0.06	0	0
NDVI	2.73E+02	5.11E+03	1.17E+03	0	0	0
NDWI	2.81E+02	5.21E+03	1.24E+03	0	0.04	0
MNDWI	−1.80E+00	2.68E+02	−4.53E+01	0	0	0.66

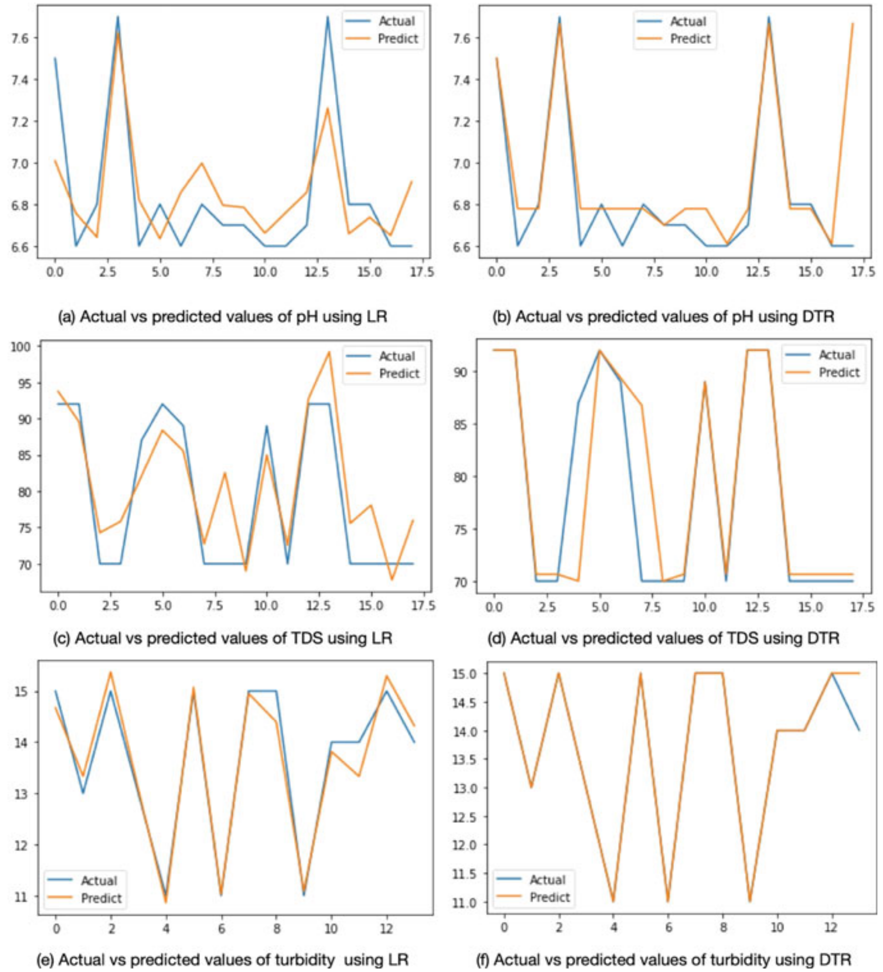

(a) Actual vs predicted values of pH using LR

(b) Actual vs predicted values of pH using DTR

(c) Actual vs predicted values of TDS using LR

(d) Actual vs predicted values of TDS using DTR

(e) Actual vs predicted values of turbidity using LR

(f) Actual vs predicted values of turbidity using DTR

Fig. 4 Actual versus predicted values for the selected water quality parameters using linear and decision tree regression

can be observed that NDVI, NDWI, and MNDWI had high coefficients for all three parameters.

Though linear regression also performed satisfactorily, the decision tree regression model showed better results for all three parameters with R^2 values above 0.90. Figure 4b, d and f also establish the superior performance of decision tree regression compared with the linear regression. For pH, band 5 which is the NIR of the Landsat dataset had the highest importance value of around 0.79. All other bands had significantly low importance values (less than 0.1) indicating the strong relation of the reflectance at the NIR band with the pH value. This also suggested that the NIR band reflectance could independently be a good characteristic for determining the pH level of water bodies. For TDS, the most important band was found to be band 6, i.e., SWIR-1 band with a value around 0.54. The next two important bands for TDS estimation were the green and red bands with values greater than 0.15. Thus, a combination of these bands could be used for TDS analysis of water samples for higher accuracy. The auxiliary band MNDWI had the highest importance value of 0.66 for turbidity analysis. The red band was the second significant band with a value of around 0.28.

4 Conclusion

Though remote sensing is used in many parts of the world for water quality monitoring, it has rarely been used in India, especially in the North-Eastern part. In this study, experiments were performed for the estimation of water quality parameters—pH, turbidity, and TDS of Deepor Beel using the Landsat dataset. For all the parameters, both linear and decision tree regression produced high accuracy with R^2 values higher than 0.70. Decision tree regression, however, showed more promising results compared with linear regression. The analysis also helped in identifying the important bands for each parameter which could be useful for designing models for the individual parameters. Nevertheless, the major challenge in the practical application of this method is the availability of good quality datasets with low cloud coverage in all seasons for North-East India. Also, the presence of water hyacinth creates a hindrance in capturing the optical properties of the water in Deepor Beel. For more effective results, the remote sensing-based method can be combined with the traditional in situ water quality monitoring techniques and the same method can be tested in other places of the world for its validity from the global perspective.

Acknowledgements This research used the in situ water quality parameter values of Deepor Beel published by the authors Badonboklang Khongthaw et al. of Assam Down Town University. We appreciate their effort in collecting the water samples and making the data available.

References

Christensen VG, Jian X, Ziegler AC (2000) Regression analysis and real- time water-quality monitoring to estimate constituent concentrations, loads, and yields in the Little Arkansas River, south-central Kansas, 1995-99 (No. 4126). US Department of the Interior, US Geological Survey

Deka SK, Goswami DC (1992) Hydrology, sediment characteristics and depositional environment of wetlands: a case study of Deepor Beel, Assam. J Assam Sci Soc 34(2):62–84

Gholizadeh MH, Melesse AM, Reddi L (2016) A comprehensive review on water quality parameters estimation using remote sensing techniques. Sensors 16(8):1298

Gitelson A, Garbuzov G, Szilagyi F, Mittenzwey KH, Karnieli A, Kaiser A (1993) Quantitative remote sensing methods for real-time monitoring of inland waters quality. Int J Remote Sens 14(7):1269–1295

Islam M, Ahmed AM, Barman B, Dakua S, Debnath D (2014) Studies on physico-chemical properties of water in some selected sites of Deepor Beel (Ramsar site), Assam, India. Clarion-Int Multi J 3(2):25–32

Kazi TG, Arain MB, Jamali MK, Jalbani N, Afridi HI, Sarfraz RA, Shah AQ (2009) Assessment of water quality of polluted lake using multivariate statistical techniques: a case study. Ecotoxicol Environ Saf 72(2):301–309

Khongthaw B, Modi A, Jokhio C, Nongrem T, et. al (2019) Assessment of spatial variations of water quality index (WQI) of Deepor Beel, Assam, India. IJESC 9(6):23143–23146

Liu H (1998) Conservation of wetlands especially as waterfowl habitat in northeast China. Chin Geogra Sci 8(3):281–288

Mabwoga SO, Chawla A, Thukral AK (2010) Assessment of water quality parameters of the Harike wetland in India, a Ramsar site, using IRS LISS IV satellite data. Environ Monitor Assess 170(1):117–128

Pekel E (2020) Estimation of soil moisture using decision tree regression. Theor Appl Climatol 139(3):1111–1119

Pereira OJ, Merino ER, Montes CR, Barbiero L, Rezende-Filho AT, Lucas Y, Melfi AJ (2020) Estimating water pH using cloud-based landsat images for a new classification of the Nhecolândia Lakes (Brazilian Pantanal). Remote Sens 12(7):1090

Pu F, Ding C, Chao Z, Yu Y, Xu X (2019) Water-quality classification of inland lakes using Landsat8 images by convolutional neural networks. Remote Sens 11(14):1674

Ritchie JC, Zimba PV, Everitt JH (2003) Remote sensing techniques to assess water quality. Photogrammet Eng Remote Sens 69(6):695–704

Teixeira Pinto C, Jing X, Leigh L (2020) Evaluation analysis of landsat level-1 and level-2 data products using in situ measurements. Remote Sens 12(16):2597

Topp SN, Pavelsky TM, Jensen D, Simard M, Ross MR (2020) Research trends in the use of remote sensing for inland water quality science: moving towards multidisciplinary applications. Water 12(1):169

Wang X, Yang W (2019) Water quality monitoring and evaluation using remote sensing techniques in China: a systematic review. Ecosyst Health Sustain 5(1):47–56

Improved Detection of Large-Sized Pedestrians Using Non-linear Scale Space and Combination of HOG and Dense LDB Features

Amlan Jyoti Das, Navajit Saikia, and Abhishek Das

Abstract Multi-scale detection in pedestrian detection plays a vital step due to its use in detecting pedestrians in different scales. However, multi-scale detection is a challenging task due to various reasons like selection of appropriate scale factor, low resolution and loss of sharp edges at deeper pyramidal levels, etc. In this paper, new pedestrian detectors are presented which uses non-linear scale space for multi-scale detection. The proposed detector uses histogram of oriented gradient features in combination with dense local difference binary features. Different classifiers like linear SVM and cascade of boosted classifiers are used to train the detector. INRIA pedestrian dataset is used to train and test the proposed detectors. The proposed system is evaluated in terms of precision versus recall and miss-rate versus FPPW/FPPI as well as computational speed. The performance of the proposed detectors is also compared with some similar existing pedestrian detectors.

Keywords Pedestrian detection · Multi-scale detection · Linear SVM · Cascade classifier · Dense local difference binary · Histogram of oriented gradients

1 Introduction

Pedestrian detection is an important domain in computer vision, and it serves as the backbone of wide range of security and surveillance applications. One of the challenges in pedestrian detection is multi-scale detection. Multi-scale detection

A. J. Das (✉)
Gauhati University, Guwahati, Assam 781014, India

N. Saikia
Assam Engineering College, Guwahati, Assam 781013, India
e-mail: navajit.ete@aec.ac.in

A. Das
HPC-AI Infrastructure Development, C-DAC, Pune, India
e-mail: abhishekd@cdac.in

J. K. Deka et al. (eds.), *Emerging Technology for Sustainable Development*,
Lecture Notes in Electrical Engineering 1061,
https://doi.org/10.1007/978-981-99-4362-3_26

is generally performed to detect pedestrians of different size. The most commonly used multi-scale detection approach is image pyramid. In image pyramid, the original image is densely down-sampled, and feature computation is done for all the windows in that level using sliding window approach. This approach does not require to train models for different size of pedestrians. In (Viola and Jones 2003; Felzenszwalb et al. 2010), the authors however have used classifier pyramid which used trained detectors for different sized pedestrians. These models are tested on different location to detect pedestrians different of different size. It results in faster detection. However, setting the appropriate scale factors during training the models is daunting task. It also requires scale invariant features which is not common including gradient histograms. Hence, image pyramid method is more popular due to its computationally less complex training procedure and its flexibility in selection of scaling factor (Dollar et al. 2010).

Histogram of Oriented Gradients (HOG) (Dalal and Triggs 2005a), Local Binary Pattern (LBP) (Tuzel et al. 2008), Haar-like features (Wojek and Schiele 2008), channel features (Dollar et al. 2009a), etc. are some of the popular handcrafted features used in pedestrian detectors. Authors have also used combination of different features (Walk et al. 2010; Wang et al. 2009; Ojala et al. 2002) for improved performance. Variants of Support Vector Machine (SVM) (Dalal and Triggs 2005a), boosted classifiers (Dollar et al. 2009a) and decision tree are some of the popular classifiers used in pedestrian detection. A detailed analysis of the performance of these classifiers is presented in Benenson et al. (2014). Detection performance and speed (Dollar et al. 2009a; Zhu et al. 2006) are two primary aspects of a pedestrian detector.

Yi Z. and Xue J. have proposed to use non-linear scale space for multi-scale detection in Yi and Xue (2014). The authors have confirmed the assumption that significant image boundaries can be restored at deeper pyramidal levels which is not obtained by using image pyramid. Due to this reason, the detector provides robustness in detecting large-sized pedestrians. This paper introduces pedestrian detectors that use non-linear scale space for improved detection of large-sized pedestrians. Combination of HOG and dense LDB features have been used for improved performance. Two popular classifiers, i.e., linear SVM and cascade of boosted classifiers, are used to analyze their performances.

The rest of the paper is organized as follows: Sect. 2 discusses some related works in the domain of pedestrian detection. Section 3 presents the proposed methodology. Section 4 presents the experimental results of the proposed detectors, and Sect. 5 provides a comparative study of the proposed detectors with some of the similar detectors. Section 6 concludes the paper.

2 Related Works

An ample amount of literature has been reported for pedestrian detection in the last two decades. These techniques are either handcrafted feature or data-driven based. However, data-driven techniques (Benenson et al. 2014; Zhang et al. 2016) use large datasets for training like Caltech (Dollar et al. 2009b) which is not required in handcrafted feature-based techniques. Therefore, in this paper, we concentrate only on the handcrafted feature-based approaches. HOG (Dalal and Triggs 2005a) is one of the most commonly used gradient-based feature descriptor. Authors have also used combination of different types of features as a single feature might not sufficient to meet the complex challenges in pedestrian detection (Mori et al. 1837). Features such as Histogram of Optical Flow (HOF) (Walk et al. 2010), color self-similarity (Walk et al. 2010), LBP (Wang et al. 2009), dense LDB (Das and Saikia 2016), etc. have been used in combination with HOG features to improve the detector performance. In Viola et al. (2003), authors have used frame differencing and Haar features to train a cascade of boosted classifiers to obtain faster detection. Authors in Ojala et al. (2002) have used color, texture and edge information. Integral Channel Feature (ICF) (Dollar et al. 2009a) is another popular feature which uses combination of gradient histograms, gradient magnitude and color channels.

The basic objective of this work is to explore the performance of a detector which uses only non-linear scale space for multi-scale detection. In this paper, we have used similar set of features as used in (Das and Saikia 2016; Das et al. 2021) where HOG and dense LDB features have been used. Different classifiers are also used to evaluate its performance. This work proposes to employ both linear SVM and cascade of boosted classifier-based detectors in combination with HOG and dense LDB features. In this paper, we propose to use the following:

- Pedestrian detector where a linear SVM is trained using HOG and dense LDB features as in Das and Saikia (2016) with non-linear scale space for multi-scale detection.
- Pedestrian detector where a cascade of boosted classifier is trained using fastHOG and dense LDB features as in Das et al. (2021) with non-linear scale space for multi-scale detection.

The section below describes the proposed methodology.

3 Proposed Methodology

Figure 1 shows the basic block diagram of the proposed pedestrian detectors. The same hybrid feature set containing HOG and dense LDB is considered in this detector as used in Das and Saikia (2016) and (Das et al. 2021). The pedestrian detector proposed in Das and Saikia (2016) and (Das et al. 2021) uses the pyramidal levels in multi-scale detection which are created linearly (Dollar et al. 2010) by down-sampling the image using filters of fixed kernel size. This leads to loss of edge information when the image is down-sampled to higher levels of the pyramid which may result in misclassification when pedestrian size in the image is large. In Sect. 1, it has already been discussed that non-linear scale space helps in detecting larger objects as it can preserve significant boundaries even at deep pyramidal.

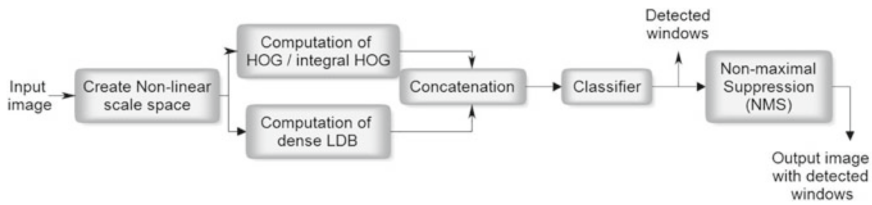

Fig. 1 System block diagram

In Yi and Xue (2014), the authors have proposed an extension to the multi-scale detection approach. In Yi and Xue (2014), the authors have confirmed the assumption that non-linear scale space preserves significant boundaries for large pedestrians at deep pyramidal levels. Hence the non-linear scale space provides robustness to detections of larger objects which is beyond the scope of the standard training window size. The functions of the different blocks are discussed as follows:

Creation of Non-linear Scale Space: The non-linear image scale space in this work is created by using FED as explained in Alcantarilla et al. (2013). The image scale space thus formed preserves strong boundaries even at higher pyramid levels. The parameters that we have used for creating a non-linear scale space using FED are shown in Table 1.

The proposed system uses 7 octave levels and 4 sublevels for creating the scale space. These values are considered for optimum performance of the system and are based on experimental observations using the INRIA pedestrian dataset. Consideration of more octave levels either resulted in decreased performance or derived images where the content could not be analyzed for small images in the dataset. Weickert diffusivity function (Weickert 2001) has been used which rapidly decreases diffusivity, and smoothing is stronger on both sides of an edge than across it. The creation of non-linear scale space by using FED is explained in Alcantarilla et al. (2013). To be noted here that any scale factor (other than 2 as considered in Alcantarilla et al. (2013)) may be considered empirically and the algorithm presented in Alcantarilla et al. (2013) should be addressed accordingly. Instead of down-sampling the image by a constant scale factor of 2, as in case of Alcantarilla et al. (2013), we have tested

Table 1 Parameters used to create non-linear scale space

Parameters	Values
Soffset	1.6
Octave levels	7
Sublevels	4
Diffusivity	Weickert
k-contrast	0.001
k-contrast percentile	0.7
k-contrast nbins	300

different down-sampling factors. We have tested different scale factors in the range of 1.1 to 1.35. The best detector performance is observed for the scale factor of 1.3.

Computation of feature set: The detector using linear SVM uses HOG and dense LDB features which are computed in the similar manner as in Das and Saikia (2016). The detector using cascade of boosted classifier however uses fastHOG (Zhu et al. 2006) and dense LDB. FastHOG uses HOG features computed using integral image, and variable block sizes are used in the same way as in Das et al. (2021). This helps in maintaining a trade-off between performance and detection speed.

Training of the linear SVM Classifier: This detector also uses INRIA pedestrian dataset for the purpose of training the linear SVM classifier. After each stage of training, hard negative mining (Dalal and Triggs 2005b) has been performed. The hard negatives (Dalal and Triggs 2005b) are extracted by using non-linear scale space and are combined to the negative training set after resizing the hard negatives to detection window size. These are used to perform the next stage of training. Five stages of iterative training provide the best performance as observed from the experimentation. The final trained classifier is used to detect pedestrians using non-linear scale space. Non-maximal suppression (Dollar et al. 2012) is applied on the detections to derive the final output.

Training of the Cascade Classifier: The cascade of boosted classifier is trained using the same set of features (combination of integral HOG and dense LDB features) and parameters as used in Das et al. (2021). The training steps are presented in Das et al. (2021). The training uses 614 positive and 1218 negative pedestrian windows in INRIA dataset.

4 Experimental Results

We test the performances of the proposed detectors in terms of miss-rate versus FPPW (per window), miss-rate versus FPPI (per image) and precision versus recall. The 288 positive test images in the INRIA pedestrian dataset are considered in the evaluation. For per window performance, the 588 pedestrian windows in the test images are mirrored to have a total of 1176 pedestrian windows.

4.1 Performance of Proposed Detector-1

The green and red curves in Fig. 2 respectively show the per window performances for the proposed detector-1 and the detector in Das and Saikia (2016). It may be observed from the Fig. that the proposed detector-1 achieves about 89% recall at 10^{-4} FPPW.

In order to evaluate per image performances, PASCAL criteria (Everingham et al. 2010) are used in order to take care of partial detections. For the proposed detector-1, Fig. 3 shows a comparison of the miss-rate versus FPPI plots for different scale

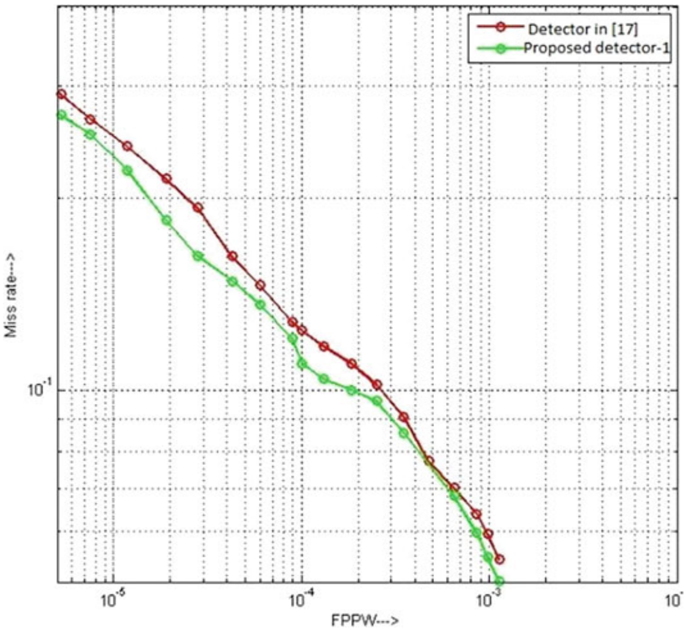

Fig. 2 Miss-rate versus FPPW plot of detector-1

factors. The experimental results show that the scale factor 1.30 performs best in terms of per image performance in our case after testing in the range from 1.05 to 1.35. The scale factors 1.14 and 1.30 yield similar detection performance, but 1.30 performs best at 10^{-1} FPPI and 10^{0} FPPI. With 1.30 scale factor, the detector achieves detection rate of 78.2% at 10^{0} FPPI and 53.7% at 10^{-1} FPPI. The log average miss-rate is 0.50. Table 2 shows the miss-rate of the detector at different FPPI values using different scale factors. Figure 4 shows the precision versus recall plots of the detector for different scale factors.

4.2 Performance of Proposed Detector-2

To study per image performance of proposed detector-2, we have tested different scale factors ranging from 1.05 to 1.35. Figure 5 shows the plot of miss-rate versus FPPI for the scale factors 1.1, 1.14 and 1.3. With 1.30 scale factor, the detector achieves the best detection rate of 76.1% at 10^{0} FPPI and 51.1% at 10^{-1} FPPI. The log average miss-rate is 0.51. Table 3 shows the miss-rates of the detector at different values of scale factor and FPPI. Figure 6 shows the comparison of precision versus recall plots for the detector-2 with different scale factors.

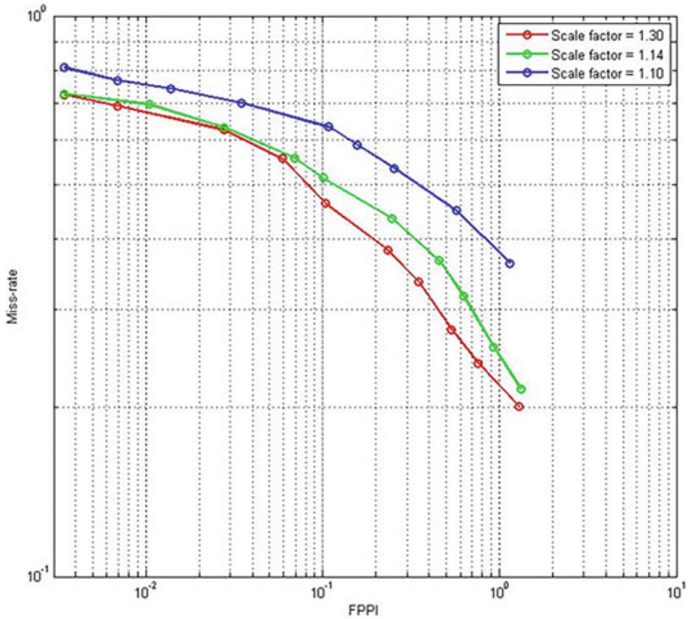

Fig. 3 Miss-rate versus FPPI plots for proposed detector-1

Table 2 Miss-rate of the detector-1 using different scale factors at different FPPI values

Scale factor/FPPI	1.1 (%)	1.14 (%)	1.30 (%)
0.01	76.2	68.7	**68.1**
0.1	62.0	51.3	**46.3**
1	38.4	26.2	**21.8**

5 Comparative Study

In performance comparison, log-average miss-rate (LAMR), miss-rate at 1 FPPI and the time required to process one frame of size of 640 × 480. Table 4 presents these evaluations for the six techniques including the proposed detectors. The proposed detectors are first compared with the detector proposed in Yi and Xue (2014) which applies the non-linear scale space. Proposed detector-1 and detector-2 have precision of 0.95 and 0.94 at recall of 0.4 corresponding to 0.7 for the detector in Yi and Xue (2014). At recall value of 0.6 and the precision values for detector-1 and detector-2 are 0.86 and 0.83 respectively corresponding to 0.45 for detector in Yi and Xue (2014). This shows that the proposed detectors perform better than the detector presented in Yi and Xue (2014).

The performances of the proposed detectors are also compared with the similar detectors using image pyramid. The performances of HOG and HOG-LBP-based detectors here are taken from Dollar et al. April (2012). It may be observed from

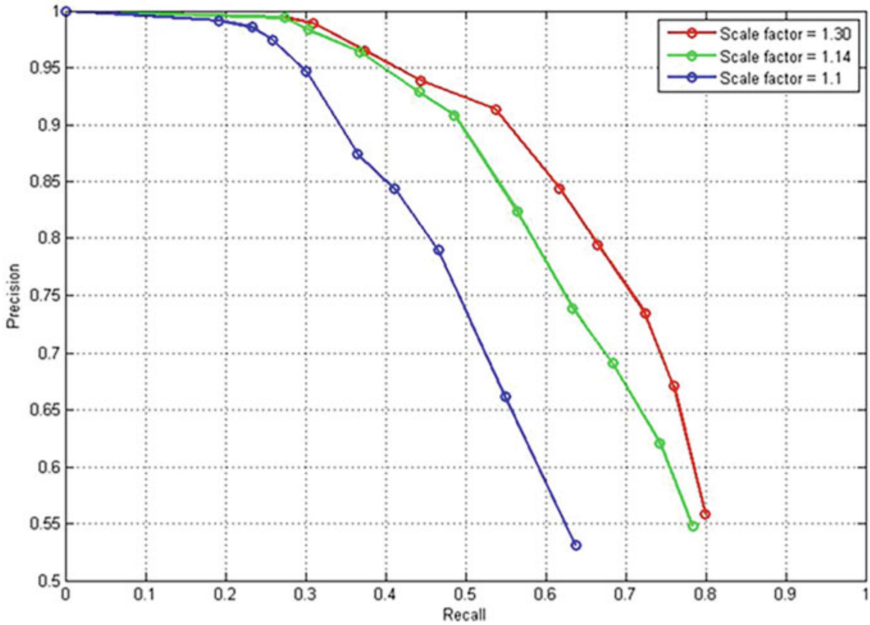

Fig. 4 Precision versus recall plots for proposed detector-1

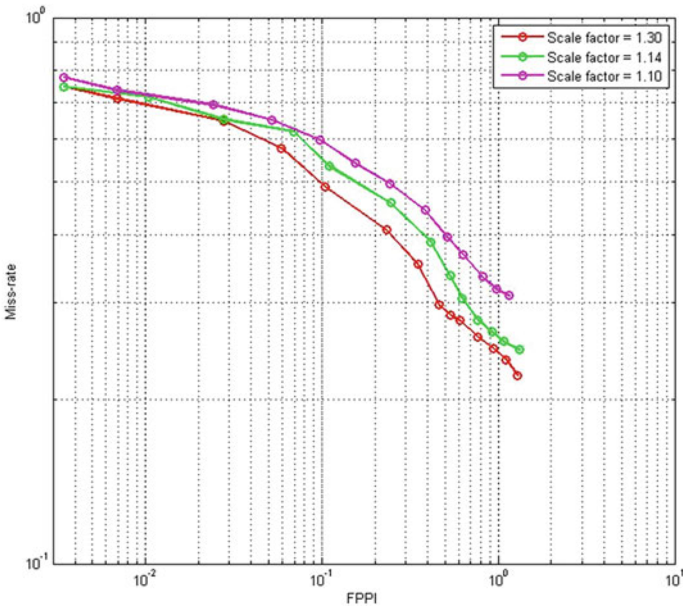

Fig. 5 Miss-rate versus FPPI plots for proposed detector-2

Table 3 Miss-rate of the detector-2 using different scale factors at different FPPI values

Scale factor/FPPI	1.1 (%)	1.14 (%)	1.30 (%)
0.01	72.2	71.2	**69.1**
0.1	59.7	55.0	**48.9**
1	31.1	26.1	**23.9**

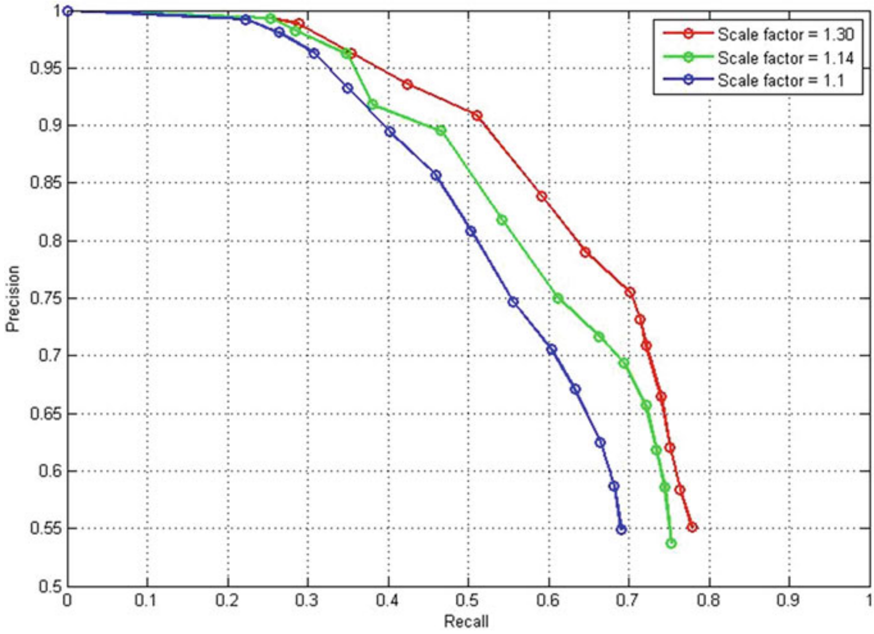

Fig. 6 Precision versus recall plots for proposed detector-2

Table 4 Comparison of performance with similar existing detectors

Detector	Classifier	Training dataset	% Miss-rate at		Sec/ frame
			1 FPPI	0.1 FPPI	
Proposed detector-1	Linear SVM	INRIA	21.8	46.3	1.8
Proposed detector-2	Cascade of boosted		23.9	48.8	0.18
HOG non-linear (Yi and Xue 2014)	Linear SVM		44	85	–
HOG (Dalal and Triggs 2005a)	Linear SVM		23	46	2.3
HOG + LBP (Wang et al. 2009)	Linear SVM		19	39	9.1
HOG + Dense LDB (Das and Saikia 2016)	Linear SVM		17	41	2.5
HOG + Dense LDB (Das et al. 2021)	Cascade of boosted		18	43	0.2

Table 4 that the proposed detector-1 and detector-2 provide performance close to HOG at 1 FPPI and 0.1 FPPI considering all pedestrian heights. However, these observed performances are marginally lower compared to HOG-LBP (Wang et al. 2009) and HOG-dense LDB (Das and Saikia 2016; Das et al. 2021). Detector-1 provides an improvement of miss-rate by about 1.2% over HOG and reduction by about 2.8% than HOG-LBP is observed. The proposed detector-1 has a miss rate of about 46.3% at 10^{-1} FPPI which is close to HOG but higher by about 7.3% than HOG-LBP. The proposed detector-2 performs inferior to proposed detector-1 which might be due to the use of integral HOG instead of traditional HOG descriptor. Both the proposed detectors perform inferior to their counterparts using image pyramid proposed in Das and Saikia (2016) and Das et al. (2021) respectively. The reason behind this inferior performance is that the scale space created by using non-linear diffusion scale space is smaller compared to image pyramid. The count of the levels and sublevels of the scale space is selected empirically. Larger values of levels lead to smoothing of the images at lower pyramidal levels, which in turn reduces the performance of the detector.

However, one of the observed advantages of the proposed detectors is that large-size pedestrians can be detected due to the consideration of non-linear scale space. The use of image pyramid does not help to detect these large-size pedestrians. Figures 7 and 8 show the detection percentage of the detectors for different pedestrian sizes at 1 FPPI and 0.1 FPPI, respectively. From the study, it is evident that the use of non-linear scale space has improved the detection percentage of the large sized pedestrians for both linear SVM and cascade classifier-based detectors. The proposed linear SVM-based detector-1 has improved detection percentage by around 14% at 1 FPPI and 3% at 0.1 FPPI compared to the detector in Das and Saikia (2016) which uses image pyramid. Similarly, there is an increase in detection rate by around 10% for 1 FPPI and 6% for 0.1 FPPI in case of the cascade-based proposed detector-2 compared to the detector proposed in Das et al. (2021).

The other advantage of the proposed detector-1 and detector-2 is that they take less time to process one frame in comparison to the other detectors. From Table 4, the proposed detector-2 takes the least time to process a frame (which is equivalent to more than 5 FPS) which may be critical in real-time applications.

6 Conclusion

This paper has introduced two pedestrian detectors employing non-linear scale space for multi-scale detection. Proposed detector-1 uses linear SVM classifier, and detector-2 uses cascade of boosted classifier. The detectors use variants of HOG combined with dense LDB features. It is observed that the proposed detectors perform better in case of large sized pedestrians compared to similar detectors with the same feature sets and using image pyramid. The proposed detectors also perform better than the existing detector which uses non-linear scale space and HOG. Another notable achievement here is the detection speed. The proposed detector-2 is found

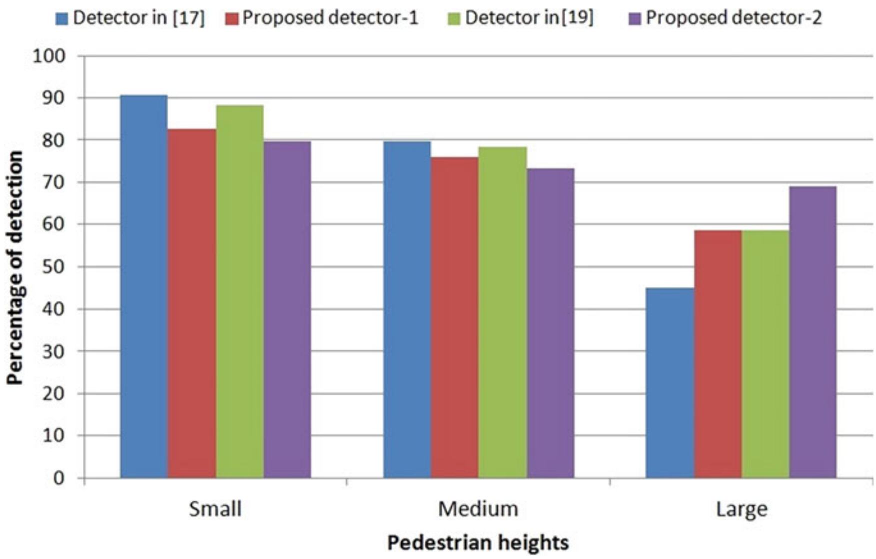

Fig. 7 Detection % for different pedestrian heights at 1 FPPI of detector-1 and detector-2

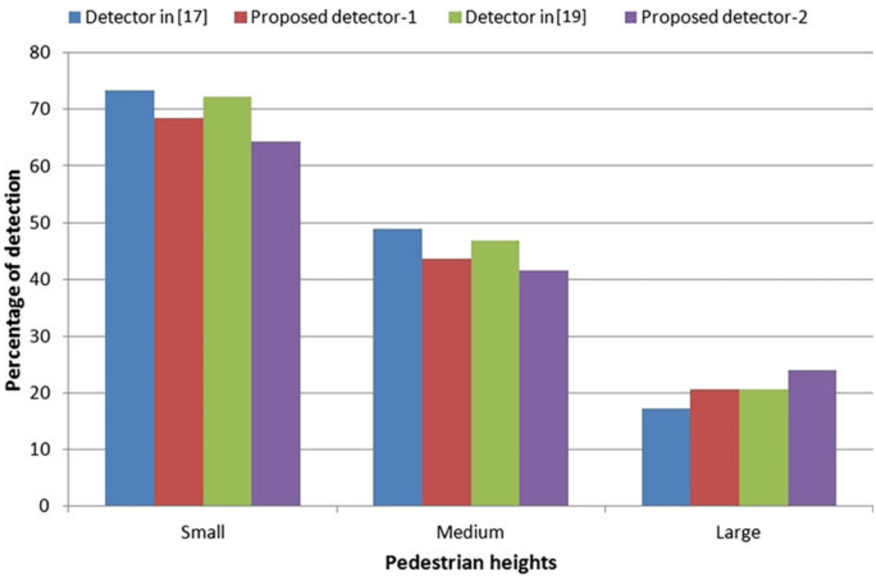

Fig. 8 Detection % for different pedestrian heights at 0.1 FPPI of detector-1 and 2

to be faster than all the similar detectors. In future work, the potential of non-linear scale space for multi-scale detection can be further explored using different feature sets and classifiers.

Acknowledgements This work is supported by the Department of Science and Technology, Govt. of India, under the INSPIRE fellowship program.

References

Alcantarilla PF, Nuevo J, Bartoli A (2013) Fast explicit diffusion for accelerated features in nonlinear scale spaces. In: Proceedings of the British machine vision conference. BMVA Press

Benenson R, Omran M, Hosang J, Schiele B (2015) Ten years of pedestrian detection, what have we learned? In: Agapito L, Bronstein MM, Rother C (eds) Computer vision - ECCV 2014 workshops. Springer International Publishing, Cham, pp 613–627

Dalal N, Triggs B (2005a) Histograms of oriented gradients for human detection. In: 2005a IEEE computer society conference on computer vision and pattern recognition (CVPR'05), vol 1, pp 886–893

Dalal N, Triggs B (2005b) Histograms of oriented gradients for human detection. In: IEEE computer society conference on computer vision and pattern recognition (CVPR'05), vol 1, pp 886–893

Das AJ, Saikia N (2016) Pedestrian detection using dense LDB descriptor combined with hog. In: 2016 international conference on information technology (InCITe)- the next generation IT summit on the theme - internet of things: connect your worlds, pp 299–304

Das AJ, Saikia N, Choudhury S (2021) Cascade-based pedestrian detector using edge and pattern features. In: Bora PK, Nandi S, Laskar S (eds) Emerging technologies for smart cities. Lecture notes in electrical engineering, vol 765. Springer, Singapore. https://doi.org/10.1007/978-981-16-1550-4_7

Dollar P, Tu Z, Perona P, Belongie SJ (2009a) Integral channel features. In: BMVC

Dollar P, Wojek C, Schiele B, Perona P (2009b) Pedestrian detection: a benchmark. In: 2009b IEEE conference on computer vision and pattern recognition, pp 304–311

Dollar P, Belongie S, Perona P (2010) The fastest pedestrian detector in the west. In: Proceedings of the British machine vision conference. BMVA Press, pp 68.1–68.11

Dollar P, Wojek C, Schiele B, Perona P (2012) Pedestrian detection: an evaluation of the state of the art. IEEE Trans Pattern Anal Mach Intell 34:743–761

Everingham M, Gool L, Williams CK, Winn J, Zisserman A (2010) The pascal visual object classes (voc) challenge. Int J Comput Vision 88:303–338

Felzenszwalb PF, Girshick RB, McAllester D (2010) Cascade object detection with deformable part models. In: IEEE computer society conference on computer vision and pattern recognition, pp 2241–2248

Mori G, Belongie S, Malik J (2005) Efficient shape matching using shape contexts. IEEE Trans Pattern Anal Mach Intell 27(11):1832–1837

Ojala T, Pietikainen M, Maenpaa T (2002) Multiresolution gray-scale and rotation invariant texture classification with local binary patterns. IEEE Trans Pattern Anal Mach Intell 24(7):971–987

Tuzel O, Porikli F, Meer P (2008) Pedestrian detection via classification on riemannian manifolds. IEEE Trans Pattern Anal Mach Intell 30(10):1713–1727

Viola P, Jones MJ (2003) Fast multi-view face detection

Viola P, Jones MJ, Snow D (2003) Detecting pedestrians using patterns of motion and appearance. In: Proceedings ninth IEEE international conference on computer vision, vol 2, pp 734–741

Walk S, Majer N, Schindler K, Schiele B (2010) New features and insights for pedestrian detection. In: 2010 IEEE computer society conference on computer vision and pattern recognition, pp 1030–1037

Wang X, Han TX, Yan S (2009) An hog-lbp human detector with partial occlusion handling. In: 2009 IEEE 12th international conference on computer vision, pp 32–39

Weickert J (2001) Efficient image segmentation using partial differential equations and morphology. Pattern Recogn 34(9):1813–1824

Wojek C, Schiele B (2008) A performance evaluation of single and multi-feature people detection. In: Rigoll G (ed) Pattern recognition. Springer Berlin Heidelberg, Berlin, Heidelberg, pp 82–91

Yi Z, Xue J (2014) Improving hog descriptor accuracy using non-linear multi-scale space in people detection. In: Proceedings of the 2014 ACM southeast regional conference. ACM, pp 9:1–9:6

Zhang L, Lin L, Liang X, He K (2016) Is faster r-cnn doing well for pedestrian detection? In: Leibe B, Matas J, Sebe N, Welling M (eds) Computer vision—ECCV 2016. Springer International Publishing, Cham, pp 443–457

Zhu Q, Yeh MC, Cheng KT, Avidan S (2006) Fast human detection using a cascade of histograms of oriented gradients. In: 2006 IEEE computer society conference on computer vision and pattern recognition, vol 2, pp 1491–1498

Cyberthreat Detection Using Machine Learning

Simanta Rajbangshi, Chemkai Wangpan, Ayushman Chaudhury, Nupur Choudhury, and Rupesh Mandal

Abstract Millions of users have been a victim of cyberattacks, and thousands of companies are affected as well. This paper proposes Machine Learning to be used as a method to improve the detection rates of cyberthreats in a network which is better than the traditional signature or anomaly-based methods. Machine Learning can be used to detect threats and protect systems in real time thereby reducing the damage caused by attacks to a very high extent. In this paper, five Supervised Machine Learning algorithms, Random Forest, Logistic Regression, SVM, Decision Tree and Naive Bayes, have been used with optimized parameters and tuning and lastly, a deep learning algorithm; Convolutional Neural Network (CNN) has been used, and the performances have been compared among them. The algorithms performed well with Random Forest model being the highest. The results achieved prove that Machine Learning can be implemented to develop a threat detection system for a network which would be much more secure compared to the existing methods of detection and prevention.

Keywords Intrusion detection system · Machine learning · Convolutional neural networks · Networking

1 Introduction

This generation is highly dependent on the internet to carry out various tasks which are considered essentials. With an increase in the number of users on the internet, the number of attacks on users on the internet is also increasing. Denial of Service (DoS) is the most popular attack that has been rising lately, also harmless attacks like probing attacks which include port scanning that give information about a system

S. Rajbangshi · C. Wangpan · A. Chaudhury · N. Choudhury (✉) · R. Mandal
Assam Don Bosco University, Guwahati, India
e-mail: nupur.choudhury@dbuniversity.ac.in

R. Mandal
e-mail: rupesh.mandal@dbuniversity.ac.in

J. K. Deka et al. (eds.), *Emerging Technology for Sustainable Development*,
Lecture Notes in Electrical Engineering 1061,
https://doi.org/10.1007/978-981-99-4362-3_27

or network have been resulted to more dangerous attacks like Privilege escalation attacks or Remote Access attacks. From the studies, it can be said that threat detection is basically a classification where the system/model has to classify a packet as safe or harmful. To secure our data from such attacks, Intrusion Detection Systems (IDS) are created which monitors and analyzes the data flowing in a network for identification of intrusions. There are two types of IDS, Signature-Based IDS or S-IDS and Anomaly-Based IDS or A-IDS. S-IDS identify threats in a network from the signatures stored in their database and can detect known attacks but fails for newer attacks. While, A-IDS creates a pattern for normal network behavior and classifies unknown networks as intrusion, but contains high false positive rates. Thus, Machine Learning is an optimal solution. The existing Intrusion Detection Systems are struggling to increase both detection speed and accuracy simultaneously, but no practical solutions are available. Thus, to combat this problem, we are doing a research work that uses Machine Learning with a deep learning algorithm to detect threats in a network. For achieving accurate attack detection, using signature-based Machine Learning is not suitable due to the limitations of using preconfigured databases and results in the failure to detect threats that are unknown to the system. Therefore, Machine Learning techniques should be adopted in our system and implemented in such a way that it works accurately and also be able to predict newer methods of attacks. Moreover, existing Machine Learning techniques using standard algorithms (Omar et al. 2013; Qu et al. 2017) or based on IoT (Costa et al. 2019) do have limitations. Massive amounts of data need to be classified in such cases. Therefore, deep learning methods (Haq et al. 2015) come into play which can provide better results and has good potential. In this research work, CNN, a deep learning algorithm which is mostly used for image processing, but not been used in the field of networking systems.

The remaining paper is constructed as follows: Sect. 2 represents the past works conducted in the field of IDS using Machine Learning or deep learning methods as well as work on the NSL-KDD dataset. Section 3 contains the description of NSL-KDD dataset and its analysis. Section 4 is the detailed information about the methodology used to conduct the research work. Section 5 describes the results achieved followed by Sect. 6 as the conclusion of our work.

2 Related Works

Our research shows that various works have been carried out in the field of Intrusion Detection Systems using Machine Learning algorithms. In 2013, Omar Salima and her team (Omar et al. 2013) carried out an analysis on three perspectives of technical challenges in IDS based on Machine Learning, namely feature extraction, classifier construction and sequential pattern prediction. Recently, a study where deep learning was used for an IDS by Qu et al. (2017) showed an IDS model based on Deep Belief Networks and using the NSL KDD dataset. They have applied long short-term memory (LSTM) architecture to RNN and trained the model using KDD

Cup'99 dataset. Another study was done by Haq and team (2015) where a statistical comparison was done to show classifier design. They used single, hybrid and ensemble algorithms in the research. A study by Hamid et al. (2016) was done where they used different machine learning methods using Weka on the KDD CUP 99 dataset. They used tenfold cross-validation to evaluate the performance in terms of True Positive Rate, False Positive Rate, precision, accuracy, etc. It also evaluates the Machine Learning models provided by Weka and describes the performance measures taken into consideration. Another related work named Internet of Things: A survey on Machine Learning-based intrusion detection approaches (Costa et al. 2019) shows the use of both new and traditional machine learning algorithms for handling security issues in IoT environments. Their system was able to detect three types of IoT attacks called jam, false and reply attack. A study by Ingre and Yadav evaluated the performance of NSL-KDD dataset using ANN. They obtained high detection rates in binary as well as multiclass classification (Li et al. 2014). A study by Bedi et al. (2020) shows class imbalance problem handling in the KDD-99 and NSL-KDD datasets using Siamese Neural Networks. The attack classes R2L and U2R being the minority have less detection rate as compared to DoS and Probe attack classes and hence proposed a Siam-IDS that can detect them without oversampling or random under sampling techniques. Sun et. al. (2018) created a dual-layer model for efficient threat detection using KDD CUP 99 dataset. They did an oversampling of the minority class using synthetic samples and used Gradient Boosting Decision Tree, KNN and Fly Optimization algorithm for separation of normal and attack classes. In 2003, Mukkamala and Sung (1822) used feature selection for intrusion detection with neural networks and SVM to rank the input features according to each specific class label. In 2014, Kumar Shrivas and Dewangan (2014) proposed ANN-based IDS with net gain ratio feature selection technique. A data mining framework was introduced by Lee et al. (1999) for the same. Chandrashekhar and Raghuveer (2013) used data mining techniques like fuzzy C-means clustering, fuzzy neural network and SVM for developing and IDS using the KDD-99 dataset. Parsaei et al. (2017) used SDN to categorize network traffic by applying different types of neural network estimators. They used data mining techniques with various ML algorithms. Ilievski and Latkoski (2021) classified network traffic using supervised ML algorithms by using a network functions virtualization environment, and decision tree performed the best. Le et al. (2018) have applied big data, ML, NFV, SDN and built a practical and strong configuration for predicting and management of behaviors in network traffic.

3 Dataset Description and Analysis

NSL KDD dataset is the corrected version of KDD CUP 99 which was first publicized by the MIT Lincoln labs at the University of California. NSL-KDD was later published by the University of New Brunswick as a revised version of KDD'99. It was proposed to remove the issues of KDD 99 dataset that contained a lot of unnecessary records. Even though the dataset is old as of now, it serves as the benchmark to compare similar IDS/IPS systems as well as Machine Learning algorithm-based system's performances. The dataset contains the record of information collected through systems like simple Intrusion detection network systems. The dataset has 43 columns and is divided into five main categories: Normal traffic, Denial of Service, Probe or Scans, User to Root and Remote to Local. The following two graphs are plotted to visualize the data distribution against different protocols and attack labels.

Statistical measurements and representation provide a better understanding of the dataset used. It can be seen that there are 22 types of attack from the Fig. 1. These attack categories are further divided into 4 types and one normal type. DOS attack presents 90% of attack types and 30% the dataset, while other attack types compromise of only 9.25% among all attack types. At the first glance, the dataset appears unbalanced, but it contains lots of information about the data packets.

In order to extract relevant feature from the dataset, we first removed any duplicate values present. We then mapped the labels as either '1' or '0' depending whether it is attack type or normal type using one-hot encoding. If features aren't selected properly, the performance of the model is highly affected. Table 1 shows the number of data points that are present categorically as well as in each protocol along with the attacks labels for analysis.

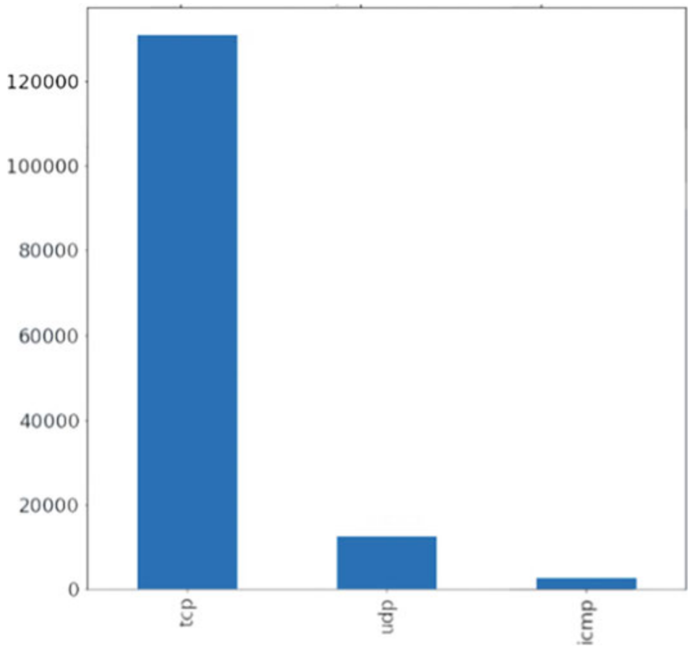

Fig. 1 Distribution of data points per protocol

Table 1 Data points in each attack label

Category	Name of attack	ICMP	TCP	UDP	Data points
DOS attacks	Back	0	956	0	45,927
	Land	0	18	0	
	Neptune	0	41,214	0	
	Pod	201	0	0	
	Smurf	2646	0	0	
	Teardrop	0	0	892	
Probe attacks	Ipsweep	3117	482	0	3633
	Nmap	981	265	247	
	Portsweep	5	2926	0	
	Satan	32	2184	1417	
Privilege escalation attacks	Buffer overflow	0	30	0	52
	Loadmoudle	0	9	0	
	Perl	0	3	0	
	Rootkit	0	7	3	
Access attacks	Ftp write	0	8	0	995
	Guess Passwd	0	53	0	
	Imap	0	11	0	
	Multihop	0	7	0	
	Phf	0	4	0	
	Spy	0	2	0	
	Warezclient	0	890	0	
	Warezmaster	0	20	0	
Normal packets		1309	53,599	12,434	67,342

4 Methodology Used

We used five supervised ML algorithms and one deep learning algorithm to compare the performances side by side. We have also used hyperparameters in each to fine-tune the algorithms for better scores compared to default parametric scores. Grid Search cross-validation method is also used which will automatically find the best model according to the parameters given. It takes higher time but provides the best parameters and results (Fig. 2).

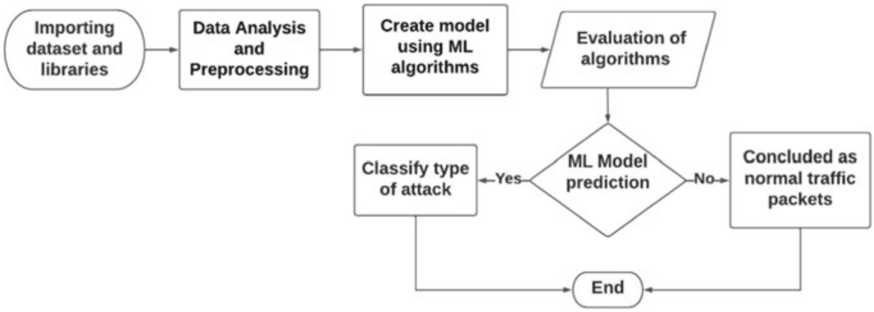

Fig. 2 Workflow diagram for the methodology used

4.1 Algorithms Used

The following six Machine Learning Algorithms have been used to compare and contrast the performances and create our model.

(1) **Decision Tree**: The maximum depth of the tree has been specified along with the number of samples that are required to split. The parameter to specify the number of cross-validation iterations has been also used and specifying the number of cpus to use. Below are the hyperparameters used:
   max_depth: 5–500, min_samples_split: 5–500, cross-validation iterations = 3, n_jobs = −1 (using all CPUs).
(2) **Random Forest**: In this model, the maximum depth is specified as well as the number of estimators which are the decision trees.
   Hyperparameters used: Max_depth: 5–1000, N_estimators: 5–500, min_samples_split = 5–500, cross-validation iterations = 3, n_jobs = −1 (using all CPUs).
(3) **Support Vector Machine (SVM)**: In this algorithm, SGD Classifier has been used with the loss function as 'hinge' which gives the linear SVM.
   Hyperparameters used: Penalty: l1, l2, Loss = hinge, cross-validation iterations: 5, n_jobs = −1 (using all CPUs).
(4) **Logistic Regression**: We again used the SGD classifier using the loss function as 'log' which represents the logistic regression function. Likewise, we have used GridSearchCV to tune the parameters and find the best model.
   Hyperparameters used: Penalty: l1, l2, Loss = log, cross-validation iterations: 5, n_jobs = −1.
(5) **Naïve Bayes**: In this algorithm, the number of iterations has been specified to make sure the accuracy can be determined properly. Also, the number of jobs to run in parallel has been specified as −1 which indicates it can use all CPUs to perform the operation.
   Hyperparameters used: Var_smoothing: 10**x for x in range (−9,3), cross-validation iterations: 5, n_jobs = −1.

(6) **Convolutional Neural Network**: For this algorithm, we have used ReLU as activation function for the first three layers and sigmoid for the output layer. We have given the learning rate as 0.9. The optimizer RMSprop has been used to create the model. Convolution Neural Network achieved very low accuracy rate and F1-score considering to the fact that CNN is best used for image processing.

4.2 Evaluation Metrics

Accuracy is the most important evaluation parameter for an IDS that is used to measure the performance of the Machine Learning models. In addition to the accuracy, we considered the true positive and false positive rate.

We have used the following metrics to evaluate our models performance:

$$\text{Accuracy} = \frac{\text{TP} + \text{TN}}{\text{TP} + \text{FP} + \text{FN} + \text{TN}} \tag{1}$$

$$\text{True Positive Rate(TPR)} = \frac{\text{True Positive}}{\text{True Positive} + \text{False Negative}} \tag{2}$$

$$\text{False Positive Rate(FPR)} = \frac{\text{False Positive}}{\text{False Positive} + \text{True Negative}} \tag{3}$$

$$\text{Precision} = \frac{\text{True Positive}}{\text{True Positive} + \text{False Positive}} \tag{4}$$

$$\text{Recall} = \frac{\text{True Positive}}{\text{True Positive} + \text{False Negative}} \tag{5}$$

$$\text{F1Score} = 2 * \frac{\text{Precison} * \text{Recall}}{\text{Precison} + \text{Recall}} \tag{6}$$

5 Results

The tested algorithms performed quite well and in comparison to each other. The models have performed really well achieving good scores with random forest topping with precision score of 97.89, recall 97.91 and F1-score of 96.05. But as the dataset used is smaller in size and contains very less data points for many attack classes, it can be difficult for the models to work in real time. Moreover, newer datasets can be developed which contain the latest information about each attack type and would increase the detection rate for newer attacks to a very high extent due to the learning

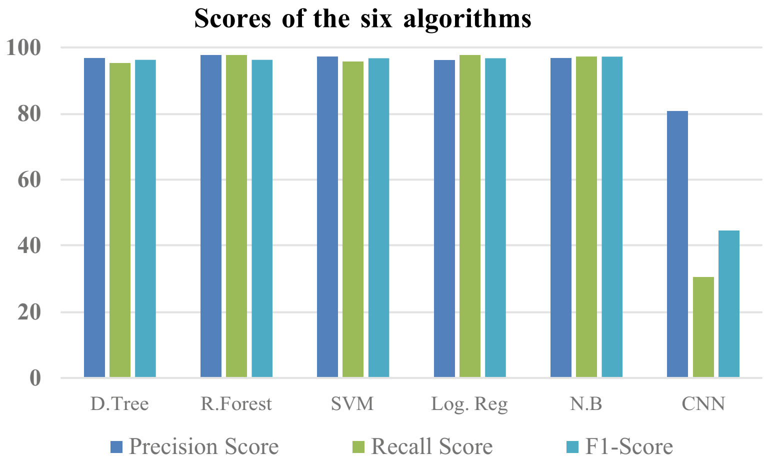

Fig. 3 Bar graph to show the scores of our tested algorithms

capabilities of Machine Learning algorithms. Also, the deep learning CNN algorithm is capable of performing better with correct parameters and better optimized datasets for neural networks (Fig. 3).

6 Conclusion

As we already know, existing threat detection systems like IDS or IPS fails to detect modern threats, and rely on signatures available in their databases to classify them as threats, meanwhile failing to detect the zero-day threats. We demonstrated how Machine learning is useful to effectively predict and detect threats in the network with great accuracy. Also, the model's performance can be improved by using the GPU libraries for deep learning instead of the CPU which results in 10 × improvement in training times. This proves that Machine Learning algorithms can be further used to detect threats in real time as well as prevent zero-day attacks to a great extent if it is optimized correctly with proper parameters and configuration.

References

Bedi P, Gupta N, Jindal V (2020) Siam-IDS: handling class imbalance problem.Intrus Detect Syst Siamese Neural Netw 171:780–789

Chandrashekhar AM, Raghuveer (2013) Fortification of hybrid intrusion detection system using variants of neural networks and support vector machines. Int J Netw Secur Appl

Costa K, Papa J, Lisboa C, Munoz R, Albuquerque V(2019) Internet of Things: a survey on machine learning-based intrusion detection approaches. Comput Netw 151. https://doi.org/10.1016/j.comnet.2019.01.023

Hamid Y, Muthukumarasamy S, Journaux L (2016) Machine learning techniques for intrusion detection: a comparative analysis 1–6. https://doi.org/10.1145/2980258.2980378

Haq NF, Onik AR, Hridoy MAK, Rafni M, Shah FM, Md. Farid D (2015) Application of machine learning approaches in intrusion detection system: a survey. Int J Adv Res Artifi Intell (IJARAI) 4(3)

Ilievski G, Latkoski P (2021) Serbian J Electric Eng 18(2):237–254

Kumar Shrivas A, Dewangan A (2014) An ensemble model for classification of attacks with feature selection based on KDD99 and NSL-KDD data set. Int J Comput Appl 99:8–13. https://doi.org/10.5120/17447-5392

Le L-V, Sinh D, Lin B-SP, Tung LP (2018) Applying big data, machine learning, and SDN/NFV to 5G traffic clustering, forecasting, and management. In: Proceedings of the 4th IEEE conference on network softwarization and workshops (NetSoft). Montreal, Canada, pp 168–176

Lee W, Stolfo SJ, Mok KW (1999) A data mining framework for building intrusion detection models. In: Proceedings of the 1999 IEEE symposium on security and privacy (Cat. No.99CB36344), pp 120–132. https://doi.org/10.1109/SECPRI.1999.766909

Li W, Yi P, Wu Y et al (2014) A new intrusion detection system based on KNN classification algorithm in wireless sensor network. J Electric Comput Eng 2014(5):1–8

Mukkamala S, Sung AH (1822) Feature selection for intrusion detection with neural networks and support vector machines. J Transp Res Board 2003:33–39

Omar S, Jebur H, Benqdara S (2013) An adaptive intrusion detection model based on machine learning techniques. International J Comput Appl70. https://doi.org/10.5120/11971-6640

Parsaei MR, Sobouti MJ, Raouf Khayami S, Javidan R (2017) Network traffic classification using machine learning techniques over software defined networks. Int J Adv Comput Sci Appl 8(7):220–225

Qu F, Zhang J, Shao Z, et al. (2017) An intrusion detection model based on deep belief network. In: Vi international conference, pp 97–101

Sun C, Lv K, Hu C, Xie H (2018) A double-layer detection and classification approach for network attacks. In: 27th international conference on computer communication and networks (ICCCN). IEEE, Hangzhou, China, pp 1–8

Medicinal Plant Classification Using Neural Network

Avilie Khate and Bobby Sharma

Abstract The earth is filled with a different kinds of medicinal plants. These medicinal plants are used in some useful ways such as formulation of drugs, herbal products made from it, and common ailments and diseases cured by making medicines out of the medicinal plants. There are many medicinal plants in the wilderness. Recognition of those medicinal plants by human sight are going to take a long time, slow, tiresome, and not accurate. As many of them are under extinction as per the IUCN records, image processing comes into play by identifying the endangered plants and helping in preserving it. The Mendeley dataset has a collection of different species of healthy medicinal herbs such as Alpinia Galanga (Rasna), Citrus Limon (Lemon), and Moringa Oleifera (Drumstick), and 30 different medicinal plants with 1500–2000 images are available in Mendeley's dataset. In each respective medicinal plant folder, 50–100 high-quality images are present. The species botanical/scientific name are named as the folder name which will be used to train the model. In this paper, it proposed a system that adopts the deep learning method to obtain high accuracy in the classification and recognition of medicinal plants. Convolutional Neural Network (CNN) is used as the system for classifying of medicinal plant images based on deep learning.

Keywords Mendeley dataset · Deep learning · Convolutional Neural Network

A. Khate (✉) · B. Sharma
Department of Computer Science and Engineering, School of Technology, Assam Don Bosco University, Guwahati, India
e-mail: aviliekhate123@gmail.com

B. Sharma
e-mail: bobby.sharma@dbuniversity.ac.in

J. K. Deka et al. (eds.), *Emerging Technology for Sustainable Development*,
Lecture Notes in Electrical Engineering 1061,
https://doi.org/10.1007/978-981-99-4362-3_28

1 Introduction

There are thousands of plants that can be found around us, many of which are utilised as medicines. Long-established methods for medications made from medicinal plants by our forefathers are used extensively within the pharmaceutical industry and research for which many lives have been saved. To this day, many indigenous people and populations employ medicinal plants. To date identifying plants successfully and correctly is done manually based on morphological characteristics (Begue et al. 2017). A professional botanist's inherent knowledge is essential for recognising and discovering unknown new plants. People use their eyes, noses, hands or other human organs to assess the shape, colour, taste, and texture of the whole plant or individual parts (leaf, flower, fruit, or bark), and then they decide the species of medicinal plants based on either reference or experience (Kan et al. 2017). Nonetheless, manually identifying medicinal plants is time-consuming and difficult, and it is highly dependent on the person's knowledge, experience, and skills about the plants. Hence, automatic classification of plants based on their characteristics is supported by many researchers researching this subject. Thanks to this many folks can now easily recognised medicinal plants. With the advancement of image processing and pattern recognition technologies, computer-based automatic image identification is now widely used in practice with the majority of them relying on machine learning techniques.

Machine learning is data analysis technique. It takes data as inputs, and it learns to spot or identify patterns before making a decision with little human intervention. It improves as a result of training. Machine learning is employed in a variety of fields, including medicine, finance, and many more. By attempting to automate the system, it decreases people's workload.

Although the methods are very similar, the systems produced so far use a different number of steps to automate the process of automatic classification. These processes entail prepping the leaves collected, performing some pre-processing to identify their unique characteristics, classifying the leaves, building the database, training for identification, and finally evaluating the results. The most important parameter in recognition accuracy is the ability to detect similar things as well as distinguish between distinct types of objects.

2 Brief Literature Review

In paper (Begue et al. 2017), computer vision algorithm was employed to extract many shape-based properties from medicinal plants leaves. Machine learning methods are then used to classify 24 distinct plant species into their correct categories. The most accurate classifier was the Random Forest classifier which had a 90.1% accuracy.

In paper (Dudi and Rajesh 2019), a medicinal plant recognition based on CNN and machine learning was proposed, and 32 species and 1800 data were used from Flavia dataset. Both testing and training were conducted using the Flavia dataset. They employed ANN, SVM, KNN, and Naïve Bayes (NB) as well as other machine learning techniques. It was achieved with a 98% accuracy.

This research, (Kan et al. 2017) proposes a useful strategy for classifying 12 different types of medicinal plant leaf photos. After pre-processing of leaf photos, the shape and texture details of the plant leaves are retrieved. Secondly, the classification efficiency of numerous models such as the BPNN (BP neural network), probabilistic neural network (PNN), K-nearest neighbour classification algorithm, and SVM (support vector machine classifier) is examined in a comparison experiment. For the image classification of medicinal plant leaves, the suggested SVM classification approach based on both shape and texture data was effective and practicable.

It was proposed in this work (Venkataraman and Mangayarkarasi 2016) that a vision-based technique is used to construct an automated system that recognises plants. Even a man who is not familiar with this sector can grasp what plants he is seeing and their therapeutic properties thanks to the system's design. The creation of the feature set, which is a key stage in recognising any plant species, is discussed in this work.

A leaf classification system based on the dual-path deep CNN is proposed in the publication (Shah et al. 2017) by Shah, Sougatta Singh et al. The remaining big operations will be carried out using the dual-path CNN.

i. Both form and texture properties are examined and investigated.
ii. The resulting features are optimised for categorisation.

It claimed that it outperformed other CNN approaches since the method they utilised had a good accuracy of around 99.28% (Flavia dataset).

References	Classifier	Accuracy (%)	Dataset	Training	Testing	Species
1	Random Forest	90.1	NM	NM	NM	24
2	ANN, KNN	98	1800	1400	320	32
3	SVM	93.3	1800	240	120	12
4	Non-classifier	*	5	*	*	1
5	Dual-Path CNN	99.28	6630	5500	800	29

3 Medicinal Plant Recognition

3.1 Classification Method

(A) VGG16

VGG16 is a CNN model that has been pre-trained using images from the ImageNet dataset. VGG16 gets its name from the fact that it contains 16 layers with different weights. It's a really huge network, with around 138 million (approximately) parameters. It has 3×3 filter convolutional layer with a stride of one, as well as an equivalent padding and max pool layer of 2×2 filter of stride 2. Throughout the architecture, the convolution and max pool layers are arranged in the same order. As illustrated in Fig. 1, VGG16 contains two FC (fully connected layers) for output, followed by a softmax. Each convolutional layer employs a fixed number of kernels with variable dimensions in each layer to conduct a simple convolution operation on the input pictures. The beginning layer of the convolution extracts edge and colour characteristics from the input images. The feature maps of the input photos are generated by these layers.

The amount, number, and size of the filters used during a single convolutional layer determine the size of the feature maps. The output of the last convolutional layer is the input to the first fully connected layer. The first two each have 4096 channels, whereas the third uses a 1000-way ILSVRC classification system and hence has 1000 channels. The softmax layer receives the output from the last FC layer. The classification is done via the softmax layer, which also calculates the probability values for each species. Rectification (ReLU) nonlinearity is present in all buried layers.

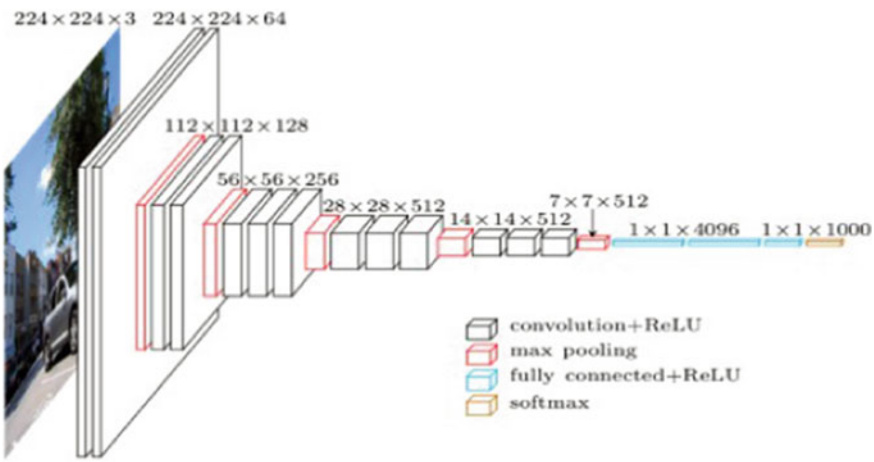

Fig. 1 VGG16 architecture

(B) VGG19

In VGG19 pictures with a fixed size of (224 * 224), RGB image is sent to the network, indicating that the matrix is of the shape (224, 224, 3). The only pre-processing is the elimination of the mean RGB value from each pixel; it utilises kernels of (3 * 3) size with a stride size of 1 pixel, allowing it to span the whole image concept. To retain the image's spatial resolution, spatial padding is utilised. Max pooling is done with two-pixel sweeps across 2 * 2 pixel window. After that, a rectified linear unit (ReLu) was employed to inject nonlinearity into the model in order to enhance classification and reduce processing time, since previous models depended on sigmoid functions, which had shown to be considerably superior. In the end, VGG19 implements three fully connected layers, the first two of which were of size 4096, followed by a layer with 1000 channels for 1000-way ILSVRC classification, and last, as seen in Fig. 2, a softmax function.

(C) RESNET

Hundreds or thousands of convolutional layers are allowed to be used in Residual Network (ResNet); also ResNet is a Convolution Neural Network. As seen in Fig. 3, ResNet stacks identity mappings, or layers that don't do anything at first, and passes over them, reusing the activations from preceding levels. Batch Normalisation is at the heart of ResNet. Batch Normalisation improves the network's performance by adjusting the input layer. The issue of covariate shift has been solved. The Identity

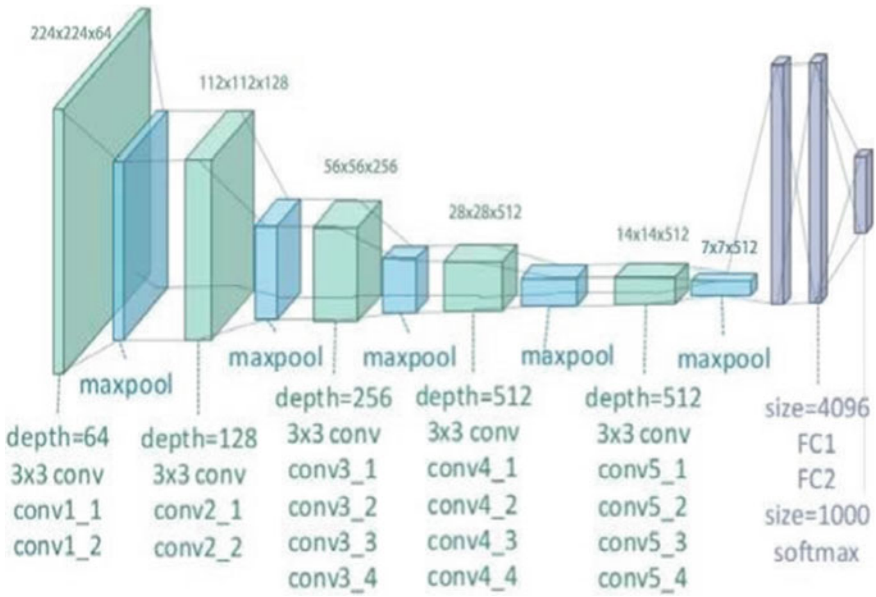

Fig. 2 VGG19 architecture

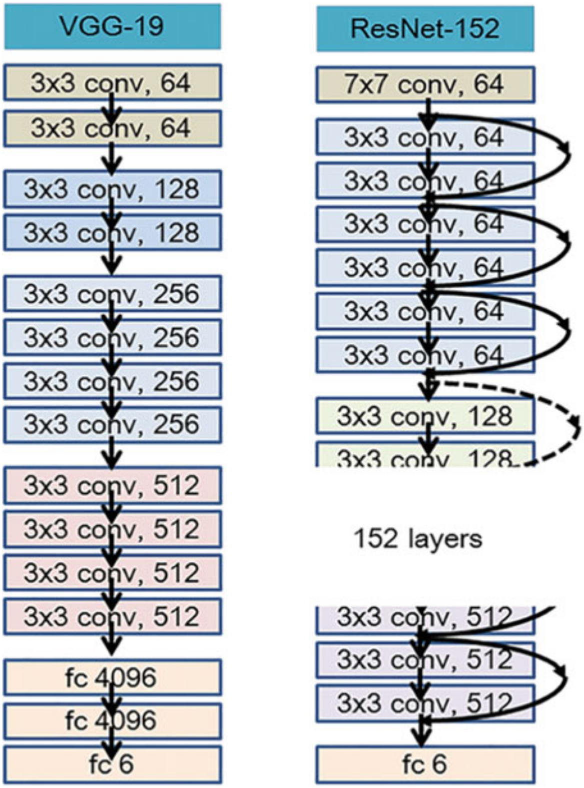

Fig. 3 ResNet architecture

Connection is used by ResNet to prevent the network against vanishing gradient concerns.

4 Experimental Result

(A) Data collection

A medicinal plant dataset (Mendeley dataset) is employed. Alpinia Galanga (Rasna), Citrus Limon (Lemon), Moringa Oleifera (Drumstick), and many other plant/herb species are included in the dataset. The dataset contains 1800 photos of 30 species. Each folder has 50–100 high-quality photos, and the folders are named by the species they contain. These datasets are then utilised to train and test the model. In the image, i.e. Figure 4, a sample data is shown.

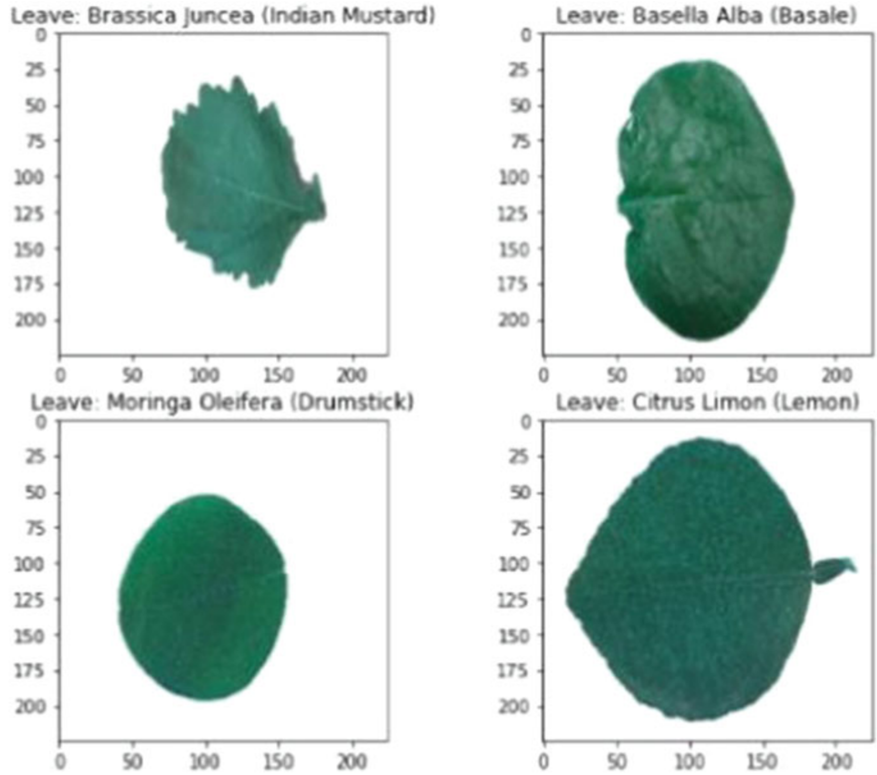

Fig. 4 Sample images of Mendeley dataset

(B) Experiment

Seventy per cent of the medicinal plant dataset is used for training, whereas 30% is used for testing. The training set contains approximately 1284 images, while the validation set contains approximately 551 images for 30 classes of Alpinia Galanga (Rasna), Amaranthus Viridis (Arive-Dantu), Artocarpus Heterophyllus (Jackfruit), Azadirachta Indica (Neem), Basella Alba (Basale), Brassica Juncea (Indian Mustard), Carissa Carandas (Karanda), Citrus Limon (Lemon), Ficus Auriculata (Roxburgh fig), Ficus Religiosa (Peepal Tree), Hibiscus Rosa-sinensis, Jasminum (Jasmine), Mangifera Indica (Mango), Mentha (Mint), Moringa Oleifera (Drumstick), Muntingia Calabura (Jamaica Cherry-Gasagase), Murraya Koenigii (Curry), Nerium Oleander (Oleander), Nyctanthes Arbor-tristis (Parijata), Ocimum Tenuiflorum (Tulsi), Piper Betle (Betel), Plectranthus Amboinicus (Mexican Mint), Pongamia Pinnata (Indian Beech), Psidium Guajava (Guava), Punica Granatum (Pomegranate), Santalum Album (Sandalwood), Syzygium Cumini (Jamun), Syzygium Jambos (Rose Apple), Tabernaemontana Divaricata (Crape Jasmine), Trigonella Foenum-graecum (Fenugreek). The dataset is then fed into the

Table 1 .

Optimiser	Epoch	Batch_size	Loss	Accuracy	Val_Loss	Val_Acc
SGD	6	32	3.3624	0.0740	3.3697	0.0661
	6	64	3.3641	0.0740	3.3698	0.0661
	10	32	3.3620	0.0672	3.3773	0.0623
	10	64	3.3607	0.0672	3.3774	0.0623
	20	32	3.3648	0.0672	3.3700	0.0623
	20	64	3.3597	0.0740	3.3693	0.0661
Adam	6	32	0.2624	0.9435	12.7012	0.2140
	6	**64**	**0.0122**	**0.9951**	**2.0098**	**0.7160**
	10	32	0.1820	0.9426	5.1858	0.3852
	10	64	0.0140	0.9961	2.2021	0.7237
	20	32	0.1461	0.9611	6.2077	0.3113
	20	64	0.0895	0.9757	3.8606	0.2335

model, which is subsequently trained and assessed using several hyperparameters such as epoch, batch size, and optimiser.

The experiment is carried out using Google Colab on a machine with an Intel Core i3 processor, 8 GB of RAM, and 2 GB of AMD M3 graphics.

We aimed to evaluate the classification with different Convolutional Neural Networks. The results of the experiment are that VGG19 gains an accuracy of 0.9964; however, its loss accuracy is higher than that of VGG16. Meanwhile, RESNET 50 did perform well as it obtained an accuracy of 0.9951; however, due to its huge loss accuracy, it is not the suitable classifier for this experiment. Finally, we recognised that VGG16 performs the best when the optimiser is of ADAM, its epoch is 20 and its batch size is 64 with an accuracy of 0.9952. For evaluation, the results of the different CNN are given in Table 1.

RESNET

Out of all the experiments in RESNET50, we find that opt = adam, epoch = 6, batch_size = 64 has the highest accuracy, i.e. 0.9951.

VGG16

Optimiser	Epoch	Batch_size	Loss	Accuracy	Val_loss	Val_acc
SGD	6	32	1.9052	0.4877	1.8079	0.3891
	6	64	0.2303	0.9426	0.2501	0.9339
	10	32	0.1398	0.9776	0.1686	0.9572
	10	64	0.2728	0.9309	0.2265	0.9416
	20	32	0.3474	0.9124	0.3055	0.9339
	20	64	0.2019	0.9611	0.5116	0.8911

(continued)

(continued)

Optimiser	Epoch	Batch_size	Loss	Accuracy	Val_loss	Val_acc
Adam	6	32	0.0828	0.9776	0.1253	0.9689
	6	64	0.0549	0.9864	0.1198	0.9611
	10	32	0.0776	0.9747	0.1851	0.9533
	10	64	0.0093	0.9971	0.1147	0.9650
	20	**32**	**0.0290**	**0.9952**	**0.0749**	**0.9728**
	20	64	0.0129	0.9971	0.1524	0.9533

Out of all the experiments in VGG16, we find that opt = adam, epoch = 20, batch_size = 64 has the highest accuracy, i.e. 0.9952.

VGG19

Optimiser	Epoch	Batch_size	Loss	Accuracy	Val_loss	Val_acc
SGD	6	32	0.0546	0.9883	0.1148	0.9650
	6	64	0.0273	0.9871	0.1128	0.9767
	10	32	0.0062	0.8948	0.0635	0.9767
	10	64	0.0100	0.9971	0.0774	0.9728
	20	32	0.0147	0.9987	0.1808	0.9300
	20	64	0.0363	0.9964	0.1805	0.9705
Adam	6	32	0.1512	0.9591	0.7713	0.8599
	6	64	0.2317	0.9292	0.6767	0.8282
	10	**32**	**0.0202**	**0.9971**	**0.5598**	**0.9572**
	10	64	0.0192	0.9971	0.4418	0.9494
	20	32	0.1231	0.9640	0.3721	0.9339
	20	64	0.0772	0.9734	0.4292	0.8949

Out of all the experiments in VGG19, we find that opt = SGD, epoch = 10, batch_size = 32 has the highest accuracy, i.e. 0.9964.

From the graph Figs. 5 and 6, we know that VGG16 is the best model since its accuracy and val_accuracy are higher than the other models at an epoch of 20, batch size of 32, and using adam as its optimiser.

5 Conclusion

In this work, we evaluated the different CNN models in classifying medicinal plants, and we recognised that out of all the models used VGG16 performed the best based on its accuracy, loss, validation loss, and validation accuracy. Besides CNN help in

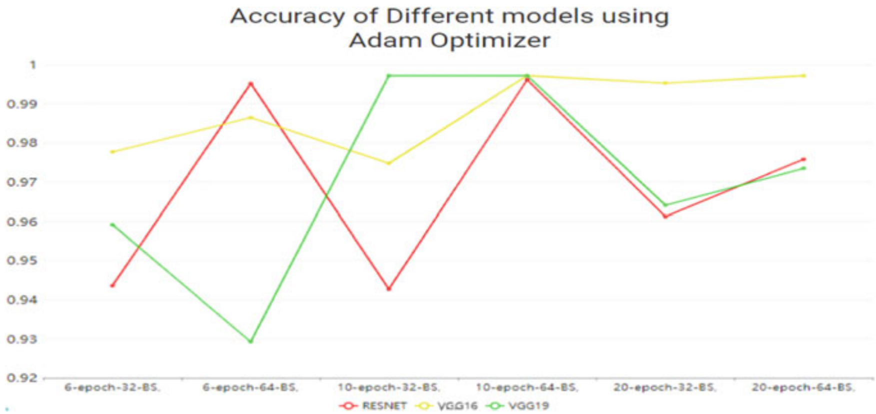

Fig. 5 Accuracy of the models at different epoch and batch size using adam optimiser

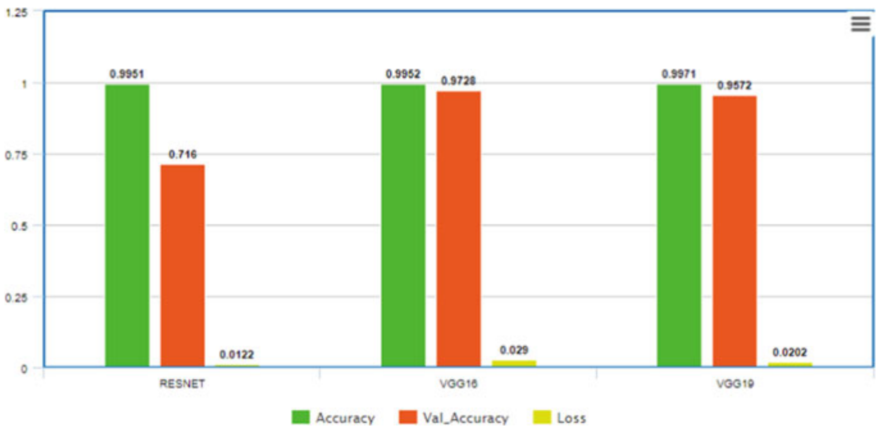

Fig. 6 Comparison of all the models at their best

medicinal plant recognition to be applied in real life as it extracts the features on its own.

In the future, different state-of-the-art models could be used in the future to improve its accuracy. Furthermore, alternative machine learning algorithms can be applied, and their performance can be compared to the current performance of CNNs.

References

Azla MAF, Chua LS, Rahmad FR, Abdullah FI, Alwi SRW (2019).https://doi.org/10.3390/computers8040077

Begue A, Kowlessur V, Singh U, Mahomoodally F, Pudaruth S (2017) Automatic recognition of medicinal plants using machine leaning techniques. Int J Adv Comput Sci Appl (IJACSA) 8(4)

Dileep MR, Pournami PN (2019) AyurLeaf: a deep learning approach for classification of medicinal plants. 978-1-7281-1895-6/19/$31.00 c 2019 IEEE

Dudi B, Rajesh V (2019) Medicinal plant based on CNN and machine learning. Int J Adv Trends Comput Sci Eng 8(4):999–1003

Gopal A, Gayatri V, Prudhveeswar Reddy S (2012) Classification of selected medicinal plants leaf using image processing. 978-1-4673-2322-2112/$31.00 ©2012 IEEE

Kan HX, Jin L, Zhou FL (2017) Classification of medicinal plant leaf image based on multi-feature extraction. Pattern Recogn Image Anal 27(3):581–587. ISSN 1054-6618

Pushpanathan K, Hanaf M, Mashohor S, Ilahi WFF (2020) Machine learning in medicinal plants recognition: a review.https://doi.org/10.1007/s10462-020-09847-0

Rajani S, Veena MN (2018) Study on identification and classification of medicinal plants. Int J Adv Sci Eng Technol 6(2)(Spl.Issue-2). ISSN(p) 2321-8991, ISSN(e) 2321-9009, http://iraj.in

Shah MP, Singha S, Awate SP (2017) Leaf classificationusing marginalized shape context and shape+texture dual-path deep convolutional neural network. 978-1-5090-2175-8/17/2017 IEEE

Venkataraman D, Mangayarkarasi N (2016) Computer vision based feature extraction of leaves for identification of medicinal values of plants. In: 2016 IEEE international conference on computational intelligence and computing research

Vo AH, Dang HT, Nguyen BT, Pham V-H (2019) Vietnamese herbal plant recognition using deep convolutional features. Int J Mach Learn Comput 9(3)

Driving Behavior Analysis Using Deep Learning on GPS Data

Saurabh Kumar Singh, Utkarsh Anand, Anurag Patel, and Debojit Boro

Abstract Aggressive drivers are often considered to violate traffic rules and adopt dangerous driving behavior. This requires the development of effective and robust classifiers for unsafe drivers. Driving behavior analysis is the classification of driving behavior based on the driver's GPS trajectory. With ever-increasing GPS trajectory data, dangerous driving behavior can be thoroughly analyzed and better classified using a deep learning model. Behavioral analytics can help us analyze and identify dangerous drivers that contribute to traffic safety and promote safe driving behavior. In this paper, we propose a novel feature extraction model using a statistical approach to extract the important features from the GPS trajectory data and label the trajectory. To overcome the dataset dependency, we propose to use a deep learning model on our labeled data and finally classify the safe and unsafe drivers. The proposed method demonstrates high accuracy with reduced computational overhead.

Keywords Driving behavior analysis · Deep learning · Feature extraction · GPS

S. K. Singh · U. Anand · A. Patel · D. Boro (✉)
Department of Computer Science and Engineering, Tezpur University, Napaam, Tezpur, Assam 784028, India
e-mail: admn@tezu.ernet.in; deb0001@tezu.ernet.in
URL: http://www.tezu.ernet.in/dcompsc/

S. K. Singh
e-mail: csb18055@tezu.ac.in

U. Anand
e-mail: csb18039@tezu.ac.in

A. Patel
e-mail: csb18058@tezu.ac.in

J. K. Deka et al. (eds.), *Emerging Technology for Sustainable Development*, Lecture Notes in Electrical Engineering 1061,
https://doi.org/10.1007/978-981-99-4362-3_29

1 Introduction

Driving behavior analysis has been a prominent problem for the past decade with ever-increasing research and development in this field. Fueled by a vast amount of user GPS trajectory data publicly made available, driving behavior analysis has been getting more attention from researchers. The increased availability of real-time vehicle trajectory data is helping in the development of effective and robust techniques for analysis. The motivation for this study is:

- According to MORTH (Ministry of Road Transport and Highways (MORTH) 2019) roughly around 70% of all road accidents in India are caused mainly due to reckless and indiscipline driving. The identification of such drivers is very necessary to keep the road safe.
- Driving pattern of a driver affects fuel consumption and emission thus having an impact on the environment. Many automotive insurance companies are adopting pay-as-you-drive or pay-how-you-drive modes for price determination. Prices are decided based on the aggressiveness of the driver.
- Identifying unsafe drivers and taking suitable action on them will help prevent accidents rather than perform post-accident analysis.
- The analysis of human driving behavior is contributing a lot toward the development of autonomous driving as in certain conditions the autonomous algorithm relies solely on human decisions.

The study involves the classification of driving behavior based on GPS trajectories. Driving behavior involves identifying patterns and potentially dangerous behaviors in the GPS trajectory data through feature extraction and behavior evaluation. The main objectives of this study are:

- To extract features like speed, acceleration, and angle for approximating event features.
- To use event feature for labeling of GPS trajectories using statistical approaches.
- To classify and predict drivers associated with unsafe driving behavior by training a machine learning model to map GPS coordinates directly with their classes.

The contributions of our work can be summarized as follows:

- Extraction of basic features like speed, acceleration, angle, and sensitive area to estimate deeper features like SASV (sensitive area speed violation), harsh turning, harsh braking, and harsh acceleration.
- Labeled the raw dataset using weighted CDF (Cumulative Distributive Functions) values of our extracted features.
- Trained a deep learning classifier on our labeled data to classify safe and unsafe drivers. Model achieved high accuracy with reduced computational overhead and overcome dataset dependency.

2 Background and Related Work

The increased real-time trajectory data available today allows learning complex driving patterns from the huge samples, unlike small data samples. Huge data samples have richer representations and high dimensions which present us with statistical and computational challenges. The trajectory data can be collected using navigation applications, most of which have built-in GPS sensor that records the real-time location of the users. GPS sensors can produce data that has a large scale of samples generated over real-time continuous datasets. Though these samples have their advantages, the data still have high noise, and extracting features or identifying patterns can be very challenging in such datasets.

Driver behavior analysis using GPS data in statistical models is quite expensive as the computation of high dimension data is not easy. Authors in Liu et al. (2015) suggest that Principal Component Analysis (PCA) will be a successful method for learning features based on GPS data assuming that the input is independent as a Gaussian distribution. Authors in Zhao et al. (2010) state that Kernel Principal Component Analysis (KPCA) showed a higher accuracy as compared to PCA. Neural Network is the most widely used approach in solving such problems. Convolutional Neural Network is considered as one of the state-of-the-art methods to model big data in the space domain. In recent studies, combining statistical and deep neural networks is a new trend in this field of study. Recently authors in Guo et al. (2018) developed a hybrid unsupervised deep learning model to study driving behavior and risk pattern. They approached the problem using an Autoencoder and Self-organized Maps (AESOM), to extract latent features and classify driving behavior. One of the approaches to solve this problem as proposed in Guo et al. (2018) is through using a combination of Autoencoder and Self-organized Maps (AESOM) for the extraction of concealed features and classification of driving behavior. Identification of harsh acceleration and deceleration or irregular maintenance of vehicle position, speeding were studied under two cases. They conducted experiments and concluded that through multi-layer autoencoders back propagation is efficient for non-linear and multi-model dimensionality reduction, whereas for a large GPS dataset, the reconstruction errors were minimal.

Previous studies have analyzed driving behavior with smartphone sensors, GPS devices, or video collection through camera/wearable devices. Geo-fencing service by IBM corporation (IBM 2019) analyzes speed, harsh acceleration, harsh breaking, harsh hard cornering with the help of GPS data of users and provides alerts to the car's dashboard screen. Another leading US insurance company called AllState (Allstate. Stay smart on the road) introduced a solution called Drivewise that rewards the driver for safe driving, which eventually promotes safe driving behavior. AllState uses driver's telematics data to analyze the behavior of the drivers based on which they reward the drivers. They also calculate a score to decide the insurance premium cost. Yu et al. (2017) proposes a system that detects abnormal driving behaviors using smartphone. The model uses SVM and Neural Network algorithms to detect the abnormality. Hard cornering and hard braking parameters are taken for behavior

Table 1 Existing methods

Approach	Algorithm	Dataset	Accuracy %
Features extraction from redundant driving behaviour data [2]	PCA and Deep Sparse Autoencoder	2-D artificial data sets	NA
Driver's mental fatigue classification, based on EEG [3]	KPCA and SVM	VR-based dynamic simulator	81.64
AESOM for feature extraction [4]	AESOM	Smartphone's GPS sensors (Shenzhen, China)	NA
Using smartphone sensor's data [7]	SVM and NN	Smartphone sensors data of 20 drivers (6 months)	95.36 (SVM), 96.88 (NN)

detection. TD Insurance (2019) a leading company in Canada collects and analyzes driving data, and assigns a driving score for each trip. It uses speed, hard braking, acceleration, and cornering to detect the behavior of the drivers. Though it collects a lot of parameters but uses only speed as the parameter to alert its drivers. Table 1 shows the main features of the existing methods.

3 Problem Statement

The driving behavior analysis problem is an identification and classification of safe and unsafe driving patterns of the drivers after observing their GPS trajectories. It is challenging to clean and process the raw dataset with the GPS trajectories into an appropriate set of features to maximize prediction accuracy. The dataset may contain noise, uneven time intervals, or inaccurate GPS locations. Therefore, to classify driving behavior it is necessary to clean the dataset for extraction of relevant features by the proposed model.

3.1 Assumptions

The proposed model has certain limitations as the dataset does not provide complete information about the state of the vehicle environment. To overcome certain limitations, we consider the below assumptions:

- The road condition is consistent throughout the trajectory.
- A particular vehicle is driven by only one person.
- The traffic condition is consistent throughout the trajectory.
- The maximum speed and class of the vehicles are the same.

- Population segment used for analysis is homogeneous, and majority of drivers are safe drivers.

4 Feature Extraction

Models and approaches as stated in Sect. 2 do not consider many parameters which are important for the precise prediction of driver behavior. Parameters like sensitive area speed violation (SASV) and turning angle on road are some of the most important parameters required for predicting driving behavior. In our method, these parameters are extracted from the GPS data and included for better prediction. The parameters are discussed in detail below.

Acceleration Events like harsh acceleration and harsh braking directly correlate to the acceleration of the vehicle. The effect of acceleration can determine and detect anomalous behavior of the driver. Acceleration can be defined as rate of change of velocity with respect to time. The value of acceleration can be calculated using the formulae given below.

$$\overline{a} = \frac{v - v_0}{t - t_0} = \frac{\Delta v}{\Delta t} \tag{1}$$

where $\overline{a}$ is the average acceleration, v is final velocity, v_0 is initial velocity, Δv is the difference between the final and initial velocity, and Δt is elapsed time which can be collected from the dataset.

If g_1, g_2 are two consecutive GPS points, then v is the velocity of GPS point g_2 and v_0 is the velocity at GPS point g_1; similarly t is the time stamp of GPS point g_2, and t_0 is the time stamp of GPS point g_1.

Angle Events like harsh turning are dependent on the change in direction with respect to speed. These events can be estimated by evaluating the change in angle of the direction of a vehicle where it is headed through its GPS coordinates. We can approximate the earth as a plane and use two-dimensional vector calculations.

Let g_1, g_2, g_3 and g_2, g_3, g_4 are the three consecutive GPS points, and $\vec{u}$ and $\vec{v}$ represent them respectively.

Then the angle between GPS points g_1 and g_2 is calculated using Eq. 2.

$$\theta = \cos^{-1}\left(\frac{\vec{u} \cdot \vec{v}}{\|\vec{u}\| \|\vec{v}\|}\right) \tag{2}$$

where $\vec{u}$ and $\vec{v}$ are two vectors derived from GPS coordinates, $\|\vec{u}\|$ and $\|\vec{v}\|$ are the magnitude of the velocity vectors, and θ is the angle between them as shown in Fig. 1. The equation represents finding angle between two vectors using dot product.

Sensitive Area Speed Violation (SASV) We propose a new way of marking the sensitive area around the vehicle trajectory. We collect and mark all the sensitive

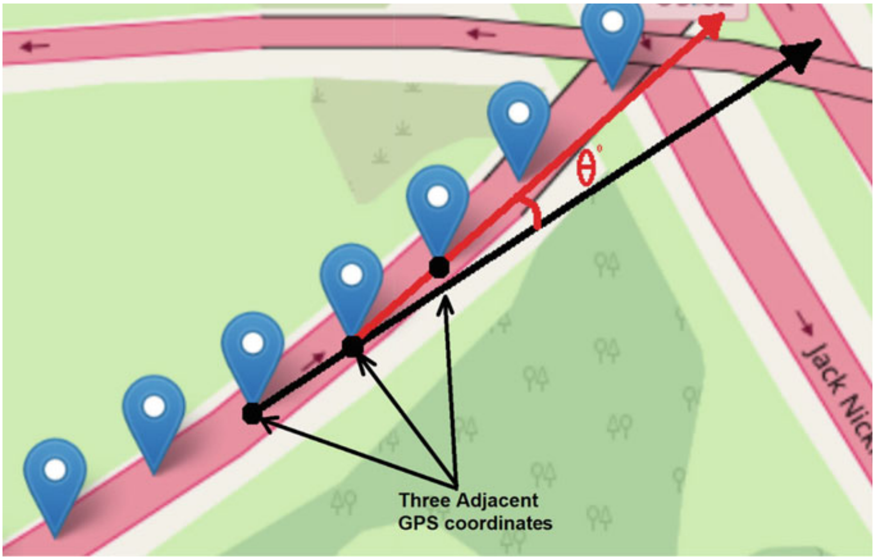

Fig. 1 Angle of direction change of the vehicle

locations such as schools, hospitals, and college GPS points from different sources on the Internet. We then take a circular area of 300 m around these marked locations as shown in Fig. 2. Then we calculate the distance between the vehicle trajectory GPS points and the sensitive marked GPS points. If the distance falls short of less than 300 m, we mark that vehicle's GPS point as sensitive point and then compare the speed of the vehicle at that GPS point. If the speed is more than the maximum allowed, we give the driver more penalty in points of speed violation.

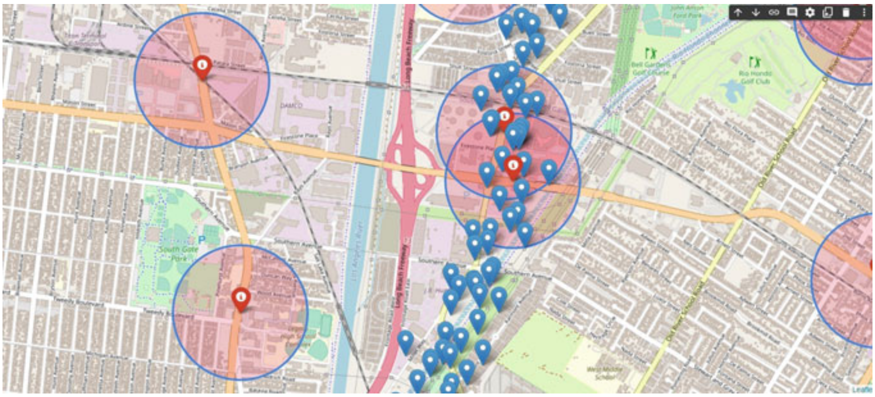

Fig. 2 Enlarged view of trajectory cascaded with sensitive zones: Red circles are sensitive areas, blue marking are recorded GPS points of trajectory

Fig. 3 Zonal division of vehicle trajectory

Calculating the distance between vehicle GPS trajectory points and GPS points of sensitive areas is computationally expensive as there are a large number of sensitive areas present in that region. Hence, we further modify our approach. Based on the vehicle trajectory, we divide a region into many zones (as shown in Fig. 3). For each GPS point in different zones, the distance is calculated only from those sensitive marked areas which fall under that particular zone. All other sensitive areas falling in other zones to which the GPS point does not belong are discarded. This approach reduces the computation time significantly.

We mark all the GPS points which are within the range of 300 m as 'sensitive area' which indicate that the point is inside one or more sensitive areas. Else, we mark it as 'normal area' to indicate the GPS point is not in the sensitive area. After marking the GPS points, we calculate the SASV feature based on speed limit of the specified area. The SASV feature is calculated by counting the occurrence of speed violation committed by the driver per kilometer.

5 Proposed Method

In this section, we propose a novel method to classify driving behavior by dividing the problem into two smaller problems. The first problem is to label the GPS trajectory data through feature extraction. To solve this problem we use statistical approaches on extracted features like harsh turn, harsh braking, and harsh acceleration to approximate a score based on the weighted sum of their CDF values. We then label the data with the help of these generated scores. The second problem is to use these labeled data to generate a model which can map the GPS trajectories directly to their classes. For this we a use publicly available state-of-the-art time-series classification model for the prediction of class labels based on only three features, viz. latitude, longitude, and speed.

5.1 Feature Extraction Model

We process the raw unlabeled dataset to remove noise and garbage values, then we extract features like acceleration, angle, and sensitive area explained in Sect. 4. The extracted features are then used to estimate the event type such as harsh acceleration, harsh braking, and harsh turning as shown in Fig. 4. Harsh acceleration and harsh braking are calculated using the acceleration feature, any sudden increase in acceleration is considered as harsh acceleration, and high retardation is considered as harsh braking. Harsh turning is calculated using the angle and speed feature; high speed and high angle change are marked as harsh turning. We calculate the score feature by estimating CDF (Mendels et al. 2018) of event features.

Score Feature To calculate the score of the driving behavior for each driver, we find its weighted sum of the CDF (area under density function of normalized event per kilometer) values of all the event features using Eq. 3.

$$\text{Score}_{s \in S(x)} = \sum_{\text{event}} \text{weight}_{\text{event}} P_{\text{event}}(X \leq x) \tag{3}$$

where x is events per kilometer, event is Event Type, $\text{weight}_{\text{event}}$ is weight of event, P_{event} is CDF value, and S is population segment. The Score feature specifies how safe a driver is compared to the general population. The higher the score value it is more likely that the driver has unsafe driving behavior. Weighted sum over CDF values on event features gave us a score to label the trajectories.

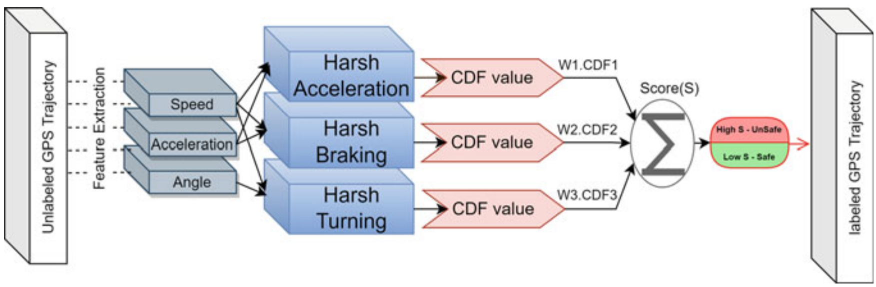

Fig. 4 Feature extraction model

5.2 Classification Model

Event feature is not present in every dataset, and large-scale calculation of these events is computationally expensive. To classify any raw GPS data which does not contains event features we trained a deep learning model MINIROCKET (Dempster et al. 2020) on our labeled dataset to predict class labels. MINIROCKET classifier is trained with only three features latitude, longitude, and speed. The trained model eliminates the need for extraction of features and delivers similar performance when compared to statistical labeling on the test data.

6 Experiment Results

In our experiment, we use a web service Google Colab, the machine configuration comes with 12 GB of RAM and 12 GB NVIDIA Tesla K80 GPU. We use DACT (Dataset of Annotated Car Trajectories) (Moosavi 2017) that contains trajectory data of 50 driver trips and a total of around 48,000 GPS points with a sampling rate of 1 s. Table 2 shows the sample description of the trajectories with their various features.

We analyze the driving behavior on two different parameters *Rule violation* and *Driving style*. To estimate the *Rule violation,* we only use the normalized value of SASV feature as shown in Table 3.

For labeling the *Driving style*, the dataset is processed with the help of the feature extraction model which combines CDF value of all event features for each driver and gives us a score relative to the general population which represents driving behavior. The CDF values and scores of few drivers are shown in Table 4. Higher scores are unsafe drivers while lower scores are safe drivers.

Using the score feature value, we assign a class label to the driver trajectory. We label higher scores as unsafe while lower scores as safe. We feed our labeled data with only three features latitude, longitude, and speed to MINIROCKET classifier and train for 100 epochs. We achieved 100% accuracy as shown in Fig. 5.

6.1 Discussion

The event feature of the dataset plays a very major role in the classification. We calculate the score feature for *Driving style* estimation using statistical methods on harsh events. We also produced a feature, 'Sensitive Area' which represents whether or not a GPS point is present within a certain range of schools and hospitals. We calculate a novel SASV feature based on the speed violation to estimate *Rule violation.* The *Driving style* and *Rule violation* play a very important role in determining driving behavior and contribute to road safety. We propose a model that classify *Driving style*

Table 2 Dataset sample

TripID	TimeStamp	Speed	Acceleration	Heading	HeadingChange	Latitude	Longitude	Annotation	SegmentType
T-1	Wed Jul 24 15:58:22 EDT 2013	29	0	84	0	39.980572	−82.953895	Null	Null
T-1	Wed Jul 24 15:58:23 EDT 2013	29	−0.28	84	0	39.980575	−82.953735	Null	Null
T-1	Wed Jul 24 15:58:24 EDT 2013	24	−1.94	84	0	39.980582	−82.953587	Null	Null
T-1	Wed Jul 24 15:58:25 EDT 2013	21	−1.39	84	0	39.980602	−82.953477	Null	Null
T-1	Wed Jul 24 15:58:26 EDT 2013	20	−0.56	90	6	39.980603	−82.953347	Null	Null
T-1	Wed Jul 24 15:58:27 EDT 2013	19	−0.28	90	0	39.9806	−82.95325	Null	Null
T-1	Wed Jul 24 15:58:28 EDT 2013	19	−0.28	90	0	39.9806	−82.95313	Segment	Slow-down

Table 3 Rule violation

Driver	Distance (km)	Occurance of violations	SASV	Rule violation
T-1	15.8364	85	5.3674	0.1959842
T-10	24.0076	470	19.577	0.7148382
T-11	12.5815	302	24.003	0.8764621
T-12	22.1294	326	14.732	0.5379062
T-13	15.9831	400	25.026	0.9138135
T-14	22.1398	432	19.512	0.7124734
T-15	20.7581	533	25.677	0.9375582
T-16	14.8016	225	15.201	0.5550505
T-17	20.7034	567	27.387	1
T-18	21.6624	324	14.957	0.5461313

Table 4 Drivers with their score and label

Driver	Calculated CDF values			Score (S)	Label
	Harsh acceleration	Harsh braking	Harsh turning		
T-18	0.9483	0.8541	0.3952	2.1977	Unsafe
T-1	0.6436	0.7281	0.846	2.2177	Unsafe
T-3	0.709	0.7607	0.78	2.2497	Unsafe
T-11	0.7729	0.6691	0.8291	2.2711	Unsafe
T-39	0.6474	0.7845	0.8663	2.2981	Unsafe
T-44	0.8038	0.8079	0.8311	2.4428	Unsafe
T-32	0.85	0.7974	0.9121	2.5595	Unsafe
T-5	0.9471	0.8783	0.7869	2.6123	Unsafe
T-16	0.932	0.8797	0.9313	2.743	Unsafe
T-35	0.9333	0.8743	0.9372	2.7447	Unsafe
T-43	0.0228	0.0974	0.3636	0.4837	Safe
T-36	0.1922	0.111	0.181	0.4842	Safe
T-37	0.1241	0.1742	0.3138	0.612	Safe

using only the GPS coordinates and speed of vehicle. The model can be used on any raw GPS data without calculating event features reducing computational expenses and complexity.

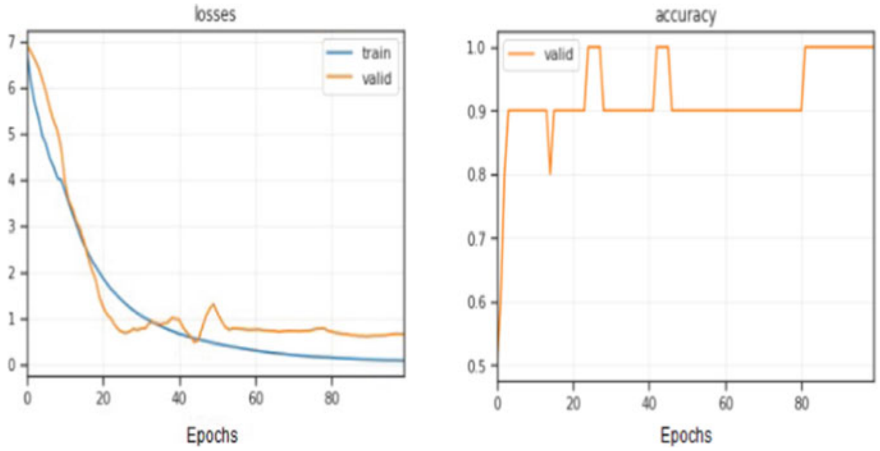

(a) Epoch vs Loss (b) Epoch vs Accuracy

Fig. 5 MINIROCKET training loss and test accuracy at 100 epochs

7 Conclusion

Availability of labeled event feature datasets is very limited. The MINIROCKET classifier gave accurate results after training over our labeled dataset. Generalizing our model to any other dataset which may not have event feature, the proposed model can directly predict *Driving style* class labels, eliminating the problem of dataset dependency. We also calculate driving behavior in terms of *Rule violation*, which estimates how many times a driver violates road safety rules. In this work we only considered speed violations based on trajectory information; however, there are other factors like lane change, vehicle overtaking, etc. In future, we look forward to work on these features and introduce new parameters for driving behavior analysis.

References

Allstate. Stay smart on the road. https://www.allstate.com/drive-wise.aspx

Dempster A, Schmidt DF, Webb GI (2020) MINIROCKET: a very fast (almost) deterministic transform for time series classification. CoRR, abs/2012.08791

Guo J, Liu Y, Zhang L, Wang Y (2018) Driving behaviour style study with a hybrid deep learning framework based on GPS data. Sustainability 10(7)

IBM: Analytics: real-world use of big data in insurance (2019). https://www.ibm.com/services/us/gbs/thoughtleadership/big-data-insurance/

Liu HL, Taniguchi T, Tanaka Y, Takenaka K, Bando T (2015) Essential feature extraction of driving behavior using a deep learning method. In: 2015 IEEE intelligent vehicles symposium (IV), pp 1054–1060

Mendels O, Bertental G, Kamara T (2018) Unsupervised driver safety estimation at scale, a collaboration with pointer telocation

Ministry of Road Transport and Highways (MORTH) (2019). Road accidents in India. https://morth.nic.in/road-accident-in-india. Last accessed 28-01-2022

Moosavi S (2017) DACT: Dataset of Annotated Car Trajectories

TDInsurance. TD MyAdvantage (2019). Myadvantage. https://www.tdinsurance.com/products-services/auto-car-insurance/my-advantage

Yu J, Chen Z, Zhu Y, Chen Y, Kong L, Li M (2017) Fine-grained abnormal driving behaviors detection and identification with smartphones. IEEE Trans Mob Comput 16(8):2198–2212

Zhao C, Zheng C, Zhao M, Liu J (2010) Classifying driving mental fatigue based on multivariate autoregressive models and kernel learning algorithms. In: 2010 3rd international conference on biomedical engineering and informatics, vol 6, pp 2330–2334

Blockchain-Based Marketplace for Farmers Using Perun Payment System

Sujit Sangram Sahoo, Mahesh Mohan Hosmane, and Vijay Kumar Chaurasiya

Abstract Agricultural sector requires a supply chain for the availability of different farm products throughout the usable premises to gain more profit. Many existing researches address the issue, but no one is comfortable with payment, authentication, and integrity. Centralized models are not flexible. Blockchain is used along with the supply chain by the current research works to decentralize the system where the scalability issue is not addressed. Our scheme is the first blockchain-based supply chain model, which can resolve the scalability issue to make the payment faster. We have used *Perun* virtual channel to resolve the issue. In faster payment in blockchain, *Perun* payment system is comparable with visa and master card also. Our scheme is user-friendly, as we use data integrity with the current date and time at sending and receiving. The proposed scheme is fully decentralized with scalable blockchain. Availability of the whole system publicly and to all the participant entities makes a public verifiable system. We have used smart contracts and analyzed the gas consumption in the result section. Performance of the resultant work shows that our scheme is cost-effective and feels like easy payment in the blockchain. The payment time in the proposed scheme is almost 99% less than the existing works. The application of the resultant work may consider for other current sectors.

Keywords Blockchain · Smart contracts · Supply chain · Virtual payment · Scalability issue

S. S. Sahoo (✉) · M. M. Hosmane · V. K. Chaurasiya
Indian Institute of Information Technology Allahabad, Prayagraj, India
e-mail: rsi2018005@iiita.ac.in

M. M. Hosmane
e-mail: mit2020054@iiita.ac.in

V. K. Chaurasiya
e-mail: vijayk@iiita.ac.in

J. K. Deka et al. (eds.), *Emerging Technology for Sustainable Development*, Lecture Notes in Electrical Engineering 1061,
https://doi.org/10.1007/978-981-99-4362-3_30

1 Introduction

Modernization in agriculture is required for sustainable growth. We need some updated technology to overcome the past problems at every step. Technology must ensure better performance and show the better result in current opportunities. The reasons behind this could be fear of adopting new techniques in agriculture, lack of awareness, and competitiveness. Again the storage warehouses (freezing storage), poorly handled marketing techniques, and a loose-ended agricultural supply chain is also responsible (Agarwal and Saxena 2018; Parwez 2013; Somashekhar et al. 2014). In our case, the technology ensures blockchain, which makes a better supply chain to increase efficiency and provide better performance. Supply chain may be any sector or industry and plays a crucial role in developing that sector. Trust between entities is the prime factor in any supply chain. Considering an agricultural supply chain in the Indian subcontinent, farmers/producers and customers/buyers are at a loss. Many mediators in the chain gain most of the profit through products. At the farmer's end, they sometimes do not get the minimum price for their products, and at the customer's side, they end up paying more the actual money to the product, which the intermediaries decide. This is how in some areas agriculture ends up being a loss-making sector.

To make it profitable, we propose a fully decentralized model for the agricultural sector and high-speed payment through blockchain. The resultant model is fully secure and does not depend on a single participant to fail. It is fully decentralized using smart contracts, and the farmers can sell the product to anyone without the help of a third party. The farmers will choose logistics for their product delivery. Similarly, the buyer is also profitable by getting the lower price directly from the farmer. All the above decentralization processes are possible with the help of smart contracts. The main issue lies in the payment process that is the scalability issue, which can be solved by Perun virtual payment channel (Dziembowski et al. 2019). Perun confirms 100,000 transactions per second while other decentralized models Bitcoin (7 transactions per second) and ethereum (30 transactions per second). Perun makes our system faster as compared to other channels and does wait for a long time to get payment, basically for farmers. The model is fully decentralized and makes sure the users are very fast and secure through blockchain. Figure 1 shows the overview of the scheme.

1.1 Centralized Versus Decentralized Supply Chain

The traceability in the agricultural supply chain is another important factor as the products are highly perishable. Hence, traceability in the supply chain plays a crucial factor in maintaining sustainability and safety in the chain (Galvez et al. 2018; George et al 2019). So, the supply chain can be classified into two broad categories based on the distribution of actors: Centralized Supply Chain (CSC) and Decentralized Supply

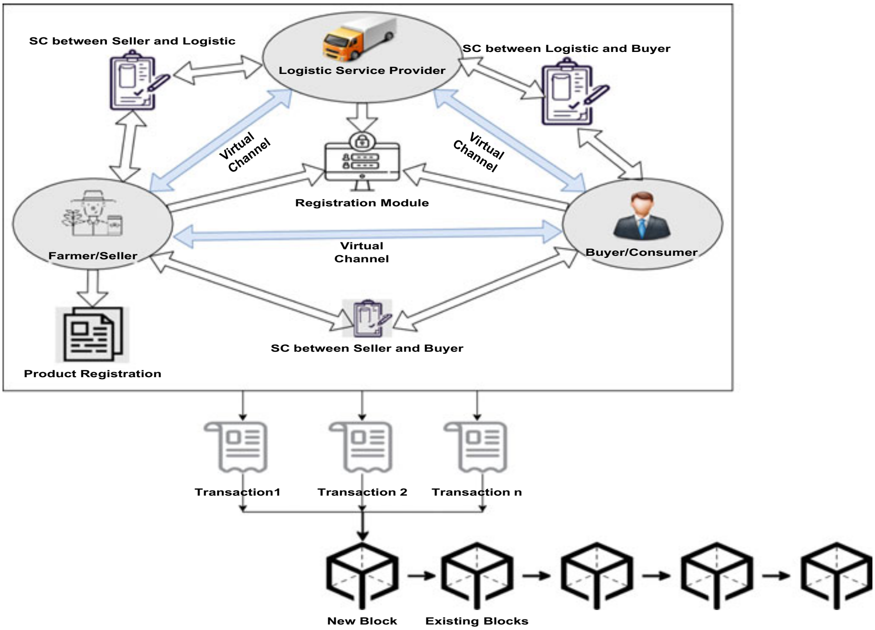

Fig. 1 Overview of proposed architecture (sc-Smart Contract)

Chain (DSC). The main aim of CSC is to maximize the profit of the supply chain, whereas, in DSC, each actor of the supply chain tries to maximize the gain of the individual (Ali et al 2018). The main disadvantage of such a model is traceability. The actors of the chain cannot verify the actions of other actors. Hence as discussed, the proposed supply chain model can be active throughout the product life-cycle and can verify. The issue of traceability and trust from the traditional supply chain is reduced in the current model.

1.2 Role of Blockchain in Supply Chain

Blockchain provides a decentralized system governed by no authority, and the anonymity of the participating entities is ensured. Technology that was designed for cryptocurrency, in later stages, extended to many sectors such as health, supply chain (Perboli et al. 2018), legal, etc. (Table 1) This was possible due to introducing a new concept known as smart contracts. Blockchain can play a significant role in uprising the true potential of a supply chain management through the inherent characteristics, such as decentralization, information being secured cryptographically, smart contracts, immutability, etc. In the traditional supply chain, this was achieved through IoT-based system, which was centralized. A centralized system can be a single point of failure and can lead to the non-availability of data at certain

Table 1 Pros and cons of centralized and decentralized supply chain

	Pros	Cons
Centralized Supply chain	Provides standardization throughout the hierarchy Centralized decisions Provides hierarchy in the system	Provides less flexibility Lack of trust in the process Delay in decision making
Decentralized supply chain	Provides decision maker equal chances Highly flexible Provides trust in the process	Impacts standardization Higher operations cost Low authoritative command

Table 2 Role of blockchain in our system

Advantages	Details
Decentralization	No central party involved in the transaction of the data or payment
Immutability	The data once lodged onto the blockchain is immutable to changes
Transparency	Every transaction is verified by consensus protocol and then committed into a block
Smart Contracts	Provides a way of implementing contracts which acts upon events
Disintermediation	Provides interconnected transaction management
Efficiency	Increases the efficiency of process without the intervention of any third party
Anonymity	The actors in the network are identified by a unique key and the transactions are anonymous
Trustless	There is no requirement of trust between the actors to make transactions
Scalability	Increase throughput of the payment

times (Khan and Salah 2018). The decentralization scheme resolves many existing issues in the centralized model. We consider decentralization in our strategy, and blockchain has decentralized our method. The products' sellers, buyers, and logistics work publicly. Any particular participant's dis-involvement cannot hamper our system. The scalability, efficiency, smart contract, and decentralization are the essential parameters for our proposed approach. Table 2 shows the role of blockchain in our system.

1.3 Use of Scalable Blockchain

The main issue persistent in the blockchain is scalability. All the blockchain technologies proposed are not faster than visa and master card transactions. They require an extended time to confirm a transaction. Bitcoin lightning network (BLN) is the first off-chain payment that resolves the particular issue (Poon and Dryja 2016). BLN has some problems like (i) the transaction moves through all the participants

Fig. 2 Perun architecture

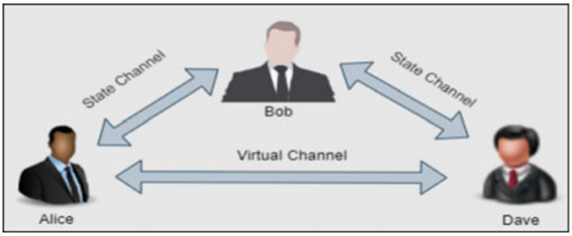

in the channel. (ii) Flood and loot attacks are possible in BLN. To overcome the issues of BLN, Dziembowski et al. 2019 have proposed a Perun virtual channel for faster payment in blockchain. The Perun channel is based on the ethereum network. Transactions on the Perun network use smart contracts. Our proposed work has used the Perun virtual channel to make faster payment in the whole model.

1.4 Virtual Channels

The on-chain transactions in the blockchain environment have inherent scalability issues, and the on-chain transaction fees may observe a high surge in peak times. This makes the micro-payments that are the usual day-to-day transaction not so attractive in the on-chain transaction mechanism, as sometimes the fee concerning the micropayment can be higher than that of the actual payment. So there was a need to build a layer-two solution that can be built on top of the existing blockchain, which can handle the off-chain transactions and support micro-payments with minimal fees, thus addressing the blockchain's scalability problem. Figure 2 shows the off-chain architecture of the Perun virtual channel. This mentioned scenario is for only three parties, which can be extended to many parties, by implementing the concept of virtual channels recursively over the state channels or virtual channels. Figure 2 show that Alice and Bob have an existing state channel between them and Bob and Dave have a state channel between them. Alice and Dave can have a virtual channel using the current state channel. Here Bob will be the conflict resolving authority, through which the transactions are routed. Bob is involved only in the creation and deletion of the virtual channel.

1.5 Smart Contract

A smart contract is an autonomous function that creates all the agreements between participant entities. It is the same as regular contracts, but the main advantage is automatic execution after its deadline. The participants create contracts anytime for their requirements in the proposed system. All the participants must follow the system's rules and make their contracts public verifiable. The miners present in the blockchain will mine after the contract period is over and automatically added to the blockchain ledger. It provides autonomy, trust, speed, and accuracy to the system by making it public verifiable.

2 Literature Survey

This section provides the literature survey on blockchain and its use case in the supply chain. As discussed in the paper by Saurabh and Dey (2021) gives the main idea of the agricultural supply chain considering the use case of the grape-vineyard supply chain. The core idea is to integrate the blockchain with IoT (using RFID), providing traceability and transparency. It gives the theoretical and conceptual framework based on the prior conjoint analysis. This paper provides a brief architecture of the supply chain entities and a procedure for entering into processes. The discussion has not cleared the Blockchain and the payment mechanism.

Feng et al. (2020) has discussed the traceability in the food supply chain using blockchain. Salah et al. (2019) considers the Soybean supply chain management, starting from seed procurement. The paper also describes the entity-relationship model of the system. The authors of the Casado-Vara et al. (2018) discuss the circular economy in the supply chain with blockchain as the core technology. They provide a MAS architecture considering the actors involved in the chain and its respective roles. Shahid et al. (2020) give an insight into the end-to-end approach of the supply chain in the agri-food industry. It discusses the entities present in the supply chain and mainly concentrates on food traceability with a review system for every entity present in the chain. It proposes storing the hash values of the blocks in the chain rather than storing the complete transaction details. They discussed the IPFS for storing the hashes of the transaction and recovering when needed and the security analysis conducted on their system. The model is developed in an Ethereum network with solidity for writing smart contracts.

Fu et al. (2020) have discussed the case study of using a supply chain in the Chinese agricultural market with IoT coupled to build a trusted network. They also discuss the drivers for the supply chain using blockchain. Saberi et al. (2019) shows how blockchain is used to build a sustainable supply chain management system considering every aspect of the chain in most of the domains. The paper describes how blockchain technology works in reality and can be integrated into the global supply chain. The document classifies the barriers to the implementation as Inter-Organization, Intra, System-related, and External barriers. A paper by Abeyratne and Monfared (2016) discusses the effect of blockchain in supply chain management. This paper also discusses the basics of blockchain technology and gives an example of the life-cycle (supply chain) of a cardboard box right from resourcing the raw materials to the waste management system. A paper by Zheng et al. (2018) provides an insight into the opportunities and challenges that are present while implementing technology. They briefly explore the architecture of blockchain, the security algorithm in it, the consensus algorithm, and the applications related to blockchain. The paper also discusses the main issues in blockchain, such as scalability, privacy, and big data analytics.

In Agarwal and Saxena (2018), the author has discussed a study on supply chain management in Indian agriculture. They briefly discuss the challenges in the supply chain management system by classifying them into challenges posed by lack of knowledge in ICT and long supply chain networks, which is lack of coordination in actors of the chain leading to wastage/loss of products. Mukherjee et al. (2021) identifies the aspects of benefits of implementing blockchain in the traditional agricultural supply chain. The benefits mentioned here are data immutability, transparency, traceability, etc. The critical point is how a sustainable agricultural supply chain be built by incorporating above-mentioned benefits. Another paper, Lindman et al. (2017), provides an insight into the blockchain technology in the digital payments system. They have discussed the organization and design issues and have posed some research questions regarding the same. Korpela et al. (2017) in their paper discuss the integration of blockchain technology to supply chain to form a new Digital Supply Chain (DSC). They provide a statistical analysis of features of blockchain such as smart contracts, data immutability in the supply chain, and a requirements gap in the current digital supply chain. They also mention cloud computing of blockchain data to accelerate the computation. We cannot find any research strategy that can be fully decentralize and scalable.

3 Proposed Methodology

This project aims to build an effective agricultural supply chain using blockchain technology. As discussed earlier, any supply chain is inefficient with decentralization in it. In a traditional supply chain, the third party or mediators can be a probable suspect for the absence of trust. We develop a marketplace for farmers without any third-party/mediators, wherein any farmer can sell their products directly to consumers/procurers. Once the deal is accepted, a logistic provider can ship the products from farmers to buyers, thereby providing a direct linkage between procurer and farmer. It also helps in increasing the traceability in the system. The process of authentication will happen by using cryptographic hash matching. We have used *Perun* virtual payment system for faster payment and resolving the scalability issue of the different existing research work. Moreover, the payment will complete only after the hash match. Overview of the detailed proposed architecture is given in Fig. 1. Our proposed solution has mainly three entities: (i) Farmer/Producer, (ii) Logistics Provider, and (iii) Procurer/Buyer.

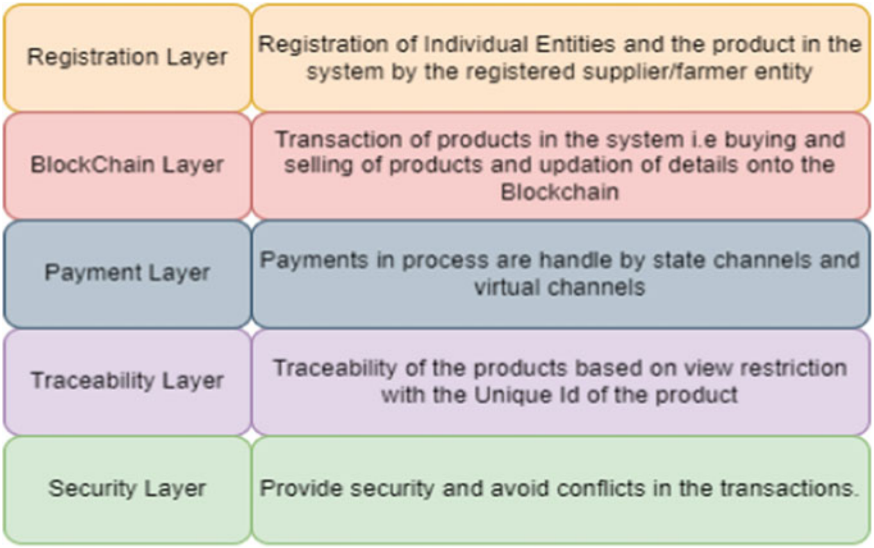

Fig. 3 Layered structure of the proposed system

3.1 Layered Structure of Our System

Our proposed solution has been divided into five layers. The layers are Registration Layer, Blockchain Layer, Payment Layer, Traceability Layer, and Security Layer. The working prospective of different layers has discussed along with the respective algorithms. Figure 3 shows the layered approach of our system.

3.2 Registration Layer

This layer is responsible for successful registration of all individual entities participate in the scheme. There are two algorithms are working inside the layer; first one is entity registration and another product registration algorithm. Our working procedure completely depends on ethereum. So that every participants must carry one ethereum wallet to complete their registration process. Algorithm 1 shows the detailed procedure of the entity registration.

Algorithm 1 Entity registration module

```
if consumerMapping[msg.sender] = true then
    Multiple registration is not allowed
else
    consumerMapping[msg.sender] = true;
    Consumer Registered Succesfully
end if
```

Once registration of entities is completed, the entity will be an active member of the network, where that can transact. In this case, the farmer can register the product on the network that can be accessible by all other participants. When the product is being registered a unique ID will be given to each product. This helps in the traceability of the product. The product registration algorithm is given in Algorithm 2.

Algorithm 2 Product registration module

```
Require: Input: Product Id,Product Name,Product Amt
unique = address(bytes20(keccak256(abi.encodePacked(msg.sender,timestamp))))
packageMapping[unique].uniqueId = unique;
packageMapping[unique].uid = true;
packageMapping[unique].itemNo = itemno;
packageMapping[unique].itemName = itemname;
packageMapping[unique].orderStatus = 0;
packageMapping[unique].producer = msg.sender;
packageMapping[unique].amt = amt;
packageMapping[unique].time = now
producerStockListMap[msg.sender].stockId.push(unique);
updateCustomerStockList(unique);
return(Product Registered Successfully);
```

3.3 Blockchain Layer

When the product is registered, it will be published in the network and intended recipients will be the buyers/procurers who are registered in the network. Buyers will be able to view the product details such as product name, produced time, product source, producer details (but it will be a cryptographic address) and the product amount. If there is a requirement of that product, then buyer will order the item and the order status of that product will be changed. The amount with respect that product will be transferred to the farmer at the same moment.

Once the product is purchased by an buyer, this information will be published in the network and the intended recipients will be the logistics provider. A successfully registered logistics provider will be able to view the accepted order of all products; however, not all details will be viewed by the logistic provider such as deal amount, etc. The logistics provider based on the source and destination available in the product details can accept the shipping orders and ship the products. The seller chooses the logistic person from the list of availability; otherwise the process will select the designated one by their reputation.

Algorithm 3 Product ordering module

Require: Input: Product UniqueId
1: **if** *consumerMapping*[*msg.sender*] = true **then**
2: packageMapping[unique].orderStatus = 1
3: packageMapping[unique].customer = msg.sender
4: packageMapping[unique].time = now
5: updateLogisticrStockList(uniqueId)
6: **else**
7: return Not a registered Consumer
8: **end if**

3.4 Payment Layer

The payment in the network is considered to be held off-chain. Perun channel network based on ethereum is considered for the payment. The payee can choose at least one payment channel for payment; otherwise the Perun channel routes the payment procedure to the active one.

Consider a situation is given in Fig. 4 where Alice needs to make the payment to Dave, but Alice doesn't have direct payment channel with Dave. But the intermediaries have channel with neighbors. This network of channels can be used to route the existing channel by creating a virtual channel between them and also create the virtual channel recursively. The payee can use the balance of the existing payment channel in the newly created virtual channel and create multiple virtual channels. In Fig. 4, we can see that the virtual channel between Alice and Dave has the total balance of 150 taken from their respective state channels (the figure is represented logically). The detailed working procedure of the payment module is discussed in Algorithm 4.

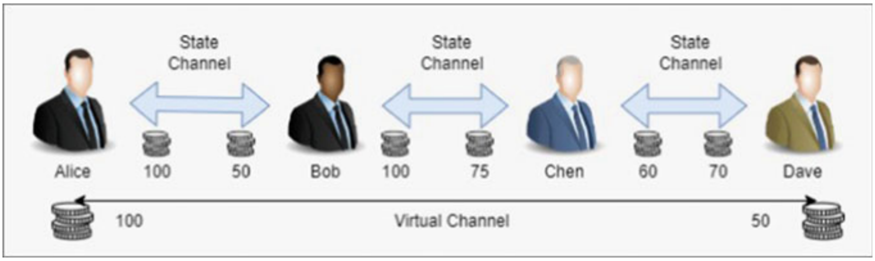

Fig. 4 Off-chain payment network

Algorithm 4 Payment module

Require: Input: Product UniqueId
if *consumerMapping*[*msg.sender*] = true **then**
  if *PaymentMethod* = On-Chain **then**
    address(packageMapping[unique].producer).transfer(packageMapping[unique].amt);
    updateLogisticrStockList(uniqueId)
  else
If direct channel available transfer the amount else initiate the process of creation virtual channels
  end if
else
  return Not a registered Consumer
end if

3.5 *Traceability Layer*

Algorithm 5 Tracking order

Require: Input: Product UniqueId
if *consumerMapping*[*msg.sender*] = true **then**
  Display Order Details
  Display order Status
  Display payment Status
  Display Delivery and Supply Time
  Display Comments
else
  return Not a registered Consumer
end if

The Algorithm 5 shows the traceability concept in the supply chain. There is a view restriction based on the actors of the chain. The Consumer and Buyer can have all the data related to product visible, but the logistic person cannot have the details of the contract. They show the status of their product at any time in the system. This layer is for the user convenient.

3.6 Security Layer

The Proof of Supply and Proof of Product Acceptance between the supplier and the logistic are ensured by depositing tokens by the individual entities into the product data in the chain. The token is hash value of entity id, product id and timestamp. The value associated with the product can be used to verify Proof of Supply and Product acceptance. The algorithm for the same is shown below. The same procedure can be used for the logistic entity also.

Algorithm 6 Proof of supply

Require: Input: Product Id,Product Name
1: supplierToken = address(bytes20(keccak256(abi.encodePacked
2: (msg.sender,timestamp,ProductId,ProductName))));
3: packageMapping[unique].uniqueId = supplierToken;
4: return(Product Supplied to Logistic Successfully);

Algorithm 7 Proof of Authentication

Require: Input: Product UniqueId
1: verification Token = address(bytes20(sha256(abi.encodePacked
2: (msg.sender,timestamp,ProductId,ProductName))));
3: **if** *verificationToken* = *storedtoken* **then**
4: Proof Accepted
5: **else**
6: Decline the proof
7: **end if**

Finally, when the logistics provider ships the product from the farmer's site to the customer's site, the customer verifies the product and accepts the product into their product list. When the product is accepted by the customer, a certain amount is transferred to the logistics provider from the customer's account as fixed by the logistics provider. The concept of Proof of Supply and Proof of Product Acceptance is also used here, only after which the amount of shipping is transferred to the Logistic from consumers account. The algorithm for the same is given in Algorithm 4.

The authentication of the acceptance as well as sending of the product has been generalized. Authentication scheme uses keccak256 as per the ethereum network. The purpose of the convenience, we have picked the current date and time at the time of product sending. The data integrity is provided by keccak256 also.

4 Result and Analysis

The implementation of the above-mentioned methodology was conducted to analyze. The configuration of the system is i5-8th gen cpu @clock speed 2.4 GHz, 8Gb RAM and a Windows 10-Home system. Truffle suite was considered to enable Ethereum Virtual Machine and develop DApp. For the visualization of front-end, a light-weight website was developed hosted locally enabling the connection between local blockchain Ganache using web3.js libraries. Ganache provides a local blockchain with pre-defined accounts each consisting of private-key and fixed cryptocurrency (Ether).

The smart contract is developed using Solidity language in Remix IDE, which helps in developing and testing the smart contracts, and truffle suite is used to deploy the contracts on the emulated Ethereum network. A metamask extension is setup in the web browser to connect with the local blockchain which is listening on certain port. Metamask extension is also used to sign the transaction that will be appended in a block, in the locally deployed ethereum network. The pre-defined accounts provide by Ganache is imported on to metamask, to create multiple users

Figure 5 shows the total gas consumed with the certain actions performed. The contract deployment cost is higher when compared to other tasks. The product registration cost is much higher compared to other functionality as lot of computation is involved in there. The Proof of Supply and Proof of Acceptance algorithm as discussed above are implemented to remove the discrepancy that are occurred during transaction. The producer is considered as a legitimate user, and each entity is identified by their respective Ethereum Address. Table 3 shows the gas consumption of different modules of our proposed work. Default gas price = 20 Gwei in ganache. 1 Gwei = 0.000000001 ether. User Registration (UR), Product Registration (PR), Product Ordering (PO), Logistic Acceptance (LA), Proof of Supply (PS), Proof of Acceptance (PA).

The proposed scheme is better than all other existing schemes in view of scalability issue and easy authentication. Degree of decentralization is higher, and the payment time is very less. Perun virtual channel is very fast for payment and comparable with visa and master card transaction systems. Authentication and data integrity use current date and time to verify the particular product and the product id verified from blockchain. The cost of our system is very low as compared with existing schemes.

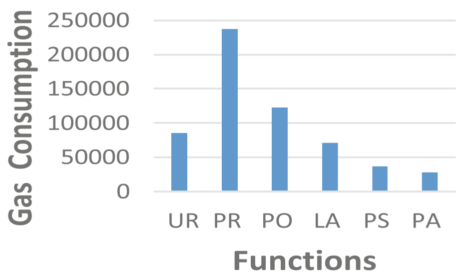

Fig. 5 Functions versus gas consumed

Table 3 Gas consumed in smart contracts

Functions	Gas consumed	Cost in ether
UR	85,360	0.0008536
PR	237,852	0.00237852
PO	122,585	0.00122585
LA	70,758	0.00070758
PS	36,404	0.00036404
PA	28,114	0.00028114

5 Conclusion

Our resultant scheme is a scalable solution for the supply chain. The proposed model is fully decentralized and conveniently used for the agricultural sector. This project provides a methodology for replacing the traditional agricultural supply chain with a blockchain-enabled smart supply chain, thus establishing direct linkage between producer and consumer, thereby eliminating the factors associated with the third party. This model can also handle the issues of traceability and transparency. The key benefits of blockchain technology, such as data immutability, smart contracts, etc., for the agricultural supply chain are also managed efficiently and effectively. Our proposed system is cost-effective and requires less time for payment. The resultant work achieves faster payment authentication, and data integrity is also user-friendly. The performance is better that shows the effectiveness of our scheme.

References

Abeyratne SA, Monfared RP (2016) Blockchain ready manufacturing supply chain using distributed ledger. Int J Res Eng Technol 5.9:1–10

Agarwal NR, Saxena A (2018) Supply chain management of Indian agriculture industry: an exploratory study. Global J Enterprise Inform Syst 10.1:45–54

Ali SM et al (2018) Examining price and service competition among retailers in a supply chain under potential demand disruption. J Retail Consum Serv 40:40–47

Casado-Vara R et al (2018) How blockchain improves the supply chain: case study alimentary supply chain. Proc Comput Sci 134:393–398

Dziembowski S et al (2019) Perun: virtual payment hubs over cryptocurrencies. In: 2019 IEEE symposium on security and privacy (SP). IEEE, pp 106–123

Feng H et al (2020) Applying blockchain technology to improve agri-food traceability: a review of development methods, benefits and challenges. J Clean Prod 260:121031

Fu H et al (2020) Blockchain-based agri-food supply chain management: case study in China. Int Food Agribus Manage Rev 23:667–679

Galvez JF, Mejuto JC, Simal-Gandara J (2018) Future challenges on the use of blockchain for food traceability analysis. TrAC Trends Anal Chem 107:222–232

George RV et al (2019) Food quality traceability prototype for restaurants using blockchain and food quality data index. J Cleaner Prod 240:118021

Khan MA, Salah K (2018) IoT security: review, blockchain solutions, and open challenges. Future Gen Comput Syst 82:395–411
Korpela K, Hallikas J, Dahlberg T (2017) Digital supply chain transformation toward blockchain integration. In: Proceedings of the 50th Hawaii international conference on system sciences
Lindman J, Tuunainen VK, Rossi M (2017) Opportunities and risks of blockchain technologies—a research agenda
Mukherjee AA et al (2021) Application of blockchain technology for sustainability development in agricultural supply chain: justification framework. Oper Manage Res 15:1–16
Parwez S (2013) Food supply chain management in Indian agriculture: issues, opportunities and further research
Perboli G, Musso S, Rosano M (2018) Blockchain in logistics and supply chain: a lean approach for designing real-world use cases. IEEE Access 6:62018–62028
Poon J, Dryja T (2016) The bitcoin lightning network: scalable off-chain instant payments
Saberi S et al (2019) Blockchain technology and its relationships to sustainable supply chain management. Int J Prod Res 57.7:2117–2135
Salah K et al (2019) Blockchain-based soybean traceability in agricultural supply chain. IEEE Access 7:73295–73305
Saurabh S, Dey K (2021) Blockchain technology adoption, architecture, and sustainable agri-food supply chains. J Cleaner Prod 284:124731
Shahid A et al (2020) Blockchain-based agri-food supply chain: a complete solution. IEEE Access 8:69230–69243
Somashekhar IC, Raju JK, Patil H (2014) Agriculture supply chain management: a scenario in India. Res J Social Sci Manage 4.07:89–99
Zheng Z et al (2018) Blockchain challenges and opportunities: a survey. Int J Web Grid Serv 14.4:352–375

Sentiment Analysis on COVID-19 Tweets: Machine Learning Approach

Janrhoni M. Kikon and Rubul Kumar Bania

Abstract Analysis of tweets accompanying a catastrophic situation is a crucial chore. Sentiment analysis is the field of study to analyze the varied opinions shared by diverse users on social networking platforms on various social phenomena. In this paper, an analysis of the sentiments on thousands of tweets collected from Kaggle on the ongoing pandemic of COVID-19 is carried out. Data preprocessing technique followed by TF-IDF approach for uni-gram and bi-gram features is extracted. Three different supervised machine learning classifiers such as Bernoulli's Naïve Bayes (BNB), Gaussian Naïve Bayes (GNB), and Random Forest (RF) models are applied. Experimental results suggest that on both the feature extraction models, i.e., uni-gram and bi-gram feature extraction techniques, RF classifier has performed better than the other two models. With 70%-30% train–test set, RF has achieved an accuracy of 90.06% to classify the tweets into *negative*, *neutral*, and *positive* classes.

Keywords COVID-19 · Sentiment analysis · Twitter · TF-IDF · Random Forest

1 Introduction

In a world governed by the internet, social media or social networking platforms such as Twitter, Facebook, Instagram, etc. have become an intrinsic part of our day-to-day life. We use these platforms to post real-time topics about various issues and thus it becomes a good data repository. We can easily put our opinions and sentiments on diverse topics and issues. Among the various microblogging websites, Twitter is the most widely used social media platform to tweet about daily worldwide activities. For instance, the worldwide known disease, Corona which was declared as pandemic by WHO on 13th March 2020. It is an infectious disease caused by the

J. M. Kikon · R. K. Bania (✉)
Department of Computer Application, North-Eastern Hill University, Tura Campus, Tura, Meghalaya 794002, India
e-mail: rubul.bania@nehu.ac.in

J. K. Deka et al. (eds.), *Emerging Technology for Sustainable Development*, Lecture Notes in Electrical Engineering 1061,
https://doi.org/10.1007/978-981-99-4362-3_31

SARS-CoV-2 virus. The number of corona cases according to world meter is estimated to be over 414,473,899 confirmed cases and 5,847,191 deaths as of February 15, 2022. The entire world started engaging themselves on different social media platforms to communicate, share and express their opinions and views regarding the various issues relating to the ongoing global pandemic. Taking the advantage of the abundance of data available on Twitter, sentiment analysis can be performed on the tweets relating to COVID-19. Sentiment analysis or opinion mining is the process of determining a chunk of text as *positive*, *negative*, or *neutral* (Machuca et al. 2020; Bania 2020). These sentiments play a vital role as it helps in determining an overview of public opinion about a certain topic. By using sentimental analysis techniques, we can interpret the sentiments or emotions of others and classify them into different categories such as *negative*, *neutral*, and *positive* which may help an organization to know people's emotions and act accordingly (Machuca et al. 2020; Bania 2020). *Positive* sentiment means that it has a positive word or sentence attached to a particular text which indicates enthusiasm, optimism, forward-looking, excitement, etc. *Negative* sentiment implies the negative opinion of a person in a particular text which indicates anger, frustration, gloomy, unenthusiastic, etc. A word or sentence in a particular text is considered as a *neutral* sentiment when the opinion of a person is neither positive nor negative. It means that the person is unbiased or doesn't express any particular feeling or opinion. This analysis depends on its expected outcomes, e.g., analyzing the text depending on its polarity and emotions, feedbacks about a particular feature, as well as analyzing the text in different languages. Incorporating the recent techniques of natural language processing (NLP) and machine learning, suitable computational models can be prepared to analyze the sentiments of individuals toward the COVID-19 pandemic. In the literature, several works can be found which have attempted to prepare such models (Machuca et al. 2020; Bania 2020; Abdulaziz et al. 2021; Alrazaq et al. 2020). Moreover, government can make use of this information in policymaking as they will be able to know how people are reacting to this new strain, what all challenges they are facing such as food scarcity, panic attacks, etc. Various profit organizations can also make a profit by analyzing various sentiments as in some of the tweet's users talk about the scarcity of masks, hand sanitizers, etc.

By motivating with above-mentioned facts, this study is undertaken with the following objectives:

i. To perform Twitter sentiment analysis and sentiment prediction on COVID-19 related tweets.
ii. To collect a large amount of data i.e., tweets for a period of time (Dataset July 25, 2020 to August 29, 2020).
iii. To categorize the text into *positive*, *neutral*, and *negative* classes.
iv. To extract features from the tweets using Term Frequency-Inverse Document Frequency (TF-IDF) and predict the tweets using supervised machine learning classifier models.

The remaining portion of this paper is organized as follows. In Sect. 2, some of the works related to this study is given. Section 3 describes the overall structure of the methodology. The experimental setup and evaluations are highlighted in Sect. 4. The paper is winded up with concluding remarks with future perspectives in Sect. 5.

2 Related Work

Majority of the research studies that cover Twitter sentiment analysis are inclined toward the machine learning algorithms. Besides the COVID-19 pandemic in recent years other epidemic/pandemic situations due to the Swine flu (2009), Ebola (2014–2017), Zika (2015 to present day) viruses have spread in different countries (Alrazaq et al. 2020). Machuca et al. (2020) have prepared a model to classify English tweets during the pandemic COVID-19 in 2020. The tweets were classified as positive or negative by applying the logistic regression algorithm. The achieved classification accuracy of the model was 78.5%. Similarly, in the year in 2020, Alrazaqet et al. (2020) have analyzed English language tweets from February 2, 2020, to March 15, 2020. They have analyzed the collected tweets using word frequencies of single (uni-grams) and double words (bi-grams) models. That study has identified 12 topics, which were grouped into four main themes: origin of the virus; its sources; its impact on people, countries, and the economy; and ways of mitigating the risk of infection. Aslam et al. (2020) have conducted a study on sentiments and emotions evoked by news headlines of COVID-19 outbreak. They extracted and classified sentiments and emotions from 141,208 headlines of global English news sources regarding the COVID-19. The headlines were classified into positive, negative and neutral sentiments after the calculation of text unbounded polarity at the sentence level score and incorporating the valence shifters. In addition, the National Research Council Canada (NRC) Word- Emotion Lexicon was used to calculate the presence of eight emotions at their emotional weight. The results reveal that the news headlines had high emotional scores with a negative polarity.

3 Methodology

The pipeline of the methodology, which is followed in this work, is shown as a block diagram in Fig. 1. It is divided into three processes, viz. data collection, data pre-processing and data analysis. The natural language processing toolkit (NLTK), which is a Python-based platform, is extensively used in this work. The data analysis phase is derived into two parts. The first part of the analytic includes sentiment analysis of the textual component of the Twitter data. Tweets are assigned sentiment scores of polarities by using different Python libraries such as TextBlob. The second part of analytic includes the feature extraction using TF-IDF (Bania 2020) technique for further prediction with supervised learning algorithms. The detailed steps of the phases of the methodology are shown in Fig. 1.

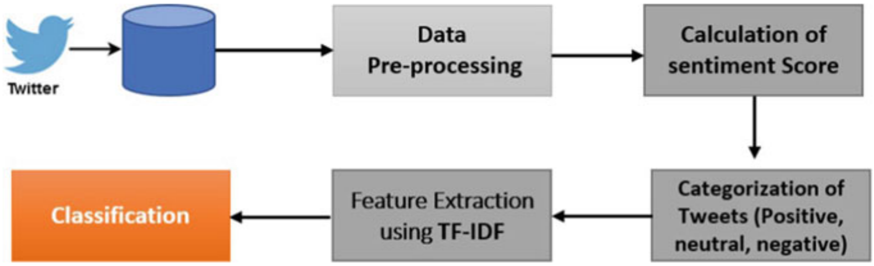

Fig. 1 Block diagram of the methodology

3.1 Data Collection and Preprocessing

We have collected the COVID-19 -related tweeter dataset from Kaggle data repository website (www.kaggle.com/datasets/gpreda/covid19-tweets). The dataset has the tweets from 25/07/2020 to 29/08/2020. There are a total 179,104 tweets available in the dataset, and sample of the data is shown in Fig. 2. Before applying the data directly to the predication models, data pre-processing task is very important as there are lots of noises present in the dataset.

In order to perform the data pre-processing task, initially non-English tweets are identified using the language field in the tweet metadata and removed them to avoid further analysis. Thereafter, we have removed the special characters (#, @), emojis, URLs, different non-printable characters from the tweets. Next, the text data needs to be converted into lower case as it is important to normalize the case of our words so that every word is in the same case and the computer doesn't process the same word as two different tokens. The stop words are also removed. Stop words are those words

	user_location	date	text
0	astroworld	2020-07-25 12:27:21	If I smelled the scent of hand sanitizers toda...
1	New York, NY	2020-07-25 12:27:17	Hey @Yankees @YankeesPR and @MLB - wouldn't it...
2	Pewee Valley, KY	2020-07-25 12:27:14	@diane3443 @wdunlap @realDonaldTrump Trump nev...
3	Stuck in the Middle	2020-07-25 12:27:10	@brookbanktv The one gift #COVID19 has give me...
4	Jammu and Kashmir	2020-07-25 12:27:08	25 July : Media Bulletin on Novel #CoronaVirus...
...	...	...	...
179100	Newton, NJ	2020-08-29 19:44:27	Wallkill school nurse adds COVID-19 monitoring...
179101	Newton, NJ	2020-08-29 19:44:27	Wallkill school nurse adds COVID-19 monitoring...
179102	T.O.	2020-08-29 19:44:23	we have reached 25mil cases of #covid19, world...
179103	Ilorin, Nigeria	2020-08-29 19:44:21	Thanks @IamOhmai for nominating me for the @WH...
179104	Ontario	2020-08-29 19:44:16	2020! The year of insanity! Lol! #COVID19 http...

Fig. 2 Sample of the dataset

that do not contribute to the deeper meaning of the phrase. Thereafter, stemming and lemmatization are both techniques used to normalize text to its core root. After performing the overall data pre-processing task, the total number of tweets which are available in the dataset is 142,334.

3.2 Tweet Categorization and Feature Extraction

After the preprocessing task, using the NLTK and TextBlob libraries the polarity of each tweet is calculated from the CSV files (Chakraborty et al. 2020; Abdulaziz et al. 2021). Sentiment analysis is basically the process of determining the attitude or the emotion of the writer, i.e., whether the sentence emotions inclined toward negative or neutral or positive directions. The "sentiment" method of TextBlob returns two properties, polarity, and subjectivity. Polarity is a float value which lies in the range of [$-$ 1, 1]. The polarity 1 means positive statement, and $-$ 1 means a negative statement and 0 means neutral.

After categorizing the tweets into their sentiment level, it is necessary to apply the learning or the prediction model. But before using any learning model, it is required to transform the Tweeter text data into numeric form. This process is known as text vectorization. It is a fundamental step in the process of machine learning for analyzing text. By looking at the computational effort and observing successful results, in this research TF-IDF technique is applied. The details of TF-IDF process can be found in Bania (2020). Once data is vectorized, the text classifier model is fed to the training data that consists of feature vectors for each text sample and decision tag. With enough training samples, the model will be able to make accurate predictions (Bania 2020; Abdulaziz et al. 2021). There are many different choices of machine learning models which can be used to train a final model.

Here in this work, we have used the Gaussian Naïve Bayes (GNB), Bernoulli's Naïve Bayes (BNB), and Random Forest (RF) models (Bania 2020).

Naïve Bayes is a well-known simple and effective method for text classification. NB is a classification technique based on Bayes' theorem with an assumption of independence among predictors. GNB is an extension of Naïve Bayes classification. It follows a Gaussian distribution which is also known as a normal distribution. It means that the predictors take continuous values and not discrete values. On the other hand, BNB is a variant of Naive Bayes. It is used for discrete data where features are only in binary form. It works on Bernoulli distribution. RF classifier is a bagging technique that falls under ensemble learning techniques. It is a combination of different decision trees which are considered as the base learners. Each decision tree is trained with feature and row sampling with a replacement concept with the same distribution.

4 Experimental Results

To get the uniform experimental results, all the methods are implemented in Python. Programs are simulated in a machine with Processor: Intel(R) Core (TM) i5-8300H CPU @ 2.30 GHz, 64-bit operating system, x64-based processor, and having Windows 10 environment. The partitioned of the dataset is performed according to a train-test (70% and 30%) spilt scheme. For RF classifier, number of estimators, i.e., the number of decision trees in the forest is set to 100 and the maximum depth of the tree is set "none". For the GNB and BNB classifiers, default setting of the "sklearn" environment is used. Four different classification validity measures (Machuca et al. 2020) such as (i) average accuracy, (ii) average precision, (iii) average recall and (iv) $F1$-score measure are used.

4.1 Result Analysis

The bar chart representation for the Kaggle dataset is shown below in Fig. 3. In the given figure, the x axis represents the type of sentiments and y axis represents the total counts of the tweet. The percentage of negative, neutral and positive tweets for the dataset is 16.36, 43.52 and 40.12%. After minutely doing the observations and with further exploration, we have figured out some of provoking words which contribute the positive and negative sentiments and those are as follows: negative sentiments with most common words, "pandemic", "isolation", "outbreak", "mask", "plasma", "lockdown", "ban", "market", "virus", "death", "breaking", "crisis", "fear", "fight", "fatality", "sad", "die", "emergency", "risk", "apocalypse", "symptoms", "hospital", "infected", "crisis", "infection". Further, the terms which generate positive sentiment includes, "positive", "care", "doctor", "recovery", "relief", "medicine", "food", "trust", "global", "love", "vaccine", "free", "God", "good", "support".

The order of the words used in English text is not random. In English, for example, we can say "She was tested positive" but not "positive tested was she". The relationships between words in texts are very complex. This can be achieved by using an approach called N-Gram.

In a sufficiently large corpus, it is likely to see "She was" and "tested positive" several times, but less likely to see "positive tested" and "tested was". These co-occurring words are known as "n-grams", where "n" is a number indicating how long a string of words you considered. This approach for language modeling assumes a tight relationship between the positions of each element in a string, calculating the occurrence of the next word with respect to the previous one.

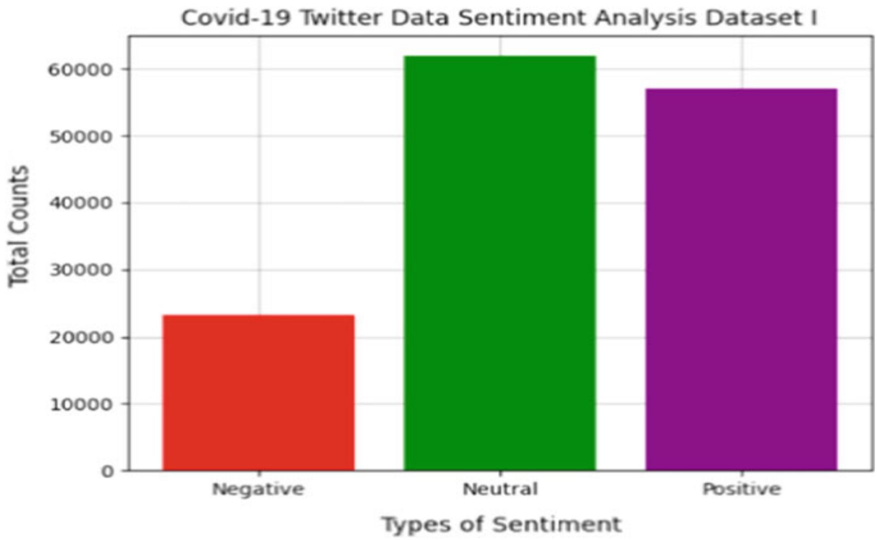

Fig. 3 Text categorization bar plot

The prediction of tweets into *negative*, *neutral*, and *positive*, experiments are carried out using train set/test set spilt applied on three popular classifiers, viz. Gaussian-NB, Bernoulli-NB, RF classifiers and Machuca et al. (2020). The total number of support of samples on the 30% of the test set for negative is 5999, for neutral is 23371 and for positive is 13331. The overall summary of the experimental results achieved on the Kaggle dataset by using 70% training and 30% test samples is reported in Table 1. From Table 1, it can be observed that for the uni-gram and bi-gram feature extraction techniques, RF model has achieved better results than the other models. The improvements in accuracy achieved by the RF model are (9.79, 2.8, 3.15%) and (32.04, 2.8, 2.68%) with respect to G-NB, B-NB and Machuca et al. methods, respectively. A confusion matrix is a technique for evaluating the performance of a classification algorithm. In Fig. 4, confusion matrix generated by the various classification models is shown. In Fig. 4, among the 42,701 testing tweets samples (30% of Dataset), 5436, 8422, 5587, and 4241 tweets were misclassified by the G-NB, B-NB, Machuca et al. and RF models. Now, we can conclude from the summarized experimental results shown in Table 1 and confusion matrix that Random Forest classifier has achieved better classification evaluation results with both bi-gram and uni-gram models compared to the other classification models.

Table 1 Experimental results with respect to accuracy, precision, recall, *F*-measure

Classifiers	Uni-gram					Bi-gram				
	–	Pre	Rec	F1-Sc	Acc	–	Pre	Rec	F1-Sc	Acc
GNB	Neg	0.57	0.67	0.61	80.27	Neg	0.17	0.89	0.29	31.08
	Neu	0.88	0.99	0.93		Neu	0.69	0.21	0.32	
	Pos	0.94	0.71	0.81		Pos	0.92	0.21	0.34	
	M-Avg	0.79	0.79	0.78		M-Avg	0.59	0.44	0.32	
	W-Avg	0.85	0.84	0.84		W-Avg	0.69	0.31	0.32	
BNB	–	Pre	Rec	F1-Sc	Acc	–	Pre	Rec	F1-Sc	Acc
	Neg	0.83	0.63	0.71	87.26	Neg	0.80	0.18	0.29	62.61
	Neu	0.88	0.95	0.91		Neu	0.58	0.97	0.72	
	Pos	0.89	0.88	0.89		Pos	0.85	0.34	0.49	
	M-Avg	0.87	0.82	0.84		M-Avg	0.74	0.50	0.50	
	W-Avg	0.87	0.88	0.87		W-Avg	0.71	0.63	0.58	
RF	–	Pre	Rec	F1-Sc	Acc	–	Pre	Rec	F1-Sc	Acc
	Neg	0.88	0.68	0.77	**90.06**	Neg	0.79	0.19	0.31	**63.12**
	Neu	0.89	0.98	0.93		Neu	0.58	0.97	0.73	
	Pos	0.95	0.90	0.92		Pos	0.87	0.35	0.50	
	M-Avg	0.91	0.85	0.87		M-Avg	0.75	0.51	0.51	
	W-Avg	0.91	0.91	0.90		W-Avg	0.72	0.63	0.58	
Machuca et al. (2020)	–	Pre	Rec	F1-Sc	Acc	–	Pre	Rec	F1-Sc	Acc
	Neg	0.93	055	0.69	86.91	Neg	0.73	0.36	0.51	60.44
	Neu	0.83	0.98	0.90		Neu	0.51	0.77	0.77	
	Pos	0.95	0.79	0.86		Pos	0.76	0.55	0.54	
	M-Avg	0.90	0.78	0.82		M-Avg	0.72	0.53	0.57	
	W-Avg	0.88	0.87	0.86		W-Avg	0.71	0.67	0.51	

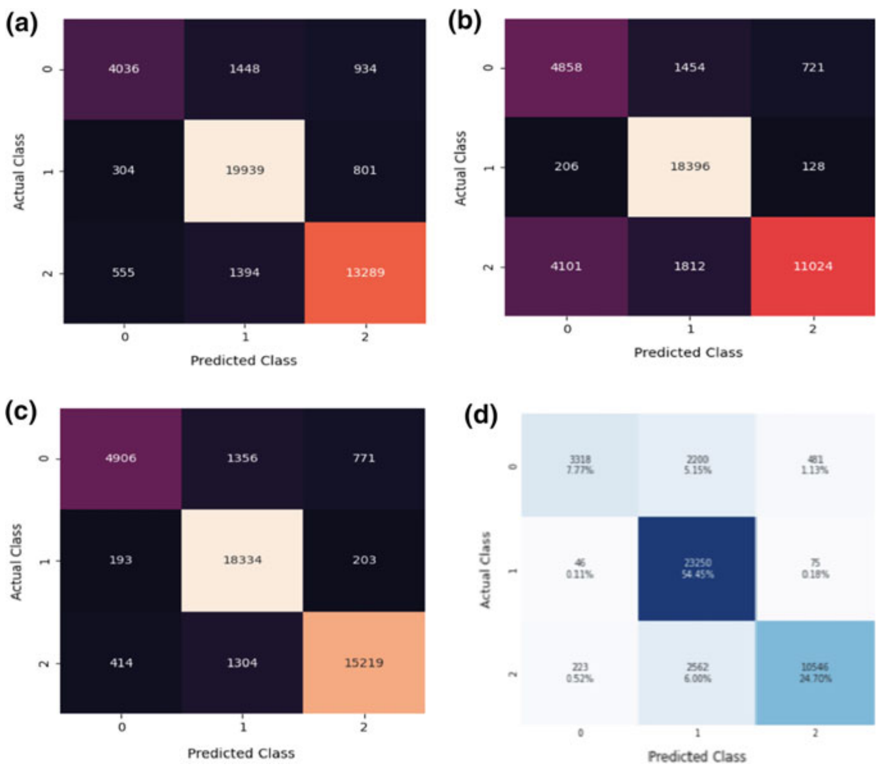

Fig. 4 Confusion matrix for **a** G-NB **b** B-NB **c** RF and **d** Machuca et al.

5 Conclusion

In this paper, we have analyzed the performance of the various supervised learning models to predict the tweets into three classes, viz. *negative*, *neutral*, and *positive*. Initially for this study, the data were collected from the Kaggle repository for the time frame of July 25, 2020 to August 29, 2020. The data are then pre-processed with the help of different Python based-libraries. Then the polarity of each tweet is calculated (using Text Blob Python library), thereby assigned the *negative*, *neutral*, and *positive* classes to the tweets. The feature extraction scheme with the uni-gram and bi-gram is performed by a well-known technique known as TF-IDF thereby different features are extracted to prepare the datasets to feed it into the prediction model. Along with three classifiers GNB, BNB, RF, the study is also compared with one of the latest state-of-the art models (Machuca et al.). The performance of the various classifiers is examined in the experimental section. We have finally observed that RF performance is better than the other classification models.

References

Abdulaziz M, Alsolamy M, Alabbas A, Alotaibi A (2021) Topic based sentiment analysis for COVID-19 tweets. (IJACSA) Int J Adv Comput Sci Appl 12:1

Alrazaq A, Alhuwail D, Househ M, Hamdi M, Shah Z (2020) Top concerns of tweeters during the covid-19 pandemic: Infoveillance study. J Med Internet Res 22(4):1–9

Aslam F, Mumtaz Awan T, Syed JH, Kashif A, Parveen M (2020) Sentiments and emotions evoked by news headlines of coronavirus disease (COVID-19) outbreak. Hum Soc Sci Commun 9(2):1–9

Bania RK (2020) COVID-19 public tweets sentiment analysis using TF-IDF and inductive learning models. INFOCOMP J Comput Sci 19(2):23–41

Chakraborty K, Bhatia S, Bhattacharyya S, Platos J, Bag R, Hassanien AE (2020) Sentiment analysis of covid-19 tweets by deep learning classifiers study to show how popularity is affecting accuracy in social media. Appl Soft Comput J 97:106754

Machuca CR, Gallardo C, Tosa RM (2020) Twitter sentiment analysis on coronavirus: machine learning approach. In: International symposium on automation, information and computing, 2–4 Dec 2020, Beijing, China

Pedrosa AL, Bitencourt L, Cazumba ML, Silva ACS (2020) Emotional, behavioral, and psychological impact of the covid-19 pandemic. Front Psychol 11:1–18

Sailunaz K, Alhajj R (2018) Emotion and sentiment analysis from twitter text. J Comput Sci 36:101003

Adder Design Using Reversible Logic

Gunajit Kalita, Navajit Saikia, and Amit Sravan Bora

Abstract Reversible logic is a prominent area of research due to its interesting characteristics. Reversible logic is also useful in low power computing. The quantum computing technique is also reversible, and so another attraction is attached with this logic. In computing, adders are very important circuit. Adders play a major role in the design of various computing devices. And so, adders are extensively studied. There are adders proposed in many literatures, even though there is always an ample scope to improve the designs. In this manuscript, two reversible gates also called microblocks are presented. Then using these gates, two new adders are designed. One of the designs is a ripple carry adder, and the other design is an improved design in terms of quantum cost and delay. These proposed circuits are constructed using reversible logic. The presented adders are compared with some available literatures on full adders, and it is found that the performance of the proposed adders is of comparable standard. Two designs of 2-bit adders are also presented, and using these deigns, *n*-bit realization of adders can be achieved.

Keywords Reversible logic · Reversible adder · Quantum cost · Garbage output · Ancilla input

1 Introduction

In traditional electronics, gates may have more than one input, but they come up with a single output only. Another issue of concern is heat dissipation. Landauer (1961) observed this issue of concern with the conventional digital electronics. He pointed out that loss of every bit of information gives rise to dissipation of at least KTln2 Joule of energy, where K is the Boltzmann constant and T is the temperature of the heat

G. Kalita (✉) · N. Saikia
Assam Engineering College, Guwahati 781013, India
e-mail: mailtogunajit@gmail.com

A. S. Bora
Monash University, Clayton, Australia

J. K. Deka et al. (eds.), *Emerging Technology for Sustainable Development*,
Lecture Notes in Electrical Engineering 1061,
https://doi.org/10.1007/978-981-99-4362-3_32

sink in Kelvin. For a large number of bits, the total power loss will increase which will generate heat undesirably. This leads to loss of information. The logic in traditional electronics is irreversible. In reversible logic, the input information are conserved (Prasad et al. 2006) in the computational process so that those can be regenerated from output (Moallem et al. 2014). These challenges can be addressed with the help of reversible logic. Reversible logic is also associated with quantum computing. Reversible logic can also be applied in other technologies like adiabatic CMOS design, optical computing, nanotechnology, etc. There are lots of work reported on reversible logic gates and circuits. Some recent works also describe design of ALU using new reversible gates (Kamaraj and Marchamy 2019). One of the important circuits in such design is adder. It is a principal part of a computer. Low power design of adder is highly desirable, and use reversible logic is helpful here.

1.1 Concept of Reversibility

Reversible logic is an n-input and n-output function $f: B^n \rightarrow B^n$ that satisfies one-to-one and on-to mapping (or bijective) among the inputs and outputs (Shende et al. 2003). A reversible logic gate with n-input and n-output lines implements a reversible logic function. Reversible circuit consists of one or more reversible gates cascaded one after another such that the number of inputs and number of outputs are same (Shende et al. 2003).

A reversible gate or circuit is initially designed by using classical digital electronics satisfying its input–output characteristics. Equivalent quantum representation for reversible gates and circuits can be derived by using elementary quantum gates. There are different libraries for elementary quantum gates, and one such popular library is the NCV gate library. This library has four gates: NOT, Controlled NOT (CNOT) or Feynman, Controlled V and Controlled V^+. These quantum gates have unity quantum cost (Barenco et al. 1995; Sasanian et al. 2012).

1.2 Performance Parameters

Some popularly used performance parameters for reversible gates and circuits are as follows.

Quantum Cost: It is the number of elementary quantum gates required to represent a reversible gate or circuit. As circuits are reversible in quantum technology, quantum cost is used as a performance measure for reversible gates and circuits (Kamaraj and Marchamy 2019; Sasanian et al. 2012). This also helps in technology mapping.

Garbage Count: In reversible circuit, garbage output is an unused output line. A garbage output appears as qubits in the equivalent quantum circuit (Kamaraj and Marchamy 2019; Barenco et al. 1995). Hence, the garbage count is expected to be minimum possible in reversible circuit.

Ancilla Count: An ancilla input is a constant input line in reversible circuit. It is desired that the ancilla count be minimum possible to reduce the number of qubits in the equivalent quantum circuit (Kamaraj and Marchamy 2019; Barenco et al. 1995).

Gate Count: Gate count is the number of gates used in a reversible circuit (Kamaraj and Marchamy 2019).

2 Background and Objectives

An adder is a digital device that adds two or more bits and yields two outputs one is sum and the other is a carry. Reversible adders are designed using reversible gate. There are some works on reversible adders reported in various literatures. In the following, a brief discussion is presented.

2.1 Literature Survey

Authors in Pain et al. (2019) show the designs of both half adder and full adder using new reversible gates. The gate is called URGL2 gate. The half adder presented here uses 2 URGL2 gates. The full adder presented here requires 5 URGL2 gates. Authors in Bhuvana and Kanchana Bhaaskaran (2018) present ripple carry adder, BCD adder and a subtractor. To design the adders, a new reversible gate called BKAS gate is proposed. This gate can act as full adder. The designs are shown for 4-bit adders. In (Rahmati and Houshmand 2017), authors present full adder using Feynman and Peres gate. Two designs are presented, design I and design II. The design I is found to be better in terms of performance parameters. Hence design I is considered for reference. The authors also have proposed n-bit full adder design approach. Author in Thapliyal (2016) presents three different design approaches of adder subtractor using reversible logic. From the presented results, first design approach is better in terms of quantum cost; however in terms of ancilla and garbage count, other two are better. In (RashaMontaser and Abdel-Aty 2018), authors present different designs of adder subtractor using reversible R gate. The manuscripts also presented various operations the circuits can performed along with a 1-bit ALU. Authors in Vandana Shukla et al. (2016), presented two design approaches for adder and subtractor circuits, these designs are shown for 8-bit circuit. The first approach uses Feynman and PFAG gate. Since the PFAG gate is a full adder gate, so for 8-bit full adder, 8 such gates are required apart from the 8 Feynman gates used for subtraction circuit along with the adder. In another literature (Thapliyal and Srinivas 2005), authors present a new gate called TSG gate. The gate can work as a full adder gate. In this manuscript, authors apply the gate as a 4:2 compressor toward the design of a 8×8 Wallace tree multiplier. Authors in Thapliyal and Vinod (2007) proposed a new gate called OTG; this gate can work as a full adder. The gate is mainly for online testability purpose. In this manuscript, authors also present another full adder for online testability, that combined the OTG gate and 4 × 4 Feynman gate. Authors name this gate as CTSG. For our reference the adder based on OTG gate is considered. In (Chattopadhyay and AnubhabBaksi 2016), authors present a design of adder. In their approach Peres gate, Toffoli gate and CNOT gates are used in an efficient way and that helps to reduce the quantum cost. Authors also calculated the performance parameters for n-bit adder. Authors in Morrison and Ranganathan (2011) propose two gates, MKG and POAG, both the gates are helpful in arithmetic and logic unit design. The MKG gate can work as full adder. In (Haghparast et al. 2008), authors present a new gate called HNG gate. This gate can act as a full adder. Authors in Haghparast and Navi (2008) present a full adder using double Feynman gate and parity preserving Toffoli gate.

2.2 Objectives

It may be observed from the above discussion that

- design of cost-efficient adder is still a challenge.
- new reversible gates are proposed to design circuits for user specific operations.

For example, new gates are introduced in Kamaraj and Marchamy (2019) to design ALU.

From these observations, the work in this manuscript aims to design

- new reversible gates that support to build cost-effective circuit.
- new adder circuits for better performance.

3 Proposed Reversible Gates

This work proposes two reversible gates, RG and RG7, in the following.

3.1 Reversible RG Gate

Definition 1*:* If A, B and C are input and X, Y and Z are output of the 3 × 3 RG gate, then

$$X = A \oplus \left(\mathrm{B}\overline{C} \oplus B\right), Y = AB + \overline{A}C, Z = B \oplus \mathrm{C}.$$

The reversible RG gate shown in Fig. 1 can perform the following Boolean operations.

- NOT: If inputs B and C are set to 1, input A is inverted at output X. Also, if input C is set to 0 and input A is set to 1, input B is inverted at output X. Similarly, if

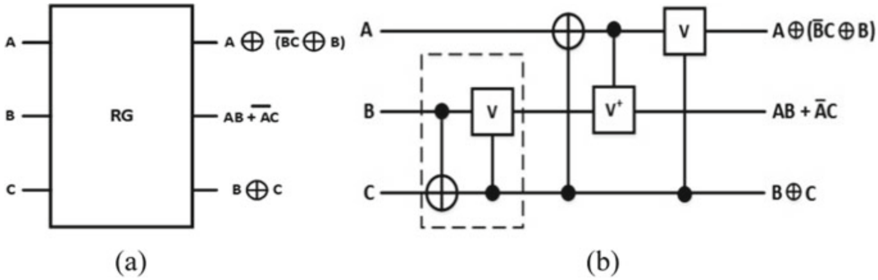

Fig. 1 **a** Block diagram and **b** quantum diagram

input C is set to 1, input B is inverted at output Z. Again, if input B is set to 0 and C is set to 1, input A is inverted at output Y.

- AND: If input C is set to 0, logical AND operation between inputs A and B is generated at output Y.
- XOR: By design, output Z generates XOR operation between inputs B and C. Also, if C is set to 1 XOR operation between A and B can be found at output X.

From the quantum diagram 1(b), it can be noticed that two CNOT (or Feynman) gates, two controlled V gate and one controlled V plus gates are used. The cost of the dotted block shown is 1. Hence, quantum cost of RG gate is 4.

3.2 Reversible RG7 Gate

Definition 2: If A, B, C and D are input and W, X, Y and Z are output of the 4×4 RG7 gate, then.

$$W = A \oplus \mathrm{B} \oplus \mathrm{C} \oplus \mathrm{D}, X = B \oplus \mathrm{C},$$
$$Y = C \oplus \mathrm{D},\ Z = (B \oplus \mathrm{C})\mathrm{D} \oplus \mathrm{BC}.$$

The RG7 gate shown in Fig. 2 can perform the following Boolean operations.

- NOT: If inputs B, C and D are set to 1, input A is inverted at output W. Again, if input C is set to 1, input B is inverted at output X. Also, if input D is set to 1, input C is inverted at output Y.
- AND: If input D is set to 0, logical AND operation between inputs B and C is generated at output Z.
- XOR: By design of the gate, logical XOR operation between inputs B and C is obtained at output X; also, XOR operation between the inputs C and D is obtained at output Y. Again, if inputs C and D are set to 0, XOR operation between inputs A and B is generated at output W.

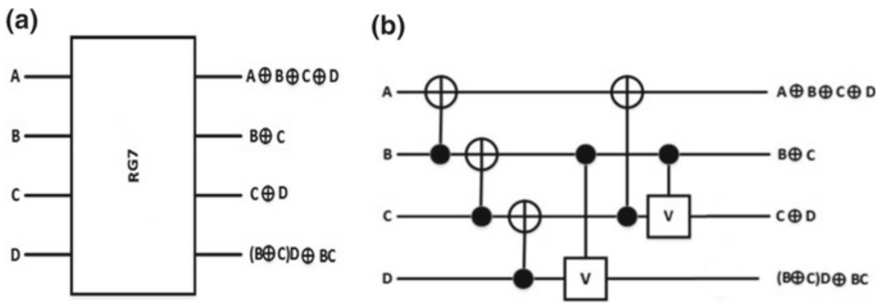

Fig. 2 **a** Block diagram and **b** quantum diagram

- XNOR: If input C is set to 1 and input D is set to 0, logical XNOR operation between inputs A and B is performed at output W.

The quantum representation of RG7 as shown in Fig. 2b uses four CNOT gates and two controlled V gates and so quantum cost of this gate is 6.

In the next section, by using these two gates reversible adders are designed and a brief discussion is presented.

4 Proposed Reversible Adders

In the following, two designs are presented. The design I uses RG7 gate and the design II uses RG and Feynman gate (FG). Feynman gate is a 2×2 gate. If the two inputs are A and B and the outputs are X and Y then, $X = A$ and $Y = A \oplus \mathrm{B}$.

4.1 Design I

This is a ripple carry adder based on reversible logic. This design uses RG7 reversible gate. The RG7 is an adder gate. If the first input is set to 0 (Fig. 2a), RG7 can operate as a full adder. The sum and carry are generated in first and last output lines, respectively.

Combining two RG7 gates, a 2-bit adder can be designed as shown in Fig. 3. If 2-bit numbers A_1A_0 and B_1B_0 are to be added, then A_0 and B_0 are given as input to the first RG7 gate with an initial carry $C_0 = 0$ then the first output line (W) at right-hand side will produce the Sum S_0 and the last output line (Z) will yield the output carry C_1. Similarly, bits A_1 and B_1 are given as input to the second RG7 gate, the sum S_1 will be generated at the first output line and the carry C_2 generates at last output line. Now, the required result is $C_2S_1S_0$. The two middle outputs (X and Y) of both the gates are unused; hence, they are garbage output. In the two gates, the first input is set as 0, these two are ancilla input. In this way, combining three gates a 3-bit adder

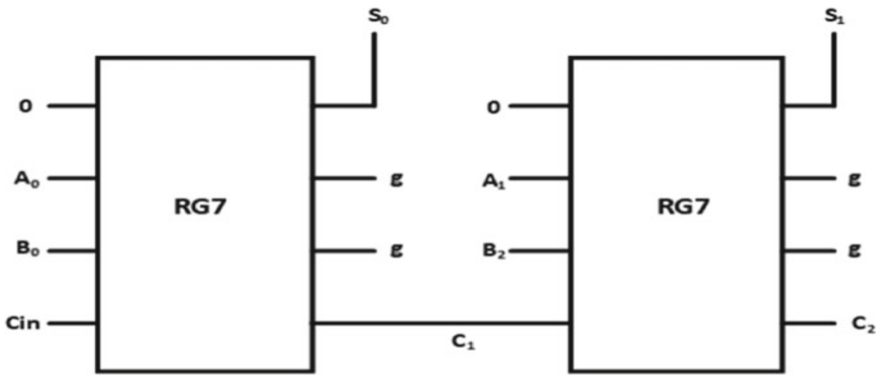

Fig. 3 2-bit adder using RG7 gate

can be realized. Likewise, cascading n such gates an n-bit adder can be designed. For n-bit adder, following parameters can be noted.

$$\begin{aligned}
&\text{Quantum cost} = 6n \\
&\text{Garbage output} = 2n \\
&\text{Gate count} = n \\
&\text{Ancilla input} = n.
\end{aligned}$$

4.2 Design II

The design II uses two RG reversible gates and one Feynman as shown in Fig. 4. A single RG gate can act as a half adder. If numbers A and B are to be added, then the third input (C) of RG gate is set to 0. And then first output line (X) of RG generates the sum and the second output (Y) generates the half carry. Thus to design a 2-bit adder, two RG gates are used. The first RG gate will add A_0 and B_0. The input carry C_0 is set to 0 (ancilla input). Then the first RG gate will produce a bit $S0$, and the output carry bit of first RG gate is given as first input to the Feynman gate (FG). Similarly, the second RG gate will add $A1$ and $B1$ and the generated bit at first output line feeds to the Feynman gate as second input. The sum bit $S1$ is generated in the output of Feynman gate (second output). The carry $C1$ is the second output of RG gate. The third output of both the RG gates is unused, also the first output of Feynman gate is not required, and hence, these are garbage output (g). Thus, result of 2-bit number A and B is $C_1S_1S_0$.

To design a 3-bit adder, one RG gate and one Feynman gate are added to the 2-bit adder. And thus, an n-bit adder can be designed and that is shown in Fig. 5. The performance parameters of the n-bit adder can be presented as following.

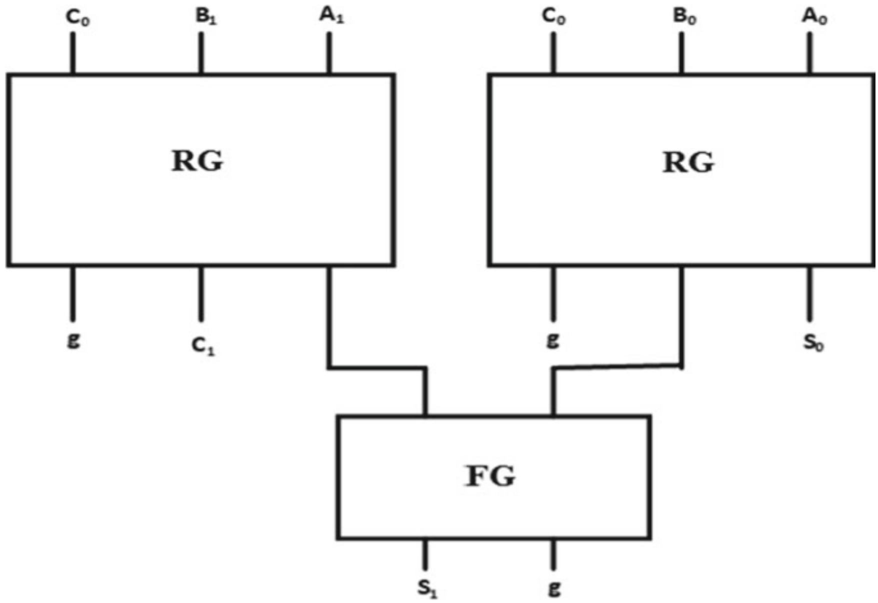

Fig. 4 2-bit adder using RG and Feynman gate

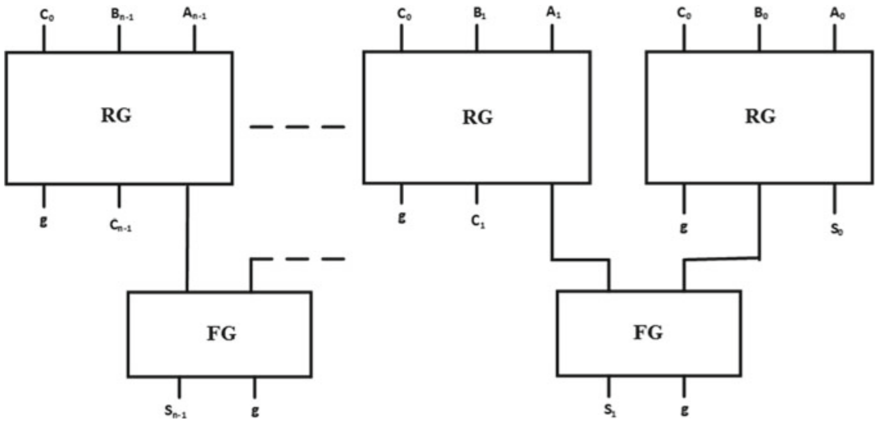

Fig. 5 N-bit adder using RG and Feynman gate

$$
\begin{aligned}
&\text{Quantum cost} = 5n - 1\\
&\text{Gate output} = 2n - 1\\
&\text{Garbage count} = 2n - 1\\
&\text{Ancilla input} = n.
\end{aligned}
$$

In the next section, performance of these designs with some available works is discussed.

5 Result Analysis

The performance comparisons of proposed reversible adders are studied with the available designs. The first one is the comparison of full adder, and the second one is a 2-bit adder.

From the above comparison as shown in Table 1, it may be noticed that the proposed design I is equivalent to the available best design. The design I can be treated as another design of comparable standard in terms of the performance parameters. The design II has same ancilla input like the best available; however, other parameters require improvement in this case. Similarly, from the Table 2, it is observed that for 2-bit adder using design II is better in terms of quantum cost. The ancilla input is equal to the best available designs shown in Table 2. The design II can be realized as n-bit adder. The design is already shown in Fig. 5.

Table 1 Performance comparison for full adder

References	Quantum cots	Gate count	Garbage count	Ancilla count
Pain et al. (2019)	20	5	10	5
Bhuvana and Kanchana Bhaaskaran (2018)	6	1	2	1
Rahmati et al. (2017)	9	3	3	2
Thapliyal (2016)	8	2	0	2
Montaser et al. (2018)	8	2	1	1
Shukla et al. (2016)	8	1	1	1
Thapliyal and Srinivas (2005)	8	1	2	1
Thapliyal and Vinod (2007)	6	1	2	1
Chattopadhyay and Baksi (2016)	8	4	1	1
Morrison and Ranganathan (2011)	6	1	2	1
Haghparast et al. (2008)	6	1	2	1
Haghparast and Navi (2008)	10	4	6	5
Proposed design I	6	1	2	1
Proposed design II	8	2	2	1

Table 2 Performance comparison of 2-bit full adder

References	Quantum cots	Gate count	Garbage count	Ancilla count
Pain et al. (2019)	20	5	10	5
Bhuvana and Kanchana Bhaaskaran (2018)	12	2	4	2
Rahmati et al. (2017)	18	6	6	4
Thapliyal (2016)	16	4	0	4
Montaser et al. (2018)	16	4	2	2
Shukla et al. (2016)	16	2	2	2
Thapliyal and Srinivas (2005)	16	2	4	2
Thapliyal and Vinod (2007)	12	2	4	2
Chattopadhyay and Baksi (2016)	16	8	2	2
Morrison and Ranganathan (2011)	12	2	4	2
Haghparast et al. (2008)	12	2	4	2
Haghparast and Navi (2008)	20	8	12	10
Proposed design I	12	2	4	2
Proposed design II	9	3	3	2

6 Conclusion

Adders are very significant component of computation. The proposed adders are found to be comparable with the available adders. The design I is equivalent to the best available adders in terms of performance parameters. The design II has better performance in terms of quantum cost. Furthermore, design II is also better in terms of ancilla input. The delay in design II is significantly lower than the design I (except the internal hardware delay). Design II slightly requires more numbers of gates. There is always a scope of improvement in a work. And to improve these designs, more investigations are required and this will be our future work.

References

Barenco A, Bennett CH, Cleve R, DiVincenzo DP, Margolus N, Shor P, Sleator T, Smolin JA, Weinfurter H (1995) Elementary gates for quantum computation. Phys Rev A 52(5):3457–3467

Bhuvana BP, Kanchana Bhaaskaran VS (2018) Quantum cost optimization of reversible adder/subtractor using a novel reversible gate. In: Conference 2018, innovations in electronics and communication engineering, lecture notes in networks and systems, vol 7. Springer, pp 111–118

Chattopadhyay A, Baksi A (2016) Low-quantum cost circuit constructions for adderand symmetric boolean functions. In: Proceedings of IEEE international symposium on circuits and systems (ISCAS), Montreal, QC, Canada

Haghparast M, Navi K (2008) Design of a novel fault tolerant reversible full adder for nanotechnology based systems. World Appl Sci J 3(1):114–118

Haghparast M, Jassbi SJ, Navi K, Hashemipour O (2008) Design of a novel reversible multiplier circuit using HNG gate in nanotechnology. World Appl Sci J 3:974–978

Kamaraj A, Marchamy P (2019) Design of integrated reversible fault-tolerant arithmetic and logic unit. Microprocess Microsyst 69:16–23

Landauer R (1961) Irreversibility and heat generation in the computing process. IBM J Res Dev 5(3):183–191

Moallem P, Ehsanpour M, Bolhassani A, Montazeri M (2014) Optimized reversible arithmetic logic units. J Electron 31:394–405

Montaser R, Younes A, Abdel-Aty M (2018) New design of reversible full adder/subtractor using R gate. Int J Theor Phys

Morrison M, Ranganathan N (2011) Design of a reversible ALU based on novel programmable reversible logic gate structures. In: Proceedings of IEEE computer society annual symposium on VLSI, Chennai, India

Pain P, Das K, Sadhu A, Kanjilal MR, De D (2019) Power analysis attack resistable hardware cryptographical circuit design using reversible logic gate in quantum cellular automata. Microsystem Technologies, Springer

Prasad AK, Shende VV, Markov IL, Hayes JP (2006) Data structure and algorithm for simplifying reversible circuits. ACM J Emerg Technol Comput Syst 2:277–293

Rahmati M, Houshmand M, Kaffashian MH (2017) Novel designs of a carry/borrow look-ahead adder/subtractor using reversible gates. J Comput Electron

Sasanian Z, Wille R, Miller D (2012) Realizing reversible circuits using a new class of quantum gates. In: Proceedings design automation conference, 06

Shende VV, Prasad AK, Markov IL, Hayes JP (2003) Synthesis of reversible logic circuits. IEEE Trans Comput Aided Des Integr Circuits Syst 22(6):710–722

Shukla V, Singh OP, Mishra GR, Tiwari RK (2016) A novel approach for reversible realization of 8-bit adder-subtractor circuit with optimized quantum cost. In: Proceedings of international conference on emerging trends in engineering, technology and science 2016, Pudukkottai, India

Thapliyal H (2016) Mapping of subtractor and adder-subtractor circuits on reversible quantum gates. Trans Comput Sci XXVII:10–34

Thapliyal H, Srinivas MB (2005) Novel 'TSG' gate and its application for Designing components of a primitive reversible/quantum ALU. In: Proceedings of 5th IEEE international conference on information communications & signal processing, Bangkok, Thailand

Thapliyal H, Vinod AP (2007) Designing efficient online testable reversible adders with new reversible gate. In: Proceedings of IEEE international symposium on circuits and systems, New Orleans, LA, USA

Anti-Spoofing System for Face Detection Using Convolutional Neural Network

Sumedha Sutradhar, Nazrul Ansari, Manosh Kumar, Nupur Choudhury, and Rupesh Mandal

Abstract The concept of face anti-spoofing is an important part in the face recognition system. It has great importance for fiscal payment and different networking systems in today's modern world. A new system has been introduced using a three-layer convolutional neural network. Accordingly, in this paper, we present a deep neural network strategy for face anti-spoofing. This paper proposes a system of detecting spoofing using convolutional neural network (CNN) classifier. The convolutional neural network system is constructed to arrest the spoofed faces from piercing in the name of genuine person. We have considered 3 layers of CNN in order to make the detection of the images in a more clear format. Self-datasets of real and fake images are created to train the neural network. The two datasets are trained singly to resolve the absolute outgrowth. The accuracy achieved by our model is quite satisfactory. The experimental results over the validation dataset and training dataset show that this system shows better performance and has demonstrated a satisfactory accuracy over other models.

Keywords Face detection · Spoofing · Cyber-attacks · Face biometrics · Convolutional neural network

1 Introduction

Online identity fraud is on the rise in recent years. Identity fraud refers to various tactics used to impersonate and commit crimes or fraud, usually related to money laundering. Although most spoofing methods are done by e-mail or computer, there are some strategies that are less well known to the public and companies, but they are more dangerous, such as facial spoofing, which involves imitating or using a person

S. Sutradhar · N. Ansari · M. Kumar · N. Choudhury (✉) · R. Mandal
Assam Don Bosco University, Guwahati, India
e-mail: nupur.choudhury@dbuniversity.ac.in

R. Mandal
e-mail: rupesh.mandal@dbuniversity.ac.in

J. K. Deka et al. (eds.), *Emerging Technology for Sustainable Development*, Lecture Notes in Electrical Engineering 1061,
https://doi.org/10.1007/978-981-99-4362-3_33

face to impersonate that person and try to trick the biometric face recognition control systems (https://www.electronicid.eu/en/blog/post/facial-spoofing-what-it-is-how-to-prevent-it-and-spoofing-detection-solutions/en). Anti-spoofing face detection is a function to prevent false facial verification by using a photo, video, mask or other area of the authorized face. The threats associated with spoofing have been growing in the recent years. With the advancement in technology, the number of malicious attacks by illegal attackers has increased manifold. Antispoofing face detection is needed to reduce the number of cyber-attacks on social media today. It will be one of the factors which would determine the future landscape of AI. Anti-spoofing is extremely necessary in order to reduce the number of cyber-thefts, protect sensitive data, mitigate fraud and to give reassurance to people regarding their personal data. In order to differentiate between which is real and which is fake it is important to impose a face recognition system. By doing this the identity frauds will decrease to a great percentage. We used CNN, which is an in-depth learning algorithm to build our model. AI includes a huge set of libraries, all of which are very efficient to implement to build a model. In-depth learning models can attain high levels of accuracy, even surpassing human performance in some cases. A vast set of labeled data and multi-layered neural network architecture are used to train the model. The structure of neural networks is determined by the human brain's structure. Neural networks are taught to do comparable duties in data as our brains do in identifying patterns and separating different sorts of information. Individual layers of the neural network can be regarded of as a filter that works from negative to concealed, increasing the chances of obtaining and delivering a positive result. The brain strives to compare new information to what we already know whenever we receive it. The model uses the technique of binary supervision in order to identify real and fake images. It ranges between 0 and 1 which is used to identify any image related frauds. In convolutional networks, the sigmoid function is utilized as activation. This unit output is guaranteed to be between 0 and 1 if the neuron activation function is a sigmoid function. The output of this unit is also null because the sigmoid is a nonlinear function. The measured input volume is a line function. The sigmoid unit is a neuron that uses the sigmoid function as its activation function (Saeed 2021).

The dataset of our project has been divided into three categories—training, testing and validation. Due to which the classification of images into real and fake has been done by model with a very satisfactory accuracy.

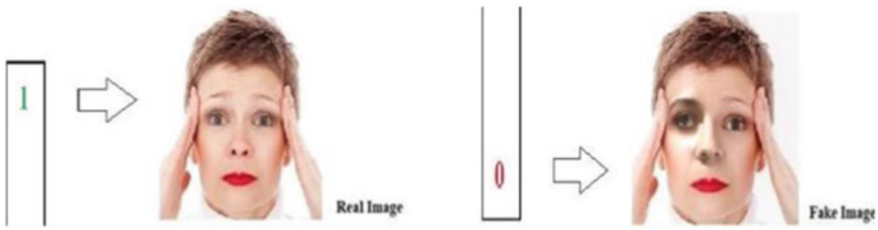

Fig. 1 Binary supervision technique used in our model

2 Background

Though spoofing and morphing sounds similar, they have certain differences between them. Spoofing can be referred to as a cybercrime similar to impersonation for trespassing a device/entity as compared to morphing which related to transformation of an image into something else using computer-assisted techniques. Spoofing also relates to conversion to a new entity whereas morphing correlates to changes in the image form or the character. The concept of anti-spoofing for face detection has been presented in different ways by various authors. Description of some of them is as follows:

2.1 Texture-Based Methods

In (Bromme et al. 2018), the authors present a full study and discovery of generalization of different methods to detect false faces based on recent deep learning methods and conventional structural description methods. Within the study of generalization, they present a new database created with different methods to create fake faces. They also propose protocols to effectively evaluate structure based and deep learning based. Geirhos et al. (2018) have shown that models are more about texture than shape Gatys et al. (2015). The gram matrix is offered as a fine description of the texture that can be used in texture generation and picture processing. (Gatys et al. 2016; Liu et al. 2020).

2.2 Motion-Based Methods

The detection of an object or its motion based on motion in a sequence of photographs is known as motion-based recognition. Methods like cyclic motion detection and recognition, lip reading, hand gesture interpretation, motion action recognition, and temporal texture categorization are some of the techniques to recognize motion (Cédras and Shah 1995). The motion of a nonrigidly articulated body exhibits periodicity, so this is used as a strong marker for classifying moving objects. In moving the classification of the object, nonrigid object movement can be proposed in a stout way. Optical flow can be considered as again an essential tool to classify the object. It is assumed that the flow in form of residue is present in the objects with rigidity while moving objects such as animals have a higher count (Patel et al. 2018). Feng et al. transmit optical flow map and Shearlet image function to CNN (Feng et al. 2016) during the deep university era. Xu et al. presented the LSTMCNN architecture to employ provisional information for binary classification in Xu et al. (2015).

In general, all previous techniques still consider face spoofing as a binary classification problem, making cross-database tests difficult to generalize. We learn the rPPG signal from face movies to collect timewise information in this study.

2.3 Image Quality and Reflectance-Based Methods

Characteristic reflection, opacity, chroma moment, and color variation have emerged in Wen et al. (2015) on liquid crystal displays (LCDs) to depict the changes in surface reflection between actual and simulated faces. To distinguish between real and fraudulent faces, (Feng et al. 2016) combines picture quality features and optical flow parameters. In addition, Fourier spectroscopy (Pinto et al. 2015) identified features that were effective in detecting facial duplication using sound information from fraudulent facial photos. These reflecting and image quality-based approaches work well for low-resolution attacks, but their effectiveness may suffer when compared against forged artifacts of higher quality (Saeed 2021).

2.4 Region-Based CNNs

With a deep learning run, CNN of the region (NCNS) has achieved a strong improvement in object detection performance. The prohibited methods of CNNS have been RCNN (Girshick et al. 2014) extracted from the suggestions of the image area, then each area of interest (King) is classified by a healthcare network. To reduce the excess CNN calculations in the NCN to accelerate and the frame has been expanded to share basic tactical functions to change investment head into (He et al. 2015). After that, the network of regional proposals (NPN) is presented in RECNN faster than (Ren et al. 2015), implementing additional speed compared to fast RCNN (Pomari et al. 2018). Faster RCNN is expanded for many different tasks due to its effectiveness in object detection (Saeed 2021).

3 Proposed Methodology

The face anti-spoofing is a binary classification issue whose purpose is to tell the difference between real and false faces. Traditional display assault detection can be broken down into two steps: the acquisition of a facial region and the extraction of features. The main idea of the proposed approach is to design a model using CNN architecture which would help to reduce identity related theft/fraud. The description of the classifier used and the step-by-step algorithm has been explained (Fig. 2):

The model will be created as a convolutional neural network (CNN) network utilizing deep learning algorithms. The data set will be represented by the target

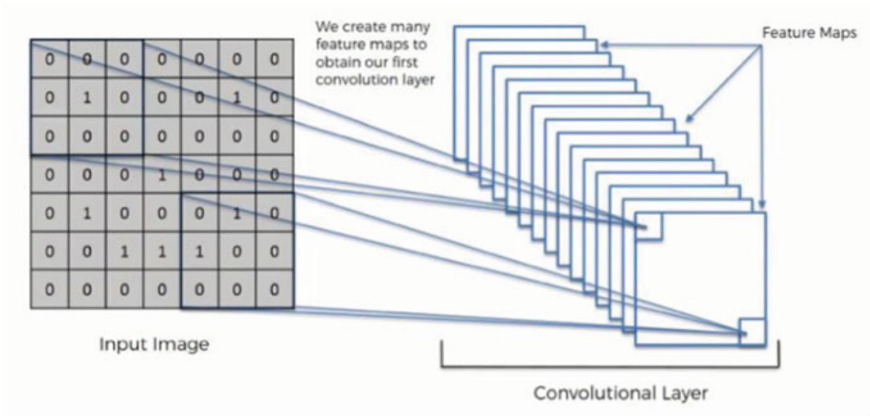

Fig. 2 Basic idea of convolution

photos, which will be extracted. With the use of traditional mathematical activities, a convolutional layer is used to extract picture functions when building CNN-shaping classes. These convolutional operations act as two-way digital filters, with each matrix block picture having the same size as the filter size being multiplied by the filter matrix. Create a function for activation. The activation function layer sits between the normal and feature map layers, and it discards undesired pixels, such as negative values, just like any other classic neural network activation function. It will utilize a nonlinear activation function called the Rectified Linear Unit because to the nonlinear nature of the image data (ReLU). The positive component of its reasoning is defined as the rectification work. We sample the array using an approach called max pooling to adjust the layer's output to minimize the size of the array at the correct step. Additional synthesis aids in rendering the representation almost invariant for tiny input translations. Create anticipation by having this neural network decide whether or not the image is a match. It's known as the 'fully connected' network to distinguish it from the convolutional method. Before constructing a completely connected network, the group's functional card data must be transformed into a single column to match as a nervous network. This is referred to as 'flattening.' Sigmoid functions and classification modules should be built (classify images). The formula used for sigmoid function is:

$$\sigma(k) = 1/(1 + \mathrm{e}^{k}) \tag{1}$$

The Sigmoid function's output is used to express a binary distribution (a probability distribution of two results). When the neural network has finished training, the dataset is examined and the confusion matrix, which comprises numerous factors through which the neural network accuracy is calculated, is retrieved.

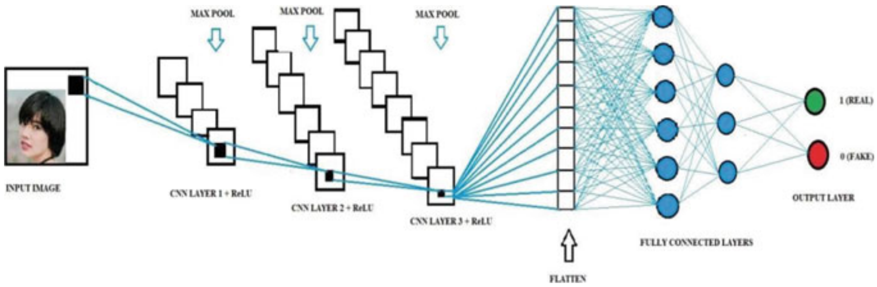

Fig. 3 Proposed three-layer CNN architecture of our model

3.1 Dataset Description

The dataset used in this work is available at https://www.kaggle.com/datasets/ciplab/real-and-fake-face-detection and is categorized into training, testing and validation. It has 960 fake images and 1081 real images. The training and validation dataset has been further into real and fake datasets, and some of the images from the validation datasets have been taken into testing dataset.

3.2 Data Preparation

The training dataset contains 1000 images in 2 classes, and the validation dataset contains 200 images in 2 classes. Explanation of our proposed architecture is as follows (Fig. 3).

3.3 Training and Working of the CNN-Based Model

An input image has been taken of size (200×200), i.e., the height and width of the image. The original sizes of the image were (600×600), but after converting it into grayscale its size reduced to (200×200). We have converted the RGB image into a grayscale image with a filter dimension of 3×3 in order to reduce the size of pixels for better accuracy.

$$\begin{aligned}&\text{Dimension of output} = [(200-3+1),\\&(200-3+1)] = [196, 196]\end{aligned} \tag{2}$$

For converting the image from RGB scale to grayscale, we do the following calculation:

$$\text{trainning} = \text{ImageDataGenerator(rescale} = 1/255) \tag{3}$$

$$\text{validation} = \text{ImageDataGenerator(rescale} = 1/255) \tag{4}$$

3.4 First CNN Layer + ReLU

The input image first goes on to the first CNN layer along with the Rectified Linear Unit (ReLU). The number of convolutional kernels is 16 and the size of the filter is (3 × 3). After the image ends processing in this layer its size becomes (200 × 200 × 16). The input image is designated by f, and our kernel is denoted by h; therefore, feature map values are calculated using the formula. The result matrix's row and column indexes are denoted by m and n, respectively [22].

$$G[m,n] = (f * h)[m,n] = \sum j \sum kh[j,k]f[m-j,n-k] \tag{5}$$

where f = input image, h = kernel and m, n = row and column index of result matrix.

3.5 ReLU Activation Function

The ReLU function is applied to increase the nonlinearity in our images. The function returns 0, if it receives any negative input and for any positive value, it returns the value back. The ReLU function's equation is as follows:

$$f(x) = \max(0, z) \tag{6}$$

After the first CNN layer, the reduced image now goes onto the max pooling layer.

3.6 Max Pooling

Pooling filters are usually always (2 × 2) pixels in size, with a 2-pixel stride

$$\text{Feature map} = 3 \times 3 = 9\,\text{pixels, Max Pool} = 2 \times 2 = 4\,\text{pixels} \tag{7}$$

3.7 Second CNN Layer + ReLU

Now, the image goes onto the second CNN layer wherein the number of convolutional kernels is 32 and the size of the filter is (3 × 3) along with this the ReLU also comes into consideration. After the image gets processed in the second CNN layer, it moves on to the max pooling layer where the same function takes place as of the above-mentioned max pooling layer.

3.8 Third CNN Layer + ReLU

The number of kernels increases to 64 as the image progresses to the third and final CNN layer, and the filter size is increased (3 × 3). Here also the ReLU comes into consideration along with the CNN layer.

3.9 Fully Connected Layer and Sigmoid Activation Function

The image is sent to the max pooling layer, and the output of the CNN layers is flattened to generate a single long feature vector. It is linked to a fully connected layer, which is the final classification model. The sigmoid activation function is preferred for classification since the likelihood of the output or prediction is only between 0 and 1 (Fig. 4).

We have listed the hyperparameters and settings used in our experiments: convolutional filter size: 3 × 3, activation function is ReLU, Optimizer: RMSprop, Learning rate:0.01. We took a conventional approach to look for similar problems and deep learning architectures which have already been shown to work. Then a suitable architecture of three layers was developed by experimentation.

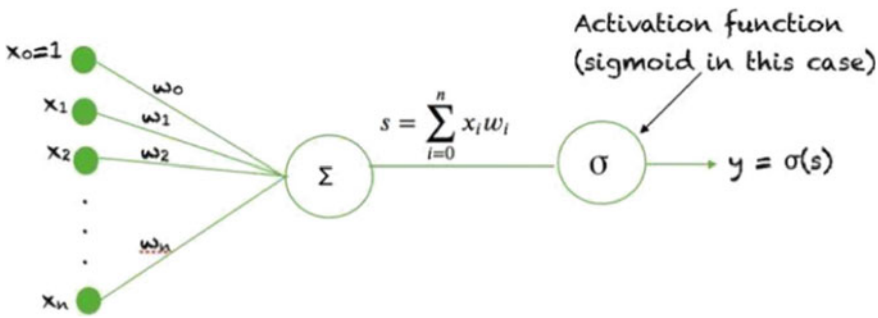

Fig. 4 A sigmoid unit in a neural network (Chen et al. 2019)

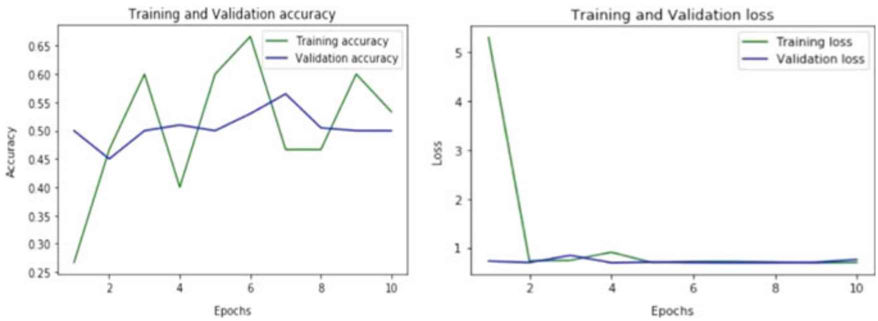

Fig. 5 Graphs above show the accuracy curves and loss curves for training and validation as shown in our model

4 Results and Discussions

The output of our project has been executed by the sigmoid function using binary classification. The accuracy which our proposed model is able to achieve is between 80 and 90% which can be achieved by increasing the number of epochs. The training and validation loss curve for showing the percentage of loss achieved by our model has been plotted. In calculating the validation loss, dropout is disabled. In this case, our training set had many ’hard’ cases to learn as compared to our validation set that had mostly ’easy’ cases to predict (Fig. 5).

We have trained our model to predict from ‘easy’ cases to check with how much accuracy is our model able to detect whether can image is real or fake. If we had considered ‘hard’ cases, then it might had been that our model would have faced overfitting due to which the predictions would have come out to be wrong or of less accuracy. To test the effectiveness of our compilation method, consider the latest method of detecting spoofing for comparison. To test, we used the same test database used to compare the proposed methods. The proposed model uses CNN with ReLU and Sigmoid activation function as compared to the DNN Model (Pomari et al’s Model) (Pomari et al. 2018). This method also do not use of a pre-built machine learning model, trains data as compared to transfer learning approach of the DNN model. The model focusses on the images with a single human face with 80–90% accuracy as compared to 96 % classaccuracy in the DNN model.

5 Conclusion

Aside from deceptive counter measures, most high-end face biometric systems are at risk of attack, as they try to increase discrimination within ownership regardless of whether the feature presented is from a live legal client or not. The project’s proposed anti-fraud method has yielded promising results on a single website, but it may be lacking in general information on the numerous settings of fraudulent attacks that can occur in real-world systems. This shows that dealing with a range of fraudulent attacks may necessitate a network of specific attackers. Additional datasets for actual and false photos can help improve system accuracy. Changing the settings used to train the data can also improve accuracy. As the field progresses, new and more difficult data should be expected. As current public information has its limitations and does not adequately cover the issue, the results suggest that future development may require complex data with a variety of high-quality spoofing attacks and appropriate protocols.

References

Bromme A, Busch C, Dantcheva A, Rathgeb C, Uhl A (eds) BIOSIG 2018, lecture notes in informatics (LNI), Gesellschaft fur Informatik, Bonn 2018

Cédras C, Shah M (1995) Motion-based recognition a survey. Image and vision computing, Elsevier, Mar 1995

Chen H et al (2019) Cascade face spoofing detector based on face anti-spoofing R-CNN and improved Retinex LBP

Facial spoofing: what it is, how to prevent it and spoofing detection solutions. https://www.electronicid.eu/en/blog/post/facial-spoofing-what-it-is-how-to-prevent-it-and-spoofing-detection-solutions/en

Feng L, Po L-M, Li Y, Xu X, Yuan F, Cheung TC-H, Cheung K-W (2016) Integration of image quality and motion cues for face anti-spoofing: a neural network approach. J vis Commun Image Represent 38:451–460

Feng L, Po L, Li Y (2016) Integration of image quality and motion cues for face anti-spoofing: a neural network approach. J vis Commun Image Represent 38(1):451–460

Gatys L, Ecker AS, Bethge M (2015) Texture synthesis using convolutional neural networks. In: Advances in neural information processing systems, pp 262–270

Gatys LA, Ecker AS, Bethge M (2016) Image style transfer using convolutional neural networks. In: Proceedings of the IEEE conference on computer vision and pattern recognition, pp 2414–2423

Geirhos R, Rubisch P, Michaelis C, Bethge M, Wichmann FA, Brendel W (2018) Imagenet-trained cnns are biased towards texture; increasing shape bias improves accuracy and robustness. arXiv preprint arXiv:1811.12231

Girshick R, Donahue J, Darrell T, Malik J (2014) Rich feature hierarchies for accurate object detection and semantic segmentation. In: Proceedings of the IEEE conference on computer vision and pattern recognition, Jun 2014, pp 580–587

He K, Zhang X, Ren S, Sun J (2015) Spatial pyramid pooling in deep convolutional networks for visual recognition. IEEE Trans Pattern Anal Mach Intell 37(9):1904–1916

Liu Z, Qi X, Torr PHS (2020) Global texture enhancement for fake face detection in the wild

Patel B, Ray N, Patel P (2018) Motion based object tracking

Pinto A, Pedrini H, Schwartz WR, Rocha A (2015) 'Face spoofing detection through visual codebooks of spectral temporal cubes.' IEEE Trans Image Proc 24(12):4726–4740

Pomari T, Ruppert G, Rezende E, Rocha A, Carvalho T (2018) Image splicing detection through illumination inconsistencies and deep learning. In: 2018 25th IEEE international conference on image processing (ICIP). Athens, pp 3788–3792

Ren S, He K, Girshick R, Sun J (2015) Faster R-CNN: towards real-time object detection with region proposal networks. In: Proceedings of the advances in neural information processing systems, pp 91–99

Saeed M (2021) A gentle introduction to sigmoid function. Aug 25, 2021 in start machine learning

Wen D, Han H, Jain AK (2015) Face spoof detection with image distortion analysis. IEEE Trans Inf Forensics Secur 10(4):746–761

Xu Z, Li S, Deng W (2015) Learning temporal features using LSTM-CNN architecture for face anti-spoofing. In: ACPR. IEEE, pp 141–145

Utilizing Greenhouse Technology Towards Sustainable Agriculture Using IoT "TechFarm"

Darsana Sandilya, Charlina Bharali, Angom Ringku, and Bobby Sharma

Abstract Greenhouse is a structure that consists of walls and gates, and a transparent roof which maintains a climatic condition that is favourable for the growth of plants inside the greenhouse. Greenhouse system is maintained by human beings which reduces the labour work inside the greenhouse. The automatic greenhouse formed by the utilization of Internet of Things helps in overcoming the problem faced by the farmers and provides with an automatic monitoring of the greenhouse system. This paper proposes an automation system that uses Arduino NANO and various sensors for detecting the moisture, temperature, light and humidity to get a rise in the production.

Keywords IoT · Arduino Nano · Raspberry Pi 3 · Humidity sensor · Water pump · Servomotor · Temperature sensor · Capacitive soil moisture sensor · Light sensor

1 Introduction

A greenhouse is a structure that is built of walls and a transparent roof and is designed to maintain regulated climatic conditions and helps to grow plants in extreme weather conditions. The greenhouse controls the key factors which include temperature, light intensity, irrigation and the humidity which creates a suitable for the plants to grow inside the greenhouse and leads to a good quality of production. The crop cultivation inside a greenhouse is highly affected the farming operations to protect fields and maximize crop production. Regular monitoring of these factors gives certain information obtaining individual effects of various factors for maximum crop production. The greenhouse has reduced the inconvenience and other issues that is caused by the traditional way of farming, which is benefitting the farmers (Figs. 1 and 2).

D. Sandilya (✉) · C. Bharali · A. Ringku · B. Sharma
Department of Computer Science and Engineering, Assam Don Bosco University, Azara, India
e-mail: darshubb5@gmail.com

B. Sharma
e-mail: bobby.sharma@dbuniversity.ac.in

J. K. Deka et al. (eds.), *Emerging Technology for Sustainable Development*,
Lecture Notes in Electrical Engineering 1061,
https://doi.org/10.1007/978-981-99-4362-3_34

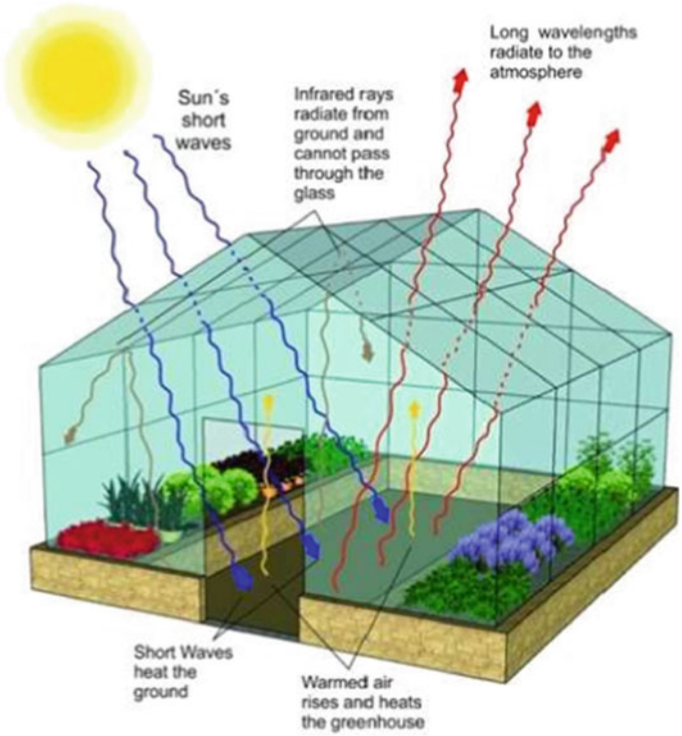

Fig. 1 Structure of a greenhouse

Greenhouse has also overcome the shortcomings in the growing qualities of a piece of land. They also enables certain crops to be grown throughout the year (Fig. 3).

In spite of being useful to the farmers in producing good quality crops and production rate, it causes troubles to the farmers, as they might not be familiar with the technology, they may fail to maintain the environment inside the greenhouse like suppose they may not be able to maintain the required climatic conditions or suppose how much water is required to irrigate the plants, which will lead to the damage of crops. This type of problems can be prevented with the help of smart greenhouse using IoT, where all the jobs will be done with the help of sensors.

2 Literature Review

In Shirsath et al. (2017), authors mention that this project is designed using Arduino, and it uses android phone to monitor the greenhouse (control it using android from remote location). It was based on SMS system (GSM-Global System for Mobile

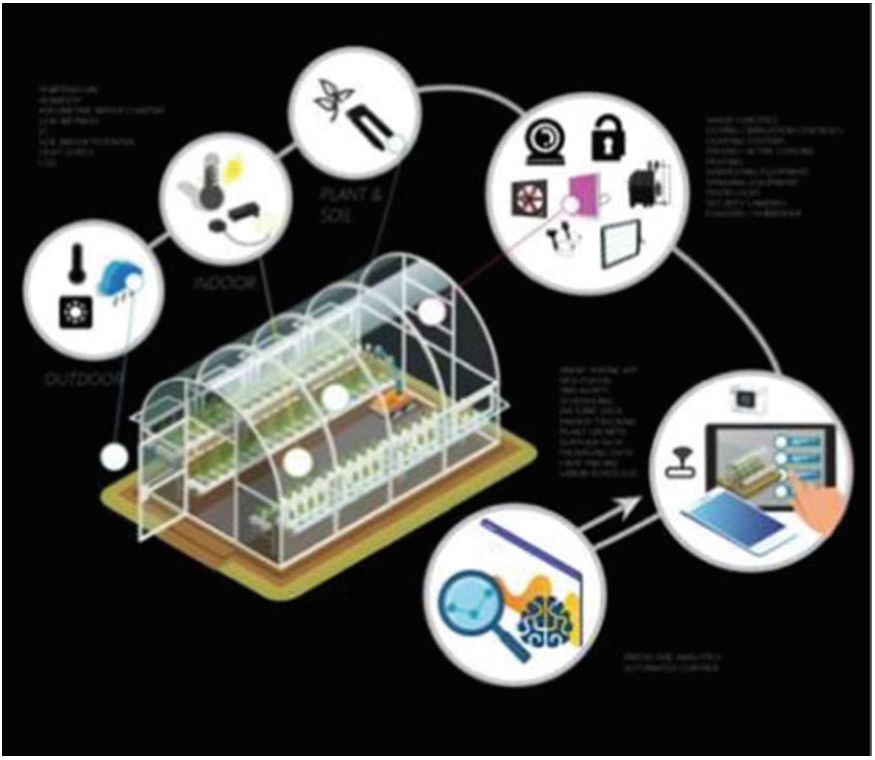

Fig. 2 IoT elements and sensors

Fig. 3 Connection of Wi-Fi

communication). This system allows the farmer for taking correct decision by studying the actual status of the sensors. But there are few limitations like,

(i) One person always had to be present in the greenhouse.
(ii) It was time consuming and costly.

In Shiyale et al. (2020), authors mention that the design of hardware for greenhouse monitoring is used to control the environment condition of given house to get good condition. In this system, the monitoring of greenhouse component consists of sensor for temperature, checking water level and soil moisture. ARDUINO UNO, GSM modem, Wi-Fi modem, water pump, DC motor, DC fan, LCD, regulator and rectifier power supply are used to detect data. They provide an instant solution for irrigation and other field activities. This system helps in improving the good production and helps in faster growth of plants. They also mentioned about reducing the wastage of water resources.

In Vatari et al. (2019), the authors mention that Internet of Things can be applied to different daily activities such as health care, smart home, etc. Bluetooth, Wi-Fi and ZigBee are widely used in Internet of Things devices but along with short transmission range, middle power consumption and weakness of interference. Hence, low power wide area network (LPWAN) for the cellular network is proposed for wide coverage, lower power consumption and massive devices with reliable communication for IoT devices. Limitations of the system are the implementation and maintenance cost.

In Microtonics Technologies (2018), the authors mention that the proposed greenhouse system can control and monitor the changes like temperature, humidity and soil moisture by combining the sensor to the Raspberry Pi, and then it gives alerts to the users using mobile application. Application that is developed helps in getting latest information about the agricultural background.

In Lavanya et al. (2019), authors mention that the greenhouse environment including Internet of Things and cloud helps to control the system and accordingly stores information. They even mentioned that implementation of the smart greenhouse condition was always advantageous. They mentioned about Arduino-based works for automatic controlling and monitoring of environmental changes.

3 Proposed Work

This paper overcomes drawbacks of the existing system. This paper proposes a new system that uses various sensor to monitor various factors inside the greenhouse. The inputs' pin of Arduino NANO helps to maintain the climatic conditions inside the greenhouse. Based on the threshold value set for the temperature, moisture, humidity and light, the Wi-Fi module present in the Raspberry Pi enables to transfer the information collected from the sensors to the server and store it in the database. Here it uses a MQTT server. The information is then passed on to the user's device through internet to monitor the system. This system allows machine-to-machine interaction rather than human-to-machine interaction (Fig. 4).

The proposed system gives an automatic form of greenhouse condition providing a secured connection among the people and noticeable things around, and it permits real-time information gathering through various open source platform. This system provides automatic controlling and monitoring and conveys the gathered sensors

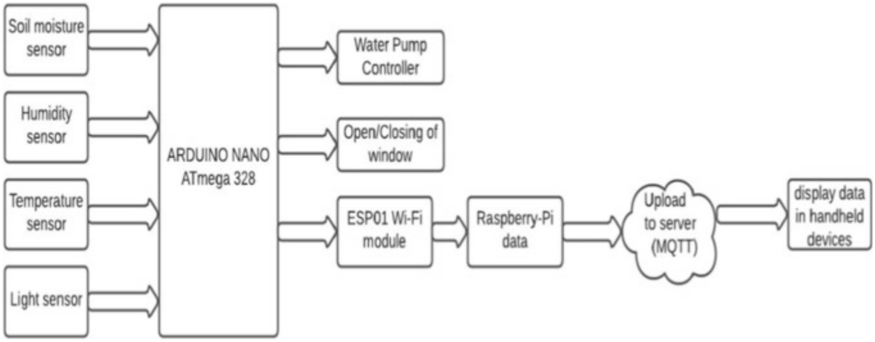

Fig. 4 Block diagram

information from the MQTT server to achieve an anytime access of the information that are detected from the green house, which enables high rate production and that is beneficial for the farmers (Figs. 5 and 6).

We use two servomotors for opening and closing of the window and one for rotating the fan. The data connected by the sensors goes to Arduino Nano, then to ESP01 and then to Raspberry Pi. We can use this model for multiple greenhouse. Soil moisture sensor is connected to analog pin, and the humidity and the temperature sensor is connected to the digital pin of the Nano. The relay module acts as a switch, depending on the light sensor it will switch on or off the LED lights. Light sensor is connected to A_4 and A_5 of the Nano board.

4 Hardware Used

Arduino Nano: The Arduino Nano is a board based on Atmega328P which is released in 2008. It provides the same connectivity as in Arduino UNO board, but it is comparatively smaller in size.

Raspberry Pi 3: Raspberry Pi is a low cost, credit card size computer that is developed in the United Kingdom. It itself is a screenless computer.

Humidity Sensor: DHT21 sensor used here is a digital module for testing humidity and temperature to ensure high reliability and stability.

Water Pump: The water pump is an essential tool to pump out water from the garden, pool, or under the ground.

Servomotor: A servomotor is a rotary device that rotates in angular or linear position with velocity and acceleration.

Temperature Sensor: The digital temperature sensor is a single-wire device that is used to measure temperature with an accuracy of $\pm$ 5%.

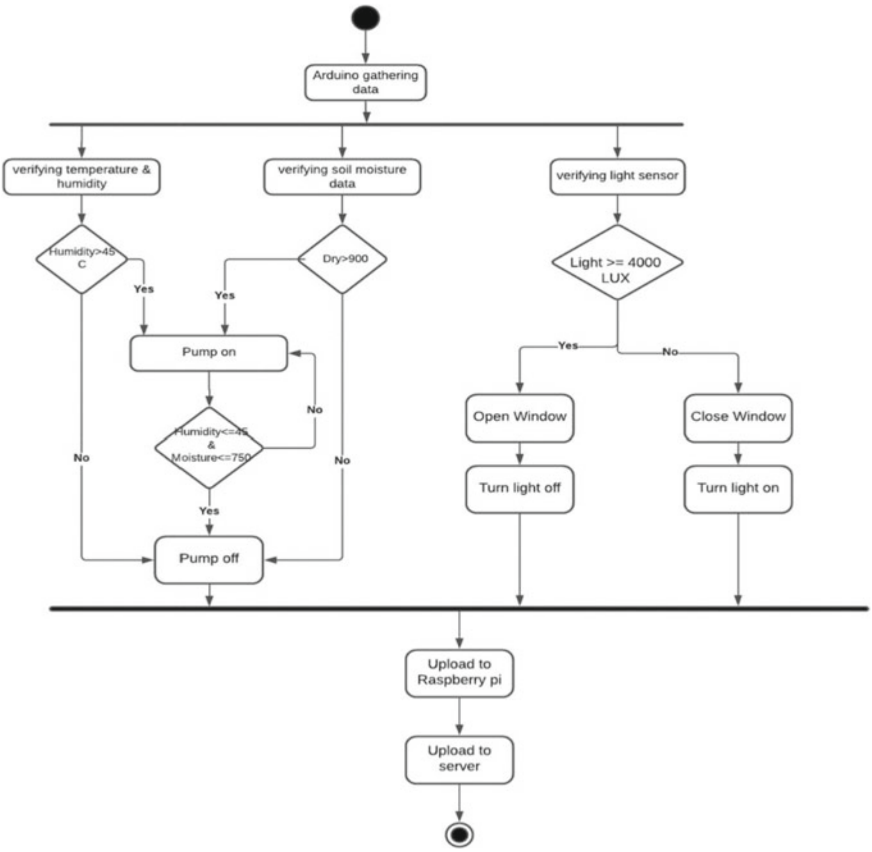

Fig. 5 Activity diagram for the system

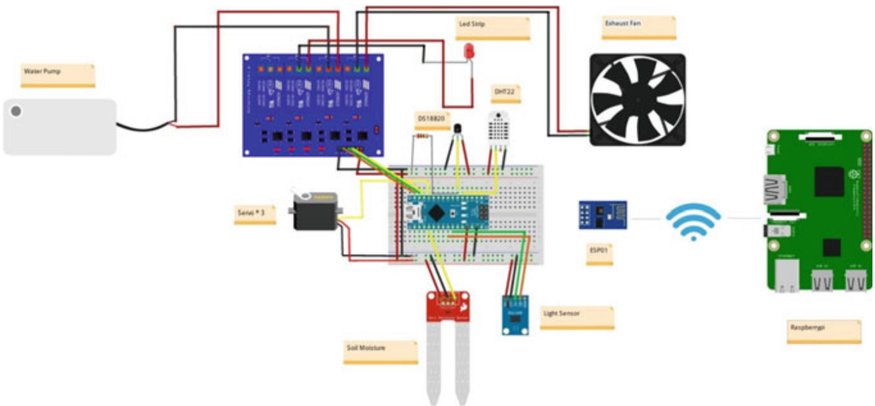

Fig. 6 Circuit diagram

Capacitive Soil Moisture: This capacitive soil moisture sensor measures the level of moisture present in the soil.

Light Sensors: Light sensor BH1750 is used to detect the various intensities of light. It can detect wide range at high temperature.

5 Result and Analysis

The connection of various hardware devices and sensors including capacitive soil moisture sensor, light sensor, Arduino NANO, Raspberry Pi, humidity and temperature sensor along with water pump and servomotor is shown in Fig. 7.

After setting up the hardware, the parameters including temperature, pressure and humidity had been observed in two scenarios, namely with greenhouse setup and without greenhouse setup.

Accordingly, data had been plotted according to Figs. 8, 9, 10 and 11.

Collected data had been analysed and found that the proposed greenhouse can be managed to have a controlled environment for proper growth of the crops. Moreover, the collected data can be kept for further analysis as well as for prediction purpose.

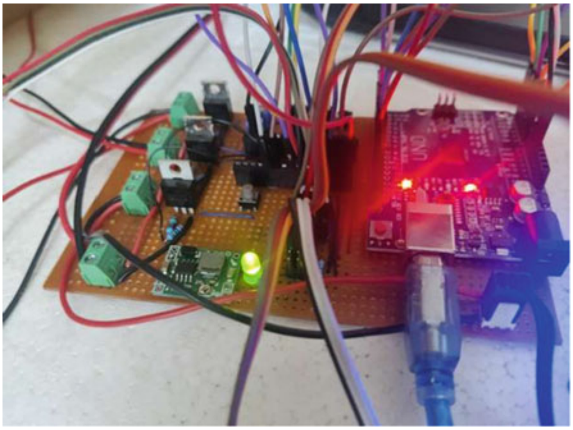

Fig. 7 Hardware setup of devices

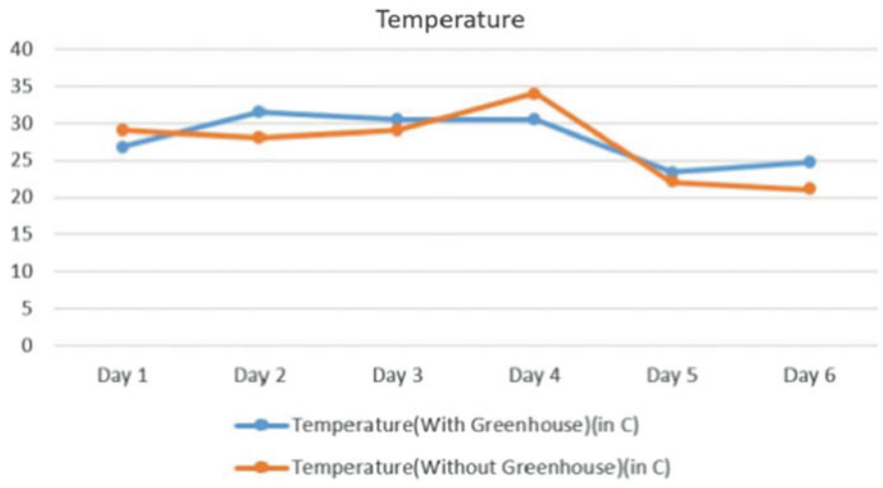

Fig. 8 Temperature graph for analysing temperature inside and outside the greenhouse

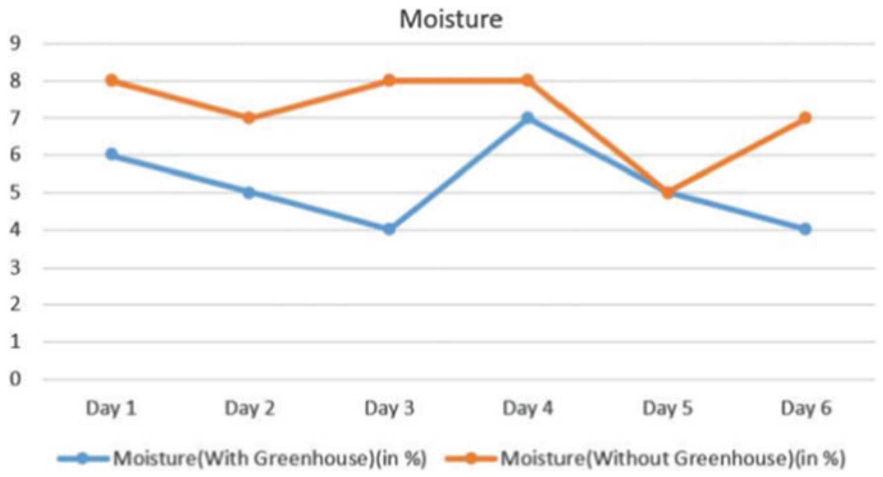

Fig. 9 Graph for analysing moisture level inside and outside the greenhouse

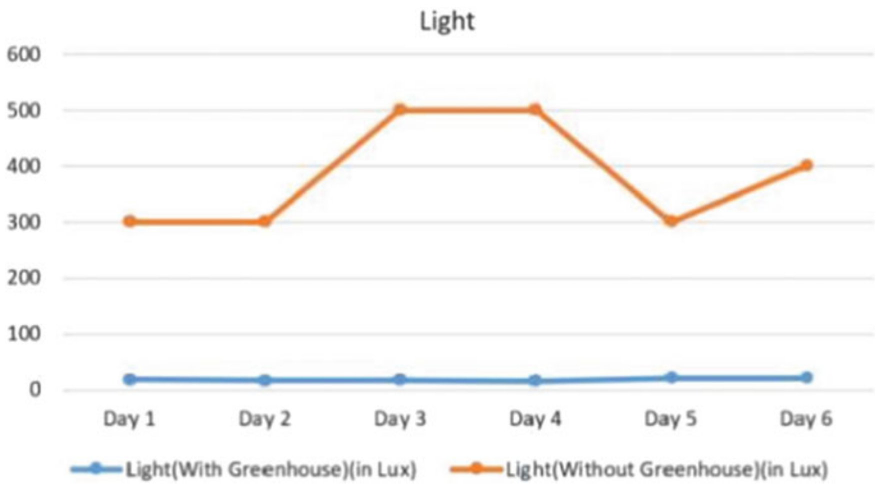

Fig. 10 Light intensity graph inside and outside the greenhouse

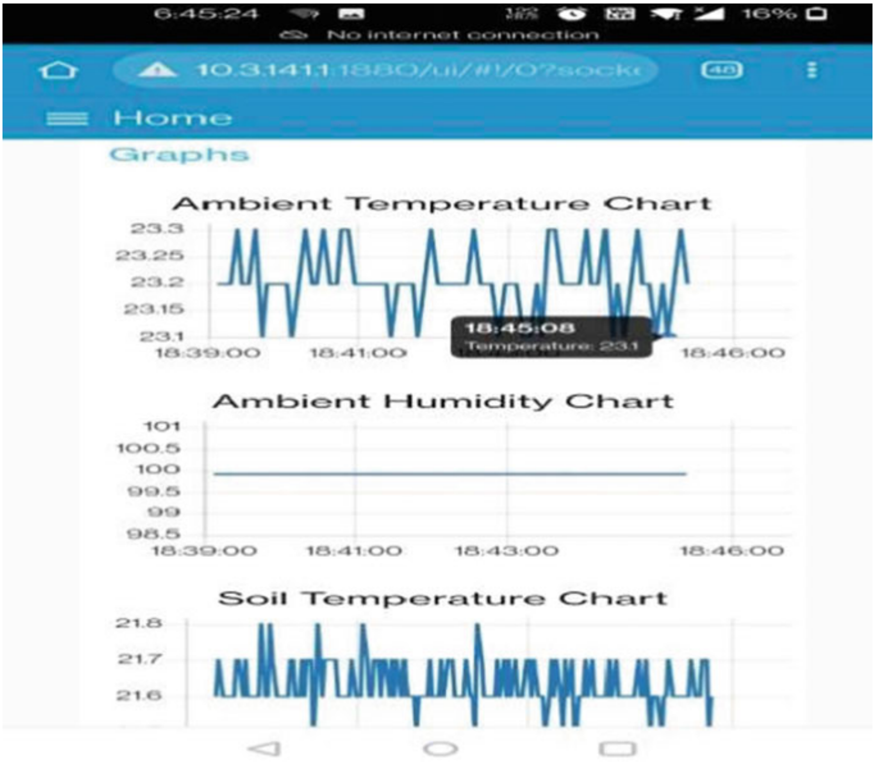

Fig. 11 User control and data representation through MQTT

6 Conclusion

This IoT-based project Utilizing Greenhouse Technology Towards Sustainable Agriculture will bring traditional agricultural systems and new Internet of Things together for complete visibility and automation. So here in the proposed system, it sends information about the temperature using the temperature sensor DHT11, soil moisture using the capacitive soil moisture sensor, humidity using humidity sensor DHT21 and lighting using BH1750. By using this information, the farmer can decide whether to water his farm or not, by turning on the motor using and also can regulate the temperature, humidity and lighting by using his mobile phone sitting at home. The farmer also does not need to worry about the gate being open or closed. Our system will close the door automatically when someone forgets to close the door which will help farmers in good production of agriculture.

References

Chang YS, Chen YH, Zhou SK (2019) A smart lighting system for greenhouse based on Narrowband-IoT. In: IMPACT, 2019. https://doi.org/10.1109/IMPACT.2018.8625804, Electronic ISSN: 2150-5942

Dedeepya P, Srinija USA, Gowtham Krishna M, Sindhusha G, Ganesh T (2019) Smart greenhouse farming based on IoT. In: ICECA, 2019. https://doi.org/10.1109/ICECA.2018.8474713, Electronic ISBN: 978-1-5386-0965-1

Fahim Y, Sarkar T (2018) A project report on IoT based smart farming system. Certificate of Approval. ISSN: 334131097. www.researchgate.net/publication.

Kodali RK, Jain V, Karagwa S (2016) IoT based smart greenhouse. In: Conference: 2016 IEEE Region 10 humanitarian technology conference (R10-HTC). https://doi.org/10.1109/R10-HTC.2016.7906846

Lavanya G, Rani C, Ganeshkumar P (2019) An automated low cost IoT based fertilizer intimation system for agriculture. Elsevier

Mahmood DM (2014) Data acquisition of greenhouse using Arduino. J Babylon Univ/pune Appl Sci 22(7):1908–1916

Microtonics Technologies (2018) IoT based greenhouse monitoring and control system project. Microtonics Technologies

Muthupavithran S, Akash S, Ranjithkumar P (2016) Greenhouse monitoring using internet of things. Int J Innov Res Comput Sci Eng (IJIRCSE) 2(3). ISSN: 2394-6364

Poyen EF, Bhattacharya K, Mondal A, Ghosh A, Bandyopadhyay R (2014) Sensor based automated shading of greenhouse. In: International conference on innovative engineering technologies (ICIET'2014), 28–29 Dec 2014, Bangkok (Thailand)

Shirsath DO, Kamble P, Mane R, Kolap A, More RS (2017) IoT based smart greenhouse automation using Arduino. Int J Innov Res Comput Sci Technol (IJIRCST) 5(2). ISSN: 2347-5552. https://doi.org/10.21276/ijircst.2017.5.2.4

Shiyale PD, Thombre H, Tyagi G, Chauhan A (2020) IoT-based smart greenhouse automation. Int J Creat Res Thoughts (IJCRT) 8(5). ISSN: 2320-2882

Sreekantha DK, Kavya AM (2017) Agriculture crop monitoring using IoT—a study. In: 2017 international conference on intelligent systems and control (ISCO). IEEE, pp 134–139

Vatari, Linlin, Vimal (2019) Automation using IoT in greenhouse environment. J Inf Technol Digit World 01(01). https://doi.org/10.36548/jitdw.2019.1.005. ISSN: 2582-418X

Vernon J (2019) Why do plants grow better in a greenhouse? Hartley Botanic

Enabling Technologies for Effective E-Waste Management

Ezan Abdullah and Khushaima Hilal

Abstract Effective or efficient management of e-waste is considered as preeminent vital challenges of the modern days. The massive scale of e-waste generated and dumped in open landfills or oceans without proper treatment poses severe threat to the environment around the globe. E-waste can be considered as one of the prime root causes of different types of pollution like air, soil, and water. Furthermore, the absence of stringent rules and regulations for proper e-waste treatment, duping, and management also adds to the problem. With these issues as a motivation factor, this paper proposes an efficient e-waste management framework for effectively managing the e-waste. The paper discusses the various issues and challenges of e-waste management. Furthermore, the role of various enabling technologies like IoT, WSN, blockchain, and artificial intelligence in effective e-waste management is also discussed. Finally, some of the best practices and future research directions are proposed.

Keywords E-waste · Blockchain · AI · WSN · Machine learning · GIS

1 Introduction

E-waste is mainly defined as the dilapidated electronic devices that are discarded or expired or they cannot be used for further purpose. It starts generating when the electronic products come to the end of life and no further more useful. E-waste is one of the root causes of globally rising problems in developing countries. E-waste consists of lots of items; some of them are computer, portable digital assistance, video, audio devices, or other electrical and computer equipment. By 2021, more than 60 thousand metric tons of e-waste produced worldwide are causing many harmful health and biological effects especially on health effects such as cancer, reproductive

E. Abdullah (✉) · K. Hilal
Department of Computer Science and Engineering, School of Engineering Science and Technology, Jamia Hamdard, New Delhi 110062, India
e-mail: khanabdullah434@gmail.com

J. K. Deka et al. (eds.), *Emerging Technology for Sustainable Development*,
Lecture Notes in Electrical Engineering 1061,
https://doi.org/10.1007/978-981-99-4362-3_35

health, genetic modification, physical impairment, asthma, tuberculosis, hormonal disorders, and cell function changes.

There are many negative effects on human health and non-living things due to dangerous waste in both ecosystem and health; certain countries show interest or the need for a universal alliance to resolve the challenges and causes of waste hazard. Gadgets have modern and advanced features and affordable price that inspire or attract buyer to invest in new devices and take over from their old devices.

Adanu et al. (2020) described that electronic waste is not the same as e-waste in a literal sense, but a big trade for those involved in the sale and reuse of e-waste. This results in significant e-waste in developing countries due to regulatory standards and poor enforcement laws when it comes to extraction, and they extract precious mineral such as gold, silver, and iron from e-waste. Countries such as Africa, Pakistan India, and Bangladesh have the highest importer of e-waste.

In the report in recent surveys, the under-developing countries are producing e-waste in twice quantity as compared to developed countries. As per the recent surveys, India is the third largest e-waste producer. As a report produced by the global e-waste monitor, the major cause or the source of e-waste generation is due to human activities. It became a major problem with urbanization and the growth of large conurbations.

The proposed system creates a smart or well-maintained e-waste system where buyers can access important safety measures in waste management and reuse their e-waste efficiently. The contribution of the paper is as follows:

- Highlighting the key issues and challenges of effective e-waste management.
- Discussing the role of enabling technologies in effective handling of e-waste.
- Proposed an architecture for effective e-waste management.
- Discussion about the future research directions.

1.1 Motivation

E-waste possesses countless threats to living and non-living things. It has a very major effect on privacy and data security. Thus, there is a necessity to hold e-waste continuously to minimize the damaging effects and minimize crimes. The unprofessional handling of e-waste and unsupervised dumping in landfills possess severe health hazards. Taking this as a motivation, this paper proposes an efficient architecture for effective handling of e-waste.

2 Related Work

This section discusses the various ultra-modern in effective e-waste management.

2.1 E-Waste Management with the Help of Blockchain

Blockchain was invented or introduced by **Satoshi Nakamoto**; it is mainly defined as a model which is used for recording information in a way that it becomes difficult, or we can say that it is impossible to modify or to do some changes or hacking the system. Blockchain is considered as a digital ledger of transactions that is distributed and duplicated across the whole network of computer systems which are the part of that blockchain. Blockchain is a type of Distributed Ledger Technology (DLT) in which transactions are written down with an unchangeable cryptographic signature called as hash. We can use blockchain for managing or tracking the e-products, and blockchain uses smart contracts to for tracking and managing.

There are many papers describes blockchain technologies for e-waste management Kouhizadeh and Sarkis (2018), Gupta and Bodi (2018), Sahoo et al. (2021), Chaudhary et al. (2021), Farizi and Sari (2021), and many other papers describes we take idea from them.

Ongena et al. (Huang and Koroteev 2021) describe that this approach depends upon smart contracts which are made using blockchain technology; with the help of this technology, they can bring administrative bureau, buyer, and stakeholders to the same blockchain program; and this will lead to improved awareness and higher clarity in the process.

The vision will authorize smart contracts to easily describe the objectives of the collection and punish the right team when needed. In blockchain, the validation of the trust which gives access to the parties to record and trace information plays an important role. In blockchain, data and information are immutable.

2.2 E-Waste Management Using Machine Learning

Many researchers have done extensive work using the machine learning for effective management of e-waste (Shaikh et al. 2020; Hussain et al. 2020; Nowakowski and Pamuła 2020; Aswani et al. 2021). Machine learning is generally known as give learning or train a machine in a way that machine can improve automatically through experience and by the use of data, or it is a study of computer algorithms and data structures. It comes under or we can say that it is a part of artificial intelligence. We can learn machines in two ways: supervised and unsupervised; the machine learning algorithm is used in various programs, i.e., ATM machines, e-mail filtering, banking sector, social networking, and where it is impractical or unrealizable to develop standard algorithm to perform the needed tasks. There are many research papers related to waste management of e-waste using machine learning. Huang and Koroteev (2021) described e-waste management using machine learning and artificial intelligence. A collection of new innovative machinery mechanized by artificial intelligence allows the industry to deliver composite waste smartly. This program uses sensors of artificial intelligence and tools to determine what is in the live migration. AI detectors are a significant real-time development for common visual solutions.

This method was the machine learning operating-driven problem-solving framework to plan energy and waste management.

The main motive of this framework is to integrate machine learning with neural network. The number of wastes is forecasted using the neural network. It is a better machine learning algo which facilitate upgrade the waste compilation on energy cost build on strained energy markets.

In the Logan City Council area of Queensland, the evaluation of monthly waste output has been certified in four expert systems algorithms including adaptive neuro-fuzzy inferences, support vector machine, ANN, and K-nearest neighbors.

According to a recent study of off-shelf IoT-based waste management associated with backend data analysis for waste disposal combined with active waste. Raspberry Pi and ultrasonic sensors are installed in waste tanks to control waste in a specific community. To separate the current and possible times of waste disposal, they use in-depth learning algorithms and the actual status of the bin.

The suggested model (MLDPAF) enhances waste execution movement that includes components recovery and energy. This method includes machine learning and neural network for the better future arrangement of waste management and energy. In this model, they predicted the waste with the help of artificial neural network that approximates the waste formation weekly as compared to each number that is considered.

2.3 E-Waste Management Using Geographical Information System (GIS) as Decision Support Tool

There are many researchers which have done extensive work using geographical information system as decision support tool for effective management of e-waste (Mangaonkar et al. 2014; Widmer et al. 2005; Shanmugapriya and Vivek 2016).

A case study has been published in Al Nuzha District, Irbid, Jordan, and showed the importance of using a GIS that is defined as a decision-making tool for municipal solid waste management planning (Gutierrez et al. 2015). With effective collection and transportation of e-waste, they reduce the time, cost, and effort required by municipalities for these services.

GIS tools typically refresh the network and create collection track for trucks, garbage collection vans, etc. The result of this model shows in each round around 2880.2 m traveling distance sharp reduction and in percent of existing in very large quantities of bins from 25% to zero.

The main purpose of this study is to organize a sample study to calculate selected methods and to expand new geospatial data-based approaches that can assist in better planning the selection process within the Great Irbid Municipality (GIM) limited assets.

In GIS, we use orthoimage of the workspace which was also used and worked to modernize maps by scanning new routes and expanding them as the formation of new characters in data.

Methodology of Using DIS

Initially, we need to collect data and adjust the data which should have to be updated each time the model used as other roadways and obstacles change over time depending on the management of the city.

Finally, a small distance was a key requirement for route adjustment to include all regional drums in such a way that we could assess the results with high quality and conclusions with high justifiability; after using hypothesis testing, statistical analysis was performed. Research provides effective ways to deal with complex decisions and increase the effectiveness of waste collection with bounded resources.

2.4 E-Waste Management Using Location Intelligence

There are many researches done on e-waste management using location intelligence (Shanmugapriya and Vivek 2016; Zhu 2014; Nowakowski et al. 2018). Gutierrez et al. (2021) described waste collection system location intelligence in this paper; they demonstrate how IoT consolidates with data access networks. This paper elaborates an efficient selective collection of waste which depends on delivering intelligence to trash cans; this technique starts working with the use of clustering and routing algorithm which minimizes the waste collection cost that is proposed.

In this process, we use the shortest path spanning tree algorithm that is used to calculate the short distance between a two-point area and GIS data for city roads. In this case, we also use a genetic algorithm, which helps to collect trajectory cycles that contain a specific set of trash cans. It fixed an integrated development problem.

The result shows that under the same conditions, we can create a waste collection system in a real waste disposal system that improves waste collection efficiency by having when waste is collected, on the same day and we can reduce the trash can element. Excessive e-waste that will not be when the garbage cans are full.

2.5 E-Waste Forensics

E-waste forensics plays a very vital role; there are lots of researchers to do research on e-waste forensics (Osibanjo and Nnorom 2007; Nnorom and Osibanjo 2008; Doyon-Martin 2015). Kapoor et al. (2021) describe e-waste forensics. In addition to ecological, social, and health effects, e-waste is also a warning to data confidentiality and security and creates related crimes. As e-waste production increases with the adoption of electronic devices, e-waste-related prohibited activities have also increased.

E-Wastes and Crimes

There are three broad categories that include the e-waste-related crimes.

(1) Smuggled e-waste business.
(2) Ecological crimes.
(3) Digital and high-tech crimes.

Smuggled E-Waste Business

A giant amount of e-waste originated by distinct countries is delivered for disposal to some under-developing countries. The transportation of e-waste among different destinations that are developed and under-developing has led to a dramatic increase in illicit trade.

Ecological Crimes

The criminal category is assigned to ban activities that affect any abuse or infringement of ecological laws, thereby ensuing in ecological destruction being punished under national laws.

Digital and High-Tech Crimes

Digital devices and media storage contain sensitive information. Therefore, we should have to take care during disposal of these devices to protect the confidentiality of data saved on them and its security. Gadgets and storage devices such as cell phones, computers, hard drive, and USBs are discontinued and joined to e-waste.

Most of the consumers are not aware of that this confidential information remains available on the devices even if it is erased or directed to the recycle bin or when the hard drive is formatted.

Another article also proposed that Ghana is the seventh largest cybercrime country in the world, and many advisers have settled a link between cybercrime and waste disposal ground (Fig. 1).

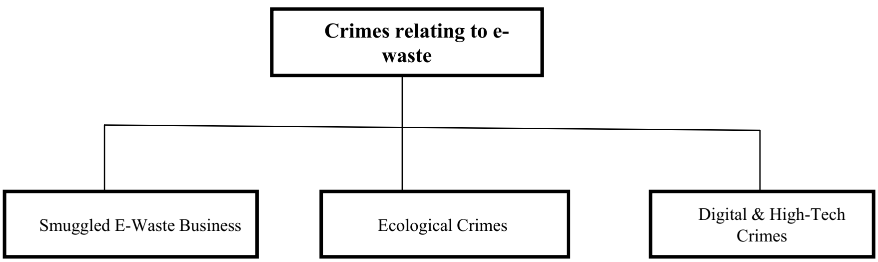

Fig. 1 E-waste-related crimes

Preventive Management Measures

In order to reduce crime, there is a very essential need to present these types of all cases in the court, leading to the execution of some of the protective measures which should have been taken to decrease the crime rate which occurs due to mismanagement of e-waste including strengthening the national legal framework by adding relevant fines, penalties, and alternative punishment.

Environmental crime is a branch of forensics science that focuses on applying scientific knowledge in detecting natural crime and any pollution of natural resources through human activities. The countrywide Green Tribunal Act 2010 turned into established to prosecute local crime to make amends for these offenses. Forensic geology, also known as geo-forensics or forensic soil technology, refers to using a selection of recognized techniques in world technological know-how to resource studies or investigations that can be subject to law. E-waste carries many threats to the environment, human fitness, society, information, safety, and privacy. Hence, there may be a need to control e-waste wisely which will reduce dangerous consequences and reduce crime. Strict rules and legislation must be applied to make sure proper and secure control and disposal of e-waste. It is also very crucial to be privy to the diverse components of e-waste which include various crimes that can position the lives of customers at amazing danger.

2.6 E-Waste Management Using Deep Learning and IoT

Several researchers have done extensive work using the integration IoT and deep learning for efficient execution of e-waste (Wang et al. 2021; Sheng et al. 2020). Rahman et al. (Sahoo et al. 2021) describe waste management system using deep learning intelligently with IoT. With the help of deep learning and IoT, we can make an agile solution for selection and real-time data monitoring. In this model, they make a combination of two parts, namely in the first element, we are able to do waste classification via convolutional neural network, and in the second component, they make constructive architecture of smart waste cans. With the help of IoT, we will display data in actual time, and structural models are becoming remarkable outcomes inside the field of waste execution. In the beginning, we can divide e-waste into two wide species of digestible and indigestible waste. We can do waste classification using deep learning technologies. After completing this, we should upgrade the IoT application to work and set up a dashboard on a web server that ensures simultaneously observing the information over the internet. When this process is completed, we cross on to educate our model with machine learning to differentiate non-digestible substances. We use database to store the data in which we store all the data related to all types of scrap, and with the help of database and security, we can reduce crimes related to e-waste forensics. The research is performed via a hard and fast development procedure to make sure an effective waste control management. In the version of waste disposal structures the usage of the Raspberry Pi in addition to the camera module along with the deep learning mechanism.

3 Challenges or Issues Related to E-Waste

3.1 Volume of E-Waste Generated

Generation of e-waste around 200+ metric tons per year causes many harmful effects, and there is no proper disposal of e-waste that occurs; developed countries send their e-waste to developing countries.

3.2 Child Labor Involvement

Mainly, poor children's lives in slum areas quit studying in early age and start working in workshops; a population around 4.5 lakh of age group (10–14 yrs.) is working in workshops. Child labor is an offensive crime but only in papers.

3.3 Ineffective Legislation

Legislation plays a very vital role in every field of every country, but there is an absence of information on most of the SPCB'S/PCC websites. A big failure occurs in the implementation of E-Waste Management and Handling Rule 2012.

3.4 Lack of Infrastructure

Infrastructure plays a very vital role in e-waste management, but there is no collection, and take back mechanisms take place only when the electronic wastes are taken by illiterate rag-pickers.

3.5 Health Hazards

E-waste management contains over the thousands of toxics which are decomposed into soil and groundwater, and they cause many harmful diseases and harms for animals also.

People dispose chemicals in dustbin like lead, CFCs, and discharged batteries into dustbins.

3.6 Lack of Incentives Schemes

The working environment in the informal recycling sector is much worse than in the legal industry than programs to encourage producers who do something to manage e-waste. Products manuals and guide books are in particular languages, and mainly people throw out them or they do not read guide books. And the information is not given on websites.

3.7 Poor Awareness and Sensitization

Only 5% of individuals think of impact on environment; rest of the 95% dispose their electrical and electronic equipment into waste or sell them at cheaper rates to rag-pickers or street vendors.

3.8 E-Waste Imports

Mainly developing countries like America, China, and Russia send their e-waste to under-developing countries like India, Sri Lanka, Pakistan, etc. which causes a big amount of cross-border flow of e-waste.

3.9 Security Incrimination

At the end of computer's life, they may contain sensitive personal information. And bank account details which if not deleted leave a chance for fraud.

3.10 Heavy Budget of Setting Up Recycling Facility

Multinational companies are not providing recycling facilities because a huge amount of money is required to make a recycling setup and less chances of profit in recycling process. Transportation cost varies from place to place; machine fuels and servicing cost also come.

3.11 Lack of Research

Due to less scholarship fund people do not do research on this topic and lack of research people do not do appropriate disposal practices

3.12 Unwillingness of Authorities

There is a lack of co-operation between the various authorities responsible for e-waste management and disposal, including the exclusion of municipalities.

4 Laws Related to E-Waste

The first international e-waste law enacted in 1989; this law is known as the Basel Convention; and the main purpose or objective of this law is to reduce the flow of hazardous waste among nations, especially this law is designed to prevent the transfer of hazardous waste from developed countries to countries they are still developing. The Basel Convention also guarantees proper environmental management of toxic and hazardous waste. This meeting has made an indirect application to e-waste due to the presence of toxic and dangerous substances up to that point.

The conference was held in 2002 with the adoption of The Mobile Phone Partnership Initiative (MPPI). Thereafter adopted the Nairobi Declaration which authorizes clerks to exercise reasonable environmental control of e-waste.

The E-waste Act was later revised in 2016 and became e-waste management laws, 2016. In 2016, for the first time the concept of Extended Manufacturing Production (EPR) was also introduced making manufacturers responsible for the safe disposal of electronic goods. The rules of e-waste management, 2016 have been changed by the Agency; video notification G.S.R. 261 (E) 14, dated 22 March 2018 to expedite the effective implementation of e-waste management in a reasonably prudent manner and to amend the collection objectives under the EPR provision.

5 Proposed Solution

As e-waste is a major worldwide problem, so we make strict guidelines and give training to all the workers which are working in scrap factories, and we create a proper criterion of using electronic products. Government should make strict laws and start awareness programs and teach people how they trash their e-waste.

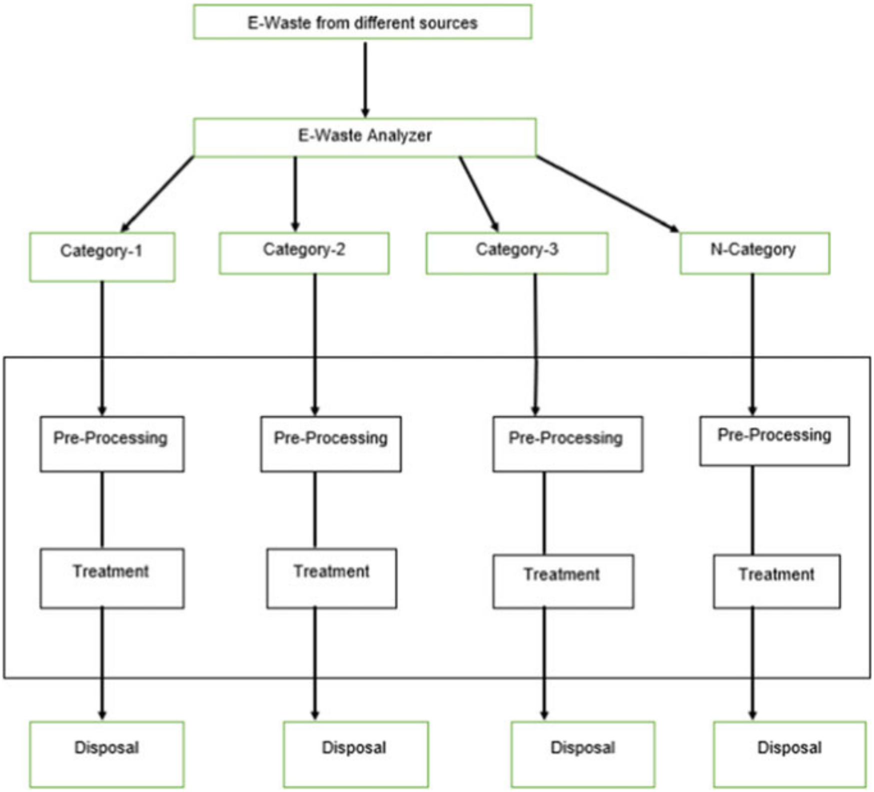

Fig. 2 E-waste management architecture

We have proposed a solution of waste management using a combination of blockchain, machine learning, and artificial intelligence. Figure 2 shows the proposed approach.

We can connect all the trash cans with a specific bar code and put object recognition system on all the trash cans; when someone put their waste to that trash can, they scan that object and send a message or an alert to the head center of that particular area; all the waste collecting vehicles work on geographical information system; with the help of this system, vehicles will cover minimum distance with a specific amount of time, and each product list is available to the head department so the stolen of e-waste is not possible all the dumping ground under CCTV surveillance and a monthly forensics survey done on dumping ground.

And on dumping ground we have to make three sections where we categorize the quality of wastes with the help of labor.

We can track or manage e-waste with the help of blockchain using smart contracts; each block of blockchain uses a block; each block has its own hash number; we can consider each block as an electronic product; when we want to trash e product, we can track them easily and do proper management of that; and with the help of machine learning using artificial intelligence, we can scan trash cans which type of e-products is disposed into it.

With the help of deep learning and IoT, we can provide a quick solution to classification and real-time monitoring. We can also make smart trash bins in which we can put multiple sensors like ultrasonic sensors for scanning the trash bins, load measurement sensor for measuring the load, and micro-controller for controlling the functions of e-waste trash bins; we can manage these sensors using cloud server and Android application. We can separate waste with the help convolutional neural network and architectural design of smart garbage boxes. The sensors first send and receive an ultrasound to measure the empty level of the garbage boxes.

We can connect dumping grounds and trash bins with the help of Bluetooth and Wi-Fi, the system will send the data via cloud server, and Bluetooth connection leads to monitor the data through the Android app.

We can classify waste convolutional neural network (CNN). It extracts features from images. CNN, because of its high accuracy, is largely used for image classification.

With the help of advanced technologies like artificial intelligence and machine learning, we can decompose e-waste in a proper manner or we can easily recycle it and use for further purpose, and we can give training to people how to recycle e-waste through video tutorials.

References

Adanu SK, Gbedemah SF, Attah MK (2020) Challenges of adopting sustainable technologies in e-waste management at Agbogbloshie, Ghana. Heliyon 6(8):e04548

Aswani T et al (2021) Automated E-waste disposal using machine learning. VIVA-Tech Int J Res Innov 1(4):1–7

Chaudhary N (2018) Electronic waste in India: a study of penal issues. Image 1:2

Chaudhary K et al (2021) Blockchain: a game changer in electronic waste management in India. Int J Integr Supply Manag 14(2):167–182

Doyon-Martin J (2015) Cybercrime in West Africa as a result of trans-boundary e-waste. J Appl Secur Res 10(2):207–220

Farizi TS, Sari RF (2021) Implementation of blockchain-based electronic waste management system with hyperledger fabric. In: 2021 2nd international conference on ICT for rural development (IC-ICTRuDev). IEEE

Gupta N, Bedi P (2018) E-waste management using blockchain based smart contracts. In: 2018 international conference on advances in computing, communications and informatics (ICACCI). IEEE

Gutierrez JM et al (2015) Smart waste collection system based on location intelligence. Procedia Comput Sci 61:120–127

Hatamleh RI et al (2020) The use of a GIS system as a decision support tool for municipal solid waste management planning: the case study of al Nuzha District, Irbid, Jordan. Procedia Manuf 44:189–196

Huang J, Koroteev DD (2021) Artificial intelligence for planning of energy and waste management. Sustain Energy Technol Assess 47:101426

Hussain A et al (2020) Waste management and prediction of air pollutants using IoT and machine learning approach. Energies 13(15):3930

Kapoor N, Sulke P, Badiye A (2021) E-waste forensics: an overview. Forens Sci Int: Anim Environ 1:100034
Kouhizadeh M, Sarkis J (2018) Blockchain practices, potentials, and perspectives in greening supply chains. Sustainability 10(10):3652
Mangaonkar N, Sabhani P, Sirsat S (2014) Green technology for avoiding E-waste with the help of GIS. In: 2014 international conference on advances in communication and computing technologies (ICACACT 2014). IEEE
Nnorom IC, Osibanjo O (2008) Electronic waste (e-waste): material flows and management practices in Nigeria. Waste Manag 28(8):1472–1479
Nowakowski P, Pamuła T (2020) Application of deep learning object classifier to improve e-waste collection planning. Waste Manag 109:1–9
Nowakowski P, Szwarc K, Boryczka U (2018) Vehicle route planning in e-waste mobile collection on demand supported by artificial intelligence algorithms. Transp Res Part D: Transp Environ 63:1–22
Osibanjo O, Nnorom IC (2007) The challenge of electronic waste (e-waste) management in developing countries. Waste Manag Res 25(6):489–501
Rahman MW et al (2020) Intelligent waste management system using deep learning with IoT. J King Saud Univ Comput Inf Sci
Sahoo S, Mukherjee A, Halder R (2021) A unified blockchain-based platform for global e-waste management. Int J Web Inf Syst
Shaikh F et al (2020) Waste profiling and analysis using machine Learning. In: 2020 second international conference on inventive research in computing applications (ICIRCA). IEEE
Shanmugapriya E, Vivek N (2016) A waste and e-waste management—an overview. In: Swarnalatha C (ed) Entrepreneurship and management: innovative construction techniques and ecological development, vol 2. Civil engineering, p 109
Sheng TJ et al (2020) An internet of things based smart waste management system using LoRa and tensorflow deep learning model. IEEE Access 8:148793–148811
Wang C et al (2021) A smart municipal waste management system based on deep-learning and Internet of Things. Waste Manag 135:20–29
Widmer R et al (2005) Global perspectives on e-waste. Environ Impact Assess Rev 25(5):436–458
Xavier LH, Adenso-Díaz B (2015) Decision models in e-waste management and policy: a review. Decis Models Eng Manag 271–291
Zhu X (2014) GIS and urban mining. Resources 3(1):235–247

Modeling and Simulation of Successful Signal Transmission Without Information Loss in Axon

Biswajit Das, Satyabrat Malla Bujar Baruah, and Soumik Roy

Abstract When a nerve signal propagates through a nerve fiber, it is subject to a number of processes, including those of the extracellular space (ECS) attenuation due to the longitudinal or axial resistance, etc. The information content of the signal is of much importance as it has to reach the desired location with maximum amount to signal having being retained throughout its journey along the fiber. Studies have shown that the nerve anatomy along with the surrounding extracellular medium plays a very important role in facilitating the signal transmission from the site of generation to distant places along the fiber. In this work, effort has been made to understand the similarity of the neuronal signal between two distinct locations of an axon. Initially, an action potential or nerve impulse is considered to be generated at a node of Ranvier, and the similarity of the signal at the subsequent node of Ranvier after propagating via a myelinated segment is computed. The results obtained show that the length of the nerve fiber has a key role to play in retaining the overall information content of the nerve signal, and also it is observed that there must be some critical length of the nerve fiber so that the information is not lost as it propagates from one region of the fiber to the other.

Keywords Nerve conduction · Extracellular conductivity · Signal similarity · Cable · Correlation

---

B. Das (✉) · S. Malla Bujar Baruah · S. Roy
Department of ECE, Tezpur University, Tezpur University Campus, Napaam, Dist-Sonitpur, Assam 784028, India
e-mail: biswajit700@tezu.ernet.in

S. Roy
e-mail: xoumik@tezu.ernet.in

J. K. Deka et al. (eds.), *Emerging Technology for Sustainable Development*,
Lecture Notes in Electrical Engineering 1061,
https://doi.org/10.1007/978-981-99-4362-3_36

1 Introduction

An action potential is generated when a nerve fiber is stimulated by an external stimulus or when it receives a signal from a neighboring neuron. The membrane potential is affected by the unequal distribution of sodium (Na^+) and potassium (K^+) ions on each side of the neuronal membrane as the carriers actively move these two ions. A nerve fiber may be myelinated or non-myelinated or it may contain regions of myelination followed by a demyelinated section. It is understood that a signal undergoes little to no attenuation as it travels through a myelinated section since a myelin layer acts as an insulator preventing ions to escape toward the external medium (Simons and nave 2016; Morell and Norton 1980). The nerve signal undergoes salutatory conduction in the presence of a myelin sheath enabling faster conduction of the neuronal impulse (Stämpfli 1954; Stadelmann et al. 2019). The part of the fiber in which an action potential is generated is called an active fiber, and a passive fiber is one which only facilitates the movement of the action potential (Scott 1975). The inward and outward migration of ions is required for the production of an action potential, which happens at places where there is no myelination, primarily at the Ranvier nodes. The shape and size of the fiber also play an important role in the signal transmission as the velocity of the signal transmission is found to be higher in a larger fiber than in a smaller one (Blijham et al. 2006; Waxman 1980; Hursh 1939); this is because a fiber with greater diameter offers little resistance to the flow of the ions along the length of the fiber. Thus, the fiber anatomy is found to play a huge role in signal transmission.

The region around a nerve fiber which is consists of pool of ions is termed as the extracellular space (ECS) (Syková and Nicholson 2008; Barros et al. 2011; Nicholson and Hrabětová 2017). The extracellular space is found to have a significant role when it comes to signal transmission through a nerve fiber as the size of the extracellular space plays a key role in signal transmission. Studies have shown that when the extracellular space is large, more signal attenuation takes place in comparison with a smaller extracellular space as a larger extracellular space offers more mobility of ions from the fiber toward the extracellular media (Bédard and Destexhe 2013; Baruah et al. 2021). Thus, the role of extracellular space shall not be neglected while dealing with nerve signal transmission. Therefore, it can be said that the overall combination of the extracellular space and fiber anatomy plays a significant role in the signal transmission via a nerve fiber.

One of the most important factors in understanding how much of the original signal is retained as it propagates along the length of the fiber is by understanding the signal similarity or correlation of the signal between the concerned segments (Pospisil and Bair 2021; Kohn et al. 2016). Correlation can be described as the extent of association between two signals at different section of the nerve fiber parts (Asuero et al. 2006; Cohen and Kohn 2011). In this work, similarity between the initially generated impulse and the signal at the successive node of Ranvier after passing through a myelinated segment is computed for different fiber length. The results show some key insights as to how the fiber length plays a significant factor in retaining the information content of the signal.

2 Proposed Model

The proposed model is based on Rall's equivalent cable model (Goldstein and Rall 1974; Rall 2011), which represent the nerve fiber as an analogous cable. In this work, an action potential is considered to be generated at the node of Ranvier which then propagates forward via a myelinated segment on to the next node of Ranvier. The representation of the proposed model is shown in Fig. 1. The equivalent electrical circuit of the proposed model is shown in Fig. 2.

In this work, the similarity between the signals at two successive node of Ranvier is computed. This similarity shows the amount of information that is retained as it passes along the nerve fiber. Figure 1 shows a basic outline of the proposed model, a signal is considered to be generated at the first node of Ranvier, and then, it gets propagated along the fiber through a myelinated segment to the next node of Ranvier. When this signal travels and enters the myelinated chamber, it undergoes passive transmission due to the nature of the channel and encounters attenuation of the signal due to the axial resistance against propagation. When this propagating signal re-enters in the next node of Ranvier, due to presence of active ion channel, re-encoding of the signal takes place corresponding to amount of current delivered to the node after propagation losses. This arrangement of structures in axon is represented with equivalent electrical circuit as shown in Fig. 2, and the active membrane is

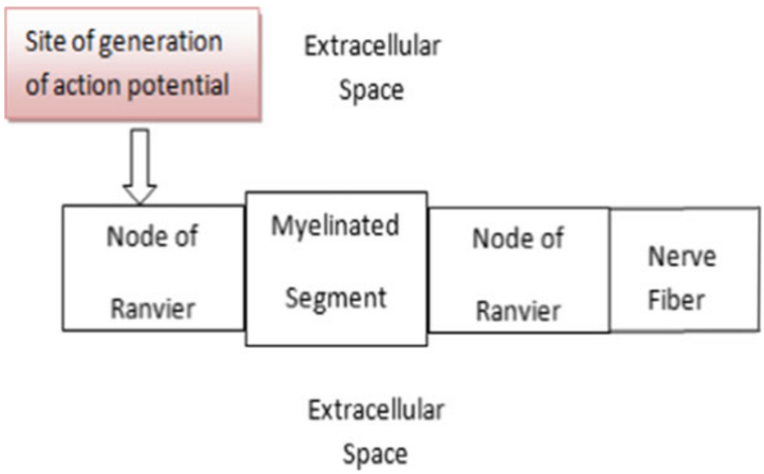

Fig. 1 Representation of the proposed method

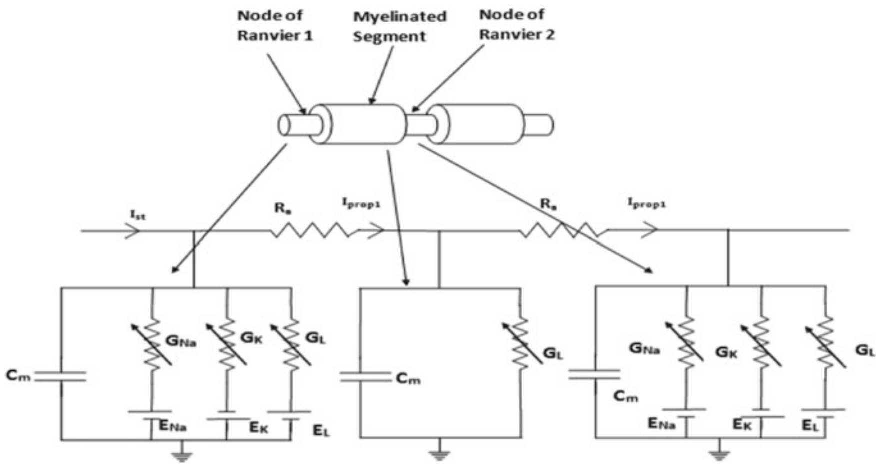

Fig. 2 Modified circuit with the H–H model on the right now is depicted by its passive elements only

inspired from the H–H model (Hodgkin and Huxley 1952), whereas the passive membrane is inspired from model discussed in Das et al. (2019).

3 Mathematical Derivations

Initially, a spike train of duration of 1–8 ms and 15–22 ms is taken as an input to the initial node of Ranvier which is given as I_{st} in Eq. 1. Since the first tank circuit is an active membrane, its resultant mathematical expression can be given by the Hodgkin and Huxley (H–H) equation which is shown as

$$I_{st} = C_m \frac{dV_m}{dt} + G_{Na}(V_m - E_{Na}) + G_K(V_m - E_K) + G_l(V_m - E_l) \tag{1}$$

Experiments by Hodgkin and Huxley have shown that the ion permeability of ions can also be represented by their ionic conductances, viz. G_{Na}, G_K, and G_L, respectively. They have also shown that these permeabilities can be further expressed as $G_{Na} = \overline{g_{Na}} m^3 h$, $G_k = \overline{g_k} n^4$, $G_L = \overline{g_l}$ where m^3 and h are the activation variable for sodium ions n^4 is the activation variable for potassium ions, respectively.

$$\frac{dn}{dt} = \propto_n (V_m)(1-n) - \beta_n(V_m)n$$
$$\frac{dm}{dt} = \propto_m (V_m)(1-m) - \beta_m(V_m)m$$
$$\frac{dh}{dt} = \propto_h (V_m)(1-h) - \beta_h(V_m)h$$

Here, $\propto_i$ and β_i are rate constants for the ith ion channel that depends on voltage but not time n, m, and h are dimensionless quantities between 0 and 1 that are associated with potassium channel activation, sodium channel activation, and sodium channel inactivation, respectively, and are represented by Boltzmann equations as functions of the membrane potential. From the Hodgkin and Huxley expression, α and β can be expressed as

$$\propto_n\,(V_m) = \frac{0.01(V_m+50)}{1-\exp\left(\frac{V_m+50}{-10}\right)},\quad \propto_m\,(V_m) = \frac{0.1(V_m+35)}{1-\exp\left(\frac{V_m+35}{-10}\right)}$$

$$\propto_h\,(V_m) = 0.07\exp\left(\frac{V_m+60}{-20}\right),\quad \beta_n(V_m) = 0.125\exp\left(\frac{V_m+60}{-80}\right)$$

$$\beta_m(V_m) = 4\exp\left(\frac{V_{m+60}}{-18}\right),\quad \beta_h(V_m) = \frac{1}{1+\exp\left(\frac{V_m+30}{-10}\right)}.$$

Here, V_m is the resting membrane potential which is about – 60 mV. These equations are empirical which is dependent on the equations describing the movement of a charged particle in an electric field, and it is the physical model of a gate moving within a channel to open and close. Now, Eq. 1 can be rearranged as follows:

$$\frac{\mathrm{d}V_{\mathrm{mnode1}}}{\mathrm{d}t} = -\frac{1}{C_m}[(\mathrm{G}_{\mathrm{Na}}(V_{\mathrm{mnode1}} - E_{\mathrm{Na}}) + G_{\mathrm{K}}(V_m - E_{\mathrm{K}}) + G_{\mathrm{l}}(V_m - E_{\mathrm{l}}) + I_{\mathrm{st}})] \tag{2}$$

The current which is leaves the first node of Ranvier acts as an input to the next section of the nerve fiber which is the myelinated segment. This current can be expressed as

$$I_{\mathrm{prop1}} = \frac{V_{\mathrm{mnode1}} - V_{\mathrm{mnodemye1}}}{R_a} + \text{Leakage current} \tag{3}$$

For a myelinated fiber, leakage current is zero, thus Eq. 3 can be rewritten as

$$I_{\mathrm{prop1}} = \frac{V_{\mathrm{mnode1}} - V_{\mathrm{mnodemye1}}}{R_a} \tag{4}$$

Here, I_{prop1} is the propagating current from the node of Ranvier to the myelinated segment. V_{mnode1} and V_{mnode2} are the two input and output node between whom the current is computed. The membrane potential is denoted by V_m. C_m stands for total membrane capacitance, which may be represented as $C_m = c_m D_i l$ in terms of specific membrane capacitance c_m. The internal diameter of the fiber is D_i, while the length of the fiber in question is l. E_{Na}, E_{K}, and E_{l} are the equivalent potentials of sodium, potassium, and leakage ions, respectively. G_{Na}, G_{K}, and G_{l} are the total membrane conductances of the sodium, potassium, and leakage ions given by Hodgkin and

Huxley. R_a is the axial resistance or the longitudinal resistance of the fiber between the two points of interest which can be expressed as

$$R_a = R_i + R_e \tag{5}$$

R_i is the total internal resistance of the fiber, and R_e is the total extracellular space resistance. These resistances can be further expressed by their characteristics resistances as $R_i = \frac{4r_i l}{\pi D_i^2}$ and $R_e = \frac{4r_e l}{\pi D_e^2}$, respectively. Here, r_i and r_e are the characteristics internal and extracellular resistances, respectively. D_e is the extracellular space diameter. Therefore, the resultant mathematical equation governing the passive propagation or the myelinated fiber can be

$$\frac{V_{\text{out}} - V_{\text{in}}}{R_a} + C_m \frac{\mathrm{d}V_{\text{out}}}{\mathrm{d}t} + \frac{V_{\text{out}} - E_1}{R_1} + I_{\text{prop1}} = 0 \tag{6}$$

Equation 6 can be rearranged as

$$\mathrm{d}V_{\text{out}} = \left(\frac{V_{\text{in}} - V_{\text{out}}}{R_a} + \frac{E_1 - V_{\text{out}}}{R_1} I_{\text{prop1}} \right) \frac{\mathrm{d}t}{C_m} \tag{7}$$

Equation 7 gives the membrane potential expression at the myelinated segment. The resultant current that exits the passive membrane can be shown as

$$I_{\text{prop2}} = C_m \frac{\mathrm{d}V_{\text{mnode2}}}{\mathrm{d}t} + \mathrm{G}_{\text{Na}}(V_{\text{mnode2}} - E_{\text{Na}}) + G_{\text{K}}(V_{\text{mnode2}} - E_{\text{K}}) + G_1(V_{\text{mnode2}} - E_1) \tag{8}$$

Rearranging Eq. 8 to obtain the resultant membrane potential can be given as

$$\frac{\mathrm{d}V_{\text{mnode2}}}{\mathrm{d}t} = -\frac{1}{C_m} \left(\frac{V_{m1} - E_{\text{Na}}}{R_{\text{Na}}} - \frac{V_{m1} - E_{\text{K}}}{R_{\text{K}}} + \frac{V_{m1} - E_1}{R_1} + I_{\text{prop2}} \right) \tag{9}$$

Now, the similarity between the signals at the two successive nodes of Ranvier is computed for different length of the fibers. Initially, a multiple spike train of time duration of 1–8 ms and 15–22 ms is taken as an input signal for a fiber of length 80 μm, and the results are computed in MATLAB, then similar experiment is conducted for a fiber of length 50 μm and input spike train of time duration 1–8 ms and 15–22 ms. The similarity between the signals at the two successive node of Ranvier is then computed to observe the signal similarity.

4 Results and Discussion

The initial node is triggered by a multiple spike train of duration 1–8 ms and 15–22 ms which then propagates along the fiber via a myelinated segment to the next node of Ranvier. The similarity between the signal at the first node of Ranvier and then the successive node of Ranvier is computed to see the amount of information that is retained by the original signal. Figure 3 shows the initial input spike train at the initial node of Ranvier, and Fig. 4 shows the spike train at the myelinated segment. It is seen that as the spike train moves from the first node of Ranvier to the passive (myelinated) region, attenuation of the signal occurs; this is due to the decremental conduction of the nerve impulse which takes place due to the presence of the longitudinal resistance along the length of the fiber. A small amount of DC shift is also observed in the passive region due to the passive membrane properties of the nerve fiber which is mainly due to the capacitive properties. Now, the spike train moves from the passive region to the next segment, i.e., to the next node of Ranvier, the resultant membrane potential plot at the second node of Ranvier is shown in Fig. 5. Figure 6 shows the overlapping signal of the initial node of Ranvier and that in the successive node of Ranvier.

From Fig. 6, it can be seen that due to salutatory conduction, the propagating signal renews itself, and the information content of the signal is very much retained with a very small amount of information loss taking place.

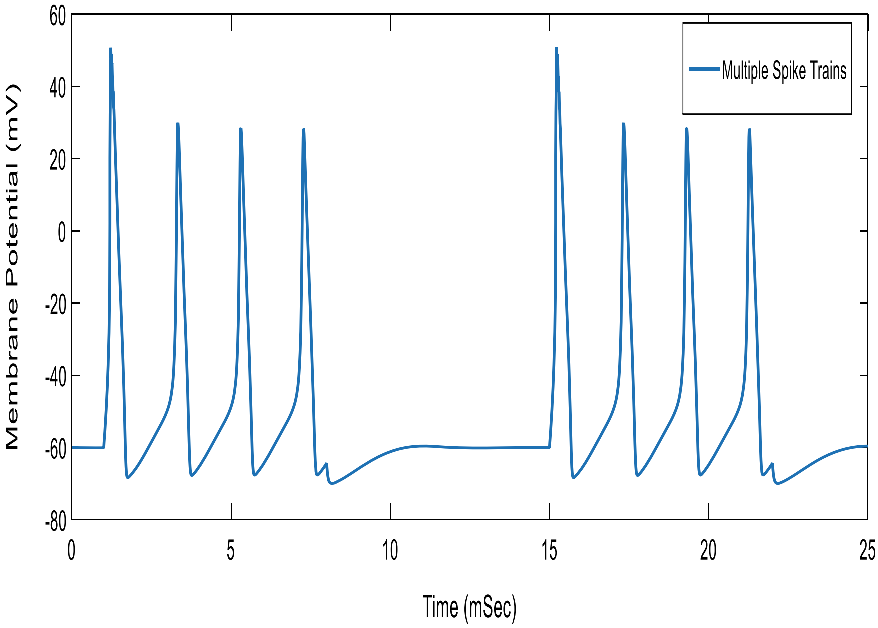

Fig. 3 Initial action potential spike trains of duration 1–8 ms and 15–22 ms at the first node of Ranvier

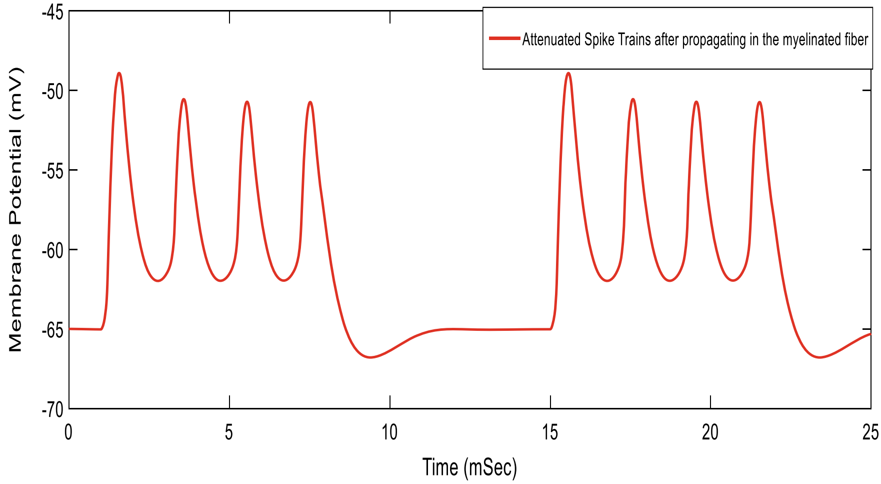

Fig. 4 Attenuated spike train after propagation in the myelinated segment

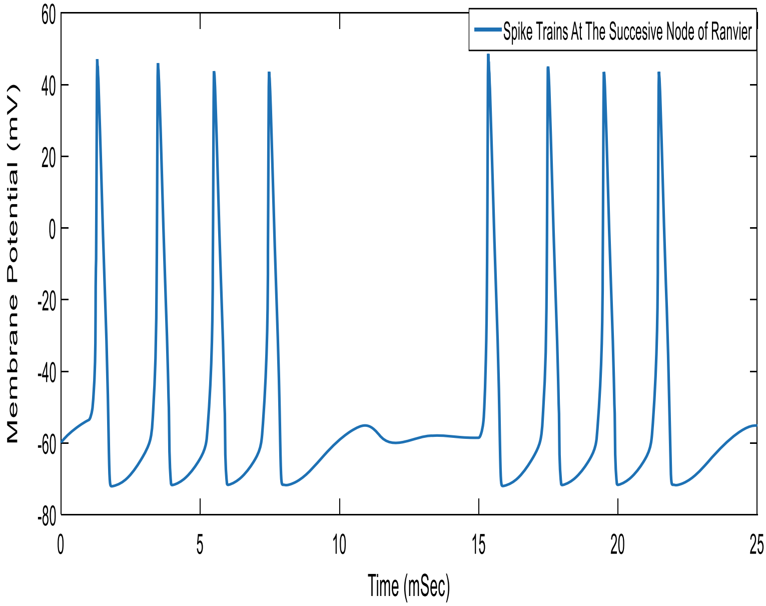

Fig. 5 Spike train at the successive node of Ranvier

Now, the work focuses on computing the same experiments for a fiber with a shorter length, i.e., length of the fiber is considered to be of 50 μm. The resultant plots generated for a fiber of 50 μm are shown from Figs. 7, 8, 9 and 10.

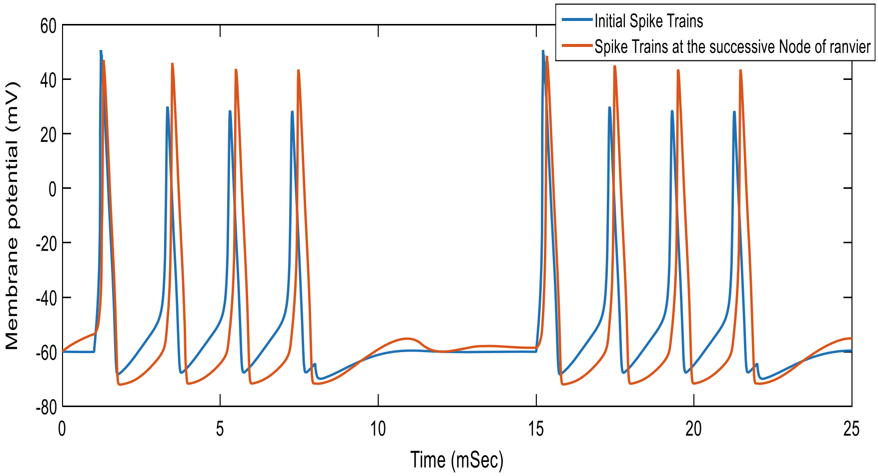

Fig. 6 Overlaying plot of the initial spike train sequence and the spike train at the successive node of Ranvier

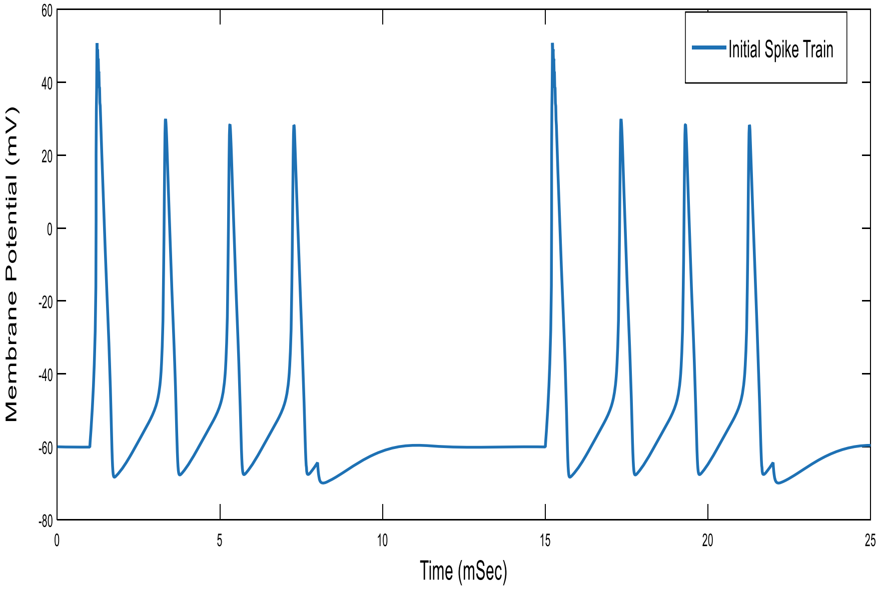

Fig. 7 Initial action potential spike trains of duration 1–8 ms and 15–22 ms at the first node of Ranvier for a fiber of length 50 μm

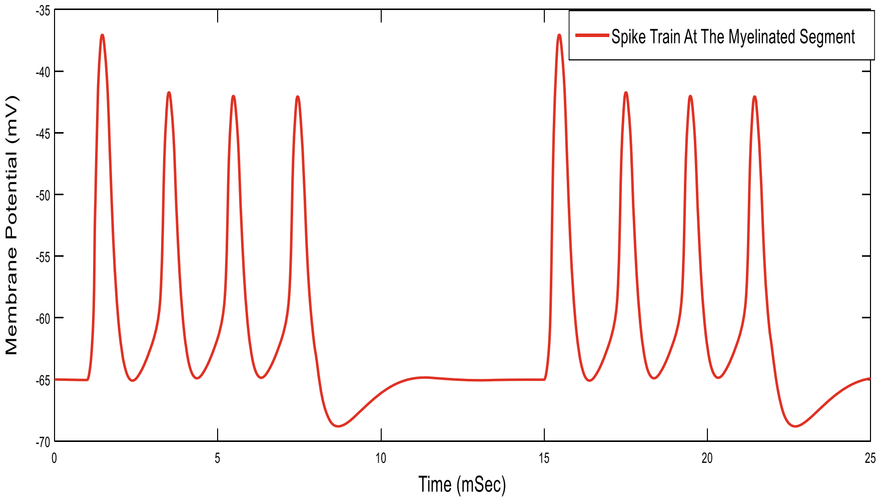

Fig. 8 Attenuated spike train after propagation in the myelinated segment for a fiber of length 50 μm

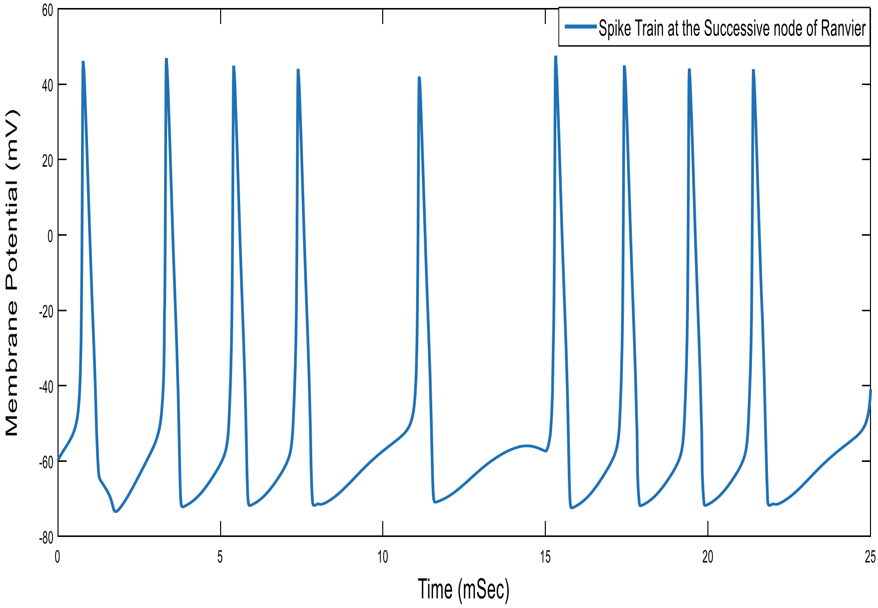

Fig. 9 Spike train at the successive node of Ranvier for a fiber of length 50 μm

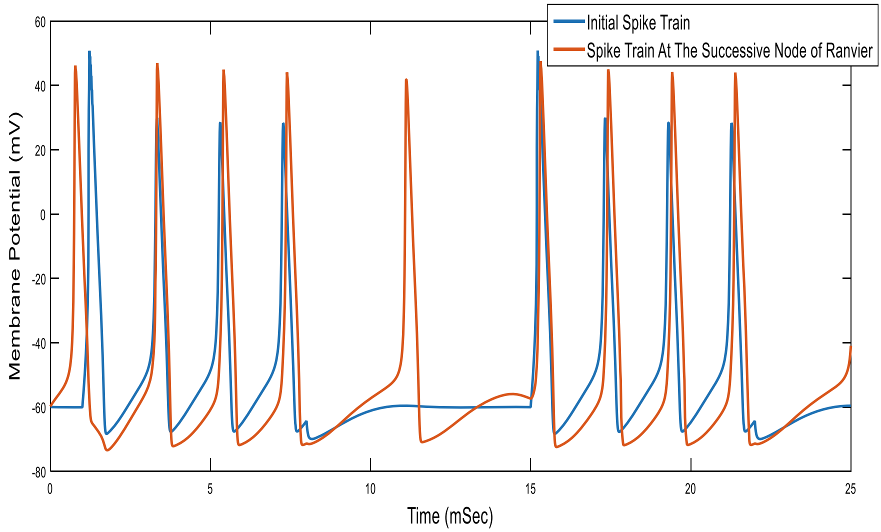

Fig. 10 Overlaying plot of the initial spike train sequence and the spike train at the successive node of Ranvier for a fiber of length 50 µm

It is observed from Figs. 9 and 10 that when a shorter fiber is considered i.e. of 50 µm length, an additional spike is generated at the second node of Ranvier which suggests information mismatch taking place. This is because the delivering current to the next node of Ranvier gets increased. It is known that, $I_{\text{inj}} = I_{\text{delivered}} + I_{\text{losses}}$ where I_{inj} is the initial current due to action potential at the inlet of the fiber, $I_{\text{delivered}}$ is the current delivered at the outlet of the fiber, and I_{losses} is the propagation loss due to axial resistance of the endoplasm such that I_{losses} is inversely proportional to the length of the fiber. Thus, the above equation infers that a shorter fiber results in a decrease in the axial resistance and a decrease in axial current propagation loss, thereby delivering high current at the outlet and vice-versa results in an additional spike get generated at the subsequent node of Ranvier. Thus, it can be said that for a shorter fiber, information mismatch might take place due to high current getting delivered at the node. Section 4.1 shows the simulation parameter considered to conduct the study.

4.1 Simulation Consideration

The simulation parameters used for the experiment are as follows: Characteristic membrane capacitance (c_{m}) is 1 µF/mm^2, resting membrane potential is − 60 mV, and length of the fiber under consideration is 80 µF and 50 µF, respectively. Internal diameter of the fiber (D_{i}) is 5 µm, and extracellular space diameter (D_{e}) is 5 µm. Equivalent potential of sodium ions (E_{Na}) is 55 mV, equivalent potential of potassium ions (E_k) is 72 mV, and equivalent potential of leakage ions (E_k) is − 50 mV. Sodium conductance (g_{Na}) is 1.2 S/mm^2, potassium conductance (g_k) is 0.36 S/mm^2, and leakage conductance (g_l) is 0.003 S/mm^2.

5 Conclusion

In this work, the similarity between two segments of a nerve fiber, i.e., between an initial node of Ranvier where the action potential generates and the subsequent node of Ranvier is computed. Initially, the length of the fiber is taken to be of 80 μm and input spike train of duration 1–8 ms and 15–22 ms is taken to trigger the fiber at the first node of Ranvier. In this case, it is found that the signal more or less tends to remain intact as it passes from the initial node to the second node via the myelinated fiber with little loss taking place. Now, a shorter fiber is considered i.e. of length 50 μm and input spike train of duration 1–8 ms and 15–22 ms is applied as an input. It is observed in this case that the information content of the signal is hampered. As the signal moves from one node of Ranvier to the other node of Ranvier, an additional spike is found to get generated at the second node. The reason for this is that since the length of the fiber is decreased, spike encoding changes significantly and since for a shorter fiber has less amount of open channels to facilitate ionic losses, high amount of current is delivered to the subsequent region of the fiber, thus resulting in generating an extra spike at the second node of Ranvier which can significantly hamper the information content of the signal. Thus, it can be said that there exists some critical length for myelinated fibers such that the signal information content is not modified and remains intact.

References

Asuero AG, Sayago A, Gonzalez AG (2006) The correlation coefficient: an overview. Crit Rev Anal Chem 36(1):41–59

Barros CS, Franco SJ, Müller U (2011) Extracellular matrix: functions in the nervous system. Cold Spring Harb Perspect Biol 3(1):a005108

Baruah SMB, Das B, Roy S (2021) Extracellular conductivity and nerve signal propagation: an analytical study. In: Proceedings of international conference on communication, circuits, and systems. Springer, Singapore, pp 399–405

Bédard C, Destexhe A (2013) Generalized cable theory for neurons in complex and heterogeneous media. Phys Rev E 88(2):022709

Blijham PJ, Ter Laak HJ, Schelhaas HJ, Van Engelen BGM, Stegeman DF, Zwarts MJ (2006) Relation between muscle fiber conduction velocity and fiber size in neuromuscular disorders. J Appl Physiol 100(6):1837–1841

Cohen MR, Kohn A (2011) Measuring and interpreting neuronal correlations. Nat Neurosci 14(7):811–819

Das B, Baruah SMB, Roy S (2019) Velocity profile of alpha (α) type and gamma (γ) type motor neuron and type III and type IV sensory neuron. In: 2019 second international conference on advanced computational and communication paradigms (ICACCP). IEEE, pp 1–6
Goldstein SS, Rall W (1974) Changes of action potential shape and velocity for changing core conductor geometry. Biophys J 14(10):731–757
Hodgkin AL, Huxley AF (1952) A quantitative description of membrane current and its application to conduction and excitation in nerve. J Physiol 117(4):500–544
Hursh JB (1939) Conduction velocity and diameter of nerve fibers. Am J Physiol Legacy Content 127(1):131–139
Kohn A, Coen-Cagli R, Kanitscheider I, Pouget A (2016) Correlations and neuronal population information. Annu Rev Neurosci 39:237–256
Morell P, Norton WT (1980) Myelin. Sci Am 242(5):88–119
Nicholson C, Hrabětová S (2017) Brain extracellular space: the final frontier of neuroscience. Biophys J 113(10):2133–2142
Pospisil DA, Bair W (2021) Accounting for biases in the estimation of neuronal signal correlation. J Neurosci
Rall W (2011) Core conductor theory and cable properties of neurons. Compreh Physiol 39–97
Scott AC (1975) The electrophysics of a nerve fiber. Rev Mod Phys 47(2):487
Simons M, Nave KA (2016) Oligodendrocytes: myelination and axonal support. Cold Spring Harb Perspect Biol 8(1):a020479
Stadelmann C, Timmler S, Barrantes-Freer A, Simons M (2019) Myelin in the central nervous system: structure, function, and pathology. Physiol Rev 99(3):1381–1431
Stämpfli R (1954) Saltatory conduction in nerve. Physiol Rev 34(1):101–112
Syková E, Nicholson C (2008) Diffusion in brain extracellular space. Physiol Rev 88(4):1277–1340
Waxman SG (1980) Determinants of conduction velocity in myelinated nerve fibers. Muscle Nerve: off J Am Assoc Electrodiagn Med 3(2):141–150

An ECG Acquisition/Local Server Unit for Remote Patient Consultation

Bidyut Bikash Borah, Satyabrat Malla Bujar Baruah, Debaraj Kakati, and Soumik Roy

Abstract With the advent of current electronics technology and access to the Internet, it is now possible to obtain distant medical diagnostics and counseling at a distance. However, because of the size and cost of such medical equipment, third-world and developing countries continue to face barriers to primary medical consultation and testing. One such medical situation is the early assessment of patients' cardiovascular well-being. An attempt has been made in this suggested framework to build and implement a low-cost ECG collection combined with a local storage server system capable of capturing and storing patient data locally. When the system is connected to the Internet, the server can send patients' ECG data to a group of registered cardiologists for immediate assessment of a patient's criticality and generate complete assessment reports of individuals by collecting tagged information from the cardiologists' responses in addition to local storage. These comprehensive assessment reports can then be printed for the patient or electronically mailed to others who need to know. This system is portable, low-cost, and seamlessly implementable into the Android UI for better usability over uninterrupted Internet service.

Keywords ECG · Remote monitoring · Portable ECG device · Patient monitoring · ECG acquisition

1 Introduction

With the advancement of contemporary medical technology and healthcare systems in recent years, the average human life expectancy has increased dramatically, resulting in a surge in the percentage of patients served by local healthcare organizations. The number of medical healthcare specialists serving such a large number of patients has a significant impact on the accessibility of medical services, either due

B. Bikash Borah (✉) · S. Malla Bujar Baruah · D. Kakati · S. Roy
Department of Electronics and Communication Engineering, Tezpur University, Napam, Sonitpur, Tezpur, Assam 784028, India
e-mail: baruah.satyabrat@gmail.com

J. K. Deka et al. (eds.), *Emerging Technology for Sustainable Development*,
Lecture Notes in Electrical Engineering 1061,
https://doi.org/10.1007/978-981-99-4362-3_37

to a limited number of patients attended per day or inaccessibility due to long-distance communication, necessitating an urgent need for IoT-based alternatives (Beaton et al. 2014; Prakash and Venkatesh 2013; Xia et al. 2013) to accommodate vulnerable members. Aside from the specialist-to-patient ratio and inaccessibility due to transit time, present COVID-19 conditions have rendered such critical care medical facilities inaccessible to the general population (Andrade 2020; Zhang et al. 2021) due to constrained inter-district and inter-state transfers. To assist such critical patients, crucial data transmission (Shahidul Islam et al. 2019; Xu 2020) and specialists' evaluation of medical records through the Internet (Kadhim et al. 2020; Shabaan et al. 2020) for immediate assessment of criticality is required (Shabaan et al. 2020). The cardiovascular care unit is one such critical medical care facility that requires a quick reaction from cardiologists to assess the patients' criticality and need for emergency medical intervention. A trivial latency in reacting to a cardiovascular patient's medical treatment may result in the traumatized person's death (Honnekeri et al. 2014; Kumar et al. 2021; Wong et al. 2019), necessitating the quick intervention of professionals to save such vital patients. According to WHO's medical surveys, cardiovascular disorders have been one of the leading causes of premature death in the majority of countries (Ma et al. 2011) around the world during the last decade, particularly in the middle and developing world (Teo and Dokainish 2017). The reasons for such high numbers in low- and middle-income countries (Mensah et al. 2013; Teo and Dokainish 2017) include a lack of access to emergency medical services and early access to such data sharing systems due to the expensive cost of such equipments (Alam et al. 2018; Dixit and Kala 2021). Thus, the availability of low-cost, easy-to-use, portable ECG systems capable of sharing patients' medical data over the Internet (Beaton et al. 2014; Saikia et al. 2020; Varshney et al. 2019) for facilitating early examination of cardiovascular as well as other medical complications and proper intervention in the identification of medical complexity could substantially reduce fatality ratios.

An attempt has been made in this proposed work to build and construct an IoT-based low-cost ECG server system that can gather crucial patients' ECG data and store the ECG medical data within the server that can be promptly shared among a group of cardiology doctors. Once the crucial data about the traumatized patient is shared among the specialists, any of the available specialists or all of the specialists can assess the severity of the patient's condition for prompt response and intervention. The proposed system contributes to providing high sensitivity and specificity in detecting electrical cardiac abnormalities. Moreover, its mobility and real-time transmission, ease of use, and cheap cost make it a good option for early cardiac treatment in clinical and community settings. Any caregiver or medical staff can efficiently operate the proposed system, so the system is also helpful for doctors who wish to monitor their patients remotely.

2 Methods

The schematic of the proposed model is shown in Fig. 1, where ECG from patients is acquired using an 'AD8232' ECG module, where three leads are used depicted using three body pads, namely in 'red', 'black', and 'green' colors, which is in turn connected to a microcontroller unit interfaced with a Wi-Fi module. This ECG unit, along with the controller and Wi-Fi module, is the main unit responsible for ECG data acquisition and connectivity with the server unit. This server unit then shares the data immediately with a group of cardiologists for immediate assessment of the patients' criticality. Details of each module have been discussed in detail in the section follows.

2.1 ECG Acquisition Module with Arduino Nano

ECG module has been interfaced with the Arduino Nano controller via 'ADC channel', and the ECG of the patient has been collected using three non-invasive leads. LA lead of the 'AD8232' module is connected to the left-hand palm of the subject, RA leads to the right-hand palm, and the RL lead is connected to the right leg, and ECG data from the patient has been recorded after every 100 ms. The process of acquisition of ECG is straightforward and is shown in Fig. 2. Acquired data from the patient has been preprocessed within the microcontroller to remove low-frequency noises, high-frequency noises, and powerline noises. The low-frequency noises due to respiration contribute to the baseline wondering of the signal, whereas muscle noise and internal noise of the electronics component contribute to the high-frequency noises and need to be removed before interpreting ECG data. This clean ECG data is

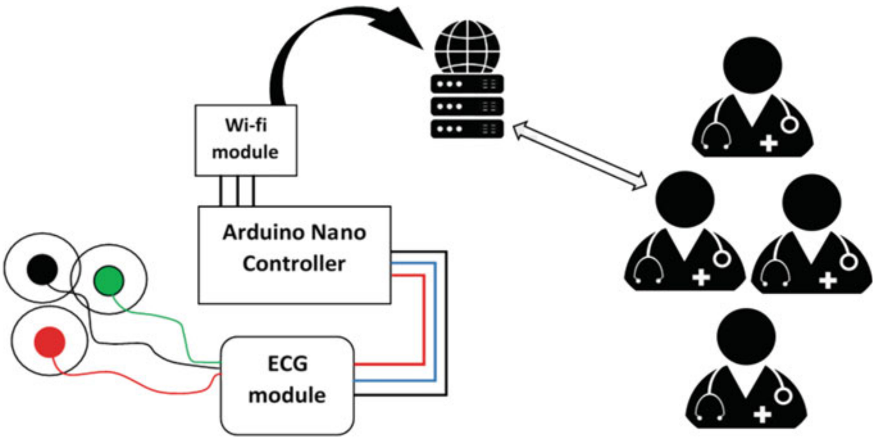

Fig. 1 Schematic of the proposed model

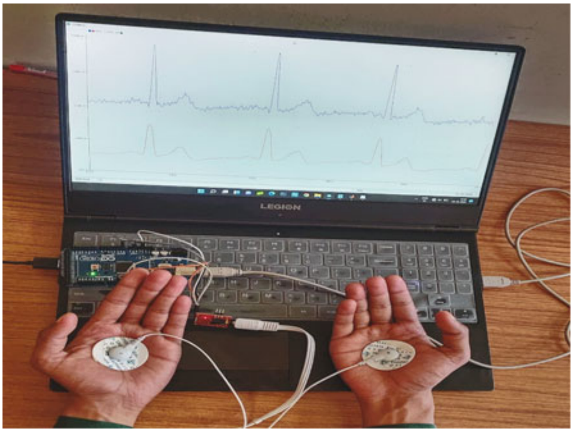

Fig. 2 Process of acquisition of ECG signal from patient

then forwarded to the Wi-Fi module to be transmitted over to the local storage server and has been discussed in detail in Sects. 2.2 and 2.3.

2.2 Interfacing Wi-Fi-Module

The Arduino NANO is equipped with an AD8232 ECG sensor module, which collects ECG data from patients, as detailed in Sect. 2.1. The Arduino Nano is also attached to an 'ESP8266' Wi-Fi module, which uses less than 1 mA to stay connected to the access point and consumes 60 μA in deep sleep mode with the RTC clock still operating. The module is set up so that it can provide great integration performance while consuming little power. Figure 3 depicts the ESP8266's power-saving operating method.

The data collected from the patients is initially saved in a buffer in the microcontroller and then processed. The Wi-Fi frame implementation method prepares a data frame for transmission to the network's main server. The created data frame comes with an application programming interface (API) key and an auto-generated unique patient id.

The prepared data frame is then sent as a string to the main server using the HTTP POST method. The method is set up so that it connects to the server first, and then, after the server gets the POST request, it delivers an HTTP 200 success code and an access token if the API Key provided is genuine. After initial authentication, this token is used to visit the server to prevent sending the same data several times, which increases the danger of being intercepted. To avoid their abuse, these tokens also expire after a certain time.

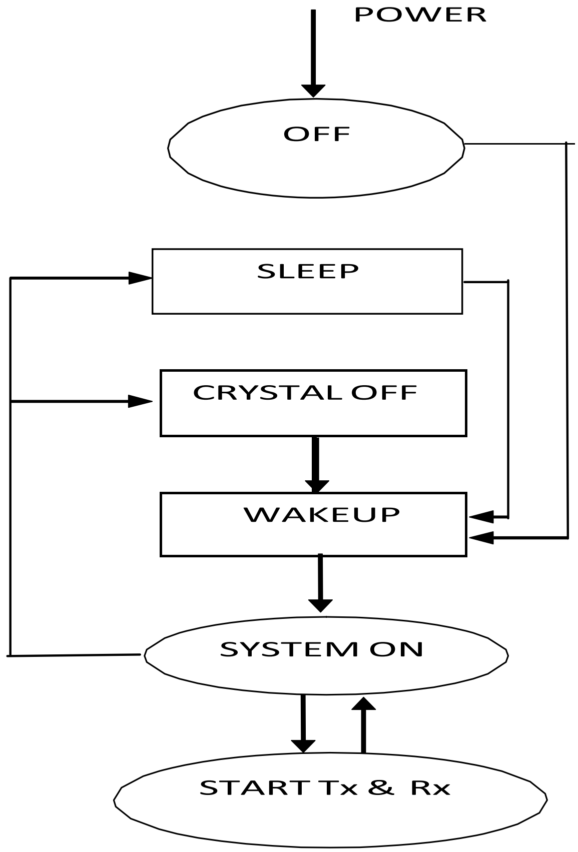

Fig. 3 Power-saving operating method

2.3 Raspberry Pi and Server Configuration

The suggested concept uses a Raspberry Pi embedded Linux board for the network's main Webserver. The Raspberry Pi server is written in PHP, and MySQL is utilized as a relational database management system (RDBMS). Patients' data is stored in a database that clinicians may access remotely.

Data is delivered from node to server and server to node through a Wi-Fi network on the Raspberry Pi server, which features an Ethernet connector for network and Internet connection to operate the Webserver. An Apache Webserver is installed on the Raspberry Pi board to construct an Embedded Webserver. The Apache server provides online distribution of website services using HyperText Transfer Protocol (HTTP). It is a widely used webserver that runs on various operating systems, including Linux, UNIX, Windows, Solaris, Mac OS X, Novell NetWare, and others. In this research, the Apache2 version was utilized to create the Webserver. When the Webserver gets an HTTP POST request from a specific node, it first performs data frame authentication. It assigns a unique token to that node before copying the data supplied by the node to the server database. The system is set up in such a manner that when new patient data is received at the server, it prompts the user for information such as name, sex, age, and so on. The information gathered may then be seen through a series of HTML/PHP/MySQL pages. It gives the user remote access to the web page for information monitoring. For delivering Internet connectivity in indoor and outdoor locations, IEEE 802.11 Wireless Local Area Network became the favored choice.

3 Results and Discussion

Shown in Fig. 4 are the different forms for report generation from local server data, which give the administrator to record additional information and tag the data with fields such as name, age, and contact information of the patient along with other associated medical records.

The administrative panel, as illustrated in Fig. 4a, offers an array of visual parameters, including the total number of doctors, the number of available doctors at the time, the total number of patients, and so on. When a new doctor registers in the system, the system has been implemented so that the administrator must go to the incoming request area and make a decision on the new doctor's requests in order to confirm their legitimacy. As shown in Fig. 4b, the system repository is configured with two different tables for patients and doctors. The ECG acquisition unit's data will be entered into the patient database using the acquisition unit's unique patient id. As illustrated in Fig. 4c, the administrator will be able to monitor a table that contains all patient details and will be able to transfer patients' data to registered doctors.

As stated in Sect. 2.3, if a new patient data is received at the local server, the system will display a screen similar to the one shown in Fig. 4d for entering supplementary patient information that may be used during diagnostics. Following submission, the system will gather ECG data from the database and generate ECG reports for the patients, as shown in Fig. 4e. For various diagnoses, the patients' ECG reports are delivered to some of the active doctors. They are manually chosen based on report routing and doctors' answers via their registered e-mail identifiers. Following diagnosis, the reports from the respective doctors are collected from the responding e-mails id's of the corresponding cardiologists, and a final report is generated using the response tags of the specialists, which can then be printed or e-mailed to the patients, as shown in Fig. 4f. A comparison of similar ECG-based telemedicine technologies existing in the current market has been compared with the proposed system and given in Table 1.

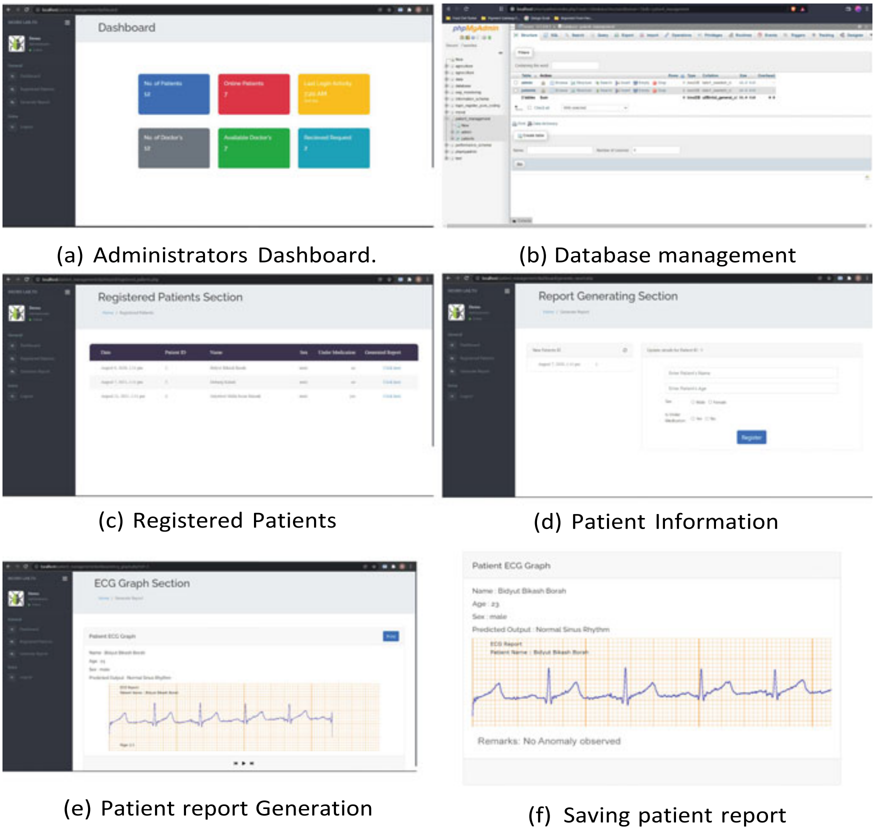

Fig. 4 Local server processes for in-bound patient database management, data processing, and remote patients' health assessment

Table 1 Comparison of existing similar ECG technology and facilities

	GE MAC600	SANKET LIFE	Spandan	Our system
Access type	ECG with offline storage	ECG with IoT and android interface	ECG with wired android device	ECG local server storage and IoT connect
Architecture	12 electrode	3 electrode	3 electrode	3 electrode
Expert's network	No	Subscription	No	Open access
Expert report	No	No	No	Yes
Cost (INR)	Rs. 60,000	Rs. 8000	Rs. 8000	–

4 Conclusion

The suggested framework is an implementation of an efficient on-site medical ECG data acquisition device integrated with a local storage server capable of storing patients' ECG data and any supplementary information required for essential patient assessment. The technology, linked to the Internet, has the advantage of instantly transmitting data to professionals for prompt assessment of the patients' criticality. The current framework stresses local storage of medical data and manual sending of medical data to off-shore or remote specialists to promptly assess the criticality of patients by connecting the local server over the Internet. Some of the processes in the proposed work are performed manually, and future work on the suggested framework focuses on automating the entire framework and expanding the framework to an android application for the convenience of users.

References

Alam ST, Hossain MM, Islam MK, Rahman MD (2018) Towards development of a low cost and portable ECG monitoring system for rural/remote areas of Bangladesh. Int J Image Graph Signal Process 10(5)

Andrade C (2020) Covid-19 and lockdown: delayed effects on health. Indian J Psychiatry 62(3):247

Beaton A, Aliku T, Okello E, Lubega S, McCarter R, Lwabi P, Sable C (2014) The utility of handheld echocardiography for early diagnosis of rheumatic heart disease. J Am Soc Echocardiogr 27(1):42–49

Dixit S, Kala R (2021) Early detection of heart diseases using a low-cost compact ECG sensor. Multimed Tools Appl 80(21):32615–32637

Honnekeri BS, Lokhandwala D, Panicker GK, Lokhandwala Y (2014) Sudden cardiac death in India: a growing concern. J Assoc Physicians India 62(12):36–40

Kadhim KT, Alsahlany AM, Wadi SM, Kadhum HT (2020) An overview of patient's health status monitoring system based on internet of things (IoT). Wirel Pers Commun 114(3)

Kumar A, Avishay DM, Jones CR, Shaikh JD, Kaur R, Aljadah M, Kichloo A, Shiwalkar N, Keshavamurthy S (2021) Sudden cardiac death: epidemiology, pathogenesis and management

Ma J, Flanders WD, Ward EM, Jemal A (2011) Body mass index in young adulthood and premature death: analyses of the us national health interview survey linked mortality files. Am J Epidemiol 174(8):934–944

Mensah GA, Sampson UK, Roth GA, Forouzanfar MH, Naghavi M, Murray CJ, Moran AE, Feigin VL (2015) Mortality from cardiovascular diseases in sub-Saharan Africa, 1990–2013: a systematic analysis of data from the global burden of disease study 2013. Cardiovasc J Afr 26(2 H3Africa Suppl):S6

Prakash S, Venkatesh V (2013) Real time monitoring of ECG signal using pic and web server. Int J Eng Technol (IJET) 5(2):1047–1053

Saikia A, Sill S, Baruah SM, Roy S, Das BR (2020) Android interface for handling ECG data from GE mac 600 ECG system. In: 2020 international conference on computational performance evaluation (ComPE). IEEE, pp 771–776

Shabaan M, Arshad K, Yaqub M, Jinchao F, Zia MS, Boja GR, Iftikhar M, Ghani U, Ambati LS, Munir R (2020) Survey: smartphone-based assessment of cardiovascular diseases using ECG and PPG analysis. BMC Med Inform Decis Mak 20(1):1–16

Shahidul Islam M, Islam MT, Almutairi AF, Beng GK, Misran N, Amin N (2019) Monitoring of the human body signal through the internet of things (IoT) based LoRa wireless network system. Appl Sci 9(9):1884

Teo KK, Dokainish H (2017) The emerging epidemic of cardiovascular risk factors and atherosclerotic disease in developing countries. Can J Cardiol 33(3):358–365

Varshney H, Allahloh AS, Sarfraz M (2019) IoT based ehealth management system using Arduino and google cloud firestore. In: 2019 international conference on electrical, electronics and computer engineering (UPCON). IEEE, pp 1–6

Wong CX, Brown A, Lau DH, Chugh SS, Albert CM, Kalman JM, Sanders P (2019) Epidemiology of sudden cardiac death: global and regional perspectives. Heart Lung Circ 28(1):6–14

Xia H, Asif I, Zhao X (2013) Cloud-ECG for real time ECG monitoring and analysis. Comput Methods Programs Biomed 110(3):253–259

Xu G (2020) IoT-assisted ECG monitoring framework with secure data transmission for health care applications. IEEE Access 8:74586–74594

Zhang J, Hayashi Y, Frank LD (2021) Covid-19 and transport: findings from a world-wide expert survey. Transp Policy 103:68–85

Proximity Coupled Planar MIMO Antenna for LTE-46/LTE-U Bands of Sub-6 GHz

P. Krishna Kanth Varma and Nagesh Kallollu Narayaswamy

Abstract For 5G applications, a novel two-port linearly polarized multiple-inputs multiple-outputs (MIMO) proximity coupled antenna is presented and discussed. The orthogonal arrangement of the antenna components enables us to achieve more than 30 dB isolation. FEM-based ANSYS high-frequency structure simulator (HFSS) electromagnetic solver is used for the modeling and simulation of this module. The suggested antenna works at a single frequency band, 5.35–5.60 GHz, thereby addressing the critical sub-6 GHz regions for 5G outdoor applications. The significant difference between co-polarization and cross-polarization levels justifies the radiation attributes of the antenna. The envelope correlation coefficient (ECC) and diversity gain (dB) are calculated to justify its MIMO antenna performance. At resonating frequency, positive gain value and radiation efficiency of more than 80% are recorded.

Keywords Multiple-input multiple-output (MIMO) · Envelope channel coefficient (ECC) · 5G · Diversity gain (DG)

1 Introduction

In today's radio system, 5G technology has sparked a stir. In the recent few years, 5G systems have seen a rise in popularity due to their superior capabilities. The first phase of 5G deployments has already begun in several emerging nations, including Japan, S Korea, and America, and numerous 5G devices have already hit the market. An

P. Krishna Kanth Varma (✉)
Department of Electronics and Communication Engineering, S.R.K.R. Engineering College, Bhimavaram, Andhra Pradesh, India
e-mail: pkkvarma@srkrec.ac.in

Visvesvaraya Technological University, Belagavi 590018, India

N. K. Narayaswamy
Department of Electronics and Communication Engineering, Nagarjuna College of Engineering & Technology, Bengaluru, India

J. K. Deka et al. (eds.), *Emerging Technology for Sustainable Development*,
Lecture Notes in Electrical Engineering 1061,
https://doi.org/10.1007/978-981-99-4362-3_38

antenna that works in the sub-6 GHz band is required by the services provided by 5G (Nadeem et al. 2018). Over the past 10 years, a great deal of research has been done on microstrip patch antennas. Planar antennas with dual/multiband capabilities have been created (Ojaroudiparchin et al. 2015). Researchers are motivated to work on the MPA because of its appealing characteristics, such as its minimal loss, lightweight, and conformity (Osseiran et al. 2014; Singh et al. 2019). There is a lot more to 5G than just the speed, and we are only getting started. 5G offers a wide range of services, including low latency communication, fast Internet, IoT applications. It was decided to divide the 5G spectrum band into three distinct bands: first, the low band (below 1 GHz), the second class of frequencies is the so-called mid bands, which range from 1 to 7 GHz. Bands with a high octave (above 24 GHz) are also known as the mm-wave (Dwivedi et al. 2022). However, even though millimeter-wave antennas are the greatest choice for achieving faster speeds, they cannot be used over long distances owing to atmospheric losses and bandwidth use. Because of its longer wavelength, mid-band designed antennas are becoming more popular and have already been used by a significant number of nations. Numerous antennas are described in the literature for use at frequencies below 6 GHz (Desai et al. 2021; Sghaier and Latrach 2021; Dwivedi et al. 2021; Saxena et al. 2020).

Today's upcoming 5G wireless technologies demand increased data transfer rates from dependable communication channels, and MIMO antenna-equipped devices are its foundation. In a fading environment, several antenna units are used at the transmitter and reception ends of a communication system to offer multipath connections that increase data transmission. Today's upcoming 5G wireless technologies demand increased data transfer rates from dependable communication channels, and MIMO antenna-equipped devices are its foundation. In a fading environment, several antenna units are used at the transmitter and reception ends of a communication system to offer multipath connections that increase data transmission.

MIMO antennas will be used in 5G systems operating in the sub-6 GHz spectrum to provide a high data throughput. The performance of MIMO systems is harmed by mutual interaction between distinct antenna components. For providing isolation between components in MIMO systems, techniques such as spatial decoupling (Rajkumar et al. 2017) and utilizing alternative decoupling structures (Ramachandran et al. 2017) have been published in the literature. A MIMO antenna design with a built-in decoupling mechanism was presented in Wang et al. (2015), with a 0.2 mm edge-to-edge spacing between the two monopoles for isolation. There is some gap between the antenna parts or some extra complexity owing to the decoupling features in the MIMO antennas stated above.

This article describes a novel dual-port MIMO antenna with linear polarization. The antenna components are oriented orthogonally to provide isolation higher than 30 dB. The suggested antenna provides isolation without the need for any extra decoupling construction or element spacing. Impedance matching is accomplished with a matched stub transmission line feed. A T-shape matching stub is proximately coupled with the patch via a split ring aperture. The other performance metrics of MIMO antennas, ECC and DG, are within the permitted range. The suggested antenna's operational frequency range of 5.35–5.6 GHz makes it an excellent choice for 5G indoor applications.

2 Design Principle and Analysis

2.1 Unit Cell Element

Figure 1a illustrates the geometry of the unit cell element used in the suggested MIMO arrangement. The radiating element is encased in a $50 \times 50 \times 1.6\ \text{mm}^3$ FR-4 epoxy substrate. Copper is used for the radiating element and ground plane. The dimensions of the recommended antenna element are given in Table 1. The antenna is composed of a T-shaped matching stub and a split ring slot-loaded conducting ground plane. To optimize the dimensions of an antenna element, both the feeding stub and the split ring slot-loaded ground plane are adjusted in terms of location and size. Before developing the unit cell radiator, the antenna's polarization purity and directional radiation properties were considered. The HFSS 18 electromagnetic solver is used to model, simulate, and optimize the proposed antenna.

2.2 Steps to Achieve Proximity Coupled Antenna Design

Figure 1c and d shows how changes in antenna design and feeding affect return loss for a single antenna element. The first phase uses a simple microstrip line with a square grounded substrate (design 1). An annular ring slot is added in the ground plane in design stage 2. In design-3, the basic microstrip line is converted into a stub impedance line feed to maintain impedance matching. Design-3 produces a sub-6 GHz resonance band. The recommended antenna design-4 results in resonance at 5.5 GHz (sub-6 GHz) with broad bandwidth and superior return loss characteristics.

2.3 2-Port MIMO Antenna

The suggested MIMO antenna system's geometrical configuration is shown in Fig. 2. A single element was used to create a two-port MIMO antenna; both antenna elements are orthogonal to one another, resulting in spatial diversity and isolation of more than 30 dB throughout the operating spectrum. The comparative analysis is carried in terms of $|S_{11}|$ (dB) and mutual coupling scattering parameters are investigated to justify the orthogonal placement orientation of unit cells (c.f. Fig. 2).

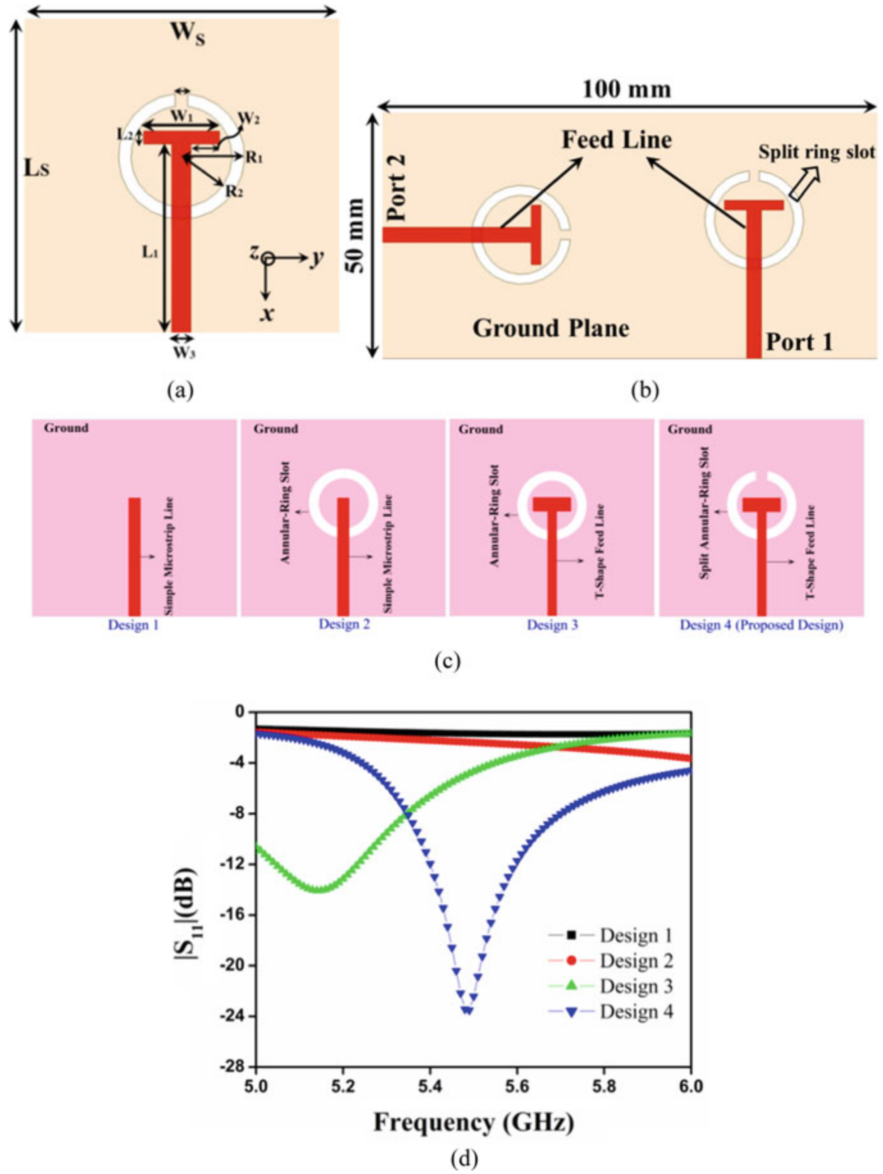

Fig. 1 Schematic design of the proposed module **a** unit cell **b** MIMO unit **c** evolution of a single patch antenna element **d** comparative $|S_{11}|$ plot for Design-1, Design-2, Design-3, and Design-4

Table 1 Geometrical specifications of the proposed design

Parameters	Dimensions (mm)	Parameters	Dimensions (mm)
L_S	50	W_s	50
L_1	30	W_1	12
L_2	2	W_2	4.5
R_1	10	W_3	3
R_2	8	H (thickness of Sub)	1.6

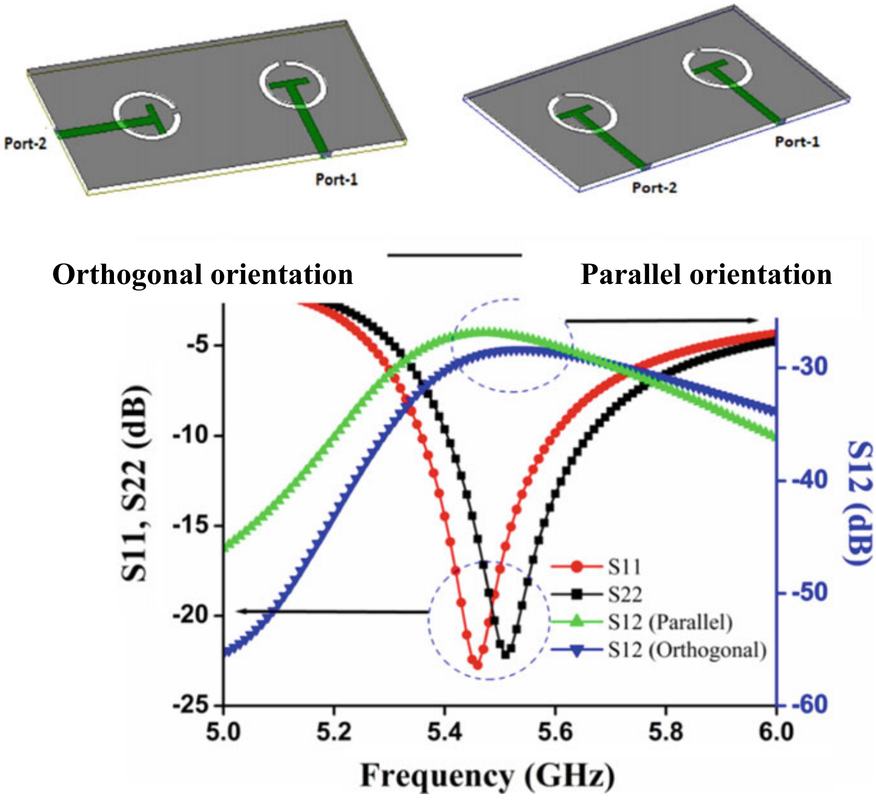

Fig. 2 Geometric configuration and scattering parameters (S11, S22, S12-parallel, and orthogonal) of the proposed MIMO antenna

2.4 Isolation Achievement and Surface Current Distribution

The electric field distribution at each port of a dual-port MIMO antenna is shown in Fig. 3. As can be seen, the current is strongest around the radiating structure's feed, meaning that these are the areas of the structure that assist the most in keeping it resonant within the desired frequency range. Furthermore, the electric field strength

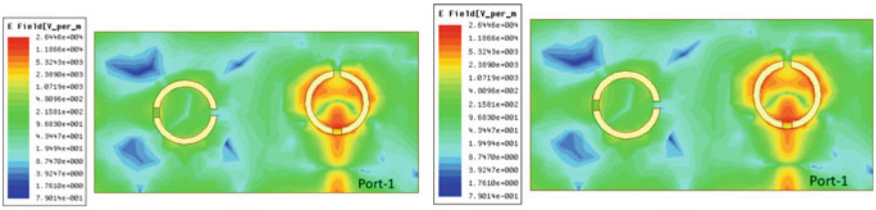

(a) (b)

Fig. 3 Electric field distributions of the proposed MIMO antenna **a** Port-1 **b** Port-2

of each antenna element's transmission line is strong. Additionally, the coupling fields between antenna components are reduced due to the orthogonal positioning of antenna elements. Figure 3a depicts the electric field distribution when only port-1 is activated, whereas Fig. 3b depicts the field strength distribution when port-2 is active.

3 Results and Discussions

Figure 4 depicts the return loss ($|S_{11}|$, $|S_{22}|$) and isolation ($|S_{12}|$, $|S_{21}|$) between the antenna elements in decibels (dB). It is obvious from Fig. 4 that a level of isolation of more than 30 dB has been attained between ports 1 and 2. The scattering parameters graphs show incoherence for both port-1 and port-2, which supports the suggested MIMO identity arrangement. As seen in Fig. 4, the suggested MIMO antenna can effectively cover the 5.5 GHz band (5.35–5.60 GHz) with a reflection coefficient less than − 10 dB (2:1 voltage standing wave ratio, VSWR).

Fig. 4 Suggested MIMO antenna's S-parameters versus frequency graph

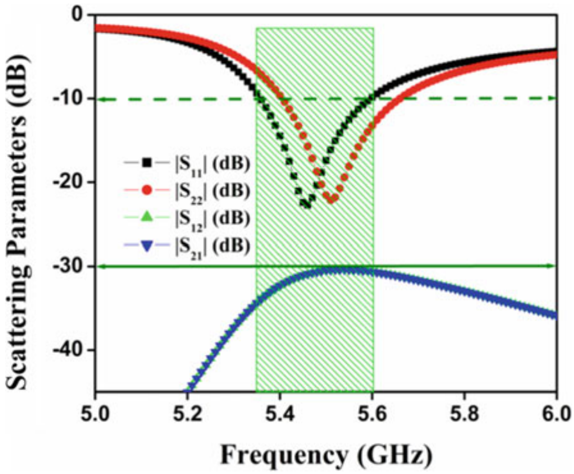

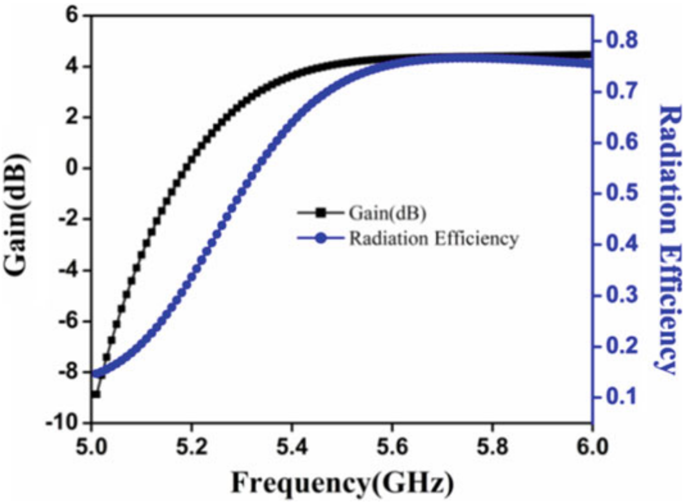

Fig. 5 Gain (dB) and radiation efficiency graph for the MIMO design

Figure 5 depicts the gain and radiation efficiency curve for the proposed antenna. The antenna's maximal gain for the aforementioned band is 3.9 dB, and its radiation efficiency is more than 75%. Figure 6 depicts the proposed antenna's two-dimensional radiation patterns (Co- and cross-polarization) in the E-plane and H-plane. The co-polarization level is 15–20 dB better than the cross-polarization level in both planes. The suggested antenna can radiate in all directions.

4 Demonstrations and Analysis of MIMO Antenna Technology

The envelope correlation coefficient (ECC) and diversity gain (DG) are investigated in this part to validate the MIMO significance of the proposed antenna. Under the assumption that the transmission environment is uniform, with isotropic incident waves dispersed in the theta-polarized and phi-polarized directions, the ECCs depicted in Fig. 7 are computed from the recorded three-dimensional complex E-field patterns and scattering parameters (Dwivedi et al. 2020). It was discovered that all of the computed ECCs were less than 0.05. The total active reflection coefficient (TARC), the envelope correlation coefficient (ECC), and the diversity gain (DG) characteristics are critical factors to consider when designing diversity/multiple-input multiple-output (MIMO) antennas and may be computed using the equations below (Sharawi 2013).

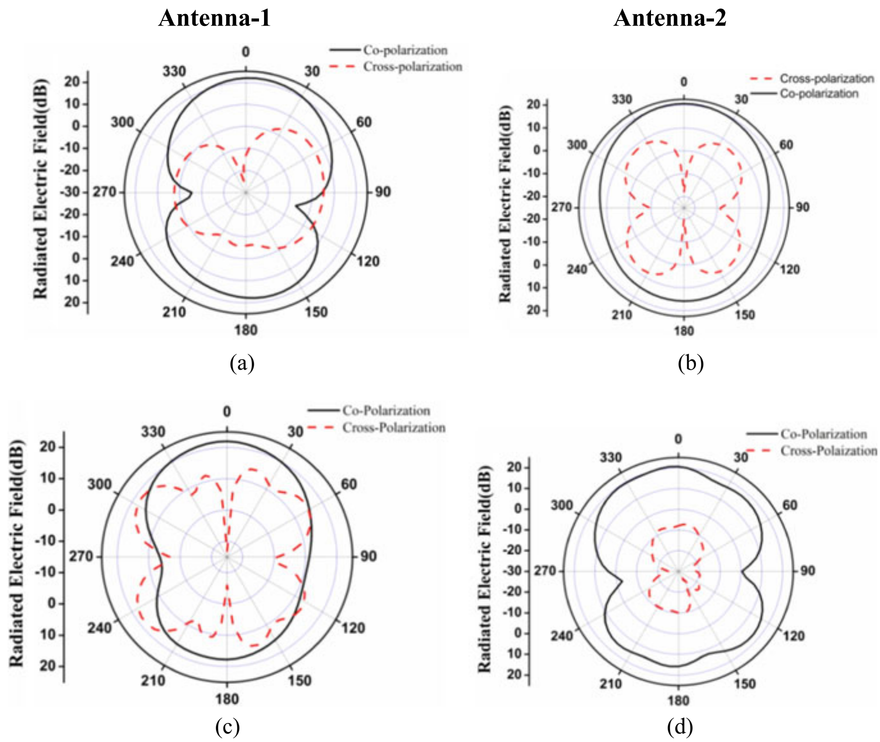

Fig. 6 Radiation patterns at 5.5 GHz **a** E-plan port-1 **b** E-plane port-2 **c** H-plane port-1 **d** H-plane port-2

$$\mathrm{ECC}_s = \left| \frac{\left|S_{11}^* S_{12} + S_{21}^* S_{22}\right|}{\left|\left(1 - |S_{11}|^2 - |S_{21}|^2\right)\left(1 - |S_{22}|^2 - |S_{12}|^2\right)\right|^{1/2}} \right|^2 \tag{1}$$

$$\mathrm{ECC}_{\text{Far - field}} = \frac{\left| \iint_{4\pi} \left[E_i(\theta, \phi) * E_j(\theta, \phi)\right] \mathrm{d}\Omega \right|^2}{\iint_{4\pi} |E_i(\theta, \phi)|^2 \mathrm{d}\Omega \iint_{4\pi} \left|E_j(\theta, \phi)\right|^2 \mathrm{d}\Omega} \tag{2}$$

$$\mathrm{DG} = \sqrt{1 - \mathrm{ECC}} \tag{3}$$

$$\mathrm{TARC} = \frac{\sqrt{\left(\left(\left|S_{11} + S_{12} e^{j\theta}\right|^2\right) + \left(\left|S_{21} + S_{22} e^{j\theta}\right|^2\right)\right)}}{\sqrt{2}} \tag{4}$$

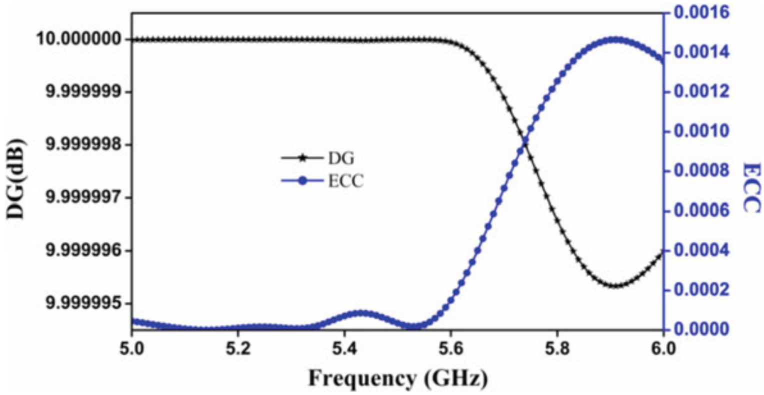

Fig. 7 ECC and DG graph for the proposed MIMO antenna

Additionally, another critical performance metric is diversity gain. The diversity gain of the proposed MIMO antenna is shown in Fig. 7. Due to the low ECC, the value of DG is found to be near to 10 dB (the optimal value) over the given frequency band.

The reflection coefficient derived from scattering characteristics is insufficient to predict antenna performance under MIMO constraints. The total active reflection coefficient (TARC) is a critical measure for understanding the radiation impact of one antenna element on the performance of other antenna elements. As seen in Fig. 8, the TARC value is less than − 20 dB over the whole operating bandwidth (5.35–5.60 GHz) and is found to be consistent across a wide variety of elevation angle values (theta).

Fig. 8 TARC of the proposed MIMO antenna

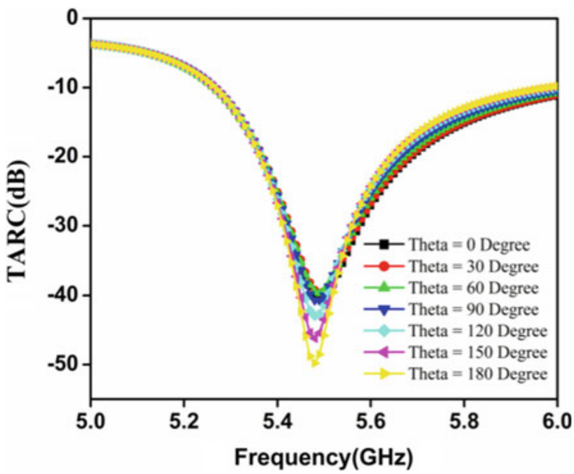

5 Conclusion

This communication describes a two-port MIMO antenna using a unique orthogonal design philosophy. The isolation strategy presented in this letter applies not just to the sub-6 GHz frequency, but also other bands. Each antenna element is a mirror of its adjacent components in both horizontal and vertical orientations. Orthogonal polarization is obtained as a consequence. The frequency range (5.35–5.60 GHz) is covered by 10-dB impedance bandwidths. The isolation between antenna elements is observed at more than 30 dB. ECC, DG, and TARC are used to demonstrate the antenna's diversity capability. The antenna has been successfully analyzed and investigated to provide the requisite properties for the sub-6 GHz band of interest. Based on the preceding investigations, it can be concluded that the suggested MIMO antenna is capable of operating in the necessary frequency spectrum for 5G wireless applications.

References

Desai A, Palandoken M, Kulkarni J, Byun G, Nguyen TK (2021) Wideband flexible/transparent connected-ground MIMO antennas for Sub-6 GHz 5G and WLAN applications. IEEE Access 9:147003–147015. https://doi.org/10.1109/ACCESS.2021.3123366

Dwivedi AK, Sharma A, Singh AK, Singh V (2020) Quad-port ring dielectric resonator based MIMO radiator with polarization and space diversity. Microw Opt Technol Lett 62:2316–2327. https://doi.org/10.1002/mop.32329

Dwivedi AK, Sharma A, Pandey AK, Singh V (2021) Two port circularly polarized MIMO antenna design and investigation for 5G communication systems. Wirel Pers Commun 120:2085–2099. https://doi.org/10.1007/s11277-021-08461-9

Dwivedi AK, Sharma A, Singh AK, Singh V. Novel design of cylindrical DRA built MIMO antenna for 5G future prospective covering (n78/n79) bands. Presented at the (2022). https://doi.org/10.1007/978-981-16-2761-3_7

Nadeem Q-U-A, Kammoun A, Debbah M, Alouini M-S (2018) Design of 5G full dimension massive MIMO systems. IEEE Trans Commun 66:726–740. https://doi.org/10.1109/TCOMM.2017.2762685

Ojaroudiparchin N, Shen M, Pedersen GF (2015) Multi-layer 5G mobile phone antenna for multi-user MIMO communications. In: 2015 23rd telecommunications forum Telfor (TELFOR). IEEE, pp 559–562. https://doi.org/10.1109/TELFOR.2015.7377529

Osseiran A, Boccardi F, Braun V, Kusume K, Marsch P, Maternia M, Queseth O, Schellmann M, Schotten H, Taoka H, Tullberg H, Uusitalo MA, Timus B, Fallgren M (2014) Scenarios for 5G mobile and wireless communications: the vision of the METIS project. IEEE Commun Mag 52:26–35. https://doi.org/10.1109/MCOM.2014.6815890

Rajkumar S, Vivek Sivaraman N, Murali S, Selvan KT (2017) Heptaband swastik arm antenna for MIMO applications. IET Microwaves Antennas Propag 11:1255–1261. https://doi.org/10.1049/iet-map.2016.1098

Ramachandran A, Mathew S, Rajan V, Kesavath V (2017) A compact triband quad-element MIMO antenna using SRR ring for high isolation. IEEE Antennas Wirel Propag Lett 16:1409–1412. https://doi.org/10.1109/LAWP.2016.2640305

Saxena S, Kanaujia BK, Dwari S, Kumar S, Choi HC, Kim KW (2020) Planar four-port dual circularly-polarized MIMO antenna for sub-6 GHz band. IEEE Access 8:90779–90791. https://doi.org/10.1109/ACCESS.2020.2993897

Sghaier N, Latrach L (2021) Design and analysis of wideband MIMO antenna arrays for 5G smartphone application. Int J Microw Wirel Technol 1–13. https://doi.org/10.1017/S1759078721000659

Sharawi MS (2013) Printed multi-band MIMO antenna systems and their performance metrics [Wireless Corner]. IEEE Antennas Propag Mag 55:218–232. https://doi.org/10.1109/MAP.2013.6735522

Singh V, Mishra B, Singh R (2019) Anchor shape gap coupled patch antenna for WiMAX and WLAN applications. COMPEL Int J Comput Math Electr Electron Eng 38:263–286. https://doi.org/10.1108/COMPEL-12-2017-0546

Wang S, Hwang L, Lee C, Hsu C, Chang F (2015) MIMO antenna design with built-in decoupling mechanism for WLAN dual-band applications. Electron Lett 51:966–968. https://doi.org/10.1049/el.2014.4352

Effective Facemask Detection Using a Few Learning-Based Recognition Methods

Atlanta Choudhury and Kandarpa Kumar Sarma

Abstract Global healthcare systems are effectively dealing with the pandemic arising out of COVID-19 virus yet there are requirements to formulate appropriate risk minimization methods. In the absence of effective medical resources, certain alternatives are recommended to stem the infection. Mask wearing is regarded to be a non-pharmaceutical intervention measure to prevent rapid spread of the virus from an infected individual. As part of measures to ensure wearing of marks in public places, certain methods of monitoring are being developed. Majority of these are based on learning-aided pattern recognition methods. This paper discusses the design of a few learning-based methods like Artificial Neural Network (ANN), Convolutional Neural Network (CNN) and Support Vector Machine (SVM) and also includes discussion on the performance of these methods which are configured and trained to find the best suitable approach for checking mask wearing in a real-time situation. It is observed that the proposed technique based on VGG-16 CNN achieves high accuracy (99.0%) during the testing phase but when implemented with SVM during training, similar results are obtained.

Keywords COVID-19 · Deep learning (DL) · Deep transfer learning (DTL) · VGG · SVM · CNN · ANN · Face mask

1 Introduction

At present, the situation due to the Coronavirus pandemic (COVID-19) is improving and the infections are declining but the disease shall be a part of human life. This disease commonly spreads through human-to-human contact. According to the World Health Organization (WHO) website (Vijitkunsawat and Chantngarm 2020), the

A. Choudhury (✉) · K. K. Sarma
Department of ECE, Gauhati University, Guwahati, Assam 781014, India
e-mail: atlantachoudhury07@gauhati.ac.in

K. K. Sarma
e-mail: kandarpaks@gauhati.ac.in

J. K. Deka et al. (eds.), *Emerging Technology for Sustainable Development*,
Lecture Notes in Electrical Engineering 1061,
https://doi.org/10.1007/978-981-99-4362-3_39

spread of virus can be avoided by mitigating the effect of the virus in the environment (Johns Hopkins University 2020; Militante and Dionisio 2020) or preventing the virus transfer from person to person by practicing physical distance and wearing face masks. Further, WHO recommended physical distancing of at least six feet or two meters between persons in crowded places and wearing a face mask both of which can significantly reduce transmission of the COVID-19 virus (Jahromi et al. 2020; Ellis 2020; Feng et al. 2020; WHO 2020). It makes necessary the requirement to develop monitoring tools so that proper measures can be undertaking regarding reinforcement of the norm of wearing masks in places of human gathering. As part of measures to ensure wearing of marks in public places, certain methods of monitoring are being developed. Majority of these are based on learning-aided pattern recognition methods. Here, we discuss the design of a few learning-based pattern recognition systems which are configured and training for effective monitoring of wearing of masks in public places. A few learning-based methods, namely Artificial Neural Network (ANN), Convolutional Neural Network (CNN) and Support Vector Machine (SVM) are designed using a cloud platform, and open-source images are used for the training, validation and testing purposes. Different performance metrics (accuracy, F1-score, precision and recall) are used to judge the performance of the proposed models. There is one distinct face mask datasets are used to train and test the model, i.e., first dataset consists of 7553 images, divided into two classes: 3725 images of faces with masks and 3828 images without masks. For all experiments, 80% of the datasets are dedicated for training and 20% for testing. When testing the model, it achieved an accuracy of 99%. In 2001, the researchers proposed the concept of the face detection by using the Haar-like features technique creating the many rectangular and compared between white and black area which their feature can changed sizes and positions to find the face area (Johns Hopkins University 2020). In 2011, the researchers proposed converting from RGB to YCbCr or HSV to find skin region. After that, they were calculated with the pixels of skin areas and the number of pixels of pictures (Militante and Dionisio 2020). In Jahromi et al. (2020), researchers presented the Region of Interest (ROI) technique to find skin region by using the Random Forest Classification algorithm and Correct Classification Rate (CCR) for error checking. As a result, outputs are highly accurate than POESIA technique which was an open-source project (Jahromi et al. 2020). In Ellis (2020), the ROI areas were processed with Principal Component Analysis (PCA) to create the feature extraction and used in K-Nearest Neighbor (KNN), Multi-Layer Perception (MLP) and SVM algorithms for creating some models to predict the outputs. In this paper, we report the design and analysis of four different methods for performing masked face detection (MFD). We specifically present the design of a few learning-based methods like ANN, CNN, VGG-16 which is a popular version of CNN and SVM. Further, the work includes discussion on the performance of these methods which are configured and trained to find the best suitable approach for checking mask wearing in a real-time situation. It is observed that the proposed technique based on VGG-16 achieves high accuracy (98.0%) during the testing phase but when implemented with SVM during training, similar results are obtained.

2 Proposed Approach

The process logic and the sequence tagging used for the region of interest (RoI) labeling are shown in Figs. 1 and 2, respectively. The data used for training the learning-based methods are first separated out for training, testing and validation with a set of images having RoIs marked and appropriately labeled necessary for supervised learning. As already mentioned, ANN in feed forward form, CNN and the VGG-16 along with the SVM are used for the classification of wearing masks or not. Before doing into further details, a brief discussion is presented regarding the learning-based methods used in this work. The VGG-16 is a special CNN version which was used to win ILSVR (ImageNet) competition in 2014. It is considered to be one of the excellent vision model architectures till date. It follows an arrangement of convolution and max pool layers consistently throughout the whole architecture as shown in Fig. 3.

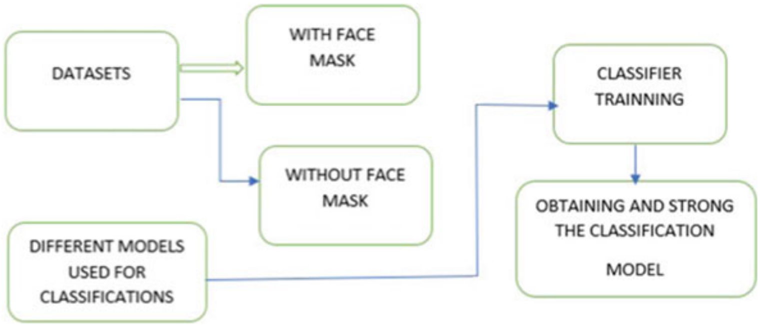

Fig. 1 Process logic of the work

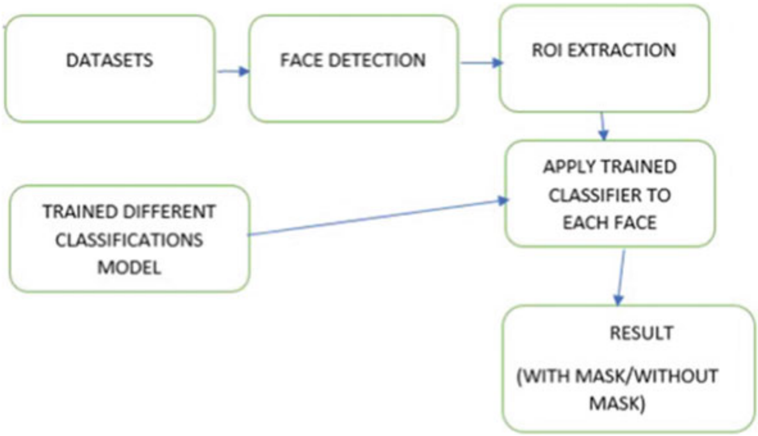

Fig. 2 Block diagram of sequence tagging and ROI

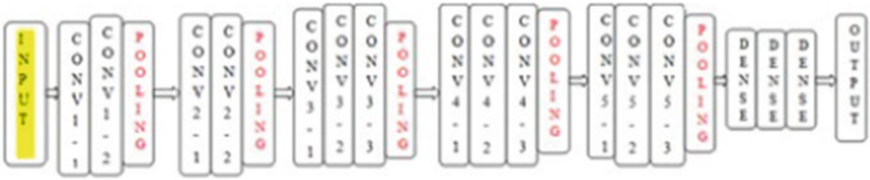

Fig. 3 Architecture of VGG-16

The SVM model (Fig. 4) is similar to logistic regression and uses a linear function $w^T X + b$. Contrary to the working of the logistic regression, the SVM does not generate probabilities, but only provides class detection. The SVM predicts that the positive class is present when $w^T X + b$ is positive. Likewise, it predicts that the negative class is present when $w^T X + b$ is negative. The SVM is dependent on the kernel function used with which machine learning algorithms are associated and are configured for prediction.

The CNN model (Fig. 5) is formed by several distinct layers that carries out multiple transformations of the inputs and generates an output linked with a classification decision while trained either using supervised or unsupervised approach.

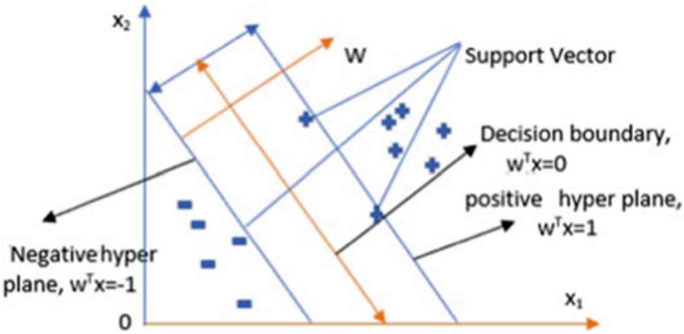

Fig. 4 SVM layout

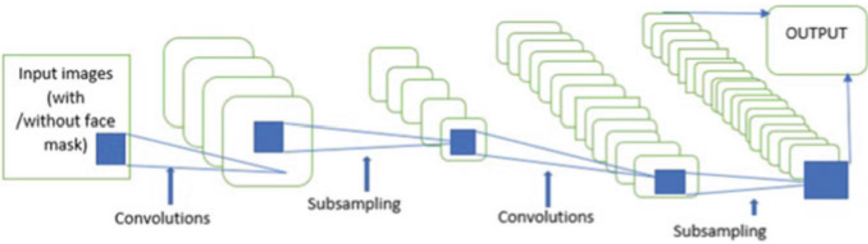

Fig. 5 CNN architecture

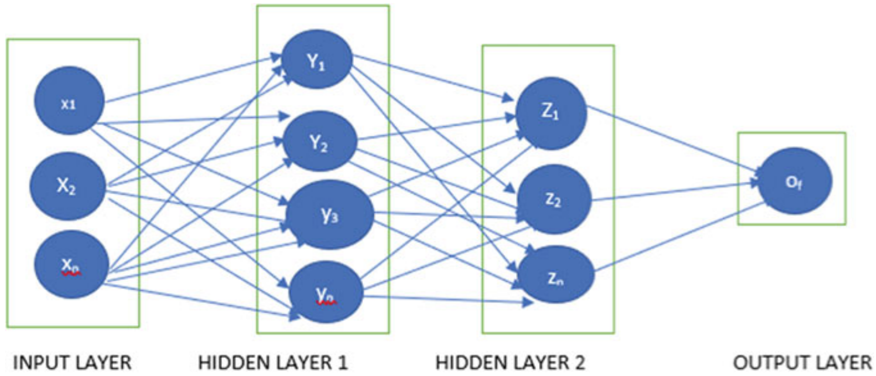

Fig. 6 ANN in feed forward form

The ANN in feed forward (Fig. 6) form is constituted by several layers and is able to perform nonlinear transforms to map inputs to output following a supervised learning paradigm using the back propagation (BP) algorithm.

All the above-mentioned methods reused to learn the applied patterns and provide classification decisions.

3 Methodology and Experimental Details

The working of the system is based on certain steps as shown in Fig. 7. There are three main components, namely the preprocessing unit, learning mechanism and the evaluation and prediction unit.

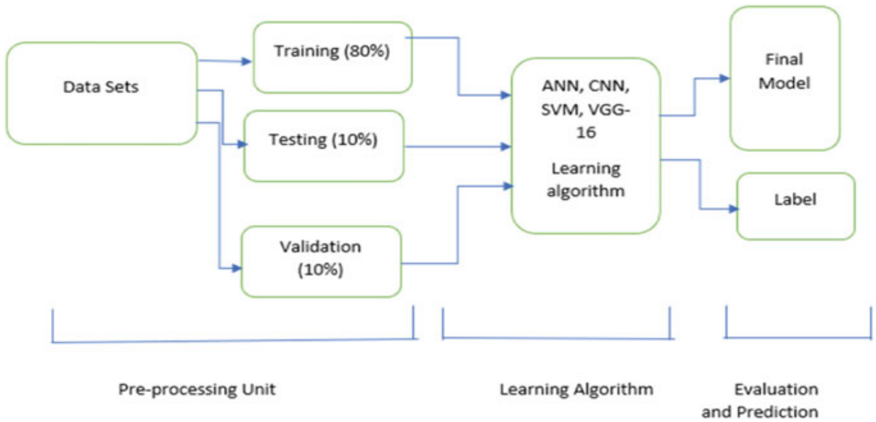

Fig. 7 Different stages of the machine learning-based face mask detection system

Fig. 8 Example of face mask datasets with mask

Fig. 9 Example of facemask datasets without datasets

3.1 Preprocessing Unit and Data Set

The preprocessing of the data is used to deal with the Kaggle dataset adopted for the work. The dataset provides both faces with and without masks on faces. It comprises about 7553 images which are grouped into a set with 3725 images for people with facemasks and 3828 images for people without masks. Also, the images are available with random sizes, colors, backgrounds, brightness and contrast variations to cover all situations. These datasets are split into 2 groups. One of them is the training set with about 6042 images (80%). The testing dataset is 755 images (10%), and the validation set is 755 images (10%) (Figs. 8 and 9).

3.2 Learning Algorithm

After receiving the information from the preprocessing section, the data are used for training of each of the learning-based system (ANN, CNN, SVM and VGG-16) and analyze the performances.

3.3 Evaluation and Prediction Unit

After completing the training process, we need to use dropout rates to prevent over-fitting. Then, we use the Mean Square Error (MSE) as the cost function to compare performance during and after training and to ascertain testing. Also, we attempt to reduce the learning rate with Adaptive Moment Estimation optimizer technique to find the best accuracy algorithm for MFD.

4 Experimental Results

Comparing the accuracy of each algorithm by using the quantitative analysis technique for the evaluation, the model accuracy and model loss graphs are shown in Figs. 10, 11, 12, 13, 14 and 15 for ANN, CNN and VGG-16 learning models, respectively.

Table 1 gives the results of different parameters calculated for those learning methods during testing. During training, the SVM shows 99% accuracy but after several rounds of testing, the performance of the VGG-16-based approach proves to be better. From result (Figs. 14 and 15; and Table 1)—efficiency. This is due to the fact that the relative feature learning and classification continuation of the VGG-16 are effective in performing the task of facemask detection despite variations in the surrounding and the inputs. The proposed systems are compared with similar existing model in terms of accuracy given in Table 2.

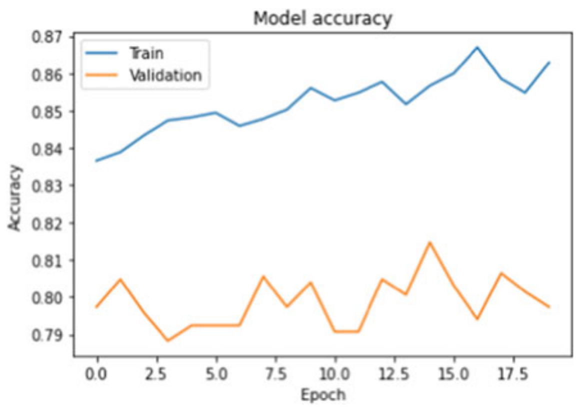

Fig. 10 Model accuracy of ANN

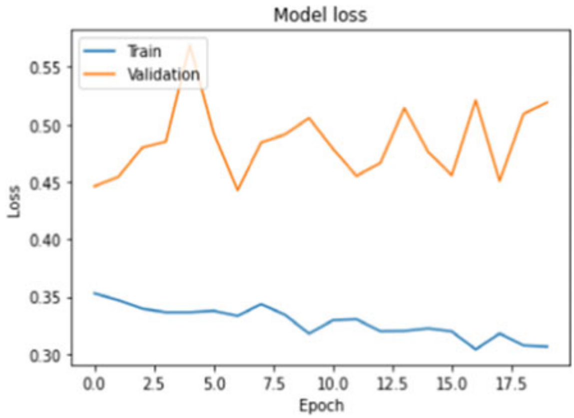

Fig. 11 Model loss ANN

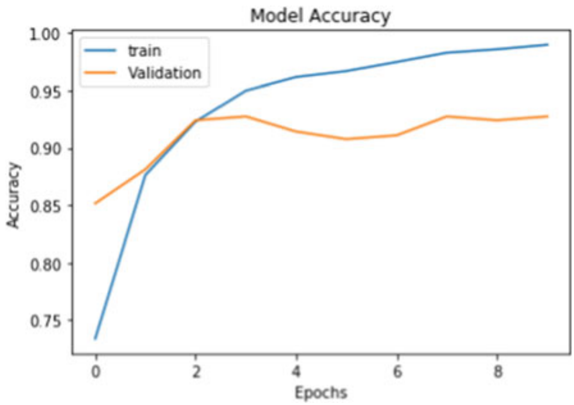

Fig. 12 CNN model accuracy

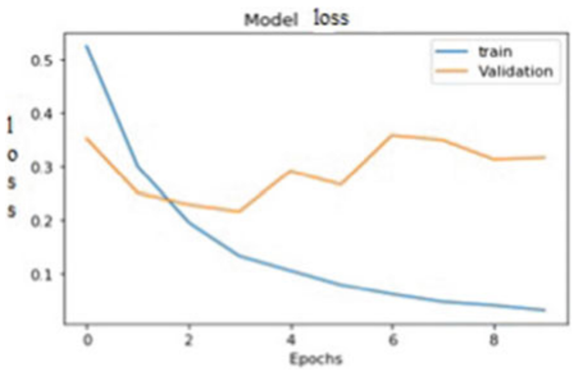

Fig. 13 CNN model loss

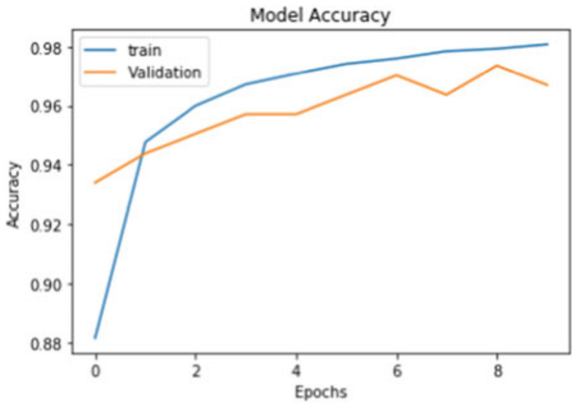

Fig. 14 VGG-16 model accuracy

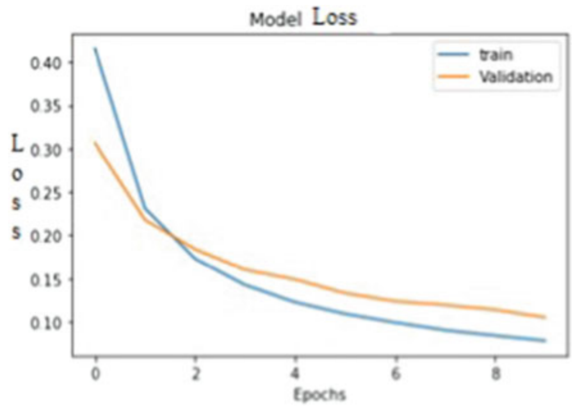

Fig. 15 VGG-16 model loss

Table 1 Performance evaluation

Sl. No.	Model	Class	Precision	Recall	F1-score	Support	Confusion matrix	Accuracy (%)
1	ANN	0	0.79	0.83	0.81	761	[634 127]	80
		1	0.82	0.78	0.8	750	[168 582]	80
2	CNN	0	0.93	0.96	0.94	761	[568 25]	94
		1	0.96	0.93	0.94	750	[43 572]	94
3	VGG-16	0	0.96	0.99	0.98	761	[588 5]	98
		1	0.99	0.96	0.98	750	[23 592]	98
4	SVM	0	0.99	0.99	0.99	761	[756 5]	96
		1	0.99	0.99	0.99	750	[6 744]	96

Table 2 Proposed system be compared with similar existing works

References	Model	Classification	Accuracy
Vijitkunsawat and Chantngarm (2020)	CNN	Yes	60%
Johns Hopkins University (2020)	CNN	Yes	–
Militante and Dionisio (2020)	VGG-16 CNN	Yes	96%
Jahromi et al. (2020)	CNN + SVM	Yes	–
Ellis (2020)	VGG-16	Yes	99.80%
Kneis (2018)	SVM	Yes	99.50%
VimaFace and Shirivastava (2022)	VGG-16	Yes	94%
Adhinata (2021)	VGG-16	Yes	92.57%
Utomo (2022)	SVM	Yes	93.30%
	Proposed model (ANN + CNN)	Yes	80%, 94%
	Proposed model (SVM)	Yes	96%
	Proposed model (VGG-16)	Yes	98%

5 Conclusion

This paper presents a few learning-based masked face detection methods designed using ANN, CNN, VGG-16 and SVM and tested for under a diverse range of situations. From the result, it can be seen that the percentage of the accuracy rate of the VGG-16-based approach has the highest efficiency. The present system can be extended to real life situations and has been validated with online testing. The proposed work can be used for various purposes like monitoring in restaurants, bus stand, railway station, airports and some other public places or social gatherings. In the future, this work can be extended for face mask detection from more standard datasets and video surveillance by using computer vision technology and deep Transfer Learning.

References

Addagarla SK, Chakravarthi GK, Anitha P (2020) Real time multi-scale facial mask detection and classification using deep transfer learning techniques. Int J Adv Trends Comput Sci Eng 9(4):4402–4408

Adhinata FD (2021) Comparative study of VGG16 and MobileNetV2 for masked face recognition. Jurnal Ilmiah Teknik Elektro Komputer dan Informatika (JITEKI) 7(2):230–237. ISSN: 2338-3070

Afkhamiaghda M, Elwakil E (2020) Preliminary modeling of Coronavirus (COVID-19) spread in construction industry. J Emerg Manag 18(7):9–17. https://doi.org/10.5055/JEM.2020.0481

Ellis R. WHO changes stance, says public should wear masks. https://www.webmd.com/lung/news/20200608/who-changes-stance-says-public-should-wear-masks. Accessed 31 Jul 2020

Feng S, Shen C, Xia N, Song W, Fan M, Cowling BJ (2020) Rational use of face masks in the COVID-19 pandemic. Lancet Respir Med 8(5):434–436. https://doi.org/10.1016/S2213-2600(20)30134-X

Jahromi R, Mogharab V, Jahromi H, Vazpour A (2020) Synergistic effects of anionic surfactants on coronavirus (SARS-CoV-2) viricidal efficiency of sanitizing fluids to fight COVID-19. bioRxiv, 2020.05.29.124107. https://doi.org/10.1101/2020.05.29.124107

Jiang X, Gao T, Zhu Z, Zhao Y (2021) Real-time face mask detection method based on YOLOv3. https://doi.org/10.3390/electronics10070837

Johns Hopkins University. COVID-19 Map-Johns Hopkins Coronavirus Resource Center. https://coronavirus.jhu.edu/map.html. Accessed 30 Jul 2020

Kneis B (2020) Face detection for crowd analysis using deep convolutional neural networks. In: Pimenidis E, Jayne C (eds) EANN 2018, CCIS 893. Springer, pp 71–80. https://doi.org/10.1007/978-3-319-98204-5_6

Krizhevsky A, Sutskever I, Hinton GE (2021) Image Net classification with deep convolutional neural networks. In: Advances in neural information processing systems, pp 1097–1105

Militante SV, Dionisio NV (2020) Deep learning implementation of facemask and physical distancing detection with alarm systems. In: The third international conference on vocational education and electrical engineering (ICVEE)

Su X, Gao M, Ren J, Li Y, Dong M, Liu X (2021) Face mask detection and classification via deep transfer learning. Multimed Tools Appl. https://doi.org/10.1007/s11042-021-11772-5

Utomo MNY (2022) Face mask-wearing detection using soft-margin support vector machine (SVM). IJID (Int J Inform Dev) 10(2):72–81. e-ISSN: 2549-7448

Vijitkunsawat W, Chantngarm P (2020) Study of the performance of machine learning algorithms for face mask detection. IEEE. ISBN: 978-1-7281-6694-0/20

VimaFace C, Shirivastava N (2022) Face and face-mask detection system using VGG-16 architecture based on convolutional neural network. Int J Comput Appl (0975-8887) 183(50)

WHO (2020) Advice on the use of masks in the context of COVID-19. Available at: https://www.who.int/publications. Accessed 31 Jul 2020 [Online]

Development and Implementation of Voice-Controlled 3D Movement of Robotic Arm Based on Embedded System

Alakesh Sarkar, Partha Bhowal, Nityananda Hazarika, Ram Kishore Roy, Hidam Kumarjit Singh, and Tulshi Bezboruah

Abstract In this paper, we propose a method for a robotic arm based on human–machine interface, which can assist physically disabled people to perform activities of their day-to-day life. The interface can be implemented in several ways, viz. by using voice command or hand gesture or through electrooculography. In the propose system, human voice command is used to control the prototype devices. An HM2007 IC is used for the voice command processing and recognition. The analog input voice command given by the user is converted to the digital output signal by the speech recognition IC. The microcontroller further processes these digital outputs for motion and directional control of the robotic arm. The paper includes the results obtained by testing the system for both speaker dependent and speaker independent cases, respectively, under noise-free and noisy environment.

Keywords Speech recognition · Robotic arm · Embedded system · Physically disabled

1 Introduction

The research in developing human–machine interfaces (HMI) for individuals with motor impairments have gain momentum in recent years. In most of the time, people with disability are relying on others to perform activities of daily life. Recent development in the field of assistive technologies has provided increase independence to those people. But there are still ample room for further improvement in these technologies. It will not only significantly improve their ability, but also contribute in

A. Sarkar · P. Bhowal · N. Hazarika (✉) · R. K. Roy · H. K. Singh · T. Bezboruah
Department of Electronics and Communication Technology, Gauhati University, Guwahati, Assam 14, India
e-mail: hazarikanitya@gmail.com

J. K. Deka et al. (eds.), *Emerging Technology for Sustainable Development*, Lecture Notes in Electrical Engineering 1061,
https://doi.org/10.1007/978-981-99-4362-3_40

increasing independence and quality of their life. The HMI primarily based on brain–computer interfaces (BCI), electrooculography (EOG) interfaces, or voice recognition (VR) (Martínez et al. 2013). These entire interfaces have their own pros and cons. Nowadays, robots are widely used in many fields starting from mechanization of work in industry to highly sensitive research in outer space exploration. Many mathematical models and scientific tools are used to create intelligent robot for rapidly expanding range of human activities. The benefit of using robot is that once it is programmed, it repeatedly performs the task with a high accuracy than that of the most experienced human operator. Robots are built and programmed to be job specific. The human–robot interaction (HRI) is one of the challenging fields of research and is still remaining a lot to contribute (Gatti et al. 2014; Gosavi et al. 2013). In (Sivaraman et al. 2021), movement of a robotic arm is achieved by using motion gloves. The arm can imitate the movement of human palm through this technique. Real-time remote controllability by means of Bluetooth module and Internet are also addressed in Sharma et al. (2018). Another way of interfacing human hand with robotic arm is through image processing technique (Lengare and Rane 2015). This technique takes real-time video of human hand and tracks it to imitate its motion in the robotic arm. Speech recognition is one of the prominent technologies for HRI and human–computer interface (HCI). Speech recognition allows us to interact with an application with our voice command. The speech recognition allows us to provide input by talking. In literature, most of the work on speech-based robotic arm control system has used voice recognition module HM2007 for speech detection (Dharaskar et al. 2012; Shankar and Raj 2017). However, the limitations of using this voice recognition module are not properly formulated.

In this work, we have developed, implemented, and tested a voice command controlled three-dimensional (3D) robotics arm movement system. Our goal is to develop an assistive technology by leveraging the human voice.

2 Implementation Details

The block diagram of the complete experimental setup of the voice-controlled robotic arm automatic manipulator is shown in Fig. 1. It consists of four sections, namely: (i) voice recognition (VR) section, (ii) microcontroller (μC) as central processing section, (iii) driver circuit section, and (iv) robotic arm manipulator section. The heart of the system is HM2007 voice recognition kit (HM2007p 2016). The user voice command through the microphone is given to the voice recognition section as analog input. This analog signal is processed and recognized by the VR unit. This unit produces output in the form of digital signal which is then applied to the μC. The μC IC AT89S52 is used as central processing unit in our system (Microcontroller AT89s51 2016). Based on each voice command, the μC generates specific control signal for the motion and direction control of the robotic arm. The robotic arm is based on three motors, rotated in three dimensions.

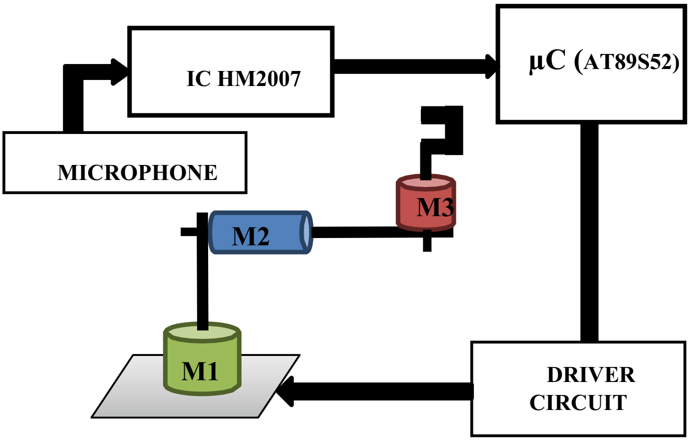

Fig. 1 Block diagram of the speech controlled robotic arm

Initially, HM2007 voice recognition kit is trained by a list of verbal vocabulary by the user. The microphone is used to pick up the command. Table 1 gives the list of voice commands used for training the kit for specific type of operation to be performed by the robotic arm. The output pins of voice recognition kit are connected correspondingly to the port 1 of the µC. The processor generates specific control signal for each command given by the user and control direction of the motor(s). The µC pins P1.0, P1.1, and P1.2 generate enable signal for Motor 1 (M1), Motor 2 (M2), and Motor 3 (M3), respectively. To control the directional movement, pin P1.3 generates signal for clockwise rotation and pin P1.4 generates signal for the anticlockwise rotation for all three motors, respectively.

Table 2 gives the pin connection of the µC with motor for directional motion. Table 3 gives the digital output of the HM2007 IC vs. the µC generated signal for each voice command.

Table 1 List of voice commands used for training the speech recognition kit for specific type of operation to be performed by the robotic arm

Voice command	Operation performed by robotic arm
RIGHT	Rotate Motor 1 in the right direction
LEFT	Rotate Motor 1 in the left direction
UP	Rotate the Motor 2 in up direction
DOWN	Rotate the Motor 2 in down direction
CLOCKWISE	Rotate the Motor 3 in clockwise direction
ANTICLOCKWISE	Rotate the Motor 3 in anticlockwise direction
STOP	Stop all

Table 2 µC pin configuration versus motor directional motion

Motor	Direction of rotation of motors	Microcontroller pins	
Motor 1	Clockwise	P1.0	P1.3
	Anticlockwise	P1.0	P1.4
Motor 2	Clockwise	P1.1	P1.3
	Anticlockwise	P1.1	P1.4
Motor 3	Clockwise	P1.2	P1.3
	Anticlockwise	P1.2	P1.4

Table 3 Digital data output of HM2007 versus microcontroller generated signal for operation

Data output of voice recognition kit								Motors movement
D7	D6	D5	D4	D3	D2	D1	D0	
0	0	0	0	1	0	0	1	09 (Right)
0	0	0	1	1	0	0	0	18 (Left)
0	0	0	0	0	1	0	1	05 (Down)
0	0	0	1	0	1	0	0	14 (Up)
0	0	0	0	0	1	1	0	03 (Clockwise)
0	0	0	1	0	0	1	0	12 (Anticlockwise)

2.1 Software Description

The Proteus simulator and Keil 51 C editor are used to simulate and debug the code. The program is written in embedded C. The generated hex code is used to burn into the µC. The flowchart of the program is given in Fig. 2.

3 Results and Discussions

The system is tested for both speaker dependent as well as speaker independent cases. The system is also tested under different environmental conditions, viz. with noise-free and noisy environment. The noise-free environment is created by testing the system in a silent and close room, where it is very hard to reach any other voice. As we don't have noise generating source at specific measured level, in order to test our system in noisy situation, we have created random noisy environment. The noisy environment is created by running all the fans and opening all the doors in the room. At the same time, 3 peoples at three sides of the speaker at a distance of 10 cm are allowed to talk in the moderate voice. First, the system is tested in noise-free environment by using the voice of the person who has trained the system and the responses are recorded and are given in Table 4. Second, the system is tested by the same trained person under noisy environment and the responses are recorded

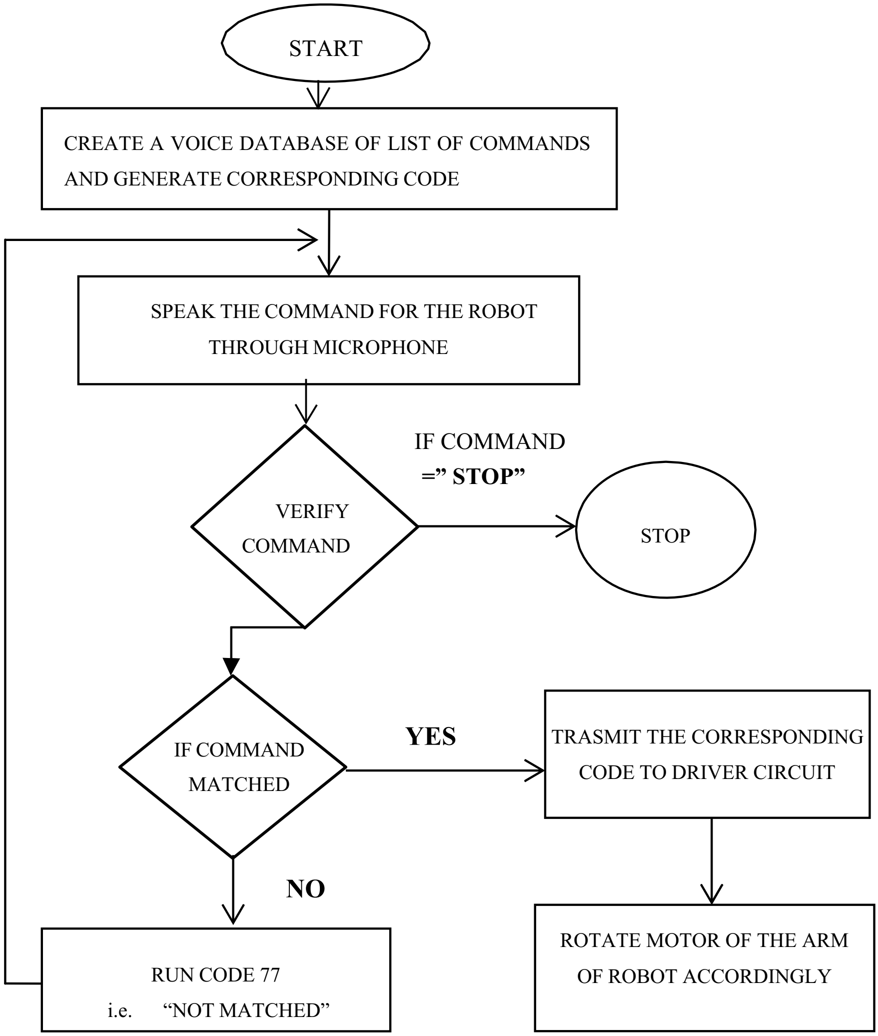

Fig. 2 Flowchart of voice-controlled robotic arm

and are given in the Table 5. Next, the system is tested under noise-free and noisy environment by the person other than who has not trained the system. The responses are recorded and are given in the Table 6 and Table 7, respectively.

Table 8 gives the recognition rate of the system for both speaker dependent and speaker independent cases, respectively, under noise-free and noisy environment.

Table 4 Testing result of robotic arm movement by voice command by trainer under noise-free environment

VOICE command (For movement of arms)	Number of trails	Recognized	Not recognized
RIGHT	10	10	0
LEFT	10	10	0
UP	10	10	0
DOWN	10	10	0
CLOCKWISE	10	10	0
ANTICLOCKWISE	10	10	0

Table 5 Testing result of robotic arm movement by voice command by trainer under noisy environment

VOICE command (For movement of arms)	Number of trials	Recognized	Not recognized
RIGHT	10	10	0
LEFT	10	10	0
UP	10	10	0
DOWN	10	10	0
CLOCKWISE	10	10	0
ANTICLOCKWISE	10	09	1

Table 6 Testing result of robotic arm movement by voice command by a person other than trainer under noiseless environment

VOICE command (For movement of arms)	Number of trails	Recognized	Not recognized
RIGHT	10	09	01
LEFT	10	10	00
UP	10	10	00
DOWN	10	07	03
CLOCKWISE	10	09	01
ANTICLOCKWISE	10	08	02

Table 7 Testing result of robotic arm movement by voice command by other than trainer under noisy environment

VOICE command (For movement of arms)	Number of trails	Recognized	Not recognized
RIGHT	10	08	02
LEFT	10	10	00
UP	10	09	01
DOWN	10	07	03
CLOCKWISE	10	09	01
ANTICLOCKWISE	10	06	04

Table 8 Recognition rate of voice-controlled robotic arm under different testing environment

Voice command under case	Environment of operation	Recognition rate in %
Speaker dependent	Noise-free environment	100
	Noisy environment	96.67
Speaker independent	Noise-free environment	80
	Noisy environment	63.33

4 Conclusions

In this study, a systematic approach to develop and implement voice-controlled 3D robotic arm has been described. The study shows that the system is highly stable with the commands of the voices of the person who had trained the system in noise-free environment. That means the system is highly speaker and noise dependent. As the noise level increases, the recognition rate of the system is prominently falls. The recognition rate of the system also depends on length of the word and the way the words are pronounced. For the word which is longer and similar in pronunciation, the recognition rate falls sharply. If there are more numbers of homonym words as command, the system recognition rate decreases.

References

Dharaskar DR, Chhabria SA, Ganorkar S (2012) Robotic arm control using gesture and voice. Int J Comput Inf Technol Bioinf (IJCITB) 1(1):41–46

Gatti J, Fonda C, Tenze L, Canessa E (2014) Voice-controlled artificial handspeak system. Int J Artif Intell Appl (IJAIA) 5(1)

Gosavi SD, Khot UP, Shah S (2013) Speech recognition for robotic control. Int J Eng Res Appl 3(5):408–413

HM2007p (2016) Datasheets. Available at: http://www.alldatasheet.com, Date Viewed: Aug 2016

Lengare PS, Rane ME (2015) Human hand tracking using MATLAB to control Arduino based robotic arm. In: 2015 international conference on pervasive computing (ICPC) 2015 Jan 8. IEEE, pp 1–4

Martínez JA, Ubeda A, Ianez E, Azorin JM, Perez-Vidal C (2013) Multimodal system based on electrooculography and voice recognition to control a robot arm. Int J Adv Robot Syst 10:1–9

Microcontroller AT89s51 (2016) Datasheets. Available at: http://www.alldatasheet.com, last accessed: Aug 2016.

Shankar SS, Raj KVA (2017) Design and fabrication of voice activated robotic arm. Int Res J Eng Technol 4:1737–1741

Sharma S, Sahai S, Joshi J, Hema N (2018) Stage-wise development of a remote-controlled robotic arm. In: 2018 fifth international conference on parallel, distributed and grid computing (PDGC). IEEE, pp 364–367

Sivaraman P, Kumar SV, Aasvitha A, Yogitha U, Varshini S, Priya GV, Krishna GM (2021) Humanoid gesture control ARM with manifold actuation by embedded system. Mater Today Proc 37:2749–2758

PRI Modulation Classification in EW Systems Using Deep Learning

Purabi Sharma and Kandarpa Kumar Sarma

Abstract The analysis of radar signals is a critical task in Electronic Warfare (EW) environments and decides the nature of counter employments. For an Electronic Support (ES) system, the challenge is to efficiently recognize the source of the threat radiation. In dense EW situations, detection of Pulse Repetition Interval (PRI) modulation modes of radar signal significantly aids the manifestation of emitter in the process of radar emitter recognition. Developments in Artificial Intelligence (AI) methods suggest that this emerging technology can be very effective for such purposes. In this direction, an automatic approach for recognizing eight kinds of complex PRI modulation types based on Continuous Wavelet Transform (CWT) and Convolutional Neural Network (CNN) is proposed. The CWT is used to decompose the PRI modulation sequence to obtain different time–frequency components, and the CNN is used to extract features from the 2D scalogram composed of temporal and spectral elements for deriving appropriate class decisions. The simulation result shows that the proposed method not only enhances the performance but is also robust in an environment with noisy content. The recognition accuracy is 98.2% with 30% spurious pulses in the simulation environment.

Keywords Electronic warfare · PRI modulation · CWT · Convolutional neural network

P. Sharma (✉) · K. K. Sarma
Department of Electronics and Communication Engineering, Gauhati University, 781014, Guwahati, Assam, India
e-mail: purabis1989@gmail.com

K. K. Sarma
e-mail: kandarpaks@gauhati.ac.in

J. K. Deka et al. (eds.), *Emerging Technology for Sustainable Development*,
Lecture Notes in Electrical Engineering 1061,
https://doi.org/10.1007/978-981-99-4362-3_41

1 Introduction

The electromagnetic environment encountered in radio frequency (RF) domain is more crowded due to the usage of advanced communication, navigation and radar systems (Niekerk and Cloete 2015; Eaves and Reedy 2012). When multiple radars transmit signals simultaneously, an Electronic Support (ES) system receives an interleaved stream of signals. The function of ES system is to separate these signals (Nishiguchi and Kobayashi 2000) and thus identify and locate the sources of hostile electromagnetic (EM) radiation for the purpose of immediate threat recognition (Sharma et al. 2020). In this direction, Pulse Repetition Interval (PRI) modulation types of radar signals hold the key and the recognition of such wave patterns play a very significant role in identifying emitters. Radar PRI modulation mode can be used to infer the function and application of the radar radiation source, which is an important basis for radiation source identification in ES system (Nishiguchi and Kobayashi 2000). Hence, recognition of PRI modulation types is crucial for the identification of radar emitter and its working pattern. However, with the diversification of radar functions and steady advancement of countermeasures, PRI modulations have become more intricate. Moreover, as PRIs mix with background noise, the complexities increase further.

There are several methods available in literature for recognition of PRI modulation types. A method based on auto-correlation and normalization is presented in Shi et al. (2016). A method based on the three features of PRI (like zero-crossing density, harmonic amplitude ratio and sign properties of difference of the waveform) sequence in time and frequency domain is discussed in Hu and Liu (2010). A method based on three-layered Artificial Neural Network (ANN) and features of PRI modulation type such as local stationarity, monotonic directionality, and symmetry is discussed in Liu and Zhang (2017). A novel method based on two-stage hierarchical classification technique and extracted sub-patterns is reported in Kauppi et al. (2010). However, its performance deteriorates when there is high ratio of noise that breaks the regularity of the sub-patterns. In (Nguyen et al. 2018), a new learning-based method called Feature-based Neural Network is used for classification of seven PRI modulation types but this method rely on a set of handcrafted features of specific PRI modulations types. In (Tang et al. 2019), a decision tree-based method is discussed for recognition of four PRI modulation types with a dependence on a large number of handcrafted thresholds, high time-latency, sensitive to the noise level and change of PRI parameters.

Overall, the key aspect to note regarding the aforementioned techniques is that these can recognize some of the basic PRI modulation modes with certain variations in approaches. However, the limitations are more or less similar that they need a significant amount of data preprocessing and computation time. Also the results are unable to adapt to environments infested with a high ratio of noisy pulses. Moreover, the learning-based methods require a careful design of features and a feature extraction process before implementing neural network. As a result, these approaches are unable to quickly respond to changes in PRI modulations and provide autonomous decision making. This backdrop provides ample of opportunities for deep neural networks (DNN)-based methods because they don't require handcrafted features, demonstrate resilience to noise, pattern and background variations, learn continuously and possess reliable adaptive capability. A CNN-based method for recognition of PRI modulation modes is reported in Li et al. (2018). In this method, different PRI sequences are directly used as an input to CNN providing a recognition accuracy of 96.1% in complex environment. However, the method has not considered the subtypes of complex PRI modulation modes. Another method based on Asymmetric Convolution Squeeze-and-Excitation (ACSE) network and features of PRI sequence in auto-correlation domain is discussed in Qu et al. (2020). The method provides a recognition accuracy of more than 95% at low SNR value but confined only to a few basic PRI modulation types.

In this paper, an automatic method based on CNN and Continuous Wavelet Transform (CWT) features to recognize eight complex PRI modulation modes is proposed. The innovation point in the proposed method is, to improve the classification performance of CNN and to incorporate the time–frequency attributes of the PRI patterns, CWT is used. The high resolution and locality in both time and frequency provide good features for the identification of similar modulation types. This method makes use of the feature representation capabilities of CNN and multi-resolution content representation ability of CWT and deals with complex variations of the identified PRI modulation modes. Additionally, this method avoids the use of sophisticated handcrafted features and does not require delicate data preprocessing. The rest of the paper is organized as follows. In Sect. 2, we present some preliminaries about PRI modulations types used in the proposed method. In Sect. 3, we present the techniques used in the proposed algorithm. In Sect. 4, experimental results of the algorithm are presented. Finally, the summary of the work and conclusion is given in Sect. 5.

2 PRI Modulation Modes

Modern multi-purpose radars create multiple sophisticated PRI patterns, each for different function. The PRI sequence of a radar pulse signal is defined as (Nguyen et al. 2018):

$$P(j) = t(j+1) - t(j),\ j = 0, 1, 2, ..., L-1$$

where '$t(j)$' is the estimated time of arrival of jth radar pulse and 'L' is the number of detected pulse. The pattern of a PRI sequence is governed by a specific PRI modulation type. In this work, the following eight different PRI modulation types used in modern radar systems are considered:

- **Constant PRI**: It is ideally a consistent value which has no variation. Constant PRI is commonly used in search and track radar (Li et al. 2018).

- **Jittered PRI**: This PRI value fluctuates randomly in the range between 1% and 30% around a certain constant PRI value following uniform or Gaussian distribution (Tang et al. 2019). Jitter PRI is used in radars as an electronic defense to reduce the effects of some types of jamming (Tang et al. 2019).
- **Dwell and Switch (D&S) PRI**: This type of PRI sequence consists of some constant PRI values. It remains on a certain value for a short duration of time before switching to another value. D&S PRI is basically used by pulse Doppler radars to resolve velocity or range ambiguities (Tang et al. 2019).
- **Staggered PRI**: In this type of PRI sequence, two or more stable PRI values appear in a cyclic order. Staggered PRI sequence is generally used to eliminate blind speeds in Moving Target Indication (MTI) radar systems (Nguyen et al. 2018).
- **Sliding PRI**: The values of sliding PRI sequence change over time, it increases continuously until an upper threshold value is reached and then quickly returns to a minimum value (Brzan et al. 2021). Basically, it resembles a sawtooth waveform (Katsilieris et al. 2017). Sliding PRI is used to prevent radar target shadowing and for constant altitude coverage during elevation scanning (Qu et al. 2020).
- **Wobulated PRI**: This type of PRI sequence varies periodically such as sinusoidal. This variation of PRI is used to avoid eclipsing for ranging and for missile guidance (Li et al. 2018).

Sliding and Wobulated PRIs are generally referred to as complex PRI modulation types. The subtypes of these complex PRI modulation types are sawtooth, sine, saturated sine and triangle (Katsilieris et al. 2017). The curves of different PRI modulation types are shown in Fig.1. In real EW environment, PRIs are vulnerable to errors and spurious pluses. As a result significant amount of distortion occurs in the original form of a PRI sequence, making the classification task extremely difficult. This situation can be overcome with a CNN that have high tolerance to noise induced variations. The method proposed in this paper can recognize all the subtypes of complex PRI modulation types (saturated sine and triangle) along with the basic PRI modulation modes, i.e., constant, jitter, sliding, staggered, D&S and Wobulated efficiently.

3 Proposed Method

In this section, the proposed method and its various stages for recognition of PRI modulation types are explained in detail. The first step in this method is to find 2D-scalogram of the input PRI sequences using CWT. These scalograms are then given as input to a CNN for classification purpose. The work flow diagram of the proposed method is shown in Fig. 2.

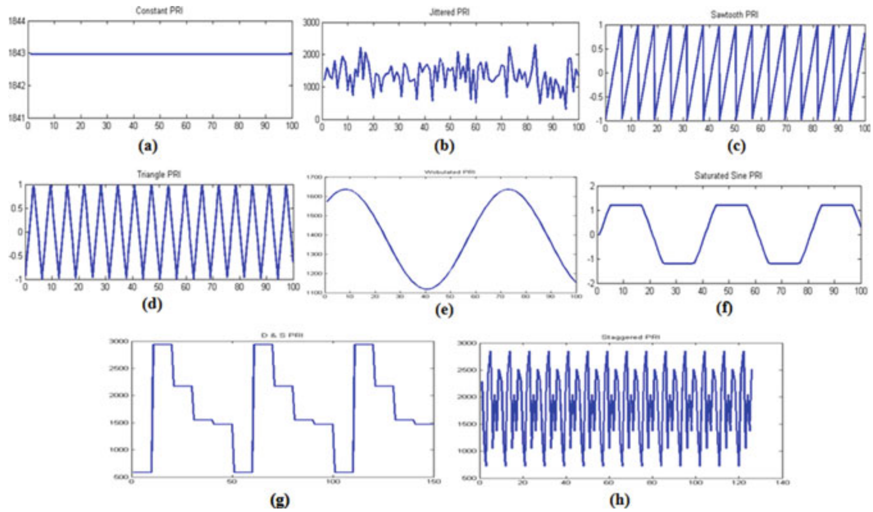

Fig. 1 PRI modulation types: **a** Constant **b** Jittered **c** Sawtooth **d** Triangle **e** Wobulated **f** Saturated sine **g** D & S **h** Staggered

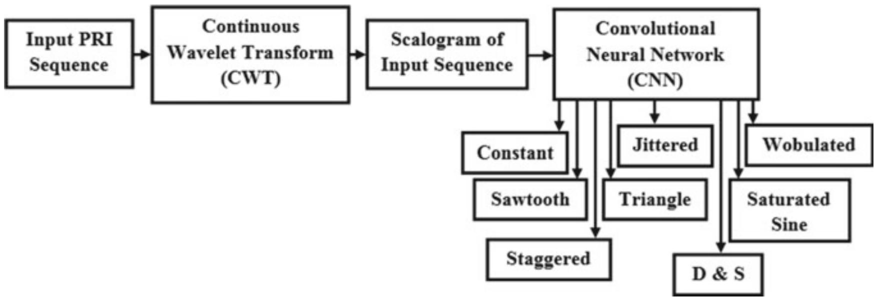

Fig. 2 Workflow diagram of the proposed method

3.1 Continuous Wavelet Transform (CWT) Features

In the proposed method, CWT of various PRI sequences is computed then using the coefficient matrix of CWT, scalogram plot is obtained. The CWT provides a multi-resolution representation of a signal by convolving it with a scaled mother wavelet (Brzan et al. 2021). The coefficients reflect the similarity between the analyzed signal and the wavelets. Thereafter, absolute of CWT coefficients is calculated to form a scalogram. The scalogram represents the spread of the signals energy as a function of time and frequency (scale) (Brzan et al. 2021). Therefore, CWT is used in the proposed method to incorporate the time–frequency attributes of the PRI patterns and to improve the classification performance of CNN. The scalogram of two different PRI modulation types is shown in Fig. 3.

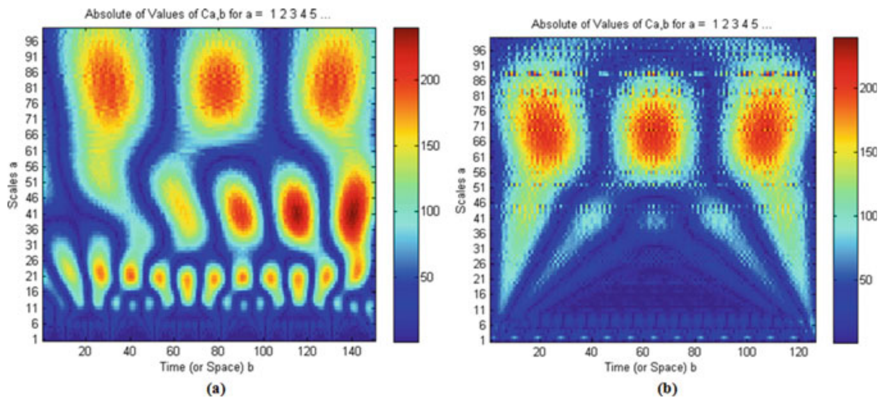

Fig. 3 Scalograms of PRI modulation types: **a** D&S **b** Staggered

3.2 CNN Architecture

CNN adopts convolutional operations to avoid tedious data preprocessing and extract discriminant features for performing classification and regression in diverse range of applications (Wang et al. 2021). The proposed CNN-based technique can provide suitable classification result even in challenging environments with spurious pulses. These features of CNN have perfectly met the requirement for PRI modulation mode recognition. A CNN has multiple layers such as convolution layers, max-pooling layers and fully connected layers. In this method, four consecutive convolution and max-pooling operations are used to extract features from the scalogram. The number of filters is increased from 8 to 64 along the convolution layers with a constant filter size of 3 × 3. The weights of the convolution kernel are trained using the back-propagation (BP) error algorithm. The Rectified Linear Unit (ReLU) is used as the nonlinear activation function for all convolution layers to increase nonlinearity in the image. A batch normalization layer is also included between each of the convolution and ReLU layers. This layer is used to normalize the feature map of each channel so as to reduce training time and sensitivity of network initialization. A filter of size 2 × 2 with a stride of 2 is used for all the max-pooling layers that downsample the dimension of feature maps by a factor of 2. Finally, for classification purpose, a fully connected layer is used followed by a nonlinear activation function called softmax that normalizes the output of fully connected layer to target class probabilities. The CNN architecture is designed according to the complexity of the data. The method is tested with various combinations of filter size and number of filter in convolution layer and max-pooling layer. Suitable results were obtained for the mentioned parameters.

4 Results and Discussion

Eight different types of PRI sequences are simulated in the proposed method. All the parameters are simulated based on the situations that may come across in a real EW scenario as reported in Li et al. (2020). In order to evaluate the performance of the proposed method, a base set of 1030 randomly generated PRI sequences are used for training and validation purposes. To give proper representation to all types of noise condition that might exist in an EW scenario, noise variations like white Gaussian noise, speckle noise and burst noise are considered in the simulated PRI sequences with SNR fluctuations in the range of −5 dB to 25 dB. Sample size is further reinforced by incorporating more variation in the training sample using bootstrapping technique. Several copies of the original sample set are generated using this technique. Out of the data generated, the original sequences are used to carry out benchmarking training of the network which involves 80% of data for CNN learning and remaining 20% for validation purpose. Another set of multiple copies of 216 randomly generated PRI sequences are used for testing the method. The pulse length for each PRI sequence is set to 300. The data generation as well as training is performed in MATLAB simulation environment. In the training algorithm of CNN, stochastic gradient descent with momentum (SGDM) is used as the optimizer and the cross-entropy is taken as the loss function. All the parameters of the CNN architecture are set based on trial–error-optimize approach to make the recognition achieve the best performance. The training progress graph of CNN architecture used in the method is shown in Fig. 4. The method successfully recognizes all the eight PRI modulation types with a recognition accuracy of 98.2%. The confusion matrix for modulation recognition is shown in Fig. 5.

Table 1 gives the comparison of proposed method with existing methods in the literature, in terms of recognition accuracy. Though the recognition accuracy of the techniques reported in the above literature is high but the downside of these methods reported in Shi et al. (2016), Hu and Liu (2010), Liu and Zhang (2017), Kauppi et al. (2010), Nguyen et al. (2018), (Tang et al. 2019) is that they requires large amount

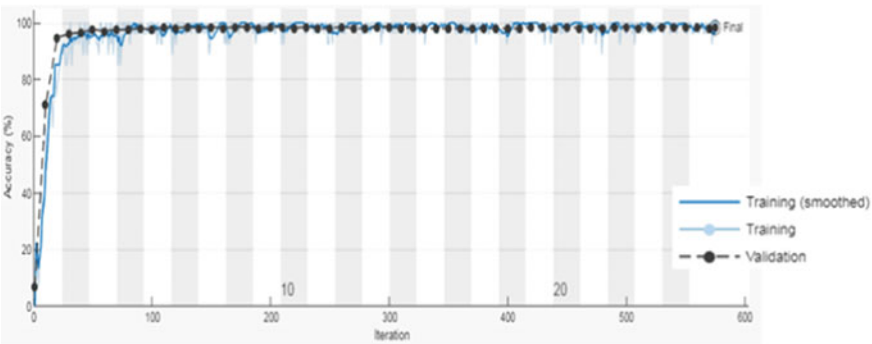

Fig. 4 Training progress graph of the CNN used in the proposed method

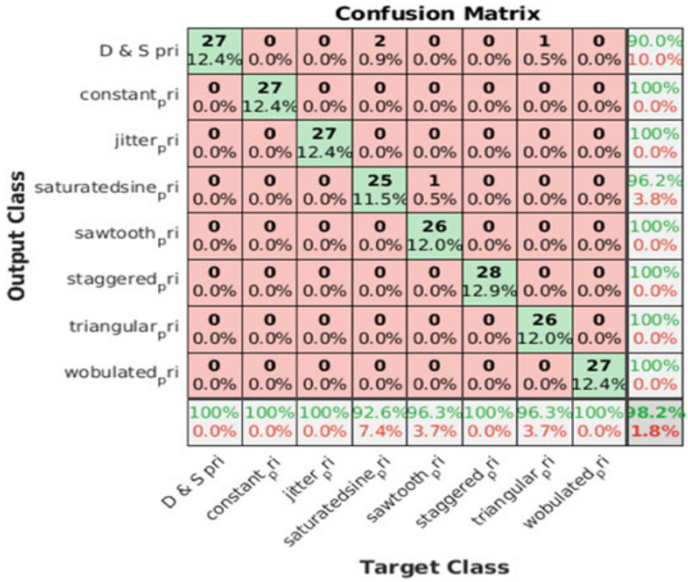

Fig. 5 Confusion matrix of CNN

Table 1 Comparison of the proposed method with existing techniques

Technique	Recognition accuracy (%)
Auto-correlation and normalization (Shi et al. 2016)	97
Time and frequency domain features of PRI sequence (Hu and Liu 2010)	100
Neural Network (Liu and Zhang 2017)	99
Feature set based on PRI sequence and Hierarchical classification (Kauppi et al. 2010)	99
Feature-based Neural Network (Nguyen et al. 2018)	99.5
Decision tree-based method (Tang et al. 2019)	96
CNN and time series PRI sequence (Li et al. 2018)	96.1
ACSE and auto-correlation features of PRI sequence (Qu et al. 2020)	> 95
Proposed method	98.2

of data preprocessing and feature extraction which is time consuming. Moreover, these methods have not considered subtypes of complex PRI modulation types. The proposed method manages to overcome all these limitations as well as achieves higher recognition accuracy than the deep learning-based method discussed in (Li et al. 2018; Qu et al. 2020).

5 Conclusion

In this paper, an automatic method based on CWT features and CNN is proposed to resolve a significant task of classification of PRI modulation in EW environment as part of an ES system. The key aspect of PRI modulation type recognition is carried out using a deep learning-based approach. The method can recognize subtypes of complex PRI modulation modes along with the basic PRI modulation modes efficiently. Simulation results show that the recognition accuracy is 98.2% and robustness to typical noise condition that exists in an EW environment. Furthermore, the use of time–frequency attributes of the PRI patterns helps to improve the classification performance of CNN and it does not require complex handcrafted features and manually done complex data preprocessing. In the future work, it is planned to incorporate topological variations in the structure of network to improve the performance of the algorithm in presence of different types of noise with low SNR value and evaluate evolving threat scenarios.

References

Brzan H, Moca VV, Ichim AM, Muresan RC (2021) Fractional superlets. In: Proceedings of 28th European signal processing conference (EUSIPCO), IEEE, Amsterdam, pp 2220–2224

Eaves J, Reedy E (2012) Principles of modern radar, Springer, Berlin

Hu G, Liu Y (2010) An efficient method of pulse repetition interval modulation recognition. In: Proceedings of international conference on communications and mobile computing (CMC). IEEE, China, pp 287–291

Katsilieris F, Apfeld S, Charlish A (2017) Correlation based classification of complex PRI modulation types. In: Proceedings of sensor signal processing for defence conference (SSPD). IEEE, UK, pp 1–5

Kauppi JP, Martikainen K, Ruotsalainen U (2010) Hierarchical classification of dynamically varying radar pulse repetition interval modulation patterns. Neural Netw 23(10):1226–1237

Li X, Huang Z, Wang F, Wang X, Liu T (2018) Toward convolutional neural networks on pulse repetition interval modulation recognition. IEEE Commun Lett 22(11):2286–2289

Li X, Liu Z, Huang Z (2020) Attention-based radar PRI modulation recognition with recurrent neural networks. IEEE Access 8:57426–57436

Liu Y, Zhang Q (2017) An improved algorithm for PRI modulation recognition. In: Proceedings of international conference on signal processing, communications and computing (ICSPCC). IEEE, China, pp 1–5

Nguyen P, Ha K, Nguyen HQ (2018) Classification of pulse repetition interval modulations using neural networks. In: 2018 IEEE symposium series on computational intelligence (SSCI). IEEE, India, pp 1739–1743

Niekerk BV, Cloete C (2015) Management information systems for electronic warfare command and decision support. J Inf Warfare 14(1):63–74

Nishiguchi K, Kobayashi M (2000) Improved algorithm for estimating pulse repetition intervals. IEEE Trans Aerosp Electron Syst 36(2):407–421

Qu Q, Wei S, Wu Y, Wang M (2020) ACSE networks and autocorrelation features for PRI modulation recognition. IEEE Commun Lett 24(8):1729–1733

Sharma P, Sarma KK, Mastorakis NE (2020) Artificial intelligence aided electronic warfare systems-recent trends and evolving applications. IEEE Access 8:224761–224780

Shi Z, Wu H, Shen W, Cheng S, Chen Y (2016) Feature extraction for complicated radar PRI modulation modes based on autocorrelation function. In: Proceedings of advance information management, communicates, electronics and automation conference (IMCEC). IEEE, China, pp 1617–1620

Tang Y, Tang M, He X, Han J, Fan X (2019) Method for automatically identifying PRI patterns of complex radar signals. J Eng 2019(20):6975–6978

Wang T, Lu C, Sun Y, Yang M, Liu C, Ou C (2021) Automatic ECG classification using continuous wavelet transform and convolutional neural network. Entropy (Basel), 23(1):119(2021). https://doi.org/10.3390/e23010119

JSCC-UFMC in Multi-User Antenna Diversity Using Hybrid Beamforming for Millimeter Wave Wireless Communications

Surajit Deka and Kandarpa Kumar Sarma

Abstract Joint source and channel coding (JSCC) has been found to be effective in ensuring better link reliability and quality of service (QoS) while using the already scarce spectrum efficiently. For better spectrum management, universal filter multi-carrier (UFMC) has been receiving greater attention for achieving high throughput. Multi-user (MU) multi-input multi-output (MIMO) antenna diversity has already been accepted to be a key element and also for upscaling data rates, while millimeter wave (MMW) has been regarded to be a critical technology for 5G wireless communication. In this paper, JSCC and UFMC have been deployed over a MUMIMO antenna diversity aided by hybrid beamforming. The composite setup is experimented with a range of scenarios including the adoption of the framework in a MMW arrangement. Experimental results involving peak-to-average power ratio (PAPR), power spectral density (PSD) and bit error rate (BER) have shown improvement in performance. Further, there is an increase in reliability in data recovery and channel capacity.

Keywords Joint source and channel coding (JSCC) · Universal filtered multi-carrier (UFMC) · Massive MIMO · Millimeter wave (MMW)

1 Introduction

The rapid emergence of smart applications in modern wireless communication technology places stringent requirement of better quality of service (QoS), higher bandwidth and spectrum efficiency. There are a few challenges faced by current and upcoming 5G technology (Hammoodi 2019). Next-generation wireless networks aim to deliver high data transmission rates of up to 20 Gb/s, low network latency of

S. Deka (✉) · K. K. Sarma
Department of Electronics and Communication Engineering, Gauhati University, Guwahati 781014, Assam, India
e-mail: dekasurajit123@gmail.com

K. K. Sarma
e-mail: kandarpaks@gauhati.ac.in

J. K. Deka et al. (eds.), *Emerging Technology for Sustainable Development*, Lecture Notes in Electrical Engineering 1061,
https://doi.org/10.1007/978-981-99-4362-3_42

up to 1 ms and the ability to service up to 1 million devices per square kilometer (Wen et al. 2018). Achieving these features will require the implementation of advanced techniques, including joint source and channel coding (JSCC), modulation schemes and antenna deployment strategies. These techniques will be crucial in optimizing the performance of the networks and ensuring that they can meet the demands of modern wireless communication.

In general, the individual coding of source and channel is common in wireless communication systems and play important roles in data transmission (Gao and Tuncel 2013). In source coding, redundant bits are removed to compress the data and in channel coding, additional data redundancy is included along with the original data in order to mitigate the effects of noise and achieve improved QoS. The implementation of separate source and channel coding (SSCC) methods can lead to increased system complexity (Tian et al. 2014). However, this complexity can be reduced by utilizing JSCC, which offers advantages such as lower computational complexity, improved reception quality, better link reliability and more efficient data representation through redundancy elimination. The use of fountain coding has been shown to be a promising technique in this regard. By combining JSCC with fountain coding, near-optimal capacity can be achieved with reduced bit error rate (BER) (Deka and Sarma 2019). In addition to these techniques, multiplexing schemes are also important.

Orthogonal frequency division multiplexing (OFDM) is a popular technology used in broadband wireless systems, such as 4G and is expected to play a significant role in 5G systems as well (Ma 2017). However, OFDM has several drawbacks, including spectral inefficiency due to the cyclic prefix, out-of-band (OOB) emissions, high peak-to-average power ratio (PAPR), inter-carrier interference (ICI) and stringent synchronization requirements (Almutairi et al. 2019). To address these issues, an efficient multi-carrier modulation technique called universal filtered multi-carrier (UFMC) has been developed by generalizing OFDM and filter bank multi-carrier (FBMC) modulation. UFMC is better suited for delay-sensitive applications and burst transmissions compared to (OFDM-) FBMC, as FBMC filters the entire band leading to data loss, while UFMC addresses this issue. Additionally, UFMC offers high spectral efficiency with lower overhead, reduced design complexity compared to FBMC and compatibility with all variations of multi-input multi-output (MIMO) antenna diversity. Therefore, UFMC is considered a suitable multi-carrier modulation technique for 5G wireless communication systems (Yarrabothu and Nelakuditi 2019).

The ever-growing demand for high data rate and more user capacity makes it necessary to use the available spectrum more efficiently. Antenna diversity approach called MIMO is one such way (Wu et al. 2009; Deka and Sarma 2020). The spectral efficiency can be enhanced by MIMO in two ways. Firstly, to communicate at the same time with several mobile station (MS) receivers, a base station (BS) transmitter is allowed. Secondly, tens or hundreds number of BS elements are allowed that increases the data streams within a cell for better communication. Multi-user (MU) version of MIMO is substituting MIMO to fulfill higher throughput requirements. MUMIMO is found to be more effective and critical for better performance of 5G wireless communication. Due to the advantage of MU and massive MIMO at the frequencies of centimeter wave (cmWave), it becomes essential for upcoming networks. Lately, 5G networks are preferring millimeter wave (MMW) bands as backbone. At these frequencies, high free-space path loss requires large array gains that can fulfill the requirement of high signal-to-noise ratio (SNR) even at minimum 100m distances (Zhang et al. 2019).

Massive MIMO poses a lot of challenges because large antenna array is used. To know the channel state information (CSI), a large number of spectral resources are used between transmit and receive antenna. The use of hybrid beamforming can adjust these problems in an efficient way. It uses digital and analog beamformers in the baseband and RF region, respectively (Buzzi et al. 2019). Further, enhancement of link reliability and channel capacity is dependent on modulation and equalization techniques. Minimum mean squared error (MMSE) equalization with successive interference cancelation (SIC) and optimal ordering gives better bit error rate (BER) performance with less computational complexity as compared to linear minimum mean squared error (LMMSE) (Park et al. 2008).

In view of the above, this paper includes the details of experiments performed using a JSCC-UFMC combination in a MUMIMO setup deployed as part of a MMW backbone. The objective is to ascertain the performance improvement derived out of such a combination, where for base station level connectivity, hybrid beamforming is used. A range of simulations has been carried out and performances recorded with multiple modulation schemes, multiple FFT size, varying filter lengths (of Kaiser and Dolph-Chebyshev (DC)) and several sub-bands of UFMC including LMMSE-based optimization and MMSE with successive interference cancelation (SIC).

The main contributions of this work are as follows:

- This work proposes the design and analyzes the performance of JSCC-UFMC-MUMIMO antenna diversity with hybrid analog/digital beamforming, where the number of antennas is more than the RF chains for the MMW carrier frequency wireless link.
- It is shown that optimal performance in terms of computational complexity without loss of spectral efficiency with the use of JSCC-UFMC is possible.
- Performance comparison between LMMSE and MMSE-SIC and an analysis where MMSE-SIC equalization technique gives satisfactory outcomes.

2 System Model and Methods

The primary objective of this work is to design of a hybrid system that integrates a JSCC block with UFMC and implemented using MUMIMO antenna diversity using hybrid beamforming. The UFMC is based upon Kaiser and DC filters which provide different performances. The objective is to determine the optimal configuration of JSCC for better link reliability, higher spectral efficiency and higher throughput. The system model of the proposed approach is shown in Fig. 1.

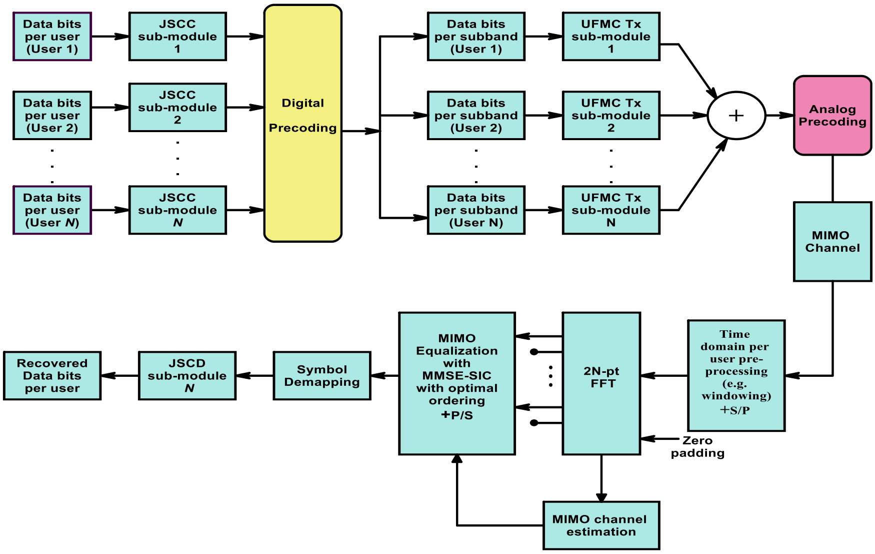

Fig. 1 Processing for the data transmission and reception

Here, as shown in the system model (Fig. 1), first the data streams are passed through JSCC block, where fountain and turbo coding stages are used. Next, as part of hybrid beamforming, digital precoding is done in combination with UFMC, where sub-blocks are used for transmitting data from each user. The data is now passed through the channel in a MUMIMO setup for which analog precoding is done. At the receiver side, a frequency to time domain transform is carried out followed by a time domain preprocessing. Next, a $2N$-fast Fourier transform (FFT) is done (along with zero padding) to support UFMC data recovery. Along with the above, CSI recovery with SIC, equalization and parallel to serial conversion are carried out. Subsequently, after symbol de-mapping and JSCC decoding (Turbo decoding with Max-Log-Map algorithm), data bits per user are recovered and presented.

2.1 *Joint Source-Channel Coding (JSCC) and Hybrid Beamforming*

For this work, JSCC is combined with hybrid beamforming to see optimal performance generated in a secured wireless link over a massive MIMO antenna diversity framework. The encoder depicted in Fig. 1 employs a turbo-fountain encoder in conjunction with the JSCC operation. Within the turbo encoder, the input data X undergoes encoding via a recursive systematic convolutional (RSC) encoder. To ensure appropriate code generation, it is recommended that the feedback of the RSC encoder be set to a primitive polynomial. This selection is advantageous as primitive polynomials generate maximum-length sequences, contributing to the desired randomness of the resulting turbo code (Deka and Sarma 2019).

The process of turbo coding generates a systematic sequence, denoted as X^s and two parity sequences, denoted as p_1 and p_2. These sequences are obtained from both the RSC encoder with and without interleaving, as shown below.

$$X^s = X_1^s, X_2^s, \ldots, X_n^s \tag{1}$$

$$X^{p_1} = X_1^{p_1}, X_2^{p_1}, \ldots, X_k^{p_1} \tag{2}$$

$$X^{P_2} = X_1^{p_2}, X_2^{p_2}, \ldots, X_k^{p_2} \tag{3}$$

where n and k are the length of systematic sequence and parity sequence.

After puncturing, all the outputs are concatenated in parallel to form the following equation as shown below

$$X^c = \left[X_1^S, X_1^{p_1}, X_1^{p_2}, \ldots, X_n^S, X_k^{p_1}, X_k^{p_2}\right] \tag{4}$$

Then the incoming data undergoes interleaving by π_i, producing a significant number of symbols that function as both a channel encoder and forward error-correcting code to counteract the impact of channel noise.

$$X^{c_1} = X_1^{c_1}, X_2^{c_1}, \ldots, X_n^{c_n} \tag{5}$$

$$X^{c_2} = X_1^{c_2}, X_2^{c_2}, \ldots, X_n^{c_n} \tag{6}$$

$$X^{c_3} = X_1^{c_3}, X_2^{c_3}, \ldots, X_n^{c_n} \tag{7}$$

The combination of the Eqs. (5), (6) and (7) gives the form of equation as

$$P = \left[X^{c_1}(:), X^{c_2}(:), X^{c_3}(:)\right] \tag{8}$$

After JSCC, the hybrid beamforming operation is performed in combination with UFMC technique. As shown in Fig. 2, the data streams L_s are maps to RF chains and the antenna elements are connected to RF chains. Here, F_{BS} is the digital precoder and.

F_{RF} is the analog precoder. Data transmission part comprises channel coding, bit mapping, splitting of data streams, baseband precoding, UFMC modulation and RF analog beamforming. Each antenna element uses phase shifters for the fully connected RF architecture.

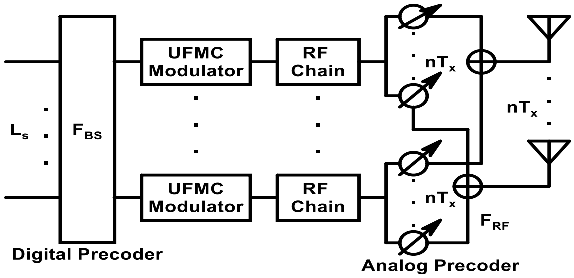

Fig. 2 Data transmission through hybrid beamforming

2.2 Universal Filtered Multi-Carrier (UFMC)

As already noted, UFMC is a preferred scheme of 5G wireless system (Yarrabothu and Nelakuditi 2019). In this work, after digital precoding, each of the data undergoes through the UFMC block which is implemented using both Kaiser and DC window. This multi-carrier technique represents side lobe attenuation with the help of FIR coefficients. To improve the performance in case of spectral leakage, the Kaiser window of FIR filter type is used. The well-known Kaiser–Bessel window is shown in Eq. (9).

$$w_K(n) \triangleq \begin{cases} I_0\left(\beta\sqrt{1-\left(\frac{n}{M/2}\right)^2}\right), & -\frac{M-1}{2} \leq n \leq \frac{M-1}{2} \\ 0, & \text{elsewhere} \end{cases} \tag{9}$$

where M is the window length, and β is the side lobe height control parameter.

Grouping of B sub-bands from K data sub-carriers is the initial design considerations of the UFMC transmitter. The UFMC sub-modules ($i = 1, \ldots, B$) taken S_i data symbols as input, where S_i comprises n_l QAM symbols. Then, an IFFT operation is taking place on each sub-band. Subsequently, each sub-band undergoes additional filtering. Afterward, to form the overall transmit vector X, the output of each UFMC module is added together given as,

$$X = \sum_{i=1}^{B} X_i = \sum_{i=1}^{B} F_i V_i S_i \tag{10}$$

where $V_i \epsilon\ \mathbb{C}^{N_{FFT}\times n_l}$ is the $IFFT$ matrix and F_i is the Kaiser filter impulse response.

2.3 MMW Channel Model for MIMO

The channel which is generally use at frequencies of sub-6 GHz is usually differs from the MIMO antenna diversity channel model at MMW (Buzzi et al. 2019). Here, the channel model and its related parameters are described briefly. Here, N_T is the number of transmit antennas and N_R is the number of receive antennas, respectively. The propagation channel $\boldsymbol{H(t)}$ with a dimension of $(\boldsymbol{N_R X N_T})$ corresponding to continuous time function with matrix-valued can be modeled here. The signal propagation in the environment of MMW MIMO channel we used $\boldsymbol{K_{cl}}$scattering clusters based on popular clustered model which comprises different propagation path $\boldsymbol{K_{ray,i}}$,where $\boldsymbol{i = 1, \ldots, K_{cl}}$, in combination with a possible LOS component. The channel impulse response $\boldsymbol{H(t)}$ can be written as

$$\boldsymbol{H(t) = \Upsilon \sum_{i=1}^{K_{cl}} \sum_{l=1}^{K_{ray,i}} \alpha_i l \sqrt{L(r_{i,l})} a_r(\phi^r_{i,l}, \theta^r_{i,l})} \\ \delta(\mathrm{t} - \boldsymbol{\tau}_{i,l}) + \boldsymbol{H_{LOS}(t)} \tag{11}$$

where $\phi^r_{i,l}$ and $\phi^t_{i,l}$ represent the azimuth angles of arrival and departure. $L(r_i, l)$ and $\alpha_{i,l}$ are the attenuation and complex path gain. $\tau_{i,l} = r_{i,l}/c$ is the propagation delay. The factors $a_r\ (\phi^r_{i,l}, \theta^r_{i,l})$ and $a_t\ (\phi^t_{i,l}, \theta^t_{i,l})$ represent the normalized receive and transmit array response vectors and $\gamma = \sqrt{\frac{N_R N_t}{\sum_{i=1}^{K_{cl}} K_{ray,i}}}$ is a normalization factor that ensures the received signal power.

3 Experimental Results

Using the parameters as given in Table 1, we have simulated the proposed system as illustrated in Fig. 1 and has been tested as mentioned above. Firstly, we discuss the results in terms of BER using JSCC-UFMC-MUMIMO with hybrid beamforming techniques in 16 × 64 MIMO antenna diversity setup with MMSE-SIC and optimal ordering equalization (for ascertaining better link reliability). Next, we highlight the BER performance using JSCC-UFMC-MUMIMO with hybrid beamforming techniques in 16 × 64 MIMO setup with LMMSE equalization (for ascertaining better link reliability) to see the performance difference obtained in terms of BER.

We present our findings as part of our proposed methodology for achieving the optimal configuration of JSCC-UFMC in conjunction with DC and Kaiser filters to minimize out-of-band (OOB) emissions while considering varying FFT sizes, QAM modulation orders and filter lengths. Then, the approach was applied to a 16 × 64 large MIMO setup, using MMSE-SIC and optimal ordering equalization to reduce system complexity, improve link reliability, increase spectral efficiency and achieve higher throughput. The results show better peak-to-average power ratio (PAPR),

Table 1 System simulation parameters, values and techniques

Parameters	Values and techniques
Communication bandwidth	500 MHz
Carrier frequency	28 GHz
Modulation order	16, 64
Joint source-channel encoder	Turbo-fountain encoder
Encoders for separate operation	Huffman and LT codes
Multicarrier technique	UFMC
Number of sub-band	8
Sub-band size	16
Filter length (L)	16, 43
$N_R X N_T$	16 × 64
Filter used	Dolph-Chebyshev and Kaiser
Number of FFT	512, 1024
Equalization	MMSE-SIC and LMMSE
Joint source-channel decoding	Turbo-fountain (Max-Log-Map)

power spectral density (PSD) and bit error rate (BER), as well as increased channel capacity.

In order to produce numerical results, we have considered the system simulation parameters, values and techniques as given in Table 1.

3.1 Performance of JSCC-UFMC-MUMIMO Using Hybrid Beamforming Techniques in 16 × 64 Setup with MMSE-SIC (Optimal Ordering Equalization) and LMMSE Equalization

Firstly, the BER performance of JSCC-UFMC-MUMIMO is depicted in Fig. 3 and Table 2 with MMSE-SIC equalization is performed. It is observed that BER performance (Table 2) improves as compared to (Table 3) with increase in values of SNR.

The PSD and frequency plots of the JSCC-UFMC-MIMO system with DC and Kaiser filter are depicted in Fig. 4. It is observed that the system with Kaiser filter provides better PSD due to the prevention of spectrum leakage. Also, it has better PSD performance on the stop band as shown in Fig. 4a and b. We also see that JSCC-UFMC provides satisfactory performance in a MUMIMO when deployed with hybrid beamforming when DC and Kaiser filters are used as part of UFMC sub-bands and channel equalization carried out using MMSE-SIC.

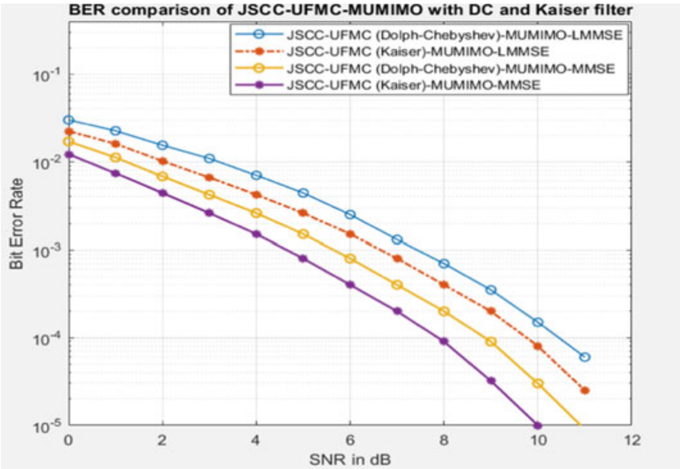

Fig. 3 BER comparison of JSCC-UFMC-MUMIMO with LMMSE and MMSE-SIC

Table 2 BER comparison of JSCC-UFMC-MUMIMO-MMSE-SIC with DC and Kaiser filter

SNR dB	BER with Kaiser filter	BER with DC filter
0	0.0122	0.0170
2	0.0044	0.0068
4	0.0015	0.0026
6	0.0004	0.0008
8	0.00011	0.00021

Table 3 BER comparison of JSCC-UFMC-MUMIMO-LMMSE with DC and Kaiser filter

SNR (dB)	BER with Kaiser filter	BER with DC filter
0	0.0223	0.0301
2	0.0102	0.0154
4	0.0052	0.0070
6	0.0015	0.0025
8	0.0004	0.0007

As discussed above, we have implemented JSCC-UFMC-MUMIMO transceivers operating at MMW frequencies combined with hybrid beamforming techniques in combination with DC and Kaiser filters to reduce OOB emission and deployed over 16 × 64 MUMIMO setup with MMSE-SIC and optimal ordering equalization with different QAM modulation orders (16-QAM and 64-QAM), FFT sizes (512 and 1024) and filter lengths (16 and 43) and compared the proposed method with existing method (Table 5) to see the performance difference and to reduce the system complexity, obtain better link reliability, higher spectral efficiency and throughput that gives less BER with increased channel capacity, better PAPR and

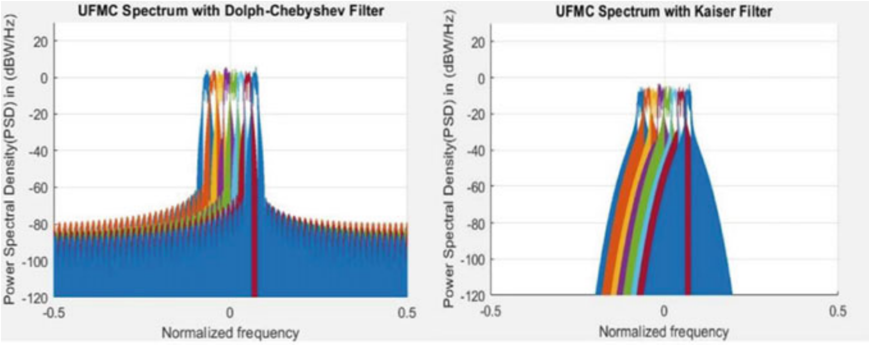

(a) (b)

Fig. 4 (**a**) PSD with DC filter and (**b**) PSD with Kaiser filter

PSD as shown in Figs. 3 and 4 and Tables 2, 3, 4 and 5. It is observed from the results that JSCC-UFMC-MUMIMO with Kaiser window with MMSE-SIC and optimal ordering equalization with 16-QAM modulation order, 512 FFT size and 16 filter length can provide better comparative results as compared to LMMSE equalization technique.

Table 4 PAPR comparison of the proposed method (JSCC-UFMC-MUMIMO-MMSE)

Sub-bands	Sub-band Size	Filter length	Modulation order	FFT size	PAPR in dB
8	16	16	16	512	7.735
		43			7.972
8	16	16	64	1024	8.105
		43			8.246

Table 5 Comparison of the proposed method with existing method (Buzzi et al. 2019)

Filter length	Modulation order	FFT size	BER (SNR = 6 dB)		PAPR in dB	
			Proposed	Existing	Proposed	Existing
16	16	512	0.001	0.011	7.735	8.057
43			0.005	0.014	7.972	8.314
16	64	1024	0.011	0.019	8.105	8.456
43			0.017	0.026	8.246	8.685

4 Conclusion

The implementation of JSCC-UFMC in MUMIMO operating at high frequencies (28 GHz) is a viable option for high data rate communication when hybrid beamforming is performed. From this work, we have observed that combinations of JSCC-UFMC-MUMIMO with Kaiser window and MMSE-SIC with optimal ordering equalization in combination with 16-QAM modulation order, 512 FFT size and 16 filter length is effective for improving QoS. The proposed approach is compared to the LMMSE equalization technique and is found to provide better results in terms of QoS enhancement and mitigation of the ill effects of parameters such as BER, PAPR and PSD associated with high data rate transmission over wireless channels.

References

Almutairi AF, Al-Gharabally M, Krishna A (2019) Performance analysis of hybrid peak to average power ratio reduction techniques in 5G UFMC systems. IEEE Access 7:80651–80660
Buzzi S et al (2019) MIMO-UFMC transceiver schemes for millimeter-wave wireless communications. IEEE Trans Commun 5(67):3323–3336
Deka S, Sarma KK (2019) Joint source channel coding with MIMO MC-CDMA for efficient communication. In: 2nd international conference on innovations in electronics, signal processing and communication (IESC). IEEE, Shillong, pp 60–65
Deka S, Sarma KK (2020) JSCC-UFMC and large MIMO technology for high data rate wireless communication. Int J Mob Comput Multimedia Commun (IJMCMC) 4(11):42–66
Gao Y, Tuncel E (2013) Separate source-channel coding for transmitting correlated gaussian sources over degraded broadcast channels. IEEE Trans Inf Theory 6(59):3619–3634
Hammoodi A (2019) Green coexistence for 5G waveform candidates: a review. IEEE Access 7:10103–10126
Ma T (2017) A novel PRCC scheme for OFDM systems over frequency-selective fading channels. IEEE Signal Process Lett 5(24):634–637
Park J, Whang Y, Kim SK (2008) Low complexity MMSE-SIC equalizer employing time-domain recursion for OFDM systems. IEEE Signal Proc Lett 15:633–636
Tian C et al (2014) Optimality and approximate optimality of source-channel separation in networks. IEEE Trans Inf Theory 2(60):904–918
Wen J et al (2018) Design of waveform shaping filter in the UFMC system. IEEE Access 2(6):32300–32309
Wu T, Lau VKN, Zhang S (2009) Design and analysis of MIMO joint source channel coding (JSCC) with limited feedback. IEEE Trans Wireless Commun 8(6):2920–2926
Yarrabothu RS, Nelakuditi UR (2019) Optimization of out-of-band emission using kaiser-bessel filter for UFMC in 5G cellular communications. China Commun 8(16):15–23
Zhang Y et al (2019) Optimal hybrid beamforming design for millimeter-wave massive multi-user MIMO relay systems. IEEE Access 7:157212–157225

Dual-Band Omnidirectional Parasitic Dielectric Resonator Antenna

Roktim Konch, Sivaranjan Goswami, Kumaresh Sarmah, and Kandarpa Kumar Sarma

Abstract A simple structured dual-band omnidirectional as well as directional parasitic coupled, quadrilateral shaped dielectric resonator antenna (DRA) feeding by a coaxial connection is presented. It consists of a FR4 substrate having a plus shaped patch, excited by a coaxial connector at the center of the structure. Four rhombus shaped DRA is diagonally placed above the microstrip line. Variation of height of the parasitic DRA affecting the antenna radiation pattern is investigated in this paper. The antenna has an omnidirectional radiation property at the first resonance frequency 3 GHz and directional radiation pattern at the second resonance frequency 4.5 GHz is also observed. The DRA is used to enhance the radiation field at resonance frequency. The proposed antenna demonstrates an omnidirectional radiation pattern at lower resonance frequency and four directional radiation patterns at second resonance frequency.

Keywords Dielectric resonator antenna (DRA) · Multi-beam radiation · Omnidirectional · Directive antennas

1 Introduction

The dielectric resonator antenna (DRA) has a number of advantages such as its high efficiency, low cost, and high degree of flexibility (Kumar and Gupta 2014; Keyrouz and Caratelli 2016; Xia et al. 2019). Omnidirectional DRAs are good for indoor wireless communications because they provide large signal coverage (Liu et al. 2021) and are popularly used as a beam searching antenna (Malik et al. 2021). Directional antennas radiate or receive great power in specific directions allowing

R. Konch (✉) · S. Goswami · K. K. Sarma
Electronics and Communication Engineering, Gauhati University, Guwahati, Assam, India
e-mail: roktim@gauhati.ac.in

K. Sarmah
Electronics and Communication Technology, Gauhati University, Guwahati, Assam, India
e-mail: kumaresh@gauhati.ac.in

J. K. Deka et al. (eds.), *Emerging Technology for Sustainable Development*,
Lecture Notes in Electrical Engineering 1061,
https://doi.org/10.1007/978-981-99-4362-3_43

increased performance, reduced interference from unwanted sources and consumes less power. In the modern communication system a secure, efficient, and reliable system is very much crucial.

Several approaches have been suggested to increase the gain (Jusoh et al. 2014) of DRAs. Arrangement of single element DRAs (Pandey et al. 2019) is the most versatile method, in which the gain value can be directly controlled by the number of elements in the array. However, increasing size, complexity, and costs of the resultant antenna are the main disadvantages. Various techniques and structured DRAs have been reported for improving the antenna performance such as wideband (Liu et al. 2021), enhanced gain (Nikkhah et al. 2013), and hybrid mode (Zou and Pan 2015; Perron et al. 2009). But, no reported work have proposed a dual-band, omnidirectional, and multi-beam antenna which is in demand for beam searching and directional communication for modern communication systems. Also the multi-beam property can be integrated to the reconfigurable (Konch et al. 2018) antennas. Therefore, the requirement of such a design in front of a new parasitic structured DRAs investigated.

In this work, the design of a dual-band, omnidirectional, and multi-beam DRAs is obtained exciting diagonally by microstrip lines. The plus shape microstrip patch is centrally excited through a coaxial connector, and above the line, four rhombus shaped DRA elements are placed. A parametric study has been conducted to observe the behavior of parasitic DRA elements with respect to different heights. The proposed antenna is designed and simulated using ANSYS HFSS.

2 Design Methodology and Proposed Antenna

The proposed structure consists of a four closely placed rhombus shaped DRA forming a quadrilateral structure, and these DRA are excited through a microstrip line placing diagonally below the individual structure as shown in Fig 1. An FR4 substrate with a height $h = 1.5$ mm, $\varepsilon r = 4.3$ is used in this design. The center of the patch is considered as the origin and the feed point is located at the origin.

The optimized dimension of the proposed antenna is given in Table 1. Here, the ground plane and FR4 substrate are equal in length and width. All the four DRAs are of equal length, width, and height, therefore only one box is required. The separation width between the four DRAs is 03 mm.

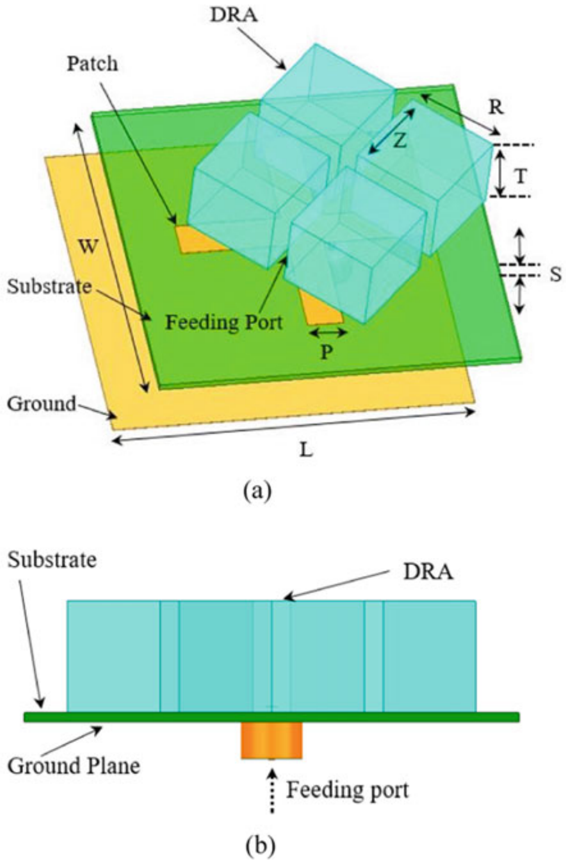

Fig. 1 Geometry of the proposed antenna **a** prospective view **b** side view of the structure

Table 1 Optimized dimension of the antenna (Units in mm)

L	W	P	S	T	R	Z
80	80	8	1.5	18	21	21

3 Simulated Results and Discussion

Figure 2 shows the simulated reflection coefficient (S11) of the proposed antenna. Two resonance frequencies are observed at around 3.0 GHz and 4.5 GHz at the reflection coefficient graph. The −10 dB impedance bandwidth is about 4.26 and 1.95%.

Figure 3 shows the simulated 3D total gain radiation pattern. At lower resonance frequency, the gain is 3.9 dB and having a well-shaped omnidirectional radiation pattern (Fig. 3a). In the second resonance frequency, the gain is 3dB and has a

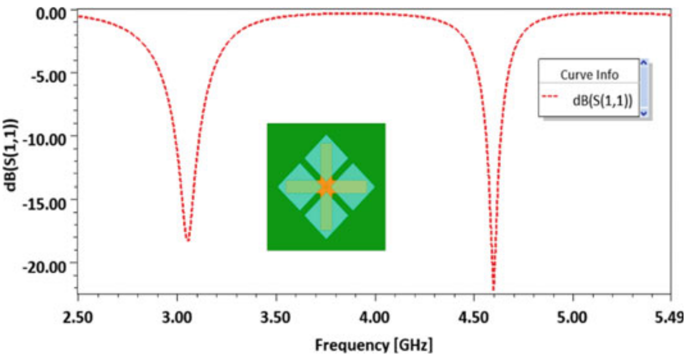

Fig. 2 Reflection coefficient (S11) of the selected model

four directional beam radiation pattern (Fig. 3b). The separation between the two resonance frequencies is in an appropriate interval, so there is no mutual interference between the dual bands. The thickness of the DRAs placed above the microstrip radiating patch affect the antenna performances, which is investigated and the details gain vs. two resonance frequencies are given in Table 2. From the experiment, it is seen that when the height of the DRA is increased the dual-band antenna gain, also gradually increasing. Although, large DRAs increase the gain, but make the device bulky, hence a careful selection is required. In this experiment, we used a Zirconium element as a dielectric resonator material. Zirconium is a solid, non-toxic, low cost, easily available material, so it is deposited in the proposed model.

Table 3 compares the proposed model with other DRA antennas in terms of DRA topology, excitation, resonance frequency, and design complexity. The proposed antenna has structural stability, rigid model and dual-band, directional, and multi-beam characteristics, which is unique and better as compared to the existing design.

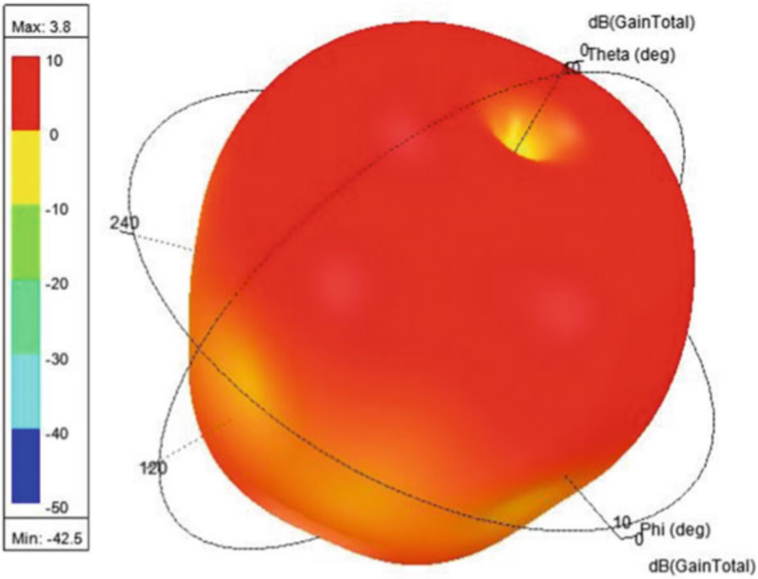

(a)

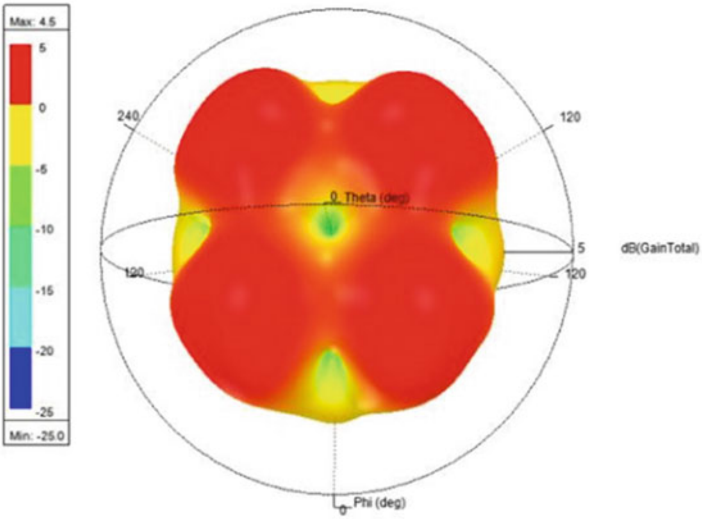

(b)

Fig. 3 Radiation patterns 3D **a** omnidirectional radiation pattern at 03 GHz **b** multi-beam radiation pattern at 4.5 GHz

Table 2 DRA height (mm) versus gain (dB)

DRA height (mm)		02	04	06	08	10	12	14	16	**18**	20
Resonance frequency	03 GHz	1.7	2.4	3	3.2	3.5	3.7	3.8	3.8	**3.9**	3.8
	4.5 GHz	4.63	4.6	4.0	4.6	4.5	4.6	4.6	4.0	**4.5**	4.5

Table 3 Comparison between the proposed structures with some other existing structures

Ref	DRA topology	Design complexity	Frequency (GHz)
Liu et al. (2021)	Ring with circular DRA	Simple	2.58
Xia et al. (2019)	Cylindrical with hollow bow	Complex	4.3–8
Pandey et al. (2019)	Rectangular	Moderate	10
Lugo et al. (2018)	Multilayer	Moderate	4.35
This work	Single layer	Simple	3, 4.5

4 Conclusion

A new single-layer planar feed compact quadrilateral DRA has been presented. It has plush-shaped printed lines, and a regular ground layer. It has been found that the radiation patterns are very stable in both the resonance frequencies. Further, the mathematical analysis and hardware implementation of the proposed model can be performed to study the design for effective implementation on four real live simulations.

References

Jusoh M, Sabapathy T, Jamlos MF, Kamarudin MR (2014) Reconfigurable four-parasitic-elements patch antenna for high-gain beam switching application. IEEE Antennas Wirel Propag Lett 13:79–82

Keyrouz S, Caratelli D (2016) Dielectric resonator antennas: basic concepts, design guide-lines, and recent developments at millimeter-wave frequencies. Int J Antennas Propag

Konch R, Sarma A, Goswami S, Sarmah K (2018) Design of a pattern reconfigurable switched parasitic array for null steering application. In: 2018 2nd international conference on electronics, materials engineering and nano-technology (IEMENTech). IEEE, pp 1–4

Kumar J, Gupta N (2014) Performance analysis of dielectric resonator antennas. Wireless Pers Commun 75(2):1029–1049

Liu X, Leung KW, Yang N (2021) Wideband horizontally polarized omnidirectional cylindrical dielectric resonator antenna for polarization reconfigurable design. IEEE Trans Antennas Propag 69(11):7333–7342

Lugo DC, Ramirez RA, Wang J, Weller TM (2018) Multilayer dielectric end-fire antenna with enhanced gain. IEEE Antennas Wirel Propag Lett 17(12):2213–2217

Malik PK, Madhav BTP, Kalkhambkar G, Amit S (2021) Smart antennas: latest trends in design and application

Nikkhah MR, Rashed-Mohassel J, Kishk AA (2013) High-gain aperture coupled rectan-gular dielectric resonator antenna array using parasitic elements. IEEE Trans Antennas Propag 61(7):3905–3908

Pandey S, Kumar D, Parkash O, Pandey L (2019) Design and development of dielectric resonator antenna using ceramic materials: an overview. Trans Indian Inst Met 72(8)

Perron A, Denidni TA, Sebak AR (2009) High-gain hybrid dielectric resonator antenna for millimeter-wave applications: Design and implementation. IEEE Trans Antennas Propag 57(10):2882–2892

Xia ZX, Leung KW, Lu K (2019) 3-D-printed wideband multi-ring dielectric resonator antenna. IEEE Antennas Wirel Propag Lett 18(10):2110–2114

Zou M, Pan J (2015) Investigation of resonant modes in wideband hybrid omnidirectional rectangular dielectric resonator antenna. IEEE Trans Antennas Propag 63(7):3272–3275

Development of Near-Real-Time Solar Generation Prediction Technique Using Weather Data

Navareen Sohkhlet and Bikramjit Goswami

Abstract This paper presents a technique for forecasting solar power generation using weather forecast data. Solar power generation mainly depends on the relative position of the sun and some extrinsic as well as intrinsic factors. Extrinsic factors, such as cloud cover, temperature, rainfall, humidity, and wind speed, are used for the prediction of solar generation. Apart from these, the intrinsic factors are also taken as inputs for the proposed prediction technique. The artificial intelligence–based techniques of linear regression, polynomial regression, and artificial neural networks are used for prediction purposes, with input data of all the months of the year 2021. After developing different AI models, their accuracies are compared before selecting the best technique for solar generation prediction. The AI model found to be accurate during the present work is applicable to all solar generation systems, for generation level prediction.

Keywords Solar generation prediction · Linear regression · Polynomial regression

1 Introduction

Solar power is one of the most promising renewable energy sources, the generation of which does not result in the emission of pollutants and greenhouse gases (Kim et al. 2017). Global warming and the energy crisis over the past few decades have motivated the use and development of alternative, sustainable, and clean energy sources (Sabzehgar et al. 2020). Solar energy or solar power is a nonconventional source or renewable source of energy and its intensity depends on the weather and sun's position concerning the panels. Electricity demand needs to be predicted for better planning of utilization. Solar energy generation varies frequently with the weather and relative solar position (Verma et al. 2016).

N. Sohkhlet · B. Goswami (✉)
Assam Don Bosco University, Assam, India
e-mail: bikramjit.goswami@dbuniversity.ac.in

J. K. Deka et al. (eds.), *Emerging Technology for Sustainable Development*,
Lecture Notes in Electrical Engineering 1061,
https://doi.org/10.1007/978-981-99-4362-3_44

Solar power forecasting is a complex process as it mainly depends on climate conditions, which change or fluctuate over time. Therefore, machine learning (ML)–based methods have been used for effective solar power generation forecasting. For improved accuracy, new and more intelligent methods are being developed (AlKandari and Ahmad 2020).

Renewable energy or nonconventional generation resources such as solar and wind behave in a stochastic fashion due to frequent weather parameter changes. Transmission and distribution losses also affect the performance of these resources. Therefore, scheduling, optimization, and management of smart grids and microgrids with a high concentration of renewable energy resources are the main issues or challenges of such grids. One of the most promising practices in scheduling the performance of smart grids is to forecast the energy production of the resources that lead to energy generation and cost-efficient replacement of the current process (Sabzehgar et al. 2020). Models based on artificial intelligence (AI) are used for optimization and control purposes due to their learning capabilities. Examples of these models include support vector machines (SVM), regression, and neural networks.

AI techniques play an important role in prediction modeling and analysis of the performance as well as in controlling renewable energy generation processes. AI techniques are used to solve complicated problems and practices in various fields of the engineering and technology. AI systems can be used as a way to solve complex problems. AI systems have been used in diverse applications of pattern recognition, manufacturing, optimization, control, robotics forecasting, power systems, signal processing, medical, and social sciences (Kumar and Kalavathi 2018). Their use in renewable energy generation forecasting is however a newer application, becoming increasingly popular nowadays.

2 Use of AI in Solar Generation Prediction

One of the simplest AI-based techniques used in generation prediction is regression analysis, which is effectively used for solar generation prediction in the present work. It is a method to determine a functional relationship of the model between predictor (independent) parameters and response (dependent). The regression analysis shows a repetitive process so that the outputs can be utilized to verify, criticize, analyze, and modify the inputs (Nalina et al. 2014). The regression approach identifies the correlation between parameters by fitting the linear equation to the data. Figure 1 shows the plot between solar generation and ambient temperature. This type of distribution of data can be analyzed using the regression technique very conveniently.

The methodology of modeling the system for the prediction of solar generation is shown in Fig. 2. It shows the stepwise procedure of the AI model developed for obtaining the forecast data considering weather conditions, such as, sunny, scattered cloud, partly sunny drizzle over, overcast, thunderstorm, etc. Another input is daily solar generation in net million units (MU) from the North Eastern Regional Load Dispatch Centre (NERLDC) for the state of Assam for the year 2021.

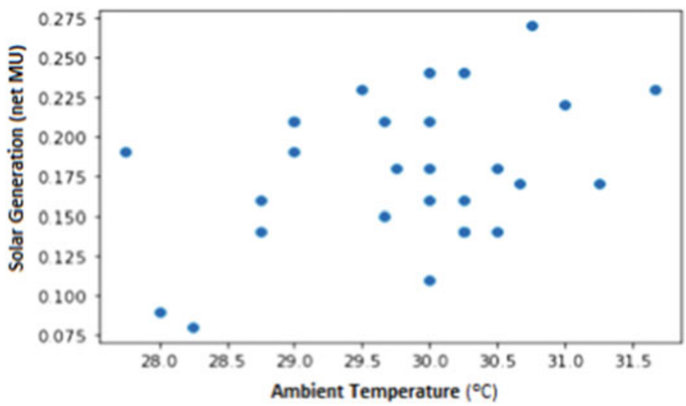

Fig. 1 The plot of solar generation versus ambient temperature

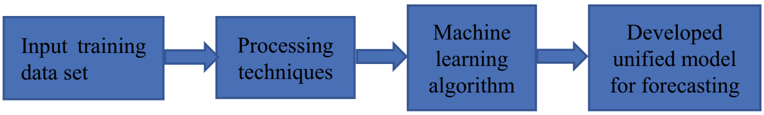

Fig. 2 Block diagram of the system model

Figure 3 shows the step-by-step methodology of training, testing, and validation of a regression-based AI model designed for predicting solar generation. The weather parameters are gathered from different authentic weather forecast websites. Initially, the solar generation is predicted using a model generated, based on the aforementioned weather parameters, using two different approaches: linear and polynomial regression techniques. Then, these estimated values are used to forecast the generated power in the grid. The estimation models are obtained from the averaged data gathered in the year 2021. An essential step in obtaining forecast models is to have two sets of data: the training and the test data sets. The training data set is used to obtain the prediction model, and the test data set is used for model evaluation.

Therefore, further weather and generation data were gathered to test the accuracy of the model. The input data are all sorted before being used. The data with null entry are eliminated, and the data are normalized to increase the accuracy of the forecast models. After utilizing these models for forecasting solar power generation, the error of each model is measured by comparing the original target data and the forecast data. The analysis and predictions are performed using Python software for programming and training regression algorithms.

As mentioned earlier, the solar energy generation forecast, utilized in this work, is done in phases. Phase one is the data preprocessing for the forecast models, which in the case of the current work includes eliminating all of the null entry data. In phase two, a model for estimating and forecasting solar generation based on weather parameters is derived. It can be comprehended from these figures that while some of

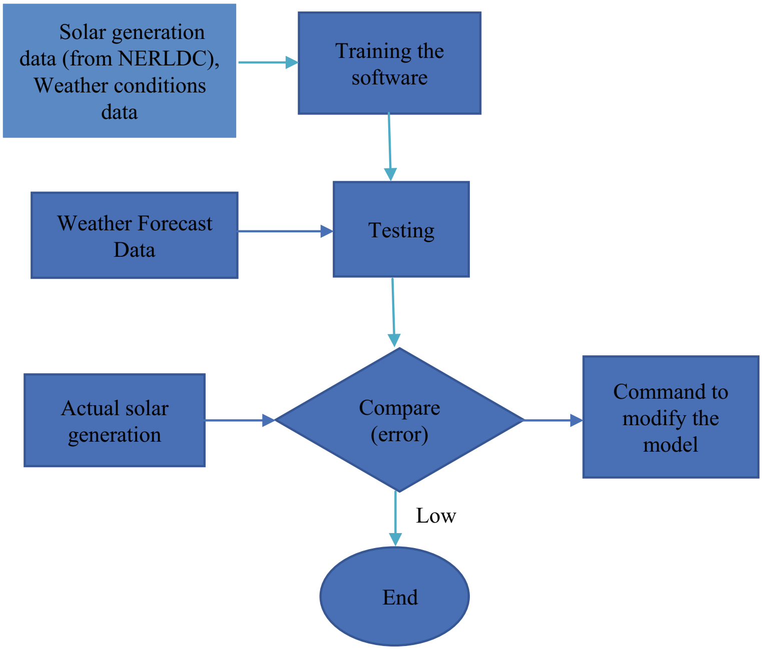

Fig. 3 Process flowchart of the AI model

the weather parameters are linearly related to solar generation, some are not. Hence, polynomial regression technique is found to be more accurate in estimating solar generation as compared to linear regression.

3 Results and Discussion

Figure 4 shows the best fit polynomial graph after the regression technique is implemented for solar generation estimation in August 2021. In the figure, the horizontal axis shows the ambient temperature, and the vertical axis shows solar generation data obtained from NERLDC for the state of Assam.

Table 1 shows the estimated solar generation considering 1-month-long data for training the regression model and predicting the solar generation of the subsequent days for the different seasons of the year 2021.

Table 1 shows the accuracy of estimated solar generation for different days of the seasons of 2021 for training and validation, using polynomial regression, thereby considering the actual solar generation (net MU) from the NERLDC website and the predicted solar generation (net MU) from the technique developed and subsequently computing the relative error. Figure 5 shows the error percentage curve by taking the actual and the predicted value obtained from the system forecasting model using

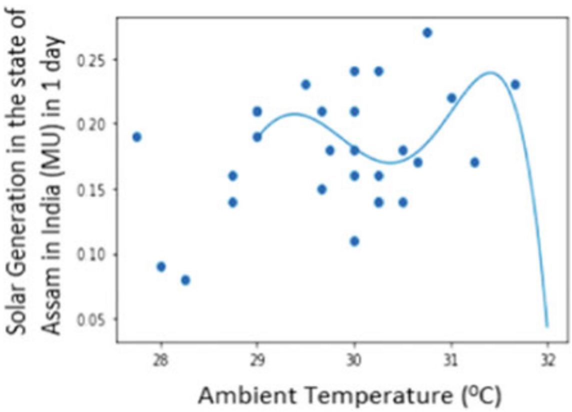

Fig. 4 Polynomial fit of solar generation vs. ambient temperature

Table 1 Estimated solar generation using polynomial regression using month-long data for different seasons in the year 2021

Training period	Estimation date	Actual solar generation (net MU)	Predicted solar generation (net MU)	Error (%)
1–28 February	1 March	0.17	0.1479	13
1–31 May	1 June	0.15	0.129	14
1–31 August	1 September	0.15	0.182	−21
1–30 September	1 October	0.29	0.23	20
1–31 October	1 November	0.20	0.21	−5

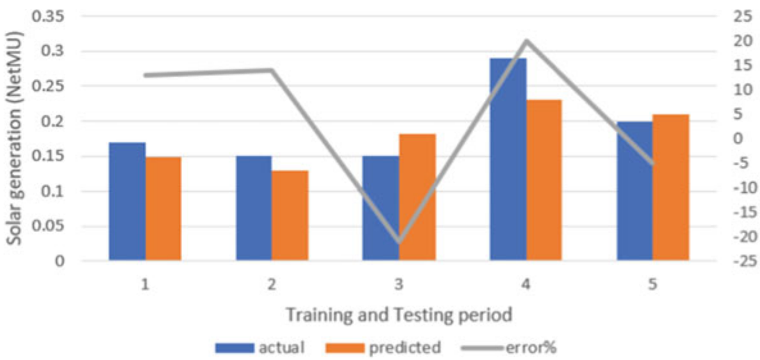

Fig. 5 Error percentage curve between the actual and the predicted solar generation in (net MU)

polynomial regression technique. The error percentage lies within the range of -5% to +20% for the period considered. Table 2 shows estimated solar generation considering data for 15 days of the year 2021 for training. The methodology used is the same as the training done using 1-month data. The accuracy calculations are also shown for the different seasonal estimations for the year. The table shows the calculation of the accuracy of different months of 2021 for training and validation using the regression algorithm, thereby considering the actual solar generation (net MU) from the NERLDC website and the predicted solar generation (net MU) from the trained regression model and obtaining the error.

Figure 6 shows the error curve by taking the actual and the predicted value obtained from the system forecasting model using polynomial regression technique for a particular period interval as shown in Table 2 and its error percentage lies within the range of −23% to +17%.

Table 3 shows estimated solar generation considering weekly data (7 days each) for the training of the prediction system for different seasons of the year 2021. In the table, the accuracy of the estimation technique considering weekly data as input (weather conditions, temperature, solar generation, etc.) for different seasons of the year 2021 for training. By comparing the actual and predicted solar generation, it can be observed that training the system with weekly data gives better accuracy. With month-long data for training, the error is slightly more than that with week-long data. With 15 days of data used for training, the error in estimating solar generation is the highest. Training the regression model with less than 7 days data leads to greater error. Hence, it is observed that the optimum period of training of the regression model for a more accurate prediction of solar generation is 7 days (1 week).Fig. 7 shows the error curve by taking the actual and the predicted values obtained from the system forecasting model using polynomial regression techniques for a particular period of interval as shown in Table 3, and its error percentage lies within the range of −25.5% to +15%.

Table 2 Estimated solar generation using polynomial regression using 15 days of data for different seasons in the year 2021

Training period	Estimation date	Actual solar generation (net MU)	Predicted solar generation (net MU)	Error (%)
1–15 January	16 January	0.06	0.089	−4.8
1–14 February	15 February	0.1	0.1236	−23
15–28 February	1 March	0.17	0.14	17
1–15 March	16 April	0.14	0.149	−6.4
1–15 May	16 May	0.02	0.018	10
1–15 July	16 July	0.19	0.1939	−2
16–31 July	1 August	0.19	0.1384	16
15–30 September	1 October	0.29	0.296	−0.2
1–15 October	16 October	0.24	0.27	−10
1–15 November	16 November	0.26	0.25	3

Fig. 6 Error percentage curve between the actual and the predicted solar generation in (net MU) using 15-day data period interval

Table 3 Estimated solar generation using polynomial regression using 7 days of data for different seasons in the year 2021

Training period	Estimation date	Actual solar generation (net MU)	Predicted solar generation (net MU)	Error (%)
1–6 October	7 October	0.26	0.28	−10
7–13 October	14 October	0.29	0.295	−1.79
21–26 October	27 October	0.26	0.221	15
1–6 November	7 November	0.29	0.2922	−0.75
14–20 November	21 November	0.24	0.236	1.6
21–26 November	27 November	0.26	0.226	13
1–6 December	7 December	0.2	0.255	−25.5
14–20 December	21 December	0.22	0.253	−15
21–26 December	27 December	0.24	0.243	−1.25

Fig. 7 Error percentage curve between the actual and the predicted solar generation in (net Mu) using 7-day data period interval

4 Conclusion

In this work, an AI-based solar generation prediction model is developed, based on the actual values of different weather parameters for the city of Guwahati, Assam, in the year 2021. The designed regression-based AI model gives accuracy in the range of 0.75–25.5% error. The model can be further improved in accuracy by incorporating more inputs, such as near-real-time remote sensed data. Moreover, as the inputs are highly nonlinear in relation, the use of artificial neural networks in the training is expected to provide more accuracy in estimating solar generation in the region. This AI-based technique also requires testing and validation for other areas of the world for the global validity of the model.

References

AlKandari M, Ahmad I (2020) Solar power generation forecasting using ensemble approach based on deep learning and statistical methods. Appl Comput Inf

Kim JG, Kim DH, Yoo WS, Lee JY, Kim YB (2017) Daily prediction of solar power generation based on weather forecast information in Korea. IET Renew Power Gener 11(10):1268–1273

Kumar KR, Kalavathi MS (2018) Artificial intelligence based forecast models for predicting solar power generation. Mater Today Proc 5(1):796–802

Nalina U, Prema V, Smitha K, Rao KU (2014) Multivariate regression for prediction of solar irradiance. In: International conference on data science and engineering (ICDSE). IEEE, pp 177–181

Sabzehgar R, Amirhosseini DZ, Rasouli M (2020) Solar power forecast for a residential smart microgrid based on numerical weather predictions using artificial intelligence methods. J Build Eng 32:101629

Verma T, Tiwana APS, Reddy CC, Arora V, Devanand P (2016) Data analysis to generate models based on neural network and regression for solar power generation forecasting. In: 7th international conference on intelligent systems, modelling and simulation (ISMS). IEEE, pp 97–100

Monitoring Soil Wetness Using Ground-Based L-Band Scatterometer

Bikramjit Goswami

Abstract Microwave scatterometers have been used in both ground-based and platform-mounted remote sensing applications. The primary use of microwave scatterometers in ground-based applications is measuring and monitoring soil moisture. However, the determination of suitable frequency of the scatterometer for detecting soil saturation for different soil types is a topic still under study. The present study is an extensive field-based experimental work done in the state of Assam in India, considering alluvium-rich soil of the Brahmaputra valley. The L-band of microwave range is considered for the field testing and determining suitable configuration of the scatterometer, for monitoring soil wetness, as presented in detail in the paper. The configuration is found to be suitable in detecting the changes in soil moisture and identifying pre-saturation conditions of the soil also.

Keywords Scatterometer · Microwave · Soil moisture · L-band

1 Introduction

Soil moisture information is useful for reservoir management, early warning of droughts as well as flood, irrigation scheduling, and crop yield forecasting. It also helps understand the initiation of convective events and to forecast the risk of flash floods, or the occurrence of fog. Quantitative measurements of soil moisture in the surface layer of soil have been most successful by using active remote sensing in the microwave region (Shukla et al. 2014).

Space-based remote sensing of soil moisture accommodates these needs by providing surface soil moisture observations on a global scale every one to two days under a variety of conditions (Berhane 2007). The ground study done using scatterometers help determine the suitable frequency, antenna polarization, look angle etc., for the purpose.

B. Goswami (✉)
Assam Don Bosco University, Guwahati, India
e-mail: bikramjit.goswami@dbuniversity.ac.in

J. K. Deka et al. (eds.), *Emerging Technology for Sustainable Development*,
Lecture Notes in Electrical Engineering 1061,
https://doi.org/10.1007/978-981-99-4362-3_45

Most soil moisture products from remote sensing satellites are capable of depicting seasonal and short-term soil moisture changes quite well. However, biases in the absolute value and dynamic range may be large when compared to in situ and modeled soil moisture data (Hou et al. 2008). Hence, it is the requirement of in-situ experiments for different soil types and ground conditions.

Various techniques based on the active microwave remote sensors of type synthetic aperture radar (SAR) provide powerful tools for soil moisture monitoring in the tropical regions, because of their all weather, day-and-night imaging, and cloud penetration capabilities (Sun et al. 2012).

Among the equipment used for backscattering coefficients measurement for ground-truth validation, scatterometer is the most common one (Goswami and Kalita 2014). Scatterometer is an active microwave sensor, having both a microwave source (transmitter) and a microwave detector (receiver) in it. A ground-based scatterometer of certain frequency can be used for measuring the response from the ground parameters. One such parameter which changes the characteristic of scattering as well as backscattering from the ground is soil moisture. This happens due to the change in dielectric constant of the soil with change in moisture content in it. Thus, the backscattering response of the ground with changes in scattering angle, polarization of the transmitter and receiver, etc., can be analyzed for determining the utility of such active microwave sensors to the ground parameters.

The backscattering coefficient measurements using scatterometers are the primary means to study the characteristics of backscatter from various terrain features. Experiments on soil moisture monitoring have also been performed using ground-based scatterometers for different frequencies, look/incident angle and polarization (Song et al. 2010). In such experiments, data collected at different frequencies, polarizations, and incident angles are analyzed and interpreted using various models also. Several integral equation methods (IEMs) have also been developed to retrieve soil moisture from the backscattering coefficient (Shubert and Ruck 1631).

The current work is an attempt to determine suitable frequency, polarization, and look angle of a L-band ground-based scatterometer for monitoring soil moisture in the fluvial plains of the Brahmaputra valley in India. The L-band is the range of frequencies in the radio spectrum from 1 to 2 GHz. L-band is at the top end of the ultra-high-frequency (UHF) band, at the lower end of the microwave range. This paper presents in detail the methodology used for soil moisture monitoring, along with the results and analysis of the experimental results obtained.

2 Methodology

The methodology used for experimenting with ground-based scatterometer for monitoring the soil moisture is presented in the following steps.

- Selection of suitable frequency range for the transmitter and receiver of the scatterometer, based on the sensitivity of the frequency range to the soil moisture monitored.
- Determination of the suitable scattering angle for monitoring the changes in the soil moisture.
- Determination of the suitable polarization configuration of the transmitter and receiver antennae for monitoring the changes in the soil moisture.
- Validation with ground-truth experimentation, by measuring the soil moisture using a probe type soil moisture sensor.

The experimental field, the soil type, and the experimental setup are shown in Fig. 1, 2, and 3, respectively. The experimental field is in the campus of Assam Don Bosco University at Azara, Guwahati, India. The latitude and longitude of the location are- 26.1294° N, 91.6205° E, respectively. The experimental setup consists of the following instruments.

- A transmitter pyramidal horn antenna
- A receiver pyramidal horn antenna
- A microwave power meter
- A microwave source
- Mounting stands for the antennas with incidence angle adjustment facility
- Waveguides and cables.

Regional level continuous soil moisture monitoring for the top layer of the ground uses technologies like microwave scatterometer, which help acquire soil moisture information from the field, with high accuracy. Similarly such experimentation has done in the current work using a L-band, ground-based bistatic scatterometer system placed in the specular direction for 25° to 70° incidence angles, varied at steps of 5° for both HH and VV polarizations. HH polarization is when both the transmitter and

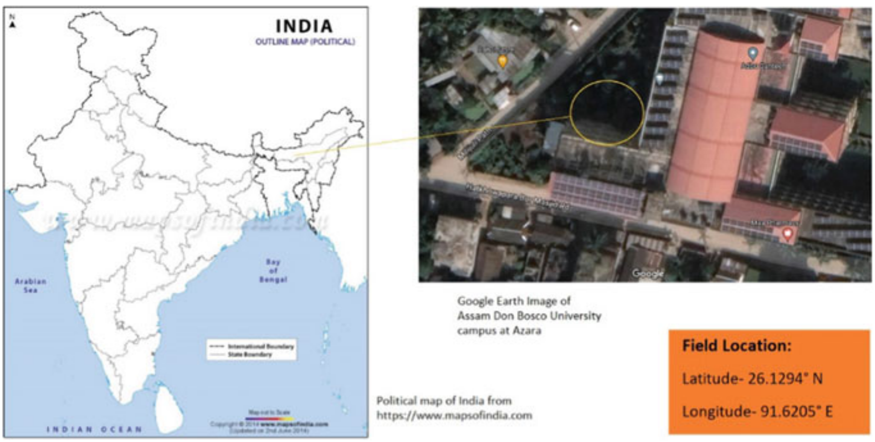

Fig. 1 The experimental field location

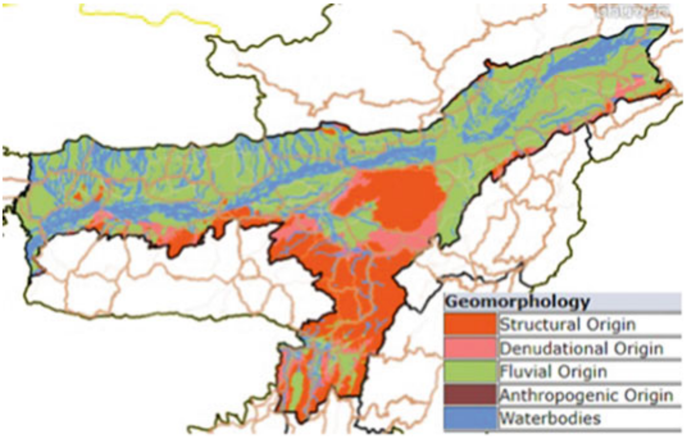

Fig. 2 Soil types of Assam as indicated in Bhuvan maps of ISRO. [bhuvan.nrsc.gov.in]

receiver antenna are of horizontal polarizations. Similarly, VV polarization is when both the transmitter and receiver antenna are of vertical polarizations.

From the initial results obtained, it is observed that, in comparison with VV configuration, i.e., both transmitter and receiver antennae kept in vertical polarization condition, the HH polarization (horizontal polarization for both transmitter and receiver) shows much better sensitivity to soil moisture. Hence, in further experimentation with the scatterometer, HH polarization is used.

3 Results and Discussion

The results of the experiments performed using L-band scatterometer with variations in the frequency in the L-band range of 1.0–2.1 GHz show the sensitivity of the different frequency ranges to the changes in soil moisture. Specifically, the variations in scatterometer responses due to soil wetness change in various locations in the Brahmaputra valley plain areas have been experimented with. The changes in sensitivity of the microwave scatterometer sensor's received power to the soil wetness variations for the fluvial soil of the Brahmaputra valley is found to be highly uniform for various locations in the entire region.

The received power values of scatterometer are monitored for the ground target by placing the transmitter and receiver antennas connected to the microwave source and the microwave power meter, respectively, as explained in the previous section. The Eq. (1) shows the relation between the received power (P_r) and the transmitted power (P_t) in simplified form.

$$P_r = \frac{P_t G \sigma}{4\pi R^2} \tag{1}$$

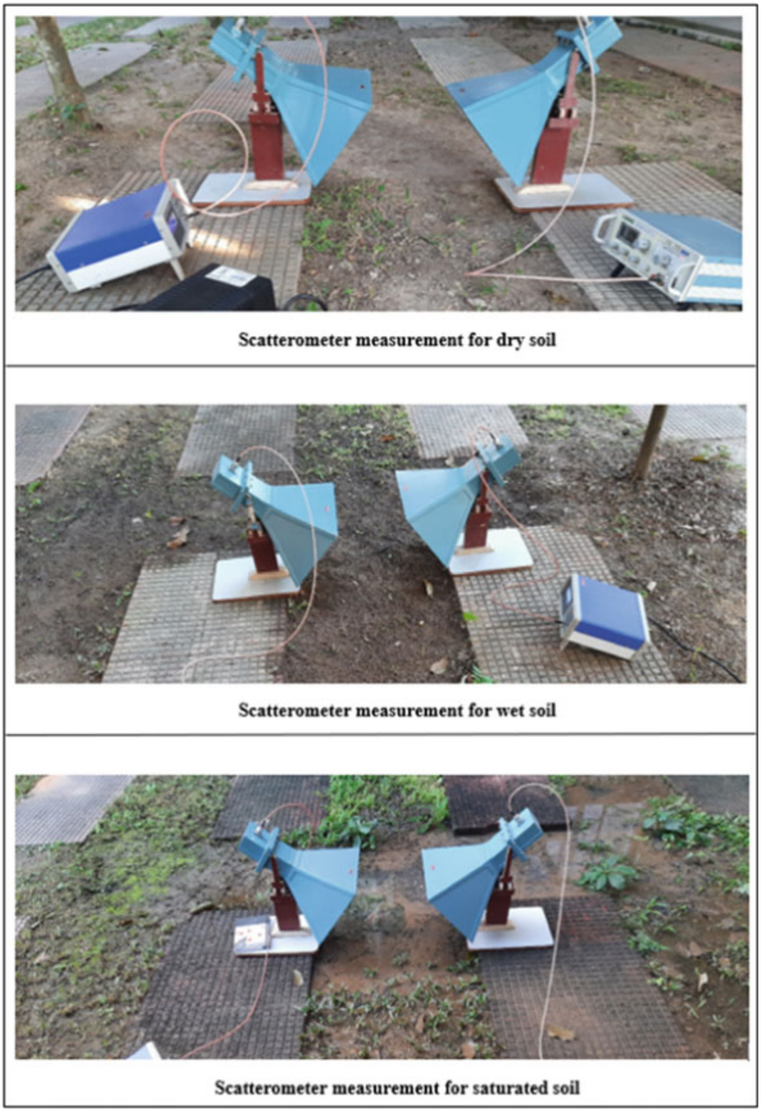

Fig. 3 The experimental setup in the field, for testing dry soil, wet soil, and saturated soil

where

G Antenna gain
σ Radar cross Section
R Range or distance between the antennae.

Table 1 shows the variations in the received power level for a constant transmit power of 23 dbm from the source, at various look/incidence angles of the scatterometer varying from 25° to 70°. For the experiment, power received for several frequencies of the source were tested. By observing the sensitivities, the frequency of around 1.75 GHz is used for the experiment, due to high sensitivity of that frequency to soil wetness. The variations show that the 45° look angle is the most sensitive setting of the scatterometer for a varying received power value with the change in soil moisture level. Therefore, for the rest of the experiments, for determining the most suitable frequency level also, the 45° incidence angle is chosen.

Table 2 shows the received power values at the specular direction (direction of the reflected wave from a smooth surface) for the scatterometer with an incidence angle of 45°, at a constant transmit power of 23 dbm. The received power variations at four different soil moisture levels are tabulated, for finding the most suitable L-band frequency range for monitoring the soil wetness. For the ranges of frequencies shown on the table, the received power levels are same for a particular soil moisture level.

Figure 4 shows the variations in received power for different frequency ranges in graphical form. Both from Table 2 and Fig. 4, it is clearly observed that 1.71 GHz to 1.78 GHz range is the most suitable frequency range for sensitive monitoring of soil moisture levels. The frequency range of 1.71–1.78 GHz is therefore used with the look angle of 45° at HH polarization for monitoring soil wetness of various fields afterward.

Table 1 Received power (P_r) variations with change in soil moisture levels at various incidence angles of the scatterometer

Sl. No.	Incident angle (in degrees)	P_r in dbm for dry soil (soil moisture of 13%)	P_r in dbm for semi-wet soil (soil moisture of 42%)	P_r in dbm for saturated soil (soil moisture of 70%)
1	25°	−2	−1	−1
2	30°	−3	−1	1
3	35°	−3	−1	0
4	40°	−2	−1	1
5	45°	−3	0	2
6	50°	−3	−1	1
7	55°	−2	−1	0
8	60°	−1	0	2
9	65°	0	1	2
10	70°	0	1	2

Table 2 Received power (P_r) variations with change in soil moisture levels at different frequency ranges within L-band

Sl. No.	Frequency range (GHz)	P_r in dbm for soil moisture of 11%	P_r in dbm for soil moisture of 38%	P_r in dbm for soil moisture of 51%	P_r in dbm soil moisture of 72%
1	1.01–1.30	−4	−2	−1	−1
2	1.31–1.43	−3	−1	0	1
3	1.44–1.48	−2	0	1	2
4	1.49 to 1.57	−2	1	1	2
5	1.58–1.62	0	1	1	3
6	1.63–1.70	1	2	4	5
7	1.71–1.78	1	3	6	8
8	1.79 to 1.88	−2	0	2	3
9	1.89 to 1.95	−3	−1	0	2
10	1.96 to 2.01	−5	−3	1	4

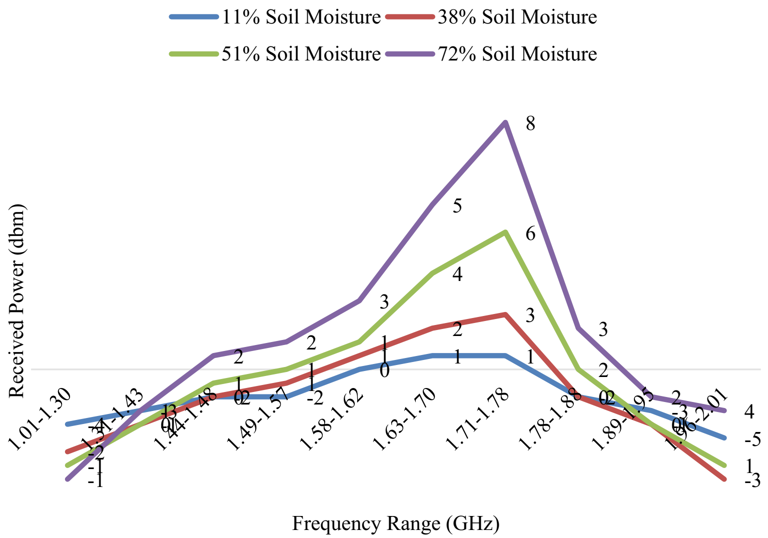

Fig. 4 Variations in received power (P_r) by the scatterometer at different soil moisture levels

From the observed results of the experiments done at different locations of the Brahmaputra valley, it is found that the high increase in soil moisture level and pre-saturation condition of the soil are indicated by a high increase in the received power values of the scatterometer at the above-mentioned configuration of the scatterometer. The same configuration may therefore be used effectively in platform-mounted, aircraft-mounted, or satellite-mounted active microwave sensors for monitoring soil moisture and pre-flood soil saturation conditions in the fluvial type soil.

4 Conclusion

Suitable configuration of L-band ground-based scatterometer can be effectively used for monitoring soil wetness in fluvial soil types. The frequency range of 1.71–1.78 GHz is the most sensitive range to soil moisture changes for such soil types. The 45° look angle for such scatterometers is found to be effective in measuring the soil moisture changes. The best configuration of scatterometer for soil wetness monitoring is therefore found to be the frequency range of 1.71–1.78 GHz with 45° incidence angle in specular direction, using HH polarization of the antennae. Microwave remote sensing sensors within this frequency range can therefore be used for monitoring the soil wetness and for detecting the pre-flood soil saturation conditions. Such experiments can be done for other soil types in other locations also, for the determination of suitable frequency and look angle of the scatterometer, applicable for monitoring soil wetness in those regions.

References

Berhane D (2007) Development of methods and techniques for land resource surveying for Eritrea (Doctoral dissertation, University of Pretoria)

Goswami B, Kalita M (2014) Radar backscattering measurement of bare soil and vegetation covered soil using X-band and full polarization. Int Arch Photogrammetry Remote Sens Spat Inf Sci 40(8):733–735

Hou AY, Skofronick-Jackson G, Kummerow CD, Shepherd JM (2008) Global precipitation measurement. In: Precipitation: advances in measurement, estimation and prediction. Springer, Berlin, pp 131–169

Shubert KA, Ruck GT (1992) Canonical representation of the radar range equation in the time domain. In: Ultrawideband radar 1631. SPIE, pp 2–12

Shukla A, Panchal H, Mishra M, Patel PR, Srivastava HS, Patel P, Shukla AK (2014) Soil moisture estimation using gravimetric technique and FDR probe technique: a comparative analysis. Am Int J Res Form Appl Nat Sci 8:89–92

Song K, Zhou X, Fan Y (2010) Retrieval of soil moisture content from microwave backscattering using a modified IEM model. Prog Electromagnet Res B 26:383–399

Sun Q, Zhang F, Shao Y, Liu L, Wang G, Bian X, Li K, Wang X (2012) S-band backscattering analysis of wheat using tower-based scatterometer. In: 2012 IEEE international geoscience and remote sensing symposium. IEEE, pp 4621–4624

An Enhanced Blockchain Consensus Mechanism Using Proof-of-Work and Proof-of-Stake

Kausthav Pratim Kalita, Jerry Casper Kharbhih, Debojit Boro, and Dhruba Kumar Bhattacharyya

Abstract Blockchain is a composite technology that combines cryptography and consensus algorithms to solve traditional distributed database synchronization problem. Due to the features like immutability and traceability, blockchain is considered to be a reliable platform to store shared information. It is an integral part of various modern multi-field infrastructures, including cryptocurrency. The popularity of blockchain gained spectacularly after the introduction of Bitcoin in the financial world. The consensus mechanism used in Bitcoin, called Proof-of-Work (PoW), also received a similar acceptance and even used in the present blockchain technologies. However, PoW has faced criticism for being less responsive to transaction throughput and for demanding huge computational power. In this paper, we make an attempt to improve the PoW mechanism by incorporating it with another popular consensus mechanism called Proof-of-Stake (PoS). From our experiments, it is observed that such a collaboration can greatly improve the block creation time in the blockchain network and also increase fairness as both higher computational power owners and higher stakeholders get a fair chance to contribute to the chain.

Keywords Blockchain · Consensus algorithms · Proof-of-Work · Proof-of-Stake

K. P. Kalita (✉) · J. C. Kharbhih
Assam Don Bosco University, Airport Road, Azara, Guwahati, Assam, India
e-mail: kausthav.kalita@dbuniversity.ac.in

J. C. Kharbhih
e-mail: jerrykharbhih@gmail.com

K. P. Kalita · D. Boro · D. K. Bhattacharyya
Tezpur University, Napaam, Tezpur, Assam, India
e-mail: deb0001@tezu.ernet.in

D. K. Bhattacharyya
e-mail: dkb@tezu.ernet.in

J. K. Deka et al. (eds.), *Emerging Technology for Sustainable Development*,
Lecture Notes in Electrical Engineering 1061,
https://doi.org/10.1007/978-981-99-4362-3_46

1 Introduction

Blockchain refers to a linked list oriented chain of information which is collectively shared by the users of a distributed network. One of the issues that blockchain tries to solves is money transfer. Let us consider an example where a person Alice staying in a country wants to transfer money to a person Bob staying in another country. This is usually done via a trusted third party. This process usually takes more than a day and also it comes with a transaction fee. Blockchain aims to do this same process without involving any trusted third party. It also helps in making the transaction faster with reduced transaction fee, making the process as cheap as possible.

In centralized systems, the central server is responsible for validating and verifying every single transaction that is generated in the governed network resulting in full dependency on one entity. This, also triggers the possibility of a single point of failure and limits the performance of the entire system. Blockchain attempts to eliminate such a restriction by allowing two parties to involve in a transaction without needing permission from any central authority. However, they need to trust the consensus mechanism of the network and agree on the decision-making rules established in the transaction confirmation process. Such an approach reduces the cost of deployment and also eliminates the performance of bottleneck associated with a centralized system.

Thus, blockchain facilitates a distributed environment where peers can exchange assets by maintaining the validation expected by the deployed consensus algorithm Zheng et al. (2018)

2 Consensus Mechanisms in Blockchain

A consensus mechanism ensures that every participant of a blockchain network agrees to the data that need to be appended in the chain. The rules in such a mechanism provide the basic regulations required to validate a block before committing it to the distributed ledger. Such a mechanism is robust enough to tolerate faulty or failing nodes.

Consensus protocols are constructed in such a way that malicious entities are unable to intrude the system and build their own chains. This is done by involving computationally intensive activities like mining or requiring the possession of large amount of assets to get the appending rights. There are a wide range of varying strategies applied in different consensus algorithm to design efficient and fault tolerating blockchain platforms. Among them, the most popular and widely used mechanisms are PoW, PoS and delegated PoS.

Table 1 Popular assets and their consensus mechanisms

Platform	Consensus mechanism
PoW	Bitcoin, Ethereum, Bitcoin Cash, Bitcoin SV, Litecoin, Monero
PoS	Ethereum classic, Zcash Tezos
Delegated PoS	EOS, Tron

If we consider the top 20 digital currencies (Coindesk 2022), the top assets that implement PoW, PoS and delegated PoS are in Table 1.

In this paper, we focus on the PoW and PoS consensus algorithms.

2.1 Proof-of-Work (PoW)

PoW is one of the earliest consensus algorithms used in the blockchain technology. This algorithm is popularly used in bitcoin where it is used for verifying the blocks before adding them to the chain (Nakamoto and Bitcoin 2008). To execute the PoW mechanism is time-consuming and costly, requiring rigorous hash generation with the help of enormous computation power. Therefore, it is a random process with low probability of satisfying the required condition. Blockchain deploys such a mechanism to enable proper validation of transactions before adding them to the distributed ledger. It enables miners in the network to indulge in a competition of solving hash puzzles to determine a nonce value that indicates their honesty and commitment to the network members. They are rewarded with incentives in return to the resources they have utilized to win the ownership of the generated block. This activity is known as mining. There is always a possibility that two miners simultaneously solve the puzzle and obtain the target hash at the same time. In such a scenario, the validating nodes accept the longest chain received by them and discard the smaller chains.

2.2 Proof-of-Stake (PoS)

PoS is another consensus algorithm that came up later as an alternative to PoW, ensuring the elimination of excessive computational effort for creating hash values. PoS requires the nodes that will verify the transaction to invest some amount of tokens as stake (Bitcoinwiki. 2022). The selection of miners is based on the amount of stake offered by the miner. Higher stake value indicates greater probability that the participant is legitimate who wants to put its assets on risk to attain the mining opportunity. However, such an approach demoralizes peers with low account balances as rich peers have greater chance of creating blocks. In order to overcome this disadvantage, various techniques have been proposed. One such approach is to randomize the selection of the next block generator (Fan and Chai 2018).

Another solution suggests determining the age of the assets put in stake which allows owners with older and larger stake balances acquire higher possibility of attaining block generation task (King and Ppcoin 2012; Ren 2014). PoS method promises to provide sufficient protection from illegitimate activities by applying the following measures.

- Preforming an attack involves gaining large share of stakes.
- The attacker is deprived of any incentives and even loses the stake that is initially offered, thus losing the trust and reputation in the network.

3 Literature Review

Blockchain technology started being popular with the introduction of a very popular cryptocurrency called Bitcoin. Satoshi Nakamoto (a pseudo name) in Nakamoto and Bitcoin (2008) proposed the first white paper on Bitcoin in 2008, where a peer-to-peer electronic cash system that uses blockchain as the backbone technology was discussed. Nakamoto explained how consensus is reached between the nodes in the distributed by using an algorithm called Proof-of-Work (PoW). The PoW will enable the nodes to perform transactions via an electronic payment system that is based on cryptographic proof rather that trust. But as highlighted in Lin and Liao (2017), Ahmed and Shilpi (2018) the main disadvantage of the PoW algorithm is that it takes a really long time to obtain the target value and to create a block. Another challenge is that if a node or a group of nodes gets control over 51% of the network, then the node or the group of nodes will be able to take control over the whole network making the network centralized (Ye et al. 2018). To combat this problem and make the creation of blocks faster, another consensus algorithm came up called Proof-of-Stake (PoS).

BitFury (2015) gives us an overview of both the consensus algorithms and also highlighted the differences in both. The main difference highlighted in the paper is that PoW requires a lot of computational power for mining a block, whereas PoS consumes less computing power. Another difference is that in PoW anyone can participate in the mining, but in the case of PoS, a node has to put something at stake which is a cryptocurrency most of the time before it gets the chance to validate a block. The more stake one puts the more chance one will get for validation of a block. This is mainly in the naive PoS. The paper also discussed about a new version of the PoS algorithm which is delegated PoS. In this algorithm, the stake holders will select delegates for validating the blocks. This makes the block generation faster. In some versions of this algorithm, even the delegates have to put some amount of money as stake so as to make sure that the delegates will not act maliciously. A cryptocurrency called PPCoin (King and Ppcoin 2012) is an example of a cryptocurrency that initially used PoW and later on migrated to PoS consensus algorithm.

Although PoS has proven that it is faster than PoW, PoS has it's own issues like nothing at stake problem which is explained in BitFury (2015). But interestingly the issues that arises in PoW does not arise in PoS and vice versa. So a combination of both can result in a better consensus algorithm that is more secure and reliable. Duong et al. (2016) introduces a hybrid system called a 2-hop blockchain that combines both the PoW and PoS algorithm. The authors mainly address the issues of the 51% attack in PoW. The proposed system consist of two rounds namely the PoW and the PoS round. PoW is used for getting the valid chain of the blockchain when a fork occurs, and PoS involves choosing a PoS holder who is given the authority of identifying and approving the most valid chain-pair in its visibility. In other words, the PoS holder will be the one that will add the block to the chain. The proposed system was called 2-hop because of the hopping from one consensus algorithm to another. Chepurnoy et al. (2017) discusses the application of a modified version of the 2-hop system in a cryptocurrency namely "TwinsCoin."

4 Proposed Methodology

In a distributed network like blockchain, there is no central authority to validate the information ingested in the platform. In such a scenario, each of the participants in the network needs to behave legitimately to achieve a trusted environment. Since the authority of adding blocks in a blockchain is equally distributed among the peers, consensus algorithms are used. The two most popularly used consensus algorithms are PoW and PoS. In this paper, we propose to combine both the algorithms to achieve a better composite algorithm that can take the benefit from each of them as well as reduce the vulnerabilities each of them provides. PoW needs huge computational power to discover the target hash required for block creation. On the other hand, PoS is more favorable for peers with large balances as richer miners attain greater opportunities to create blocks. Thus, our proposed method targets the following:

- PoW runs only for specific rounds while searching for the target hash value. The number of rounds allowed is decided by a value termed as MaxHashCount (MHC). If the target hash is not obtained within MHC, the network shifts to PoS.
- In PoW, the difficulty level is increased when the current average time recorded is lesser than the expected average time. The expected average time is termed as MaxAverageTime (MAT). But once the recorded average time exceeds MAT, the network shifts to PoS.
- PoS runs only for a specific number of rounds after which the network shifts back to PoW. The number of rounds allowed in PoS is termed as CountValue (CV).

4.1 Algorithm Design

The method proposed in our work is represented by the logical procedure mentioned in Algorithm 1. Our main aim is to run PoW in the initial stage and keep it running until the average block creation time (AT) exceeds MAT. After every successful round of PoW, AT is calculated and compared with MAT. If AT crosses MAT then the consensus is shifted to PoS which runs for predetermined rounds referred as CV. Initially, it selects a node that has the highest amount of stake in the first round, and then in the next round, the node with the second highest stake is taken into consideration. This continues till all the CV number of nodes get a chance to be a validator. This approach will prevent the rich node to become a validator in all the consecutive rounds preventing centralization of the system and providing a wider opportunity for block creation. Once the CV rounds are over, then the consensus is moved backed to PoW and the same procedure is repeated. In such an approach, the miners who have invested in mining hardware as computing resources as well as validators with high stake values both get benefited, yet, preventing them from dominating the network and enjoying monopoly. Ignoring the risk of centralization of power in a blockchain network often exposes the provision for attacks like double-spending (Natoli and Gramoli 2016) and 51% attack. Thus, the algorithm protects against such vulnerabilities.

We introduced MHC which determines the maximum number of iterations allowed to find the target hash value in PoW. This is done to ensure that the network does not consume an enormous amount of time in finding the target nonce as it significantly affects the block creation time and gradually affects AT. If the target nonce is not discovered within MHC, the network shifts to PoS. MHC is determined by using the following approach: Suppose, the previous block creation times are t_1, t_2,, t_{n-1}. Once the next round gets over, AT is calculated as given:

$$\frac{[t_1 + t_2 + \ldots + t_{n-1}] + t_n}{n} = \text{AT} \tag{1}$$

Now, we want AT not to exceed MAT. Thus, we can write:

$$\frac{[t_1 + t_2 + \ldots + t_{n-1}] + t_n}{n} \leq \text{MAT} \tag{2}$$

$$t_n \leq (n \times \text{MAT}) - \sum_{p=1}^{n-1} t_p \tag{3}$$

From Eq. 3, we can obtain the time bound within which the next block needs to be created in order to prevent AT from exceeding MAT. Finally, we can determine MHC by multiplying t_n with the hashrate observed in the network:

$$\text{MHC} = t_n \times \text{hashrate} \tag{4}$$

Algorithm 1 Optimized consensus mechanism

1: Initialization of n nodes in the network, N $\rightarrow$ set of accepted nodes for PoS
2: Let *ni* represent i^{th} node having balance *bi* and proposed stake *si*
3: Set MaxAverageTime (MAT) = α; MaxHashCount(MHC) = μ; Difficulty (D) = δ; let $\delta = \delta k$
4: Let AverageTime (AT) = 0
5: Set Flag = 1 /* 1 indicate PoW and 0 indicate PoS */
6: **if** Flag = = 1 **then**
7:     result = PoW() /* proof-of-work algorithm runs*/
8:     /* result = 1 indicates that the target hash is obtained*/
9:     /* result = 0 indicates that the target hash is not obtained*/
10:     **if** result = = 1 **then**
11:         AT is updated /* using **Eq. 1***/
12:     D is updated as follows:
13:     **if** AT < α **then**
14:             $\delta k = \delta k + 1$
15:             μ is updated /* using **Eq. 4***/
16:         **else**
17:             Flag = 0
18:             Reset D: $\delta k = \delta$
19:         **goto** step 6
20:     **else**
21:         Flag = 0
22:         Reset D: $\delta k = \delta$
23: **else**
24:     Set CountValue(CV) = χ; counter: C = 0
25:     **while** C is less than χ **do**
26:         PoS() /* proof-of-stake algorithm runs */
27:         AT is updated
28:         C = C + 1
29:     μ is updated
30:     Flag = 1
31:     **goto** step 6

5 Result Analysis

5.1 Experiment Setup

To establish the testbed, a blockchain network is created in the Python language (version = 3.9.10). Multiple processes are run in a standalone machine with the help of the Flask application framework (version = 2.0.3) developed in Python. All the hashing operations done in our experiments are calculated using SHA256 algorithm provided by the *hashlib* package in Python. Since the peers are running in a single machine, MAT is configured to 1 s. Initially, MHC is set to 2^{32}. After each round of PoW, MHC is updated with the help of the Eq. 4. The blockchain network is initiated with PoW consensus algorithm. PoW is continued until the round where PoW fails to achieve the target nonce with MHC. In such a case, the network shifts to PoS which runs for definite amount of time as configured in CV. Then, the network moves back to PoW with updated value of MHC. The total number of successful rounds run with the proposed algorithm in our test environment is 200. Once the simulation with proposed algorithm is over, the network is deployed with the primitive PoW consensus algorithm alone and compared with the composite one.

5.2 Results and Observations

Our experiment was conducted in two phases. In the first phase, only PoW was selected as the consensus algorithm. The PoW consensus algorithm was deployed without using any of the new parameters that were introduced in our proposed algorithm (PA). In the second phase, PA was deployed with parameters such as MHC.

In Fig. 1, the cumulative time for both the phases are plotted. It can be seen in the graph that both phases take approximately same amount of time to create 200 blocks. However, PA takes a steady path, whereas PoW witnesses excessive fluctuation in some rounds. This indicates that in certain rounds of PoW, block creation took comparatively huge amount of time than the rest. Such a variation is not observed in PA.

In Fig. 2, a similar pattern is observed for the moving average time of PoW and PA. In the first phase, the plot of the moving average time in PoW is not steady as

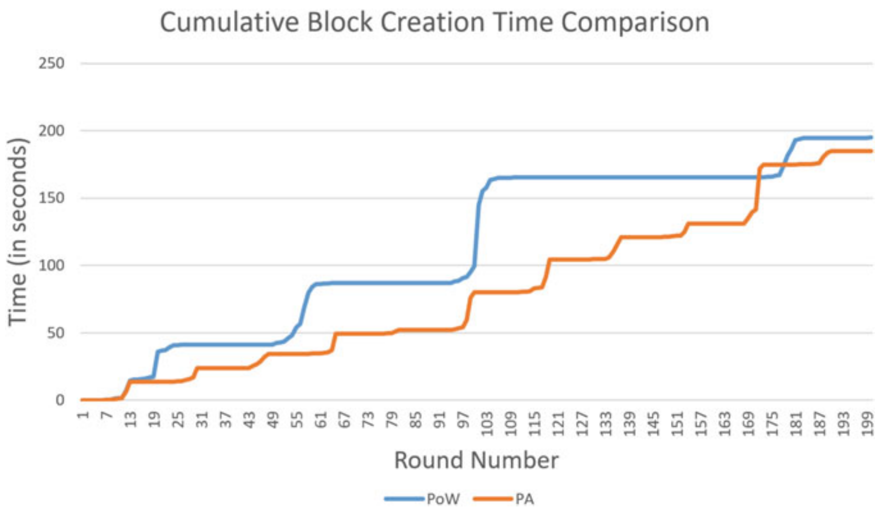

Fig. 1 Cumulative block creation time comparison between PoW and PA

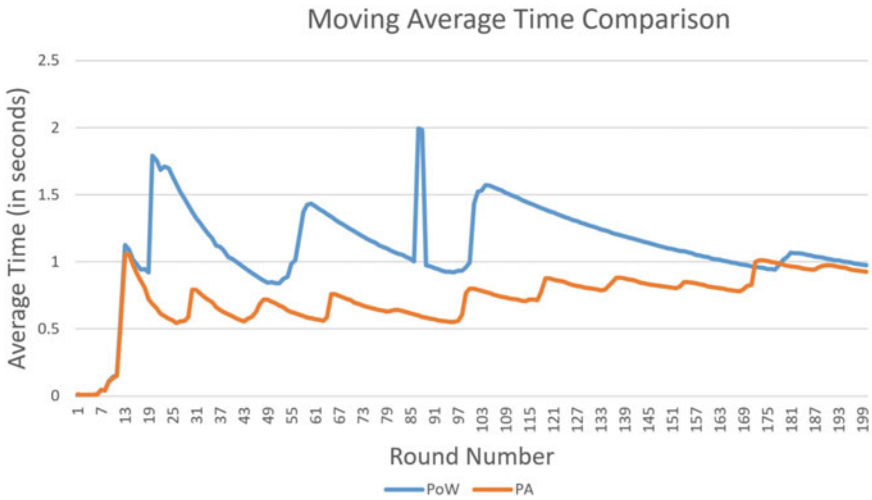

Fig. 2 Moving average time comparison between PoW and PA

the difficulty level through the simulation had to be frequently adjusted. On the other hand, the plot of the moving average time in PA is very close to being steady. The reduction in variation is caused by the shifts between PoW and PoS.

Figure 3 indicates the consensus algorithm (either PoW or PoS) that was running when the block was created in that round. This graph reflects information about the second phase where PA was deployed. It can be observed from the figure that both PoW and PoS alternatively share the network for block creation. Such an alternation prevents resourceful miners from continuously appending the chain and also disrupts rich stakeholders from winning the right to mine new blocks continuously.

The share of participation of both the consensus algorithms is shown in Fig. 4. The graph shows that the majority of the rounds deployed PoW for block creation. Such a share of distribution is because the rounds executed by PoW is not restricted by a fixed value unlike in PoS. However, the contribution from PoS is noteworthy as it contributed to keeping the cumulative block creation time and running average time steadily.

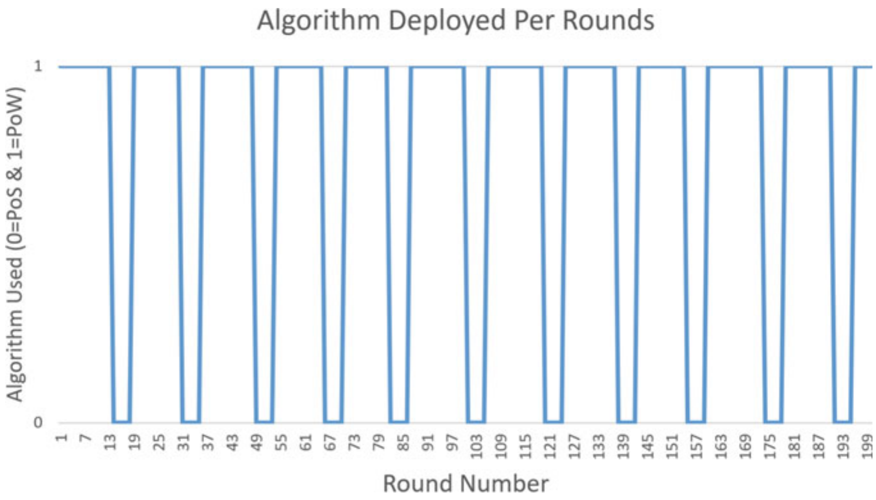

Fig. 3 Algorithm deployed per round in PA

Fig. 4 Participation of PoW and PoS in PA

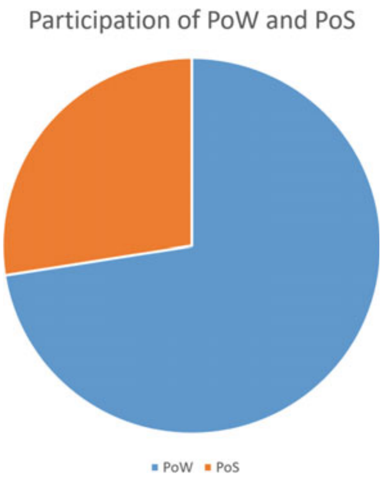

6 Conclusion

Blockchain is an attractive domain of research and innovation in the world today. In a trustless distributed environment, blockchain has shown promising potentials of being the best bet of people dealing with the value-sensitive commodities. Behind every blockchain technology, there is always a consensus algorithm that plays an extremely important role in a distributed environment. There are many such algorithms proposed today by various researchers. Some are still in the research stage, while some like PoW, PoS, Ripple etc., are currently used in the world today by

Bitcoin, Ethereum, Ripple etc. Our proposed system uses an optimized version of the PoW along with PoS consensus algorithm that can be implemented practically in a computer with an average system configuration and also maintaining the security aspect. The work reflected in this paper is aimed at extracting the benefits of both the popular consensus algorithms and construct a new approach to benefit the miners, validators and the blockchain network at large.

References

Ahmed I, Shilpi MA (2018) Blockchain technology a literature survey. Int Res J Eng Technol (IRJET) 5(10):2395–56

Bitcoinwiki (2022) https://en.bitcoin.it/wiki/Proof of Stake. Last Accessed on: 17 Apr 2022

BitFury G (2015) Proof of stake versus proof of work. White paper

Chepurnoy A, Duong T, Fan L, Zhou HS (2017) TwinsCoin: a cryptocurrency via proof-of-work and proof-of-stake. IACR Cryptol Eprint Arch 2017:232

Coindesk. https://www.coindesk.com/coindesk20. Last accessed on: 17 Apr 2022

Duong T, Fan L, Zhou HS (2016) 2-hop blockchain: combining proof-of-work and proof-of-stake securely. Cryptology ePrint Archive, Report 2016/716

Fan X, Chai Q (2018) Roll-DPoS: a randomized delegated proof of stake scheme for scalable blockchain-based internet of things systems. In: Proceedings of the 15th EAI international conference on mobile and ubiquitous systems: computing, networking and services 5 Nov 2018, pp 482–484

King S, Nadal S (2012) Ppcoin: peer-to-peer crypto-currency with proof-of-stake. self-published paper, 19 Aug 2012, 19:1

Lin IC, Liao TC (2017) A survey of blockchain security issues and challenges. IJ Netw Secur 19(5):653–659

Nakamoto S, Bitcoin A (2008) A peer-to-peer electronic cash system. Bitcoin.–URL https://bitcoin.org/bitcoin.pdf

Natoli C, Gramoli V (2016) The blockchain anomaly. In: 2016 IEEE 15th international symposium on network computing and applications (NCA) 31 Oct 2016. IEEE, pp 310–317

Ren L (2014) Proof of stake velocity: building the social currency of the digital age. Self-published white paper

Ye C, Li G, Cai H, Gu Y, Fukuda A (2018) Analysis of security in blockchain: case study in 51%- attack detecting. In: 2018 5th international conference on dependable systems and their applications (DSA) 22 Sep 2018. IEEE, pp 15–24

Zheng Z, Xie S, Dai HN, Chen X, Wang H (2018) Blockchain challenges and opportunities: a survey. Int J Web Grid Serv 14(4):352–375

A Remote Health Monitoring System for the Elderly Based on Emerging Technologies

C. M. M. Mansoor, Sarat Kumar Chettri, and H. M. M. Naleer

Abstract In the background of a rapidly aging population, the widespread deployment of smart wearable devices might help ease the societal burden created by the growing demand for healthcare and support among the elderly. Despite the fact that technology plays an important part in attaining these goals, any solution needs to be planned, implemented, and verified via domain expertise. This chapter examines the technologies that are employed in healthcare. Machine Learning (ML), Cloud Computing, Big Data, the Internet of Things (IoT), Artificial Intelligence (AI) and remote and wearable sensor network devices are among the technologies studied. Similarly, the data for a research article are gathered from a previously published study 92 papers from reputable publications. The essay also includes a systematic review technique. In addition, the study was prompted by Cloud Computing and IoT technology because of its high accuracy rate, manageable interface, and effective and efficient outcomes. They will need both financial and technical aid to collaborate with healthcare specialists and provide both the technology, knowledge needed for treatments to be beneficial.

Keywords Cloud computing · Big data · Internet of Things · Machine learning

C. M. M. Mansoor (✉)
Department of Information Technology, South Eastern University of Sri Lanka, Oluvil, Sri Lanka
e-mail: mansoorr@seu.ac.lk

S. K. Chettri
Department of Computer Applications, Assam Don Bosco University, Guwahati, India
e-mail: sarat.chettri@dbuniversity.ac.in

H. M. M. Naleer
Department of Computer Science, South Eastern University of Sri Lanka, Oluvil, Sri Lanka
e-mail: hmmnaleer@seu.ac.lk

J. K. Deka et al. (eds.), *Emerging Technology for Sustainable Development*,
Lecture Notes in Electrical Engineering 1061,
https://doi.org/10.1007/978-981-99-4362-3_47

1 Introduction

Elderly populations are at an increasing amount in many nations throughout the globe. Biological variables and disorders have a significant role in healthy aging (Özsungur 2021). Many choose to remain in their homes rather than go to a healthcare facility. Remote health monitoring is one of the most growing sectors, owing to its advantages over standard hospitalization procedures (Liu et al. 2016; Reviews 2020).

Telemedicine (Mohammed et al. 2019) that uses ICT to allow coordination among diverse persons to facilitate their cooperative efforts in diagnosing or treating a condition (Albahri et al. 2018; Grossi et al. 2020). Dementia has a huge effect on society, patient quality of life (Lv et al. 2019). Personal home care exacerbates the nursing shortage and adds to the nursing effort (Liu et al. 2019). A high-resolution GPS, Complementary Metal-Oxide Semiconductor (CMOS) image sensor, magnetometer, accelerometer, microphone, ambient light sensor, and gyroscope. These sensors may be used to assess a variety of health metrics, including HR Variability (HRV), Heart Rate (HR), Respiration Rate (RR) issues (Majumder and Deen 2019). The surveilling character allow caretakers to remotely watch the movements, activities of elders might lead to conflict (Berridge et al. 2020). Polypharmacy is as a patient's usage of drugs, while others define it as the optimization of pharmaceuticals to allow a patient to take multiple acceptable medications (Al-Dahshan et al. 2020; Alsuwaidan et al. 2019; Miyabayashi et al. 2019; Lv et al. 2010).

When a situation is serious, the Contact Emergency Center (CEC) will use an ambulance or an Unmanned Aerial Vehicle (UAV) to administer first assistance to the patient (Fakhrulddin et al. 2019; Lee and Kim 2020).

2 Literature Review

With an aging population and higher life expectancies, seniors are in greater need of care and innovative healthcare (Caner and Cilasun 2019). The COVID-19 epidemic is excessively affecting elders. Those aged 60 and up had a greater mortality rate (Yassine 2021). Remote patient monitoring in healthcare applications, IoT-based smart home technologies without jeopardizing security standards/posing a huge number of dangers (Talal et al. 2019).

Smart Health Technologies are the result of a natural synergy between m-Health and smart cities from the perspective of ICT. IoT technologies are connected with medical systems in order to give individuals in need (Guisado-Fernández et al. 2019). AI health-monitoring technology play a new role in bridging human resource shortages in caring for the elderly (Ho 2020). Living with chronic illnesses that typically coincide with aging is directly tied to maintaining a particular degree of well-being (Adami et al. 2021). RHM is a continuous health data monitoring technique. Physiological nursing are all part of this. As a result, IoMT facilitates quick, remote, real-time and trustworthy diagnosis of a variety of diseases and decision-making. This process receives, analyzes, and monitors a significant volume of data (Al Shorman et al. 2020). Sensors, RFID, GPS, infrared, and wearable technology are examples of sensing devices and technologies included in the IoT (Wang et al. 2019). Although Patient Acceptance (ACC) has a helpful influence (Zhou et al. 2019). The capacity of smart gadgets to engage with users and communicate with one another in an IoT-based smart home environment is being envisioned as a key resource to improve the quality of life experienced by elders (Thakur and Chia 2019; Kruse et al. 2020). Heart rate, temperature data on an LCD and delivers an automated alert to caregivers/surgeons. The Big Data Analytics (BDA) and IoT are key tools for gaining knowledge, support for improving the lives of elders by enhancing the role of ICT (Wang et al. 2019).

A deep learning model employing knowledge-based methodologies was used, results were analyzed and compared to the Support Vector Machine (SVM) method (Sodhro et al. 2020). Individual data may be easily transferred or duplicated between the local Solid POD and the cloud Solid POD (Chen 2019). "HeartAround," a complete homecare system interviews and qualitative analysis, the System Usability Scale (SUS) technique (Panagopoulos et al. 2019). A monitoring system based on RFID with Ultra-High Frequency (UHF) has been presented as a solution to this problem. The caregiver keep an eye on without interfering with the elder's daily activities. In addition, the caretaker has remote access to the system. Then, caregiver can monitor the elder at all times (Bin Eddy Yusuf et al. 2020). IoT-based communications and DS-based machine learning/classification to identify ADLs conducted by the aging in order to highlight perhaps worrying actions and notify the apt healthcare staffs (Yassine 2021). Active, mid, and passive RFID tags are the three types of tags available (Deep et al. 2020).

3 Methodology

This study was conducted with a qualitative approach systematic review from the preceding five years. The collected data were analyzed to look at the uses, advantages, disadvantages of certain health technology. To gather the data, following technologies utilized: AI, Cloud (Pham et al. 2016; Monteiro et al. 2018), IoT (Xl et al.; Iranpak et al. 2021), Big Data (Author 2016), Wearable sensors (Dias 2018) and ML.

3.1 Criteria for Selecting and Excluding Articles

A first recovered records was carried out by one of the writers. After analyzing individual titles and abstracts, duplicate articles were deleted, records were discarded. The included studies were examined by second author, who assessed the full-text papers/eligibility. Journal, conference papers were omitted because we believed these two venues were more likely to contain current, relevant scientific papers related to our survey.

1. The article is a conference or journal paper written in English.
2. Papers published or reported between 2019 and 2022
3. The major focus on wearable sensors/IoT for monitoring elderly adults.
4. Telemedicine in healthcare is the major focus in one or more of the following areas:

   I. Services in the medical field
   II. Network failure and disaster management
   III. Telemedicine patient triage
   IV. Telemedicine sensors
   V. Prioritization of patients in telemedicine
   VI. Telemedicine security.

We discarded publications that did not meet our eligibility criteria after three rounds of filtering and screening. We provide health services, patient prioritization, patient assessment, emergency preparedness, network issues, telemedicine sensors, protection.

3.2 Research Question

The following are the research questions for the article needed for this study analysis.

- How technologies influencing in elder's healthcare?
- Which developing technology aids in illness prediction and diagnosis?

Based on the previous characteristics criteria, 92 research papers were finished to extract the essential data.

4 Results and Discussion

According to Table 1, numerous technologies are employed. The deep analysis, as shown in the table illustrates the technologies, suggested or approved technologies, illnesses. The papers (Hamim 2021; Hassen et al. 2019; Study et al. 2019; Lousado 2020; Debauche et al. 2019; Saha et al. 2021; Ibrahim 2019) are used IoT as the main technology. Subtechnologies of various types are employed in the distant remote monitoring for aged people. Especially, Bluetooth devices, cellphones with mobile networks (3G/4G and, in the future, 5G), DS18B20 temperature sensor, Arduino Nano, wireless networks, sensors are used in this technology. In reference (Thar et al. 2019; Li et al. 2019; Durán-Vega et al. 2019) are used Wearable sensors as the main technology. Reference (Thar et al. 2019) mentioned a Ambient Assistive

Table 1 Results of the previous table

Paper	Suggested technologies	Used technologies under main technologies	Diseases	Advantages
Thar et al. 2019)	Wearable sensors, Smart phone app	Ambient Assistive Living, fitness trackers, wearable biometric sensors	Diabetes, heart disease, blood pressure	Delivering remote monitoring, minimizing hospitalization. A successful health solution monitors older individuals in real-time
Hamim 2021)	IoT	Heart pulse sensor, body temperature, galvanic skin Response sensor	Measure pulse rate, galvanic skin response and body temperature	Watching the patient's health data over time using an application
Hassen et al. 2019)	IoT, cloud computing	Android app Fog server, My-signals HWV2	Diabetes, heart disease, Alzheimer's	Effective, simple to use, understand, implying that it enhance the level of the geriatric health sector
Li et al. 2019)	Smart wearable systems	Electronic care surveillance-wearable, smart garments, implanted, skin, wearable devices	Location, vital signs, body movement, and fall prevention	Users would be able to get real-time-time anywhere they get input on their bodily state and at any time as healthcare technology advances
Tanabe, et al. 2018)	Robotic Smart Home	Mobility, operational, transfer, information assist systems	Leg problems	People may enjoy comfort thanks to a home health monitoring system linked to the IoT
Yu et al. 2019)	Unobtrusive sensors	Motion, pressure and wearable sensors	Diabetes and pressure	Providing elderly people with a reduced cost, pleasant, and user-friendly living environment
Study et al. 2019)	IoHT	Edge computing	Health diagnosis	Getting actual acquired source data, IoHT efficiency, responsive

(continued)

Table 1 (continued)

Paper	Suggested technologies	Used technologies under main technologies	Diseases	Advantages
Petere et al. 2016)	Cloud Platform (sensors)	Glucometer, airflow, micro controller and a gateway	Observable metrics, neurological disorder	Makes a connection elderly people, allowing you to connect with them and remotely check their wellbeing
Lousado 2020)	IoT, Long Range (LoRa) Technologies	Bluetooth devices, smartphones mobile wireless networks, sensors	SARS-CoV-2 pandemic	Evaluation of individuals' medical health, as has been repetitively noticed in the media in the present pandemic context
Durán-Vega et al. 2019)	Wearable Device, Mobile App	Biometric bracelet connected to a mobile app	Heart rate, temperature, oxygenation heart rate	Simple to learn and use by users, giving a preliminary indication enhance the effectiveness of the elder healthcare system
Sapci and Sapci 2019)	AI	Intelligent algorithm and software engineering, as well as robotics technologies	Aged people heart rate, temperature, activities and behaviors	Designed to keep track of the care of older people
Klaib et al. 2019)	IoMT, cloud Technologies	Tobii technology, Azure cloud	Eye problem elderly and special needs people	Precise gaze estimations, video capture system mobility, and totally remote recordings
Debauche et al. 2019)	Fog IoT, Cloud IoT	Sensor network, local smart gateway, heartrate sensor	Oxygen saturation, EMG, respiration, blood pressure, glucose level	All through the communication between the sensor and the patient, data privacy protection and confidentiality are maintained

(continued)

Table 1 (continued)

Paper	Suggested technologies	Used technologies under main technologies	Diseases	Advantages
Al Nahian et al. 2020)	AI, big data	A camera, an RFID reader, and a radar sensor Smartwatches, wristbands, and waistbands	Neurological disorder	Deal with elderly people's expression recognition, medical condition projections, and actual fall tracking
Kumar and Sekhar 2015)	Android smart phone	Pulse oximeter sensor, Temperature sensor, Bluetooth module	Heart rate, oxygen saturation level in blood and temperature related	To use an Android mobile application, the doctor may keep a constant eye on the condition of the patient
Saha et al. 2021)	IoT	Arduino Nano, ATmega328 microcontroller, and DS18B20 temperature sensor	Body temperature related, chronic diseases	Information is collected and processed in order to provide appropriate feedback to patients with or without mobility help who are indoors
Syed et al. 2019)	IoMT (Internet of Medical Things)	AAL (Ambient Assisted Living)	Left ankle, right arm, and chest diseases	When opposed to digital computation, parallel processing enables more scalability and better performance in recognizing the movement sensed by distinct body parts
Ibrahim 2019)	IoT and big data	Artificial neural network, MapReduce	All diseases	Assist in the deployment of advanced health, resulting in enhanced healthcare delivery and accessibility

(continued)

Table 1 (continued)

Paper	Suggested technologies	Used technologies under main technologies	Diseases	Advantages
Shahzad et al. 2018)	Cloud computing	Electrocardiography sensors, blood pressure sensors, and glucometers	Chronic diseases	Through modeling of private cloud computing, improvements were developed to monitor and track real-time medical data, limited in an approved region
Tasneem Usha et al. 2019)	Android application	GSM and GPS modules	All diseases	Through an Android app, you may observe real-time activities, remotely monitor the patient's status, get emergency notifications, and track their whereabouts

Living technologies, fitness trackers, wearable biometric sensors technologies are used under the main technology. Reference (Li et al. 2019) Electronic care surveillance devices and wireless sensor networks. Reference (Durán-Vega et al. 2019) includes, biometric bracelet connected to a mobile application are sub technologies. In reference (Al Nahian et al. 2020; Ibrahim 2019) are used big data is the main technology used for Remote Monitoring. Reference (Klaib et al. 2019; Shahzad et al. 2018) used Cloud technology (Klaib et al. 2019). Paper described used techniques are Tobii technology, Azure cloud.

We propose IoT as the finest among other technologies based on the table. Due to their great accuracy, wearable sensors and AI are the finest solutions for remote monitoring healthcare system.

5 Conclusion

Various technology alternatives are now being investigated throughout the globe in order to improve healthcare services (Mohapatra et al. 2019). We aimed to address a vacuum in health status. The articles, on the other hand, contained information on how elder may preserve their social contacts and be engaged in their everyday lives and users will benefit from remote monitoring to minimize chronic and diet-related disease, enhance cognitive performance, improve emotional health and live healthier lives overall. Most of the papers include IoT, mobile applications, sensors and wearable devices. The remote healthcare monitoring system lowers healthcare costs by minimizing the need for human help and improving life for elders. As elder get more comfortable with Remote technology, it's feasible that building designed solutions to solve age-related physical hurdles take priority over the existing technical avoiding obstacles. Accordance to that, whether in the form of these reviews, could concentrate on the human elements of IoT for elderly care. The compromise between technical ability in terms of performance, accuracy, modalities, and human needs for safety, longevity, in certain cases, esthetics, is always shifting and might be examined.

References

Adami I et al (2021) Monitoring health parameters of elders to support independent living and improve their quality of life

Al Nahian MJ, Ghosh T, Uddin MN, Islam MM, Mahmud M, Kaiser MS (2020) Towards artificial intelligence driven emotion aware fall monitoring framework suitable for elderly people with neurological disorder. In: Lecture notes in computer science (including subseries Lecture notes in artificial intelligence and lecture notes in bioinformatics), vol 12241 LNAI, September, pp 275–286. https://doi.org/10.1007/978-3-030-59277-6_25

Al Shorman O, Al Shorman B, Al-Khassaweneh M, Alkahtani F (2020) A review of internet of medical things (IoMT)-based remote health monitoring through wearable sensors: a case study for diabetic patients. Indones J Electr Eng Comput Sci 20(1):414–422. https://doi.org/10.11591/ijeecs.v20.i1.pp414-422

Albahri OS et al (2018) Systematic review of real-time remote health monitoring system in triage and priority-based sensor technology: taxonomy, open challenges, motivation and recommendations. J Med Syst 42(5):80. [Online]. Available http://www.embase.com/search/results?subaction=viewrecord&from=export&id=L621351533%0A. https://doi.org/10.1007/s10916-018-0943-4

Al-Dahshan A, Al-Kubiasi N, Al-Zaidan M, Saeed W, Kehyayan V, Bougmiza I (2020) Prevalence of polypharmacy and the association with non-communicable diseases in Qatari elderly patients attending primary healthcare centers: a cross-sectional study. PLoS One 15(6):1–13. https://doi.org/10.1371/journal.pone.0234386

Alsuwaidan A et al (2019) A comprehensive overview of polypharmacy in elderly patients in Saudi Arabia. Geriatrics 4(2):1–10. https://doi.org/10.3390/geriatrics4020036

Author SD (2016) Monitoring mobile patients using predictive analysis by data from wearable sensors, pp 332–335

Berridge C, Wetle TF, Bowers BJ (2020) Why older adults and their children disagree about in-home surveillance technology, sensors, and tracking. Gerontologist 60(5):926–934. https://doi.org/10.1093/geront/gnz068

Bin Eddy Yusuf SS, Abbas Helmi RA, Bin Abdullah MI, Jamal A (2020) Towards elderly monitoring management system using IOT. In: 2020 IEEE symposium on industrial electronics and applications, pp 1–7. https://doi.org/10.1109/ISIEA49364.2020.9188191

Caner A, Cilasun SM (2019) Health care services and the elderly: utilization and satisfaction in the aftermath of the Turkish health transformation program. Gerontol Geriatr Med 5:233372141882286. https://doi.org/10.1177/2333721418822868

Chen H (2019) Ubi-care: a decentralized ubiquitous sensing healthcare system for the elderly living support. In: Proceedings of IEEE 17th international conference on dependable, autonomic and secure computing, IEEE 17th international conference on pervasive intelligence and computing, IEEE 5th international conference on cloud and big data computing, 4th international conference on cyber science and technology congress, pp 543–547. https://doi.org/10.1109/DASC/PiCom/CBDCom/CyberSciTech.2019.00108

Debauche O, Mahmoudi S, Manneback P, Assila A (2019) Fog IoT for health: a new architecture for patients and elderly. Procedia Comput Sci 160:289–297. https://doi.org/10.1016/j.procs.2019.11.087

Deep S, Zheng X, Karmakar C, Yu D, Hamey LGC, Jin J (2020) A survey on anomalous behavior detection for elderly care using dense-sensing networks. IEEE Commun Surv Tutorials 22(1):352–370. https://doi.org/10.1109/COMST.2019.2948204

Dias D (2018) Wearable health devices—vital sign monitoring, systems and technologies. https://doi.org/10.3390/s18082414

Durán-Vega LA, Santana-Mancilla PC, Buenrostro-Mariscal R, Montesinos-López OA (2019) An IoT system for remote health monitoring in elderly adults through a wearable device and mobile application

Fakhrulddin SS, Gharghan SK, Al-Naji A, Chahl J (2019) An advanced first aid system based on an unmanned aerial vehicles and a wireless body area sensor network elderly persons in outdoor environments. Sensors (Switzerland) 19(13). https://doi.org/10.3390/s19132955

Grossi G, Lanzarotti R, Napoletano P, Noceti N, Odone F (2020) Positive technology for elderly well-being: a review. Pattern Recognit Lett 137(xxxx):61–70. https://doi.org/10.1016/j.patrec.2019.03.016

Guisado-Fernández E, Giunti G, Mackey LM, Blake C, Caulfield BM (2019) Factors influencing the adoption of smart health technologies for people with dementia and their informal caregivers: scoping review and design framework. JMIR Aging 2(1). https://doi.org/10.2196/12192

Hamim M (2021) IoT based remote health monitoring system for patients and elderly people, June 2021. https://doi.org/10.1109/ICREST.2019.8644514

Hassen B, Inf H, Syst S, Ben Hassen H, Dghais W, Hamdi B (2019) An E-health system for monitoring elderly health based on Internet of Things and Fog computing. Heal Inf Sci Syst. https://doi.org/10.1007/s13755-019-0087-z

Ho A (2020) Are we ready for artificial intelligence health monitoring in elder care? BMC Geriatr 20(1):1–7. https://doi.org/10.1186/s12877-020-01764-9

Study SAC, Ianculescu M, Alexandru A, Nicolau N-D, Neagu G, Bica O (2019) IoHT and edge computing, warrants of optimal responsiveness of monitoring applications for. In: 2019 22nd international conference on control systems and computer science, pp 655–661. https://doi.org/10.1109/CSCS.2019.00118

Ibrahim A (2019) Smart healthcare. 4(2):93–109. https://doi.org/10.1108/PRR-08-2019-0027

Iranpak S, Shahbahrami A, Shakeri H (2021) Remote patient monitoring and classifying using the internet of things platform combined with cloud computing. J Big Data. https://doi.org/10.1186/s40537-021-00507-w

Kariapper RKAR, Nafrees ACM, Razeeth MSS, Pirapuraj P (2020) Emerging smart university using various technologies: a survey analysis. Test Eng Manag 82(1):17713–17723

Klaib AF, Alsrehin NO, Melhem WY, Bashtawi HO (2019) IoT smart home using eye tracking and voice interfaces for elderly and special needs people. 14(7):614–621. https://doi.org/10.12720/jcm.14.7.614-621

Kruse C, Fohn J, Wilson N, Nunez E, Hall E, Marcos S (2020) Utilization barriers and medical outcomes commensurate with the use of telehealth among older adults: systematic review. 8:1–24. https://doi.org/10.2196/20359

Kumar MA, Sekhar YR (2015) Android based health care monitoring system

Lee LN, Kim MJ (2020) A critical review of smart residential environments for older adults with a focus on pleasurable experience. Front Psychol 10:1–15. https://doi.org/10.3389/fpsyg.2019.03080

Li J, Ma Q, Chan AHS, Man SS (2019) Health monitoring through wearable technologies for older adults: smart wearables acceptance model. 75:162–169. https://doi.org/10.1016/j.apergo.2018.10.006

Liu P et al (2019) The effect of smart homes on older adults with chronic conditions: a systematic review and meta-analysis. Geriatr Nurs (Minneap) 40(5):522–530. https://doi.org/10.1016/j.gerinurse.2019.03.016

Liu L, Stroulia E, Nikolaidis I, Miguel-Cruz A, Rios Rincon A (2016) Smart homes and home health monitoring technologies for older adults: a systematic review. Int J Med Inform 91:44–59. https://doi.org/10.1016/j.ijmedinf.2016.04.007

Lousado P (2020) Monitoring and support for elderly people using LoRa communication technologies: IoT concepts and applications

Lv H, Yang G, Zhou H, Huang X, Yang H, Pang Z (2019) Teleoperation of collaborative robot for remote dementia care in home environments. IEEE J Transl Eng Heal Med 8:2020. https://doi.org/10.1109/JTEHM.2020.3002384

Lv Z, Xia F, Wu G, Yao L, Chen Z (2010) iCare: a mobile health monitoring system for the elderly. https://doi.org/10.1109/GreenCom-CPSCom.2010.84

Majumder S, Deen MJ (2019) Smartphone sensors for health monitoring and diagnosis. Sensors (Switzerland) 19(9):1–45. https://doi.org/10.3390/s19092164

Miyabayashi I, Washio M, Yanagimoto T, Fortin E, Yasumura S (2019) Population aging and health of older people in Japan: introduction of health issues and care system for the elderly, pp 1–16. https://doi.org/10.1007/978-981-13-1762-0_1

Mohammed KI et al (2019) Real-time remote-health monitoring systems: a review on patients prioritisation for multiple-chronic diseases, taxonomy analysis, concerns and solution procedure. J Med Syst 43(7). https://doi.org/10.1007/s10916-019-1362-x

Mohapatra S, Mohanty S, Mohanty S (2019) Chapter 7—Smart healthcare: an approach for ubiquitous healthcare management using IoT. Elsevier Inc.

Monteiro K, Santos GL, Santos W, Endo PT (2018) Developing an e-health system based on IoT, fog and cloud computing. In: 2018 IEEE/ACM international conference on utility and cloud computing companion (UCC Companion), pp 17–18. https://doi.org/10.1109/UCC-Companion.2018.00024

Özsungur F (2021) Gerontechnological factors affecting successful aging of elderly. Aging Male 23(5):520–532. https://doi.org/10.1080/13685538.2018.1539963

Panagopoulos C, Menychtas A, Tsanakas P, Maglogiannis I (2019) Increasing usability of homecare applications for older adults: a case study. Designs 3(2):1–18. https://doi.org/10.3390/designs3020023

Petere E et al (2016) In: 2016 20th international conference on system theory, control and computing (ICSTCC), joint conference of SINTES 20, SACCS 16, SIMSIS 20, 13–15 Oct 2016, Sinaia, Romania, pp 543–548

Pham M, Mengistu Y, Do HM, Sheng W, Member S (2016) Cloud-based smart home environment (CoSHE) for home healthcare

Reviews C (2020) Remote health monitoring of long-term seizure under stress. J Crit Rev 7(12):2374–2377. https://doi.org/10.31838/jcr.07.12.378

Saha R, Biswas S, Sarmah S, Karmakar S, Das P (2021) A working prototype using DS18B20 temperature sensor and Arduino for health monitoring. SN Comput Sci 2(1):1–21. https://doi.org/10.1007/s42979-020-00434-2

Sapci AH, Sapci HA (2019) Innovative assisted living tools, remote monitoring technologies, artificial intelligence-driven solutions, and robotic systems for aging societies: systematic review. 2:1–16. https://doi.org/10.2196/15429

Shahzad A, Lee YS, Lee M, Kim Y, Xiong N (2018) Real-time cloud-based health tracking and monitoring system in designed boundary for cardiology patients, vol 2018

Sodhro AH et al (2020) Towards wearable sensing enabled healthcare framework for elderly patients. In: IEEE international conference on communications, 2020-June. https://doi.org/10.1109/ICC40277.2020.9149286

Syed L, Jabeen S, Manimala S, Alsaeedi A (2019) Smart healthcare framework for ambient assisted living using IoMT and big data analytics techniques. Futur Gener Comput Syst 101:136–151. https://doi.org/10.1016/j.future.2019.06.004

Talal M et al (2019) Smart home-based IoT for real-time and secure remote health monitoring of triage and priority system using body sensors: multi-driven systematic review. J Med Syst 43(3). https://doi.org/10.1007/s10916-019-1158-z

Tanabe S et al (2018) Designing a robotic smart home for everyone, especially the elderly and people with disabilities, pp 1–5

Tasneem Usha R, Sazid Sejuti F, Islam S (2019) Smart monitoring service through self sufficient healthcare gadget for elderly. In: Proceedings—2019 IEEE international symposium on smart electronic systems (iSES), pp 276–279. https://doi.org/10.1109/iSES47678.2019.00068

Thakur N, Chia, Han YY (2019) Framework for an intelligent affect aware smart home environment for elderly people. Int J Recent Trends Hum Comput Interact 9:23

Thar MA, Carl B, Asim M, Kolivand H, Fahim M, Waraich A (2019) Remote health monitoring of elderly through wearable sensors, pp 24681–24706

Tun SYY, Madanian S, Mirza F (2021) Internet of things (IoT) applications for elderly care: a reflective review. Aging Clin Exp Res 33(4):855–867. https://doi.org/10.1007/s40520-020-01545-9

Wang J et al (2019) Mobile and connected health technology needs for older adults aging in place: cross-sectional survey study. JMIR Aging 2(1):1–9. https://doi.org/10.2196/13864

K. XL, D. Q. L. Xl, N. Dql, D. Hgx, V. Dql, and D. Hgx, IoT healthcare monitoring systems overview for elderly population

Yassine A (2021) Health monitoring systems for the elderly during COVID-19 pandemic: measurement requirements and challenges. IEEE Instrum Meas Mag 24(2):6–12. https://doi.org/10.1109/MIM.2021.9400963

Yu J, An N, Hassan T (2019) A pilot study on a smart home for elders based on continuous in-home unobtrusive monitoring technology, pp 1–14. https://doi.org/10.1177/1937586719826059

Zhou M, Zhao L, Kong N, Campy KS, Qu S, Wang S (2019) Factors influencing behavior intentions to telehealth by Chinese elderly: an extended TAM model. Int J Med Inform 126:118–127. https://doi.org/10.1016/j.ijmedinf.2019.04.001

Blockchain with Adjustable Proof-of-Work Consensus Mechanism for Mobile Devices

Kausthav Pratim Kalita, Eric Rani, Debojit Boro, and Dhruba Kumar Bhattacharyya

Abstract Nowadays, most of the major industries, such as healthcare, are losing millions of valuable data and information, and therefore, many of these major industries have implemented blockchain technology in order to save and secure their valuable data since blockchain's major feature is to store information in an immutable and permanent manner. Blockchain provides greater transparency, enhanced security, instant traceability, increased efficiency, and speed. Though when we talk about blockchain, it is mainly the mining of transactions that draws our attention and of course, mining thus consumes huge computational power. In this chapter, we have implemented a lightweight blockchain in smartphones. We have built a simple blockchain that can store the contents of any smartphone user and this lightweight blockchain can perform all the operations that a normal blockchain does, like the mining of transactions, updating the chain, and checking if there is any pending transaction. From our experimental study, we have observed that implementing blockchain in smartphones does consume a huge computational power, that is, the smartphone starts to heat up and the battery power decreases rapidly.

Keywords Blockchain · Proof-of-work · Mobile devices

K. P. Kalita (✉) · E. Rani
Assam Don Bosco University, Airport Road, Azara, Guwahati, Assam, India
e-mail: kausthav.kalita@dbuniversity.ac.in

E. Rani
e-mail: ericrani07@gmail.com

K. P. Kalita · D. Boro · D. K. Bhattacharyya
Tezpur University, Napaam, Tezpur, Assam, India
e-mail: deb0001@tezu.ernet.in

D. K. Bhattacharyya
e-mail: dkb@tezu.ernet.in

J. K. Deka et al. (eds.), *Emerging Technology for Sustainable Development*,
Lecture Notes in Electrical Engineering 1061,
https://doi.org/10.1007/978-981-99-4362-3_48

1 Introduction

Blockchain was first introduced into this world by a person named *Satoshi Nakamoto* who published a white paper on bitcoin in 2008. The paper discusses a peer-to-peer electronic cash system that regulated using the blockchain technology. Blockchain is defined as a decentralized system, that is, it does not requires any third party organization to process a transaction. It is a distributed ledger that records information in such a way that makes it difficult for hacker or intruder to get hold of the information that is stored in the ledger, put simply it is also impossible to alter or changed the information that is stored in the ledger. Information stored in blockchain is immutable and the data cannot be changed once the transaction has occurred (Zheng et al. 2017). Blockchain technology has been applied in many fields like Internet of Things (IoT), cryptocurrency, healthcare, and supply chain but in recent trends it has been seen that blockchain for smartphones had drawn a lot of attention and the main attraction is the possibility of mining bitcoin from a smartphone device. Of course there is a lot of negative impacts on the smartphones such as overheating, battery damage and decreasing device performance (Bardinova et al. 2020). Mining of bitcoin requires huge computational power and thus can be performed by super computers. Mining is one of the key concepts, behind the Bitcoin protocol, in which valid transactions are collected into blocks and are added to the ledger by linking it to the previously accepted blocks. The network thus formed is the blockchain, where transactions are ingested using consensus algorithms, preventing users from reusing the utilized bitcoins for a different transaction (O'Dwyer and Malone 2014). The term lightweight implies a transaction or blockchain operation that takes less computational power and cost to implement the basic unit of blockchain referred as blocks. Several transaction are organized into blocks and every block contains a header, a timestamp, hash of its immediate block and also hash of the previous block. This way it create a sequential linkage between data blocks on the blockchain, which confirms irreversibility and ensure that data is tamper proof (Uddin et al. 2019).

This chapter will show the implementation of a lightweight blockchain in smartphones and also the graphical representation for every transaction that is created against its nonce value. The rest of the paper is organized as follows. Section 2 discusses blockchain uses in smartphones. Section 3 presents the implementation and result. Section 4 concludes the paper.

2 Literature Review

Bitcoin (Nakamoto 2008) paved the way for the researchers to apply proof-of-work consensus algorithm in various applications. Initial works around the concept was done in preventing junk mails from getting sent by malicious spammers. In paper (Dwork and Naor 1992), the authors propose the idea of presenting a complex computational problem to the sender who has to undergo the processing time to solve the problem. Receivers accept a mail only after the computation is completed by the sender. Similar computation-driven puzzles are applied in wide range of domains (Franklin and Malkhi 1997; Juels 1999; Serjantov and Lewis 2003). In Back (1997), the author introduces the method where the sender has to accomplish the challenge of finding an input which produces a cryptographic hash preceding with fixed length of zeros. The method allows quick verification of a time consuming solution. In recent years, many strategies are implemented to improve the proof-of-work consensus algorithm for better efficiency and reduced centralization caused by mining pools. Once such example is the EthHash model (Sharma et al. 2020) implemented in the Ethereum network. However, this model is still dependent on large scaled mining resources to bring consensus among the peers for chain generation. Researchers have come up with many different variants of proof-of-work with the intention of improving the algorithm for better results (Tromp 2014; King 2013; Miller et al. 2015; Eyal et al. 2016; Sompolinsky and Zohar 2013, 2015; Tang et al. 2017). In the field of fog and cloud computing, blockchains can be applicable only if their embedded consensus algorithms are executable with limited resources. The same objective is desirable in case of IoT. In Kumar et al. (2019), the authors propose an approach where proof-of-work is improvised to be applicable in fog and cloud computing. In Jiao et al. (2019), an auction-based model is proposed where miners belonging to a mobile blockchain network can offload the computational task of proof-of-work to fog or cloud computing services.

3 Proposed Methodology

Blockchain runs in a network with the help of a consensus mechanism that determines the entry of a new block of information into the chain. In any cryptocurrency-based blockchain network, the objective is to let the peers undergo a competition to create a new block. This leads to the application of consensus algorithms that are time-consuming and challenging. Such rigorous competition is not usually required when blocks have to be maintained by peers within an organization or whose objective is just to maintain a ledger between or among a small group of peers. So, if a blockchain needs to be maintained at the individual level and not at the machine level, portable devices like smartphones can be utilized for such installation. Here, individual-level indicates that the user of the network can maintain his/her node through a personal gadget like a smartphone instead of depending on expensive machines.

We propose a consensus mechanism that takes the proof-of-work consensus algorithm and makes it less time and resource-consuming. The idea is to maintain a blockchain that allows the creation of blocks by two participating parties in turn. Broadly speaking, it can be said that the blocks are created in a round-robin fashion. This allows active participation of both the peers and, thus, becomes very secure against tampering. The peers in the network can validate the blockchain before it commits new sets of transactions. The primary validation involves verifying that the

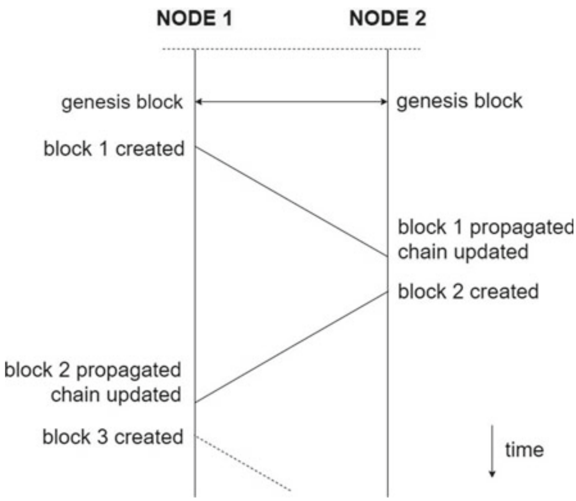

Fig. 1 Message passing sequence in the proposed model

previous block is created by the other peer. Such a technique is applicable in various use cases where data needs to be shared between parties that do not trust each other.

In Fig. 1, the sequence of message passing is demonstrated. At first, the genesis block is shared between the two peers. It holds the basic information to uniquely define the blockchain and can include the configurations and metadata that is followed throughout the lifetime of the chain. In configuration settings, one of the most essential information is the allotment of block miners. Since there are two participants, they are configured using odd and even numbers of the block. In the figure, $NODE_1$ is assigned as an odd node. Thus, it is responsible for creating all the odd-numbered blocks in the chain. Hence, $NODE_2$ is responsible for generating all the even blocks. Apart from the configurations, the genesis block also holds the metadata which indicates the structure of transactions that is allowed while creating a block.

In the proposed model, the core idea of proof-of-work remains the same which is to find the target nonce. But, since the blockchain is aimed at installing in mobile devices, the difficulty level is kept minimal with a threshold value. The idea behind proof-of-work is to let the network search for the target value which results in the consumption of time and resources. Due to this high resource-hungry mechanism, it becomes very difficult and challenging to become a successful miner. In our scenario, the peers know their turns and, thus, become involved only when their turns arrive. Yet, the proof-of-work is necessary in our case as it prevents any of the peers from making a fraudulent chain. The pseudo-codes for odd block miners and even block miners are shown in Pseudo-code 1 and Pseudo-code 2 respectively.

Pseudo-code 1 Logic for Odd Block Miner

```
nonce ← 0
data ← blockData
if count is odd then
    while hash(dataWithNonce) ≠ target_hash do
        nonce ← nonce + 1
        dataWithNonce ← concatenate(data, nonce)
    end while
end if
count ← count + 1
```

Pseudo-code 2 Logic for Even Block Miner

```
nonce ← 0
data ← blockData
if count is even then
    while hash(dataWithNonce) ≠ target_hash do
        nonce ← nonce + 1
        dataWithNonce ← concatenate(data,nonce)
    end while
end if
count ← count + 1
```

3.1 Maintaining the Average Block Creation Time

It is necessary to maintain the average time in creation new blocks in the blockchain. It helps in maintaining the uniform increase of length of the blockchain and also provides an indication about the time the network takes in updating a new block in the chain. Let this average time be ∂. When a new block is created, the mining time is stored in an array of previous values of mining duration and the updated average time is calculated. If this updated average time is lower than ∂ then the difficulty level (τ) is increased whereas if that time is higher than ∂ then τ is decreased. This is how the difficulty is adjusted in the algorithm. The overall logic is represented in the pseudo-code mentioned in Pseudo-code 3.

Pseudo-code 3 Applying τ and ∂

```
nonce ← 0
difficulty_bits ← 0
if difficulty_bits > τ then
    difficulty_bits = difficulty_bits − 1
end if
ComputePoW ()
UpdatedAverageTime = ComputeAverageTime()
if UpdatedAverageTime > ∂ then
    difficulty_bits = difficulty bits – 1
end if
if UpdatedAverageTime < ∂ then
    difficulty_bits = difficulty_bits + 1
end if
```

4 Experiments and Results

An experimental setup was constructed to implement the proposed model. Since the aim was to attain a consensus algorithm that can be applied to mobile devices, a setup consisting of two smartphones was built. These two smartphones were phones with very basic features having common random access memory and storage sizes. A block diagram is shown in Fig. 2 to provide knowledge on the components and their respective configurations.

As shown in the figure, two smartphones were chosen with basic specifications of 4 GB random access memory and 64 GB of storage. These configurations are very minimal in comparison to the expensive resources required in cryptocurrency mining. Thus, we could not expect these portable machines to do high-end computations. But, due to the controlled manner in which difficulty was maintained, the resources we considered were sufficient.

The blockchain application was coded in Python3 using the python module called Flask. The Flask framework enables us to create web servers that can be accessed using exposed endpoints. Every module created in the development had an endpoint that could be accessed using HTTP methods like GET and POST. The application was developed in a Windows OS-based computer and once it was ready it was shifted to the available smartphones.

4.1 Obtaining Threshold Difficulty

The first step in the experiment was in deciding on the difficulty level up to which the mining should be considered. To find this value, two separate blockchains of length $= 32$ were created through the mining process in the two devices. Let the

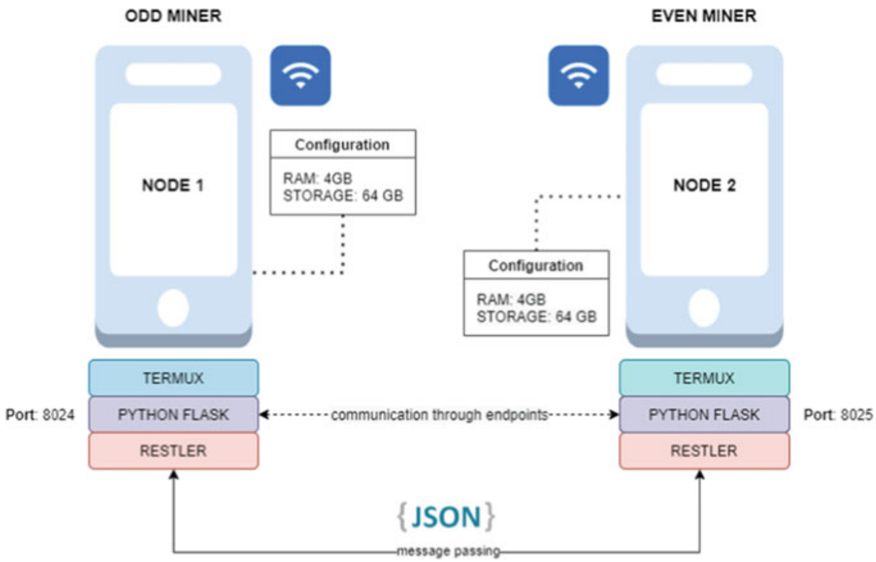

Fig. 2 Experimental setup

two mining phases be called $MINE\ SET_1$ and $MINE\ SET_2$. In a single $MINE\ SET$, the difficulty was sequentially incremented by 1 in the proceeding blocks. That is, if the first block's difficulty was set to 0, the next block's difficulty was set to 1. This procedure helped in determining the difficulty level after which the devices were taking a much longer duration in discovering the target hash values compared to the previous level. In Fig. 3, it was observed that the hash rates in $MINE\ SET_1$ and $MINE\ SET_2$ continued to have higher values from round 27 onward. This indicated that the devices were finding it harder to obtain the nonce for the target hashes with the difficulty level set to 26 or more.

Figure 4a gave a clear indication that during all the higher block mining duration, the hashrates were always high. This implies that the devices become constantly resource hungry when the block mining time increases. From Fig. 4b it can be observed that the block mining time increases when the difficulty levels are set high. This concludes that the higher plots seen in Fig. 4a belong to the last few mining rounds in $MINE\ SET_1$. Similar results were observed in $MINE\ SET_2$ as well. Another observation made in this experiment is that a sudden escalation of mining time is observed in round 28 in the Fig. 4b. To identify a good value of τ, a decisive approach needs to be adopted in determining the value where difficulty level must be stopped.

To decide on the peak difficulty value, the product of hash rate and time is chosen as it indicates the total hashes obtained in a particular mining process. Total hash is contributed by the hash rate as well as the duration of that hash rate. Thus, this value gives a clear picture on when to stop raising the difficulty level in the mining activity. For $MINE\ SET_1$, the Fig. 5 shows that a constant growth of hash counts starts from round 30. From these graphs too, it is convincing to state that difficulty

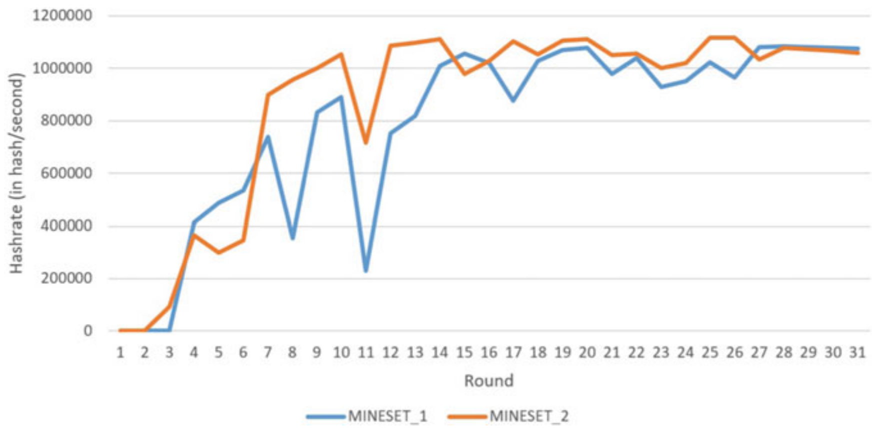

Fig. 3 Hashrate comparison graph

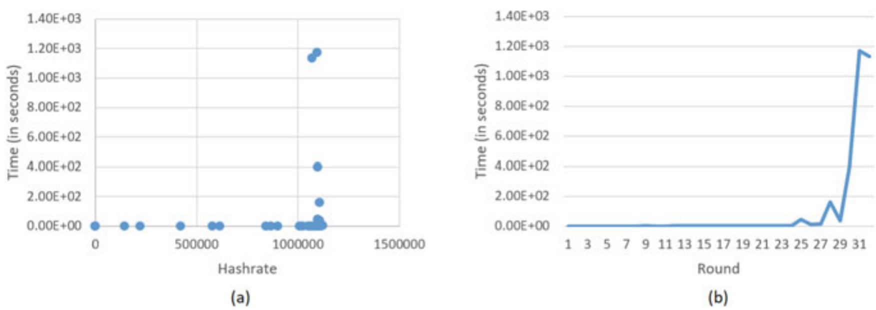

Fig. 4 **a** Hashrate w.r.t Time. **b** Block Mining Time in each round

= 29 (the difficulty level of round 30) can be chosen as an optimal threshold level for the blockchain network.

4.2 Results Obtained

The threshold difficulty value obtained through the method shown in the previous section was applied to the blockchain code and then the network was started. $NODE_1$ and $NODE_2$ shared the genesis blocks and began to run the mining process in their respective turns. $NODE_1$ mined the odd blocks and $NODE_2$ mined the even blocks. The expected average time was set to 30 s. Values like nonce, hash rates, block mining duration, and average block creation times were recorded for 50 blocks. Figure 6a shows the resultant graph of time and average time. Another similar test was conducted with expected average time of 1 min. The figure is shown in Fig. 6b.

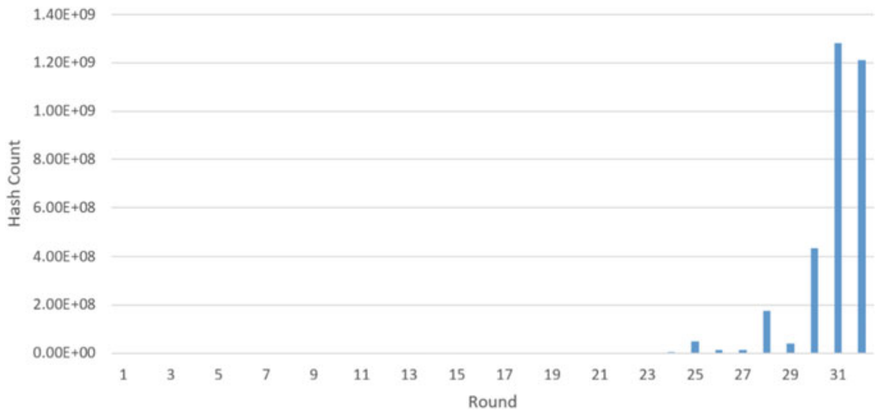

Fig. 5 Hash count in each round

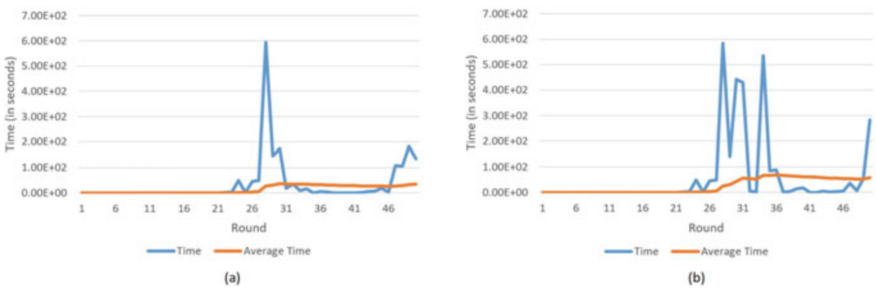

Fig. 6 **a** Time versus average time per round (expected average time = 30 s). **b** Time versus average time per round (expected average time = 60 s)

From both the results it is observed that the average time is controlled properly within the algorithm and the mining time remains restricted to a value that was desirable after analyzing the graph of Fig. 3. Lastly, the hash rates in every round in both the tests is shown in Figs. 7a, b which indicates the devices went through the mining process with manageable computational resource.

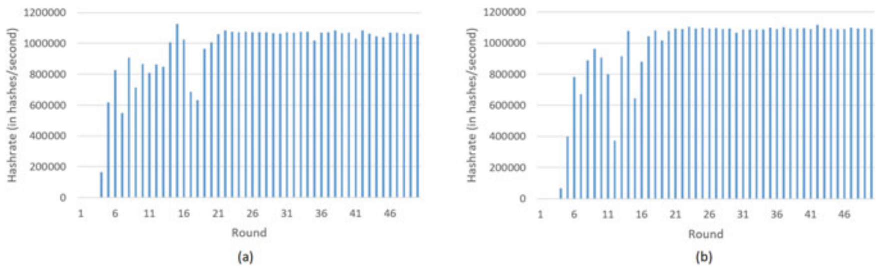

Fig. 7 **a** Hashrate in each round (expected average time = 30 s). **b** Hashrate in each round (expected average time = 60 s)

5 Conclusion

Consensus algorithm is the backbone of any blockchain application. There are various types of consensus mechanisms applied in blockchains and proof-or-work is one of the oldest and most popular consensus mechanism of all. Yet, its dependability in high computational power demotivates it from being used in portable devices. In this paper, we attempt to make proof-of-work applicable in mobile devices by keeping the mining difficulty manageable enough for less resourceful devices to perform the mining process with efficiency and speed.

References

Back A (1997) Hashcash. http://www.cypherspace.org/adam/hashcash/

Bardinova Y, Zhidanov K, Bezzateev S, Komarov M, Ometoy A (2020) Measurements of mobile blockchain execution impact on smartphone battery. Data 5(3):66

Dwork C, Naor M (1992) Pricing via processing or combatting junk mail. In: Annual international cryptology conference, Springer, pp 139–147

Eyal I, Gencer AE, Sirer EG, Van Renesse R (2016) Bitcoin-ng: a scalable blockchain protocol. In: 13th USENIX symposium on networked systems design and implementation (NSDI 16), pp 45–59

Franklin MK, Malkhi D (1997) Auditable metering with lightweight security. In: International conference on financial cryptography. Springer, pp 151–160

Jiao Y, Wang P, Niyato D, Suankaewmanee K (2019) Auction mechanisms in cloud/fog computing resource allocation for public blockchain networks. IEEE Trans Parallel Distrib Syst 30(9):1975–1989

Juels A (1999) Client puzzles: a cryptographic countermeasure against connection depletion attacks. In: Proceedings on networks and distributed system security symposium (NDSS)

King S (2013) Primecoin: Cryptocurrency with prime number proof-of-work. July 7th, 1(6). Available at https://c3.coinlore.com/pdf/primecoin-white-paper.pdf

Kumar G, Saha R, Rai MK, Thomas R, Kim TH (2019) Proof-of-work consensus approach in blockchain technology for cloud and fog computing using maximization-factorization statistics. IEEE Internet Things J 6(4):6835–6842

Miller A, Kosba A, Katz J, Shi E (2015) Nonoutsourceable scratch-off puzzles to discourage bitcoin mining coalitions. In: Proceedings of the 22nd ACM SIGSAC Conference on Computer and Communications Security 2015, pp 680–691

Nakamoto S (2008) Bitcoin: A Peer-to-Peer Electronic Cash System. Available at SSRN: https://ssrn.com/abstract=3440802 or https://doi.org/10.2139/ssrn.3440802

O'Dwyer KJ, Malone D (2014) Bitcoin mining and its energy footprint. In: Hamilton Institute National University of Ireland Maynooth, ISSC 2014/CIICT 2014, Limerick, June 26–27

Serjantov A, Lewis S (2003) Puzzles in p2p systems. In: 8th CaberNet Radicals Workshop, Corsica

Sharma DK, Pant S, Sharma M, Brahmachari S (2020) Cryptocurrency mechanisms for blockchains: models, characteristics, challenges, and applications. In: Handbook of research on blockchain technology. Academic Press, 323–348

Sompolinsky Y, Zohar A (2013) Accelerating bitcoin's transaction processing. Fast Money Grows on Trees, Not Chains. IACR Cryptology EPrint Archive, vol. 881. Available at https://eprint.iacr.org/2013/881

Sompolinsky Y, Zohar A (2015) Secure high-rate transaction processing in bitcoin. In: International conference on financial cryptography and data security. Springer, pp 507–527

Tang S, Liu Z, Chow SS, Liu Z, Long Y, Liu S (2017) Forking-free hybrid consensus with generalized proof-of-activity. IACR Cryptol 2017:367

Tromp J (2014) Cuckoo Cycle: a memory-hard proof-of-work system. IACR Cryptol Arch 2014:59

Uddin MA, Stranieri A, Gondal I, Balasurbramanian V (2019) A lightweight blockchain based framework for underwater IoT. Electronics 8(12):1552

Zheng Z, Xie S, Dai H, Chen X, Wang H (2017) An overview of blockchain technology: architecture, consensus, and future trends. In: 2017 IEEE 6th International Congress on Big Data

LoRa-Enabled IoT Framework for Flash Flood Crisis Management

Rupesh Mandal, Bobby Sharma, and Dibyajyoti Chutia

Abstract This chapter proposes a framework which is based on Internet of Things (IoT) and Long Range (LoRa) communication framework which helps to collect relevant data from inundated areas and make the data available for use by the disaster management authority and for the general population. This chapter also presents a detailed review of IoT- and LoRa-based contributions in the domain of detection and analysis of flash flood. The proposed framework has the potential of reducing the dependency over internet to transmit data over long ranges during disaster by using LoRa and its associated protocols. The entire framework is integrated with a number of sensors in three distinct layers which would be used to collect data which are relevant for the occurrence of flashflood. Overall, this system would be highly advantageous for the protection, prevention and rescue of lives and property during flash floods.

Keywords Flash flood · Internet of Things · LoRa

1 Introduction

Floods, Tsunamis, earthquakes, storms and other such Natural hazards pose a severe threat which affects not only the lives but also resources and property all over the world (Dilley et al. 2005). If not carefully monitored and effective measures for mitigation are considered in such situations these events would give rise to natural

R. Mandal (✉) · B. Sharma
Assam Don Bosco University, Guwahati, India
e-mail: rupesh.mandal@dbuniversity.ac.in

B. Sharma
e-mail: bobby.sharma@dbuniversity.ac.in

D. Chutia
North Eastern Space Application Centre, Shillong, India
e-mail: d.chutia@nesac.gov.in

J. K. Deka et al. (eds.), *Emerging Technology for Sustainable Development*,
Lecture Notes in Electrical Engineering 1061,
https://doi.org/10.1007/978-981-99-4362-3_49

disasters which might pose a severe challenge in terms of economic growth, destruction of urban environment as well as social disruptions (CRED 2019; Kuenzer et al. 2013). Records have reported that flood is considered as one of the most frequently occurring natural hazard which accounts for around 41% of all the natural disasters that has been occurring all over the world since the past decade (Mosquera-Machado and Dilley 2009). One common form of flood which has been creating a havoc in the urban environment is the flash flood. In India, most recently, these flash floods occur throughout the year which is primarily caused due to Excessive rainfall, increasing water levels and differences in pressure from the coastal areas which generates precipitation (Hansson et al. 2008).

In India urban areas of different states and cities refer to such a hub from where the economic situation of a city or state could be identified. This urban sprawl across the world has immense contribution to several changes worldwide in the ecological processes of the environment which primarily includes biodiversity, greenhouse gas emissions, quality of the water, etc. which causes much more vulnerability. Several problems related to housing, management of waste, management of sewage, etc. are created due to the rapid growth in the population of the urban areas. One important aspect would be to reclaim the land which lies beside water bodies such as Guwahati, Assam, India which is situated near the mighty river Brahmaputra. One very prominent city of Kolkata which is the Salt Lake City also faces similar situations (Tingsanchali 2012). However, this reclamation of land has created a problem of seasonal floods in the urban areas which is responsible for interrupting and slowing down the development of the city and the various related processes for up to days. Mumbai in India however has developed various warning as well as the evacuation systems which are primarily dependent on network for communication, which is not present in advanced cities like Delhi, Bangalore, Kolkata, etc. (Rafiq et al. 2016). IoT-related frameworks for the management of flood seen to have minimum contribution toward its purpose as the drawbacks in terms of expense, communication, integration of the system and decision making arises along with the lack of capability to use this technology in all possible flood situations. IoT has been utilized in several areas which includes healthcare, defense, communication as well as disaster management in various countries. The data which has been collected from various IoT devices such as the mobile phones, different types of sensors, data from the satellite etc. along with AI could be utilized in cases of prediction which would lead to the prevention of the loss of lives.

For India to be a smart country, it is essential that the framework which are dependent on relief and recovery should be shifted to the framework which includes integrated management system for flood that will collectively include the various stakeholders from the disaster Management Authority along with the people by considering the latest technology. These integrated systems could be technically supported via various domains such as data analytics, IoT, cloud computing, machine learning, embedded systems as well as communication networks which would effectively contribute to the detection, prediction and prevention of losses during flood related situations which would eventually be utilized for the purpose of saving lives and properties during such a disaster. IoT would aid in the development of a smart environment and indirectly convert the whole country into a smart nation. A compact and effective network for the management of flood could be formed if a greater number of IoT components could be added and connected with the network generating huge opportunity to develop an integrated system for the same purpose. All of these could be possibly realized due to the ubiquitous communication capabilities, latest sensor-based technology as well as the real time data analysis of the data collected from such type of sensor-based devices. Some of the conventional processes of data analysis which have given rise to the management of flood in the urban areas are as follows.

1.1 Statistical Analysis of Data

Here past flood or the data related to the disaster is used to predict the significant issues related to flood occurrence and also analyze the effects. Based on the various data which is being generated, different types of statistical models were being analyzed. However, this approach is not sufficient under all circumstances as there are exponential changes when it is related to the form of flood as well as the frequency that depends upon monsoon or rainfall for different times of the year and greenhouse gas emissions etc. (Brennan et al. 2016).

1.2 Impact of Social Media

During the disaster, social media such as Google, Tweeter, Facebook etc. has reduced the time and delay of communication to a great extent and has made it easier for the information dissemination in a faster rate. A significant contribution has been made by the social media (Srikanth 2012) where the details and the information related to the pre and the post disaster or the flood is disseminated along with the location. However, the primary drawbacks of these approach could be lack of connectivity during disaster and fake or partial information which are posted for the sake of false publicity (Velev and Zlateva 2012).

1.3 Geographic Information System (GIS)

GIS is used for information collection, storage and finally display the data which is related to the surface of the earth from the geo satellites that are revolving around the planet earth. This data is used to identify the flood affected zones and the various significant damages. This data requires high performance computing in order to analyze the data by professionals in order to predict the nature of damage apart from loss of lives by the disaster and has a challenge in storage (Kourgialas and Karatzas 2011; Qi 2011).

2 Related Work

Throughout the world there are significant efforts which are made globally in order to develop robust and cost-effective solution which involves monitoring of flood. Researchers are working on some of the common approaches which involves computer vision and its impact in floods (Ko and Kwak 2012). These applications which are based on the cameras that are used for surveillance comprises of minimum cost and has a wider aerial zone for coverage which would enable the identification of flood at different points which has more advantage than fixed type of sensors (Kanwal et al. 2017). Wireless sensors integrated with the Internet of Things (IoT) technology is another method of monitoring and the prediction of flood. Computational models along with IoT which includes Artificial Neural Network (ANN's) (Bande and Shete 2017) have introduced newer directions which allows the designing of software and hardware which could be potentially used for extracting real-time data in terms of water level which would be needed for the monitoring as well as forecasting of flood (Barthélemy et al. 2019). IoT has been greatly on demand as well as has gained enormous popularity in the last 10 years particularly in the domain of applications in Smart city which involves the monitoring of the drainage networks in the urban areas by making use of wireless sensors (Keung et al. 2018).

Water level can be measured and identified by making use of different types of sensors such as the improvements of the early warning systems (Krzhizhanovskaya et al. 2011). In a similar attempt, Baczyk et al. (2016) represented the advantages and the disadvantages of using sensors for monitoring and measuring the level of water. One such sensor is known as the pressure transducer. These transducers could measure up to 0.001 m accuracy in the level of water which are compatible with most of the controllers for the logging of data or its visualization in the real time. On the other side these pressure transducers require the arrangement and the calibration which might get disturbed due to any displacement in the vertical direction in respect to the point of installation which would eventually lead to the degradation of the level of accuracy of the entire experiment which might have resulted from the changes in the hydrostatic pressure (Krzhizhanovskaya et al. 2011). Moreover, in addition to this some more sensors might be necessary for monitoring of the air pressure for the adjustment of the output of the pressure transducers. Additionally, one another option may be Rangefinder sensors which cannot be submerged inside water. These sensors have minimum cost which make the entire process affordable for those scenarios in which multiple sensors needs to be deployed for monitoring a large area. However, these sensors need manual calibration that depends on the distance at which it is places from the water level that it needs to measure (Rachman et al. 2008). Principally, these rangefinders or the ultrasonic sensors transmits or throws a signal and then the time in between the send and the receive signals are calculated when it comes to monitoring of the water levels (Hagedorn 1992). In a similar manner the radar sensors and the optical sensors is utilized for the monitoring of flood and the satellite is used for assessment (Hagedorn 1992). The comparison between optical and the radar sensors are done by Lin et al. (2016) where it was identified that the optical sensor data is available on a wide range. One such source which is popularly used for extraction of data is the Landsat. However, there is a major disadvantage with this system which is that these sensors are not capable of penetrating through the clouds, on the other hand the radars which makes use of microwaves has the capacity of penetrating through the clouds. Even after that the optical sensors are a popular choice for the domain of image acquisition which as they are cheaper as compared to radar. However, in the study it was identified that accurate results of the assessment of the flood can be achieved by combining both the radar and the optical sources. In a similar attempt Khan et al. (2018) worked on a novel technique in order to forecast the occurrence of flash floods which was done by the observation in the increment of the moisture level of soil as well as the carbon dioxide sensors. It has been concluded that if there is an increased reading of both the sensors then there is possibility of flash flood occurrence. This experiment was carried out on the seashore and it was analyzed that the level of carbon dioxide goes up during the upwards thrust of the waves. In order to validate the scenario a moisture sensor was used for measuring the content of moisture in the sand and the readings of the sensors indicates that they could be utilized for prediction of the flash flood. In addition to it, the number of fake alarms which might be present was reduced by the application of the multilayer perceptron (MLP) algorithm. Noar and Kamal (2017) in their work explained the usage of the Blynk platform which could be utilized for the connection of the ultrasonic sensors long with internet for the generation of information on a real time basis that could be witnessed in a mobile phone. This approach makes use of NodeMCU for connecting the sensors with the internet and extract the real-time information about the status of water level. In addition to this Purkovic et al. (2019) worked with the design and development of a ultrasonic sensor involving minimum cost which was used with other sensors from EnOcean. The data transmission was done in every 5 min and the highest range that the sensor could sense was 10 m having a resolution of 10 mm. However, the results were not discussed in this paper. In another work Kafli and Isa (2017) worked in an IoT framework which included several sensors like the humidity, rangefinders, GPS sensor and carbon monoxide in order to monitor the water level which was used to measure real-time water level and generate early warnings to the local community. In another work Chandanala et al. (2013) proposed an approach for making the wireless system in a more energy efficient manner by optimization of the network coding parameters and the duty cycling. Prediction of flood was done by the execution of active monitoring by making use of ultrasonic sensors or sonars for measuring the level of water as well as a sensor which was used for the measurement of precipitation i.e., the intensity at which the rainfall has occurred. It is considered to be a cost effective and an efficient mechanism for monitoring of the sites with multiple sensors which are prone to flood in the realtime (Lin et al. 2006). Thekkil and Prabakaran (2017) in their work along with Balaji et al. (2017) who worked in a similar domain made use of ZigBee as well as GSM for transmitting the data i.e. the images which were obtained from the cameras for generating the warnings related to flood. These experiments were also supported using Scale Invariant Feature Transform (SIFT) algorithm for the facilitating monitoring of flood in an automated manner. Similarly, Pratama et al. (2017) made use of Mamdani fuzzy logic along with the ZigBee as well as water level sensors for the identification and transmission of flood related data. These experiments suggests that the maximum level of error of the approach worked upon ranges up to 5%. In another attempt Al-Assadi et al. (2009) worked with a microchip based solution which made use of an array of piezolelectric sensors which is utilized for measuring the pressure that is being exerted by the water as well as ZigBee for the data transmission as well as reception. The sensors were then embedded and a protype was created on the Altera's Cyclone Board where it was suggested that the sensors were placed in an extremely calculated manner for the accurate prediction of flood. Ogie et al. (2017) in their work proposed a solution which suggested the best location for placing the sensors for the measurement of water level and it was seen that the sensors were placed in optimal positions and considerable emphasis was given to the relevant study as it an important context to have awareness of the level of water in a larger area of affect.

3 Proposed System

This paper focusses on the development of a framework for the identification of flash flood in the urban areas and using that data to create an analytical model for the same.

The entire framework, workflow and the design of base stations and the water level sensing nodes is depicted in the Figs. 1, 2 and 3, respectively. This framework primarily comprises of three different layers as follows.

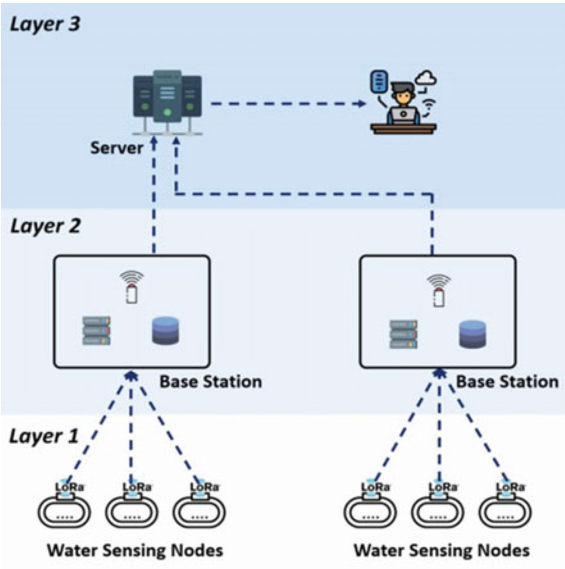

Fig. 1 Architecture of the proposed system

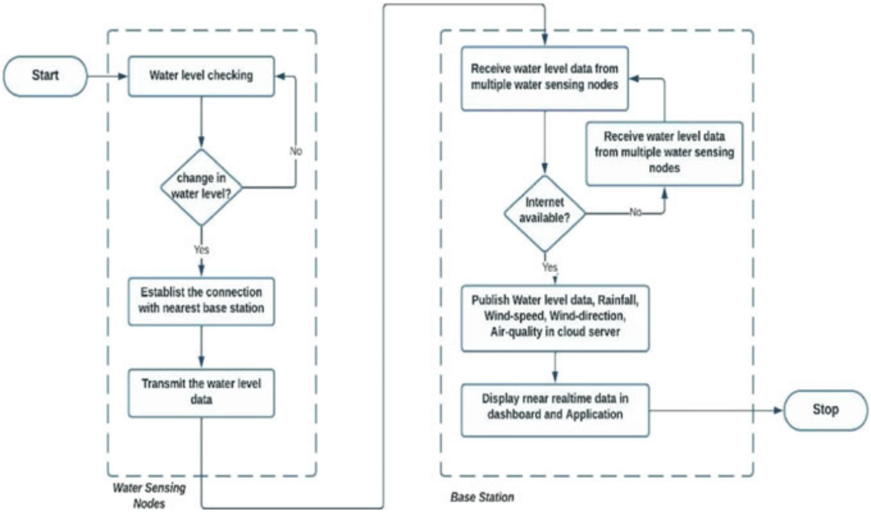

Fig. 2 Workflow of the proposed system

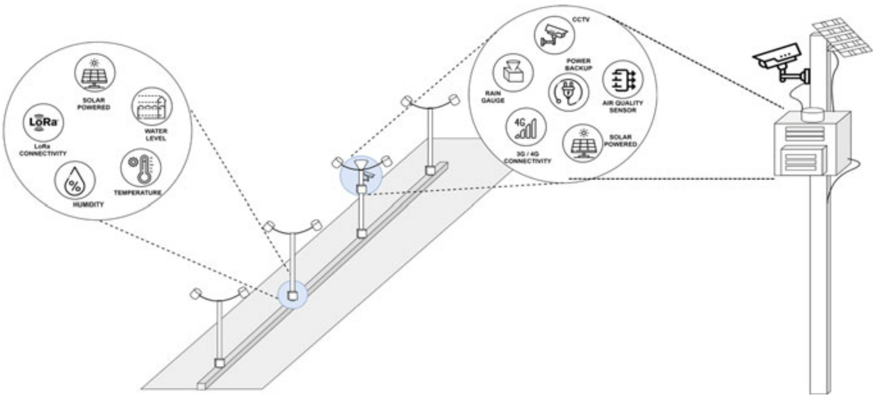

Fig. 3 Design of water sensing nodes (left) and base station (right)

A. **Layer 1:** This layer comprises of the water sensing nodes which are mounted 2.5 m above ground level; would be able to measure the height of the water level during a water-locked situation. These nodes would be powered by solar panel supported batteries. These water sensing nodes would also have an Arduino based microcontroller which is integrated with a LoRa communication module which acts a sender if the water level data to the Base station in the second layer. These nodes have the capacity of data communication without internet connectivity to the base station which might be situated at a radius of 3 km.
B. **Layer 2**: This layer comprises of a Raspberry Pi board which is responsible for data collection from multiple water sensing nodes and pushes them to the server

situated in Layer 3. The microprocessor is also integrated with two different microcontrollers which is responsible of taking the data from layer 1 as input using the LoRa module and also generates different sensor-based readings for parameters such as temperature, humidity, rainfall in cm, wind direction and wind speed, air quality sensors as well as a camera. The components of the base station are also responsible for storing the data until the internet connectivity resumes during disasters and then can push the data once the con nectivity resumes.

C. **Layer 3:** This layer comprises of the clouds server where data is pushed from the layer 2 and is displayed over an android application for the users. The respective authority for the same could view the data in a dashboard which could be further utilized for future analysis.

The workflow of the system is represented in Fig. 2. As the proposed system comprised of two categories of devices i.e., water sensing nodes and base station, the workflow starts from the water sensing nodes, which acts as a transmitter and it at first checks for change in the water level. If there is no change in the water level the nodes sit ideal and in case, there is a change then only the node establishes and send the data packet to the base station. The base station on the other hand receives multiple packets from different water sensing nodes at different time intervals. The base station is integrated with other sensor which records data for Rainfall (in centimeter), Wind Speed, Wind Direction, Air Quality Index (PM1.0, PM2.5 and PM10), Temperature, Humidity and Atmospheric pressure. It then checks for the availability of internet connectivity, if available then the all the data (nodes and base station data) will be posted to the server. If internet link is down, then the data will be logged to a local CSV file which will be pushed later to the server once internet link is available. With this approach the precious data during disaster can be saved and can be utilized for further analysis.

4 Conclusion

The proposed system would be helpful in making the data and identifying the flash flood affected areas in a city and also has the potential to guide the residents to choose an effective alternative for their travel or evacuation. The entire system is developed using LoRa which has been successful in removing significant dependency over internet for data transmission. The data which would be obtained from this system could be utilized for developing a prediction model generating an effective lead time which could help the disaster management authority of the state to take necessary steps for the evacuation of lives and traffic management in a smooth manner. Further different machine learning algorithms could be applied over the generated data to perform an analysis on the data which is obtained from the IoT framework and derive a suitable model which would not only make lives and management easier but would also prevent the loss of lives and property.

References

Al-Assadi WK, Gandla S, Sedigh S, Dugganapally IP (2009) Design of a flood prediction system. In: Proceedings of the 2009 12th International IEEE Conference on Intelligent Transportation Systems, St. Louis, MO, USA, 4–7 October 2009

Baczyk A, Piwinski J, Kłoda R, Grygoruk M (2016) Survey on river water level measuring technologies: Case study for flood management purposes of the C2-SENSE project. In: Proceedings of the International Conference on Systems, Control and Information Technologies, Warsaw, Poland, 20–21 May 2016

Balaji V, Akshaya A, Jayashree N, Karthika T (2017) Design of ZigBee based wireless sensor network for early flood monitoring and warning system. In: Proceedings of the 2017 IEEE Technological Innovations in ICT for Agriculture and Rural Development (TIAR), Chennai, India, 7–8 April 2017

Bande S, Shete VV (2017) Smart flood disaster prediction system using IoT and neural networks. In: Proceedings of the 2017 International Conference on Smart Technologies for Smart Nation (SmartTechCon), Bangalore, India, 17–19 August 2017

Barthélemy J, Verstaevel N, Forehead H, Perez P (2019) Edge-computing video analytics for real-time traffic monitoring in a smart city. Sensors 19:2048

Brennan M, O'Neill E, Brereton F, Dreoni I, Shahumyan H (2016) Exploring the spatial dimension of community-level flood risk perception: a cognitive mapping approach. Environ Hazards 15(4):279–310

Chandanala R, Zhang W, Stoleru R, Won M (2013) On combining network coding with duty-cycling in flood-based wireless sensor networks. Ad Hoc Netw 11:490–507

CRED (2019) EM-DAT: the OFDA/CRED international disaster database. Catholic University of Leuven, Brussels, Belgium

Dilley M, Chen RS, Deichmann U, Lerner-Lam AL, Arnold M (2005) Natural disaster hotspots: a global risk analysis. The World Bank, Washington

Hagedorn P, Wallaschek J (1992) Travelling wave ultrasonic motors, Part I: working principle and mathematical modelling of the stator. J Sound Vib 155:31–46

Hansson K, Danielson M, Ekenberg L (2008) A framework for evaluation of flood management strategies. J Environ Manage 86(3):465–480

Kafli N, Isa K (2017) Internet of Things (IoT) for measuring and monitoring sensors data of water surface platform. In: Proceedings of the 2017 IEEE 7th International Conference on Underwater System Technology: Theory and Applications (USYS), Kuala Lumpur, Malaysia, 18–20 December 2017

Kanwal K, Liaquat A, Mughal M, Abbasi AR, Aamir M (2017) Towards development of a low cost early fire detection system using wireless sensor network and machine vision. Wirel Pers Commun 95:475–489

Keung KL, Lee CK, Ng KK, Yeung CK (2018) Smart city application and analysis: Real-time urban drainage monitoring by IoT sensors: a case study of Hong Kong. In: Proceedings of the 2018 IEEE International Conference on Industrial Engineering and Engineering Management (IEEM), Bangkok, Thailand, 16–19 December 2018

Khan TA, Alam M, Kadir K, Shahid Z, Mazliham SM (2018) A novel approach for the investigation of flash floods using soil flux and CO_2: an implementation of MLP with less false alarm rate. In: Proceedings of the 2018 2nd International Conference on Smart Sensors and Application (ICSSA), Kuching, Malaysia, 24–26 July 2018

Ko B, Kwak S (2012) Survey of computer vision-based natural disaster warning systems. Opt Eng 51:70901

Kourgialas NN, Karatzas GP (2011) Flood management and a GIS modelling method to assess flood-hazard areas—a case study. Hydrol Sci J 56(2):212–225. https://doi.org/10.1080/02626667.2011.555836

Krzhizhanovskaya V, Shirshov G, Melnikova N, Belleman R, Rusadi F, Broekhuijsen B, Gouldby B, Lhomme J, Balis B, Bubak M et al (2011) Flood early warning system: design, implementation and computational modules. Proc Comput Sci 4:106–115

Kuenzer C, Guo H, Huth J, Leinenkugel P, Li X, Dech S (2013) Flood mapping and flood dynamics of the Mekong delta: ENVISAT-ASAR-WSM based time series analyses. Remote Sens 5:687–715

Lin YB, Lai JS, Chang KC, Li LS (2006) Flood scour monitoring system using fiber Bragg grating sensors. Smart Mater Struct 15:1950

Lin L, Di L, Yu EG, Kang L, Shrestha R, Rahman MS, Tang J, Deng M, Sun Z, Zhang C et al (2016) A review of remote sensing in flood assessment. In: Proceedings of the 2016 Fifth International Conference on Agro-Geoinformatics (Agro-Geoinformatics), Tianjin, China, 18–20 July 2016

Mosquera-Machado S, Dilley M (2009) A comparison of selected global disaster risk assessment results. Nat Hazards 48:439–456

Noar NAZM, Kamal MM (2017) The development of smart flood monitoring system using ultrasonic sensor with Blynk applications. In: Proceedings of the 2017 IEEE 4th International Conference on Smart Instrumentation, Measurement and Application (ICSIMA), Putrajaya, Malaysia, 28–30 November 2017

Ogie R, Shukla N, Sedlar F, Holderness T (2017) Optimal placement of water-level sensors to facilitate data-driven management of hydrological infrastructure assets in coastal mega-cities of developing nations. Sustain Cities Soc 35:385–395

Pratama A, Munadi R, Mayasari R (2017) Design and implementation of flood detector using wireless sensor network with Mamdani's fuzzy logic method. In: Proceedings of the 2017 2nd International conferences on Information Technology, Information Systems and Electrical Engineering (ICITISEE), Yogyakarta, Indonesia, 1–2 November 2017

Purkovic D, Coates L, Hönsch M, Lumbeck D, Schmidt F (2019) Smart river monitoring and early flood detection system in Japan developed with the EnOcean long range sensor technology. In: Proceedings of the 2019 2nd International Colloquium on Smart Grid Metrology (SMAGRIMET), Split, Croatia, 9–12 April 2019

Qi H, Altinakar MS (2011) GIS-based decision support system for integrated flood management under uncertainty with two dimensional numerical simulations. Environ Model Softw 26(6):817–821

Rachman S, Pratomo I, Mita N (2008) Design of low cost wireless sensor networks-based environmental monitoring system for developing country. In: Proceedings of the 2008 14th Asia Pacific Conference on Communications, Tokyo, Japan

Rafiq F, Ahmed S, Ahmad S, Khan AA (2016) Urban floods in India. Int J Sci Eng Res 7(1):721–734

Srikanth A (2012) Social media can solve many problems during natural disasters. http://infworm.com/social-mediacan-solve-many-problems-during-naturaldisasters/

Thekkil TM, Prabakaran N (2017) Real-time WSN based early flood detection and control monitoring system. In: Proceedings of the 2017 International Conference on Intelligent Computing, Instrumentation and Control Technologies (ICICICT), Kannur, India, 6–7 July 2017

Tingsanchali T (2012) Urban flood disaster management. Proc Eng 32:25–37

Velev D, Zlateva P (2012) Use of social media in natural disaster management. In: ICITE2012 (HongKong), vol 39, pp 41–45

Crowd Size Estimation: Smart Gathering Management

Ishita Swami and Nimish Sunil Das

Abstract Linear increase in population which results in overcrowding has become an unavoidable element in any public gathering. Public safety under such condition has become a very vital problem in areas like streets, malls and railway stations during weekends, festive seasons, holidays, concerts, etc., normally or in any pandemic situation. The massive disasters that can occur includes numerous instances of fatality where people gather in form of throng. In present time, surveillance cameras are deployed to maintain peace, security and manage crowd, as surveillance videos for proper analysis of crowd activities is an important issue for communal harmony and security; however, some major limitations in video surveillance system are that includes picture getting blurred, peculiarities among person cannot be identified automatically with respect to surroundings during live video streaming, along with that to save the information a lot of storage spaces is also required and hence it becomes costly to run and maintain. The present study proposes a method that is based on principle of Histogram of Oriented Gradients (HOG) and OpenCV that efficiently keeps in track count of the people in the scene which helps in efficient crowd management. OpenCV-based method used for crowd estimation written in Python used in this study in order to count the number of heads in live streaming and helps in crowd management according to requirement in an economical way.

Keywords Fatality · CCTV · Video surveillance · OpenCV · Motion detection · Streaming · Python · Algorithm

I. Swami (✉)
Department of Computer Engineering, LJ Institute of Engineering and Technology, Ahmedabad, India
e-mail: swami.ishita.10@gmail.com

N. S. Das
Department of Electronics and Communication Engineering, LJ Institute of Engineering and Technology, LJK University, Ahmedabad, India
e-mail: nimish.das@ljinstitutes.edu.in

J. K. Deka et al. (eds.), *Emerging Technology for Sustainable Development*, Lecture Notes in Electrical Engineering 1061,
https://doi.org/10.1007/978-981-99-4362-3_50

1 Introduction

In recent years, the human population has been growing at an alarming rate hence the rise in growth has indirectly given rise the frequent crowd gathering. The motive of assembly ha as major result in crowded behavior and wide-range assets. There is a scope of the tremendous amount of scientific research in public service, security, safety, and computer vision for the analysis of mobility and behavior of the crowd. The task of detecting a face within the crowd is difficult as of showing variance in human faces including pose, color, expression, position, orientation, and illumination. Due to such crisis, there is large crowd confusion, resulting in pushing, mass-panic, stampede, and results in control loss to prevent these tragedies, there is a requirement for automatic detection of such critical and unusual situations in the dense crowd. Which will help, to make emergency controls and appropriate decision making for maintaining security and safety. Hence this makes Crowd detection one of the most challenging as well as important tasks in visual surveillance systems. This system can be used for not only detection but also to count people, and crowd level, and also warns of the presence of a dense crowd.

To prevent these fatalities, automatic detection of critical and unusual situations in dense crowds is a must. As a result, definitely will help, to make emergency controls and appropriate decisions for security and safety. Crowd detection is one of the most challenging tasks in visual surveillance systems (Chaudhari and Ghotkar 2018; Saleh et al. 2015).

Need for Crowd Detection: Hiring human beings for crowd estimation is certainly not feasible in remote areas as it requires a lot of investment of time and cost. Using this method can lead to human errors. To avoid such errors, crowd detection systems are needed (Yamin 2019).

Applications or Requirement of Crowd Estimation

Headcount in densely populated areas: Population across the planet is increasing rapidly. Maintenance of peace and order at places like airports, railway stations, and places of large gatherings has gained prime importance. The count of people is very important in any system that manages the crowd. In any system, there might be the unavoidable point of high people density where early detection will avoid blockage and unhealthy outcomes. Counting methods are facing challenges due to large variations in illumination. As the CMS is evolving, difficulties in counting are getting reduced to some extent.

Public Events Management: Sports events, music, other Concerts, political gathering as well as rallies are studied about people densities at different points at different times. This becomes useful in crowd movement optimization. Religious events like Kumbh (Yamin 2019) provide a challenging task crowd management system. Kumbh is organized in a cycle of 12 years and its venue changes every 3 years occurring at Allahabad, Haridwar, Ujjain, and Nashik (Char Dham Yatra 2017). Millions of people gather at Kumbh. As Kumbh venues are situated on banks of mighty rivers, crowd density becomes thin. However, the crowd on Mauni Amavasya (Wikipedia

Allahabad Kumbh Mela 2018) can be very huge and stampedes have been observed. In 2013 about 20 million had a holy dip at the function of Ganga, Yamuna, and Saraswati at Allahabad. With such a large gathering we need are optimized crowd detection and management system.

Military Applications: The number of count of soldiers along with a count of military machinery such as tanks, fighter planes and their motion, etc. can be estimated and projected through the proper crowd management system. This prediction and data can strengthen any armed force and gives an advantage over the enemy.

Disaster Management: There are various overcrowding conditions at the time of food distribution or overcrowding in shelters hence proper management of resources at such time such systems can be very helpful and efficient without any stamped.

Suspicious-Activity Detection: To have successful events with any uncertain activities such as terror attacks, crowd monitoring, and management systems are utilized. Few of these methods which can be used for proper detection and monitoring of such unusual activities can be tracked and solved avoiding any causality.

Safety Monitoring: Nowadays CCTV monitoring systems are usually installed at a large scale in various areas such as religious places, airports, and public locations which helps for better crowd monitoring and management (Building Crowd Counting Model Python 2019), say for example if developed a system that is capable of analyzing behaviors and congestion time slots which helps to ensure safety and security (Khan et al. 2020; Al-Salhie et al. 2014).

Crowd Artificial Intelligence: The analysis and use of crowd movement, also known as swarm intelligence, can contribute to the modelling of group behavior based on biological and artificial models, among other things (Crowd Analysis 2023).

2 Different Methods to Do Crowd Detection

Crowd detection can be done either by use of a sensor-based system or an image processing and detection system.

2.1 Crowd Detection Using Sensors

Managing densely populated places has always proven to be a difficult task. Because the successful management of such events is heavily reliant on the application of advanced technologies, the use of advanced technologies is highly recommended. There have been numerous instances in which the application of cutting-edge technology has resulted in significantly enhanced crowd management. There have been numerous advancements in the development of recognition and sensor devices in recent years. Such technologies, when combined with appropriate backend database systems, have the potential to significantly improve crowd management operations. Managing huge groups of people is a difficult, time-consuming, and expensive endeavor. One of the most often utilized technologies is the use of RFID tags. The use of RFID tags, in conjunction with other supported wireless technologies, can help to alleviate several challenges associated with crowd management. Many activities of daily life are currently managed and administered by such technologies, which are already being utilized to manage and administer them. These technologies have not yet been evaluated for their effectiveness in managing large groups of people, which is a constant source of concern for the industry. A popular information exchange technology, radio frequency identification (RFID) is widely used in a variety of fields including electronic passports, animal tracking, supply chains, industrial automation, mining security, hospital and asset management systems, medicines, and other fields. Existing positioning methods, such as GPS, are insufficient for indoor applications due to the inability of the terminal to receive a signal from satellites. Using an RFID positioning system for locating things or people at a crowded event can help to strengthen and improve the capability of positioning systems for use in indoor applications, which is very beneficial. Basic RFID is a threshold-based system that may be used for human-based categorization systems in busy areas and can also be used to locate tags that have been lost or stolen. The RFID scanners are installed in a fixed location, and each tag can be assigned to a certain individual. Anyone individual from the group can acquire an appropriate number of tags by providing identity data at the established registration counter. Members of the rest group can gather tags from that particular individual. If a person goes missing, it can be quickly identified by utilizing the unique tag identification number, and the total number of individuals in the crowd may be estimated by counting the total number of tags distributed (Soman and Jacob 2018).

Although this system has several disadvantages, such as the fact that only a few RFID tags may not be detected in a very dense crowd because the detecting sensor network unit may not be deployed in all locations due to a lack of available space, it has some advantages. Even though they have few limits, these notions have revolutionized the tracking and retrieval of information from obscure locations. Also, these technologies have opened up a plethora of possibilities for the Internet of Things (IoT), which has prepared the way for an array of new applications.

RFID tags and labels are particularly specific to the type of material and size of your assets, which is one of the few additional disadvantages. For example, if an RFID antenna comes into touch with metal, it will be disabled, and as a result of the interference, the tag will not transmit at all. In addition, if RFID is to be used on metal, a particular type of tag with a block will be required to avoid interference with the antenna from occurring. Liquid materials can also interfere with signal reception and degrade the dependability of transmitted signals. A metal shopping cart loaded with beverages via an RFID scanner will not detect precisely or will not result in a reliable scan, which is one of the reasons why RFID isn't used in grocery stores.

2.2 Crowd Detection Using Image Processing

This section describes the different state of the art of such image processing algorithms which are used for crowd estimation and their related applications. It also gives different approaches to crowd estimation and the state of the art, every single approach has been described below in brief to get us an idea about different aspects and approaches which can be utilized for crowd detection and Estimation for better management in different aspects.

(a) *Crowd estimation in small crowd*: It is an easier method for accounting the count in large crowds. The first and foremost step involved in processing is to detect the foreground blobs with the help of background subtraction. The method used is based on Multiple Gaussians. To obtain homogenous blobs, tuning of algorithms and Morphological dilation of blobs is done to fill the consistent gaps because of unavoidable statistical shortcomings of algorithms. The camera calibrations are achieved by the Tsai algorithm which gives a set of parameters that can be used to project. The blob projection will result in a map plane called the Ground plane. When an object is present far from the camera, its projected size becomes bigger and becomes evident as the angle of the camera decreases. This can be reduced by placing the ground plan at an approximate height of the person and taking the intersected area of those projections along with a parallel plane. The latter plane is called the Head plane. When blobs are constructed, the spaces are filled by morphological dilation (Senst et al. 2014). Hence the points lost due to the initial ground-plane projection are restored by the growing region, and the blob dimensions are affected much. The head plane should be adjusted practically, considering the two following facts. (1) Objects which are below Head Plane are removed by the double projection. (2) Only that HPH that is very manages with the first projected area issues at dissimilar distances partially. The count is obtained from the intersected area of those two projections. Further operations are performed on every blob and added to get the count for the present frame. The total count estimation is then given by subjecting it to sudden oscillations. Then it was heuristically smoothened by using the simplest Finite Impulse Response Filter (FIR), namely the Simple Moving Average (SMA) filter. As the background is estimated at first, the count is always 0 initially. The outcome gives estimation accuracy requirements which are around 20% (Morerio et al. 2012).

(b) *Pixel Counting*: The pixel counting system considers the geometric correction which is generally ignored by other methods. It gives the relation for the ground plane and geometric correction. The performance of this method relies on the foreground segmentation result. Assuming certain conditions the authors formulated a certain rule of proportionality given as N (persons) = a*N (pixels). If the crowd density is moderate and occlusion is not a factor of importance, the above relationship still holds good but with a constant fixed term and few other parameters: N (persons) = a*N(pixels) + b. Another important parameter to be considered is the perspective distortion which can be corrected by using geometric correction. It first computes the scale for the lowest level plane (GC) and then discusses its applicability to the estimation. After the application of the robust segmentation algorithm, mask determination is done as the segmentation results in false foreground regions. The Region of Interest (ROI) is accounted for manually and the mask is designed. It can also be found by using the accumulation of the foreground pixels. The authors also developed a method that is adaptive to time variation and can be used for the unusual crowd.

(c) *Motion estimation and motionless detection method*: This method addresses the problems and provides solutions for motion estimation and also a motionless detection method is developed to handle followed challenges: real-time constraints, deformable objects, and occlusion. This method is an optical technique that suits crowd monitoring. The block matching technology is the basis for motion detection and estimation. This method uses three techniques as shown below: Matching techniques: This method converts images into blocks and according to a similitude criterion it compares two subsequent images. A similitude function was chosen based on "add the differences in absolute value". The size of the block provides good results at the cost of sensitivity. Hence to reduce computational complexity they chose a smaller block size. The matching is done only along the edges. Hence, they could not succeed in improving the computational time required to precede images online. Frequential techniques: This method suits spatial time-related surfaces which is a constant phase to obtain the two motion components. A set of Gabor filters are convolved with the image and using this technique they get the displacement vectors. The disadvantage here is that it is time-consuming. Differential techniques: This method is based on the assumption that the brightness of a moving point is constant concerning time. The proposed system implements the modified Horn and Schunk method in which the velocity vectors have a very small change between the consecutive images. A global crowd motion direction is obtained by using these results. To process the segmentation in good context two filters namely spatial filtering and temporal filtering are used. In the motionless detection, a module finds all those places where the motion is in action. By eliminating the respective areas and filtering the results stationery persons/objects can be located. The computation takes place only when there is no existence of motion. As a result, the stop duration gets a delay at every occlusion. To prevent the occlusion rate is recorded for a given frequency and the duration is corrected using the information. The accuracy of this system is found to be around 93%.

(d) *Granular computing-based image segmentation*: In this method crowd segmentation-based framework uses granular computing (GCS) to validate the issue of crowd segmentation to be analyzed in a discrete hierarchy of granular, and to map issues to small problems. It shows it can make pixels into proper atomic structure granules by dissolving the correlation in the pixel granules. In GrC-based crowd segmentation (GCS), in which granules are the fundamental thing, each step follows a non-identical level of granularity. This is done to obtain the capability of people to detect at various granular levels with the aim of mapping issues to manageable small problems. An extended version of the

Local Binary Patterns (LBP) operator called uniform patterns is used to confront variance in gyration of captured microstructures. The granularity skeleton structures are logically atomic regions in the frame that gives the natural separated areas in between different structures of humans and background. The main aim of the atomic regions is to possess a pixel total process flexible to various crowd scenes. So, this will be the best group diverse structure in the scene for robust crowd segmentation. This method primarily analyses heavily crowded images by adapting principles of GrC to segmentation of crowd problems at different granular levels.

(e) *Parallel Virtual Machine (PVM)*: This technique estimates the crowd density in real-time which is done based on crowd image textures. In this method, input pictures are segmented in the form of classes of crowd density. The classification is then processed using a filtering technique (low pass) depending on the previous images from the incoming image sequences. The first stage involved in this method is the categorization of every pixel obtained from the sequence of images into one of the previously recognized texture classes. This process of classifying each pixel is carried out based on the method of Self Organized Maps (SOM). The SOM uses the feature vectors of the textures taken from co-existed matrices. As the classification of various pixels takes a lot of time in the real-time environment, the method is extended using a distributed algorithm called Parallel Virtual Machine (PVM). The steps involved in this algorithm are: initially, the master processer cuts the input image into n pieces called fragments (where n refers to the count of slave nodes in the bundle). Then each of the broken image fragments is put into the slave processor. The function of the slave processer is to perform the classification of the texture of the image fragments by adapting a sequential algorithm. Further, the slave processor sends the allocated pieces to the master. Lastly, the master arranges every fragment into a terminal texture-segmented image. Texture segments and histograms are calculated as a feature vector and SOM neural network carries out the classification of the input images into their crowd density classes. The method proposed is experimented on a sequence of approximately 10,000 images captured sequentially from a tape that is recorded in a region of the airport. The technique was tested on different classes like the VH class, VL class, and the H class, and the best results were shown for the VH class (95% accuracy).

(f) *SVR model*: This procedure evaluates crowd density and individuals in images. Due to alterations in the crowd images, the density may differ across the vision's field. To overcome this problem, images are separated into small patches of the same dimensions called patches, and this number of patches is determined. The information is extracted from various places regarding headcount, confidences, and absolute errors from the given patch. Further, to improve the count accuracy, the authors introduced cascade training of head images, with a selection of bounding boxes covering all the positions and orientations of the human heads. This method is a fusion of three systems: head detection, Fourier analysis, and feature extraction. Head detection is done using a HOG-based feature descriptor. This method is used to differentiate the local object and outline it by using edge detection and intensity gradients. The image is then segmented into tiny spatial regions called patches for which 1-dimension histogram gradients or edge orientations of the given pixels are calculated. The human head appears as small dots in high-density crowd images. To overcome this problem, Fourier analysis of the image is done which is accurate in detecting human heads. Fourier transform of all the patches is obtained to get information about positions and large changes in the intensity values. The high frequencies in these patches are filtered out by Butterworth's low pass filter. The target size is chosen as a trade-off between better results and increased time of detection. Fourier analysis is accurate for crowded patches but not for non-crowded patches. To solve this problem, the confidence of the patch is calculated and combined with the results of the determined Fourier model. The interests point in the images are then detected using SIFT features. The descriptors of these points frame the base strategy which classifies crowd and non-crowd objects. This also uses the K-means clustering technique. Once the number of patches is obtained, the e-SVR model is done and is used to train the patches on their ground truths. The model is tested on crowd databases (Sneha et al. 2018). Below given are some specific methods used in Image processing used for an object as well person detection methods:

(1) Detection-based methods: For counting and identifying people in an image, a moving window-like detector is used. Such methods are not suited for crowded images as objects are not visible. These methods suit better for face detection as low-level features are extracted and pre-trained classifiers are required. (2) Regression-based methods: Regression-based method crops the patches from the image and then, for all patches low-level features are extracted. (3) Density estimation-based methods: A density map is created for the objects. Then algorithm learns a linear mapping between the object density map and the extracted features. (4) CNN-based methods: As CNN-based methods are suited for classification and regression. End- to end regression model is built instead of looking at the patches. It inputs the entire image and generates the crowd count and crowd density map (Building Crowd Counting Model Python 2019).

3 Implementation

Crowd estimation can be achieved only after the detection of no person in the crowd that number will aid in the precise estimation of the crowd. To do so we are using the image processing technique now the technique that has been used is implemented firstly on a still image and then on a live video, as the base logic algorithm is somewhat different in both cases. In the case of a still image, objects are counted, and added to these objects are counted by label/class. In the case of live footage sequence of frames is analyzed at a time. Given below is the General flow chart that has been utilized for detecting people from the given still images. The entire process mentioned in the

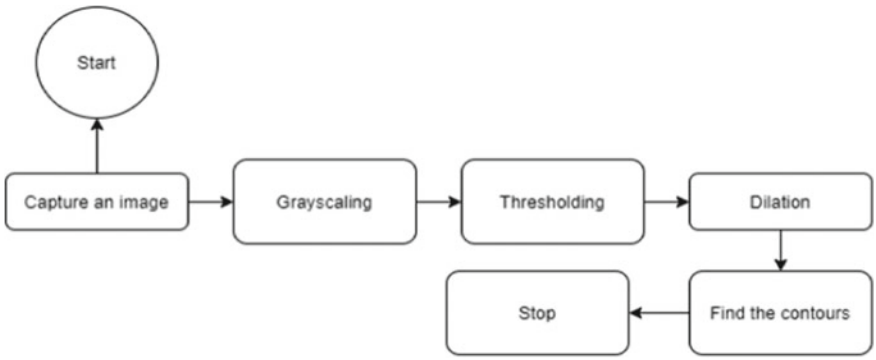

Fig. 1 Flowchart for detecting people from an image

flow chart is divided into segments according to their functions and outcome. Detail description of each segment is given (Fig. 1).

3.1 *Implementation of Still Images and Real-Time Video Streaming*

This section of Implementation consists of five sections as shown in the figure flowchart, each part has got its role of processing images and getting to the final result of headcount, most steps for still image processing and videos are almost the same. The approach can be roughly concluded as: (1) Loading, (2) Pre-Processing, (3) Processing, (4) Segmentation.

3.1.1 Input Feeding

In the case of still image crowd detection, the input image is captured and loaded to the system to perform the image processing technique, while in the case of real-time crowd detection, the live video stream is loaded as input in case of live streaming crowd detection for further processing.

3.1.2 Pre-processing

In this section few processes are done to synchronize the image for proper processing.

Gray scaling: A digital image usually contains both color information and luminance or grayscale. If you remove the color information, you are left with grayscale, resulting in a black and white image. A digital image is composed of groups of three pixels with colors red, green, and blue (RGB), also called channels in digital

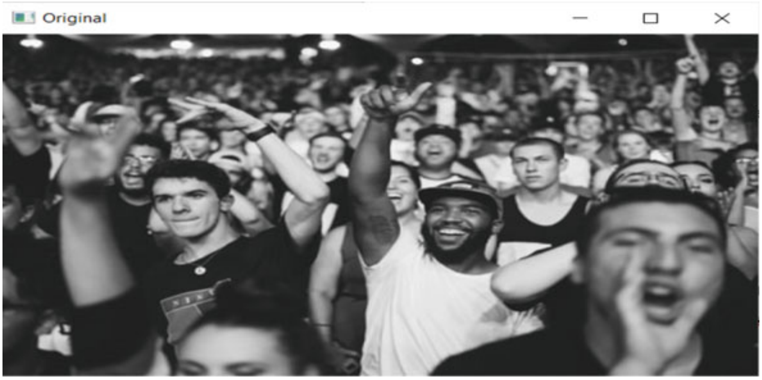

Fig. 2 Grayscale image

imaging. Each channel also contains a luminance value to determine how light or dark the color is. To get a grayscale image, the color information from each channel is removed, leaving only the luminance values, and that is why the image becomes a pattern of light and dark areas devoid of color, essentially a black and white image. Grayscale simplifies the algorithm and reduces computational requirements. Indeed, color may be of limited benefit in many applications, and introducing unnecessary information could increase the amount of training data required to achieve good performance (Fig. 2).

Thresholding implementation on images: Thresholding is generally used for image segmentation. This method is a kind of image segmentation that separates objects by altering grayscale images into binary images. After the image is gray scaled threshold value was used to classify the pixel values.*cv2.THRESH. BINARY_INV* was preferred as the pixel intensity was less than the threshold. The image thresholding technique is the most appropriate in images with high stages of contrast. The thresholding procedure can be stated as

$$T = T[a, b, p(a, b), f(a, b)] \tag{1}$$

where T represents the threshold value, the coordinates points of threshold value (a, b), and the grayscale image pixels are $p(a, b)$, $f(a, b)$. The resulting binary thresholding image is displayed in Fig. 3.

After thresholding dilation process and removal of black distortion were performed: To estimate the crowd from the image, the dilation technique was used to have connected the nearest regions so that it outputs one region per person (Fig. 4).

Then contours were found: To count the persons and record the position of the person's contours were found same procedure would be repeated in live streaming detection. The contours were detected using cv2.findContours with morphological transformations. Cv2.RETR_EXTERNAL detected the outer contour and cv2.CHAIN_APPROX_NONE algorithm was applied to make contours. The

Fig. 3 Thresholded image after gray scaling

Fig. 4 Dilated image

features of contours like perimeter, area, bounding box, and centroid were found, and entry and exit contours were printed on the frame. The centroid was extracted using the formula. This contour count was utilized for headcounts.

$$Cx = M[\text{`}m10'] / M[\text{`}m00']$$

$$Cy = M[\text{`}m01'] / M[\text{`}m00']$$

3.1.3 Motion Analysis: This Section is Concerned with Live Streaming Crowd Detection

While building the OpenCV Crowd estimator the camera module was continuously capturing the frames and these frames were processed with HOG to detect the objects

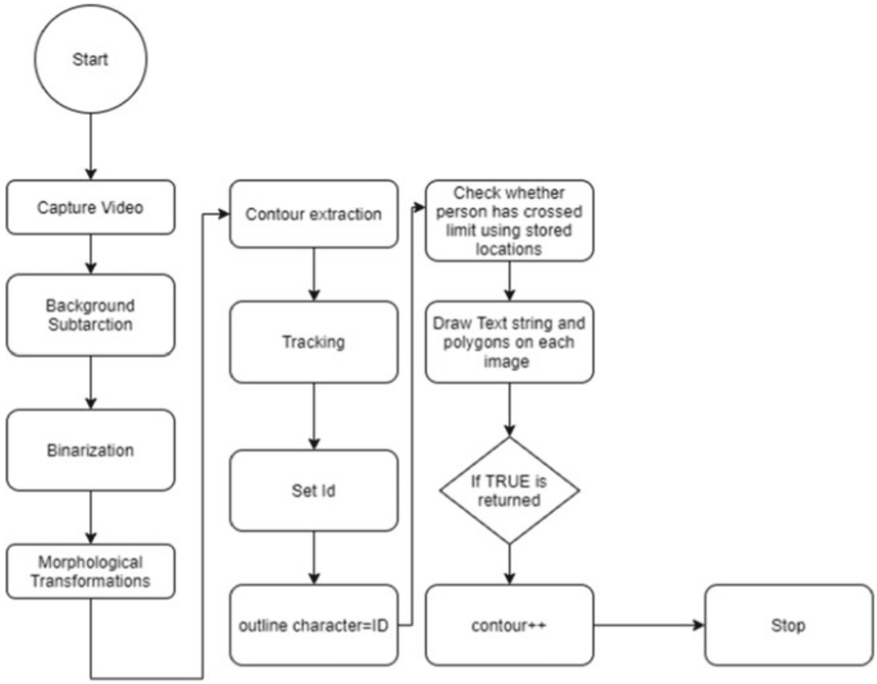

Fig. 5 Flowchart for motion analysis

in the images (Fig. 5). The process of Counting People in the live video consists of the following steps:

Reading the live captured video: Each photo frame was read from the video. To capture live video from the camera id '0' was passed to the Video Capture object. The captured properties like area and the threshold were printed on the console and entry and exit lines as red and blue with count on the frame. The algorithm inputted the background pixels and set a Gaussian distribution to each. The algorithm identifies the background from the Gaussian mixture. Then the elements were structured for morphogenic filters.

Pre-processing

(a) *Background Subtraction*: The foreground and background of the image were identified by performing background subtraction. For background subtraction, the MOG2 subtractor was used so that continuously the background gets calculated. After the background subtraction shadow (grey) was taken out and the video stream was made clear (Fig. 6).
(b) *Thresholding*: After performing background subtraction, using the THRESH_BINARY function the image was binarized. The below given formula is utilized for binarizing the image (Extended Image Processing 2000).

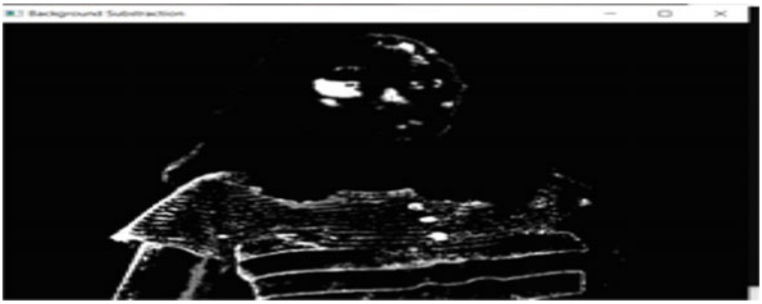

Fig. 6 Result of background subtraction

$$\mathrm{dst}(x, y) = \begin{cases} \mathrm{maxValue} \ \text{if}\ \mathrm{src}(x, y) > \mathrm{T}(x, y) \\ 0 \qquad\qquad\ \text{otherwise} \end{cases}$$

(c) *Morphological transformations*: Erosion and Dilation were applied to binarized images. For erosion and dilation kernel value was specified to calculate the value of each pixel. Erosion also referred to as (opening) expanded the black portion of the image to the white portion and dilation also referred to as (closing) expanded the white portion of the image to the black portion (Fig. 7).

(d) *For extracting contours*: The contours were detected using cv2.findContours with morphological transformations. Cv2.RETR_EXTERNAL detected the outer contour and cv2.CHAIN_APPROX_NONE algorithm was applied to make contours. The features of contours like perimeter, area, bounding box, and centroid were found, and entry and exit contours were printed on the frame. The centroid was extracted using the formula:

$$Cx = M[\text{`}m10'] / M[\text{`}m00']$$
$$Cy = M[\text{`}m01'] / M[\text{`}m01']$$

Fig. 7 Masked image

The contour of the head is the most suitable feature then by using this as a locus, a low-level filtering is applied to approximate the position of the head or in other words the person itself. This system finds application in environments where a dynamic frame of reference can be used in maintaining access records of a building and detection of persons in a crowd.

3.1.4 Tracking

Tracking simply lists out the coordinates before the person. To track the person in a frame and to get the details like direction (up/down):

1. Firstly, an ID was fed and stored in the initial location of the image.
2. Then in the subsequent frame outline of the character was matched with the set ID and the coordinates of the person were saved.
3. If the person passes the limit in the image all the stored locations were used to assess whether the person is moving up/down.
4. After the contours were detected text string was drawn on frames and images polygons were drawn on each image.
5. To make sure that the person is moving in up and down in the frame. Two imaginary lines were created that indicated when the direction of the person was evaluated (line up and line down). While evaluating whether the person had crossed line-up or line-down in the proper direction if TRUE was returned the counter got incremented, that is, on headcount increases that means one person is counted that's how persons are counted within the crowd (Fig. 8).

Fig. 8 Line up and line down

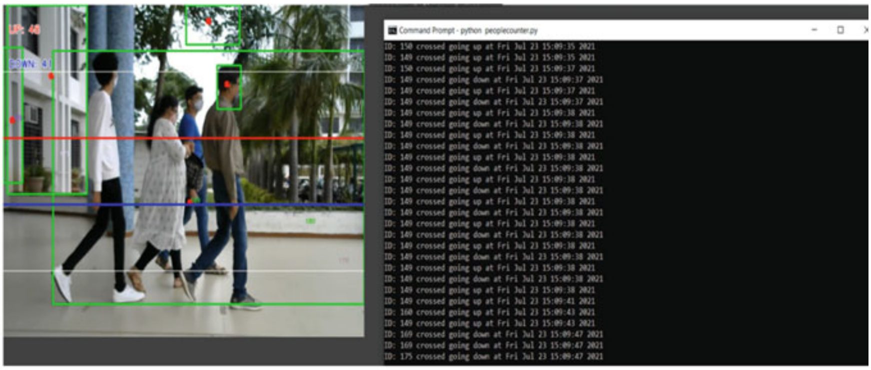

(a)

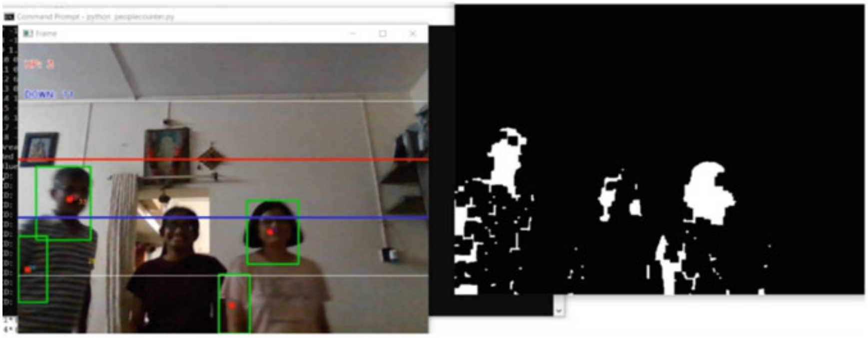

(b)

Fig. 9 **a** Livestreaming snapshot of people moving along with data on the console. **b** Livestreaming snapshot of people moving along with mask and data console.

4 Experimental Results

Masked, original frames with final results were printed on the console. It can be seen in the frame for each up and down collective ID is generated and the count is added not only that along that one can get the count time based as date and time of each contour can be saved and utilized for later analysis (Fig. 9).

5 Conclusion

This paper discusses a real-time computer vision-based system for detection, tracking, and verification of humans in an unpredictive environment in detail. Detecting an individual flawlessly in a live video has become an important topic of research nowadays and it has numerous research applications. The task becomes difficult when we have to process images from CCTV which provide low resolution. Our system is robust and efficient. Robustness has been obtained by the amalgamation of two algorithms and each algorithm uses an independent process of recognizing humans. The proposed technique provided good performance in a difficult environment where there are no still images instead input to the system is video sequences. In this paper, as a people counter is designed using HOG and OpenCV to generate an efficient people counter, developed the conceptual project where you can supply the input as video, image, or even a live camera, with help of a count of persons we can limit crowd by setting the threshold at certain detection of the count of persons to avoid any adverse situation.

References

Al-Salhie L, Al-Zuhair M, Al-Wabil A (2014) Multimedia surveillance in event detection: crowd analytics in Hajj. In: Proceedings of the design, user experience, and usability, Crete, Greece, 22–27 June 2014, pp 383–392

Building Crowd Counting Model Python (2019) https://www.analyticsvidhya.com/blog/2019/02/building-crowd-counting-model-python/

Char Dham Yatra (2017) Sacred Yatra. http://www.sacredyatra.com/badrinath-pilgrimage-stats.html. Accessed 23 Jul 2018

Chaudhari MD, Ghotkar AS (2018) A study on crowd detection and density analysis for safety control. Int J Comput Sci Eng 6(4):424–428

Crowd Analysis (2023) https://en.wikipedia.org/wiki/Crowd_analysis

Extended Image Processing (2000) https://docs.opencv.org/3.4.12/df/d2d/group__ximgproc.html

Khan K, Albattah W, Khan RU, Qamar AM, Nayab D (2020) Advances and trends in real-time visual crowd analysis, MDPI. Sensors 20:5073. https://doi.org/10.3390/s20185073

Morerio P et al (2012) People count estimation in small crowds. In: 2012 IEEE ninth international conference on advanced video and signal-based surveillance, pp476–480

Saleh SA, Suandi SA, Ibrahim H (2015) Recent survey on crowd density estimation and counting for visual surveillance. Eng Appl Artif Intell 41:103–114. https://doi.org/10.1016/j.engappai.2015.01.007

Senst T et al (2014) Crowd analysis in non-static cameras using feature tracking and multi-person density. In: 2014 IEEE international conference on image processing (ICIP), pp 6041–6045

Sneha PK, Rabichith SNS, Borra S (2018) Crowd density estimation using image processing: a survey. Int J Appl Eng Res 13:6855–6864

Soman A, Jacob S (2018) An efficient and decisive crowd management system based on RFID technology. Int J Adv Res Ideas Innov Technol 4(2):4

Wikipedia Allahabad Kumbh Mela (2018) https://en.wikipedia.org/wiki/Allahabad_Kumbh_Mela. Accessed 13 Aug 2018

Yamin M (2019) Managing crowds with technology: cases of Hajj and Kumbh Mela. Int j Inf Technol 11:229–237. https://doi.org/10.1007/s41870-018-0266-1

Determination of Crop Suitability Based on Soil pH Using Image Processing and ANN

Vidya I. Hadimani, Keerti Naregal, Roopa Hubballi, and Savita Bakare

Abstract Indian economy is largely agriculture based. With the increasing population, there is need for technological advancements in the field of agriculture to increase the yield and to satisfy the entire population. Determination of soil pH is important in finding the crop suitability. Soil pH measures the acidity or alkalinity of the soil. Soil has various elements like nitrogen, phosphorus, potassium, calcium, magnesium etc. Their varying amount determines the soil pH and the color of the soil. Crop suitability and the amount of nutrients available is based on the range of soil pH. In our work, RGB-based soil pH detection and crop suggestion system is developed which makes use of image processing techniques and ANN, in finding out the pH value and composite nutrients of the soil. The system provides 95% accuracy compared to laboratory results. This system is fast, simple and cost-effective means to provide soil pH values for the captured soil images and can be used for various applications. Our application suggests the suitable crops based on the pH value.

Keywords Soil pH · Image processing · RGB · Crops · ANN

1 Introduction

India practices agriculture since ages and soil plays a major role in agriculture. The properties of soil can be categorized as chemical and physical. In the chemical properties pH value is of prime importance and in physical we have characteristics like moisture content, texture, etc., which determine the soil quality (Barman et al. 2018). The soil pH is a measure of acidity and alkalinity in soils. The soil health is known by the nutrients contained in it and its pH value which ranges from 1 to 14 on the scale. Usually soils have pH ranging from 3 to 10. The pH value 7 is neutral, below 7 value indicates that the soil is acidic and above 7 the soil is alkaline in nature. If the

V. I. Hadimani (✉) · K. Naregal · R. Hubballi · S. Bakare
Department of CSE, K.L.E. Dr. M. S. Sheshgiri College of Engineering and Technology, Belagavi, India
e-mail: vidyahadimani@klescet.ac.in

J. K. Deka et al. (eds.), *Emerging Technology for Sustainable Development*,
Lecture Notes in Electrical Engineering 1061,
https://doi.org/10.1007/978-981-99-4362-3_51

soil is highly acidic or highly alkaline it is not suitable for the growth of the crops. The nutrients contained in soil is actually affected by the soil pH. In acidic soil having pH below 6.0: the nutrients such as potassium, nitrogen and phosphorus are less in quantity. In alkaline soil having pH of more than 7.5, phosphorus, manganese, and iron are less in quantity (Kumar et al. 2014). The RGB colors are the visual properties of the soil which helps in finding the pH value of soil (Sudha et al. 2017).

There are mainly two types of traditional methods for the classification of soil: laboratory testing and in-situ investigation. The latter included ground water investigation, drilling and sampling and in situ testing. The tests such as Vane shear test, standard penetration test, pressure meter test and cone penetration test are the in situ tests (Chandan 2018). With many years of experience the experts analyze the texture of the soil with handfeel and visually inspecting the soil (Chung et al. 2012).

The crop to be grown can be suggested based on the soil pH value. The soil is highly acidic in the pH range 3.5–4.0 and highly alkaline in range 8.5–9.0, hence are not suitable for any crop. The soil pH range and depending on that the suitable crops that can be grown are given here: for range 4.5–6.0, crop suggested are rice, soybean, wheat, peanut, pea and potato. For range 6.0–6.5, crop suggested are rice, soybean, wheat, beetroot, corn and sweet potato. For range 6.5–7.5, the crop suggested are soy bean, wheat, barley, cotton, vegetables, oats, mushrooms and oil seeds. And crops suitable for range 7.5–8.5 are oil seeds, vegetables, oats, mushrooms, cucumber, cotton and garlic (Nair 2019).

2 Literature Survey

Authors in Kumar et al. (2014) did an experiment on the 50 soil samples of Nathnagar block of Bhagalpur district. They used the below equation to compute the soil pH index value for each of the samples taken using the pH meter.

$$\text{Soil pH index} = \frac{\text{Red/Green}}{\text{Blue}}$$

For clicking the images digital camera was used and the images were saved in JPEG format. Then these JPEG images were converted to the .img files to compute the digital values. Images were transformed to analyze the RGB layer with the help of TNT Mips technique. The soil pH values obtained by measuring and from the equation, were correlated. The pH value of soil was determined by Digital image processing technique. Digital photographs were used for the determination and analysis of soil pH.

The Rapid Soil Testing kit and Soil Test Kit were used to determine the nutrients and pH level of the soil. The technique used was Artificial Neural Network. Author's program used 670 samples of captured images amongst which 130 images each for Phosphorus, Nitrogen, Potassium and pH while 50 images each for Zinc, Magnesium and Calcium. The neural network architecture includes 5 hidden layers. For the training 70% of images are used, 15% for testing and 15% for validation. The training went on till the network's mean squared error went below 1×10^{-10}. The program was implemented using MATLAB. Also an improvement was suggested by the proponents of recommending the fertilizer for a specific crop (Puno et al. 2017).

Authors of paper (Kumawat et al. 2017) have used three sensors and they inserted those at three different levels in the soil i.e. at top level, middle level and deep in the soil. If the two upper sensors did not detect the moisture the irrigation gets started for some time period. The data of soil moisture is continually sent on the cloud using IOT. This data could be accessed through website or through Bluetooth on an Android application when offline. The irrigation system could be controlled through this App. In an another system, with the help of phone camera the soil images are acquired, pH of soil is determined and depending on this the crop suggestion is made to help the farmers.

In paper (Aziz 2016), a database was used of an already collected data from another study which tabulated the pH value of soil based on the color (RGB) of the soil for 50 samples. Authors compared the soil color values of current sample with that of the color values of samples which were already stored in the database and computed the minimum error to determine the pH value for the current sample.

The neural network was trained using the data in the database. The neural network comprised of three layers. The input layer took the RGB values from the current soil sample, processes these values in the hidden layer consisting of 10 neurons and produces the pH value for the current sample in the output layer. This network used 70% of data samples (34 in number) for training itself, 15% of data samples (8 in number) were used for the validation and 15%(8 samples) for testing.

Paper (Wani et al. 2021) determined the soil pH value using the machine learning classifiers multilayer perceptron, support vector machine, Naïve Bayes and J48 classifiers. Authors used 40 image samples collected from Kaggle. The pH calculated using the above mentioned classifiers in digital image processing techniques are validated by the lab tested pH values of the soil image samples. The classification model is trained by the sample datasets and the results are produced. From the results it is analyzed that with Naïve Bayes and MLP 95% accuracy is achieved for RGB color space, with Naïve Bayes and MLP 95% accuracy is obtained for YCbCr color space and with Random Forest and MLP also 95% accuracy is achieved for LUV color space.

A brief review paper (Srivastava et al. 2021) discusses two types of computer based classification of soil which are computer-vision and image processing based techniques and deep learning and machine learning based techniques. The image processing and computer-vision based techniques consider texture, color and particles size of soil samples. Paper includes a few databases created by researchers which consider various illumination and environmental conditions for image capturing. Techniques of Deep learning ANN, CNN, BPNN were used for crop suggestion based on soil. A bar graph is added which compares the efficiencies of various classification techniques used for soil characterization. The classification techniques compared were BPNN, ANN, CNN, Random Forest, SVM, Quadratic Regression and PCA. Among these CNN gave the highest accuracy of 99.59%. This paper highlights some drawbacks of Deep learning approach and discusses four challenges faced in future work of soil classification.

The various techniques were proposed using digital image processing for determining the soil pH value in Chilke et al. (2017). The methodology proposed includes image capturing through digital camera or mobile phone or scanner. The next step is preprocessing of images which included image resizing, image enhancement to improve contrast improvement, filtering to remove noise, color space conversion. The techniques proposed for segmentation of image were ostu threshold algorithm, penalized fuzzy c-mean clustering, fuzzy c-mean clustering, k-mean clustering. For extraction of feature the methods proposed were gray level co-occurrence matrix, color co-occurrence method, wavelet transform, leaf color extraction using H and B components, Gabor filter. Finally, methods for classification included were principle component analysis (PCA), probabilistic neural network, fuzzy logic, k-nearest neighbor classifier, artificial neural network, genetic algorithm, support vector machine (SVM).

An Android application which accepts an image, processes it and computes the soil pH was proposed by the authors (Nair 2019). They tried their system on eight different types of soil of Kerala and using image processing found the pH value based on RGB colors. For different colored soil RGB value ranges were: for Dark brown colored soil 113–98–30 to 207–186–157, light-yellow soil 128–105–27 to 229–210–152, green soil 152–122–52 to 189–164–113. The values for soil pH were 7.30–7.50, 6.80–7.04 and 5.58–6.58 for dark brown, greenish and yellowish soil, respectively. And the respective pH index values were 0.0070–0.0261, 0.0084–0.0239 and 0.0071–0.0451. Their system also suggested the crops based on soil pH value.

3 Proposed Model

The block diagram of the proposed model is shown in Fig. 1.

The processing of the image is done in multiple stages. First image is acquired with the use of a digital camera or smartphone or a scanner. Next the image is processed by removing noise and filtering it and thus enhancing the image. In the following step feature extraction and detection is done, these steps are repeated for training and for testing.

3.1 Soil Image Acquisition and Preprocessing

It is very important that the images captured are clear and have minimal noise so that they can be used for further processing. The images are going to form a database and will be the training set for the new images for which the application is intended. If the image is blurred or has issues, then even with image enhancements it may be

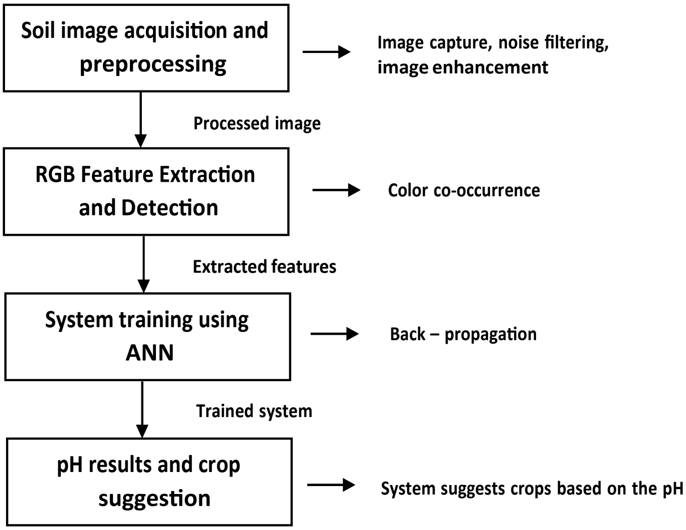

Fig. 1 Flow diagram for training phase and testing phases

difficult to get the required data. Preprocessing of the image involves enhancement of the image, resizing it, noise filtering and removal etc. To convert the RGB image to grayscale the RGB values of each pixel are taken and average is computed.

The average computation can be simple taking (R + G + B)/3 or a human perceived value can be obtained by taking a weighted average as usually the green component dominated.

3.2 RGB Feature Extraction and Detection

This is an important phase as it is key player in determining the pH value. Feature include color, color distribution which forms the texture. Various methods are available for feature extraction, we use color co-occurrence method as it is simple and provides good accuracy. The database is built with the help of sample images which are obtained and these in turn will form the training set of the new images which will be acquired (Fig. 2).

3.3 System Training Using ANN

Soil test kit is used to determine nutrients and pH level of soil. 50 images are taken for each of the parameter under study and the data set is created. These images form the training set input. The training system makes use of a back propagation Neural

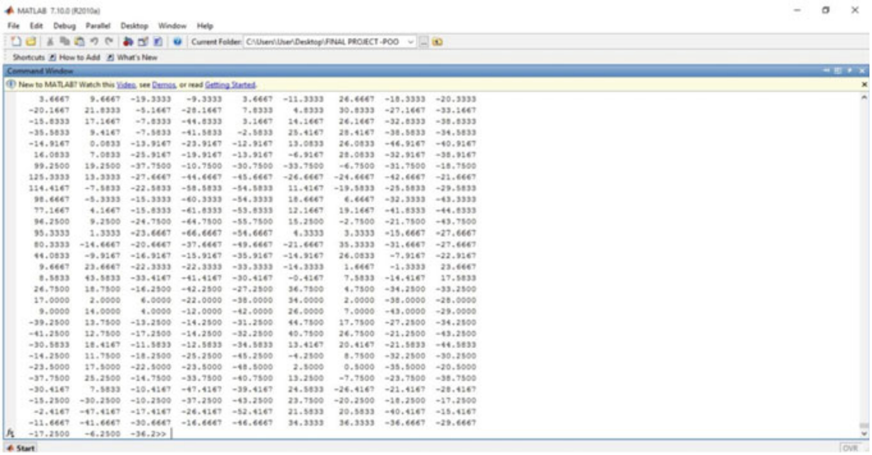

Fig. 2 Feature extraction of images

Network which enhances the accuracy of the system. Each parameter has different inputs and is variedly quantified.

Input data is represented in the form of matrix. The parameters considered are Nitrogen, Phosphorus, Potassium and pH. 50 images are considered for each of the parameter, which are used to train the neural network. A four layer network is used, the first input layer has R, G, B followed by two hidden layers and an output layer.

Using back-propagation method the neural network is trained by fine-tuning the weights using the chain-rule. Layer-wise weights adjustment are done based on the error.

The back-propagation algorithm is used to train the neural network. The weights are initially set and the results are obtained for pH, if the expected and the lab obtained results differ much, the weights are adjusted and the process is repeated till the error gets minimized to 0.12.

3.4 pH Results and Crop Suggestion

The trained system produces the pH and the N, P, K nutrient values as a result and based on these values, the suitable crop to be grown are suggested by the proposed system. The trained system is tested for the sample soil images and found to be efficient and its working is 95% accurate.

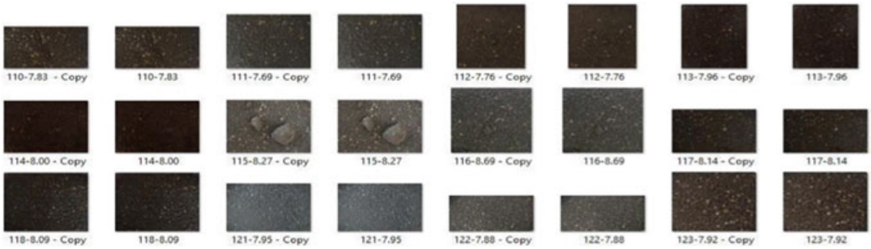

Fig. 3 Images for training the system

4 Results and Analysis

The implementation of the proposed system is done using the MATLAB software. GUI of the system is created which has different options for training dataset, testing, classification and extraction of the classified images. A set of images are stored in a folder in order to train the system. Special features from the image are extracted and stored in a matrix. ANN with four layers is used, which helps in the classification and training of the system (Fig. 3).

The different features are extracted while training the input dataset. RGB features are extracted and arranged in a matrix. These features will be compared with the image to be tested. Once the training set is done for all the images, we can move further for the Testing Phase.

Training images are given to the neural network initially and weights are adjusted for the ANN using iterative learning algorithm. The training process is repeated iteratively till the root mean square error is <0.12.

Table 1 shows the results of the software obtained and lab obtained values. ANN software method mentioned in the table is the proposed method shown in Fig. 1. The pH, N, P, K values are generated by the software, for the given samples. The results obtained match closely with the lab values, with accuracy of 95%.

Table 2 displays the suitable crops for growth based on the soil pH.

5 Conclusion and Future Work

The proposed model could give good results for the determination of soil pH and nutrients. The soil images are taken as input, MATLAB software is used for the processing of the images. User friendly graphic interface helps in easy uploading of images and checking for the pH. The obtained results are compared with laboratory obtained values and system provides 95% accuracy. The obtained results help in finding the crop suitability. The application developed is currently a standalone system working on a desktop/laptop. As part of future work the system can be deployed on a smartphone which will enable capture of live images and check the

Table 1 Result of pH, N, P, K levels

Soil image sample	Lab method				ANN software method			
	pH	N	P	K	pH	N	P	K
1	7.5	L	H	M	7.4	L	H	M
2	8.3	L	H	M	8.1	L	H	M
3	6.5	L	H	M	6.5	L	H	M
4	7.9	L	H	H	7.8	L	H	H
5	8.8	L	H	M	8.62	L	H	M
6	7.7	L	H	M	7.6	L	H	M
7	8.6	L	M	H	8.6	L	M	H
8	8.1	L	H	M	8.0	L	H	M
9	7.5	L	H	M	7.4	L	H	M
10	8.2	L	H	M	8.11	L	H	M

L Low, *M* Moderate, *H* High

Table 2 Crop suitability based on soil pH

Soil pH	Type of soil	Crops suitable to grow
6.0–6.5	Slightly acidic	Garlic, corn, pumpkins, beetroot, cauliflower, rice, sweet pepper, carrot, tomato, wheat, cucumbers, soybean, celery, sweet potato
6.5–7.5	Neutral	Mushrooms, fruits, kale, brussel sprouts, potatoes, asparagus, lettuce, soybean, pulses, sweet peas, oil seeds, cabbage, wheat, vegetables, cotton, oats, barley, radishes, broccoli, beans, rice, tobacco
7.5–8.5	Slightly alkaline	Cotton, brussel sprouts, garlic, celery, turnips, turnip greens, mushrooms, vegetables, cabbage, cucumber, oil seeds, oats, cauliflower, mustard greens

pH, nutrients and determine crop suitability. Such an application with good accuracy can be used for many applications like agriculture (to find crop suitability), horticulture, gardening, fertilizer suggesting etc.

References

Aziz M (2016) Determine the pH of soil by using neural network based on soil's colour. *Int J Adv Res Comput Sci Softw Eng* 6(11):51–54

Azizi A, Gilandeh YA (2020) Classification of soil aggregates: a novel approach based on deep learning. Soil Tillage Res 199:104586

Barman U, Choudhury RD, Talukdar N, Deka P, Kalita I, Rahman N (2018) Predication of soil pH using HSI colour image processing and regression over Guwahati, Assam, India. J Appl Nat Sci 10(2):805–809

Chandan TR (2018) Recent trends of machine learning in soil classification: a review. Int J Comput Eng Res 8:25–33

Chilke BJ, Koawale NB, Chandran DM (2017) Determination of soil pH by using digital image processing technique—a review. In: International conference on recent trends in engineering science and technology, vol 5 (ICRTEST 2017)

Chung SO, Cho KH, Kong JW, Sudduth KA, Jung KY (2012) Soil texture classification algorithm using RGB characteristics of soil images. J Fac Agric Kyushu Univ 57:393–397

Honawad SK, Chinchali SS, Pawar K, Deshpande P (2017) Soil classification and suitable crop prediction. IOSR J Comput Eng

Kumar V, Vimal BK, Kumar R, Kumar M (2014) Determination of soil pH by using digital image processing technique. J Appl Nat Sci 6(1):14–18

Kumawat S, Bhamare M, Nagare A, Kapadnis A (2017) Sensor based automatic irrigation system and soil pH detection using image processing. Int Res J Eng Technol (IRJET) 4:3673–3675

Mengistu AD, Alemayehu DM (2018) Soil characterization and classification: a hybrid approach of computer vision and sensor network. Int J Electr Comput Eng 8:989–995

Nair MG (2019) Determination of soil pH using digital image processing. Int J Inf Syst Comput Sci 8(2):84–88

Puno JC, Sybingco E, Dadios E, Valenzuela I, Cuello J (2017) Determination of soil nutrients and pH level using image processing and artificial neural network. In: IEEE

Srivastava P, Shukla A, Bansal A (2021) A comprehensive review on soil classification using deep learning and computer vision techniques. Multimed Tools Appl 80:14887–14914

Sudha R, Aarti S, Anitha S, Nanthini K (2017) Determination of soil pH and nutrient using image processing. Int J Comput Trends Technol

Wani T, Dhas N, Sasane S, Nikam K, Abin D (2021) Soil pH prediction using machine learning classifiers and color spaces. In: Joshi A et al. (eds) Machine learning for predictive analysis, lecture notes in networks and systems. Springer, p 141